AWARD NUMBER: W81XWH-15-1-0193

TITLE: Combinatorial Therapies for Neurofibroma and MPNST Treatment and Prevention

PRINCIPAL INVESTIGATOR: Steven L. Carroll, MD, PhD

CONTRACTING ORGANIZATION: Medical University of South Carolina
Charleston, SC 29412

REPORT DATE: APRIL 2019

TYPE OF REPORT: FINAL

PREPARED FOR: U.S. Army Medical Research Acquisition Activity
Fort Detrick, Maryland 21702-5012

DISTRIBUTION STATEMENT: Approved for Public Release;
Distribution Unlimited

The views, opinions and/or findings contained in this report are those of the author(s) and should not be construed as an official Department of the Army position, policy or decision unless so designated by other documentation.

REPORT DOCUMENTATION PAGE

Form Approved
OMB No. 0704-0188

Public reporting burden for this collection of information is estimated to average 1 hour per response, including the time for reviewing instructions, searching existing data sources, gathering and maintaining the data needed, and completing and reviewing this collection of information. Send comments regarding this burden estimate or any other aspect of this collection of information, including suggestions for reducing this burden to Department of Defense, Washington Headquarters Services, Directorate for Information Operations and Reports (0704-0188), 1215 Jefferson Davis Highway, Suite 1204, Arlington, VA 22202-4302. Respondents should be aware that notwithstanding any other provision of law, no person shall be subject to any penalty for failing to comply with a collection of information if it does not display a currently valid OMB control number. **PLEASE DO NOT RETURN YOUR FORM TO THE ABOVE ADDRESS.**

1. REPORT DATE	2. REPORT TYPE	3. DATES COVERED
APRIL 2019	FINAL	1AUG2015 - 31JAN2019

4. TITLE AND SUBTITLE
Combinatorial Therapies for Neurofibroma and MPNST Treatment and Prevention

5a. CONTRACT NUMBER

5b. GRANT NUMBER
W81XWH-15-1-0193

5c. PROGRAM ELEMENT NUMBER

6. AUTHOR(S)
Steven L. Carroll, MD, PhD

Email: carrolst@musc.edu

5d. PROJECT NUMBER

5e. TASK NUMBER

5f. WORK UNIT NUMBER

7. PERFORMING ORGANIZATION NAME(S) AND ADDRESS(ES)
.
Medical University of South Carolina
Charleston, SC 29425

8. PERFORMING ORGANIZATION REPORT NUMBER

9. SPONSORING / MONITORING AGENCY NAME(S) AND ADDRESS(ES)
U.S. Army Medical Research and Materiel Command
Fort Detrick, Maryland 21702-5012

10. SPONSOR/MONITOR'S ACRONYM(S)

11. SPONSOR/MONITOR'S REPORT NUMBER(S)

12. DISTRIBUTION / AVAILABILITY STATEMENT
Approved for Public Release; Distribution Unlimited

13. SUPPLEMENTARY NOTES

14. ABSTRACT
We hypothesize that tamoxifen, trifluoperazine or combined tamoxifen-trifluoperazine therapy will effectively treat established neurofibromas and MPNSTs and prolong survival. We also hypothesize that prophylactic treatment with these drugs will prevent neurofibroma and MPNST pathogenesis. To test these hypotheses, we will: 1) determine whether tamoxifen, trifluoperazine or tamoxifen-trifluoperazine therapy effectively inhibits tumor cell proliferation and survival in established neurofibromas and MPNSTs and prolongs the survival of mice with these tumors and 2) determine whether prophylactic therapy with tamoxifen and/or trifluoperazine will prevent the pathogenesis of neurofibromas and MPNSTs. These preclinical trials will be performed using robust mouse models of neurofibroma (Krox20-Cre;Nf1flox/- mice) and MPNST (P0-GGFβ3;Trp53+/- mice) pathogenesis. In Aim 1, mice with established neurofibromas and MPNSTs will be challenged with vehicle, tamoxifen, trifluoperazine or combined tamoxifen-trifluoperazine therapy and we will establish which of these treatments maximally inhibits tumor cell proliferation and survival and improves long term survival. In Aim 2, we will begin treatment of Krox20-Cre;Nf1flox/- and P0-GGFβ3;Trp53+/- mice with vehicle, tamoxifen, trifluoperazine or tamoxifen-trifluoperazine prior to the development of tumors and continue this treatment to 15 months of age. We will then determine if these prophylactic therapies prevent neurofibroma and MPNST pathogenesis or reduce the number and size of tumors in our mice.

15. SUBJECT TERMS-

Nothing listed

16. SECURITY CLASSIFICATION OF:			17. LIMITATION OF ABSTRACT	18. NUMBER OF PAGES	19a. NAME OF RESPONSIBLE PERSON
					USAMRMC
a. REPORT	b. ABSTRACT	c. THIS PAGE			19b. TELEPHONE NUMBER *(include area code)*
U	U	U	UU	222	

Table of Contents

Page

1. Introduction……. 3

2. Keywords……. 3

3. Accomplishments……..…….. 3-27

4. Impact……...…… 27

5. Changes/Problems...…..…… 27-28

6. Products…….…….…..……. 28-30

7. Participants & Other Collaborating Organizations……... None

8. Special Reporting Requirements…… None

9. Appendices…… 31-224

INTRODUCTION

We hypothesize that tamoxifen, trifluoperazine or combined tamoxifen-trifluoperazine therapy will effectively treat established neurofibromas and MPNSTs and prolong survival. We also hypothesize that prophylactic treatment with these drugs will prevent neurofibroma and MPNST pathogenesis. To test these hypotheses, we will: 1) determine whether tamoxifen, trifluoperazine or tamoxifen-trifluoperazine therapy effectively inhibits tumor cell proliferation and survival in established neurofibromas and MPNSTs and prolongs the survival of mice with these tumors and 2) determine whether prophylactic therapy with tamoxifen and/or trifluoperazine will prevent the pathogenesis of neurofibromas and MPNSTs. These preclinical trials will be performed using robust mouse models of neurofibroma (Krox20-Cre;*Nf1*$^{flox/-}$ mice) and MPNST (P_0-GGFβ3;*Trp53*$^{+/-}$ mice) pathogenesis. In Aim 1, mice with established neurofibromas and MPNSTs will be challenged with vehicle, tamoxifen, trifluoperazine or combined tamoxifen- trifluoperazine therapy and we will establish which of these treatments maximally inhibits tumor cell proliferation and survival and improves long term survival. In Aim 2, we will begin treatment of Krox20-Cre;*Nf1*$^{flox/-}$ and P_0-GGFβ3;*Trp53*$^{+/-}$ mice with vehicle, tamoxifen, trifluoperazine or tamoxifen-trifluoperazine prior to the development of tumors and continue this treatment to 15 months of age. We will then determine if these prophylactic therapies prevent neurofibroma and MPNST pathogenesis or reduce the number and size of tumors in our mice.

KEYWORDS: NF1; neurofibroma; malignant peripheral nerve sheath tumor; calmodulin inhibitor; estrogen receptor inhibitor; therapeutic targets.

ACCOMPLISHMENTS

Although we made extensive progress on our original approved Statement of Work, we were forced to modify our original experimental plan as we encountered unexpected difficulty with the imaging modalities that we originally proposed to use to identify mice with tumors. Consequently, we used an alternative approach to identifying the mice of interest. However, this also led to mandated protocol approval delays in the latter stages of this project and so we are still in the process of analyzing the effects of tamoxifen and trifluoperazine on our mouse cohorts. These parts of the project are indicated below as being “in progress” and are being supported with funds provided by my endowed Chair.

Below, I will first indicate the two Specific Aims of our project and the tasks and subtasks within each Aim. Below each subtask, I will describe the progress that we have made in that subtask. ***As some of these subtasks required identical approaches, the description of the work done for that subtasks may at times appear to be similar to the description previously provided for highly analogous subtasks.*** In addition to this progress, our investigations of the mechanisms of action of tamoxifen and trifluoperazine in MPNSTs led to unexpected findings indicating that two receptor tyrosine kinases, erbB3 and IGF1R, are important therapeutic targets in MPNSTs and that currently available therapeutic agents targeting these receptors are effective against MPNSTs. Consequently, in this report, I will also detail these important new findings which indicate that existing pharmaceuticals can be repurposed to treat MPNSTs.

Specific Aims and Studies in Approved Statement of Work

Specific Aim 1: Test the hypothesis that tamoxifen, trifluoperazine or tamoxifen-trifluoperazine therapy effectively inhibits tumor cell proliferation and survival in established neurofibromas and MPNSTs and prolongs the survival of mice with these tumors.

Specific Aim 2: Test the hypothesis that prophylactic therapy with tamoxifen and/or trifluoperazine will prevent the pathogenesis of neurofibromas and MPNSTs.

Task 1. To determine whether tamoxifen, trifluoperazine or combined tamoxifen/trifluoperazine therapy inhibits tumor cell proliferation and survival in MPNST bearing P_0-GGFβ3;Trp53$^{+/-}$ mice (months 1-36):

a. ***Obtain regulatory review and approval for these studies (months 1-2)***

Submission of the necessary protocols for regulatory review and approval was submitted in month 1, but approval was delayed for 3-4 months by the review process.

b. ***Perform studies with tamoxifen and trifluoperazine to establish maximum tolerated doses of these agents in C57BL/6 mice (months 2-4)***

As a result of our extensive previous experience with preclinical trials in mouse models, we are well aware that the maximal tolerated dose (MTD) for a specific drug often differs in mice with different genetic backgrounds. Consequently, before beginning the full study, it was necessary that we will first determine the MTD for tamoxifen and trifluoperazine in C57BL/6 mice (the genetic background of the Krox20-Cre;*Nf1*$^{flox/-}$ and P0-GGFβ3;*Trp53*$^{+/-}$ mice that are being used for our preclinical trials) and, if necessary, adjust the doses that will be used in our studies following the guidelines outlined in our preliminary studies. We began by determining the MTD for tamoxifen and trifluoperazine when administered via intraperitoneal injection to C57BL/6J mice, following a ‘‘3 + 3’’ regimen. Under this regimen, groups of three mice were treated with each agent for 1 month, following a dosing regimen in which animals received 5 consecutive days of intraperitoneally injected drug, with 2 days rest in between. This dose was increased in a step-wise fashion until adverse effects such as weight loss, alterations in grooming behavior, or death were observed. At this point, 3 additional mice were treated with the same dose to verify its effect on these animals; if it has the same effect, the dose immediately below the dose that produces toxic effects is considered to be the maximum tolerated dose. For all mice, blood was collected via cardiac puncture, centrifuged to separate the cells from the serum and the serum was frozen in aliquots at -80°C if needed in the future to measure levels of markers of the function of key organs [e.g., liver (ALT and AST enzyme levels) and kidney (blood urea nitrogen (BUN) and creatinine)]. Complete necropsies were performed on all mice and detailed histologic analyses were performed on organs most commonly affected by therapeutic agents (brain, liver, kidney, small and large intestine, lung). We found that tamoxifen administered at the maximum dose we tested primarily had negative effects on small and large intestine, which was evident as blunting of intestinal villi. We did not see any overt histologic changes in any of the tissues we examined from mice receiving the MTD of trifluoperazine. We completed the MTD studies with both observational and pathological assessment and established that the maximal tolerated dose of tamoxifen in C57BL/6J mice was 30 mg/kg and that for trifluoperazine was 20 mg/kg.

c. ***Establish cohorts of P_0-GGFβ3;Trp53$^{+/-}$ mice, identify MPNST bearing mice with PET scans and randomize mice into cohorts for treatment with vehicle, tamoxifen, trifluoperazine or tamoxifen and trifluoperazine (months 3-18)***

For the interim analysis, our biostatistician recommended that we look for an effect size of at least 2 (following the measures outlined below) in the treatment versus control groups. One-

way ANOVA with a Dunnett test for adjustment of pair-wise comparisons (compared to the control group) will be used for sample size calculation. We determined that 20 mice per group would give us 95% power to detect at least an effect size of 2 between the treatment groups and the control (vehicle) group, given 5% type I error. We also recognize NIH's recent recommendation that animal experiments include both male and female animals to avoid a sex bias. Consequently, our original experimental design was that each cohort would include 20 male and 20 female mice; male and female mice are analyzed both independently and in a stratified fashion. In accordance with these goals, we have established the full cohort of P0-GGFβ3;*Trp53*$^{+/-}$ mice necessary for Task 1 and are currently following them to identify MPNST-bearing mice which are then randomized into treatment cohorts. We completed our in vivo pharmacodynamic studies to determine the appropriate treatment schedule and found inhibition of pERK and pSGK for approximately 24 hours with no change in pAKT-S473 (Figure 1).

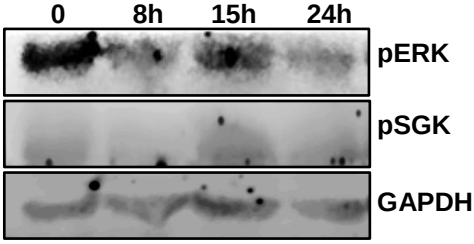


FIGURE 1. Pharmacodynamic studies of tamoxifen and trifluoperazine treatment. Western blot analysis of two targets downstream of drug treatment to show in vivo drug efficacy. Tissue was harvested from animals at 8, 15 and 24 hours after combinatorial treatment at the MTD compared to an untreated control.

In our initial research plan, we proposed identifying MPNST-bearing mice using a combination of PET imaging and monitoring of clinical signs that we had established as reliable indicators of tumorigenesis in several of our previously published studies. However, a large series of studies we have now performed with our genetically engineered mouse models have convinced us that PET does not have sufficient specificity to reliably identify MPNST-bearing mice (i.e., while this modality can recognize the neoplasms of interest, our necropsy examinations indicate that these imaging methods can be fooled, particularly when attempting to identify MPNSTs early in their course; the same turned out to be true for MRIs). We have also noted that this occurs most commonly when the results of the imaging studies and examination of clinical signs are discordant; the clinical signs are simply more reliable. In addition, our imaging facility has been crippled by problems with their instrumentation. Consequently, we modified our approach to identifying MPNST-bearing mice and focused on using clinical signs for the initial identification of MPNST-bearing mice. In this circumstance, our primary readout for drug effectiveness is survival times following the initiation of therapy and changes in proliferation and apoptotic indices as originally proposed.

d. ***Evaluate the effectiveness of the therapeutic regimens described in c (months 12-18)***

As is apparent from the Tasks outlined above, the experiments performed during the last funding period are long-term experiments in which we start the therapies and then follow the mice through the treatment period (see below for more information on our progress in these experiments). Consequently, the long-term nature of these experiments gave us the time to expand upon our tamoxifen and trifluoperazine studies by attempting to more precisely define what signaling molecules downstream of these drugs' target (which our evidence to date indicates is calmodulin) are particularly important modulators of MPNST proliferation and survival. We have previously identified a number of tamoxifen and trifluoperazine downstream effectors by performing kinomics analyses [Brosius et al *Journal of Neuropathology and Experimental Neurology* 73: 1078-1090 (2014)]. However, this approach only identified targets whose phosphorylation was altered by tamoxifen or trifluoperazine treatment; it did not functionally establish which of these targets was actually driving proliferation and survival. To identify the calmodulin-regulated pathways that were required for MPNST proliferation and/or

survival, we have completed functional genome scale shRNA screens on three NF1-associated MPNST cell lines (T265-2c, 90-8 and S462 cells) and a sporadic MPNST line (2XSB cells). These screens utilized a lentiviral library targeting 15,277 genes (Cellecta Decipher™) with each gene typically targeted by at least 5 to 6 shRNAs (a total of 82,500 lentiviral vectors). For those "drop out" assays, the representation of each barcode was quantified in successfully transduced MPNST cells after initial selection and again after 5-7 population doublings. Quantification of the barcodes in the initial and final time point yielded fold depletion values for each shRNA which were then used to calculate a gene-level score for each gene. The hit cutoff value was determined by generating a normal distribution based on the median of each empirical dataset. Genes with quant log scores greater than the 95th percentile of the normal distribution were considered hits for each screen.

We are currently analyzing our screen to identify those candidate signaling molecules downstream of tamoxifen and trifluoperazine. However, while performing these analyses and considering the implications of the findings from our Cellecta screens, we realized that we had generated findings that had additional therapeutic implications for MPNSTs. Loss-of-function mutations of the *NF1* tumor suppressor gene, which encodes the Ras inhibitor neurofibromin, are present in all NF1-associated MPNSTs and a major subset of sporadic and radiation-induced MPNSTs. In the absence of neurofibromin, Ras activation is unopposed, resulting in Ras hyperactivation. Given this, it was reasonable to expect that agents targeting Ras or Ras-regulated cytoplasmic signaling cascades would be effective against MPNSTs. However, attempts to treat MPNSTs in this manner have thus far been unsuccessful. This reflects the fact that multiple Ras proteins are hyperactivated in MPNSTs and that the key Ras-regulated signaling pathways in these tumors are poorly understood. This led us to hypothesize that an alternative approach, namely targeting the upstream proteins that drive Ras hyperactivation in *NF1*-null MPNSTs would be effective against MPNSTs. Prior to testing this hypothesis, though, we had to identify the key Ras activating proteins in MPNSTs. Several previously generated lines of evidence have suggested that one or more receptor tyrosine kinases (RTKs) fulfill this role in MPNSTs. What we realized was that our Cellecta screens would also allow us to identify the RTKs that are essential for MPNST pathogenesis. As a very large number of drugs have been developed that target RTKs, these therapeutic agents could potentially be rapidly adapted to treat MPNSTs in NF1 patients with these neoplasms.

The Cellecta Decipher™ libraries we used target all of the 58 RTKs encoded by the human genome. After calculating gene-level scores as described above, we then extracted the gene-level scores for the RTKs from this dataset and compared them to the gene-level scores for all other genes targeted by the shRNA library to identify the RTKs that were particularly important for proliferation and/or survival.

Many drugs (e.g., the pan-erbB inhibitor canertinib) simultaneously target multiple members of an RTK subfamily, a feature that can be exploited when multiple RTKs in the same subfamily contribute to tumor growth. To determine whether there were RTK subfamilies in which multiple members drove MPNST proliferation and/or survival, we first considered the gene-level scores of the genes in each subfamily as a group and compared the groups to one another to establish whether the depletion of specific RTK subfamilies disproportionately inhibited MPNST proliferation and survival (Figure 1.1). We found that the AXL (MERTK, AXL, TYRO3) and Muscle Associated Receptor Tyrosine Kinase (MUSK) subfamilies played an especially prominent role in MPNST proliferation and/or survival, as multiple members of these subfamilies were depleted in all four of the MPNST lines we screened. The Tyrosine Kinase with Immunoglobulin and Epidermal Growth Factor Homology Domains (TIE; contains TIE1 and TIE2/TEK), vascular endothelial growth factor receptor (VEGFR; contains VEGFR1/FLT1, KDR/VEGFR2 and VEGFR3/FLT4), Lemur Tyrosine Kinase (LMR; contains LMR1/AATK, LMR2/LMTK2, LMR3/LMTK3 and STYK1), Epidermal Growth Factor Receptor (EGFR; contains EGFR, ERBB2, ERBB3 and ERBB4) and Insulin Receptor (INSR, IGF1R, INSRR) subfamilies

also commonly drove MPNST growth, as these subfamilies were depleted in three of the screened MPNST cell lines. The Discoidin Domain Receptor Tyrosine Kinase (DDR; contains DDR1 and DDR2) subfamily was depleted in two cell lines and the Retinoic Acid Receptor-Related Orphan Receptor (ROR) (ROR1, ROR2), RYK/MET (MET, MST1R, RYK), SEV (ALK, LTK, ROS1), Tropomyosin-Related Kinase TRK (NTRK1, NTRK2 and NTRK3), FGFR (FGFR1-4) and ephrin (EPHA1-8, EPHA10, EPHB1-4 and EPHB6) subfamilies were depleted in only one MPNST cell line.

We also noted that there were individual members in several RTK subfamilies whose knockdown potently impaired MPNST proliferation and/or survival. A comparison of the gene-level scores of all 58 RTKs to the gene-level scores of all 15,377 genes examined in our shRNA screens showed that 22 RTKs were represented in the top 5% or 10% of the most depleted hits in at least one cell line. EGFR and ERBB3 were depleted hits in the EGFR family for the T265-2c screen as well as multiple members of the ephrin (EPHA1, 6, 10 and EPHB1) and insulin receptor (INSR and IGF1R) subfamilies as well as AXL (TYRO3), FGFR (FGFR3), VEGFR (KDR), and TIE (TIE1) subfamilies. Multiple hits in the VEGFR (KDR and FLT4) and TIE (TIE1 and TEK) subfamily occurred in the 2XSB subfamily as well as hits in EGFR (ERBB3), EPH (EPHB2), FGFR (FGFR4) and LMR (STYK1) subfamilies. The EPH (EPHA6 and EPHA10)
and VEGFR (KDR and FLT4) subfamilies contained multiple hits in the S462 screen as well as EGFR (ERBB3), insulin receptor (IGF1R), and TRK (NTRK1). Again, the EPH (EPHA1, EPHA4, EPHA8) subfamily contained most of the hits in the 90-8 screen with only the SEV (LTK), insulin receptor (IGF1R), and TRK (NTRK3) subfamilies were represented as depleted hits. Most notably, ERBB3 was our most commonly depleted hit, being a top 5% hit in three of the four cell lines tested. The EGFR family contained genes that were depleted overall compared to all of the other genes in the screen in all cell lines except 90-8.

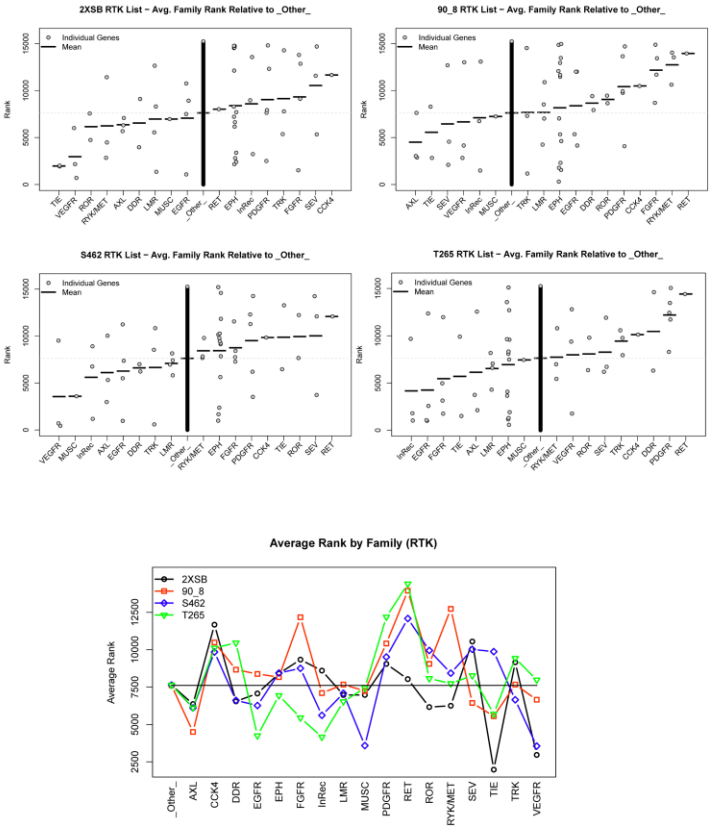


FIGURE 1.1. Graphic representation of the effects of individually ablating each of the 58 RTKs in human MPNST cells; these are grouped into individual RTK families (e.g., all four EGFR/erbB receptors). The four graphs above show the data for individual MPNST cell lines. The composite graph below incorporates the findings from all four lines for a comparison of which RTK families are reproducibly required for MPNST proliferation and/or survival.

To determine whether the RTKs identified by our Cellecta screens were activated in specific MPNST lines, we prepared cell lysates from two MPNST cell lines derived from NF1-associated tumors (T265-2c and S462 cells) and a sporadic MPNST cell line (2XSB cells). These cultures were maintained in serum-free medium prior to harvesting so that Schwann cell mitogens present in high concentrations in serum [e.g., platelet-derived growth factor (PDGF)] would not bias the results of our analyses. Each MPNST lysate was used to probe arrays of antibodies that recognized 49 of the 58 known RTKs. Following the capture of RTKs from the lysates, the

RTK antibody arrays were probed with anti-phosphotyrosine antibodies to identify the captured RTKs that were phosphorylated.

The affinity of anti-phosphotyrosine antibodies such as 4G10, PY20 and p-TYR100 can be altered by the protein sequence around the phosphorylation site. Consequently, we probed replicate arrays with either the antibody provided with the arrays or with PY20 antibody. We found that the antibody provided by the array manufacturer identified a relatively restricted subset of the RTKs, whereas the PY20 antibody detected these same RTKs as well as a number of others which were phosphorylated in MPNSTs. The phosphorylated RTKs detected with one or both antibodies are summarized in Table 1. 32 RTKs were both present and constitutively phosphorylated in all three MPNST cell lines. Of note, these proteins included a number of receptors that have been implicated in MPNST pathogenesis including the EGF receptor, three neuregulin-1 (NRG1) receptor subunits (erbB2, erbB3, erbB4), the hepatocyte growth factor receptor (HGFR) c-Met, the stem cell factor receptor (SCFR) c-Kit, platelet-derived growth factor (PDGF) receptors and insulin-like growth factor-1 receptor (IGF1R) . Upon completion of this analysis we identified not only several RTKs previous implicated but also identified a number of constitutively phosphorylated RTKs which have not been previously linked to MPNST pathogenesis.

These receptors included Axl, Dtk, Mer, multiple

TABLE 1. Kinases phosphorylated within human MPNST cells.

Kinase	MPNST cells lines where phosphorylated		
EGFR	2XSB, S462, T265-2c	**Tie-1**	
erbB2	2XSB, S462, T265-2c	**Tie-2**	2XSB, S462, T265-2c
erbB3	2XSB, S462, T265-2c	**TrkA**	2XSB, S462, T265-2c
erbB4	2XSB, S462, T265-2c	**TrkB**	2XSB, S462, T265-2c
FGFR1	2XSB, S462, T265-2c	**TrkC**	2XSB, S462, T265-2c
FGFR2a	2XSB, S462, T265-2c	**VEGFR1**	2XSB, T265-2c
FGFR3	2XSB, S462, T265-2c	**VEGFR2**	2XSB, T265-2c
FGFR4	2XSB, S462, T265-2c	**VEGFR3**	2XSB, T265-2c
Insulin R	2XSB, S462, T265-2c	**MuSK**	2XSB, T265-2c
IGF1R	2XSB, S462, T265-2c	**EphA1**	2XSB, S462, T265-2c
Axl	2XSB, S462, T265-2c	**EphA2**	
Dtk	2XSB, S462, T265-2c	**EphA3**	
Mer	2XSB, S462, T265-2c	**EphA4**	
HGFR	2XSB, S462, T265-2c	**EphA6**	
MSPR	2XSB, S462, T265-2c	**EphA7**	2XSB, S462, T265-2c
PDGFRa	2XSB, S462, T265-2c	**EphB1**	2XSB, S462, T265-2c
PDGFRb	2XSB, T265-2c	**EphB2**	
SCFR	2XSB, S462, T265-2c	**EphB4**	2XSB, S462, T265-2c
Flt-3	2XSB, S462, T265-2c	**EphB6**	
M-CSFR	2XSB, T265-2c	**ALK**	2XSB, S462, T265-2c
c-Ret	2XSB, T265-2c	**DDR1**	2XSB, S462, T265-2c
ROR1		**DDR2**	2XSB, S462, T265-2c
ROR2	**2XSB, S462, T265-2c**	**EphA5**	2XSB, T265-2c
RYK	2XSB, S462, T265-2c	**EphB3**	

fibroblast growth factor receptor (FGFRs), Tie-2, the Trk family of high affinity neurotrophin receptors, receptor-like tyrosine kinase (RYK), anaplastic lymphoma receptor tyrosine kinase (ALK), DDR1, DDR2 and multiple ephrin receptors (EphA1, EphA7, EphA10, EphB1 and EphB4). In addition, several RTKs were phosphorylated in two of the three MPNST cell lines we examined. We recognize that these latter RTKs may promote pathogenesis in functionally distinct subsets of MPNSTs. Importantly, however, all of the RTKs that were identified as phosphorylated in these arrays were also "hits" in our Cellecta screens.

We then identified pharmacologic inhibitors that targeted each of the RTKs that were identified in our Cellecta screens and/or were phosphorylated so as to establish which drugs were effective against MPNSTs. All of the inhibitors that we selected are either FDA approved or are currently in clinical trials (Table 2). The concentrations that were tested were chosen based on the IC_{50} for each target. Each inhibitor was tested in 4 MPNST cells lines plated at 10,000 cells/well in DMEM10. 72 hours after treatment with inhibitor or DMSO (vehicle control), the number of viable cells was assessed using MTT assays. Canertinib (a broad-spectrum erbB inhibitor), picropodophyllin (an IGF1R inhibitor) and lestaurtinib (targets FLT3, STAT and TRK1/2/3) treated cultures all demonstrated dramatic, concentration-dependent decreases in cell number (Figure 2 A-C) in all cell lines tested. Modest effects on cell number were observed with intedanib treatment (Figure 2D) in the NF1 associated lines, while the sporadic cell line 2XSB was resistant to these effects. Amuvatinib treatment (Figure 2E) also produced modest reductions in cell number in a concentration dependent manner in all of the cell lines. A few of the inhibitors showed limited efficacy in treating MPNSTs. Sunitinib was moderately effective at reducing cell number in T265-2c cells at higher concentrations. Similarly, crizotinib had limited effects in S462 and T265-2c cells. Contrary to previous data, we saw no effects on cell number with nilotinib treatment. These differences are likely accounted for by the differences in inhibitor concentrations utilized in this work are all in the nanomolar range, whereas the previous study utilized nilotinib in the micromolar range.

Table 2. Co-activated RTKs in human MPNST cell lines and corresponding inhibitors

Phosphorylated RTK	Inhibitor targeting kinase
EGFR, erbB2, erbB3, erbB4	Canertinib (CI-1033)
Fibroblast growth factor receptor (FGFR 1-4)	Intedanib (Nintedanib)
Insulin receptor	
Insulin-like growth factor receptor (IGF1R)	Picropodophyllin (PPP)
Axl	Amuvatinib
Dtk	
Mer	
Hepatocyte growth factor receptor (HGFR or c-Met)	Crizotinib
Platelet-derived growth factor receptor (PDGFR a and b)	Sunitinib, nilotinib, intedanib
Anaplastic lymphoma kinase (ALK)	Crizotinib
Flt-3	Sunitinib
Macrophage colony stimulating factor (MCSFR)	Sunitinib
Tie-2	
Trk-A, Trk-B, TrkC	Lestaurtinib
Vascular endothelial growth factor receptor	Sunitinib
EphA1, EphA10, EphB1, EphB4	
Ryk	

To determine if these inhibitors acted by inhibiting MPNST proliferation, we challenged human MPNST cells with a subset of the inhibitors. Using ^{3}H-thymidine incorporation assays, we found that the results paralleled those observed in the viability assays. Consequently, at least part of the effects we observed were due to inhibition of proliferation.

To directly examine the effect these drugs have on MPNST cell survival, we next assessed the survival of treated MPNST cell survival using flow cytometry for Annexin V, a protein that detects phosphatidylserine when it translocates to the extracellular membrane leaflet during initiation of apoptosis, and the viability stain 7-AAD. For these experiments, T265-2c MPNST cells were treated with the IC_{50} of canertinib, lestaurtinib, or PPP or a combination of the inhibitors. We found that individual treatments were largely cytostatic, as cell treated with any of the inhibitors in isolation showed no difference in viability when compared to vehicle treatment. However, when treated with canertinib in combination with either lestaurtinib or PPP, approximately half of the tumor cells underwent apoptosis (Figure 3). Collectively, these data suggest that inhibition of single RTKs is largely cytostatic in MPNSTs, while combinations of these drugs are instead cytotoxic.

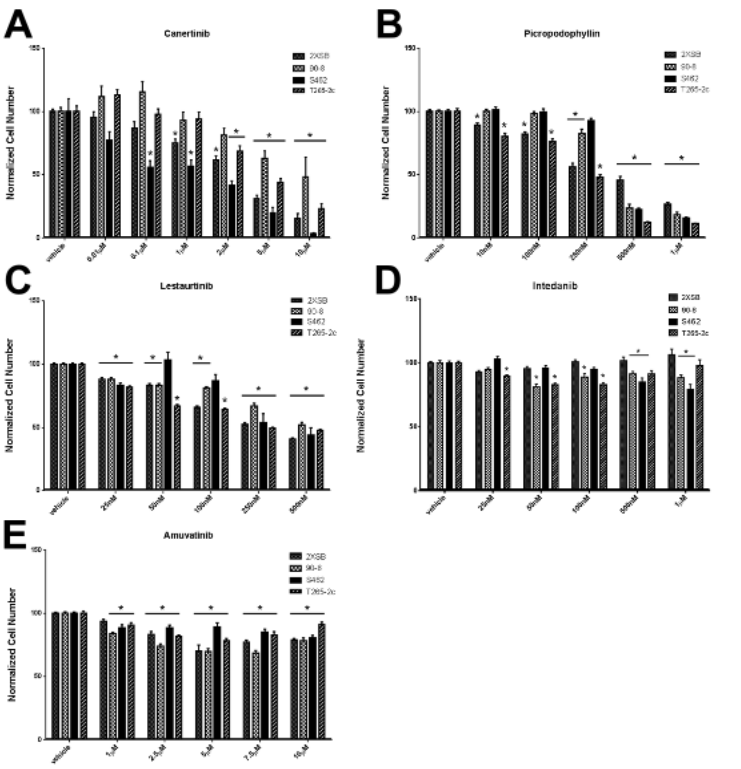


FIGURE 2. Treatment of NF1 associated and sporadic MPNSTs with inhibitors targeting various RTKs results in decreased cell number. **A**. Canertinib, a pan-erbB inhibitor, inhibited cell growth in a concentration dependent manner. **B.** The IGF1R inhibitor picropodophyllin had similar effects on MPNST cell counts *in vitro*. **C.** Lestaurtinib, a pan-Trk receptor inhibitor produced a maximum 50% reduction in tumor cell number. **D.** Modest effects on cell number were observed in 90-8, S462, and T265-2c cells with pan-FGFR inhibition. **E.** Treatment of MPNST cell lines with the Axl inhibitor amuvatinib also produce modest effects on tumor cell counts. (*p<0.05 compared to vehicle control).

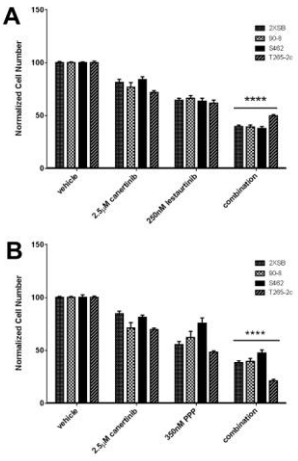


FIGURE 3. Individual RTK inhibition is largely cytostatic, whereas dual treatment is cytotoxic. Flow cytometry of treated T265-2c cells shows decreased viability compared to vehicle or either monotherapy **(A)**. In support of this, we observed significant increases in annexin-V positive cells **(B)** suggesting that dual treatment induces apoptosis. (*p<0.05 compared to vehicle control or individual treatments).

Next, we investigated the effectiveness of these inhibitors as combinatorial treatments *in vitro*. Drugs that inhibited MPNST proliferation as primary therapeutics were used at their IC_{50}. However, it was also possible that inhibitors that did not have an effect as primary therapeutics could be useful as combinatorial treatments due to compensatory signaling. The full concentration curve of these inhibitors was tested in combination with the IC_{50} of canertinib. We found that combinatorial treatment with canertinib and picropodophyllin or canertinib and lestaurtinib decreased MPNST cell number additively when compared to monotherapy or vehicle control (Figure 4). These data confirm previous studies that suggested that the erbB family of receptors and IGF1 receptor signaling both contribute to MPNST pathogenesis.

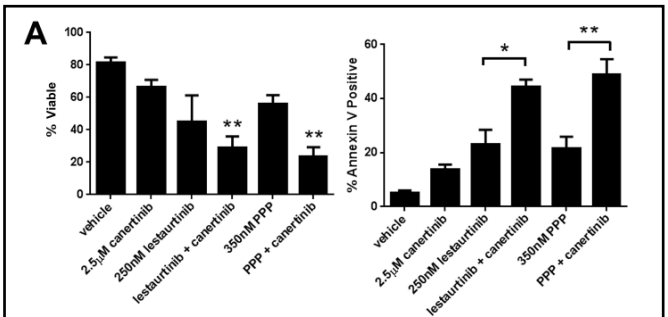


FIGURE 4. Combinatorial treatment of NF1 associated and sporadic MPNST cell lines results in further decreases in cell number. **A.** Dual treatment with lestaurtinib and canertinib reduced tumor cell number to a greater extent than either monotherapy. **B.** Combinatorial therapy with PPP and canertinib at their IC_{50} also more effectively decreased MPNST cell number when compared to either individual treatment. (*p<0.05 compared to vehicle control).

It has previously been demonstrated that inhibition of multiple RTKs in glioblastomas is required to abrogate downstream signaling and thereby prevent resistance to monotherapy. This raised the question of whether erbB kinases, the IGF-1 receptor and Trk receptors cooperate to drive Ras activation in NF1-null MPNSTs. To test this possibility, we examined the effects of monotherapy with canertinib, picropodophyllin or lestaurtinib or combinatorial treatment with canertinib plus either picropodophyllin or lestaurtinib exerted on Ras activation and Erk-1/2 phosphorylation. We found that canertinib and picropodophyllin both produced decreases in Ras activity in S462 cells (picropodophyllin > canertinib; Figure 5A). Surprisingly, however, lestaurtinib had no effect on Ras activation and combinatorial therapy with canertinib and lestaurtinib produced a reduction in Ras activation similar to that seen with canertinib treatment alone. In contrast, treatment with canertinib and PPP together ablated Ras activation (Figure 5A), indicating that both erbB kinases and the IGF-1 receptor promote Ras activation. In keeping with the effects of these drugs on Ras activation, we found that Erk phosphorylation was reduced by treatment with canertinib or picropodophyllin, but not by lestaurtinib (Figure 5B); likewise, combinatorial therapy with canertinib and lestaurtinib reduced phospho-Erk levels to an extent similar to that seen with canertinib alone. As with Ras, combinatorial therapy with canertinib and picropodophyllin completely abolished Erk phosphorylation. The observations from these completed experiments suggest that lestaurtinib inhibits MPNST proliferation and survival via effects on a signaling pathway other than the Ras-Erk signaling cascade.

Finally, we are currently treating mice xenografted with human MPNST cells with canertinib alone, lestaurtinib alone or a combination of canertinib and lestaurtinib. Our initial experiments indicate that the combination of canertinib and lestaurtinib profoundly inhibits xenograft growth

and that it does so better than either agent alone.

Although our findings clearly indicate that erbB3 is important for MPNST proliferation and survival, the fact that canertinib, which is a broad-spectrum erbB inhibitor, is also effective against MPNSTs raises the question of whether other erbB receptors are also important for MPNST pathogenesis. We and others have shown that MPNSTs variably express erbB1 (the EGF receptor), erbB2, erbB3 and erbB4. These erbB kinases are constitutively activated in MPNST cells and promote their proliferation and migration. Further, when we overexpressed an erbB3/erbB4-specific ligand [the neuregulin-1 (NRG1) isoform glial growth factor-β3 (GGFβ3)] in the Schwann cells of transgenic mice (P_0-GGFβ3 mice), these animals developed neurofibromas that transformed into MPNSTs *in vivo* with genomic abnormalities analogous to those seen in human MPNSTs. Our subsequent genetic complementation experiments showed that NRG1 promotes MPNST pathogenesis by activating erbB3 and erbB4-mediated signaling cascades that are dysregulated by neurofibromin loss.

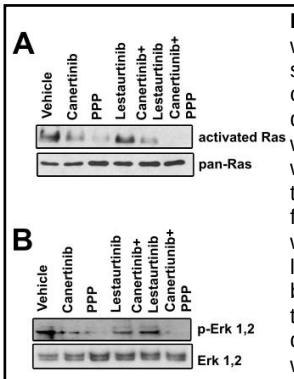


FIGURE 5. Combinatorial treatment with canertinib and PPP decreases signaling via the Ras/Erk signaling cascade. **A** Ras pull-down assays demonstrate decreased Ras activity with either canertinib or PPP, but not with lestaurtinib. Combinatorial treatment with PPP and canertinib further diminished this signal, whereas combining canertinib and lestaurtinib provided no added benefit. **B** As seen with Ras, dual treatment with canertinib and PPP decreased phosphorylation of Erk1,2 when compared to either individual treatment.

These observations present a conundrum, though—NRG1 activates both erbB3 and erbB4 and these receptors are often coexpressed in MPNSTs. Consequently, it is not clear which of them drives MPNST pathogenesis. This distinction has important mechanistic and therapeutic implications. NRG1 binds to erbB4 with an affinity an order of magnitude greater than that of erbB3 and, when activated, erbB4 has greater tyrosine kinase activity. ErbB4 also responds to several ligands (NRG3, NRG4, betacellulin, epiregulin, heparin-binding EGF) that do not activate erbB3. As their intracellular domains contain distinct docking sites for cytoplasmic signaling molecules, the downstream signaling pathways activated by erbB4 differ from those regulated by erbB3. Further, erbB4, unlike other erbB kinases, can be proteolytically cleaved post-activation, releasing a cytoplasmic fragment that functions as a transcriptional regulator. It is thus likely that if erbB4 promotes MPNST pathogenesis, it does so via mechanisms different from erbB3. If erbB4 promotes MPNST pathogenesis, it would also represent a potential target for new therapeutic agents such as the monoclonal anti-erbB4 antibodies that are currently in development. Consequently, we tested the hypothesis that erbB4 promotes MPNST pathogenesis and that it does so by activating cytoplasmic signaling cascades distinct from those regulated by erbB3.

Our previous analyses of two MPNST cell lines and six tumor samples indicated that erbB4 was variably expressed in these neoplasms. To determine how commonly erbB4 is expressed in MPNSTs *in vivo* and examine its distribution in these tumors, we immunostained thirty surgically resected human MPNSTs. Twenty-five tumors (83%) were positive for erbB4 and demonstrated prominent membranous (Figure 6A, erbB4 stain; Figure 6B, control non-immune IgG stain) and/or nuclear (Figure 6C) immunoreactivity. The membranous staining was often punctate, consistent with our previous observations in MPNST cells. Intratumoral variability was evident, with both erbB4-positive and –negative tumor cells present in the same neoplasm. Upon scoring the number of erbB4 positive tumor cells in each MPNST, we found that in most (16/25) tumors, the majority [>75% (4+; Fig. 6D) or 50-75% (3+; Fig. 6E)] of the tumor cells were erbB4 immunoreactive. In another seven tumors, erbB4 staining was less widely distributed, with 25-50% of the tumor cells being erbB4 positive (2+; Fig. 6F). The remaining two erbB4-positive MPNSTs contained <10-25% erbB4-immunoreactive cells (data not shown).

To compare erbB4 expression in MPNST cells to that in non-neoplastic human Schwann cells, we performed real time PCR quantification of *ERBB4* mRNA levels in 16 MPNST cell lines (Fig. 6G), with MCF7 cells serving as a positive high expressing control. Eleven lines had *ERBB4* expression greater than that in Schwann cells, with the highest levels observed in

MPNST642, NMS2, NMS2-PC and T265-2c cells, and intermediate expression levels in 2XSB, sNF02.2, S462, 90-8TL, MPNST2, sNF96.2, and sNF94.3 cells. Four lines (ST88-14, STS-26T, HS-PSS, Hs-Sch2) had *ERBB4* expression that was slightly lower than Schwann cells. A comparison of erbB4 protein and mRNA expression in a selected subset of MPNST lines showed that all of the lines that expressed *ERBB4* mRNA also had detectable erbB4 protein (Fig. 6H). However, *ERBB4* mRNA levels were not necessarily predictive of erbB4 protein levels, suggesting that post-translational factors regulate erbB4 protein levels in MPNST cells.

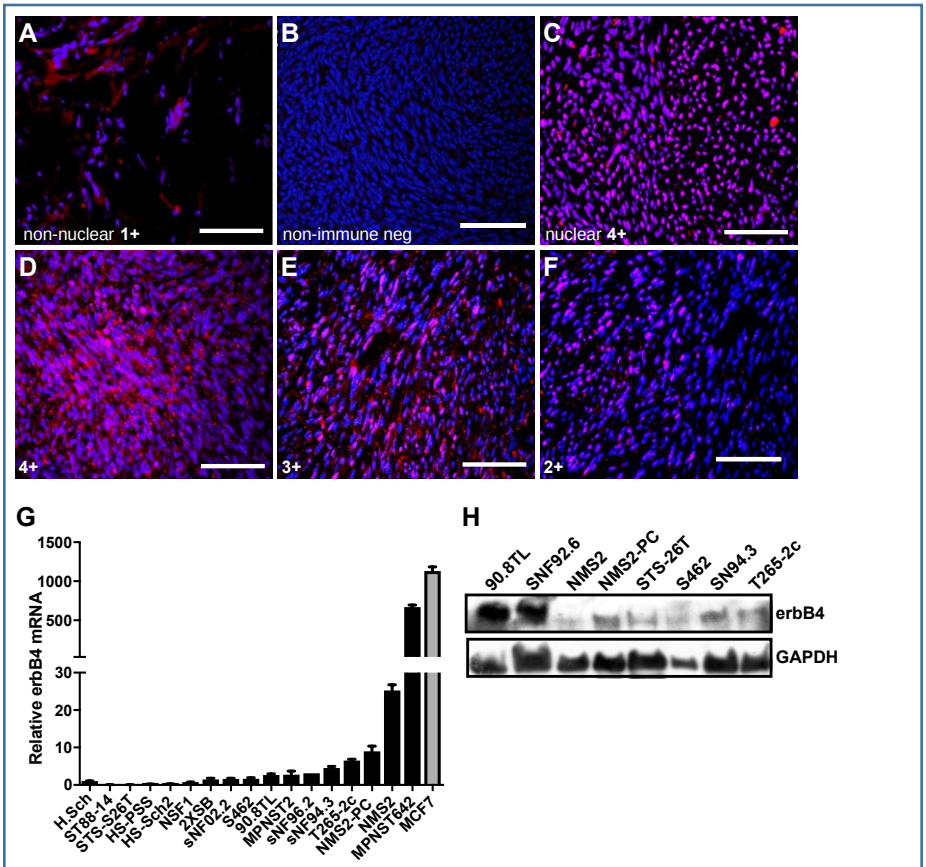


FIGURE 6. ErbB4 is commonly expressed in human MPNSTs and MPNST-derived cell lines. A-F) Representative images of erbB4 immunostaining of FFPE sections of human MPNSTs demonstrates different grades of erbB4 staining compared to isotype matched negative control (B). A subset of erbB4 positive tumor samples displayed prominent nuclear staining (C, F) and others displayed exclusive non-nuclear membranous staining (A). Red channel (Alexa 565, erbB4). Blue channel (Hoechst, nuclei). G) Real time PCR analysis showing relative mRNA expression of erbB4 mRNA using non-isoform discriminatory PCR primers; mRNA levels are shown relative to human Schwann cells. GAPDH mRNA was used as the loading control for normalization. H) ErbB4 protein expression of by immunoblot analysis of whole cell lysates derived from human MPNST derived cell lines. GAPDH was used as a loading control.

Alternative splicing of *ERBB4* mRNAs results in the production of functionally distinct protein variants that contain different juxtamembrane domains (JMa, JMb variants) and either include or lack a sequence in the autophosphorylation domain of the receptor (CYT1 and CYT2 variants, respectively). JMa variants, unlike JMb isoforms, can undergo proteolytic cleavage to release a 120kDa fragment that acts as a transcriptional regulator. The CYT1 sequence contains a p85 docking site that allows erbB4-mediated activation of the PI3 kinase/Akt signaling cascade. To determine which *ERBB4* splice variants are predominantly expressed in MPNST cells, we performed real-time PCR with isoform specific primer/probe sets. We found that most MPNST cell lines had higher expression of JMa than JMb variants while CYT1 and CYT2 variant expression was comparable across our panel of cell lines.

To determine whether erbB4 promotes the proliferation and survival of human MPNST cells, we targeted *ERBB4* expression using siRNAs in cell lines (S462 and T265-2c) with increased erbB4 mRNA and protein expression compared to Schwann cells (Fig. 7A). MTT and ^{3}H-thymidine incorporation assays showed that cultures with transient *ERBB4* knockdown contained smaller numbers of viable cells relative to cultures receiving nonsense control siRNAs (Fig. 7B), a change due, at least in part, to decreased proliferation (Fig. 7C). Stable knockdown of *ERBB4* in MPNST642 cells, tumor cells with a very high level of *ERBB4* mRNA expression and protein expression, similarly showed reductions in erbB4 protein levels (Fig. 7D) and the

number of viable cells (Fig. 7E).

Our previously described P_0-GGFβ3;*Trp53*$^{+/-}$ genetically engineered mouse (GEM) model develops MPNSTs *de novo* with complete penetrance [20]; like human MPNSTs, these GEM tumors and early passage cultures derived from them express erbB4 (Figure 7F). We therefore decided to use this model to further dissect erbB4's role in MPNST pathogenesis *in vivo*. Unfortunately, however, we could not generate P_0-GGFβ3;*Trp53*$^{+/-}$ mice with germline *Erbb4* deletion as germline *Erbb4* loss produces cardiac defects that result in embryonic lethality. The approach of introducing floxed *Erbb4* alleles into MPNSTs and deleting them with CreER^{T2} was also problematic as our initial experiments indicated that mosaicism would complicate the interpretation of these experiments. We therefore tried crossing P_0-GGFβ3;*Trp53*$^{+/-}$ mice to mice in which *Erbb4*$^{-/-}$ lethality is rescued by re-expressing erbB4 in the heart (*Erbb4*$^{-/-}$;α-MHC-*Erbb4* mice). However, out of 65 pups expected to have the desired P_0-GGFβ3;*Trp53*$^{+/-}$;*Erbb4*$^{-/-}$;α-MHC-*Erbb4* genotype, we obtained only one pup with this genotype and it did not produce any progeny.

We thus took the alternative approach of producing P_0-GGFβ3;*Trp53*$^{+/-}$;*Erbb4*$^{flox/flox}$ mice, with the goal of deleting *Erbb4 ex vivo*, grafting the cells back into mice and then assessing the effects of *Erbb4* ablation on tumor growth. The survival of P_0-GGFβ3;*Trp53*$^{+/-}$;*Erbb4*$^{flox/flox}$ mice (average survival, 210 days; Figure 7G) was indistinguishable from that of P_0-GGFβ3;*Trp53*$^{+/-}$ mice. Peripheral nervous system tumors were present in nearly 100% of the P_0-GGFβ3;*Trp53*$^{+/-}$;*Erbb4*$^{flox/flox}$ mice; these tumors were most commonly associated with trigeminal nerves, with some evident in sciatic nerve or dorsal root ganglia. The tumors in P_0-GGFβ3;*Trp53*$^{+/-}$;*Erbb4*$^{flox/flox}$ mice were markedly hypercellular MPNSTs with brisk mitotic activity (Figure 7H) and immunoreactivity for S100β and nestin (Figure 7 I-K). As tumor penetrance and lifespan in P_0-GGFβ3;*Trp53*$^{+/-}$;*Erbb4*$^{flox/flox}$ mice and P_0-GGFβ3; *Trp53*$^{+/-}$; mice was similar, we

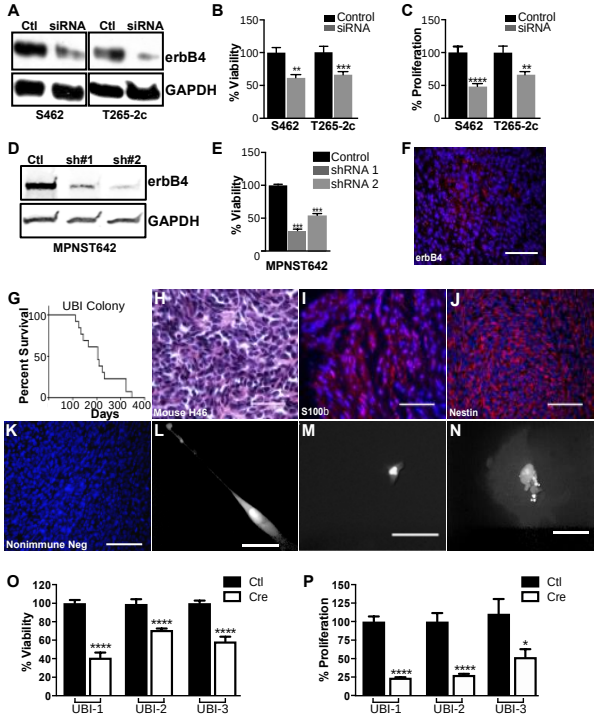


FIGURE 7. Loss of ErbB4 in human and mouse MPNST cells inhibits proliferation and survival. A) Immunoblots demonstrating reduced erbB4 expression in T265-2c and S462 cells transfected with erbB4 siRNA relative to cells transfected with non-targeting controls. B, C) Compared to non-targeting controls, erbB4 knockdown cells had decreased numbers of viable tumor cells (B) and decrease cellular proliferation (C). D) Immunoblot of MPNST642, a high erbB4 expressing cell line, demonstrating shRNA targeting of erbB4 expression. E) Compared to non-targeting shRNA controls, erbB4 shRNA knockdown cells had decreased numbers of viable tumor cells **, *p*-value≤0.01; ***, *p*-value≤0.001; ****, *p*-value≤0.0001. F) Representative erbB4 immunostaining of P_0-GGFβ3;*Trp53*$^{+/-}$;*Erbb4*$^{flox/flox}$ GEM mouse tumors showing erbB4 positivity compared to isotype matched negative controls (K). These representative erbB4 immunostains also show punctate membranous staining, with immunoreactivity present in almost all tumor cells (4+ staining). G) Kaplan-Meier survival curve of $^{/flox}$ mice shows that these animals survive an average of 210 days, similar to the parent line P_0-GGFβ3;*Trp53*$^{+/-}$ mice. H) Like their parent line, P_0-GGFβ3;*Trp53*$^{+/-}$;*Erbb4*$^{flox/flox}$ mice develop hypercellular neoplasms comprised of atypical spindled cells with numerous mitotic figures. As in human MPNSTs, these tumors are also immunoreactive for both S100β (I) and nestin (J). K) Isotype-matched negative control for erbB4 staining of mouse tumors. L) MPNST cells with intact *Erbb4* alleles (non-recombined) have a spindled morphology similar to that of wild-type Schwann cells, whereas knockout cells (M) are more ameboid. N) Nuclear blebbing was evident in a subset of *Erbb4*-ablated tumor cells. O, P) Decreased cellular viability (O) and proliferation (P) was observed in the *Erbb4* knockout cells (Cre) compared to the control cells from three independent tumor cultures. *, *p*-value≤0.05; ****p*-value≤0.0001 for comparisons of recombined (*Erbb4 -)* with non-recombined (*Erbb4+)* alleles. Red channel (Alexa 565, erbB4). Blue channel (Hoechst, nuclei).

concluded that the floxed *Erbb4* alleles did not impede tumorigenesis or worsen the survival of these mice.

To determine what effects erbB4 loss had in these tumors, we established early passage P_0-GGFβ3;*Trp53*$^{+/-}$;*Erbb4*$^{flox/flox}$ MPNST cultures, transduced them with adenovirus expressing eGFP or eGFP-Cre recombinase. eGFP-positive cells were isolated via FACS from each treatment group. PCR analyses verified the presence of recombined *Erbb4* alleles and *Erbb4* mRNA reductions in the presence of Cre recombinase, but not in controls. *Erbb4* ablation did not reduce the expression of *Egfr*, *Erbb2* or *Erbb3* mRNAs indicating that the changes described below are unlikely to reflect indirect effects on the expression of other erbB family members. The purified tumor cells were viable but demonstrated morphologic changes. In contrast to the spindled morphology of cells with intact *Erbb4* alleles (Figure 7L), the *Erbb4* knockout cells were ameboid with shorter, thicker processes and often showed nuclear blebbing (Figure 7M-N). To determine whether *Erbb4* ablation in P_0-GGFβ3;*Trp53*$^{+/-}$;*Erbb4*$^{flox/flox}$ MPNSTs inhibited viability, we performed MTT assays on transduced cultures of three independently arising MPNSTs. We found that cultures transduced with Cre-expressing adenovirus showed decreased numbers of viable cells compared to cells infected with the control vector (Figure 7O). As in human MPNST cells, ^{3}H-thymidine incorporation assays demonstrated that this decrease in cell numbers was due, in part, to reduced proliferation (Figure 7P).

To examine the effects of *Erbb4* ablation *in vivo*, the three distinct P_0-GGFβ3;*Trp53*$^{+/-}$;*Erbb4*$^{flox/flox}$ early passage MPNST cultures previously assessed by MTT and ^{3}H-thymidine incorporation assays (Figure 7O-P) were transduced with eGFP- or eGFP-Cre expressing adenovirus, FACs sorted and then orthotopically allografted in the sciatic nerves of nude mice. The grafts were excised 35 days post-grafting, and their masses and volumes determined. Grafts of *Erbb4*-ablated tumor cells showed up to an 80% reduction in volume and mass relative to grafts of cells transduced with eGFP-expressing adenovirus (Figure 8A, B). The cellularity of the *Erbb4*-null tumors was lower than that of the eGFP controls (Figure 8C, D) and the *Erbb4* knockout cells had more prominently vacuolated cytoplasm. To determine whether this decrease in graft mass and volume reflected decreased tumor cell proliferation or survival, we quantified the Ki67 and TUNEL labeling indices in five *Erbb4*-ablated and five control grafts established from each of the three early-passage cultures. In all instances, there were statistically significant decreases in Ki67 labeling in the *Erbb4*-null grafts relative to eGFP controls (Figure 8E). In addition, the *Erbb4*-ablated allografts demonstrated a 3-4-fold increase in the percentage of TUNEL positive cells relative to the control grafts (Figure 8F). *Erbb4* loss thus results in both decreased proliferation and increased apoptosis in these grafts.

During our gross examination of the grafts, we noted that the *Erbb4* ablated grafts were paler than the controls, raising the question of whether vascular density was decreased in the grafts lacking *Erbb4*. Upon immunostaining our grafts for the vascular marker CD31, we found that the vascular density in the *Erbb4* ablated grafts (Figure 8K-M) did indeed appear to be lower than that in the control allografts (Figure 8G-J). Quantification of the vascular densities in these grafts showed that the vascular density in the *Erbb4* ablated grafts was approximately half that of the control grafts (Figure 8N). As *Erbb4* is intact in the vasculature within these grafts, this suggests that the decreases in vascular density observed in *Erbb4* ablated grafts are an indirect effect of *Erbb4* loss in MPNST cells via mechanisms such as erbB4-mediated enhancement of the production and/or secretion of angiogenic factors by MPNST cells.

Although MPNSTs co-express erbB3 and erbB4, our demonstration that *Erbb4* ablation decreased proliferation, survival and angiogenesis in MPNSTs indicates that these receptors are not functionally redundant and suggest that erbB4 activates distinct signaling cascades essential for MPNST tumorigenesis. As many growth factors, including NRG1, activate Ras, we first asked whether *Erbb4* ablation diminished the erbB-dependent Ras hyperactivation we have previously observed in P_0-GGFβ3;*Trp53*$^{+/-}$ MPNSTs. To answer this question, we generated lysates from early passage P_0-GGFβ3;*Trp53*$^{+/-}$;*Erbb4*$^{flox/flox}$ MPNST cells transduced with eGFP or eGFP-Cre expressing adenovirus, pulled down the activated Ras proteins with Raf-1 and then probed the captured Ras proteins using a pan-Ras antibody (Figure 9A). Surprisingly, we found that Ras activation was not reduced by *Erbb4* ablation, indicating that *Erbb4* loss impairs MPNST proliferation and survival via effects on Ras-independent pathways.

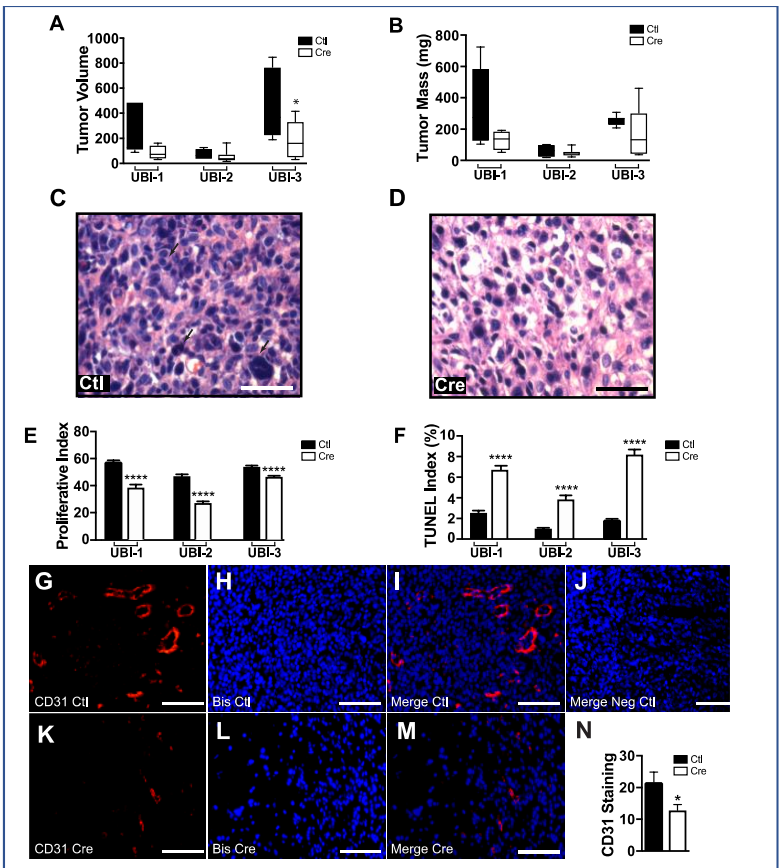


FIGURE 8. *Erbb4* ablation inhibits allograft growth and alters tumor histopathology in Nude mice. A, B) *Erbb4*-null cells from three separate tumor lines show reduced graft volume and mass compared to erbB4 expressing controls. *, *p*-value≤0.05. C-D) Representative histologic images of a UBI GFP control tumor (C) and a UBI Cre tumor (D). Arrows in C indicate the multinucleated cells that are commonly seen in these tumors-Check figure arrow. Note that these multinucleated cells are virtually absent in the *Erbb4*-null grafts. E) Quantification of Ki67 labeling indices in three allografted tumor lines. F) Quantification of TUNEL labeling indices in the same tumor lines. ****, *p*-value≤0.0001 for comparisons of recombined *Erbb4* allele (erbB4 -) grafts to grafts with non-recombined *Erbb4* alleles (erbB4+). G-M) Representative CD31 staining of control erbB4 positive tumors (G, J) and erbB4 negative tumors (H, L) with Hoechst counterstain (J,N) for cell nuclei detection. A non-immune isotype matched primary was used as a negative control (J). P) Quantification of representative immunofluorescent images using FIJI. . *, *p*-value≤0.05; ****p*-value≤0.0001 for comparisons of recombined (*Erbb4 -)* with non-recombined (*Erbb4+)* alleles.

To identify the erbB4-regulated signaling cascades potentially driving proliferation, survival and angiogenesis in MPNSTs, we stimulated *Erbb4* intact and *Erbb4*-null GGFβ3;*Trp53*$^{+/-}$;*Erbb4*$^{flox/flox}$ MPNST cells with 10nM NRG1β for 5 minutes, a time that our preliminary analyses indicated was sufficient to maximally activate NRG1β-responsive signaling pathways. Lysates from these cells were used to probe arrays containing phosphorylation site-specific antibodies that query 43 different cytoplasmic kinases and other key proteins. We then asked which of these proteins showed altered phosphorylation following NRG1β stimulation and *Erbb4* ablation.

We first identified the NRG1β responsive proteins and kinases in *Erbb4* intact GGFβ3;*Trp53*$^{+/-}$;*Erbb4*$^{flox/flox}$ MPNST cells; as NRG1β activates both erbB3 and erbB4, alterations in the phosphorylation of the proteins queried by our arrays in these cells could

reflect the action of either erbB3 or erbB4. Kinases whose phosphorylation levels were changed by at least 1.5-fold compared to unstimulated cells were considered NRG1β responsive. Using this criterion, we identified 16 NRG1β responsive sites with increased phosphorylation and 2 NRG1β responsive events in which the phosphorylation of the targeted protein was decreased (Figure 9B). The proteins in which NRG1β increased phosphorylation included Akt (T308), RSK, PRAS40 [also known as AKT1S1 (Akt1 substrate 1)], Src, Hck, Fyn, STAT3 (S727 and Y705), PYK2, PLCγ1, p53 (S46) and Chk-2; of particular note, given that we have previously shown that Ras is activated in P_0-GGFβ3;*Trp53*$^{+/-}$ MPNSTs by NRG1, we found that the phosphorylation of ERK was also increased by NRG1β stimulation in these experiments. In contrast, the phosphorylation of S473 in pAKT (unlike T308, another activation site in Akt, where phosphorylation was increased by NRG1β; see above), JNK, STAT5a/b (Y694/Y699) and β-catenin was decreased following NRG1β stimulation. However, since decreased phosphorylation of β-catenin results in increased transcriptional activity, this latter change reflects increased activation of the β-catenin pathway downstream of NRG1β.

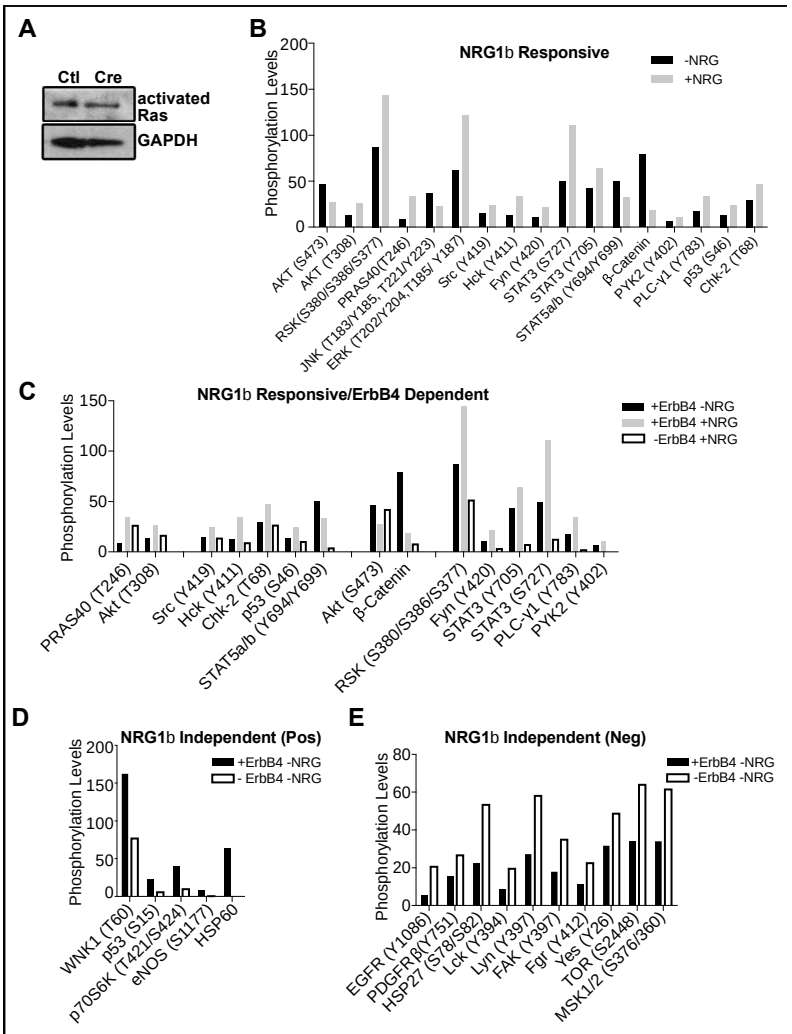


FIGURE 9. *Erbb4* is not essential for Ras hyperactivation, but does increase the phosphorylation of a number of other cytoplasmic kinases. A) A comparison of Ras activation in *Erbb4*-null (Cre) and *Erbb4*-expressing control (Ctl) UBI MPNST cells shows that *Erbb4* loss does not affect Ras activation. B) Graphical representation of quantified kinase arrays comparing the levels of baseline phosphorylation to NRG1 stimulated phosphorylation in *Erbb4*-expressing UBI MPNST cells. The graph includes the subset of kinases whose phosphorylation was altered following NRG1β stimulation. C) Graphical representation of quantified kinase arrays comparing the levels of baseline phosphorylation of control *Erbb4*- intact cells to NRG1 stimulated *ErbB4*-intact and *Erbb4-null* UBI MPNST cells to determine NRG1 dependent and *ErbB4* dependent kinases. D) Quantification of a subset of the non-responsive kinases *ErbB4*-intact compared to *ErbB4*-ablated to identify targets positively regulated by *ErbB4* independent of stimulation. E) Quantification of a subset of the non-responsive kinases *ErbB4*-intact compared to *ErbB4*-ablated to identify compensatory targets resulting from *ErbB4*-ablation independent of stimulation. Quantification of the kinases differentially phosphorylated was quantified per the manufacturer's protocol using ImageJ.

To determine which phosphorylation events noted above required NRG1β-mediated activation of erbB4, we compared the stimulated the phosphorylation profile of *Erbb4* intact cells to that of *Erbb4* ablated cells (Figure 9C). We found that two of the 18 NRG1β-responsive phosphorylation events were partially dependent on the presence of *Erbb4* (PRAS40, Akt-T308) suggesting that erbB3 and erbB4 redundantly regulate these PI3K pathway proteins downstream of NRG1β through distinct heterodimers. The phosphorylation of six kinases (Src, Hck, Chk-2, p53-S46, STAT5a and b) was completely dependent on NRG1β and intact *Erbb4*, indicating that NRG1β-driven phosphorylation of these targets is mediated, directly or indirectly, by erbB4. Interestingly, several of the changes we observed suggested that erbB3 and erbB4 play opposing roles in activating some signaling pathways in MPNSTs. For instance, the phosphorylation of STAT5a/b at Y694/699, two sites that are required for activation, was weakly (0.66 fold down) decreased by NRG1β in the presence of *Erbb4*. However, in the absence of *Erbb4*, NRG1β stimulation resulted in an almost

complete loss of STAT5a/b activation, suggesting that erbB4 opposes erbB3-mediated inhibition of STAT5a/b. The reduction in pAkt-S473 phosphorylation observed in response to NRG1β stimulation (Figure 6B) was also rescued by *Erbb4* ablation, with pAkt-S437 returning to baseline levels in the presence of NRG1β. In contrast, the reduction in β-catenin phosphorylation levels observed in response to NRG1β stimulation was further exaggerated when *Erbb4* was ablated, suggesting both erbB3 and erbB4 activate this signaling cascade. The remaining six NRG1β -responsive proteins (RSK, Fyn, STAT3-Y705/S727, PLCγ-1, PYK2) had phosphorylation that was enhanced by erbB4, both in the presence and absence of exogenous NRG1β (Figure 9C). This latter observation may reflect erbB4 activation mediated by endogenous NRG1β expressed by the tumor cells themselves or, alternatively, the action of other erbB4 ligands expressed by the MPNST cells that similarly activate downstream signaling cascades.

We next asked whether there were additional proteins whose phosphorylation was dependent upon *Erbb4* but unaffected by NRG1β stimulation. We identified 15 proteins whose phosphorylation was not altered when challenged with exogenous NRG1β but that were sensitive to *ErbB4* ablation. *Erbb4* ablation decreased the phosphorylation of five of these proteins [WNK1, p53 (S15), p70S6K, eNOS, and HSP60; Figure 9D), suggesting that *Erbb4* is a key upstream activator of these kinases. *Erbb4* loss increased the phosphorylation of the other ten proteins in a NRG1β independent manner suggesting that erbB4 negatively regulates the activation of these proteins. This latter group of proteins included two RTKs, EGFR and PDGFRβ, as well as HSP27, five Src-related kinases (Lck, Lyn, FAK, Fgr, Yes), mTOR and MSK1/2 kinases (Figure 9E). The majority of these proteins are associated with the plasma membrane and their activation in the absence of erbB4 may be a direct result of altered receptor heterodimerization and cellular architecture at the plasma membrane.

Gene ontology analyses of both the NRG1β-dependent and –independent targets of erbB4 indicated that the biological pathways regulated by erbB4 promote migration and survival (Figure 10). Specifically, these analyses indicated that the erbB4/NRG1β-dependent kinases drive proliferation and cell communication, response to stress, migration, survival and response to nitrogen compounds, whereas the NRG1β-independent actions of erbB4 include migration, survival and blood vessel cell migration. Importantly, the results of these gene ontology analyses are consistent with our experimental findings demonstrating that erbB4 promotes survival, proliferation and angiogenesis in MPNST cells.

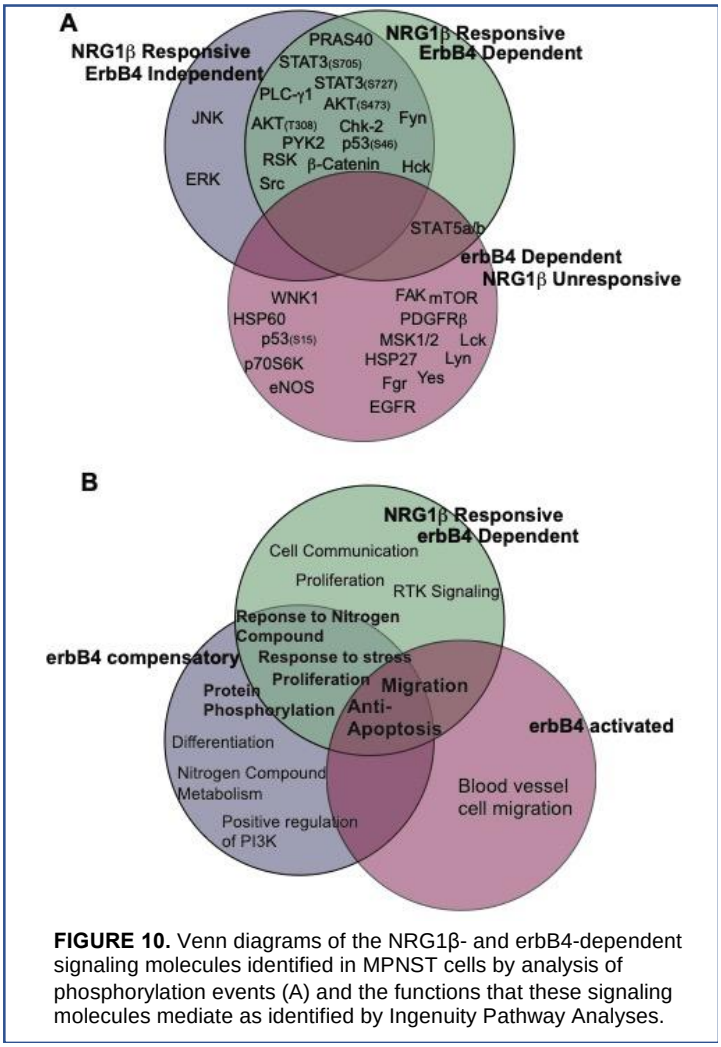


FIGURE 10. Venn diagrams of the NRG1β- and erbB4-dependent signaling molecules identified in MPNST cells by analysis of phosphorylation events (A) and the functions that these signaling molecules mediate as identified by Ingenuity Pathway Analyses.

To directly assess whether the proteins whose phosphorylation is altered by *Erbb4* loss include molecules that promote MPNST proliferation and/or survival, we inhibited the actions of four of these proteins (WNK1, PLCγ, STAT3 and STAT5a). Although our shRNAs effectively knocked down WNK1 expression in T265-2c and S462 cells, MTT assays did not show a reproducible decrease in the number of viable cells following knockdown (Figure 11A). In contrast, the PLCγ inhibitor U73122 inhibited the viability of T265-2c, S462 and MPNST462 cells in a concentration-dependent manner (Figure 11B). Likewise, the STAT3 inhibitor Cas285986-31-4 also inhibited the viability of three MPNST cell lines in a concentration-dependent manner (Figure 11C). The STAT5 inhibitor 5,15-DPP also decreased the number of viable cells in cultures of these lines in a concentration-dependent manner, although its effects were not as pronounced as those of the STAT3 inhibitor (Figure 11D). We conclude that PLCγ, STAT3 and STAT5 are among the erbB4 targets that mediate the proliferation and/or survival of MPNST cells (Figure 12).

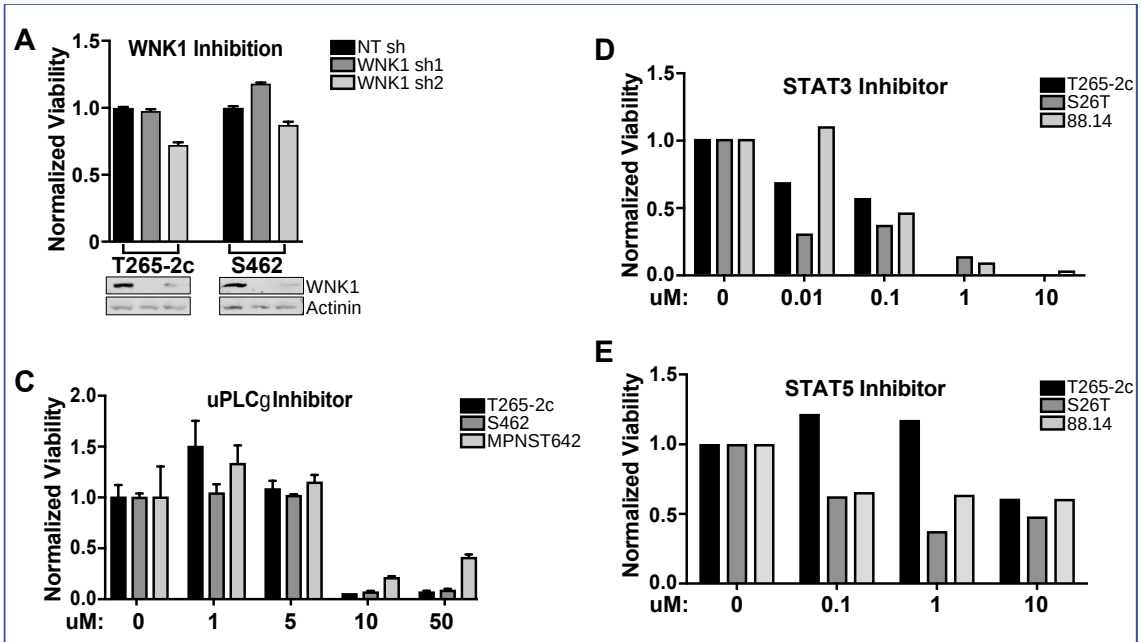


FIGURE 11. MPNSTs are sensitive to inhibition of specific erbB4 activated signaling pathways. A) Downregulation of WNK1 expression did not affect cell viability. Cell viability was assessed six days after shRNA selection. Values represent cell viability after 72 hours normalized to 0 hr. After normalization, cell viability for each WNK1 knockdown was compared to non-targeting control. B-D) Cell viability was assessed in three log phase MPNST cell lines in the presence of designated inhibitor. Values represent cell viability after 72 hours of drug treatment normalized to 0 hr. After normalization, cell viability for each drug dose was compared to vehicle control. PLC-γ inhibition effects cell viability in a dose dependent manner (B). STAT3 inhibition significantly affects cell viability (C). STAT5 inhibition modestly affects cell viability (D).

In summary, multiple erbB4 splice variants are commonly expressed in MPNSTs. Acting in a cell-autonomous manner, these erbB4 variants promote the proliferation and survival of tumor cells. ErbB4 receptors expressed by MPNST cells also indirectly promote angiogenesis in MPNSTs. Despite our anticipation that erbB4 would drive Ras activation, we found that erbB4 instead promotes MPNST pathogenesis via Ras-independent effects; these signaling events include alterations in the PI3K/Akt/mTOR and PLC-γ signaling cascades, activation of transcription via STAT proteins, and the phosphorylation of other molecules with oncogenic potential, such as HSP60. Our findings thus identify erbB4 and key erbB4-dependent signaling pathways as potentially important chemotherapeutic targets in MPNSTs. Future studies will be needed to further investigate the role of the other erbB4 targets that we have identified in MPNST pathogenesis. It will also be of great interest to establish the relative contributions that canonical membrane-based erbB4 signaling and transcriptional signaling by the erbB4 intracellular domain make to the development of these aggressive spindle cell neoplasms.

e. ***Perform diagnostic, histochemical and immunohistochemical analyses of proliferation and cell death in tumor cohorts (months 18-36; in progress).***

As noted above, the changes we had to make in our screening process to identify the mice of interest (i.e., MPNST-bearing mice) led to delays in the latter stages of this project. Consequently, we are still in the process of analyzing the effects of tamoxifen and trifluoperazine on established malignant peripheral nerve sheath tumors in our mouse cohorts. I cannot yet say what effects our therapeutic regimens are having on MPNST proliferation and survival as our experimental protocol requires that we complete the therapeutic regimen for all of our cohorts and perform the tumor analyses prior to breaking our codes for each cohorts. These efforts are being supported with funds provided by my endowed Chair.

Task 2. To determine whether tamoxifen, trifluoperazine or combined tamoxifen/trifluoperazine therapy inhibits tumor cell proliferation and survival in neurofibroma bearing Krox20-Cre;Nf1$^{flox/-}$ mice (months 1-36):

a. ***Obtain regulatory review and approval for these studies (months 1-2)***

Submission of the necessary protocols for regulatory review and approval was submitted in month 1, but approval was delayed for 3-4 months by the review process.

b. ***Establish cohorts of Krox20-Cre;Nf1$^{flox/-}$ mice, identify neurofibroma bearing mice with MRI scans and randomize mice into cohorts for treatment with vehicle, tamoxifen, trifluoperazine or tamoxifen and trifluoperazine (months 3-18)***

For the interim analysis, our biostatistician recommended that we look for an effect size of at least 2 (following the measures outlined below) in the treatment versus control groups. One-way ANOVA with a Dunnett test for adjustment of pair-wise comparisons (compared to the control group) will be used for sample size calculation. We determined that 20 mice per group would give us 95% power to detect at least an effect size of 2 between the treatment groups and the control (vehicle) group, given 5% type I error. We also recognize NIH's recent recommendation that animal experiments include both male and female animals to avoid a sex bias. Consequently, our original experimental design was that each cohort would include 20 male and 20 female mice; male and female mice will be analyzed both independently and in a stratified fashion. In accordance with these goals, we have established the Krox20-Cre;*Nf1*$^{flox/-}$ mice necessary for Task 2; work with these mice is still ongoing, as the genotype of these animals is more complicated than that of P0-GGFβ3;*Trp53*$^{+/-}$ mice and thus takes longer to generate. Krox20-Cre;*Nf1*$^{flox/-}$mice are also being followed to identify neurofibroma-bearing mice which are then randomized into treatment cohorts.

In our initial research plan, we proposed identifying neurofibroma-bearing mice using a MRI scans and monitoring of clinical signs that we had established as reliable indicators of tumorigenesis in several of our previously published studies. However, a large series of studies we have now performed with our genetically engineered mouse models have similarly convinced us that MRI does not have sufficient specificity to reliably identify tumor-bearing mice (as with MPNSTs, these modalities can recognize the neoplasms of interest, but our necropsy examinations indicate that this imaging method can be fooled, particularly when attempting to identify tumors early in their course). Again, like MPNSTs, we have found that this occurs most commonly when the results of the imaging studies and examination of clinical signs are discordant; the clinical signs are simply more reliable. In addition, our imaging facility has been crippled by problems with their instrumentation. Consequently, we have modified our approach to identifying neurofibroma-bearing mice and are now focusing on using clinical signs for the initial identification of neurofibroma-bearing mice. In this circumstance, our primary readout for

drug effectiveness is survival times following the initiation of therapy and changes in proliferation and apoptotic indices as originally proposed.

c. ***Evaluate the effectiveness of the therapeutic regimens described in c (months 12-18; in progress)***
d. ***Perform diagnostic, histochemical and immunohistochemical analyses of proliferation and cell death in tumor cohorts (months 18-36; in progress)***

As noted above, the changes we had to make in our screening process to identify the mice of interest (i.e., neurofibroma-bearing mice) led to delays in the latter stages of this project. Consequently, we are still in the process of analyzing the effects of tamoxifen and trifluoperazine on established neurofibroma tumors in our mouse cohorts. I cannot yet say what effects our therapeutic regimens are having on neurofibroma proliferation and survival as our experimental protocol requires that we complete the therapeutic regimen for all of our cohorts and perform the tumor analyses prior to breaking our codes for each cohorts. These efforts are being supported with funds provided by my endowed Chair.

Task 3. To determine whether tamoxifen, trifluoperazine or combined tamoxifen/trifluoperazine therapy extends the survival of MPNST bearing P_0-GGFβ3;Trp53$^{+/-}$ mice (months 1-36):

a. ***Obtain regulatory review and approval for these studies (months 1-2)***

Submission of the necessary protocols for regulatory review and approval was submitted in month 1, but approval was delayed for 3-4 months by the review process.

b. ***Establish cohorts of P_0-GGFβ3;Trp53$^{+/-}$ mice, identify MPNST bearing mice with PET scans and randomize mice into cohorts for treatment with vehicle, tamoxifen, trifluoperazine or tamoxifen and trifluoperazine (months 3-18)***

For the interim analysis, our biostatistician recommended that we look for an effect size of at least 2 (following the measures outlined below) in the treatment versus control groups. One-way ANOVA with a Dunnett test for adjustment of pair-wise comparisons (compared to the control group) will be used for sample size calculation. We determined that 20 mice per group would give us 95% power to detect at least an effect size of 2 between the treatment groups and the control (vehicle) group, given 5% type I error. We also recognize NIH's recent recommendation that animal experiments include both male and female animals to avoid a sex bias. Consequently, our original experimental design was that each cohort would include 20 male and 20 female mice; male and female mice will be analyzed both independently and in a stratified fashion. In accordance with these goals, we have established the full cohort of P0-GGFβ3;*Trp53*$^{+/-}$ mice necessary for Task 3 and are currently following them to identify MPNST-bearing mice which are then randomized into treatment cohorts.

As described above, we originally proposed identifying MPNST-bearing mice using a combination of PET imaging and monitoring of clinical signs that we had established as reliable indicators of tumorigenesis in several of our previously published studies. However, a large series of studies we have now performed with our genetically engineered mouse models have convinced us that PET does not have sufficient specificity to reliably identify tumor-bearing mice We have also noted that this occurs most commonly when the results of the imaging studies and examination of clinical signs are discordant; the clinical signs are simply more reliable. Consequently, we have also modified our approach in this subtask to identifying MPNST-bearing mice and are now focusing on using clinical signs for the initial identification of MPNST-

bearing mice. In this circumstance, our primary readout for drug effectiveness is survival times following the initiation of therapy and changes in proliferation and apoptotic indices as originally proposed.

c. ***Evaluate the effectiveness of the therapeutic regimens described in c (months 12-18; in progress)***
d. ***Perform diagnostic, histochemical and immunohistochemical analyses of proliferation and cell death in tumor cohorts (months 18-36; in progress)***

As noted above, the changes we had to make in our screening process to identify the mice of interest (i.e., MPNST-bearing mice) led to delays in the latter stages of this project. Consequently, we are still in the process of analyzing the effects of tamoxifen and trifluoperazine on tumors in our mouse cohorts. I cannot yet say what effects our therapeutic regimens are having on MPNST proliferation and survival as our experimental protocol requires that we complete the therapeutic regimen for all of our cohorts and perform the tumor analyses prior to breaking our codes for each cohorts. These efforts are being supported with funds provided by my endowed Chair.

Task 4. To determine whether tamoxifen, trifluoperazine or combined tamoxifen/trifluoperazine therapy inhibits tumor cell proliferation and survival in neurofibroma bearing Krox20-Cre;Nf1$^{flox/-}$ mice (months 1-36):

a. ***Obtain regulatory review and approval for these studies (months 1-2)***

Submission of the necessary protocols for regulatory review and approval was submitted in month 1, but approval was delayed for 3-4 months by the review process.

b. ***Establish cohorts of Krox20-Cre;Nf1$^{flox/-}$ mice, identify neurofibroma bearing mice with MRI scans and randomize mice into cohorts for treatment with vehicle, tamoxifen, trifluoperazine or tamoxifen and trifluoperazine (months 3-18)***

For the interim analysis, our biostatistician recommended that we look for an effect size of at least 2 (following the measures outlined below) in the treatment versus control groups. One-way ANOVA with a Dunnett test for adjustment of pair-wise comparisons (compared to the control group) will be used for sample size calculation. We determined that 20 mice per group would give us 95% power to detect at least an effect size of 2 between the treatment groups and the control (vehicle) group, given 5% type I error. We also recognize NIH's recent recommendation that animal experiments include both male and female animals to avoid a sex bias. Consequently, our original experimental design was that each cohort would include 20 male and 20 female mice; male and female mice will be analyzed both independently and in a stratified fashion. In accordance with these goals, we have established the Krox20-Cre;*Nf1*$^{flox/-}$ mice necessary for Task 4; work with these mice is still ongoing, as the genotype of these animals is more complicated than that of P0-GGFβ3;*Trp53*$^{+/-}$ mice and thus takes longer to generate. Krox20-Cre;*Nf1*$^{flox/-}$mice are also being followed to identify neurofibroma-bearing mice which are then randomized into treatment cohorts.

In our initial research plan, we proposed identifying tumor-bearing mice using a combination of MRI scans and monitoring of clinical signs that we had established as reliable indicators of tumorigenesis in several of our previously published studies. As described above, however, a large series of studies we have now performed with our genetically engineered mouse models

have convinced us that neither PET or MRI has sufficient specificity to reliably identify neurofibroma-bearing mice. Also as noted above, we have also noted that this occurs most commonly when the results of the imaging studies and examination of clinical signs are discordant; the clinical signs are simply more reliable. Consequently, we have modified our approach in this subtask to identifying neurofibroma-bearing mice and are now focusing on using clinical signs for the initial identification of neurofibroma-bearing mice. Our primary readout for drug effectiveness in this subtask is survival times following the initiation of therapy and changes in proliferation and apoptotic indices as originally proposed.

c. ***Evaluate the effectiveness of the therapeutic regimens described in b (months 12-18; in progress)***
d. ***Perform diagnostic, histochemical and immunohistochemical analyses of proliferation and cell death in tumors (months 18-36; in progress)***

As noted above, the changes we had to make in our screening process to identify the mice of interest (i.e., neurofibroma-bearing mice) led to delays in the latter stages of this project. Consequently, we are still in the process of analyzing the effects of tamoxifen and trifluoperazine on tumors in our mouse cohorts. I cannot yet say what effects our therapeutic regimens are having on neurofibroma proliferation and survival as our experimental protocol requires that we complete the therapeutic regimen for all of our cohorts and perform the tumor analyses prior to breaking our codes for each cohorts. These efforts are being supported with funds provided by my endowed Chair.

Task 5. To determine whether prophylactic therapy with tamoxifen, trifluoperazine or combined tamoxifen/trifluoperazine therapy prevents neurofibroma and MPNST pathogenesis in Krox20- Cre;Nf1$^{flox/-}$ and P$_0$-GGFβ3;Trp53$^{+/-}$ mice, respectively (months 18-36):

a. ***Obtain regulatory review and approval for these studies (months 1-2)***

Submission of the necessary protocols for regulatory review and approval was submitted in month 1, but approval was delayed for 3-4 months by the review process.

b. ***Establish cohorts of Krox20-Cre;Nf1$^{flox/-}$ and P$_0$-GGFβ3;Trp53$^{+/-}$ mice (months 18-22)***

In our original grant application, we had proposed to establish the cohorts of Krox20-Cre;*Nf1*$^{flox/-}$ and P0-GGFβ3;*Trp53*$^{+/-}$ mice required for this Task in the latter half of this project. However, in light of the delay in getting our animal protocol approved by ACURO, we went ahead and began establishing these cohorts earlier. In light of our current experience with Krox20- Cre;*Nf1*$^{flox/-}$ mice, we also plan to begin the prophylactic long-term drug treatments at a slightly later age than we originally proposed. Krox20-Cre;*Nf1*$^{flox/-}$ mice survive for approximately 11-12 months with morbidity beginning around 8 months. We had initially proposed starting drug treatment for these studies at 6 weeks of age. In the best interest of the animals, we will instead begin treatment 2 months prior to onset of morbidity for both mouse models to reduce the trauma to the mice from IP drug treatment.

For the interim analysis, our biostatistician recommended that we look for an effect size of at least 2 (following the measures outlined below) in the treatment versus control groups. One-way ANOVA with a Dunnett test for adjustment of pair-wise comparisons (compared to the control group) will be used for sample size calculation. We determined that 20 mice per group would give us 95% power to detect at least an effect size of 2 between the treatment groups

and the control (vehicle) group, given 5% type I error. We also recognize NIH's recent recommendation that animal experiments include both male and female animals to avoid a sex bias. Consequently, our original experimental design was that each cohort would include 20 male and 20 female mice; male and female mice will be analyzed both independently and in a stratified fashion. In accordance with these goals, we have established the full cohort of P0-GGFβ3;*Trp53*$^{+/-}$ mice necessary for Task 5 and are currently following them to identify MPNST-bearing mice which are then randomized into treatment cohorts. We have established the Krox20-Cre;*Nf1*$^{flox/-}$mice necessary for Task 5; work with these mice is still ongoing, as the genotype of these animals is more complicated than that of P0-GGFβ3;*Trp53*$^{+/-}$ mice and thus takes longer to generate. Krox20-Cre;*Nf1*$^{flox/-}$mice are also being followed to identify neurofibroma-bearing mice which are then randomized into treatment cohorts.

The same imaging issues noted above in previous Tasks also apply to this Task. Consequently, in this Task we have also modified our approach to identifying tumor-bearing mice and are now focusing on using clinical signs for the initial identification of tumor-bearing mice. In this subtask, our primary readout for drug effectiveness is survival times following the initiation of therapy and changes in proliferation and apoptotic indices as originally proposed.

c. ***Treat cohorts with vehicle, tamoxifen, trifluoperazine or tamoxifen and trifluoperazine (months 22-36; in progress)***

d. ***Evaluate the effectiveness of the therapeutic regimens described in b (months 22-36; in progress)***

e. ***Perform diagnostic, histochemical and immunohistochemical analyses of proliferation and cell death in tumors, if tumors are present (months 30-36; in progress)***

As noted above, the changes we had to make in our screening process to identify the mice of interest (i.e., neurofibroma or MPNST-bearing mice) led to delays in the latter stages of this project. Consequently, we are still in the process of analyzing the effects of tamoxifen and trifluoperazine on tumors in our mouse cohorts. I cannot yet say what effects our therapeutic regimens are having on neurofibroma MPNST proliferation and survival as our experimental protocol requires that we complete the therapeutic regimen for all of our cohorts and perform the tumor analyses prior to breaking our codes for each cohorts. These efforts are being supported with funds provided by my endowed Chair.

Opportunities for Training and Professional Development

Nothing to Report

Dissemination of Results to Communities of Interest

Manuscripts

Carroll SL. The challenge of cancer genomics in rare nervous system neoplasms: malignant peripheral nerve sheath tumors as a paradigm for cross-species comparative oncogenomics. *The American Journal of Pathology* 2016; 186(3): 464-477. PMID: 26740486 PMCID: PMC4816695

Hanemann CO, Blakeley JO, Nunes FP, Robertson K, Stemmer-Rachamimov A, Mautner V, Kurtz A, Ferguson M, Widemann BC, Evans DG, Ferner R, **Carroll SL**, Korf B, Wolkenstein P, Knight P, Plotkin SR and the REiNS International Collaboration. Current status and recommendations for biomarkers and biobanking in neurofibromatosis. *Neurology* 2016; 87(7 Supplement 1): S40-48. DOI:

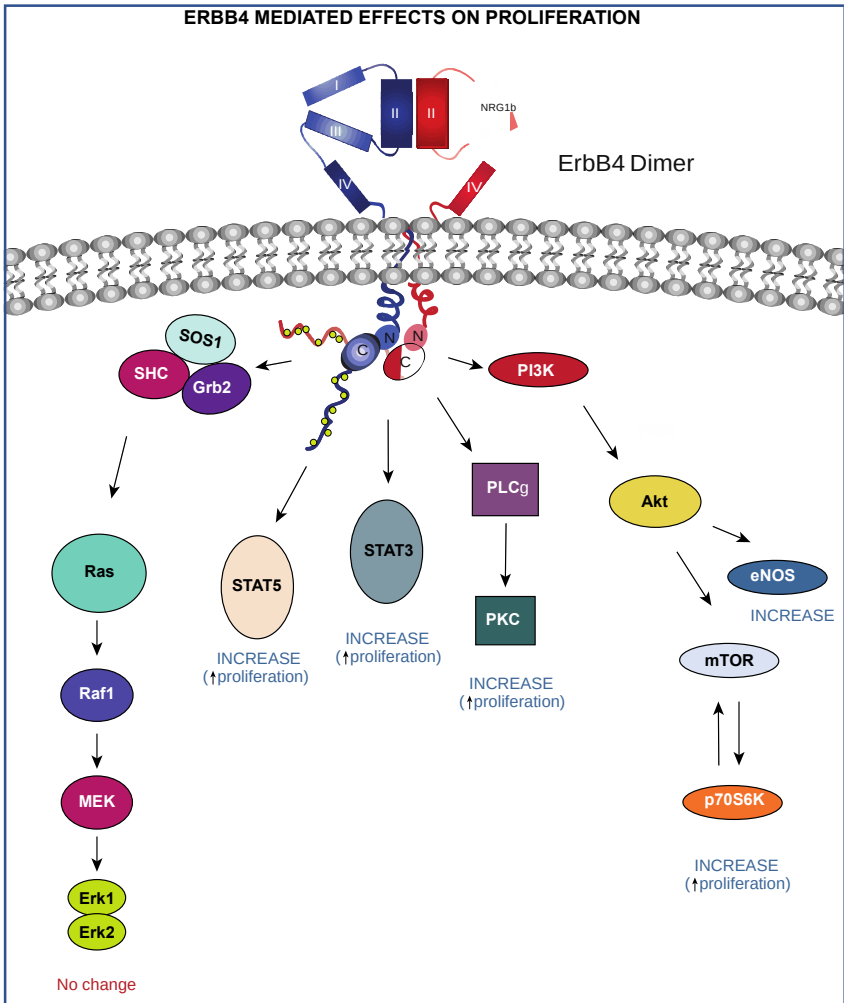


FIGURE 12. Schematic highlighting the signaling cascades that are dependent on erbB4 in MPNSTs. The STAT3/5 and PI3K pathway is positively regulated by erbB4 in a NRG1β-dependent manner.

10.1212/WNL.0000000000002932. PMID: 27527649 PMCID: PMC5578360

Jackson JD, Market JM, Li L, **Carroll SL** and Cassady KA. STAT1 and NFκB inhibitors diminish basal interferon stimulated gene expression and increase productive infection of oncolytic HSV in malignant peripheral nerve sheath tumor cells. *Molecular Cancer Research* 2016; 14(5): 482-92., PMID: 26883073, PMCID: PMC4867290

Graham CD, Kaza N, Klocke BJ, Gillespie GY, Shevde LA, **Carroll SL** and Roth KA. Tamoxifen induces cytotoxic autophagy in human glioblastoma cells. *Journal of Neuropathology and Experimental Neurology* 2016; 75(10): 946-954., PMID: 27516117, PMCID: PMC5029439

Graham CD, Kaza N, Pruitt HC, Gibson LM, Klocke BJ, Shevde LA, **Carroll SL** and Roth KA. BH3 mimetics suppress CXCL12 expression in human malignant peripheral nerve sheath tumor cells. *Oncotarget* 2017; 8(5): 8670-8678, PMID: 28055968 PMCID: PMC5352431

Longo JF, Weber SM, Turner-Ivey BP and **Carroll SL**. Recent advances in the diagnosis and treatment of neurofibromatosis type 1 (NF1) – associated peripheral nervous system neoplasms. *Advances in Anatomic Pathology* 2018; 25(2): 353-368. PMID: 29762158

Ortonne N, Wolkenstein P, Stemmer-Rachamimov A, Korf BR, Plotkin S, Riccardi VM, Miller DC, Huson S, Peltonen J, Rosenberg A, **Carroll SL**, Jackson R, Stathis M, Verma S, Mautner V, Upadhyaya M and Blakeley JO. Cutaneous neurofibromas: current clinical and pathologic issues. *Neurology* 2018; 91 (2 Supplement 1): S5-S13. PMID: 129987130.

Bianchetti I, Siegelin MD, **Carroll SL** and Roth KA Usp9X regulates cell death in malignant peripheral nerve sheath tumors. *Scientific Reports* 2018; 8(1): 17390. Doi: 10.1038/s41598-018-35806-5. PMID: 30478285, PMCID: PMC6255814.

Sun B, Wang G, Liu H, Liu P, Twal WO, Cheung H, **Carroll SL**, Ethier SP, Mevers EE, Clardy J, Roberts T, Chen C, Li Q, Wang L, Yang M, Zhao JJ, Wang Q. Oridonin, a TCM plant extract, inhibits aberrant AKT activation in breast cancer. *Oncotarget* 2018; 9: 23878-23889. PMID: 29844859. PMCID: PMC 5963618

Rice FL, Houk, Wymer JP, Gosline SJC, Guinney J, Ratner N, Jankowski M, LaRosa S, Dockum M, Storey JR, **Carroll SL**, Albrecht PJ and Riccardi VM. The evolution and multi-molecular properties of NF1 cutaneous neurofibromas originating from C-fiber sensory endings and terminal Schwann cells at normal sites of sensory terminations in the skin. *PLoS One* 2019;14(5):e0216527. doi: 10.1371/journal.pone.0216527. eCollection 2019. PMID: 31107888. PMCID: PMC6527217

Black L, Longo JF and **Carroll SL**. The family misfit: mechanisms of erbB3 action in human neoplasia. *American Journal of Pathology* 2019; 189(10): 1898-1912. PMID: 31351986

Brosius SN, Longo JF, Black L, Worley SJ, Roth KA and **Carroll SL**. ErbB4 promotes malignant peripheral nerve sheath tumor pathogenesis via Ras-independent mechanisms. *Cell Communication and Signaling* 2019; 17:74, https//doi:org/10.1186/s12964-019-0388-5., PMID: 31291965.

Abstracts

Znoyko IY, Longo JF, **Carroll SL** and Wolff DJ. Amplified allelic imbalance—a genetic signature of malignant peripheral nerve sheath tumors (MPNST). *Cancer Genomics Consortium 2015 Meeting.*

Zarovni N, Ferruzzi P, Guazzi P, Zocco D, Fondelli C, Carroll S, Longo J and Chiesi A. Identification of specific exosome-associated markers as early detectors of malignant transformation from neurofibroma to MPNST. *International Society for Extracellular Vesicles 2015*

Prechtl A, Brossier N, Barnes S, Wilson L, Brosius S, Byer S and **Carroll S.** R-Ras subfamily proteins elicit distinct physiologic effects and phosphoproteome alterations in neurofibromin-null MPNST cells. *FASEB Journal* 2015, PMID: 25946318, PMCID: PMC4433624

Natasa Zarovni, Davide Zocco, Paolo Guazzi, Elisa Lari, Antonieta Corrado, Giorgia Radano, Judy Longo, **Carroll SL** and Chiesi A. Development of blood exosomes based immunoassays and PCR tests for active surveillance of neurofibromatosis patients and early detection of malignant peripheral nerve sheet tumors (MPNST). *International Society for Extracellular Vesicles 2016*.

Larissa E, Cronin M, Skirzewski M, Karavanova I, Vullhorst D, **Carroll S** and Buonanno A. Analysis of neurodevelopment and schizophrenia-relevant behaviors in ErbB4 mutant mice lacking the Cyt-1 isoform. *Society for Neuroscience Abstracts* 2018 (In press).

Weber SM, Longo JF, Brosius SN and **Carroll SL** Combinatorial therapy with tamoxifen and trifluoperazine decreases the formation and progression of malignant peripheral nerve sheath tumors using complementary mechanisms. 2018 (In press).

Presentations

“Molecular Mechanisms Driving the Pathogenesis of NF1-Associated PNS Neoplasms”, MUSC Department of Pathology and Laboratory Medicine Faculty Grand Rounds (June 22, 2016)

"Neurofibromatosis Type 1 Syndrome and Associated Tumors", International Society of Bone and Soft Tissue Pathology Symposium on "Tumor Syndromes in Bone and Soft Tissue Pathology", United States and Canadian Academy of Pathologists 106th Annual Meeting (San Antonio, TX; March 5, 2017)

“Modeling Malignant Peripheral Nerve Sheath Tumors in Genetically Engineered Mice Overexpressing Neuregulin-1 in Schwann Cells”, Neurofibromatosis Animal Model Workshop and Animal Model Pathology Consensus Conference sponsored by the Children’s Tumor Foundation (Palm Springs, CA; October 4-5, 2018)

Medical University Science Café (presentation for the general public) on "Neurofibromatosis" (Charleston, SC; February 12, 2019)

IMPACT

Impact on the development of the principal discipline(s) of the project

We have completed a global survey of the role that each of the 58 receptor tyrosine kinases encoded in the human genome play in the proliferation and survival of MPNST cells. These results firmly establish IGF1R, erbB3 and erbB4 as key therapeutic targets in MPNSTs. Further, our preclinical trials with canertinib and lestaurtinib show that these agents, which are currently in clinical trials for other cancer types, are effective against MPNSTs. We have also comprehensively examined the role that 15,277 genes play in MPNST proliferation and survival. These results have defined the role that numerous other genes play in these processes and thus provide a number of candidate therapeutic targets that the NF1 research community can exploit to develop effective new therapies.

Impact on other disciplines

Nothing to Report

Impact on technology transfer

Nothing to Report

Impact on society beyond science and technology

Nothing to Report

CHANGES/PROBLEMS

Changes in approach and reasons for change

As noted above, we encountered unexpected problems with our imaging modalities for tumor identification. Consequently, we used our previously described clinical signs to identify tumor- bearing mice instead.

Actual or anticipated problems or delays and actions or plans to resolve them

As noted above, we did experience a delay in getting ACURO to approve our animal protocol. As a result of this delay, we moved up our schedule for Task 5.

Changes that had a significant impact on expenditures

Nothing to report.

Significant changes in use or care of human subjects, vertebrate animals, biohazards, and/or select agents

Nothing to Report

PRODUCTS

MANUSCRIPTS, ABSTRACTS and PRESENTATIONS

Manuscripts

Carroll SL. The challenge of cancer genomics in rare nervous system neoplasms: malignant peripheral nerve sheath tumors as a paradigm for cross-species comparative oncogenomics. *The American Journal of Pathology* 2016; 186(3): 464-477. PMID: 26740486 PMCID: PMC4816695

Hanemann CO, Blakeley JO, Nunes FP, Robertson K, Stemmer-Rachamimov A, Mautner V, Kurtz A, Ferguson M, Widemann BC, Evans DG, Ferner R, **Carroll SL**, Korf B, Wolkenstein P, Knight P, Plotkin SR and the REiNS International Collaboration. Current status and recommendations for biomarkers and biobanking in neurofibromatosis. *Neurology* 2016; 87(7 Supplement 1): S40-48. DOI: 10.1212/WNL.0000000000002932. PMID: 27527649 PMCID: PMC5578360

Jackson JD, Market JM, Li L, **Carroll SL** and Cassady KA. STAT1 and NFκB inhibitors diminish basal interferon stimulated gene expression and increase productive infection of oncolytic HSV in malignant peripheral nerve sheath tumor cells. *Molecular Cancer Research* 2016; 14(5): 482-92., PMID: 26883073, PMCID: PMC4867290

Graham CD, Kaza N, Klocke BJ, Gillespie GY, Shevde LA, **Carroll SL** and Roth KA. Tamoxifen induces cytotoxic autophagy in human glioblastoma cells. *Journal of Neuropathology and Experimental Neurology* 2016; 75(10): 946-954., PMID: 27516117, PMCID: PMC5029439

Graham CD, Kaza N, Pruitt HC, Gibson LM, Klocke BJ, Shevde LA, **Carroll SL** and Roth KA. BH3 mimetics suppress CXCL12 expression in human malignant peripheral nerve sheath tumor cells. *Oncotarget* 2017; 8(5): 8670-8678, PMID: 28055968 PMCID: PMC5352431

Longo JF, Weber SM, Turner-Ivey BP and **Carroll SL**. Recent advances in the diagnosis and treatment of neurofibromatosis type 1 (NF1) – associated peripheral nervous system neoplasms. *Advances in Anatomic Pathology* 2018; 25(2): 353-368. PMID: 29762158

Ortonne N, Wolkenstein P, Stemmer-Rachamimov A, Korf BR, Plotkin S, Riccardi VM, Miller DC, Huson S, Peltonen J, Rosenberg A, **Carroll SL**, Jackson R, Stathis M, Verma S, Mautner V, Upadhyaya M and Blakeley JO. Cutaneous neurofibromas: current clinical and pathologic issues. *Neurology* 2018; 91 (2 Supplement 1): S5-S13. PMID: 129987130.

Bianchetti I, Siegelin MD, **Carroll SL** and Roth KA Usp9X regulates cell death in malignant peripheral nerve sheath tumors. *Scientific Reports* 2018; 8(1): 17390. Doi: 10.1038/s41598-018-35806-5. PMID: 30478285, PMCID: PMC6255814.

Sun B, Wang G, Liu H, Liu P, Twal WO, Cheung H, **Carroll SL**, Ethier SP, Mevers EE, Clardy J, Roberts T, Chen C, Li Q, Wang L, Yang M, Zhao JJ, Wang Q. Oridonin Inhibits aberrant Act activation in breast cancer. *Oncotarget* 2018; 9: 23878-23889. PMID: 29844859. PMCID: PMC 5963618

Rice FL, Houk, Wymer JP, Gosline SJC, Guinney J, Ratner N, Jankowski M, LaRosa S, Dockum

M, Storey JR, **Carroll SL**, Albrecht PJ and Riccardi VM. The evolution and multi-molecular properties of NF1 cutaneous neurofibromas originating from C-fiber sensory endings and terminal Schwann cells at normal sites of sensory terminations in the skin. *PLoS One* 2019;14(5):e0216527. doi: 10.1371/journal.pone.0216527. eCollection 2019. PMID: 31107888. PMCID: PMC6527217

Black L, Longo JF and **Carroll SL**. The family misfit: mechanisms of erbB3 action in human neoplasia. *American Journal of Pathology* 2019; 189(10): 1898-1912. PMID: 31351986
Brosius SN, Longo JF, Black L, Worley SJ, Roth KA and **Carroll SL**. ErbB4 promotes malignant peripheral nerve sheath tumor pathogenesis via Ras-independent mechanisms. *Cell Communication and Signaling* 2019; 17:74, https//doi:org/10.1186/s12964-019-0388-5., PMID: 31291965.

Longo JF, Brosius SN, Black L, Worley SJ, Roth KA and **Carroll SL**. ErbB4 promotes malignant peripheral nerve sheath tumor pathogenesis via Ras-independent mechanisms. *Cell Communication and Signaling* 2019; 17:74, https//doi:org/10.1186/s12964-019-0388-5., PMID: 31291965.

Abstracts

Znoyko IY, Longo JF, **Carroll SL** and Wolff DJ. Amplified allelic imbalance—a genetic signature of malignant peripheral nerve sheath tumors (MPNST). *Cancer Genomics Consortium 2015 Meeting.*

Zarovni N, Ferruzzi P, Guazzi P, Zocco D, Fondelli C, Carroll S, Longo J and Chiesi A. Identification of specific exosome-associated markers as early detectors of malignant transformation from neurofibroma to MPNST. *International Society for Extracellular Vesicles 2015*

Prechtl A, Brossier N, Barnes S, Wilson L, Brosius S, Byer S and **Carroll S.** R-Ras subfamily proteins elicit distinct physiologic effects and phosphoproteome alterations in neurofibromin-null MPNST cells. *FASEB Journal* 2015, PMID: 25946318, PMCID: PMC4433624

Natasa Zarovni, Davide Zocco, Paolo Guazzi, Elisa Lari, Antonieta Corrado, Giorgia Radano, Judy Longo, **Carroll SL** and Chiesi A. Development of blood exosomes based immunoassays and PCR tests for active surveillance of neurofibromatosis patients and early detection of malignant peripheral nerve sheet tumors (MPNST). *International Society for Extracellular Vesicles 2016*.

Larissa E, Cronin M, Skirzewski M, Karavanova I, Vullhorst D, **Carroll S** and Buonanno A. Analysis of neurodevelopment and schizophrenia-relevant behaviors in ErbB4 mutant mice lacking the Cyt-1 isoform. *Society for Neuroscience Abstracts* 2018 (In press).

Weber SM, Longo JF, Brosius SN and **Carroll SL** Combinatorial therapy with tamoxifen and trifluoperazine decreases the formation and progression of malignant peripheral nerve sheath tumors using complementary mechanisms. 2018 (In press).

Presentations

“Molecular Mechanisms Driving the Pathogenesis of NF1-Associated PNS Neoplasms”, MUSC Department of Pathology and Laboratory Medicine Faculty Grand Rounds (June 22, 2016)

"Neurofibromatosis Type 1 Syndrome and Associated Tumors", International Society of Bone and Soft Tissue Pathology Symposium on "Tumor Syndromes in Bone and Soft Tissue Pathology", United States and Canadian Academy of Pathologists 106th Annual Meeting

(San Antonio, TX; March 5, 2017)

“Modeling Malignant Peripheral Nerve Sheath Tumors in Genetically Engineered Mice Overexpressing Neuregulin-1 in Schwann Cells”, Neurofibromatosis Animal Model Workshop and Animal Model Pathology Consensus Conference sponsored by the Children’s Tumor Foundation (Palm Springs, CA; October 4-5, 2018)

Medical University Science Café (presentation for the general public) on "Neurofibromatosis" (Charleston, SC; February 12, 2019)

LICENSES APPLIED FOR AND/OR ISSUED

Nothing to Report

DEGREES OBTAINED THAT ARE SUPPORTED BY THIS AWARD

Nothing to Report

DEVELOPMENT OF CELL LINES, TISSUE OR SERUM REPOSITORIES

Developed a new sporadic MPNST cell line (2XSB cells); a manuscript describing this cell line is in preparation. The line will be deposited with ATCC after submission of the manuscript so that it is generally available to the community of investigators studying MPNSTs

DATABASES AND ANIMAL MODELS

Nothing to Report

FUNDING APPLIED FOR BASED ON WORK SUPPORTED BY THIS AWARD

2018 - 2023 NINDS 1RO1NS109655
Therapeutic Targeting of Receptor Tyrosine Kinase Hierarchies in Schwann Cell Neoplasms

2018 - 2021 DOD NF170059
Development of Effective Combinational Therapies That Target MPNST Heterogeneity

2019-2021 DOD NF180050
Therapeutic Targeting of Receptor Tyrosine Kinase Hierarchies in MPNSTs

EMPLOYMENT OR RESEARCH OPPORTUNITIES APPLIED FOR AND/OR RECEIVED BASED ON EXPERIENCE/TRAINING SUPPORTED BY THIS AWARD

Nothing to Report

The American Journal of Pathology, Vol. 186, No. 3, March 2016



ELSEVIER

The American Journal of PATHOLOGY

ajp.amjpathol.org

Neuropathology Theme Issue

REVIEW

The Challenge of Cancer Genomics in Rare Nervous System Neoplasms



Malignant Peripheral Nerve Sheath Tumors as a Paradigm for Cross-Species Comparative Oncogenomics

Steven L. Carroll

From the Department of Pathology and Laboratory Medicine, Medical University of South Carolina, Charleston, South Carolina

Accepted for publication October 20, 2015.

Address correspondence to Steven L. Carroll, M.D., Ph.D., Department of Pathology and Laboratory Medicine, 171 Ashley Ave., MSC 908, Medical University of South Carolina, Charleston, SC 29425-9080. E-mail: carrolst@musc.edu.

Comprehensive genomic analyses of common nervous system cancers provide new insights into their pathogenesis, diagnosis, and treatment. Although analogous studies of rare nervous system tumors are needed, there are major barriers to performing such studies. Cross-species comparative oncogenomics, identifying driver mutations in mouse cancer models and validating them in human tumors, is a promising alternative. Although still in its infancy, this approach is being applied to malignant peripheral nerve sheath tumors (MPNSTs), rare Schwann cell–derived malignancies that occur sporadically, after radiotherapy, and in neurofibromatosis type 1. Studies of human neurofibromatosis type 1–associated tumors suggest that *NF1* tumor suppressor loss in Schwann cells triggers cell-autonomous and intercellular changes, resulting in development of benign neurofibromas; subsequent neurofibroma-MPNST progression is caused by aberrant growth factor signaling and mutations affecting the $p16^{INK4A}$-cyclin D1-CDK4-Rb and $p19^{ARF}$-Mdm2-p53 cell cycle pathways. Mice with *Nf1*, *Trp53*, and/or *Cdkn2a* mutations that overexpress the Schwann cell mitogen neuregulin-1 or overexpress the epidermal growth factor receptor validate observations in human tumors and, to various degrees, model human tumorigenesis. Genomic analyses of MPNSTs arising in neuregulin-1 and epidermal growth factor receptor-overexpressing mice and forward genetic screens with *Sleeping Beauty* transposons implicate additional signaling cascades in MPNST pathogenesis. These studies confirm the utility of mouse models for MPNST driver gene discovery and provide new insights into the complexity of MPNST pathogenesis. *(Am J Pathol 2016, 186: 464–477; http://dx.doi.org/10.1016/j.ajpath.2015.10.023)*

Our understanding of the mechanisms underlying the development of common types of nervous system tumors has expanded exponentially over the past decade. In large part, this is because a cadre of investigators and consortia such as The Cancer Genome Atlas have comprehensively identified the genomic abnormalities in large cohorts of neoplasms such as glioblastomas,[1,2] ependymomas,[3–8] medulloblastomas,[9,10] and diffuse intrinsic pontine gliomas.[11–13] These studies have provided key insights that are fundamentally altering both the diagnosis and treatment of central nervous system tumors. For diagnosis, it is now clear that for some tumor types, mutational status is more predictive of prognosis than classic pathologic criteria.[14] As a result, the International Society of Neuropathology-Haarlem Working Group, which is developing the upcoming version of the *Diagnostic Manual for Tumours of the Central Nervous System*, has proposed a diagnostic approach that integrates pathologic and molecular findings to better predict patient outcomes.[15] It is also now

Supported by NIH National Institute of Neurological Diseases and Stroke grant R01 NS048353; NIH National Cancer Institute grant R01 CA122804; the Department of Defense grants X81XWH-09-1-0086, W81XWH-11-1-0498, W81XWH-12-1-0164, W81XWH-14-1-0073, and W81XWH-15-1-0193; and The Children's Tumor Foundation grants 2014-04-001 and 2015-05-007.

Disclosures: None declared.

This article is part of a review series on neuropathology.

Copyright © 2016 American Society for Investigative Pathology. Published by Elsevier Inc. All rights reserved.
http://dx.doi.org/10.1016/j.ajpath.2015.10.023

evident that there are several molecular subtypes of glioblastomas,[16] ependymomas,[5–8] diffuse intrinsic pontine gliomas,[11,17–19] and medulloblastomas,[20–22] each of which depends on distinct signaling cascades and thus potentially sensitive to different therapeutic agents. As a result, many academic centers are now performing oncogenomic testing to predict which drugs are potentially effective against a patient's tumor.

It is reasonable to expect that globally defining the genomic abnormalities that occur in large cohorts of rare nervous system cancers would similarly affect the care of patients with those neoplasms. However, there are important barriers to performing such analyses. The Cancer Genome Atlas typically tries to study 500 examples of each tumor type, using frozen tissue and a matched germline DNA; this cohort size will capture driver mutations present in at least 5% of that tumor type. In practice, the number of tumor samples that must be collected is much larger, because many samples will be rejected during quality assurance. In addition, The Cancer Genome Atlas prefers tumors from patients who have not yet received chemotherapy or radiotherapy, which reduces the pool of available tumor samples. Because large numbers of samples are needed and rare cancers that meet these criteria are encountered only a few times annually even in large medical centers, it is likely that investigators from different institutions will have to pool their tumor collections if these studies are to be performed. However, assembling even a small collection of rare tumor specimens requires several years, and many investigators are reluctant to donate their tumor collections to large consortia because of a concern that the effort invested in their collection will not be recognized. Consequently, human factors will also impede the collection of large numbers of rare human cancer specimens.

This should not dissuade us from performing comprehensive genomic analyses on all of the rare nervous system tumors we can collect; the information we will derive from these studies will undoubtedly be invaluable. However, to maximize the value of information derived from relatively small numbers of human tumors, we will need to partner these studies with other approaches. Recognizing this, many investigators are beginning to use genetically engineered mouse models to identify driver genes potentially relevant to the pathogenesis of rare tumor types. Here, I review how this approach has been used to probe the pathogenesis of malignant peripheral nerve sheath tumors (MPNSTs).

MPNSTs are rare Schwann cell–derived neoplasms that represent approximately 5% of the soft tissue sarcomas diagnosed annually.[23] Although MPNSTs occur sporadically, after radiotherapy and in individuals with the autosomal dominant tumor susceptibility syndrome neurofibromatosis type 1 (NF1), our current understanding of the mechanisms responsible for MPNST pathogenesis in humans is derived almost exclusively from studies of NF1-associated MPNSTs. I begin by discussing the mechanisms responsible for the pathogenesis of plexiform neurofibromas, the benign precursors that give rise to MPNSTs in NF1 patients, and their transformation into MPNSTs. I then consider key genetically engineered mouse models that were created to validate observations in human MPNSTs, what we have learned from these models, and their relative suitability for MPNST driver gene discovery. I finish by reviewing the initial genomic analyses that have been performed with these mouse MPNST models.

Pathogenesis of Human Neurofibromas and MPNSTs

NF1 Tumor Suppressor Gene and Its Role in Plexiform Neurofibroma Pathogenesis

NF1 is the most common genetic disease that affects the human nervous system, occurring in 1 in every 3500 newborn infants.[24] Although completely penetrant, the manifestations of NF1 are highly variable, even in the same family. NF1 patients commonly have learning disabilities, pigmentary lesions of the iris (Lisch nodules) and skin (axillary freckling, café-au-lait macules), bone dysplasias, and glial neoplasms in brain (optic gliomas, glioblastomas), large peripheral nerves (plexiform neurofibromas, MPNSTs), and skin (dermal neurofibromas). Less frequently, these individuals develop other tumors such as pheochromocytomas, rhabdomyosarcomas, leiomyosarcomas, and juvenile myelomonocytic leukemia. In NF1 patients, one allele of neurofibromin 1 (*NF1*), a tumor suppressor gene that contains 60 exons and spans 282,751 bp on chromosome 17 (17q11.2), is inactivated. Nonsense mutations,[25] missense mutations,[25] frameshift mutations,[25] or mutations that affect RNA splicing[26] are the usual means of *NF1* inactivation; these mutations tend to cluster in exons 10a to 10c and 37, but they can be found anywhere in the *NF1* coding sequence. Complete deletion of the *NF1* gene also occurs, but is rare, being seen in only 5% of NF1 patients.[27]

Although the *NF1* gene was cloned in 1990, the functions performed by neurofibromin, the 2818-amino acid polypeptide encoded by this gene, are still incompletely understood. We do know that neurofibromin inactivates members of the Ras family of small GTP-binding proteins.[24] This function is mediated by a centrally located domain (amino acids 1203 to 1549) within neurofibromin that is homologous to the *Saccharomyces cerevisiae* GTPase-activating proteins (GAPs) IRA1 and IRA2. Ras proteins are activated on binding GTP; the neurofibromin Ras GAP domain stimulates an intrinsic GTPase activity in Ras proteins, causing them to cleave a phosphate from the bound GTP and inactivate themselves. Other domains in neurofibromin, namely the cysteine/serine-rich domain and a tubulin-binding domain located amino terminal to the Ras GAP domain, modulate its Ras GAP activity.[24] The cysteine/serine-rich domain and TBD have opposing actions; phosphorylation of the cysteine/serine-rich domain by protein kinase Cα results in enhanced Ras GAP activity, whereas the interaction of tubulin with the tubulin-binding domain inhibits neurofibromin's Ras GAP function.

A bipartite domain that contains both a region analogous to the yeast protein Sec14p and a pleckstrin homology domain is present carboxy terminal to the Ras GAP domain. Although it was suggested that this domain binds glycerophospholipids and interacts with other as yet unidentified proteins, the biological significance of these hypothetical interactions remains unknown. The carboxy terminus of neurofibromin also contains a focal adhesion kinase (FAK)−interacting domain that allows neurofibromin to modulate substrate interactions. Curiously, although neurofibromin has no known nuclear functions, a nuclear localization signal is present within the FAK-interacting domain. Conversely, some neurofibromin functions are not yet linked to specific domains in this protein. For example, although neurofibromin loss results in changes in cAMP and calcium signaling, it is not yet known which neurofibromin domains regulate these events.

Most investigators examining neurofibromin's tumor suppressor function have focused on the role of the Ras GAP domain. However, there is reason to think that other domains in neurofibromin also contribute to tumor suppression. For instance, neurofibromin is a member of a family of Ras GAPs that includes RASA1 (p120GAP), PLXNB2, RASA2 (Gap1^{m}), RASA3 (GAP1^{IP4BP}), RASA4 (CAPRI), RASAL1, SYNGAP (p135SynGAP), DAB2IP, RASAL2, and IQGAP1-3. Although several of these proteins are expressed ubiquitously, they do not compensate for neurofibromin loss in *NF1*-null tumors. Further, none of these other Ras GAPs produce a tumor susceptibility syndrome when mutated, indicating that loss of their Ras GAP activity is not sufficient for tumorigenesis. A comparison of the structure of neurofibromin to that of other Ras GAPs shows that, other than their Ras GAP domains, the domains present in other members of this protein family differ from those in neurofibromin. Given the structural and functional differences between neurofibromin and other Ras GAPs, it is thus possible that both the Ras GAP and other domains in neurofibromin are required for tumor suppression.

Shortly after the cloning of the *NF1* gene, it was recognized that plexiform neurofibroma pathogenesis is initiated when a second-hit mutation inactivates the remaining functional *NF1* gene in a cell within the Schwann cell lineage,[24] resulting in a loss of neurofibromin expression and Ras hyperactivation.[24] This led to the prediction that drugs targeting Ras signaling would be effective against *NF1*-null nerve sheath tumors. Unexpectedly, however, the farnesyltransferase inhibitor tipifarnib, which blocks a post-translational modification critical for Ras activity, did not inhibit the progression of plexiform neurofibromas.[28] In retrospect, this clinical trial likely failed because the Ras activation that follows neurofibromin loss is more complex than that seen in tumors with an activating mutation of a single Ras protein. Neurofibromin inhibits both the classic Ras (H-, N-, and K-Ras) and R-Ras (R-Ras, R-Ras2/TC21, and M-Ras) subfamilies.[24] As it happens, multiple members of both subfamilies (H-Ras, N-Ras, K-Ras, R-Ras, and R-Ras2) are simultaneously expressed and activated in MPNST cells. Further, these subfamilies have both overlapping and distinct functions in MPNST cells (Figure 1). Classic Ras and R-Ras proteins both contribute to MPNST proliferation. However, only classic Ras proteins promote the survival of MPNST cells, whereas R-Ras proteins drive their migration.[29] Within the classic Ras subfamily, though, there appears to be functional redundancy; ablation of one subfamily member results in increased expression and activation of another subfamily member with little, if any, effect on proliferation. Tipifarnib inhibits only H-Ras, because other post-translational modifications such as geranylgeranylation allow K-Ras and N-Ras to be

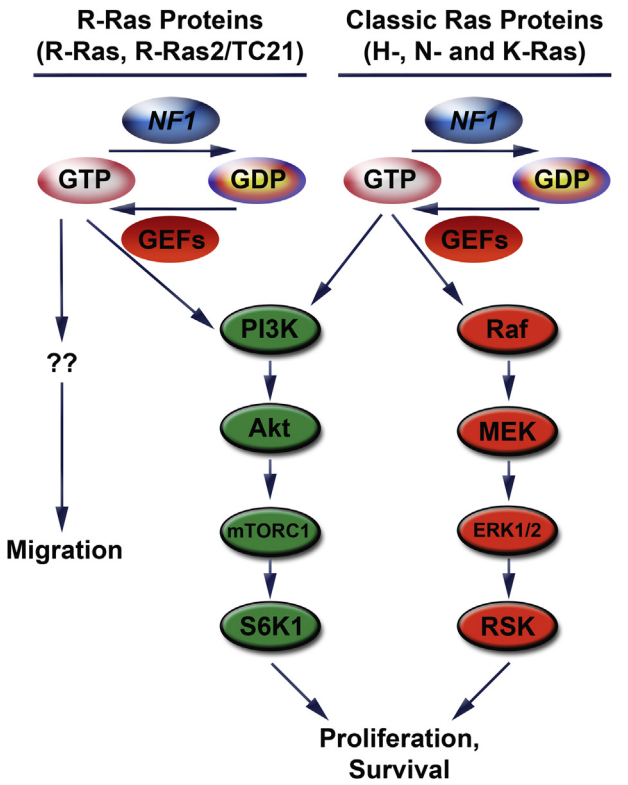


Figure 1 In plexiform neurofibromas and MPNSTs, neurofibromin loss deregulates multiple proteins from both the classic Ras and R-Ras subfamilies. NF1 stimulates an intrinsic GTPase activity in Ras proteins, causing them to cleave a phosphate from bound GTP and inactivate themselves. Ras is reactivated when guanine nucleotide exchange factors (eg, Sos), which themselves are activated by stimuli such as growth factors, cause Ras to release GDP and bind a new molecule of GTP. Despite their similar regulation, classic Ras and R-Ras proteins have overlapping (proliferation) and distinct (migration, survival) effects. This reflects the ability of different Ras families to differentially activate signaling pathways. Classic Ras proteins activate the Raf/MEK/ERK1/2/RSK and PI3K/Akt/mTORC1/S6K1 pathways, thereby enhancing proliferation and survival. It is known that R-Ras proteins can activate the PI3K pathway as well, but little is known about the cytoplasmic pathways they activate to promote migration. Note that, for the sake of simplicity, the illustration of the PI3K pathway was simplified, and some key regulators of this pathway are not shown (eg, Rheb, TSC1/2). ERK, extracellular signal-related kinase; GEF, guanine nucleotide exchange factor; MEK, mitogen-activated protein ERK kinase; MPNST, malignant peripheral nerve sheath tumor; mTOR, mammalian target of rapamycin; NF1, neurofibromin; PI3K, phosphatidylinositol 3-kinase; RSK, ribosomal S6 kinase.

appropriately activated[30] and thus circumvent inhibition by tipifarnib. Consequently, treatment with this drug likely resulted in compensatory activation of other, tipifarnib-resistant Ras proteins. Indeed, the simultaneous activation and intrafamily functional redundancy of Ras proteins in *NF1*-null MPNST cells suggests that it will be difficult to target these proteins therapeutically. Consequently, some laboratories have asked whether targeting signaling pathways downstream of Ras such as mitogen-activated protein extracellular signal-related kinase (ERK) kinase (MEK)[31,32] and the phosphatidylinositol 3-kinase (PI3K)-Akt-TSC2-mammalian target of rapamycin (mTOR)-S6 kinase[33,34] would be more effective therapeutically. Although initial results indicate that this is the case, note that the full repertoire of Ras-dependent signaling pathways activated in *NF1*-null peripheral nerve sheath tumors has not yet been defined. Indeed, a recent study that examined changes occurring in the phosphoproteome after inhibition of classic Ras signaling[29] showed that classic Ras signaling controlled multiple additional signaling cascades in MPNSTs. It will be important to determine which of these signaling cascades contribute to tumorigenesis and whether they are further dysregulated by additional mutations arising during neurofibroma-MPNST progression.

Because *NF1* loss occurs in Schwann cells, it might be expected that NF1-null nerve sheath tumors would be primarily composed of neoplastic Schwann cells. Paradoxically, however, neurofibromas are histologically complex lesions composed of $NF1^{-/-}$ Schwann cells intermingled with multiple other cell types, including $NF1^{+/-}$ Schwann cells, fibroblasts, perineurial-like cells, vasculature, mast cells, macrophages, and a poorly defined CD34-immunoreactive population. Further, animal models (see *Currently Available Mouse Models of Neurofibroma and MPNST Pathogenesis*) indicate that at least some of these other cell types are essential for neurofibroma pathogenesis. This admixture of cell types occurs, in part, because *NF1*-null Schwann cells demonstrate enhanced expression of paracrine signaling factors that recruit other cell types into the nascent neurofibroma. Although the nature of these paracrine signaling factors is incompletely understood, there is good evidence that at least one of them is stem cell factor (SCF, also known as Kit ligand), a protein that promotes the migration, survival, maturation, and activation of mast cells.[35,36] *NF1* loss enhances SCF expression, with $NF1^{-/-}$ Schwann cells secreting sixfold higher levels of SCF than $NF1^{+/-}$ or wild-type Schwann cells.[37] Intriguingly, changes in *NF1* copy number also affects mast cell physiology; $NF1^{+/-}$ mast cells show enhanced proliferation, survival, and migration when challenged with SCF.[38,39] The hyperresponsiveness of $NF1^{+/-}$ mast cells also has cascading effects on other cell types in the developing neurofibroma. For instance, SCF-induced secretion of transforming growth factor-β is exaggerated in $NF1^{+/-}$ mast cells.[40] When challenged with transforming growth factor-β, $NF1^{+/-}$ fibroblasts show increased production of collagen relative to wild-type fibroblasts, potentially explaining the dense collagenous deposits evident in human neurofibromas. Considered together, these observations suggest a model in which *NF1* loss in Schwann cells results in both cell autonomous (eg, enhanced proliferation) and nonautonomous (recruitment of other $NF1^{+/-}$ cell types) effects that interact to drive neurofibroma pathogenesis. This hypothesis is consistent with observations from several laboratories showing that multiple $NF1^{+/-}$ cell types, including Schwann cells,[41] fibroblasts,[40,42] and keratinocytes,[43] show altered proliferative responses relative to their wild-type counterparts.

Genomic Abnormalities Mediating Neurofibroma-MPNST Progression

The transformation of a neurofibroma into a MPNST requires the accumulation of additional mutations, many of which affect tumor suppressor genes. Mutations that affect the $p16^{INK4A}$-cyclin D1-cyclin-dependent kinase (CDK)4-Retinoblastoma (Rb) and $p19^{ARF}$-Mdm2-p53 cell cycle regulatory pathways were among the first linked to MPNST pathogenesis. *CDKN2A* mutations occur in up to 50% of MPNSTs[44,45] and are especially deleterious because they dysregulate both of these cell cycle regulatory pathways. This is because *CDKN2A* encodes both $p16^{INK4A}$, which inhibits CDK4 and CDK6, and $p19^{ARF}$, a protein that inhibits Mdm2, an E3 ubiquitin-protein ligase which tags p53 for proteasomal degradation. However, these pathways can be disabled in other ways in MPNSTs. For instance, expression of Rb protein is lost in 25% of MPNSTs.[46,47] Deletions and other loss of function mutations of *TP53* are also common, occurring in up to 75% of MPNSTs.[24] Tumor suppressor mutations that affect other essential signaling cascades such as the PI3K-Akt-TSC2-mTOR-S6 kinase pathway have also been identified in MPNSTs. For instance, loss of the phosphate and tensin homologue tumor suppressor, an inhibitor of the PI3K-Akt-TSC2-mTOR-S6 pathway, is evident in approximately 60% of MPNSTs.[48,49] Epigenetic repression of tumor suppressors also plays a role in MPNST pathogenesis, as demonstrated by the recent finding that expression of Ras association domain family member 1, isoform A (*RASSF1A*) is silenced in MPNSTs by DNA methylation.[50]

The discovery of candidate oncogenes in MPNSTs was driven primarily by a search for therapeutic targets. As part of this effort, several laboratories have explored the possibility that aberrant growth factor signaling is a key upstream mediator of Ras activation in MPNSTs. These studies identified several growth factors and growth factor receptors that potentially contribute to neurofibroma and MPNST pathogenesis, including the epidermal growth factor (EGF) receptor,[24] neuregulin-1 (NRG1),[24] platelet-derived growth factor,[24] hepatocyte growth factor, and its c-Met receptor,[24] the insulin-like growth factor 1 receptor,[51] transforming growth factor-β1,[52] lysophosphatidic acid,[53] midkine,[52] Kit ligand and its c-Kit receptor,[24] CXCR4 and its CXCL12 ligand,[54] basic fibroblast growth factor, and vascular endothelial growth factor.[55] However, the strength of the evidence

supporting a role for each of these candidate molecules is highly variable, ranging from merely showing that a factor or receptor is present to showing strong genomic or functional evidence. As genomic evidence, genes encoding several receptor tyrosine kinases, including the EGF receptor, the NRG1 co-receptor erbB2, c-Kit, c-Met, and the platelet-derived growth factor receptor-α, are amplified in subsets of MPNSTs.[24] Consistent with these genomic observations, pharmacologic inhibitors of the EGF receptor, NRG1 receptors, c-Kit, platelet-derived growth factor receptors, and c-Met inhibit the proliferation and/or invasion of MPNST cells.[24] However, several important questions remain unanswered about the role these molecules play in MPNST pathogenesis. Of particular importance, it is not yet known whether there are distinct subsets of MPNSTs that depend on different growth factors for their growth or, alternatively, whether each of these growth factors play distinct, critically important roles in the same tumor.

Since multiple oncogenes and tumor suppressor genes have already been implicated in MPNST pathogenesis, it is reasonable to ask whether comprehensive genomic analyses of MPNSTs are likely to identify substantial numbers of currently unknown mutations that promote the pathogenesis of these tumors. A consideration of the chromosomal abnormalities in MPNSTs shows that the pathogenic abnormalities identified thus far represent only a fraction of the genomic changes in these tumors. Cytogenetic and array comparative genomic hybridization (aCGH) studies of human NF1-associated MPNSTs indicate that these neoplasms have highly complex hypodiploid or near-triploid genomes. This complexity has made it quite difficult to identify recurrent copy number changes that contain potential driver genes. Nonetheless, some such regions were identified; for instance, losses occur repeatedly in sites on chromosomes 1p, 9p, 11, 12p, 14q, 17q, 18, 22q, X, and Y, with focal gains commonly observed on chromosome 7, 8q, and 15q.[56–65] Consistent with the tumor suppressor mutations identified in MPNSTs, some repetitive losses, such as 17q (the *NF1* gene) and 9p (*CDKN2A*), affect genes implicated in MPNST pathogenesis. However, for most of the regions of recurrent gain or loss, the driver gene or genes within these intervals have not been identified.

Only two studies have examined the genomes of human MPNSTs at nucleotide resolution. Zhang et al[66] performed whole genome sequencing on four NF1-associated MPNSTs and matched buffy coats. They found that these tumors had a median of 60 tumor-specific small insertions-deletions and nonsynonymous single nucleotide polymorphisms that affect protein-coding sequences. Intriguingly, all four of the MPNSTs also had inactivating mutations of *SUZ12*, a gene encoding a chromatin-modifying protein that forms part of polycomb repressive complex 2 (PRC2). Targeted sequencing of an additional 42 formalin-fixed, paraffin-embedded MPNST specimens (31 NF1-associated, 11 sporadic) showed that both NF1-associated and sporadic MPNSTs had mutually exclusive mutations in *SUZ12* or genes that encode other proteins that interact with PRC2 (*EED*, *AEBP2*, *EPC1*, *EZH2,* or *RBBP7*). *SUZ12* mutations were not present in the neurofibromas from which some of these MPNSTs were derived, indicating that *SUZ12* mutations occur during malignant progression. Lee et al[67] performed whole exome sequencing, DNA copy number analyses, and whole transcriptome sequencing on 15 MPNSTs, including six NF1-associated, four sporadic, and four radiation-associated tumors. In these tumors and a subsequent validation cohort of 37 formalin-fixed, paraffin-embedded specimens, PRC2 mutations were evident in 70% of NF1-associated MPNSTs, 92% of sporadic MPNSTs, and 90% of radiation-induced MPNSTs. In keeping with the role of PRC2 in establishing and maintaining epigenetic regulation via methylation of histone H3, H3K27me3 immunoreactivity was lost in MPNSTs with mutation of PRC2 components and the transcriptomes of PRC2-wild type and -mutant MPNSTs were distinct.

At present, it is unclear whether the pathogenesis of sporadic, radiation-induced, and NF1-associated MPNSTs is driven by distinct mechanisms. Although NF1-associated and sporadic MPNSTs share some common pathogenic mechanisms (eg, EGF receptor amplification and activation of the PI3K-Akt-mTOR and MEK signaling cascades), a report that two sporadic MPNST cell lines (STS-26T and YST-1 cells) have intact *NF1* genes[68] has given the impression that *NF1* mutation distinguishes between these two groups of neoplasms. An examination of currently available data shows that this conclusion is incorrect. Subsequent to the report that STS-26T cells have intact NF1 genes, it was found that these cells actually have a deletion within *NF1*.[69] My laboratory has found that YST-1 cells have a genome quite distinct from that of MPNST cells, suggesting that they were incorrectly identified as an MPNST cell line (unpublished data). Further, one of the whole exome sequencing studies found *NF1* mutations in 82% (18 of 22) of the sporadic and radiation-induced MPNSTs examined.[67] Finally, it is not yet known whether sporadic MPNSTs with intact *NF1* genes have other mutations that affect NF1-regulated signaling pathways; this possibility is consistent with observations from some genetically engineered mouse models (see *Currently Available Mouse Models of Neurofibroma and MPNST Pathogenesis*). Thus, we cannot yet conclude that sporadic and NF1-associated MPNSTs arise via distinct mechanisms. Indeed, the fact that transcriptome profiles distinguishing these tumor types have not yet been found (despite multiple attempts)[70] is consistent with the possibility that the mechanisms driving the pathogenesis of sporadic and NF1-associated MPNSTs are quite similar.

Using Cross-Species Comparative Oncogenomics to Investigate MPNST Pathogenesis

Selecting an Animal Model That Maximizes the Advantages of Cross-Species Comparative Oncogenomics

Cross-species comparative oncogenomics is an approach in which a mouse cancer model is used to identify the somatic

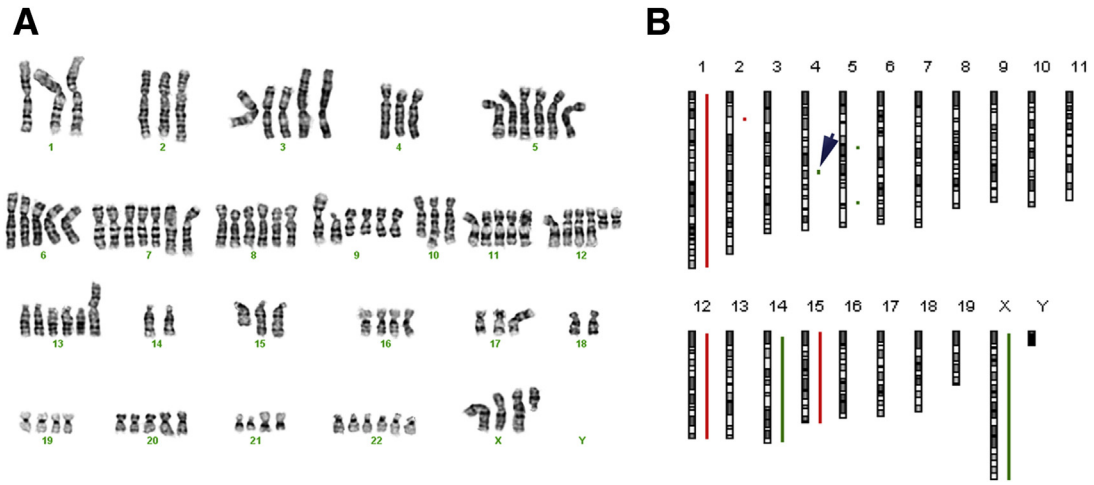


Figure 2 Comparison of the genomes of a representative human MPNST and a mouse (P_0-GGFβ3) MPNST. **A:** This human MPNST contained two major populations, one with 89 chromosomes and the other with 101 chromosomes. This highly complex karyotype was interpreted as 89 approximately 101<4n>,XXX,-X,-1,der(1)t(1;9)(q41;q21)x2,-2,der(2)(2pter->2p14::2q37->2p11.2::2q32->2qter),+der(3)(3qter->3p11::?::15q21->15qter),-4,+5,der(7)t(2;7)(q23;q22),+8,der(9)t(1;9)(q41;q13)x4,+i(9)(q10),-10,der(10)t(9;10)(q21;q25),+i(12)(p10),+add(13)(p11.2),-15,add(15)(q22)x2,-17,der(17)t(9;17)(q21;p11.1),add(17)(p11.2),-18,-18,add(20)(q12),der(21)t(19;21)(q13.3;p11.1)[cp15]. **B:** Array CGH analysis of an MPNST from P_0-GGFβ3 mouse B233. In this ideogram, gains are indicated in red and losses in green. This genome is much simpler than that of the human MPNST shown in **A**, with only four whole chromosome gains or losses and four focal copy number variations. The **arrowhead** indicates a copy number loss that ablated the *Cdkn2a/Cdkn2b* gene. MPNST, malignant peripheral nerve sheath tumor.

mutations that drive tumorigenesis, and the relevance of these mutations is then validated in the human counterpart of the mouse cancer. Because validation can be performed with formalin-fixed, paraffin-embedded tissue specimens, the size of the human tumor cohort available for validation is effectively amplified. The use of mouse cancer models also offers advantages that facilitate rapid identification of driver mutations. First, the genome of inbred mouse strains has less variability than human genomes. This means that somatic mutations in a mouse cancer are being identified against a relatively uniform genetic background rather than one with the extreme variability typical of humans. Second, there are intrinsic differences in the stability of human and mouse cancer genomes.[71] Human cancer genomes are typically structurally complex, with numerous regions of focal chromosomal gain and loss; however, only a small subset of these copy number changes affect driver genes (Figure 2). In contrast, mouse cancer genomes tend to have whole chromosome gains or losses, with few focal copy number variations. Those focal gains or losses that do occur in mouse tumors arise under strong selective pressure and are more likely to contain a driver gene.[72] Finally, because key driver genes and their associated pathways are evolutionarily conserved, driver mutations in mouse cancer models are usually relevant to the pathogenesis of their human counterpart. As evidence, cross-species comparative oncogenomic studies with the use of several genetically engineered mouse cancer models[3,73–80] or murine cancers produced by insertional mutagenesis with the *Sleeping Beauty* transposon system[64,81–83] have proven highly effective for identifying novel oncogenes and tumor suppressor genes relevant to human tumor pathogenesis.

To completely understand peripheral nerve sheath tumorigenesis, we need to identify the driver mutations responsible for neurofibroma pathogenesis, the transformation of a neurofibroma into a MPNST, and the progression from a low-grade MPNST to a high-grade malignancy. Ideally, cross-species comparative oncogenomics would thus be performed with animal models that recapitulate the process of tumorigenesis seen in humans and develop neurofibromas and MPNSTs that have genomic abnormalities mirroring those seen in their human counterparts. A variety of approaches were used to create genetically engineered mouse models that could be used for these studies (Table 1); these approaches included knocking out *Nf1* and other tumor suppressor genes, overexpressing the growth factor NRG1, and overexpressing the EGF receptor. Given the central role that *NF1* mutation plays in human neurofibroma and MPNST pathogenesis, one might expect that *Nf1* knockout models would be the natural choice for cross-species comparative oncogenomics studies. However, there are important limitations to currently available *Nf1* knockout models, and cancer genomics studies performed thus far have instead used the NRG1 and EGF receptor overexpression models. To explain these observations, it is useful to consider the strengths and weaknesses of these mouse models.

Currently Available Mouse Models of Neurofibroma and MPNST Pathogenesis

Mice with genetic ablation of the *Nf1* gene were first created in 1994, when two laboratories independently created mice with deletion of exon 31 ($Nf1^{\Delta 31/+}$ mice).[84,85] Surprisingly,

Table 1 Genetically Engineered Mouse Models of Neurofibroma and MPNST Pathogenesis

Model	Transgenic Mouse Model	Phenotype	Limitations
Nf1 knockout models	$Nf1^{\Delta 31/\Delta 31}$	Die of cardiac failure by embryonic day 13.5	Early death prevents observation of tumorigenic effects of *Nf1* loss
	$Nf1^{\Delta 31/+}$	Develop pheochromocytomas (15% incidence); also show accelerated development of other non-NF1 tumors compared with wild-type mice	No neurofibromas or MPNSTs observed
	Krox20-Cre;$Nf1^{flox/flox}$	Schwann cell hyperplasia	No neurofibromas or MPNSTs observed
	Krox20-Cre;$Nf1^{flox/-}$	Plexiform neurofibroma development by 1 year of age (showing importance of both $Nf1^{+/-}$ and $Nf1^{-/-}$ cells in neurofibroma formation)	Neurofibromas in this model do not transform into MPNSTs
Tumor microenvironment models	*Krox2-Cre;*$Nf1^{flox/flox}$ transplanted with $Nf1^{+/-}$ bone marrow	Developed plexiform neurofibromas infiltrated by donor mast cells (demonstrating importance of Nf1 haploinsufficiency in hematopoeitic lineage for neurofibroma formation)	Other $Nf1^{+/-}$ cell types within the hematopoietic lineage (eg, macrophages) may contribute to neurofibroma development
	$Nf1^{flox/+}$; *Krox2-Cre* transplanted with $Nf1^{+/+}$ bone marrow	No neurofibromas developed (showing importance of Nf1 haploinsufficiency in hematopoeitic lineage for neurofibroma formation)	
MPNST formation driven by dual tumor suppressor loss	*trans*-Linked $Nf1^{+/-}$;$p53^{+/-}$	Develop non-MPNST sarcomas characteristic of *p53* LOH	No MPNST formation
	cis-Linked $Nf1^{+/-}$;$p53^{+/-}$	Developed MPNSTs (~30% incidence)	No neurofibroma precursor lesion
	$Nf1^{+/-}p16^{Ink4a-/-}$	Accelerated development of tumors characteristic of $p16^{INK4a}$ loss	No MPNST formation
	$Nf1^{+/-}p19^{Arf-/-}$	Accelerated development of tumors characteristic of $p19^{Arf}$ loss	No MPNST formation
	$Nf1^{+/-}p16^{Ink4a}/p19^{Arf-/-}$	Developed MPNSTs (~30% incidence)	No neurofibroma precursor lesion
PNS tumor formation driven by dysregulated growth factor signaling	P_0-*GGF*β*3*	Neurofibroma formation with progression to MPNSTs by 6 to 10 months	Although genetic complementation indicates that protumorigenic effect of NRG1 is in the *Nf1* signaling cascade, tumors are not *Nf1* null and other, as yet unknown, non-RasGAP neurofibromin functions that contribute to tumorigenesis may not be modeled
	P_0-*GGF*β*3;Trp53*$^{+/-}$	MPNSTs develop *de novo* and with complete penetrance by 6 to 9 months; also model MPNST progression from WHO grade II to IV	No neurofibroma precursor lesion
	CNPase-hEGFR	Schwann cell hyperplasia with mast cell recruitment and fibrosis	Neurofibroma formation exceedingly rare at advanced age; no MPNSTs observed
	Cnp-hEGFR;*Trp53*$^{+/R270H}$	Develop both neurofibromas and MPNSTs	See discussion in text
	Cnp-hEGFR;*Dhh*-Cre;*Pten*$^{flox/+}$	Develop neurofibromas	Neurofibromas do not transform into MPNSTs
	Cnp-hEGFR;*Dhh*-Cre;*Pten*$^{flox/flox}$	Develop MPNSTs *de novo*	No neurofibroma precursor lesion

GAP, GTPase-activating protein; LOH, loss of heterozygosity; MPNST, malignant peripheral nerve sheath tumor; NF1, NF1, neurofibromatosis type 1; NRG, neuregulin; WHO, World Health Organization.

although $Nf1^{\Delta 31/+}$ mice were viable and fertile, they did not develop neurofibromas; these animals showed only some of the more rare manifestations of NF1 such as leukemias and pheochromocytomas. Mice homozygous for this mutation ($Nf1^{\Delta 31/\Delta 31}$ mice) died at embryonic day 13.5 secondary to cardiac failure, and they displayed abnormally developed skeletal muscle, kidneys, and liver. However, nervous system pathology was limited to neuronal hyperplasia in sympathetic ganglia and, less commonly, exencephaly; neurofibromas were not evident.

One possible explanation for the absence of neurofibromas in *Nf1*$^{\Delta 31/+}$ mice was that the frequency of second hit *Nf1* mutations in the Schwann cells of these animals was rate limiting. Consequently, investigators next tried to create mice with a conditional knockout of *Nf1* in Schwann cells (*Krox20*-Cre;*Nf1*$^{flox/flox}$ mice).[86] These mice showed only mild Schwann cell hyperplasia, indicating that *Nf1* loss in Schwann cells was not sufficient for neurofibroma pathogenesis. However, mice with complete *Nf1* loss in Schwann cells and *Nf1* haploinsufficiency in all other cell types (*Krox20*-Cre;*Nf1*$^{flox/-}$ mice) developed multiple neurofibromas in their cranial nerves and spinal nerve roots by 1 year of age. The contrasting phenotypes of *Krox20*-Cre;*Nf1*$^{flox/flox}$ and *Krox20*-Cre;*Nf1*$^{flox/-}$ mice provided the first experimental evidence that an *Nf1* haploinsufficient tumor microenvironment was essential for neurofibroma pathogenesis. This concept (and the important role played by mast cells) was given further support by the subsequent demonstration that lethally irradiated *Krox20*-Cre;*Nf1*$^{flox/flox}$ mice grafted with *Nf1*$^{+/-}$ bone marrow developed multiple neurofibromas infiltrated by donor mast cells.[87] *Krox20*-Cre;*Nf1*$^{flox/-}$ mice thus provided important new insights into the process of neurofibroma pathogenesis. Disappointingly, however, the neurofibromas in these animals only rarely transform and give rise to MPNSTs, and so *Krox20*-Cre;*Nf1*$^{-/flox}$ mice cannot be used to identify the driver genes responsible for the malignant transformation of neurofibromas and MPNST progression.

The lack of malignant transformation in the neurofibromas of *Krox20*-Cre;*Nf1*$^{-/flox}$ mice could, like the absence of neurofibromas in *Nf1*$^{\Delta 31/+}$ mice, reflect a low rate of mutation in other key tumor suppressor genes involved in MPNST pathogenesis. To test this possibility, mice carrying null mutations of both *Nf1* and *Trp53* on the same (*cis*-linked *Nf1*$^{+/-}$;*Trp53*$^{+/-}$ mice) and different (*trans Nf1*$^{+/-}$;*Trp53*$^{+/-}$ mice) copies of chromosome 11 were created.[88,89] In mice, the most common mechanism of second hit mutation is whole chromosome loss. Consistent with this, 30% of *cis*-linked *Nf1*$^{+/-}$;*Trp53*$^{+/-}$ mice developed MPNSTs by 5 months of age, whereas *trans Nf1*$^{+/-}$;*Trp53*$^{+/-}$ mice typically died at 10 months of age with other tumor types characteristic of *Trp53*$^{+/-}$ mice. Likewise, 26% of *Nf1*$^{+/-}$ mice that also have homozygous mutations affecting both key *Cdkn2a* functions (*Nf1*$^{+/-}$;*p16*$^{Ink4a-/-}$;*p19*$^{Arf+/-}$ mice) also develop MPNSTs.[90] Intriguingly, mice with mutations affecting only one of the two transcripts encoded by the *Cdkn2a* locus (*Nf1*$^{+/-}$;*p16*$^{Ink4a-/-}$ or *Nf1*$^{+/-}$;*p19*$^{Arf-/-}$ mice) do not develop MPNSTs,[90,91] indicating that both the p16^{INK4A}-cyclin D1-CDK4-Rb and the p19^{ARF}-Mdm2-p53 pathways must be dysregulated for MPNST pathogenesis to occur. These models provide strong experimental evidence that the *Nf1*, *Trp53*, and *Cdkn2a* genes play an important role in MPNST pathogenesis. However, in all of these models, MPNSTs arise *de novo* rather than from a neurofibroma precursor, and so they cannot be used to study transformation. Because a series of tumors from these animals have not been rigorously graded, it is also unclear whether they are appropriate models for identifying genes responsible for MPNST progression.

Although several growth factors and growth factor receptors contribute to neurofibroma and MPNST pathogenesis, only two of these molecules have been overexpressed in the Schwann cells of genetically engineered mice to directly examine their role in tumorigenesis. One of these is NRG1, a growth factor that regulates Schwann cell proliferation, survival, migration, and maturation during development. We have shown that NRG1 and all three of its receptors (the erbB2, erbB3, and erbB4 receptor tyrosine kinases) are co-expressed in human neurofibromas and MPNSTs; the resulting constitutive activation of these receptors drives the proliferation,[92] survival,[93] and migration[94] of human MPNST cells. To determine whether inappropriate activation of the NRG1/erbB signaling is sufficient to induce tumorigenesis, we created transgenic mice in which a secreted NRG1 isoform is overexpressed in Schwann cells (P_0-GGFβ3 mice). On both an outbred C57BL/6J × SJL/J background and when backcrossed onto a C57BL/6J background for five to eight generations, >90% of P_0-GGFβ3 mice develop multiple neurofibromas in cranial, sympathetic, and spinal nerves that recapitulate the pathology of human plexiform neurofibromas. In 70% to 80% of P_0-GGFβ3 mice, one or more neurofibromas transform into MPNSTs.[95,96] Further, P_0-GGFβ3 MPNSTs have mutations in the p16^{INK4A}-cyclin D/CDK4-Rb and p19^{ARF}-Mdm-p53 pathways that parallel those seen in human MPNSTs. In addition, Ras is hyperactivated in P_0-GGFβ3 MPNSTs in an erbB-dependent manner. However, immunoblot analyses[96] and whole exome sequencing (unpublished data) showed that *Nf1* is not mutated in P_0-GGFβ3 MPNSTs, which raised the question of whether NRG1 promoted tumorigenesis via its effects on the *Nf1* signaling cascade or instead activated another pathway that cooperated with the *Nf1* signaling pathway to drive neoplasia. An opportunity to distinguish between these possibilities presented itself when it was noted that tumorigenesis was suppressed in P_0-GGFβ3 mice bred onto a C57BL/6J background for ≥15 generations (inbred P_0-GGFβ3 mice). To determine whether NRG1 interacts with *Nf1* or *Trp53* loss, cohorts of inbred P_0-GGFβ3;*Nf1*$^{+/-}$ and P_0-GGFβ3;*Trp53*$^{+/-}$ mice were established and examined for evidence of tumor formation.[97] Although no tumors were seen in P_0-GGFβ3;*Nf1*$^{+/-}$ mice, virtually all of the P_0-GGFβ3;*Trp53*$^{+/-}$ mice developed MPNSTs. The MPNSTs in P_0-GGFβ3;*Trp53*$^{+/-}$ mice, like those in *cis*-linked *Nf1*$^{+/-}$;*Trp53*$^{+/-}$ mice, arose *de novo*, demonstrating that NRG1 overexpression could substitute for *Nf1* loss and thus must promote tumorigenesis through the same signaling cascade affected by *Nf1* loss. Further, P_0-GGFβ3;*Trp53*$^{+/-}$ MPNSTs originated as lesions with the pathologic features of human World Health Organization grade II MPNSTs and subsequently progressed to become World Health Organization grade III and IV lesions. Thus, P_0-GGFβ3 mice develop both neurofibromas and MPNSTs, recapitulate the process of neurofibroma-MPNST progression seen in human, and have

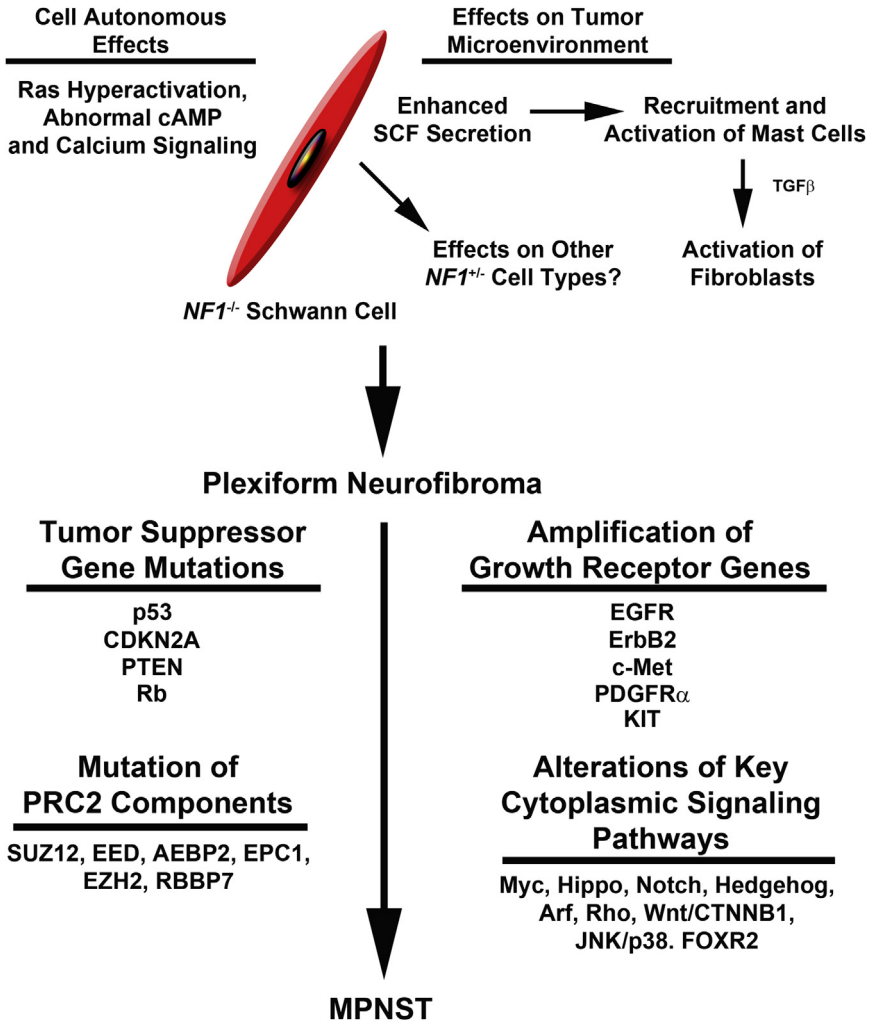


Figure 3 Overview of our current understanding of neurofibroma- MPNST pathogenesis is based on both human and mouse studies. The upper half of the diagram indicates the cell autonomous and nonautonomous consequences of NF1 loss and how this leads to neurofibroma pathogenesis. Additional events involved in the transformation of a neurofibroma to an MPNST are indicated below. Although multiple events are indicated here, note that it is quite possible that many of these abnormalities may be specific to as yet undefined MPNST subtypes. Consistent with this, initial comparisons of PRC2-mutant and wild-type MPNSTs indicated that some of the indicated tumor suppressor mutations were specifically associated with PRC2 mutant tumors. EGFR, epidermal growth factor receptor; MPNST, malignant peripheral nerve sheath tumor; PDGFR, platelet-derived growth factor receptor; PRC2, Polycomb repressive complex 2; PTEN, phosphate and tensin homologue; TGF, transforming growth factor.

tumor suppressor mutations analogous to those in human MPNSTs. In addition, P_0-GGFβ3 and P_0-GGFβ3;*Trp53*$^{+/-}$ mice model the evolution of MPNSTs as they progress from low to high grade.

Transgenic mice that overexpress the EGF receptor (erbB1) in Schwann cells [2′,3′-cyclic nucleotide 3′ phosphodiesterase (*Cnp*)-hEGFR mice) have also been generated.[98] Although the EGF receptor is in the same family as the NRG1 receptors, the phenotype of *Cnp*-hEGFR mice is more subtle than that of P_0-GGFβ3 mice. *Cnp*-hEGFR mice show Schwann cell hyperplasia, dissociation of Schwann cells from axons, increased numbers of intraneural mast cells, and fibrosis, but frank neurofibroma formation is rare, indicating that inappropriate expression of the EGF receptor is not sufficient for tumorigenesis. Nonetheless, the phenotype of *Cnp*-hEGFR mice does not exclude a role for the EGF receptor in neurofibroma and MPNST pathogenesis. As evidence, MPNST pathogenesis is impaired in *cis*-linked *Nf1*$^{+/-}$;*Trp53*$^{+/-}$ mice that also carry a hypomorphic EGF receptor mutation (*EGFR*$^{wa-2}$ mice). There is also evidence that inappropriate expression of the EGF receptor interacts with key tumor suppressor mutations to promote peripheral nervous system tumorigenesis. Crossing *Cnp*-hEGFR mice with *Nf1*$^{+/-}$ mice does not enhance tumorigenesis, much as was seen in inbred P_0-GGFβ3;*Nf1*$^{+/-}$ mice. However, *Cnp*-hEGFR mice with partial (*Cnp*-hEGFR;*Dhh*-Cre;*Pten*$^{flox/+}$ mice) or complete (*Cnp*-hEGFR;*Dhh*-Cre;*Pten*$^{flox/flox}$ mice) deletion of *Pten* in Schwann cells[99] develop neurofibromas and MPNSTs, respectively. Likewise, *Cnp*-hEGFR mice that also express a dominant-negative *Trp53* mutant (*Cnp*-hEGFR;*Trp53*$^{+/R270H}$ mice) develop neurofibromas and MPNSTs.[100]

Whole Genome aCGH and Forward Genetic Screens in Mouse MPNST Models

Two distinct approaches were used thus far to identify candidate driver genes in mouse MPNSTs, each of which is designed to take advantage of the distinct phenotypes of P_0-GGFβ3 and *Cnp*-hEGFR mice. The first approach parallels that used by The Cancer Genome Atlas and uses whole genome aCGH, whole exome sequencing, and transcriptome sequencing to identify candidate driver mutations. Although findings from whole exome sequencing and

transcriptome sequencing experiments have recently been presented at national meetings, only aCGH results are published,[96,97,100] and so I focus on those experiments here.

Consistent with previous studies in other mouse tumors, whole genome aCGH in P_0-GGFβ3 MPNSTs showed that the genomes of these mouse tumors were simpler than that of their human counterparts.[96] Copy number variations that involve whole chromosomes or chromosome arms were common, occurring an average of 5.3 times (range, 3 to 10 times) per tumor genome. A smaller number of focal copy number gains or losses were also evident in each P_0-GGFβ3 MPNST. An examination of the genes within 44 focal copy number gains or losses (26 gains, 18 losses) showed that 22 of these regions contained a total of 39 genes previously implicated in human neoplasia. One of the most common losses, which was present in >50% of the MPNSTs, was deletion of the *Cdkn2a* locus. The functions of the other genes were varied and included loci that encoded proteins regulating proliferation (*Myc*, *Strn*, *Tpd52*), chromatin remodeling (*Ep400*), progress through the cell cycle (*Chfr*, *Chek2*, *Cdk2ap1*, *Cdk4*), apoptosis (*Bbc3/PUMA*, *XIAP*, *Ddit3/GADD153*), transcriptional control (*Ncoa3*, *Nr4a3*, *Zscan22*), cell motility (*Sept6*, *Vcl*), and metabolism (*Aldob*, *Mars*, *Alad*). Genes encoding members of key cytoplasmic signaling pathways such as Hippo (*Stk4*), Notch (*Dtx3*), Hedgehog (*Gli1*), Arf (*Agap2*), Rho (*Arhgap9*), and PI3 kinase (*Pten*) were also repeatedly affected. Interestingly, several regions of recurrent copy number gain or loss did not contain any genes previously implicated in cancer pathogenesis, indicating that these regions may contain as yet unknown oncogenes or tumor suppressor genes.

MPNSTs from P_0-GGFβ3;$Trp53^{+/-}$ and *Cnp*-EGFR;$Trp53^{+/R270H}$ mice have also been studied by whole genome aCGH.[97,100] Examination of a series of P_0-GGFβ3;$Trp53^{+/-}$ MPNSTs that included World Health Organization grade II, III, and IV neoplasms showed that grade II tumors had fewer unbalanced copy number variations than grade IV lesions. Surprisingly, however, the number of copy number variations in grade III MPNSTs were not intermediate between grade II and IV neoplasms; instead, approximately one-half of the grade III MPNSTs had gains and losses that occurred with a frequency analogous to the grade IV tumors, with the remainder resembling the grade II MPNSTs. Although many of the candidate driver genes within the focal copy number variation in P_0-GGFβ3;$Trp53^{+/-}$ MPNSTs were also seen in P_0-GGFβ3 MPNSTs (eg, *Myc*), some genes encoding members of other signaling pathways (*Prkcdbp*, *Mapk1*, *Rap1gds1*, *Arap*, *Crkl*) were affected in P_0-GGFβ3;$Trp53^{+/-}$ MPNSTs, raising the question of whether tumorigenesis in this mouse model involves distinct signaling cascades. The genomes of *Cnp*-EGFR;$Trp53^{+/R270H}$ MPNSTs had a complexity similar to that seen in P_0-GGFβ3 MPNSTs. Again, *Myc* was among the genes recurrently amplified in these tumors; however, the signaling pathways affected in *Cnp*-EGFR;$Trp53^{+/R270H}$ MPNSTs included the Erk5, phospholipase C, tec kinase, and ephrin cascades.

The second approach that was used to identify driver genes in MPNSTs relies on the use of the *Sleeping Beauty* transposon system to accelerate tumorigenesis in *Cnp*-hEGFR and *Cnp*-EGFR;$Trp53^{+/R270H}$ mice.[101] Examination of the common integration sites in 269 neurofibromas and 106 MPNSTs identified 695 and 87 genes, respectively, that were recurrently present in these tumors; 37 of these genes were detected in both neurofibromas and MPNSTs. Intriguingly, tumor suppressor genes predominated in these neoplasms, with 67 potential tumor suppressor genes and 20 candidate oncogenes identified. This collection of genes was then compared with archived aCGH, single nucleotide polymorphism array, RNA expression microarray, and methylome data from human Schwann cells, neurofibromas, and MPNSTs to identify a subset of genes potentially relevant to human neurofibroma and MPNST pathogenesis. In addition to driver genes known to be important for human MPNST pathogenesis (*NF1*, *CDKN2A*, *PTEN*), three signaling cascades (PI3K/AKT/mTOR, MAPK/ERK/JNK/p38, and Wnt/CTNNB1) were identified that were both repetitively targeted by *Sleeping Beauty* and potentially relevant to human tumorigenesis. These comparisons also identified the forkhead-box transcription factor *FOXR2* as an oncogene potentially important for the development of MPNSTs. Thus, forward genetic screens with *Sleeping Beauty* transposons clearly identified genes relevant to the pathogenesis of human MPNSTs, underscoring the effectiveness of using mouse models to understand the pathogenesis of human peripheral nerve sheath tumors.

Conclusions and Future Directions

Although cross-species comparative oncogenomic studies of MPNSTs are still in their infancy, these analyses have already begun to provide new insights into the mechanisms responsible for the development of these deadly neoplasms (Figure 3). However, there are some important caveats that need to be considered as we move forward. First, the observation that different signaling pathways are being affected in different mouse MPNST models raises the question of whether particular mouse models are modeling specific MPNST subtypes. Consequently, it likely will be important to study multiple mouse models to assess this possibility. Second, it must be remembered that the identification of driver genes in mouse MPNSTs via whole exome sequencing, aCGH, and transcriptome sequencing is computational (as it is in comparable studies of human MPNSTs). Consequently, it is essential that candidate driver genes be functionally validated by a variety of approaches, including those described in the sections above. Third, it should be recognized that cross-species comparative oncogenomics will probably not effectively identify some important types of mutations such as fusion genes. This potential limitation reflects the fact that mouse MPNSTs do

not demonstrate the extreme degree of chromothripsis[102] and subsequent rejoining of chromosomal breaks seen in human MPNSTs. Nonetheless, it is increasingly evident that cross-species comparative oncogenomics is a promising approach to the challenges of performing genomics in rare tumor types and undoubtedly will be increasingly important as we turn our attention to these problematic neoplasms.

Acknowledgments

I thank Drs. Jody Fromm Longo and Amanda Prechtl for their helpful comments on this manuscript.

References

1. Cancer Genome Atlas Research Network: Comprehensive genomic characterization defines human glioblastoma genes and core pathways. Nature 2008, 455:1061–1068
2. Parsons DW, Jones S, Zhang X, Lin JC, Leary RJ, Angenendt P, Mankoo P, Carter H, Siu IM, Gallia GL, Olivi A, McLendon R, Rasheed BA, Keir S, Nikolskaya T, Nikolsky Y, Busam DA, Tekleab H, Diaz LA Jr, Hartigan J, Smith DR, Strausberg RL, Marie SK, Shinjo SM, Yan H, Riggins GJ, Bigner DD, Karchin R, Papadopoulos N, Parmigiani G, Vogelstein B, Velculescu VE, Kinzler KW: An integrated genomic analysis of human glioblastoma multiforme. Science 2008, 321:1807–1812
3. Johnson RA, Wright KD, Poppleton H, Mohankumar KM, Finkelstein D, Pounds SB, Rand V, Leary SE, White E, Eden C, Hogg T, Northcott P, Mack S, Neale G, Wang YD, Coyle B, Atkinson J, DeWire M, Kranenburg TA, Gillespie Y, Allen JC, Merchant T, Boop FA, Sanford RA, Gajjar A, Ellison DW, Taylor MD, Grundy RG, Gilbertson RJ: Cross-species genomics matches driver mutations and cell compartments to model ependymoma. Nature 2010, 466:632–636
4. Modena P, Lualdi E, Facchinetti F, Veltman J, Reid JF, Minardi S, Janssen I, Giangaspero F, Forni M, Finocchiaro G, Genitori L, Giordano F, Riccardi R, Schoenmakers EF, Massimino M, Sozzi G: Identification of tumor-specific molecular signatures in intracranial ependymoma and association with clinical characteristics. J Clin Oncol 2006, 24:5223–5233
5. Witt H, Mack SC, Ryzhova M, Bender S, Sill M, Isserlin R, et al: Delineation of two clinically and molecularly distinct subgroups of posterior fossa ependymoma. Cancer Cell 2011, 20:143–157
6. Wani K, Armstrong TS, Vera-Bolanos E, Raghunathan A, Ellison D, Gilbertson R, Vaillant B, Goldman S, Packer RJ, Fouladi M, Pollack I, Mikkelsen T, Prados M, Omuro A, Soffietti R, Ledoux A, Wilson C, Long L, Gilbert MR, Aldape K; Collaborative Ependymoma Research Network: A prognostic gene expression signature in infratentorial ependymoma. Acta Neuropathol 2012, 123:727–738
7. Mack SC, Witt H, Piro RM, Gu L, Zuyderduyn S, Stutz AM, et al: Epigenomic alterations define lethal CIMP-positive ependymomas of infancy. Nature 2014, 506:445–450
8. Pajtler KW, Witt H, Sill M, Jones DT, Hovestadt V, Kratochwil F, et al: Molecular classification of ependymal tumors across all CNS compartments, histopathological grades, and age groups. Cancer Cell 2015, 27:728–743
9. Parsons DW, Li M, Zhang X, Jones S, Leary RJ, Lin JC, et al: The genetic landscape of the childhood cancer medulloblastoma. Science 2011, 331:435–439
10. Jones DT, Jager N, Kool M, Zichner T, Hutter B, Sultan M, et al: Dissecting the genomic complexity underlying medulloblastoma. Nature 2012, 488:100–105
11. Khuong-Quang DA, Buczkowicz P, Rakopoulos P, Liu XY, Fontebasso AM, Bouffet E, Bartels U, Albrecht S, Schwartzentruber J, Letourneau L, Bourgey M, Bourque G, Montpetit A, Bourret G, Lepage P, Fleming A, Lichter P, Kool M, von Deimling A, Sturm D, Korshunov A, Faury D, Jones DT, Majewski J, Pfister SM, Jabado N, Hawkins C: K27M mutation in histone H3.3 defines clinically and biologically distinct subgroups of pediatric diffuse intrinsic pontine gliomas. Acta Neuropathol 2012, 124:439–447
12. Schwartzentruber J, Korshunov A, Liu XY, Jones DT, Pfaff E, Jacob K, et al: Driver mutations in histone H3.3 and chromatin remodelling genes in paediatric glioblastoma. Nature 2012, 482:226–231
13. Wu G, Broniscer A, McEachron TA, Lu C, Paugh BS, Becksfort J, Qu C, Ding L, Huether R, Parker M, Zhang J, Gajjar A, Dyer MA, Mullighan CG, Gilbertson RJ, Mardis ER, Wilson RK, Downing JR, Ellison DW, Baker SJ; St. Jude Children's Research Hospital–Washington University Pediatric Cancer Genome Project: Somatic histone H3 alterations in pediatric diffuse intrinsic pontine gliomas and non-brainstem glioblastomas. Nat Genet 2012, 44:251–253
14. Aldape K, Zadeh G, Mansouri S, Reifenberger G, von Deimling A: Glioblastoma: pathology, molecular mechanisms and markers. Acta Neuropathol 2015, 129:829–848
15. Louis DN, Perry A, Burger P, Ellison DW, Reifenberger G, von Deimling A, Aldape K, Brat D, Collins VP, Eberhart C, Figarella-Branger D, Fuller GN, Giangaspero F, Giannini C, Hawkins C, Kleihues P, Korshunov A, Kros JM, Beatriz Lopes M, Ng HK, Ohgaki H, Paulus W, Pietsch T, Rosenblum M, Rushing E, Soylemezoglu F, Wiestler O, Wesseling P; International Society of Neuropathology–Haarlem: International Society Of Neuropathology–Haarlem consensus guidelines for nervous system tumor classification and grading. Brain Pathol 2014, 24:429–435
16. Verhaak RG, Hoadley KA, Purdom E, Wang V, Qi Y, Wilkerson MD, Miller CR, Ding L, Golub T, Mesirov JP, Alexe G, Lawrence M, O'Kelly M, Tamayo P, Weir BA, Gabriel S, Winckler W, Gupta S, Jakkula L, Feiler HS, Hodgson JG, James CD, Sarkaria JN, Brennan C, Kahn A, Spellman PT, Wilson RK, Speed TP, Gray JW, Meyerson M, Getz G, Perou CM, Hayes DN; Cancer Genome Atlas Research Network: Integrated genomic analysis identifies clinically relevant subtypes of glioblastoma characterized by abnormalities in PDGFRA, IDH1, EGFR, and NF1. Cancer Cell 2010, 17:98–110
17. Paugh BS, Broniscer A, Qu C, Miller CP, Zhang J, Tatevossian RG, Olson JM, Geyer JR, Chi SN, da Silva NS, Onar-Thomas A, Baker JN, Gajjar A, Ellison DW, Baker SJ: Genome-wide analyses identify recurrent amplifications of receptor tyrosine kinases and cell-cycle regulatory genes in diffuse intrinsic pontine glioma. J Clin Oncol 2011, 29:3999–4006
18. Puget S, Philippe C, Bax DA, Job B, Varlet P, Junier MP, Andreiuolo F, Carvalho D, Reis R, Guerrini-Rousseau L, Roujeau T, Dessen P, Richon C, Lazar V, Le Teuff G, Sainte-Rose C, Geoerger B, Vassal G, Jones C, Grill J: Mesenchymal transition and PDGFRA amplification/mutation are key distinct oncogenic events in pediatric diffuse intrinsic pontine gliomas. PLoS One 2012, 7:e30313
19. Saratsis AM, Kambhampati M, Snyder K, Yadavilli S, Devaney JM, Harmon B, Hall J, Raabe EH, An P, Weingart M, Rood BR, Magge SN, MacDonald TJ, Packer RJ, Nazarian J: Comparative multidimensional molecular analyses of pediatric diffuse intrinsic pontine glioma reveals distinct molecular subtypes. Acta Neuropathol 2014, 127:881–895
20. Pugh TJ, Weeraratne SD, Archer TC, Pomeranz Krummel DA, Auclair D, Bochicchio J, et al: Medulloblastoma exome sequencing uncovers subtype-specific somatic mutations. Nature 2012, 488:106–110
21. Northcott PA, Shih DJ, Peacock J, Garzia L, Morrissy AS, Zichner T, et al: Subgroup-specific structural variation across 1,000 medulloblastoma genomes. Nature 2012, 488:49–56

22. Kool M, Korshunov A, Remke M, Jones DT, Schlanstein M, Northcott PA, Cho YJ, Koster J, Schouten-van Meeteren A, van Vuurden D, Clifford SC, Pietsch T, von Bueren AO, Rutkowski S, McCabe M, Collins VP, Backlund ML, Haberler C, Bourdeaut F, Delattre O, Doz F, Ellison DW, Gilbertson RJ, Pomeroy SL, Taylor MD, Lichter P, Pfister SM: Molecular subgroups of medulloblastoma: an international meta-analysis of transcriptome, genetic aberrations, and clinical data of WNT, SHH, Group 3, and Group 4 medulloblastomas. Acta Neuropathol 2012, 123:473–484
23. Lewis JJ, Brennan MF: Soft tissue sarcomas. Curr Probl Surg 1996, 33:817–872
24. Carroll SL: Molecular mechanisms promoting the pathogenesis of Schwann cell neoplasms. Acta Neuropathol 2012, 123:321–348
25. Messiaen LM, Callens T, Mortier G, Beysen D, Vandenbroucke I, Van Roy N, Speleman F, Paepe AD: Exhaustive mutation analysis of the NF1 gene allows identification of 95% of mutations and reveals a high frequency of unusual splicing defects. Hum Mutat 2000, 15:541–555
26. Wimmer K, Roca X, Beiglbock H, Callens T, Etzler J, Rao AR, Krainer AR, Fonatsch C, Messiaen L: Extensive in silico analysis of NF1 splicing defects uncovers determinants for splicing outcome upon 5' splice-site disruption. Hum Mutat 2007, 28:599–612
27. Wimmer K, Yao S, Claes K, Kehrer-Sawatzki H, Tinschert S, De Raedt T, Legius E, Callens T, Beiglbock H, Maertens O, Messiaen L: Spectrum of single- and multiexon NF1 copy number changes in a cohort of 1,100 unselected NF1 patients. Genes Chromosomes Cancer 2006, 45:265–276
28. Widemann BC, Dombi E, Gillespie A, Wolters PL, Belasco J, Goldman S, Korf BR, Solomon J, Martin S, Salzer W, Fox E, Patronas N, Kieran MW, Perentesis JP, Reddy A, Wright JJ, Kim A, Steinberg SM, Balis FM: Phase 2 randomized, flexible crossover, double-blinded, placebo-controlled trial of the farnesyltransferase inhibitor tipifarnib in children and young adults with neurofibromatosis type 1 and progressive plexiform neurofibromas. Neuro Oncol 2014, 16:707–718
29. Brossier NM, Prechtl AM, Longo JF, Barnes S, Wilson LS, Byer SJ, Brosius SN, Carroll SL: Classic Ras proteins promote proliferation and survival via distinct phosphoproteome alterations in neurofibromin-null malignant peripheral nerve sheath tumor cells. J Neuropathol Exp Neurol 2015, 74:568–586
30. Appels NM, Beijnen JH, Schellens JH: Development of farnesyl transferase inhibitors: a review. Oncologist 2005, 10:565–578
31. Jessen WJ, Miller SJ, Jousma E, Wu J, Rizvi TA, Brundage ME, Eaves D, Widemann B, Kim MO, Dombi E, Sabo J, Hardiman Dudley A, Niwa-Kawakita M, Page GP, Giovannini M, Aronow BJ, Cripe TP, Ratner N: MEK inhibition exhibits efficacy in human and mouse neurofibromatosis tumors. J Clin Invest 2013, 123:340–347
32. Watson AL, Anderson LK, Greeley AD, Keng VW, Rahrmann EP, Halfond AL, Powell NM, Collins MH, Rizvi T, Moertel CL, Ratner N, Largaespada DA: Co-targeting the MAPK and PI3K/AKT/mTOR pathways in two genetically engineered mouse models of schwann cell tumors reduces tumor grade and multiplicity. Oncotarget 2014, 5:1502–1514
33. Johannessen CM, Reczek EE, James MF, Brems H, Legius E, Cichowski K: The NF1 tumor suppressor critically regulates TSC2 and mTOR. Proc Natl Acad Sci U S A 2005, 102:8573–8578
34. Johannessen CM, Johnson BW, Williams SM, Chan AW, Reczek EE, Lynch RC, Rioth MJ, McClatchey A, Ryeom S, Cichowski K: TORC1 is essential for NF1-associated malignancies. Curr Biol 2008, 18:56–62
35. Hirota S, Nomura S, Asada H, Ito A, Morii E, Kitamura Y: Possible involvement of c-kit receptor and its ligand in increase of mast cells in neurofibroma tissues. Arch Pathol Lab Med 1993, 117:996–999
36. Ryan JJ, Klein KA, Neuberger TJ, Leftwich JA, Westin EH, Kauma S, Fletcher JA, DeVries GH, Huff TF: Role for the stem cell factor/KIT complex in Schwann cell neoplasia and mast cell proliferation associated with neurofibromatosis. J Neurosci Res 1994, 37:415–432
37. Yang FC, Ingram DA, Chen S, Hingtgen CM, Ratner N, Monk KR, Clegg T, White H, Mead L, Wenning MJ, Williams DA, Kapur R, Atkinson SJ, Clapp DW: Neurofibromin-deficient Schwann cells secrete a potent migratory stimulus for Nf1+/- mast cells. J Clin Invest 2003, 112:1851–1861
38. Ingram DA, Yang FC, Travers JB, Wenning MJ, Hiatt K, New S, Hood A, Shannon K, Williams DA, Clapp DW: Genetic and biochemical evidence that haploinsufficiency of the Nf1 tumor suppressor gene modulates melanocyte and mast cell fates in vivo. J Exp Med 2000, 191:181–188
39. Ingram DA, Hiatt K, King AJ, Fisher L, Shivakumar R, Derstine C, Wenning MJ, Diaz B, Travers JB, Hood A, Marshall M, Williams DA, Clapp DW: Hyperactivation of p21(ras) and the hematopoietic-specific Rho GTPase, Rac2, cooperate to alter the proliferation of neurofibromin-deficient mast cells in vivo and in vitro. J Exp Med 2001, 194:57–69
40. Yang FC, Chen S, Clegg T, Li X, Morgan T, Estwick SA, Yuan J, Khalaf W, Burgin S, Travers J, Parada LF, Ingram DA, Clapp DW: Nf1+/- mast cells induce neurofibroma like phenotypes through secreted TGF-beta signaling. Hum Mol Genet 2006, 15:2421–2437
41. Kim HA, Rosenbaum T, Marchionni MA, Ratner N, DeClue JE: Schwann cells from neurofibromin deficient mice exhibit activation of p21ras, inhibition of cell proliferation and morphological changes. Oncogene 1995, 11:325–335
42. Atit RP, Crowe MJ, Greenhalgh DG, Wenstrup RJ, Ratner N: The Nf1 tumor suppressor regulates mouse skin wound healing, fibroblast proliferation, and collagen deposited by fibroblasts. J Invest Dermatol 1999, 112:835–842
43. Korkiamaki T, Yla-Outinen H, Koivunen J, Karvonen SL, Peltonen J: Altered calcium-mediated cell signaling in keratinocytes cultured from patients with neurofibromatosis type 1. Am J Pathol 2002, 160: 1981–1990
44. Kourea HP, Orlow I, Scheithauer BW, Cordon-Cardo C, Woodruff JM: Deletions of the INK4A gene occur in malignant peripheral nerve sheath tumors but not in neurofibromas. Am J Pathol 1999, 155:1855–1860
45. Nielsen GP, Stemmer-Rachamimov AO, Ino Y, Moller MB, Rosenberg AE, Louis DN: Malignant transformation of neurofibromas in neurofibromatosis 1 is associated with CDKN2A/p16 inactivation. Am J Pathol 1999, 155:1879–1884
46. Mawrin C, Kirches E, Boltze C, Dietzmann K, Roessner A, Schneider-Stock R: Immunohistochemical and molecular analysis of p53, RB, and PTEN in malignant peripheral nerve sheath tumors. Virchows Arch 2002, 440:610–615
47. Mantripragada KK, Spurlock G, Kluwe L, Chuzhanova N, Ferner RE, Frayling IM, Dumanski JP, Guha A, Mautner V, Upadhyaya M: High-resolution DNA copy number profiling of malignant peripheral nerve sheath tumors using targeted microarray-based comparative genomic hybridization. Clin Cancer Res 2008, 14:1015–1024
48. Gregorian C, Nakashima J, Dry SM, Nghiemphu PL, Smith KB, Ao Y, Dang J, Lawson G, Mellinghoff IK, Mischel PS, Phelps M, Parada LF, Liu X, Sofroniew MV, Eilber FC, Wu H: PTEN dosage is essential for neurofibroma development and malignant transformation. Proc Natl Acad Sci U S A 2009, 106:19479–19484
49. Bradtmoller M, Hartmann C, Zietsch J, Jaschke S, Mautner VF, Kurtz A, Park SJ, Baier M, Harder A, Reuss D, von Deimling A, Heppner FL, Holtkamp N: Impaired Pten expression in human malignant peripheral nerve sheath tumours. PLoS One 2012, 7:e47595
50. Danielsen SA, Lind GE, Kolberg M, Holand M, Bjerkehagen B, Sundby Hall K, van den Berg E, Mertens F, Smeland S, Picci P, Lothe RA: Methylated RASSF1A in malignant peripheral nerve sheath tumors identifies neurofibromatosis type 1 patients with inferior prognosis. Neuro Oncol 2015, 17:63–69
51. Yang J, Ylipaa A, Sun Y, Zheng H, Chen K, Nykter M, Trent J, Ratner N, Lev DC, Zhang W: Genomic and molecular

characterization of malignant peripheral nerve sheath tumor identifies the IGF1R pathway as a primary target for treatment. Clin Cancer Res 2011, 17:7563–7573
52. Carroll SL, Stonecypher MS: Tumor suppressor mutations and growth factor signaling in the pathogenesis of NF1-associated peripheral nerve sheath tumors: II. The role of dysregulated growth factor signaling. J Neuropathol Exp Neurol 2005, 64:1–9
53. Nebesio TD, Ming W, Chen S, Clegg T, Yuan J, Yang Y, Estwick SA, Li Y, Li X, Hingtgen CM, Yang FC: Neurofibromin-deficient Schwann cells have increased lysophosphatidic acid dependent survival and migration-implications for increased neurofibroma formation during pregnancy. Glia 2007, 55:527–536
54. Mo W, Chen J, Patel A, Zhang L, Chau V, Li Y, Cho W, Lim K, Xu J, Lazar AJ, Creighton CJ, Bolshakov S, McKay RM, Lev D, Le LQ, Parada LF: CXCR4/CXCL12 mediate autocrine cell- cycle progression in NF1-associated malignant peripheral nerve sheath tumors. Cell 2013, 152:1077–1090
55. Zietsch J, Ziegenhagen N, Heppner FL, Reuss D, von Deimling A, Holtkamp N: The 4q12 amplicon in malignant peripheral nerve sheath tumors: consequences on gene expression and implications for sunitinib treatment. PLoS One 2010, 5:e11858
56. Forus A, Weghuis DO, Smeets D, Fodstad O, Myklebost O, van Kessel AG: Comparative genomic hybridization analysis of human sarcomas: I. Occurrence of genomic imbalances and identification of a novel major amplicon at 1q21-q22 in soft tissue sarcomas. Genes Chromosomes Cancer 1995, 14:8–14
57. Lothe RA, Karhu R, Mandahl N, Mertens F, Saeter G, Heim S, Borresen-Dale AL, Kallioniemi OP: Gain of 17q24-qter detected by comparative genomic hybridization in malignant tumors from patients with von Recklinghausen's neurofibromatosis. Cancer Res 1996, 56: 4778–4781
58. Mechtersheimer G, Otano-Joos M, Ohl S, Benner A, Lehnert T, Willeke F, Moller P, Otto HF, Lichter P, Joos S: Analysis of chromosomal imbalances in sporadic and NF1-associated peripheral nerve sheath tumors by comparative genomic hybridization. Genes Chromosomes Cancer 1999, 25:362–369
59. Mertens F, Rydholm A, Bauer HF, Limon J, Nedoszytko B, Szadowska A, Willen H, Heim S, Mitelman F, Mandahl N: Cytogenetic findings in malignant peripheral nerve sheath tumors. Int J Cancer 1995, 61:793–798
60. Mertens F, Dal Cin P, De Wever I, Fletcher CD, Mandahl N, Mitelman F, Rosai J, Rydholm A, Sciot R, Tallini G, van Den Berghe H, Vanni R, Willen H: Cytogenetic characterization of peripheral nerve sheath tumours: a report of the CHAMP study group. J Pathol 2000, 190:31–38
61. Berner JM, Sorlie T, Mertens F, Henriksen J, Saeter G, Mandahl N, Brogger A, Myklebost O, Lothe RA: Chromosome band 9p21 is frequently altered in malignant peripheral nerve sheath tumors: studies of CDKN2A and other genes of the pRB pathway. Genes Chromosomes Cancer 1999, 26:151–160
62. Schmidt H, Wurl P, Taubert H, Meye A, Bache M, Holzhausen HJ, Hinze R: Genomic imbalances of 7p and 17q in malignant peripheral nerve sheath tumors are clinically relevant. Genes Chromosomes Cancer 1999, 25:205–211
63. Schmidt H, Taubert H, Meye A, Wurl P, Bache M, Bartel F, Holzhausen HJ, Hinze R: Gains in chromosomes 7, 8q, 15q and 17q are characteristic changes in malignant but not in benign peripheral nerve sheath tumors from patients with Recklinghausen's disease. Cancer Lett 2000, 155:181–190
64. Schmidt H, Taubert H, Wurl P, Bache M, Bartel F, Holzhausen HJ, Hinze R: Cytogenetic characterization of six malignant peripheral nerve sheath tumors: comparison of karyotyping and comparative genomic hybridization. Cancer Genet Cytogenet 2001, 128:14–23
65. Kresse SH, Skarn M, Ohnstad HO, Namlos HM, Bjerkehagen B, Myklebost O, Meza-Zepeda LA: DNA copy number changes in high-grade malignant peripheral nerve sheath tumors by array CGH. Mol Cancer 2008, 7:48
66. Zhang M, Wang Y, Jones S, Sausen M, McMahon K, Sharma R, Wang Q, Belzberg AJ, Chaichana K, Gallia GL, Gokaslan ZL, Riggins GJ, Wolinksy JP, Wood LD, Montgomery EA, Hruban RH, Kinzler KW, Papadopoulos N, Vogelstein B, Bettegowda C: Somatic mutations of SUZ12 in malignant peripheral nerve sheath tumors. Nat Genet 2014, 46:1170–1172
67. Lee W, Teckie S, Wiesner T, Ran L, Prieto Granada CN, Lin M, Zhu S, Cao Z, Liang Y, Sboner A, Tap WD, Fletcher JA, Huberman KH, Qin LX, Viale A, Singer S, Zheng D, Berger MF, Chen Y, Antonescu CR, Chi P: PRC2 is recurrently inactivated through EED or SUZ12 loss in malignant peripheral nerve sheath tumors. Nat Genet 2014, 46:1227–1232
68. Miller SJ, Rangwala F, Williams J, Ackerman P, Kong S, Jegga AG, Kaiser S, Aronow BJ, Frahm S, Kluwe L, Mautner V, Upadhyaya M, Muir D, Wallace M, Hagen J, Quelle DE, Watson MA, Perry A, Gutmann DH, Ratner N: Large-scale molecular comparison of human schwann cells to malignant peripheral nerve sheath tumor cell lines and tissues. Cancer Res 2006, 66:2584–2591
69. Pasmant E, Luscan A, Varin J, Laurendeau I, Parfait B, Vidaud D: Relevance of MPNST cell lines as models for NF1 associated-tumors. J Neurooncol 2013, 114:353–355
70. Carroll SL, Ratner N: How does the Schwann cell lineage form tumors in NF1? Glia 2008, 56:1590–1605
71. Maser RS, Choudhury B, Campbell PJ, Feng B, Wong KK, Protopopov A, et al: Chromosomally unstable mouse tumours have genomic alterations similar to diverse human cancers. Nature 2007, 447:966–971
72. Plaat BE, Molenaar WM, Mastik MF, Hoekstra HJ, te Meerman GJ, van den Berg E: Computer-assisted cytogenetic analysis of 51 malignant peripheral-nerve-sheath tumors: sporadic vs. neurofibromatosis-type-1-associated malignant schwannomas. Int J Cancer 1999, 83:171–178
73. Young NP, Crowley D, Jacks T: Uncoupling cancer mutations reveals critical timing of p53 loss in sarcomagenesis. Cancer Res 2011, 71: 4040–4047
74. Yu H, Tardivo L, Tam S, Weiner E, Gebreab F, Fan C, Svrzikapa N, Hirozane-Kishikawa T, Rietman E, Yang X, Sahalie J, Salehi-Ashtiani K, Hao T, Cusick ME, Hill DE, Roth FP, Braun P, Vidal M: Next-generation sequencing to generate interactome datasets. Nat Methods 2011, 8:478–480
75. Maser RS, Choudhury B, Campbell PJ, Feng B, Wong KK, Protopopov A, et al: Chromosomally unstable mouse tumours have genomic alterations similar to diverse human cancers. Nature 2007, 447:966–971
76. Garber M, Grabherr MG, Guttman M, Trapnell C: Computational methods for transcriptome annotation and quantification using RNA-seq. Nat Methods 2011, 8:469–477
77. Endersby R, Zhu X, Hay N, Ellison DW, Baker SJ: Nonredundant functions for Akt isoforms in astrocyte growth and gliomagenesis in an orthotopic transplantation model. Cancer Res 2011, 71: 4106–4116
78. Varela I, Klijn C, Stephens PJ, Mudie LJ, Stebbings L, Galappaththige D, van der Gulden H, Schut E, Klarenbeek S, Campbell PJ, Wessels LF, Stratton MR, Jonkers J, Futreal PA, Adams DJ: Somatic structural rearrangements in genetically engineered mouse mammary tumors. Genome Biol 2010, 11:R100
79. Kim M, Gans JD, Nogueira C, Wang A, Paik JH, Feng B, Brennan C, Hahn WC, Cordon-Cardo C, Wagner SN, Flotte TJ, Duncan LM, Granter SR, Chin L: Comparative oncogenomics identifies NEDD9 as a melanoma metastasis gene. Cell 2006, 125:1269–1281
80. Zender L, Spector MS, Xue W, Flemming P, Cordon-Cardo C, Silke J, Fan ST, Luk JM, Wigler M, Hannon GJ, Mu D, Lucito R, Powers S, Lowe SW: Identification and validation of oncogenes in liver cancer using an integrative oncogenomic approach. Cell 2006, 125:1253–1267
81. Uren AG, Kool J, Matentzoglu K, de Ridder J, Mattison J, van Uitert M, Lagcher W, Sie D, Tanger E, Cox T, Reinders M, Hubbard TJ, Rogers J, Jonkers J, Wessels L, Adams DJ, van

Lohuizen M, Berns A: Large-scale mutagenesis in p19(ARF)- and p53-deficient mice identifies cancer genes and their collaborative networks. Cell 2008, 133:727–741
82. Starr TK, Allaei R, Silverstein KA, Staggs RA, Sarver AL, Bergemann TL, Gupta M, O'Sullivan MG, Matise I, Dupuy AJ, Collier LS, Powers S, Oberg AL, Asmann YW, Thibodeau SN, Tessarollo L, Copeland NG, Jenkins NA, Cormier RT, Largaespada DA: A transposon-based genetic screen in mice identifies genes altered in colorectal cancer. Science 2009, 323: 1747–1750
83. Dupuy AJ, Rogers LM, Kim J, Nannapaneni K, Starr TK, Liu P, Largaespada DA, Scheetz TE, Jenkins NA, Copeland NG: A modified sleeping beauty transposon system that can be used to model a wide variety of human cancers in mice. Cancer Res 2009, 69: 8150–8156
84. Brannan CI, Perkins AS, Vogel KS, Ratner N, Nordlund ML, Reid SW, Buchberg AM, Jenkins NA, Parada LF, Copeland NG: Targeted disruption of the neurofibromatosis type-1 gene leads to developmental abnormalities in heart and various neural crest-derived tissues. Genes Dev 1994, 8:1019–1029
85. Jacks T, Shih TS, Schmitt EM, Bronson RT, Bernards A, Weinberg RA: Tumour predisposition in mice heterozygous for a targeted mutation in Nf1. Nat Genet 1994, 7:353–361
86. Zhu Y, Ghosh P, Charnay P, Burns DK, Parada LF: Neurofibromas in NF1: Schwann cell origin and role of tumor environment. Science 2002, 296:920–922
87. Yang FC, Ingram DA, Chen S, Zhu Y, Yuan J, Li X, Yang X, Knowles S, Horn W, Li Y, Zhang S, Yang Y, Vakili ST, Yu M, Burns D, Robertson K, Hutchins G, Parada LF, Clapp DW: Nf1-dependent tumors require a microenvironment containing Nf1+/– and c-kit-dependent bone marrow. Cell 2008, 135:437–448
88. Cichowski K, Shih TS, Schmitt E, Santiago S, Reilly K, McLaughlin ME, Bronson RT, Jacks T: Mouse models of tumor development in neurofibromatosis type 1. Science 1999, 286: 2172–2176
89. Vogel KS, Klesse LJ, Velasco-Miguel S, Meyers K, Rushing EJ, Parada LF: Mouse tumor model for neurofibromatosis type 1. Science 1999, 286:2176–2179
90. Joseph NM, Mosher JT, Buchstaller J, Snider P, McKeever PE, Lim M, Conway SJ, Parada LF, Zhu Y, Morrison SJ: The loss of Nf1 transiently promotes self-renewal but not tumorigenesis by neural crest stem cells. Cancer Cell 2008, 13:129–140
91. King D, Yang G, Thompson MA, Hiebert SW: Loss of neurofibromatosis-1 and p19(ARF) cooperate to induce a multiple tumor phenotype. Oncogene 2002, 21:4978–4982
92. Stonecypher MS, Byer SJ, Grizzle WE, Carroll SL: Activation of the neuregulin-1/ErbB signaling pathway promotes the proliferation of neoplastic Schwann cells in human malignant peripheral nerve sheath tumors. Oncogene 2005, 24:5589–5605
93. Kohli L, Kaza N, Lavalley NJ, Turner KL, Byer S, Carroll SL, Roth KA: The pan erbB inhibitor PD168393 enhances lysosomal dysfunction-induced apoptotic death in malignant peripheral nerve sheath tumor cells. Neuro Oncol 2012, 14:266–277
94. Eckert JM, Byer SJ, Clodfelder-Miller BJ, Carroll SL: Neuregulin-1 beta and neuregulin-1 alpha differentially affect the migration and invasion of malignant peripheral nerve sheath tumor cells. Glia 2009, 57:1501–1520
95. Huijbregts RP, Roth KA, Schmidt RE, Carroll SL: Hypertrophic neuropathies and malignant peripheral nerve sheath tumors in transgenic mice overexpressing glial growth factor beta3 in myelinating Schwann cells. J Neurosci 2003, 23:7269–7280
96. Kazmi SJ, Byer SJ, Eckert JM, Turk AN, Huijbregts RP, Brossier NM, Grizzle WE, Mikhail FM, Roth KA, Carroll SL: Transgenic mice overexpressing neuregulin-1 model neurofibroma-malignant peripheral nerve sheath tumor progression and implicate specific chromosomal copy number variations in tumorigenesis. Am J Pathol 2013, 182:646–667
97. Brosius SN, Turk AN, Byer SJ, Brossier NM, Kohli L, Whitmire A, Mikhail FM, Roth KA, Carroll SL: Neuregulin-1 overexpression and Trp53 haploinsufficiency cooperatively promote de novo malignant peripheral nerve sheath tumor pathogenesis. Acta Neuropathol 2014, 127:573–591
98. Ling BC, Wu J, Miller SJ, Monk KR, Shamekh R, Rizvi TA, Decourten-Myers G, Vogel KS, DeClue JE, Ratner N: Role for the epidermal growth factor receptor in neurofibromatosis-related peripheral nerve tumorigenesis. Cancer Cell 2005, 7:65–75
99. Keng VW, Watson AL, Rahrmann EP, Li H, Tschida BR, Moriarity BS, Choi K, Rizvi TA, Collins MH, Wallace MR, Ratner N, Largaespada DA: Conditional inactivation of Pten with EGFR overexpression in Schwann cells models sporadic MPNST. Sarcoma 2012, 2012:620834
100. Rahrmann EP, Moriarity BS, Otto GM, Watson AL, Choi K, Collins MH, Wallace M, Webber BR, Forster CL, Rizzardi AE, Schmechel SC, Ratner N, Largaespada DA: Trp53 haploinsufficiency modifies EGFR-driven peripheral nerve sheath tumorigenesis. Am J Pathol 2014, 184:2082–2098
101. Rahrmann EP, Watson AL, Keng VW, Choi K, Moriarity BS, Beckmann DA, Wolf NK, Sarver A, Collins MH, Moertel CL, Wallace MR, Gel B, Serra E, Ratner N, Largaespada DA: Forward genetic screen for malignant peripheral nerve sheath tumor formation identifies new genes and pathways driving tumorigenesis. Nat Genet 2013, 45:756–766
102. Kloosterman WP, Koster J, Molenaar JJ: Prevalence and clinical implications of chromothripsis in cancer genomes. Curr Opin Oncol 2014, 26:64–72

Current status and recommendations for biomarkers and biobanking in neurofibromatosis

C. Oliver Hanemann, MD, PhD
Jaishri O. Blakeley, MD
Fabio P. Nunes, MD, MMSc
Kent Robertson, MD
Anat Stemmer-Rachamimov, MD
Victor Mautner, MD
Andreas Kurtz, PhD
Michael Ferguson, MD
Brigitte C. Widemann, MD
D. Gareth Evans, MD
Rosalie Ferner, MD
Steven L. Carroll, MD, PhD
Bruce Korf, MD, PhD
Pierre Wolkenstein, MD
Pamela Knight
Scott R. Plotkin, MD, PhD
For the REiNS International Collaboration

Correspondence to Dr. Hanemann: Oliver.Hanemann@plymouth.ac.uk

ABSTRACT

Objective: Clinically validated biomarkers for neurofibromatosis 1 (NF1), neurofibromatosis 2 (NF2), and schwannomatosis (SWN) have not been identified to date. The biomarker working group's goals are to (1) define biomarker needs in NF1, NF2, and SWN; (2) summarize existing data on biomarkers in NF1, NF2, and SWN; (3) outline recommendations for sample collection and biomarker development; and (4) standardize sample collection and methodology protocols where possible to promote comparison between studies by publishing standard operating procedures (SOPs).

Methods: The biomarker group reviewed published data on biomarkers in NF1, NF2, and SWN and on biobanking efforts outside these diseases via literature search, defined the need for biomarkers in NF, and developed recommendations in a series of consensus meetings.

Results: We describe existing biomarkers in NF and report consensus recommendations for SOP and a minimal clinical dataset to accompany samples derived from patients with NF1, NF2, and SWN in decentralized biobanks.

Conclusions: These recommendations are intended to provide clinicians and researchers with a common set of guidelines to collect and store biospecimens and for establishment of biobanks for NF1, NF2, and SWN. *Neurology*® 2016;87 (Suppl 1):S40–S48

GLOSSARY

5-S-CD = 5-S-cysteinyldopa; **ADM** = adrenomedullin; **MIA** = melanoma inhibitory activity; **MPNST** = malignant peripheral nerve sheath tumors; **NF1** = neurofibromatosis 1; **NF2** = neurofibromatosis 2; **PNF** = plexiform neurofibromas; **REiNS** = Response Evaluation in Neurofibromatosis and Schwannomatosis; **sAXL** = soluble growth factor receptor Axl; **SOP** = standard operating procedure; **SWN** = schwannomatosis.

The neurofibromatoses—neurofibromatosis 1 (NF1), neurofibromatosis 2 (NF2), and schwannomatosis (SWN)—are genetically distinct neurocutaneous syndromes that share many features. All 3 conditions demonstrate wide variability in disease manifestations, and are characterized by progressive, lifelong, and potentially life-threatening complications. Standard treatment is limited to surgery for most tumor manifestations. Given the unmet need for nonsurgical therapies, there have been >20 clinical trials performed between 1993 and 2014 for NF1 and NF2 with varying measures of response. Few studies have documented evidence of clinical efficacy for investigational agents.[1] To date, no biomarker-driven trials have been performed in NF.

The Response Evaluation in Neurofibromatosis and Schwannomatosis (REiNS) International Collaboration was created in 2011 to define and develop the most informative, reliable, and meaningful endpoints for clinical trials for NF. The REiNS group is composed of several working groups.[2] The biomarker working group, which includes neurologists, oncologists, geneticists,

Supplemental data at Neurology.org

From Plymouth University (C.O.H.), Peninsula Schools of Medicine and Dentistry, The Institute of Translational and Stratified Medicine, Plymouth, UK; Department of Neurology (J.O.B.), Johns Hopkins University Medical School, Baltimore, MD; Department of Pediatrics (F.P.N.) and Department of Pediatrics, School of Medicine (K.R., M.F.), Indiana University; Tailored Therapeutics (F.P.N.), Eli Lilly and Company, Indianapolis, IN; Department of Pathology (A.S.-R.), Neuro-oncology (S.R.P.), Massachusetts General Hospital, Boston; Neurologische Klinik (V.M.), Uniklinik Eppendorf, Hamburg; Berlin-Brandenburg Center for Regenerative Therapies (A.K.), Charité Universitätsmedizin Berlin, Germany; Seoul National University (A.K.), College of Veterinary Medicine and Research Institute for Veterinary Science, Republic of Korea; NCI (B.C.W.), Pediatric Oncology Branch, Bethesda, MD; Genomic Medicine (D.G.E.), University of Manchester, UK; National Neurofibromatosis Service (R.F.), Department of Neurology, Guy's and St. Thomas' NHS Foundation Trust, London UK; Department of Pathology and Laboratory Medicine (S.L.C.), Medical University of South Carolina, Charleston; and Heflin Center for Genomic Sciences (B.K.), University of Alabama at Birmingham; Dermatology (P.W.), GHU Henri Mondor, Paris, France; Children's Tumor Foundation (P.K.), New York.

REiNS International Collaboration members are listed on the *Neurology*® Web site at Neurology.org.

Go to Neurology.org for full disclosures. Funding information and disclosures deemed relevant by the authors, if any, are provided at the end of the article.

© 2016 American Academy of Neurology

© 2016 American Academy of Neurology. Unauthorized reproduction of this article is prohibited.

pathologists, dermatologists, pediatricians, and basic scientists, has the goals to (1) define biomarker needs in NF1, NF2, and SWN; (2) summarize existing data on biomarkers in NF1, NF2, and SWN; (3) outline initial recommendations for sample collection and biomarker development; and (4) harmonize sample collection and processing protocols where possible to allow for data comparison between studies by publishing standard operating procedures (SOPs).

This article summarizes the progress toward these goals. The biomarker group has concentrated on biomarkers in blood, urine, and tissue. Imaging biomarkers are discussed separately by the REiNS imaging working group.[3]

METHODS The biomarker group first performed a literature search, and reviewed and summarized existing data on biomarkers in NF1, NF2, and SWN. The group then met during a series of meetings in collaboration with the Children's Tumor Foundation (1) to establish SOPs for sample collection of NF tissue specimens that facilitate data comparison between studies and (2) to develop a minimal clinical dataset that would accompany each sample. The working group anticipates that these recommendations will be updated periodically as new information on biomarkers becomes available. Detailed assay protocols will be available on the REiNS Web site (www.reinscollaboration.org).

RESULTS Biomarkers are used for early detection of disease or in disease classification (diagnostic biomarkers), in predicting response or adverse events (predictive biomarkers), in defining optimal drug dose (metabolic/pharmacodynamic biomarkers), or in forecasting progression or recurrence (outcome biomarkers).[4] Previous natural history studies in NF1 and NF2 have clearly demonstrated a high degree of variability in disease phenotype and tumor behavior in these conditions.[5] This variability introduces complexity into the identification of valid biomarkers for NF and schwannomatosis. For example, a biomarker could potentially correlate with the presence of the genetic syndrome (e.g., NF1, NF2, or schwannomatosis), of a specific tumor type (e.g., gastrointestinal stromal tumor in NF1), with a nontumor phenotype of NF (e.g., pain severity in schwannomatosis), with cumulative disease burden (e.g., whole body tumor burden), with disease progression (e.g., growth of plexiform neurofibroma in NF1), or with malignant transformation (e.g., malignant peripheral nerve sheath tumor from plexiform neurofibroma). Given the overlap in many of these phenotypes, validating these biomarkers for individual disease manifestations will require careful phenotyping of patients.

Diagnostic biomarkers in NF. Historically, NF1, NF2, and schwannomatosis have been diagnosed using established clinical criteria. Advances in molecular techniques over the last 2 decades have led to the availability of genetic diagnosis for these conditions.[6,7] The sensitivity of genetic analysis for diagnosis of NF depends on the founder status and the clinical phenotype (segmental vs generalized) but ranges from 30% for sporadic schwannomatosis to >95% for NF1. When a causative genetic alteration in the *NF1*, *NF2*, *SMARCB1*, or *LZTR1* genes is identified, it can be used as diagnostic biomarker for related family members. In clinical practice, this information is used by reproductive endocrinologists for prenatal diagnosis or preimplantation genetic diagnosis and by genetic counselors for presymptomatic diagnosis of family members. However, additional diagnostic biomarkers will undoubtedly be useful to identify patients with specific disease features, such as plexiform neurofibromas or optic gliomas.

Outcome biomarkers in NF. Similarly, there is great variability in clinical outcomes for patients with NF. For example, while optic pathway glioma occurs in about 15% of individuals with NF1, only about 1/3 of these tumors are symptomatic, and less will progress and require active treatment.[8] Optic pathway gliomas will even spontaneously regress without treatment. This variability in outcome highlights the need to develop outcome biomarkers for NF disease manifestations. Outcome biomarkers provide evidence about the patient's disease outcome independent of any specific intervention. A validated outcome biomarker would be valuable to determine the long-term risk for dermal neurofibromas and malignant peripheral nerve sheath tumors in patients with NF1, for risk of complete deafness in patients with NF2, and for risk of severe chronic pain in patients with schwannomatosis.

Predictive biomarkers in NF. Over the last decade, there has been an explosion of clinical trials for NF-related tumors and conditions. The opportunity to study novel agents in NF opens the possibility of developing and incorporating biomarker studies into early clinical trials. To date, clinical trials run through the Neurofibromatosis Clinical Trials Consortium have included studies of pharmacodynamic biomarkers and predictive biomarkers. As drugs with activity against NF become available, these studies will provide valuable information about which patients are likely to require treatment in the future and which are likely to respond to therapy.

Existing data on biomarkers in NF1, NF2, and SWN. During development, biomarkers pass through a series of stages, including early research and development (exploratory biomarker), demonstration and validation (probable biomarker), characterization and qualification (known biomarker), and surrogacy (biomarker can substitute for clinical endpoint). For the neurofibromatoses, all

© 2016 American Academy of Neurology. Unauthorized reproduction of this article is prohibited.

Table 1 Exploratory biomarker studies published for neurofibromatosis 1 (NF1)

Biomarker	Correlate with	NF patients, n	Controls, n	Result	Reference
Diagnostic biomarkers					
MIA	NF1 status	42	22	Greater in NF1 than in unaffected controls	9
	Tumor load			Greater in NF1 with PNF than in NF1 without PNF	
	MPNST			Greater in patients with NF1 with higher tumor burden	
				No difference between patients with NF1 with or without MPNST	
MIA 5-S-CD	NF1 status	25	14	MIA greater in NF1 than in unaffected controls	10
	PNF status			No difference in MIA between patients with NF1 with or without PNF	
	Age			MIA levels correlate with age	
				5-S-CD greater in NF1 than in unaffected controls	
				5-S-CD does not correlate with age	
ADM	MPNST	32	25	Higher ADM levels in NF1 with MPNST than in NF1 with PNF	11
				No difference between patients with NF1 with or without PNF	
				Higher ADM levels in patients with NF1 ± PNF than in controls	
IL-6, IFN-γ, TNF-α, EGFR	NF1 status	104	41	Serum concentrations of IL-6, IFN-γ, and TNF-α were significantly higher in NF1 than in healthy controls	14
	MPNST status			Serum concentrations of EGFR were significantly lower in NF1 than in healthy controls	
IGFBP-1, RANTES	NF1 status	104	41	Serum concentrations of IGFBP-1 and RANTES were significantly higher in patients with NF1 with MPNST than in those without MPNST	14
	MPNST status			Serum IGFBP-1 correlated with internal tumor load	
	Internal tumor load				
Fetal antigen 1	NF1	13	177	Statistically significant difference between median values	12
				Not able to distinguish between groups	
sAXL	NF1 diagnosis, presence of NF1	72	46	Increased in patients with NF1 compared to controls	13
				Increased in patients with NF1 with PNF compared to those without	
RASSF1A methylation	MPNST	20 MPNTS methylated, 12 unmethylated		MPNST with RASSF1 methylated had worse prognosis than unmethylated, $p = 0.014$	15
miR-204	MPNST	12 NF1, 10 NF1 + MPNST		Downregulation of miR-204 downregulated in MPNST	16
Predictive biomarkers					
FOXM1	Survival	38 MPNST		High FOXM1 protein expression was predictor of poor survival for patients with NF1 with MPNST	17
CDK4	Survival	38 MPNST		*CDK4* copy number gain by aCGH was predictor of poor survival for patients with NF1 with MPNST	17
Survivin/TK1, TOP2A	Survival with MPNST	64 NF1 with MPNST		Stratifies MPNST into high and low risk	20

Abbreviations: 5-S-CD = 5-S-cysteinyldopa; aCGH = array comparative genomic hybridization; ADM = adrenomedullin; EGFR = epidermal growth factor receptor; IFN = interferon; IL = interleukin; MIA = melanoma inhibitory activity; miR = microRNA; MPNST = malignant peripheral nerve sheath tumors; PNF = plexiform neurofibromas; sAXL = soluble growth factor receptor Axl; TNF = tumor necrosis factor.

biomarkers published to date are considered exploratory; none has been validated to achieve probable biomarker status. Thus far, all published biomarker studies have been performed in the setting of NF1 (table 1); there are no published data on biomarkers in NF2 or schwannomatosis. These exploratory studies are all limited by a variety of technical issues such as limited statistical power, lack of an independent validation set, and lack of longitudinal data.

Diagnostic biomarkers in NF1.

- Melanoma inhibitory activity (MIA)—In a study of 42 patients with NF1 and 22 healthy controls,[9] MIA serum levels were significantly

© 2016 American Academy of Neurology. Unauthorized reproduction of this article is prohibited.

greater in patients with NF1 (15.2 ng/mL) than in controls (4.5 ng/mL), in patients with NF1 with plexiform neurofibromas (PNF) than in those without PNF, in patients with NF1 with high numbers of cutaneous or subcutaneous neurofibromas than in those without such tumors, and in patients with NF1 with greater internal tumor load than in those with low internal tumor load. In contrast, serum levels of MIA were not significantly different between patients with NF1 with and without malignant peripheral nerve sheath tumors (MPNST). MIA as a biomarker for NF1 was also investigated by another group.[10] This group added the analysis of the metabolite 5-S-cysteinyldopa (5-S-CD). They found concordant results with higher MIA levels in 25 patients with NF1 compared with 14 controls (13.1 vs 9.3 ng/mL) but did not find significantly different levels between patients with NF1 with or without PNF (15.1 vs 12.0 ng/mL, respectively). In their study, serum 5-S-CD levels were significantly higher in patients with NF1 than in controls and did not correlate with age. Hence, MIA does not appear to be a robust biomarker for distinguishing unaffected controls from patients with NF1 or between patients with NF1 with or without MPNST. Further work is needed to explore the utility of 5-S-CD to distinguish between groups.

- Adrenomedullin (ADM)—In a study of 32 patients with NF1 and 25 control patients,[11] serum ADM levels were significantly greater in patients with NF1 with MPNST (0.24 ng/mL, n = 5) than in patients with NF1 with PNF (0.18 ng/mL, n = 17); however, there was significant overlap in ADM levels between the cohorts. ADM levels were also significantly higher in patients with NF1 with or without MPNST (0.18 ng/mL, n = 27) than in controls (0.07 ng/mL, n = 25). No significant differences were noted between patients with NF1 with or without PNF. Although the data for ADM data are more promising than those for MIA, the current data do not indicate that ADM is a reliable biomarker in NF1 and further studies are warranted.
- Fetal antigen 1—In a study of 13 adult patients with NF1 and 177 adult controls,[12] the median fetal antigen 1 levels were significantly higher in the serum of patients with NF1 (30.6 ng/mL) than in control patients (24.9 ng/mL), although there was considerable overlap between the groups.[12]
- Soluble growth factor receptor Axl (sAXL)—In a study of 72 patients with NF1 and 46 healthy controls, serum levels of sAXL were significantly increased in patients with NF1 (23 ng/mL) compared with controls (16 ng/mL). Patients with plexiform neurofibromas had significantly higher levels of sAXL (26 ng/mL, n = 36) than patients with NF1 without plexiform neurofibromas (18 ng/mL, n = 36) although there was still some overlap between groups.[13]
- Systematic screen of multiple serum biomarkers[14]—The authors evaluated 104 patients with NF1 and 41 healthy controls and proposed 4 candidate biomarkers that were statistically significantly different in patients with NF1 vs unaffected individuals (interleukin-6, interferon-γ, epidermal growth factor receptor, tumor necrosis factor–α) and 2 biomarker candidates that were statistically significantly different in patients with NF1 with and without MPNST (insulin-like growth factor binding protein 1 and RANTES).
- Danielsen et al.[15] analyzed the promoter methylation of *RASSF1A* in primary tumor. The authors reported significantly different survival data for 32 patients with methylated or unmethylated *RASSF1A* at 5 years.
- MiRNA studies in NF1 and non-NF1 MPNSTs have been performed using cell lines and tissues. This study identified the downregulation of miR-204 as a novel diagnostic biomarker and potential therapeutic target for patients with NF1 with MPNSTs.[16]

All the above-mentioned studies were aimed at identifying diagnostic biomarkers.

Predictive and pharmacodynamic biomarkers.

- Candidate gene alterations in tumor specimens—Using high-resolution array-based comparative genomic hybridization in 38 MPNSTs (23 with NF1 and 15 without NF1), the authors identified candidate gene alterations that were then validated at the DNA, RNA, and protein levels.[17] Candidate genes in regions of copy number gain and associated (predicted) with poor survival included *SOX5*, *NOL1*, *MLF2*, *FOXM1*, *FKBP1*, *CDK4*, *TSPAN31*, *ERBB2*, *MYC*, and *TP53.* In multivariate analysis, FOXM1 protein expression and *CDK4* copy number gain were the most significant independent genomic biomarkers for poor survival in patients with MPNSTs.
- Aurora kinase A, which is important in mitotic spindle assembly and nonmitotic related cell differentiation, is a potential therapeutic target in MPNSTs. Recent studies in primary MPNSTs have demonstrated that pharmacologic aurora kinase inhibition results in MPNST cells

© 2016 American Academy of Neurology. Unauthorized reproduction of this article is prohibited.

Neurology 87 (Suppl 1) August 16, 2016

© 2016 American Academy of Neurology. Unauthorized reproduction of this article is prohibited.

Table 2 Recommended minimal clinical dataset

Demographics						
Date:						
Sex	☐ male	☐ female				
Birth	☐ month	☐ year				
Diagnosis of NF1, NF2, or schwannomatosis	☐ infancy	☐ childhood	☐ adolescence	☐ adulthood	☐ unknown	
Inheritance	☐ parent affected	☐ parent not affected	☐ unknown			
Mosaicism	☐ patient is mosaic	☐ patient not mosaic	☐ unknown			
Germline mutation	☐ not tested	☐ tested + unknown	☐ determined: (specify __)			
Clinical status						
Status	☐ alive	☐ deceased				
WHO performance status	☐ 0	☐ 1	☐ 2	☐ 3	☐ 4	
Pain	☐ not a problem	☐ occasional	☐ disabling			
Treatment directed at tumor	☐ no specific therapy	☐ chemotherapy	☐ surgery	☐ radiation	☐ targeted therapy (specify)	☐ clinical trial (specify)
NF1						
≥6 Café-au-lait macules	☐ absent	☐ present	☐ unknown			
Skin fold freckling	☐ absent	☐ present	☐ unknown			
Iris Lisch nodules	☐ absent	☐ present	☐ unknown			
Dermal neurofibromas	☐ absent	☐ scattered	☐ dense	☐ unknown		
Subcutaneous nodular neurofibromas	☐ absent	☐ scattered	☐ dense	☐ unknown		
Diffuse dermal neurofibromas	☐ absent	☐ scattered	☐ dense	☐ unknown		
Spinal neurofibromas	☐ not imaged	☐ absent	☐ 1–3 levels	☐ all levels (cervical, thoracic, lumbar, sacral)	☐ unknown	
Plexiform neurofibromas	☐ present	☐ absent by MRI	☐ absent clinically, but no MRI	☐ unknown		
Optic glioma	☐ unknown	☐ absent	☐ present, asymptomatic	☐ present, symptomatic, not treated	☐ present, symptomatic, treated	
Heart defect	☐ unknown	☐ absent	☐ present (specify)			
Vascular disease	☐ unknown	☐ absent	☐ present (specify)			
Puberty onset	☐ prepubertal	☐ precocious	☐ normal	☐ late	☐ unknown	
Stature	☐ <5th centile	☐ 5th–95th centile	☐ >95th centile	☐ unknown		
Peripheral neuropathy	☐ unknown	☐ absent	☐ present			
Aqueductal stenosis	☐ unknown	☐ absent	☐ present			
Long bone dysplasia	☐ unknown	☐ absent	☐ present			
Sphenoid dysplasia	☐ unknown	☐ absent	☐ present			
Scoliosis	☐ unknown	☐ absent	☐ present			
Intellectual disability	☐ unknown	☐ absent	☐ present			

Continued

Table 2 Continued

NF1					
Learning disability	☐ unknown	☐ absent	☐ present		
Attention deficit disorder	☐ unknown	☐ absent	☐ present		
Pheochromocytoma	☐ unknown	☐ absent	☐ present		
Glomus tumor	☐ unknown	☐ absent	☐ present		
MPNST	☐ unknown	☐ absent	☐ present		
Glioma (not optic glioma)	☐ unknown	☐ absent	☐ present		
GIST	☐ unknown	☐ absent	☐ present		
Leukemia	☐ unknown	☐ absent	☐ present		
Breast cancer	☐ unknown	☐ absent	☐ present		
Other tumors	☐ unknown	☐ absent	☐ present (specify ___)		
NF2					
Vestibular schwannoma	☐ MRI not done	☐ absent by MRI	☐ unilateral	☐ bilateral	☐ unknown
Meningioma	☐ MRI not done	☐ absent by MRI	☐ single	☐ multiple	☐ unknown
Glioma/ependymoma	☐ MRI not done	☐ absent by MRI	☐ present	☐ unknown	
Spinal schwannoma	☐ MRI not done	☐ absent by MRI	☐ single	☐ multiple	☐ unknown
Dermal schwannoma	☐ unknown	☐ absent	☐ present		
Nonvestibular cranial schwannoma	☐ MRI not done	☐ absent by MRI	☐ present (specify)	☐ unknown	
Lenticular opacity	☐ unknown	☐ absent	☐ present		
Schwannomatosis					
Schwannomas (nonvestibular)	☐ only by imaging evidence	☐ 1 pathologically confirmed	☐ 2 or more, at least 1 pathologically confirmed	☐ unknown	
Number of schwannomas	☐ single	☐ scattered	☐ dense	☐ unknown	
Vestibular schwannomas	☐ not imaged	☐ absent by imaging	☐ unilateral	☐ bilateral	☐ unknown
Meningiomas	☐ not imaged	☐ absent by imaging	☐ single	☐ multiple	☐ unknown
Other schwannomatosis-related tumors (please specify)	☐ not investigated	☐ absent	☐ present	☐ unknown	

Abbreviations: GIST = gastrointestinal stromal tumors; MPNST = malignant peripheral nerve sheath tumors; NF1 = neurofibromatosis 1; NF2 = neurofibromatosis 2.

© 2016 American Academy of Neurology. Unauthorized reproduction of this article is prohibited.

exiting the cell cycle with cessation of growth.[18] The copy number and expression of the gene product *HMMR* was found to be a functional marker of responsiveness to aurora kinase inhibition. A variety of less well-defined and reproducible prognosticators are summarized in a review by Farid et al.[19]

- Recently, gene expression analysis of 30 MPNSTs and subsequent immunohistochemical staining of 64 MPNSTs revealed a composite set of survivin (BIRC5), thymidine kinase 1 (TK1), and topoisomerase 2-α (TOP2A) immunohistochemical staining, which stratifies MPNST into high and low risk[20] independent of age, sex, tumor size, grade, NF1 status, and surgical remission.
- Blakeley et al.[21] have detected lower blood circulating levels of hepatocyte growth factor in patients with NF2 who responded to bevacizumab. This is the first evidence that a blood biomarker could be used predictively to stratify patients with NF2 (n = 13) with the highest likelihood of treatment benefit.

RECOMMENDATIONS FOR SAMPLE COLLECTION AND METHODOLOGY The REiNS biomarker group discussed potential barriers to biomarker research for NF. These barriers include the low prevalence of NF1, NF2, and schwannomatosis, which makes coordinated studies technically difficult and expensive; the extreme variability of these conditions requires expert clinical researchers to accurately phenotype patients. Based on this discussion, the group endorsed the following goals to advance the study of biomarkers within the NF community:

1. Build a prospective biorepository of curated samples. The aim would be to collect longitudinal samples from each patient to facilitate the development of early detection and prognostic markers.
2. Standardize tissue collection at participating institutions. The aim would be to collect all tissues using an identical protocol that meets standards set forth by the American Association for Cancer Research–Food and Drug Administration–National Cancer Institute Cancer Biomarker Collaborative[4] and would be linked via a shared, anonymized registry (on a Web site). Participating sites would share common consent, SOPs, quality control (see supplemental data on the *Neurology*® Web site at Neurology.org), minimal clinical dataset, and database.
3. Annotate samples with an agreed minimal clinical dataset. The goal is to link anonymously the phenotypic data to deidentified samples in the biorepository. A proposed minimal clinical dataset developed at a consensus meeting in October 2014 is shown in table 2. The group anticipates that modifications of this dataset may be required in the future to optimize the utility of biomarker research.
4. Incorporate the decentralized biorepository into existing biorepositories that are used for diagnostic purposes. The biomaterial could thus be used for both diagnosis and research and is not necessarily restricted to an upfront definition of the amount of surplus tissue. Patient care takes preference when allocating the amount of samples used for biomarker investigations.
5. Provide open access to deposited biomarkers to facilitate research. The aim would be to have samples and data open to all qualified researchers with approval of an institutional review board. A biorepository council would govern database requests.
6. An operational and an executive committee will govern requests and audit implementation of SOPs and quality control measures.
7. Incorporate biomarker collection into clinical studies. When feasible, sample collection should be incorporated into prospective clinical trials and natural history studies to help develop pharmacodynamic and predictive biomarkers.
8. Incorporate biomarker collection into routine clinical visits. Patients receiving routine care should be invited to participate in prospective sample collection during routine clinic visits.

RECOMMENDATIONS FOR BIOMARKERS BASED ON EXISTING DATA

1. Validate individual biomarkers as well as cocktails/signatures of biomarkers.
2. For ongoing and planned NF trials, studies of drug metabolism/pharmacodynamic biomarkers should be drug-specific.
3. For malignant tumors such as MPNST, explore and validate cDNA, cRNA, and circulating tumor cells as biomarkers.
4. Validate use of extracellular vesicles (exosomes) based on encouraging preliminary data as biomarkers of cancer.[22]
5. Using candidate approach, focus on the clinically relevant questions, i.e., total tumor load, presence of plexiform neurofibroma, evidence of malignant transformation, and taking into account the statistical significance in published studies. We recommend validating the following biomarker candidates in patients with NF1: BIRC5/TK1/TOP2A immunohistochemistry, ADM, interferon-γ, IGFBP-1, and sAXL.
6. Complement candidate biomarker approach with systematic unbiased approach. Encourage well-powered studies using systematic unbiased approaches, including genomics (DNA, RNA, miRNA next-generation sequencing), metabolomics, and proteomics; that is, further screening with metabolomics, proteomics, expression arrays, and miRNA.

© 2016 American Academy of Neurology. Unauthorized reproduction of this article is prohibited.

AUTHOR CONTRIBUTIONS

C.O. Hanemann: drafting the manuscript, study concept, interpretation of data, development of recommendations and SOPs. Jaishri Blakeley: study concept, review of manuscript, interpretation of data. Fabio Nunes: study concept, review of the manuscript, development of recommendations, development of SOPs. Kent Robertson: study concept, review of manuscript, development of SOPs. Anat Stemmer-Rachamimov: study concept, review of manuscript, development of SOPs. Victor Mautner: study concept, review of manuscript. Andreas Kurtz: study concept, review of manuscript, development of SOPs. Michael Ferguson: study concept, review of manuscript, development of SOPs. Brigitte C. Widemann: study concept, review of manuscript. Gareth Evans: study concept, review of manuscript. Rosalie Ferner: review of manuscript, interpretation of data. Steven L. Carroll: drafting of manuscript, development of autopsy, surgical pathology, and blood biobanking protocols. Bruce Korf: interpretation of data, reviewing manuscript, drafting minimal clinical dataset. Pierre Wolkenstein: review of manuscript. Pam Knight: study concept, review of manuscript. Scott Plotkin: study concept, drafting of manuscript, review of manuscript.

ACKNOWLEDGMENT

The authors thank Children's Tumor Foundation (CTF) for support and Xandra O. Breakefield, Massachusetts General Hospital, for advising on the manuscript.

STUDY FUNDING

No targeted funding reported.

DISCLOSURE

O. Hanemann receives support from Dr. Hadwen Trust and Brain Tumour Research. J. Blakeley has received research support from GlaxoSmithKline, Sanofi-Aventis, and Lily Pharmaceuticals. She has consulted for Abbvie. F. Nunes receives support from Eli Lilly and Company. K. Robertson receives research support from Novartis, NIH, Department of Defense, and Leukemia Lymphoma Society Translational Research Program, and serves on a medical advisory board for General BioTechnology—Cook Biomedical. A. Stemmer-Rachamimov receives support from Children's Tumor Foundation, Dana Farber Cancer Institute, and NIH, and serves on the editorial board of *Journal of Clinical Pathology*. V. Mautner reports no disclosures relevant to the manuscript. A. Kurtz receives support from Seoul National University, College of Veterinary Medicine, Novartis, and Nolitolib, and serves on the editorial board of *International Journal of Stem Cells*. M. Ferguson serves as an assistant professor with Indiana University. B. Widemann receives research support through NCI CCR Intramural Research Program. G. Evans received support from AstraZeneca and has served on the board of *Familial Cancer Journal*. R. Ferner receives funds from the Children's Tumor Foundation, European Neurofibromatosis Association, and Springer Publishing Group. S. Carrol received funding from the Department of Defense, NIH/National Cancer Institute, NIH/NINDS, and Children's Tumor Foundation. He serves on the editorial boards of *Journal of Neuropathology and Experimental Neurology*, *Neuro-Oncology*, *The American Journal of Pathology*, and *Brain Research Bulletin*. B. Korf receives funding from NIH, Department of Defense, Children's Tumor Foundation, Tuberous Sclerosis Alliance, and March of Dimes. He serves on the board of Novartis, Accolade, and Children's Tumor Foundation Medical Advisory Committee, and advises for the Neurofibromatosis Therapeutic Acceleration Project. He has served as editor for *Current Protocols in Human Genetics* and *Annual Reviews of Genetics and Genomics*. He has received funding from the American College of Medical Genetics and Genomics, American Academy of Pediatrics, Cambridge HealthTech Institute, Illumina, and Sequenome. He has received publishing royalties from Wiley Blackwell and Elsevier. P. Wolkenstrein serves on the advisory board of Abbvie and Pierre Fabre Dermatologie and consults for Laboratoire d' Uriage and Laboratoire Expansciences. He receives research support from Novartis and the French Government (PHRC 2010). P. Knight reports no disclosures relevant to the manuscript. S. Plotkin receives research support from Children's Tumor Foundation, NIH, and the Department of Defense Neurofibromatosis Clinical Trials Consortium. Go to Neurology.org for full disclosures.

Received November 17, 2015. Accepted in final form March 30, 2016.

REFERENCES

1. Plotkin SR, Stemmer-Rachamimov AO, Barker FG, et al. Hearing improvement after bevacizumab in patients with neurofibromatosis type 2. N Engl J Med 2009;361:358–367.
2. Plotkin SR, Blakeley JO, Dombi E, et al. Achieving consensus for clinical trials: the REiNS International Collaboration. Neurology 2013;81:S1–S5.
3. Dombi E, Ardern-Holmes SL, Babovic-Vuksanovic D, et al. Recommendations for imaging tumor response in neurofibromatosis clinical trials. Neurology 2013;81:S33–S40.
4. Khleif SN, Doroshow JH, Hait WN; AACR-FDA-NCI Cancer Biomarkers Collaborative. AACR-FDA-NCI Cancer Biomarkers Collaborative consensus report: advancing the use of biomarkers in cancer drug development. Clin Cancer Res 2010;16:3299–3318.
5. Ferner RE. Neurofibromatosis 1 and neurofibromatosis 2: a twenty first century perspective. Lancet Neurol 2007;6:340–351.
6. Lloyd SK, Evans DG. Neurofibromatosis type 2 (NF2): diagnosis and management. Handb Clin Neurol 2013;115:957–967.
7. Ferner RE, Huson SM, Thomas N, et al. Guidelines for the diagnosis and management of individuals with neurofibromatosis 1. J Med Genet 2007;44:81–88.
8. Listernick R, Ferner RE, Liu GT, Gutmann DH. Optic pathway gliomas in neurofibromatosis-1: controversies and recommendations. Ann Neurol 2007;61:189–198.
9. Kolanczyk M, Mautner V, Kossler N, et al. MIA is a potential biomarker for tumour load in neurofibromatosis type 1. BMC Med 2011;9:82.
10. Yoshida Y, Furumura M, Tahira M, Horie T, Yamamoto O. Serum biomarker in neurofibromatosis type 1. J Dermatol Sci 2012;67:155–158.
11. Hummel TR, Jessen WJ, Miller SJ, et al. Gene expression analysis identifies potential biomarkers of neurofibromatosis type 1 including adrenomedullin. Clin Cancer Res 2010;16:5048–5057.
12. Jensen CH, Schroder HD, Teisner B, Laursen I, Brandrup F, Rasmussen HB. Fetal antigen 1, a member of the epidermal growth factor superfamily, in neurofibromas and serum from patients with neurofibromatosis type 1. Br J Dermatol 1999;140:1054–1059.
13. Johansson G, Peng PC, Huang PY, et al. Soluble AXL: a possible circulating biomarker for neurofibromatosis type 1 related tumor burden. PLoS One 2014;9:e115916.
14. Park SJ, Sawitzki B, Kluwe L, Mautner VF, Holtkamp N, Kurtz A. Serum biomarkers for neurofibromatosis type 1 and early detection of malignant peripheral nerve-sheath tumors. BMC Med 2013;11:109.
15. Danielsen SA, Lind GE, Kolberg M, et al. Methylated RASSF1A in malignant peripheral nerve sheath tumors identifies neurofibromatosis type 1 patients with inferior prognosis. Neuro Oncol 2015;17:63–69.
16. Gong M, Ma J, Li M, Zhou M, Hock JM, Yu X. MicroRNA-204 critically regulates carcinogenesis in malignant peripheral nerve sheath tumors. Neuro Oncol 2012;14:1007–1017.
17. Yu J, Deshmukh H, Payton JE, et al. Array-based comparative genomic hybridization identifies CDK4 and FOXM1 alterations as independent predictors of survival in malignant peripheral nerve sheath tumor. Clin Cancer Res 2011;17:1924–1934.

© 2016 American Academy of Neurology. Unauthorized reproduction of this article is prohibited.

18. Mohan P, Castellsague J, Jiang J, et al. Genomic imbalance of HMMR/RHAMM regulates the sensitivity and response of malignant peripheral nerve sheath tumour cells to aurora kinase inhibition. Oncotarget 2013;4:80–93.
19. Farid M, Demicco EG, Garcia R, et al. Malignant peripheral nerve sheath tumors. Oncologist 2014;19:193–201.
20. Kolberg M, Holand M, Lind GE, et al. Protein expression of BIRC5, TK1, and TOP2A in malignant peripheral nerve sheath tumours: a prognostic test after surgical resection. Mol Oncol 2015;9:1129–1139.
21. Blakeley JO, Ye X, Duda DG, et al. Efficacy and biomarker study of bevacizumab for hearing loss resulting from neurofibromatosis type 2-associated vestibular schwannomas. J Clin Oncol 2016;34:1669–1675.
22. Kros JM, Mustafa DM, Dekker LJ, Sillevis Smitt PA, Luider TM, Zheng PP. Circulating glioma biomarkers. Neuro Oncol 2015;17:343–360.

© 2016 American Academy of Neurology. Unauthorized reproduction of this article is prohibited.

Neurology®

Current status and recommendations for biomarkers and biobanking in neurofibromatosis

C. Oliver Hanemann, Jaishri O. Blakeley, Fabio P. Nunes, et al.

Neurology 2016;87;S40-S48
DOI 10.1212/WNL.0000000000002932

This information is current as of August 15, 2016

Updated Information & Services	including high resolution figures, can be found at: http://www.neurology.org/content/87/7_Supplement_1/S40.full.html
Supplementary Material	Supplementary material can be found at: http://www.neurology.org/content/suppl/2016/08/15/WNL.0000000000002932.DC1.html http://www.neurology.org/content/suppl/2016/08/15/WNL.0000000000002932.DC2.html
References	This article cites 22 articles, 9 of which you can access for free at: http://www.neurology.org/content/87/7_Supplement_1/S40.full.html##ref-list-1
Subspecialty Collections	This article, along with others on similar topics, appears in the following collection(s): **Neurofibromatosis** http://www.neurology.org//cgi/collection/neurofibromatosis
Permissions & Licensing	Information about reproducing this article in parts (figures,tables) or in its entirety can be found online at: http://www.neurology.org/misc/about.xhtml#permissions
Reprints	Information about ordering reprints can be found online: http://www.neurology.org/misc/addir.xhtml#reprintsus

Neurology ® is the official journal of the American Academy of Neurology. Published continuously since 1951, it is now a weekly with 48 issues per year. Copyright © 2016 American Academy of Neurology. All rights reserved. Print ISSN: 0028-3878. Online ISSN: 1526-632X.

AMERICAN ACADEMY OF NEUROLOGY®

Signal Transduction

Molecular Cancer Research

STAT1 and NF-κB Inhibitors Diminish Basal Interferon-Stimulated Gene Expression and Improve the Productive Infection of Oncolytic HSV in MPNST Cells

Joshua D. Jackson[1], James M. Markert[1,2,3], Li Li[1], Steven L. Carroll[4], and Kevin A. Cassady[2,5]

Abstract

Interferon-stimulated genes (ISG) encode diverse proteins that mediate intrinsic antiviral resistance in infected cells. Here it was hypothesized that malignant peripheral nerve sheath tumor (MPNST) cells resist the productive infection of oncolytic herpes simplex virus (oHSV) through activation of the JAK/STAT1 pathway and resultant upregulation of ISGs. Multiple human and mouse MPNST cells were used to explore the relationship between STAT1 activation and the productive infection of $\Delta\gamma_1 34.5$ oHSVs. STAT1 activation in response to oHSV infection was found to associate with diminished $\Delta\gamma_1 34.5$ oHSVs replication and spread. Multiday pretreatment, but not cotreatment, with a JAK inhibitor significantly improved viral titer and spread. ISG expression was found to be elevated prior to infection and downregulated when treated with the inhibitor, suggesting that the JAK/STAT1 pathway is active prior to infection. Conversely, upregulation of ISG expression in normally permissive cells significantly decreased oHSV productivity. Finally, a possible link between NF-κB pathway activation and ISG expression was established through the expression of inhibitor of kB (IκB) which decreased basal STAT1 transcription and ISG expression. These results demonstrate that basal ISG expression prior to infection contributes to the resistance of $\Delta\gamma_1 34.5$ oHSVs in MPNST cells.

Implications: Although cancer-associated ISG expression has been previously reported to impart resistance to chemotherapy and radiotherapy, these data show that basal ISG expression also contributes to oncolytic HSV resistance. *Mol Cancer Res; 14(5); 482–92. ©2016 AACR.*

Introduction

Malignant peripheral nerve sheath tumors (MPNST) are a highly aggressive cancer of the peripheral nervous system derived from cells of the Schwann cell lineage. Patients have a median survival of 26 months following diagnosis (1). Beyond advances in surgical resection, further treatment with chemotherapy and radiation has not demonstrated an overall benefit to survival (2, 3). A promising alternative approach is the use of conditional replicating oncolytic herpes simplex viruses type 1 (oHSV) to treat MPNSTs. These oHSVs have been safely used in clinical trials in a number of cancer types, however, the tumor response has varied and we anticipate this would be true for patients with MPNSTs. We have previously demonstrated that MPNST cell lines exhibit variable oHSV susceptibility (4), and we have sought to understand the potential mechanisms of resistance that are detrimental to oHSV therapy.

Tumor resistance to oHSV has been attributed to oncogenic signaling cascade changes, namely, Ras-mediated suppression of protein kinase R (PKR) in the infected cells (5). PKR is a host antiviral kinase that limits $\gamma_1 34.5$ deleted oHSV late-gene expression and replication (6). In brief, HSV produces double-stranded RNA during viral gene expression which induces PKR dimerization, autophosphorylation, and activation. Activated PKR phosphorylates eukaryotic initiation factor α (eIF2α), leading to translational arrest in the infected cell. Wild-type HSV counters translational arrest by expressing the neurovirulence gene $\gamma_1 34.5$ which encodes a multifunctional viral protein, infected cell protein 34.5 (ICP34.5). ICP34.5 recruits a host phosphatase, protein phosphatase 1 alpha (PP1α), to dephosphorylate eIF2α thus restoring protein translation in the infected cell. Though wild-type HSV causes lethal encephalitis in the central nervous system (CNS), deletion of one or both copies of the diploid $\gamma_1 34.5$ gene attenuates neurogenic virulence. It is believed that malignant cells partially complement the loss of $\gamma_1 34.5$ through oncogenic processes such as Ras-induced suppression of PKR.

In addition to PKR, cells express a diverse set of pattern recognition receptors (PRR) that detect pathogen-associated molecular patterns such as viral nucleic acids. Stimulation of

[1]Department of Neurosurgery, University of Alabama at Birmingham, Birmingham, Alabama. [2]Department of Pediatrics, University of Alabama at Birmingham, Birmingham, Alabama. [3]Department of Cell, Developmental and Integrative Biology, University of Alabama at Birmingham, Birmingham, Alabama. [4]Department of Pathology and Laboratory Medicine, Medical University of South Carolina, Charleston, South Carolina. [5]Nationwide Children's Hospital and The Ohio State University, Columbus, Ohio.

Note: Supplementary data for this article are available at Molecular Cancer Research Online (http://mcr.aacrjournals.org/).

Corresponding Author: Kevin A. Cassady, Nationwide Children's Hospital and The Ohio State University, 700 Children's Drive, Columbus, OH 43205. Phone: 614-722-2798; Fax: 614-722-2798; E-mail: Kevin.Cassady@Nationwidechildrens.org

doi: 10.1158/1541-7786.MCR-15-0427

©2016 American Association for Cancer Research.

AACR

certain PRRs including DEAD (Asp-Glu-Ala-Asp) box polypeptide 58 (DDX58; commonly known as retinoic acid-inducible gene I; RIG-I), interferon induced with helicase C domain 1 (IFIH1; commonly known as melanoma differentiation antigen 5; MDA5), transmembrane protein 173 (TMEM173; commonly known as stimulator of interferon genes; STING), and members of the Toll-like receptor family ultimately lead to the activation of transcription factors which promote expression of the type I IFNs IFNα and IFNβ which are potent antiviral cytokines. Secreted type I IFN interacts with transmembrane IFNα receptors (IFNAR) in an autocrine and paracrine manner leading to the activation of the intracellular Janus kinases JAK1 and TYK2. Activation of JAK1 and TYK2 leads to phosphorylation of signal transducer and activator of transcription 1 (STAT1) and STAT2, which together with interferon regulatory factor 9 (IRF9) form the heterotrimeric transcription factor interferon-stimulated gene factor 3 (ISGF3). The ISGF3 complex localizes to the nucleus where it promotes transcription of several hundred interferon-stimulated genes (ISG) that contain interferon-stimulated response elements (ISRE) in their promoter regions. ISGs have diverse functions, modulating viral and cellular functions to promote intrinsic antiviral resistance. ISGs can directly inhibit mechanisms unique to certain viruses (e.g., myxovirus resistance 1, MX1), inhibit cellular processes involving transcription and translation (e.g., PKR; and 2′-5′-oligoadenylate synthetase 1, OAS1), or increased expression of PRRs and IFN/STAT1 signaling modulators to promote amplification of the antiviral response (e.g., RIG-I; MDA5; interferon-induced protein with tetratricopeptide repeats 3, IFIT3).

The research presented here tests the hypothesis that ISG upregulation contributes to oHSV resistance in a subset of MPNST tumor lines. Our results show that: (i) PKR activation is not specifically associated with oHSV-resistant phenotypes; (ii) STAT1 activation is observed in 10 of 21 MPNST cell lines and is statistically associated with diminished productivity of both a first generation $\Delta\gamma_1$34.5 oHSV and a second generation $\Delta\gamma_1$34.5 oHSV, C134, capable of evading PKR-mediated translational arrest; (iii) resistant MPNST cell lines exhibit greater ISG expression than oHSV-sensitive lines prior to oHSV infection suggesting they are primed toward an antiviral state; (iv) pretreatment of resistant MPNST tumor lines with a small-molecule JAK inhibitor reduces basal ISG expression and improves viral replication and spread; (v) conversely, either IFN stimulation or stable ISGF3 overexpression in MPNST cell lines increased ISG expression leading to decreased oHSV productivity; and finally (vi) we have provided evidence that basal expression of ISGs may be dependent on the NF-κB signaling network.

Materials and Methods

Cell lines and viruses

Human MPNST cell lines or their firefly luciferase–expressing derivatives (-luc; ref. 4) as well as MPNSTs lines derived from a genetically engineered mouse model (7) have been previously described. All MPNST cell lines were maintained in growth media containing DMEM with 10% FBS and 10 mmol/L L-glutamine (Sigma-Aldrich). The African green monkey kidney cell line Vero was obtained from the ATCC and maintained in minimum essential medium with 5% bovine growth serum. All viruses except M201 have been described previously (4, 8) and are summarized in Supplementary Table S1. M201 is an oHSV with CMVp–GFP inserted between UL3 and UL4, and murine IL12 inserted in $\gamma_1$34.5 locus and was constructed using homologous recombination with M002 (mIL-12 virus) viral DNA (8) and pCK1029 plasmid DNA using a method described previously (6). Sequential plaque purification was performed using Vero cells using eGFP expression and candidate viruses were verified by southern blot analysis (data not shown).

Reagents

The small-molecule inhibitors ruxolitinib and TPCA-1 (Selleckchem) were stored as 10 mmol/L aliquots in DMSO (Sigma-Aldrich). Primary antibodies were obtained as follows: p-T446-PKR (3076), p-S51-eIF2α (3398), eIF2α (2103), p-Y701-STAT1 (9167), STAT1 (9172), MDA5 (5321), RIG-I (3743), p-S536–NF-κB/P65 (3033), NF-κB/P65 (3987) IκB (4814), p-MEK1/2 (2338), MEK1/2 (4694), p-ERK1/2 (4376), and ERK1/2 (9102) from Cell Signaling Technology; MX1 (13750), OAS1 (14955), IFIT3 (15201), STAT2 (16674), and IRF9 (14167) from Proteintech; HSV ICP4 (H1A021, Virusys Corporation), PKR (sc707, Santa Cruz Biotechnology), and β-actin (A2228, Sigma-Aldrich). Horseradish peroxidase–conjugated goat anti-mouse (Immunopore) and goat anti-rabbit antibodies were used as secondary antibodies.

Viral productivity assays

Viral recovery (replication) assays have been described previously (4) with the following modifications: virus inoculation was performed in 150 μL regular growth media (10% FBS) for 1 hour followed by addition of growth media up to 1 mL per well in 24-well plates. Viral spread assays have been described previously (4). In brief, cells were seeded 1.5×10^5 per well in 24-well plates and infected at an multiplicity of infection (MOI) of 0.1 with GFP-expressing viruses or mock infected (media alone). After 48 hours, we performed flow cytometry to assess the percentage of cells positive for viral GFP. Flow Cytometry Absolute Count Standard fluorescent beads (Bangs Laboratories) were added to the final suspension of cells to calculate the ratio of cells surviving infection compared with mock-infected samples. All samples were collected in triplicate and the means reported.

Lentivirus construction and transduction

Cloning methods and construction of lentivector plasmids are provided as supplemental information. Lentivirus production has been described previously (4). Stable cell lines were produced via lentiviral transduction of the target cell lines. Hygromycin (Sigma-Aldrich) selection (300 μg/mL) was applied not earlier than 48 hours after transduction.

Western blotting

Cellular lysates were collected on ice in RIPA buffer (10 mmol/L Tris-Cl pH 8.0, 1 mmol/L EDTA, 1% Triton X100, 0.1% sodium deoxycholate, 0.1% SDS, 140 mmol/L NaCl) with protease inhibitor cocktail (Roche) and diluted in 4x sample buffer (240 mmol/L Tris-Cl pH 6.8, 40% glycerol, 4% SDS, 20% β-mercaptoethanol, 0.04% bromophenol blue). Samples were denatured at 98°C for 5 minutes, chilled on ice, separated by PAGE, and transferred to a nitrocellulose membrane (Thermo Fisher Scientific) and blocked for 1 hour at room temperature with 5%

dry milk (S.T. Jerrell Company) or BSA (Thermo Fisher Scientific). Membranes were incubated overnight at 4°C with primary antibody diluted in TBS with 0.1% Tween-20 (TBST). Membranes were repeatedly washed with TBST, incubated for 1 hour with secondary antibody diluted in TBST (1:20,000) at room temperature, and subsequently washed with TBST. Membranes were wetted with SuperSignal West Pico Chemiluminescent Substrate (Thermo Fisher Scientific) and exposed to X-ray film (Research Products International).

Luciferase assays

The STS26T-luc and ST8814-luc cell lines used in reporter assays have been previously transduced with firefly luciferase under a constitutive cytomegalovirus (CMV) promoter. These cell lines were transduced via lentivirus with a nanoluciferase reporter (with a C-terminal PEST sequence; Promega) under the control of either ISRE or NF-κB promoters. Luminescence assays were performed in opaque 96-well plates with the Nano-Glo Dual Luciferase Reporter Assay (Promega) according to the manufacturer's instructions. Luminescence was measured using a FLUOStar Optima (BMG LABTECH) plate reader. Nanoluciferase activity was normalized to that of firefly luciferase and reported as arbitrary units. Data were collected in triplicate or quadruplicate.

Statistical analysis

Statistical analysis was performed using Prism 5 (GraphPad Software). One-tailed Mann–Whitney *U* test was used for analysis involving multiple cell lines. Student *t* test was used for inhibitor and transduction experiments within individual cell lines. For all analyses, the cutoff for statistical significance was set at $P < 0.05$. The following notation was used: ns, $P > 0.05$; *, $P \leq 0.05$; **, $P \leq 0.01$; ***, $P \leq 0.001$.

Results

PKR activation in response to oHSV infection

To assess the contribution of antiviral signaling pathways to oHSV resistance in MPNSTs, we assessed PKR activation and eIF2α phosphorylation in response to a $\Delta\gamma_1$34.5 oHSV (R3616, kindly provided by Dr. Bernard Roizman, University of Chicago, Chicago, IL). The relevant characteristics of R3616 and other viruses used in the following experiments are provided in Supplementary Table S1. We first determined the susceptibility of 8 human and 13 mouse MPNST cell lines by viral recovery assay 24 hours after cells were infected at a MOI of 1. Titers of recovered virus ranged from 7.9×10^3 to 4.1×10^5 plaque-forming units (PFU) for human cell lines and 1.5×10^3 to 2.0×10^5 PFU for mouse lines (Fig. 1A and B). Although mouse lines yielded 3-fold lower average titers of virus than human-derived lines (3.2×10^4 and 9.5×10^5 PFU, respectively), the distributions of human and mouse lines were statistically indistinguishable (Supplementary Fig. S1). Immunoblots against phosphorylated PKR (p-PKR) and p-eIF2α in human cell lines, or p-eIF2α in mouse cell lines, revealed PKR activation and eIF2α phosphorylation following R3616 infection (Fig. 1C and D) at 12 hours postinfection in nearly all cell lines tested. There was no apparent difference in p-PKR/p-eIF2α between cell lines with high or low viral recovery. We conclude that activation of PKR is not sufficient to exclusively define the resistant phenotypes observed in MPNST cell lines.

Activation of STAT1 in response to oHSV infection and association with viral productivity

Because deletion of the HSV $\gamma_1$34.5 gene increases HSV-1 sensitivity to type I IFNs (9) which activate STAT1, we hypothesized that oHSV-induced STAT1 activation was associated with decreased viral productivity in MPNST cells. We determined that 6 hours postinfection was the optimal time to observe STAT1 Y701 phosphorylation (Supplementary Fig. S2). R3616 infection induced STAT1 activation in 3 of 8 (38%) human (Fig. 2A) and in 7 of 13 (54%) mouse cell lines (Fig. 2B). When exposed to exogenous IFNβ (200 IU/mL) STAT1 Y701 phosphorylation was evident in all human MPNST cell lines indicating that mechanisms for signal transduction were functional (Supplementary Fig. S3). When R3616 titers from all MPNST cell lines were sorted into STAT1-unresponsive (pSTAT1−) and STAT1-responsive (pSTAT1+) groups, cell lines which were STAT1 responsive were associated with significantly lower viral recovery (Fig. 2C). To further test the association of the STAT1 response of each cell line with viral productivity, we assessed viral spread within an *in vitro* monolayer. In this assay, the percentage of cells infected with an eGFP-expressing $\Delta\gamma_1$34.5 virus (C101) in a multistep infection (MOI = 0.1, 48 hours postinfection) was measured by flow cytometry. In general, MPNST cell lines tended to be resistant to the spread of C101 in the multistep assay, however, permissive cell lines which supported spread were associated with an unresponsive STAT1 phenotype (Fig. 2D). To determine whether differences in STAT1 activation was cytoprotective following oHSV infection, we measured the number of gated cells by flow cytometry at 48 hours postinfection following multistep infection with C101 and compared the counts to mock-infected cells. The results showed a trend toward higher cell counts (lower cytotoxicity) after C101 infection in STAT1-responsive cell lines, however, similar to the previous assessment, the majority of cell lines were resistant to the cytotoxic effects of C101 (Fig. 2E).

To identify whether the STAT1 response was associated with diminished oHSV productivity in the setting of a $\Delta\gamma_1$34.5 oHSV capable of PKR evasion, we repeated the spread and cytotoxicity studies using C134, a chimeric $\Delta\gamma_1$34.5 oHSV expressing the human CMV IRS1 gene product which inhibits PKR-mediated translational arrest. Immunoblots against PKR and eIF2α verified that C134 inhibited PKR-induced eIF2α phosphorylation in MPNST tumor cells (Fig. 3A) similar to what has been observed in other cell lines (10). In a viral spread assay with C154 (an eGFP-expressing variant of C134), we found that similar to the results with C101, the spread and cytotoxic effect of C154 was significantly diminished in STAT1-responsive cell lines (Fig. 3B and C). Next, to identify whether the productivity of wild-type HSV-1 was associated with STAT1 response, we repeated the spread and cytotoxicity assays with a wild-type HSV-1(F) that expresses eGFP (M2001). The results show that unlike $\Delta\gamma_1$34.5 oHSVs, the STAT1 response was not significantly associated with wild-type HSV-1 spread or cytotoxicity in the MPNST cell lines (Fig. 3D and E). Both viral spread and cytotoxicity induced by M2001 was generally high in all cell lines compared with the $\Delta\gamma_1$34.5 attenuated viruses.

These results demonstrate that the restricted productivity of $\Delta\gamma_1$34.5 oHSVs is significantly associated with the capacity of a cell to activate the STAT1 signaling cascade in response to $\Delta\gamma_1$34.5 oHSV infection. This association exists irrespective of PKR-mediated translational arrest inasmuch as the spread

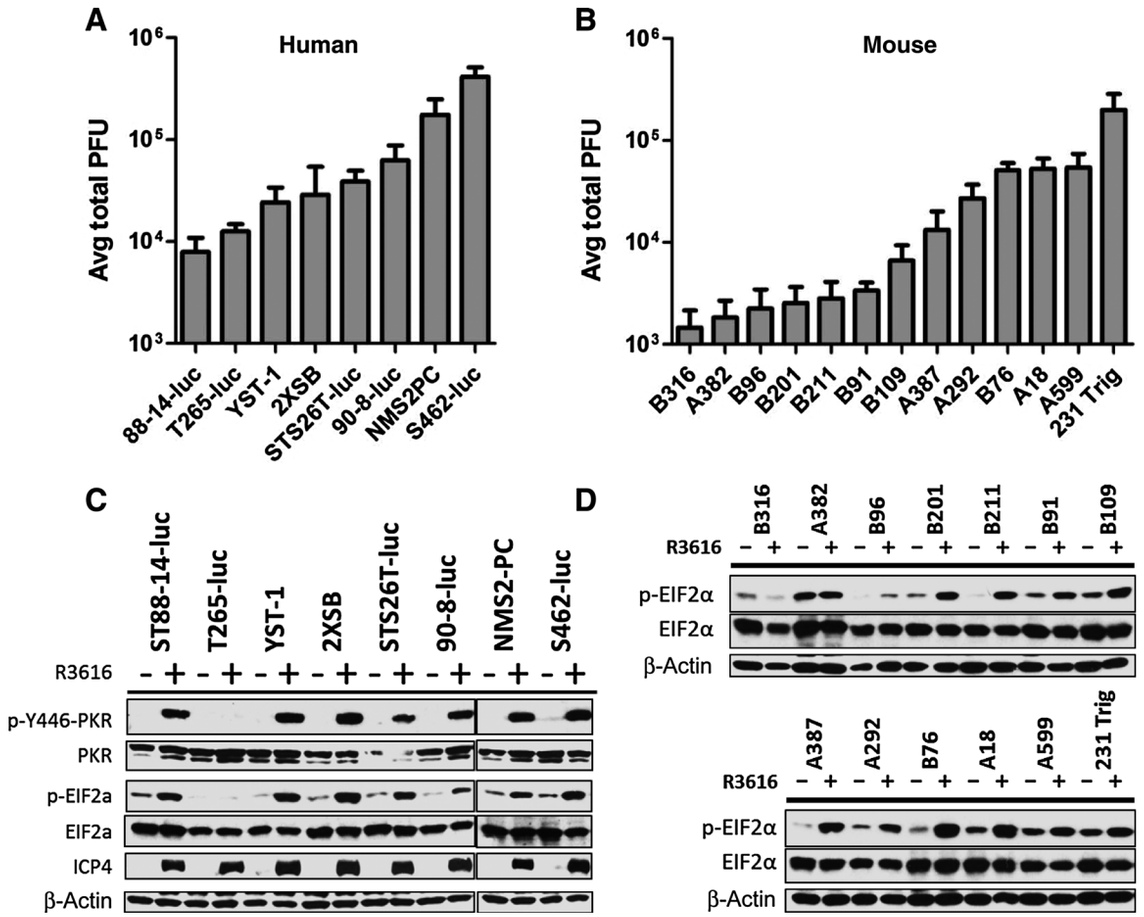


Figure 1.
oHSV productivity and activation of the PKR response. Human- (A) and mouse- (B) derived MPNST cell lines were infected with R3616 (MOI = 1, 24 hours postinfection) and viral recovery measured using standard titration methods. Data were collected in triplicate and the titers are reported as the average total PFU with SD. PKR and eIF2α in human cell lines (C) or eIF2α alone in mouse cell lines (D) was assessed by Western blot analysis for phosphorylation in response to mock or R3616 (MOI = 1, 12 hours postinfection) infection.

and cytotoxicity of C134, a $\Delta\gamma_1$34.5 HSV capable of PKR evasion, is also restricted in these STAT1-responsive cell lines. In contrast, the productivity of wild-type HSV-1 was not associated with the capacity for a STAT1 response in similar assays.

Modulation of STAT1 activation by the JAK inhibitor ruxolitinib

Next, to determine whether the observed STAT1 activation was directly responsible for diminished $\Delta\gamma_1$34.5 viral productivity in resistant MPNST cell lines, we inhibited STAT1 Y701 phosphorylation using the JAK1/2 inhibitor ruxolitinib. We hypothesized that by inhibiting this response, $\Delta\gamma_1$34.5 oHSV productivity could be improved. To test this hypothesis, we treated the oHSV-resistant MPNST cell lines STS26T-luc and ST8814-luc with 250 nmol/L ruxolitinib (Rux) or vehicle (DMSO) following $\Delta\gamma_1$34.5 oHSV infection. Cotreatment with ruxolitinib did not improve $\Delta\gamma_1$34.5 oHSV infection and spread compared with DMSO in multistep (low MOI) assay with C101 (Fig. 4A) despite the fact that ruxolitinib cotreatment prevented STAT1 Y701 phosphorylation (Fig. 4G). In viral recovery assays, ruxolitinib cotreatment did not improve R3616 replication in a single-step (MOI = 1) assays (Fig. 4B), but did slightly improve R3616 replication in multistep (MOI = 0.1) replication assays in both cell lines (Fig. 4C).

Multistep replication assays, using a low virus/cell ratio and longer time points (24 vs. 48 hours postinfection), challenge the virus to undergo multiple rounds of replication and spread beyond the initially infected cells. The modest increases in viral titer observed in the multistep assay (Fig. 4C), but not the single-step assay, led us to hypothesize that uninfected cells in the multistep assay benefitted to some degree from "pre-treatment" with ruxolitinib prior to becoming infected. To further test the effects of pretreatment, the above experiments were repeated by exposing cells to ruxolitinib for 48 hours followed by removal of the inhibitor prior to infection and addition of DMSO following infection. The results show that pretreatment alone with ruxolitinib (Rux + DMSO) significantly improved the spread of C101 (Fig. 4D) as well as titers of R3616 in both single-step and multistep assays in both cell lines (Fig. 4E and F) compared with DMSO pretreatment (DMSO + DMSO). Interestingly, pretreatment alone, whereby cells were washed of ruxolitinib prior to infection did not inhibit subsequent oHSV-induced STAT1

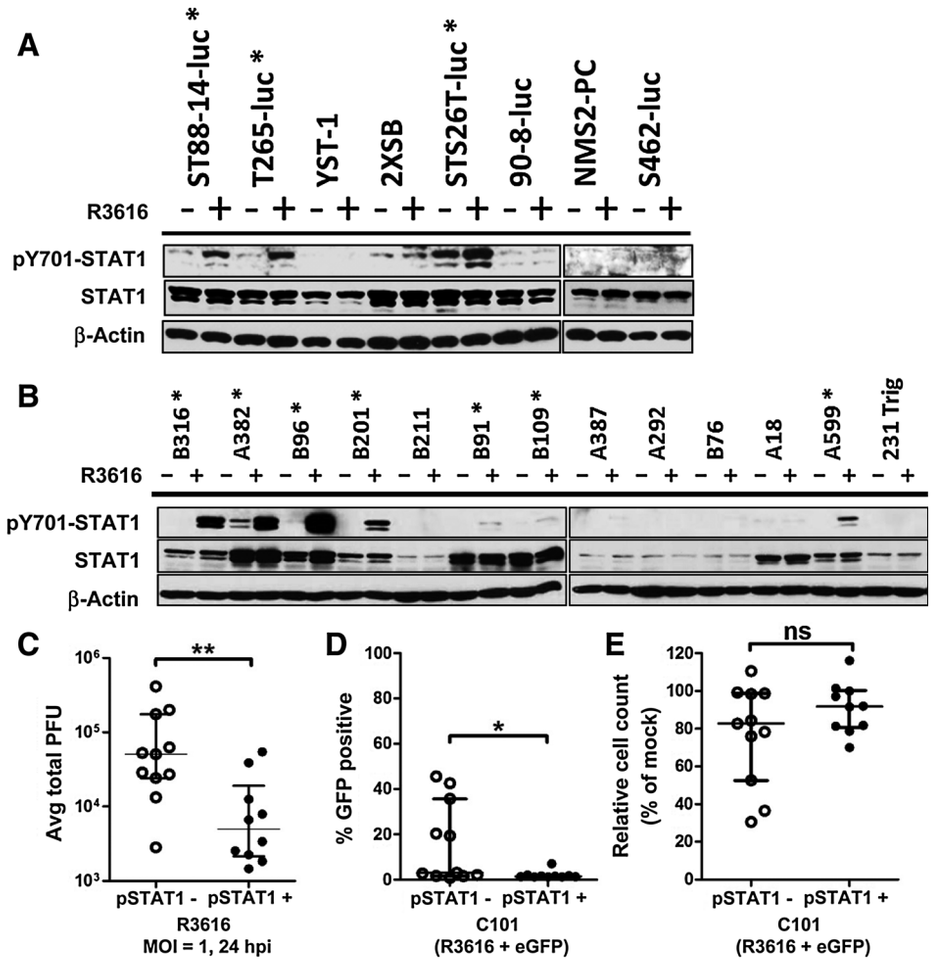


Figure 2.
STAT1 response to oHSV infection and association with viral productivity. STAT1 phosphorylation in response to R3616 infection (MOI = 1, 6 hours postinfection) was assessed by Western blot analysis in human (A) and mouse (B) cell lines. Cell lines considered STAT1 responsive are marked with an asterisk. The mean viral titers (from Fig. 1A and B) from each cell line were sorted into STAT1-unresponsive and STAT1-responsive groups and tested for statistical significance using the Mann–Whitney *U* test with the median and interquartile range plotted (C). Cell lines were assessed in a multistep infection assay (MOI = 0.1, 48 hours postinfection) with C101 for the percentage of cells positive for GFP (D) and the infected cell count as a percentage of the mock-infected cell count (E). Data were collected in triplicate and the mean reported. Cell lines were sorted on the basis of their STAT1 response and tested for statistical significance using the Mann–Whitney *U* test with the medians and interquartile range plotted.

phosphorylation (Fig. 4G). Sequential pretreatment and cotreatment with ruxolitinib (Rux +Rux) further improved viral spread beyond pretreatment alone (Fig. 4D), however, it did not significantly improve viral replication in either the single-step or multistep viral recovery assays (Fig. 4E and F). Similar improvements were obtained with a M002 series oHSV (8; Supplementary Fig. S4). To explain the unique effects of pretreatment, we hypothesized that ruxolitinib inhibited low-level stimulation and activation of the JAK/STAT pathway in the STS26T-luc and ST8814-luc cell lines. To test this hypothesis, we stably transduced these cell lines with a nanoluciferase reporter under the control of a series of ISRE promoter elements and showed that ruxolitinib diminished the basal (uninfected) ISRE reporter activity in a concentration-dependent manner relative to DMSO (Fig. 4H). An assessment of protein expression by Western blot analysis revealed that the expression of five representative ISGs (MDA5, RIG-I, MX1, IFIT3, and OAS1) decreased following 48-hour treatment with ruxolitinib as compared with DMSO (Fig. 4I). We conclude that basal STAT1/ISRE promoter activity leads to ISG expression which negatively impacts the productive infection of oHSVs.

Effect of ISG upregulation on oHSVs

To determine the extent to which basal ISGs expression occurs among other MPNST cell lines, we evaluated the relative levels of five ISGs (MDA5, RIG-I, MX1, IFIT3, and OAS1) by immunoblot in all human MPNST cell lines. The results show that for the five probed ISGs, greater protein expression was detected in the cell lines ST8814-luc, T265-luc, 2XSB, STS26T-luc, and 90-8-luc whereas YST-1, NMS2-PC, and S462-luc had low or undetectable ISG expression (Fig. 5A). The low ISG expression in S462-luc is notable as this cell line was the most permissive to oHSV infection producing the highest viral titers of MPNST cell lines tested. We hypothesized that higher basal ISG expression would increase oHSV resistance in S462-luc. To test this, S462-luc cells were exposed to different concentrations of IFNβ for 24 hours and probed for ISGs by Western blot analysis. Figure 5B shows the associated increase in ISG expression with increasing concentrations of IFNβ, whereas IFNβ-treated cells which were infected with C101 in a multistep assay were less supportive of cell to cell spread in a manner dependent on the concentration of IFNβ. Because ISGs are only transiently expressed in S462-luc in response to IFNβ (data not shown) we stably coexpressed the ISGF3 component transcription factors (STAT1, STAT2, and IRF9), a strategy which has previously been reported to elevate basal ISG expression (11). Overexpression of ISGF3 in S462-luc similarly resulted in increased ISG expression (Fig. 5C) and was associated with greater than 10-fold reduction of R3616 titers in both

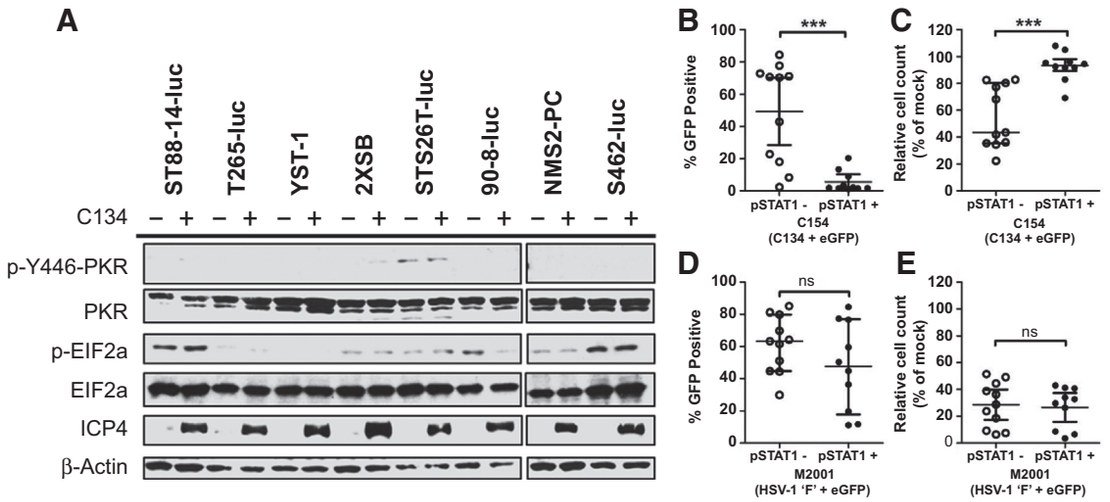


Figure 3.

PKR activation with C134 and association of productivity with STAT1 response. PKR and eIF2α in human cell lines (A) was assessed by Western blot analysis for phosphorylation in response to mock or C134 (MOI = 1, 12 hours postinfection) infection. Cell lines were assessed in a multistep infection assay (MOI = 0.1, 48 hours postinfection) with C154 and M2001 for the percentage of cells positive for GFP (B and D) and the infected cell count as a percentage of the mock-infected cell count (C and E). Data were collected in triplicate and the mean reported. Cell lines were sorted based on their STAT1 response and tested for statistical significance using the Mann–Whitney *U* test with the medians and interquartile range plotted.

single-step and multi-step replication assays (Fig. 5D). We conclude that elevated ISG expression in MPNST cell lines diminishes oHSV productivity.

NF-κB signaling and basal ISG expression

Recent reports have implicated the transcription factor NF-κB, specifically the p65/RelA subunit, in promoting low-level expression of IFNβ resulting in higher basal ISG expression (12). We hypothesized that MPNST cell lines with constitutively active NF-κB increased ISG expression in oHSV-resistant cell lines. To assess this, immunoblots were performed and showed relatively high p65 phosphorylation in the resistant cell lines STS26T-luc and ST8814-luc (Fig. 6A) suggesting elevated NF-κB activity. To identify whether basal ISRE transcriptional activity and ISG expression was related to NF-κB transcriptional activity, we stably expressed nuclear factor of kappa light polypeptide gene enhancer in B-cell inhibitor, alpha (NFKBIA; commonly known as inhibitor of κB; IκB), a native inhibitor of NF-κB, with S32A/S36A mutations that prevent proteasomal degradation and act as an NF-κB "super repressor." The results show that IκB super repressor (IκB-SR) expression decreases both NF-κB and ISRE reporter activity (Fig. 6B). In contrast, control transduction had no effect upon NF-κB or ISRE activity. IκB-SR expression also led to decreased expression of ISGs (Fig. 6C). Together these results suggest that constitutive stimulation of the NF-κB pathway can be related to the basal stimulation of ISRE elements and ISG expression.

Previous reports have shown that the small-molecule inhibitor TPCA-1, a dual inhibitor of IkB kinase (IKK; a positive regulator of NF-κB) and JAK1, can benefit the productivity of the oncolytic viruses vesicular stomatitis virus (VSV) and encephalomyocarditis virus (EMCV; refs. 13, 14). We hypothesized that TPCA-1 could also benefit oHSV by downregulating expression of ISGs. Indeed, TPCA-1 inhibited the activity of both NF-κB (Fig. 6D) and ISRE (Fig. 6E) nanoluciferase reporters in a concentration-dependent manner and reduced ISG expression in the treated cells (Fig. 6F). To test the effect of TPCA-1 on oHSV productivity, we used combinations of pretreatment and cotreatment with TPCA-1 or DMSO, similar to the ruxolitinib studies described above. As with ruxolitinib, cotreatment (DMSO + TPCA1) with TPCA-1 did not significantly improve $\Delta\gamma_1$34.5 infection and spread, however, pretreatment (TPCA1 + DMSO) was sufficient to significantly improve the spread of both of the $\Delta\gamma_1$34.5 recombinants C101 and M201 in the ST8814-luc and STS26T-luc cell lines (Fig. 6G and H). Interestingly, in contrast to the C101 and M201, the $\Delta\gamma_1$34.5 PKR evasion virus C154 benefited from either TPCA-1 cotreatment or from pretreatment alone (Fig. 6I). Pretreatment followed by cotreatment (TPCA1 + TPCA1) further improved spread in the majority of conditions tested.

Discussion

The oHSVs engineered within our laboratory are derived from HSV-1 mutants with dual deletions of the $\gamma_1$34.5 neurovirulence gene rendering them safe to administer in the CNS (15). Although normal cells restrict $\Delta\gamma_1$34.5 oHSV replication, a partial explanation for the oncolytic selectivity of $\Delta\gamma_1$34.5 HSVs for cancerous tissue is that malignant transformation of these cells results in an aberrant antiviral response that complements viral loss of the $\gamma_1$34.5 gene. However, despite the wide variety of cancer types that are susceptible to oHSVs, resistance is commonly observed. In an *in vivo* setting, resistance can be attributed to inefficient delivery methods, low interstitial penetration, tumor heterogeneity, and activation of the innate and adaptive immune response. However, resistance is observed *in vitro*. This implies that the cancer cells themselves can independently restrict or resist oHSV infection and replication through intrinsic mechanisms.

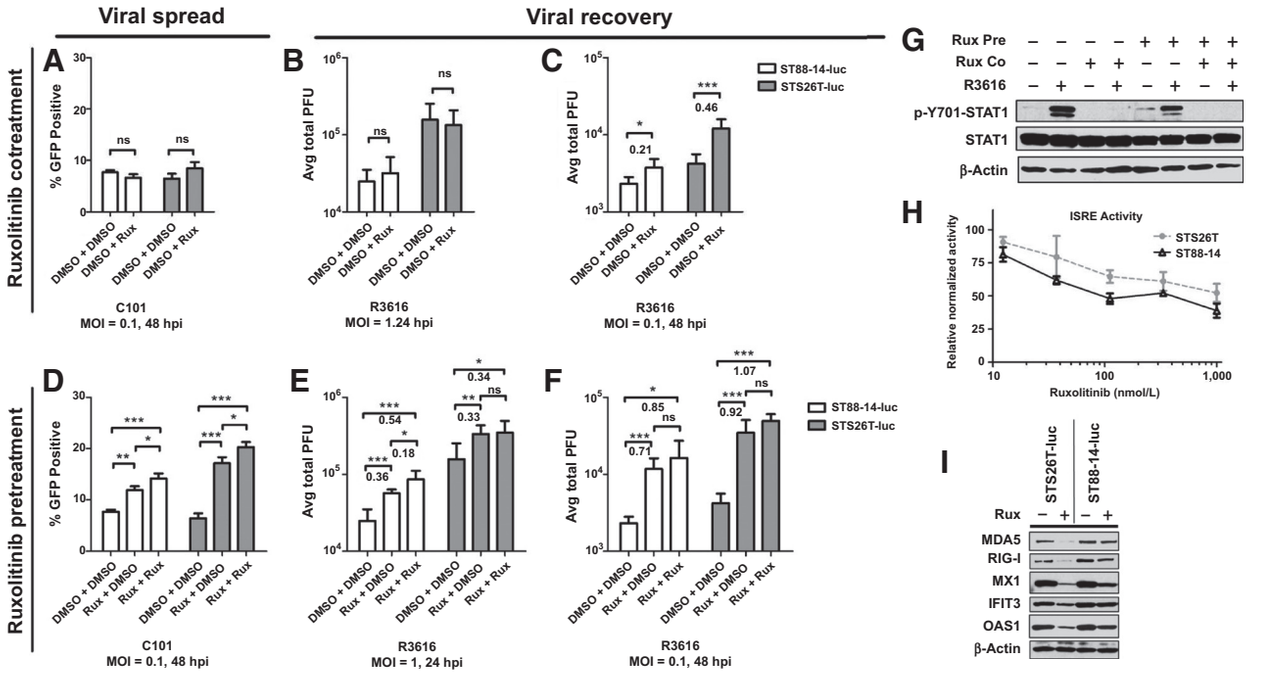


Figure 4.
Effect of JAK inhibitor ruxolitinib on viral productivity, basal ISRE activity, and ISG expression. Cell lines were pretreated with either DMSO or 250 nmol/L ruxolitinib (Rux) for 48 hours prior to infection. One hour after oHSV infection, each group was further cotreated with DMSO or ruxolitinib (250 nmol/L). GFP-expressing virus C101 was used to assess effects on oHSV spread by multistep infection (MOI = 0.1, 48 hours postinfection; A and D). Multistep (MOI = 0.1, 48 hours postinfection; B and E) and single-step (MOI = 1, 24 hours postinfection; C and F) infection with R3616 was used to assess viral recovery. Data for spread and recovery assays were collected in triplicate and the SD reported. For viral recovery, the log-fold change is reported under the significance indicator. Phosphorylation of STAT1 was observed by Western blot analysis in ST88-14-luc treated with combinations of DMSO and ruxolitinib (G). ISRE activity was measured by dual luciferase assays after 24-hour treatment with various concentrations of ruxolitinib (H). ISRE nanoluciferase activity was normalized to that of firefly luciferase and final values reported as the percentage of DMSO-treated cells. Expression of ISGs MDA5, RIG-I, MX1, IFIT3, and OAS1 in cell lines treated with DMSO or ruxolitinib (250 nmol/L) for 48 hours was observed by Western blot analysis (I).

Our previous work showed that the abundance of viral entry receptors was not responsible for restricted oHSV replication and growth in MPNST tumor cells (4). This suggests that an intracellular response contributes to intrinsic oHSV restriction. There are conflicting reports regarding the role of Ras signaling and its benefit to oHSV in the context of MPNSTs (16, 17). Our determination of the MEK/ERK status (Supplementary Fig. S5) shows that this pathway can be activated in both permissive and resistant MPNST cell lines similar to what was reported by Mahller and colleagues (16). Together with our observations regarding PKR, this suggests that Ras/MEK/ERK and PKR status are not sufficient to explain oHSV resistance in MPNST cells. Furthermore, an oHSV capable of evading the PKR response, C134, was also restricted in resistant MPNST cell lines despite inhibiting PKR activation. Although PKR-mediated translational arrest is a critical obstacle, it appears not to be the sole impediment to $\Delta\gamma_1 34.5$ oHSV replication in MPNST cells.

We demonstrated that viral productivity in MPNST tumor lines was inversely associated with an oHSV-induced STAT1 response; however, STAT1 inhibition using ruxolitinib during HSV infection did not improve oHSV replication and spread. Instead, ruxolitinib pretreatment was necessary and sufficient to improve oHSV productivity. One potential explanation for the observable STAT1 response in oHSV-resistant cells is that these cells have a greater basal upregulation of ISGs. A subset of ISGs are pattern recognition receptors (e.g., MDA5 and RIG-I) which lead to the expression of type I IFN and subsequent phosphorylation of STAT1 in response to infection. This capacity to respond to oHSV infection with STAT1 phosphorylation may therefore reflect (or act as a surrogate marker for) the coexpression of other ISGs which are directly antagonistic to oHSV replication and spread. Therefore, suppressing the STAT1 response at the time of infection with ruxolitinib cotreatment is insufficient to improve oHSV replication because basal ISG accumulation is sufficient to impart this viral resistance. The downregulation of basal ISRE activity and ISG expression following ruxolitinib pretreatment supports the hypothesis that reduced accumulation of antiviral effectors is sufficient to improve oHSV infection and spread. The presence of faint p-Y701 STAT1 staining in some of the uninfected resistant MPNST cell lines (e.g., STS26T-luc and A382 in Fig. 2A) supports the possibility that basal STAT1 activity contributes to the expression of ISGs in these cell lines. Finally, consistent with our observation that viral productivity of both $\Delta\gamma_1 34.5$ (9, 18) and C134 ($\Delta\gamma_1 34.5$ IRS1) are associated with the capacity for a STAT1 response, these viruses have been previously been reported to be sensitive to type I IFN pretreatment (9, 18) whereas wild-type HSV-1 remains insensitive to those effects (9, 18).Although basal expression of ISGs has been previously documented in a number of tumor-derived cell lines (19–23),

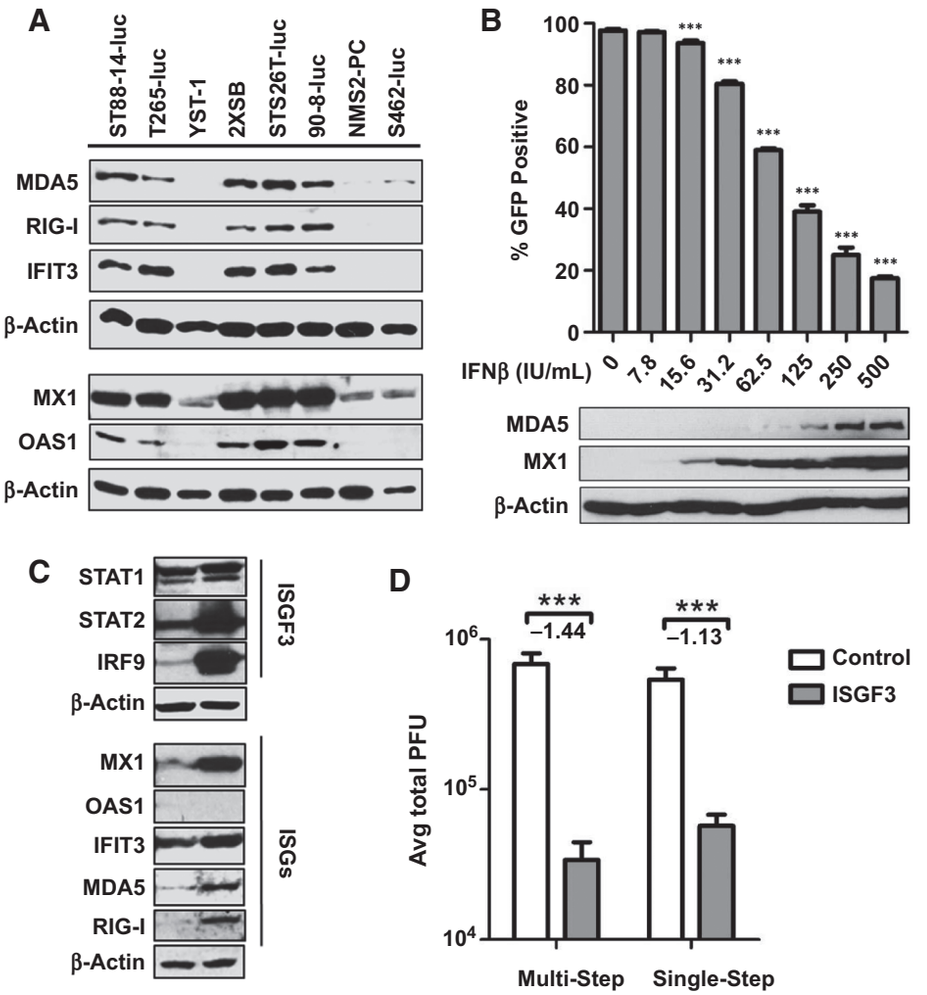


Figure 5.
Basal expression of ISGs in MPNST cell lines and effect of increased ISG expression on viral productivity. Basal expression of ISGs in all human MPSNT cell lines was assessed by Western blot analysis (A). S462-luc cells were treated with IFNβ for 24 hours and subsequently probed by immunoblot for ISGs (B) or infected with C101 at MOI = 0.2. Infected cells were then assessed by FACS for the percentage of cells positive for viral eGFP at 48 hours postinfection (B). S462-luc was stably transduced with a control lentivirus (DsRed2) or lentiviruses encoding the transcription factors STAT1-FLAG, STAT2, and IRF9 which compose the ISGF3 complex were assessed for ISG expression by Western blot analysis (C). Multistep (MOI = 0.1, 48 hours postinfection) and single-step (MOI = 1, 24 hours postinfection; D) viral recovery assays with R3616 were conducted in control and ISGF3 transduced cell lines. In each described assay, data were collected in triplicate and the SD reported. The log-fold change is reported under the significance indicator.

this has not been shown for MPNSTs. However, in the context of oHSV infection, Mahller and colleagues showed through gene expression analysis that the "JAK/STAT pathway" and "Tyrosine Phosphorylation of STAT protein" were significantly upregulated in response to G207 (a lacZ-expressing variant of R3616) in a panel of MPNST cell lines (24). Interestingly, knockdown of suppressor of cytokine signaling 1 (SOCS1), a negative regulator of STAT1, decreased the viral titers of the G207 by more than 10-fold in the highly permissive cell line S462.

Activation of the JAK/STAT pathway and ISG expression limits other oncolytic viruses including vesicular stomatitis virus (13, 19, 22, 23,25), measles virus (20), Newcastle disease virus (21), respiratory syncytial virus (26), Semliki Forest virus (27), and adenovirus (28, 29). In several of these studies, inhibitors of JAK/STAT1 signaling enhanced viral productivity (19, 22, 23, 25,27). With respect to HSV, a head and neck squamous cell carcinoma, which became radioresistant through the upregulation of STAT1 and other ISGs, suppressed the replication of oHSV R3616 by 40-fold compared with the original tumor (30). Haseley and colleagues found that overexpression of the extracellular matrix protein cysteine-rich 61 (CYR61) induced upregulation of type I IFNs and ISGs which suppressed oHSV productivity in glioma cells (31). Although $\Delta\gamma_1$34.5 HSVs are known to be sensitive to exogenous IFN (9, 18), presumably through the upregulation of ISGs by STAT1, these appear to be the only reports in the literature between a cancer-associated STAT1/ISG signature and resistance to oHSV.

The STAT1/ISG expression signature has been detected in a number of patient tumor specimens including glioblastoma (32, 33), squamous cell carcinoma (34), melanoma (35), leukemia (36), breast (36–38), ovarian (36), and pancreatic (28) cancers suggesting that cancer-associated STAT1/ISG expression is not an *in vitro* artifact. In these reports, it is not possible to determine whether the STAT1 signature is a phenotype driven by the intrinsic nature of the tumor cells (autocrine activation) or whether expression of this signature occurs in response to inflammatory stimuli from the surrounding microenvironment (paracrine activation). Regardless of the mechanism, STAT1 and ISG expression signatures have been implicated in the resistance of cancer to radiation (30, 39, 40) and chemotherapy (39, 41, 42). ISG expression in MPNSTs may offer a possible explanation for the lack of efficacy by these treatment modalities in patients with MPNSTs (2, 3).

It has been shown that innate immune effectors including microglia, macrophages, and natural killer cells actively restrict

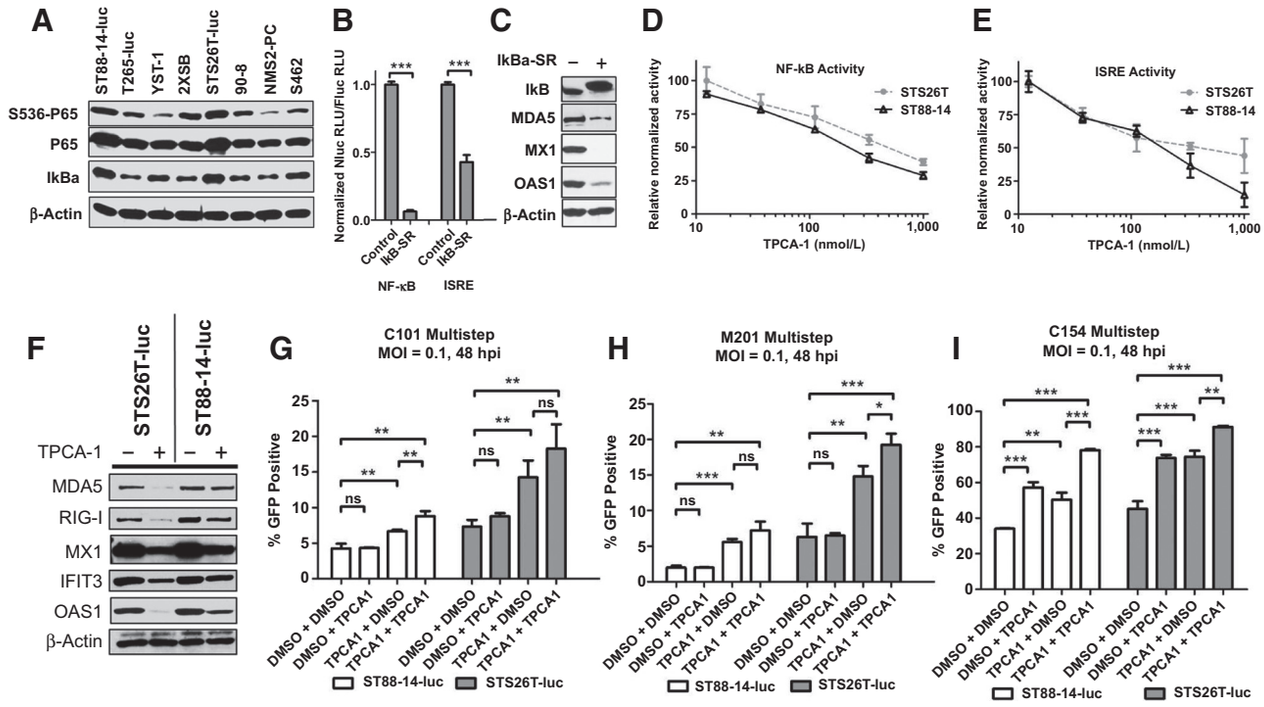


Figure 6.
Relationship of NF-κB to basal ISG expression. Phosphorylation of P65/RelA was assessed in human cell lines by Western blot analysis (A). The cell line ST88-14-luc expressing either NF-κB or ISRE luciferase reporters were stably transduced with the inhibitor of kB super repressor (IkB-SR) and nanoluciferase (Nluc) activity measured (B). Firefly luciferase (Fluc) normalized data were collected in quadruplicate and SD reported. IkB-SR transduced ST88-14-luc was probed for IkB and ISG expression by Western blot analysis (C). NF-κB (D) and ISRE (E) luciferase activity was measured in response to the small-molecule inhibitor TPCA-1. Firefly luciferase normalized data were collected in triplicate and the percentage of activity relative to DMSO treatment was reported with SD. Expression of ISGs was probed in TPCA-1 treated cell lines (250 nmol/L, 96 hours) by Western blot analysis (F). Cell lines were pretreated with either DMSO or 250 nmol/L TPCA-1 (Rux) for 96 hours prior to infection. One hour after oHSV infection, each group was further cotreated with DMSO or TPCA-1 (250 nmol/L). GFP-expressing viruses C101 (G), M201 (H), and C154 (I) were used to assess effects on oHSV spread by multistep infection (MOI = 0.1, 48 hours postinfection). Data were collected in triplicate and the SD reported.

replication of oncolytic HSV *in vivo* (43, 44). However, oncolytic viruses may be beneficial as an immunotherapy by provoking an immune response, specifically involving natural killer cells and cytotoxic T cells, leading to recognition and clearance of the tumor, despite the detriment to viral replication and oncolysis (45, 46). Indeed, paradoxical responses to oHSV have been reported whereby tumor cells which were characterized as oHSV resistant *in vitro* were more susceptible to the antitumor effect of oHSV *in vivo* (46). Although we have demonstrated associated STAT1 activation to be detrimental to oHSV productivity *in vitro*, it will be necessary to identify how tumor cells that are STAT1-responsive interact with the peripheral immune elements in this context because the efficacy of certain immunotherapies and the recruitment of CTLs is dependent upon the type I IFN response (47). In addition, the use of powerful immunosuppressants such as JAK inhibitors may counteract the effects of immunotherapy or diminish the safety profiles which have been previously established for oHSV.

Finally, the driver for basal ISG expression in tumor cells remains incompletely understood. Virally induced NF-κB activation is known to promote IFNβ transcription (48), but the extent to which the constitutive NF-κB activation, which is commonly overserved in certain cancers, affects IFNβ expression is unclear. There is some evidence that upstream signaling components of the NF-κB pathway, independent of NF-κB–driven gene expression, may be involved in STAT1 cross-talk (49, 50). Further work is needed to determine the prevalence of NF-κB–related ISG expression and the complete mechanism in MPNSTs.

In conclusion, our current research has identified a previously unexplored component of MPNST resistance to $\Delta\gamma_1 34.5$ oHSVs. We believe the novel finding of basal ISG expression in MPNST cells may have further implications for MPNST biology and their treatment with conventional antitumor therapies.

Disclosure of Potential Conflicts of Interest

J.M. Markert has ownership interest (including patents) in oHSV, K.A. Cassady has patent interests in oHSV. No potential conflicts of interest were disclosed by the other authors.

Authors' Contributions

Conception and design: J.D. Jackson, J.M. Markert, S.L. Carroll, K.A. Cassady
Development of methodology: J.D. Jackson, S.L. Carroll, K.A. Cassady
Acquisition of data (provided animals, acquired and managed patients, provided facilities, etc.): J.D. Jackson, J.M. Markert, L. Li, S.L. Carroll, K.A. Cassady
Analysis and interpretation of data (e.g., statistical analysis, biostatistics, computational analysis): J.D. Jackson, K.A. Cassady
Writing, review, and/or revision of the manuscript: J.D. Jackson, J.M. Markert, S.L. Carroll, K.A. Cassady

Administrative, technical, or material support (i.e., reporting or organizing data, constructing databases): J.M. Markert, K.A. Cassady
Study supervision: J.M. Markert, K.A. Cassady

Acknowledgments

The authors thank the UAB Comprehensive Flow Cytometry Core, UAB Heflin Genetics Center for Genomic Science, and Dr. Bernard Roizman (University of Chicago, Chicago, IL) for providing R3616.

Grant Support

Funding for this research was provided through DOD-W81XWH-10-NFRP-IIRA-NF1001157, P20 CA151129-03, P01 CA71933-15, and P50 CA97247-05.

The costs of publication of this article were defrayed in part by the payment of page charges. This article must therefore be hereby marked *advertisement* in accordance with 18 U.S.C. Section 1734 solely to indicate this fact.

Received October 19, 2015; revised January 29, 2016; accepted February 4, 2016; published OnlineFirst February 16, 2016.

References

1. Kolberg M, Høland M, Ågesen TH, Brekke HR, Liestøl K, Hall KS, et al. Survival meta-analyses for>1800 malignant peripheral nerve sheath tumor patients with and without neurofibromatosis type 1. Neuro Oncol 2013; 15:135–47.
2. Wong WW, Hirose T, Scheithauer BW, Schild SE, Gunderson LL. Malignant peripheral nerve sheath tumor: analysis of treatment outcome. Int J Radiat Oncol Biol Phys 1998;42:351–60.
3. Zehou O, Fabre E, Zelek L, Sbidian E, Ortonne N, Banu E, et al. Chemotherapy for the treatment of malignant peripheral nerve sheath tumors in neurofibromatosis 1: a 10-year institutional review. Orphanet J Rare Dis 2013;8:127.
4. Jackson JD, McMorris AM, Roth JC, Coleman JM, Whitley RJ, Gillespie GY, et al. Assessment of oncolytic HSV efficacy following increased entry-receptor expression in malignant peripheral nerve sheath tumor cell lines. Gene Ther 2014;21:984–90.
5. Farassati F, Yang A-D, Lee PW. Oncogenes in Ras signalling pathway dictate host-cell permissiveness to herpes simplex virus 1. Nat Cell Biol 2001;3: 745–50.
6. Cassady KA. Human cytomegalovirus TRS1 and IRS1 gene products block the double-stranded-RNA-activated host protein shutoff response induced by herpes simplex virus type 1 infection. J Virol 2005;79:8707–15.
7. Kazmi SJ, Byer SJ, Eckert JM, Turk AN, Huijbregts RP, Brossier NM, et al. Transgenic mice overexpressing neuregulin-1 model neurofibroma-malignant peripheral nerve sheath tumor progression and implicate specific chromosomal copy number variations in tumorigenesis. Am J Pathol 2013;182:646–67.
8. Parker JN, Gillespie GY, Love CE, Randall S, Whitley RJ, Markert JM. Engineered herpes simplex virus expressing IL-12 in the treatment of experimental murine brain tumors. Proc Natl Acad Sci U S A 2000;97: 2208–13.
9. Cheng G, Brett M-E, He B. Val 193 and Phe 195 of the γ 1 34.5 protein of herpes simplex virus 1 are required for viral resistance to interferon-α/β. Virology 2001;290:115–20.
10. Shah A, Parker J, Gillespie G, Lakeman F, Meleth S, Markert J, et al. Enhanced antiglioma activity of chimeric HCMV/HSV-1 oncolytic viruses. Gene Ther 2007;14:1045–54.
11. Cheon H, Holvey-Bates EG, Schoggins JW, Forster S, Hertzog P, Imanaka N, et al. IFNbeta-dependent increases in STAT1, STAT2, and IRF9 mediate resistance to viruses and DNA damage. EMBO J 2013; 32:2751–63.
12. Basagoudanavar SH, Thapa RJ, Nogusa S, Wang J, Beg AA, Balachandran S. Distinct roles for the NF-κB RelA subunit during antiviral innate immune responses. J Virol 2011;85:2599–610.
13. Cataldi M, Shah NR, Felt SA, Grdzelishvili VZ. Breaking resistance of pancreatic cancer cells to an attenuated vesicular stomatitis virus through a novel activity of IKK inhibitor TPCA-1. Virology 2015;485: 340–54.
14. Du Z, Whitt MA, Baumann J, Garner JM, Morton CL, Davidoff AM, et al. Inhibition of type I interferon-mediated antiviral action in human glioma cells by the IKK inhibitors BMS-345541 and TPCA-1. J Interferon Cytokine Res 2012;32:368–77.
15. Chou J, Kern ER, Whitley RJ, Roizman B. Mapping of herpes simplex virus-1 neurovirulence to gamma 134.5, a gene nonessential for growth in culture. Science 1990;250:1262–6.
16. Mahller YY, Rangwala F, Ratner N, Cripe TP. Malignant peripheral nerve sheath tumors with high and low Ras-GTP are permissive for oncolytic herpes simplex virus mutants. Pediatr Blood Cancer 2006;46:745–54.
17. Farassati F, Pan W, Yamoutpour F, Henke S, Piedra M, Frahm S, et al. Ras signaling influences permissiveness of malignant peripheral nerve sheath tumor cells to oncolytic herpes. Am J Pathol 2008;173: 1861–72.
18. Cassady KA, Saunders U, Shimamura M. $\Delta\gamma$134. 5 herpes simplex viruses encoding human cytomegalovirus IRS1 or TRS1 induce interferon regulatory factor 3 phosphorylation and an interferon-stimulated gene response. J Virol 2012;86:610–4.
19. Paglino JC, van den Pol AN. Vesicular stomatitis virus has extensive oncolytic activity against human sarcomas: rare resistance is overcome by blocking interferon pathways. J Virol 2011;85:9346–58.
20. Berchtold S, Lampe J, Weiland T, Smirnow I, Schleicher S, Handgretinger R, et al. Innate immune defense defines susceptibility of sarcoma cells to measles vaccine virus-based oncolysis. J Virol 2013;87:3484–501.
21. Wilden H, Fournier P, Zawatzky R, Schirrmacher V. Expression of RIG-I, IRF3, IFN-β and IRF7 determines resistance or susceptibility of cells to infection by Newcastle Disease Virus. Int J Oncol 2009;34:971–82.
22. Escobar-Zarate D, Liu Y, Suksanpaisan L, Russell S, Peng K. Overcoming cancer cell resistance to VSV oncolysis with JAK1/2 inhibitors. Cancer Gene Ther 2013;20:582–9.
23. Moerdyk-Schauwecker M, Shah NR, Murphy AM, Hastie E, Mukherjee P, Grdzelishvili VZ. Resistance of pancreatic cancer cells to oncolytic vesicular stomatitis virus: role of type I interferon signaling. Virology 2013;436:221–34.
24. Mahller Y, Sakthivel B, Baird W, Aronow B, Hsu Y, Cripe T, et al. Molecular analysis of human cancer cells infected by an oncolytic HSV-1 reveals multiple upregulated cellular genes and a role for SOCS1 in virus replication. Cancer Gene Ther 2008;15:733–41.
25. Liu Y-P, Suksanpaisan L, Steele MB, Russell SJ, Peng K-W. Induction of antiviral genes by the tumor microenvironment confers resistance to virotherapy. Sci Rep 2013;3:2375.
26. Echchgadda I, Chang T-H, Sabbah A, Bakri I, Ikeno Y, Hubbard GB, et al. Oncolytic targeting of androgen-sensitive prostate tumor by the respiratory syncytial virus (RSV): consequences of deficient interferon-dependent antiviral defense. BMC Cancer 2011;11:43.
27. Ruotsalainen J, Kaikkonen M, Niittykoski M, Martikainen M, Lemay C, Cox J, et al. Clonal variation in interferon response determines the outcome of oncolytic virotherapy in mouse CT26 colon carcinoma model. Gene Ther 2015;22:65–75.
28. Monsurrò V, Beghelli S, Wang R, Barbi S, Coin S, Di Pasquale G, et al. Antiviral state segregates two molecular phenotypes of pancreatic adenocarcinoma: potential relevance for adenoviral gene therapy. J Transl Med 2010;8:10.
29. Liikanen I, Monsurrò V, Ahtiainen L, Raki M, Hakkarainen T, Diaconu I, et al. Induction of interferon pathways mediates in vivo resistance to oncolytic adenovirus. Mol Ther 2011;19:1858–66.
30. Khodarev NN, Beckett M, Labay E, Darga T, Roizman B, Weichselbaum RR. STAT1 is overexpressed in tumors selected for radioresistance and confers protection from radiation in transduced sensitive cells. Proc Natl Acad Sci U S A 2004;101:1714–9.
31. Haseley A, Boone S, Wojton J, Yu L, Yoo JY, Yu J, et al. Extracellular matrix protein CCN1 limits oncolytic efficacy in glioma. Cancer Res 2012;72: 1353–62.
32. Duarte CW, Willey CD, Zhi D, Cui X, Harris JJ, Vaughan LK, et al. Expression signature of IFN/STAT1 signaling genes predicts poor survival outcome in glioblastoma multiforme in a subtype-specific manner. PLoS One 2012;7: e29653.

33. Cosset É, Petty TJ, Dutoit V, Cordey S, Padioleau I, OttenHernandez P, et al. Comprehensive metagenomic analysis of glioblastoma reveals absence of known virus despite antivirallike type I interferon gene response. Int J Cancer 2014;135:1381–9.
34. Laimer K, Spizzo G, Obrist P, Gastl G, Brunhuber T, Schäfer G, et al. STAT1 activation in squamous cell cancer of the oral cavity. Cancer 2007;110: 326–33.
35. Schultz J, Koczan D, Schmitz U, Ibrahim SM, Pilch D, Landsberg J, et al. Tumor-promoting role of signal transducer and activator of transcription (Stat) 1 in late-stage melanoma growth. Clin Exp Metastasis 2010; 27:133–40.
36. Einav U, Tabach Y, Getz G, Yitzhaky A, Ozbek U, Amariglio N, et al. Gene expression analysis reveals a strong signature of an interferon-induced pathway in childhood lymphoblastic leukemia as well as in breast and ovarian cancer. Oncogene 2005;24:6367–75.
37. Perou CM, Sørlie T, Eisen MB, van de Rijn M, Jeffrey SS, Rees CA, et al. Molecular portraits of human breast tumours. Nature 2000;406: 747–52.
38. Perou CM, Jeffrey SS, Van De Rijn M, Rees CA, Eisen MB, Ross DT, et al. Distinctive gene expression patterns in human mammary epithelial cells and breast cancers. Proc Natl Acad Sci U S A 1999;96:9212–7.
39. Fryknäs M, Dhar S, Öberg F, Rickardson L, Rydåker M, Göransson H, et al. STAT1 signaling is associated with acquired crossresistance to doxorubicin and radiation in myeloma cell lines. Int J Cancer 2007;120:189–95.
40. Tsai M-H, Cook JA, Chandramouli GV, DeGraff W, Yan H, Zhao S, et al. Gene expression profiling of breast, prostate, and glioma cells following single versus fractionated doses of radiation. Cancer Res 2007;67: 3845–52.
41. Patterson S, Wei S, Chen X, Sallman D, Gilvary D, Zhong B, et al. Novel role of Stat1 in the development of docetaxel resistance in prostate tumor cells. Oncogene 2006;25:6113–22.
42. Luszczek W, Cheriyath V, Mekhail TM, Borden EC. Combinations of DNA methyltransferase and histone deacetylase inhibitors induce DNA damage in small cell lung cancer cells: correlation of resistance with IFN-stimulated gene expression. Mol Cancer Ther 2010;9:2309–21.
43. Kurozumi K, Hardcastle J, Thakur R, Yang M, Christoforidis G, Fulci G, et al. Effect of tumor microenvironment modulation on the efficacy of oncolytic virus therapy. J Natl Cancer Inst 2007;99:1768–81.
44. Ikeda K, Ichikawa T, Wakimoto H, Silver JS, Deisboeck TS, Finkelstein D, et al. Oncolytic virus therapy of multiple tumors in the brain requires suppression of innate and elicited antiviral responses. Nat Med 1999; 5:881–7.
45. Workenhe ST, Simmons G, Pol JG, Lichty BD, Halford WP, Mossman KL. Immunogenic HSV-mediated oncolysis shapes the antitumor immune response and contributes to therapeutic efficacy. Mol Ther 2014;22:123–31.
46. Leddon JL, Chen C-Y, Currier MA, Wang P-Y, Jung FA, Denton NL, et al. Oncolytic HSV virotherapy in murine sarcomas differentially triggers an antitumor T-cell response in the absence of virus permissivity. Mol Ther Oncolytics 2015;1.
47. Corrales L, Gajewski TF. Molecular pathways: targeting the stimulator of interferon genes (STING) in the immunotherapy of cancer. Clin Cancer Res 2015;21:4774–9.
48. Wang J, Basagoudanavar SH, Wang X, Hopewell E, Albrecht R, García-Sastre A, et al. NF-κB RelA subunit is crucial for early IFN-β expression and resistance to RNA virus replication. J Immunol 2010;185:1720–9.
49. Ng S-L, Chua MA, McWhirter SM, García-Sastre A, Maniatis T. Multiple functions of the IKK-related kinase IKKε in interferon-mediated antiviral immunity. Science 2007;315:1274–8.
50. Nguyen H, Chatterjee-Kishore M, Jiang Z, Qing Y, Ramana CV, Bayes J, et al. IRAK-dependent phosphorylation of Stat1 on serine 727 in response to interleukin-1 and effects on gene expression. J Interferon Cytokine Res 2003;23:183–92.

J Neuropathol Exp Neurol
Vol. 75, No. 10, October 2016, pp. 946–954
doi: 10.1093/jnen/nlw071

ORIGINAL ARTICLE

Tamoxifen Induces Cytotoxic Autophagy in Glioblastoma

Christopher D. Graham, PhD, Niroop Kaza, PhD, Barbara J. Klocke, MS, G. Yancey Gillespie, PhD, Lalita A. Shevde, PhD, Steven L. Carroll, MD, PhD, and Kevin A. Roth, MD, PhD

Abstract

Glioblastomas (GBMs) are the most common and aggressive primary human malignant brain tumors. 4-Hydroxy tamoxifen (OHT) is an active metabolite of the tamoxifen (TMX) prodrug and a well-established estrogen receptor (ER) and estrogen-related receptor antagonist. A recent study from our laboratory demonstrated that OHT induced ER-independent malignant peripheral nerve sheath tumor (MPNST) cell death by autophagic degradation of the prosurvival protein Kirsten rat sarcoma viral oncogene homolog. Because both MPNST and GBM are glial in cell origin, we hypothesized that OHT could mediate similar effects in GBM. OHT induced a concentration-dependent reduction in cell viability that was largely independent of caspase activation in a human GBM cell line and 2 patient-derived xenolines. Further, OHT induced both cytotoxic autophagy and a concentration-dependent decrease in epidermal growth factor receptor (EGFR) protein levels. A GBM cell line expressing EGFR variant III (EGFRvIII) was relatively resistant to OHT-induced death and EGFRvIII was refractory to OHT-induced degradation. Thus, OHT induces GBM cell death through a caspase-independent, autophagy-related mechanism and should be considered as a potential therapeutic agent in patients with GBM whose tumors express wild-type EGFR.

Key Words: Autophagy, Epidermal growth factor receptor (EGFR), Glioblastoma, Tamoxifen.

INTRODUCTION

Glioblastoma (GBM) is the most common and aggressive human primary malignant brain tumor with a median survival of 12–15 months in optimally treated patients and an overall 5-year survival rate of <5% (1). This tumor type consists predominantly of malignant glial astrocytes (2), although a recent report suggests a potential role for neuronal dedifferentiation in maintenance of heterogeneous GBM (3). Resistance to apoptosis is considered a hallmark of all cancer types (4) and GBM is particularly resistant to this death mechanism, in large part due to altered expression or mutations of apoptosis-related proteins such as p53, BCL-2, and BCL-X_L (5–7). Further, the DNA alkylating agent temozolomide (TMZ), currently the chemotherapeutic standard for GBM (8), extends patients' median survival by only 3 months (9). The poor response of GBM to TMZ is attributed to elevated expression (via promoter hypomethylation) of the DNA repair protein O^6-methylguanine-DNA methyltransferase (MGMT) (10, 11), resulting in specific repair of O^6-alkylguanine adducts generated by TMZ (12). Therefore, more effective chemotherapeutic options, particularly therapies that do not rely on induction of apoptosis, are needed for patients with GBM.

4-Hydroxy tamoxifen (OHT) is an active metabolite of the tamoxifen (TMX) prodrug (13) and a well-established estrogen receptor (ER) estrogen-related receptor antagonist (13, 14). Previous studies from our laboratory and others indicate a potential utility of OHT to induce tumor cell death independent of apoptosis (15, 16). An investigation into the effects of OHT on malignant peripheral nerve sheath tumors (MPNSTs) found an ER-independent inhibition of cell proliferation (15) and a subsequent study from our laboratory demonstrated and characterized OHT-induced MPNST cell death as nonapoptotic and mediated at least in part by autophagic degradation of the prosurvival protein Kirsten rat sarcoma (KRAS) (16). Given that MPNST and GBM tumors are both comprised of glial cells, we hypothesized that OHT may induce similar death mechanisms in GBM.

Autophagy is a conserved homeostatic mechanism that mediates the sequestration and removal of damaged organelles, misfolded proteins, and various other cellular components bound for lysosomal degradation (17, 18). Autophagy is also initiated in response to stress signals resulting from nutrient deprivation and/or growth factor withdrawal (19). Although normally considered to be a cell survival response, autophagy has also been shown to mediate cell death under certain circumstances (20). In addition to our published obser-

From the Department of Pathology (CDG, NK, BJK, LAS, SLC, KAR); and Department of Neurosurgery, University of Alabama at Birmingham (GYG), Birmingham, Alabama

Send correspondence to: Kevin A. Roth, MD, PhD, Columbia University Medical Center, Department of Pathology and Cell Biology, New York, NY 10032; E-mail: kar2208@cumc.columbia.edu

Present address: Steven L. Carroll, Department of Pathology and Laboratory Medicine, Medical University of South Carolina, Charleston, South Carolina.

Present address: Kevin A. Roth, Department of Pathology and Cell Biology, Columbia University Medical Center, New York, NY, USA.

This work was supported by National Cancer Institute grant CA134773 (K.A.R.) and Department of Defense grants W81XWH-14-1-0073 (K.A.R.), W81XWH-09-1-0086 (S.L.C.), and W81XWH-15-1-0193 (S.L.C.). Funding sources for this study had no involvement in study design, collection/analysis/interpretation of data, writing of the report, or decision to publish.

Conflict of interest: The authors have no duality or conflicts of interest to declare.

Supplementary Data can be found at http://www.jnen.oxfordjournals.org.

© 2016 American Association of Neuropathologists, Inc. All rights reserved.

Downloaded from http://jnen.oxfordjournals.org/ by guest on September 20, 2016

vations that OHT induces cytotoxic autophagy in MPNST cells (16), several studies have demonstrated that inhibition of autophagy *in vitro* (21) and *in vivo* (22–24) can suppress cell death induced by hypoxia/ischemia and in normal development. These studies implicate the autophagic process as a potential chemotherapeutic target for apoptosis-resistant malignancies.

Considering the pleiotropic effects of OHT, it is likely that 1 or more ER-independent mechanisms contribute to its observed cytotoxic action in hormonally insensitive neoplasms. In the context of GBM, TMX's mechanism of action has long been considered inhibition of Ca^{2+} signaling through protein kinase C (PKC) (25–28). Since Ca^{2+} can activate both PKC and calmodulin, we examined both signaling arms and effects were compared with OHT.

In this report, we extend our previous observation that OHT induces a reduction in epidermal growth factor receptor (EGFR) levels in MPNST and established GBM cell lines (16) by demonstrating OHT-mediated caspase-independent cell death in human GBM patient-derived xenolines (PDXs). Further, OHT-induced GBM cell death was accompanied by accelerated degradation of EGFR and this effect was recapitulated by inhibition of Ca^{2+} signaling. Importantly, a GBM cell line expressing EGFR variant III (EGFRvIII) was relatively resistant to OHT-induced death and EGFRvIII was refractory to OHT-induced degradation, suggesting that the potential use of OHT in GBM patients should be limited to those tumors expressing wild-type (WT) EGFR.

MATERIALS AND METHODS

Antibodies and Other Reagents

Primary antibodies were obtained from the following sources: LC3 (Abgent, San Diego, CA #AM1800a), EGFR (EMD Millipore, Billerica, MA #06-847), EGFRvIII (Biorbyt, Berkeley, CA #orb47907), ATG5 (Cell Signaling, Danvers, MA #8540), GAPDH (Cell Signaling, #2118), AKT (Cell Signaling #9272), phosphorylated AKT (pAKT) S473 (Cell Signaling #9271), pAKT T308 (Cell Signaling #4056), and β-tubulin (Santa Cruz Biotechnology, Dallas, TX #sc-9104). Secondary antibodies were HRP-conjugated goat anti-rabbit (Bio-Rad, Hercules, CA #1662408) and horse anti-mouse (Cell Signaling #7076). OHT was obtained from EMD Millipore (#579002). BOC-aspartyl (Ome)-fluoromethyl ketone (BAF) was purchased from MP Biomedicals (Santa Ana, CA #03FK011). Bafilomycin A1 (Baf A1) was purchased from AG Scientific (San Diego, CA #B1183). Staurosporine was obtained from Sigma (St Louis, MO # S5921). Ro-31-8220 (Ro-31) was purchased from Tocris (Bristol, UK #125314-64-9); trifluoperazine (TFP) and cycloheximide (CHX) were purchased from Sigma (#T8516 and #C1988, respectively).

Cell Culture

U87MG cells (referred to hereafter as U87) were cultured in DMEM containing 1% penicillin/streptomycin (Invitrogen, Carlsbad, CA), 1% L-glutamine (Sigma), and 10% fetal bovine serum (Fisher Scientific, Waltham, MA). U87MG cells stably expressing EGFRvIII (U87vIII) were provided by Dr G Yancey Gillespie of the University of Alabama at Birmingham. The origin of U87vIII cells has been previously described by Mishima et al (29). JX6 and X1016 GBM PDXs were obtained from Dr G. Yancey Gillespie (IRB approval X050415007) and cultured in neurobasal media (Fisher Scientific #21103-049) supplemented with EGF (Fisher Scientific #PHG0311, 10 ng/mL) and fibroblast growth factor (Fitzgerald, Acton, MA #30R-AF014, 10 ng/mL). The genetic characteristics of our human GBM PDXs are as follows: X1016: Classical, WT *EGFR*, WT *CDK4*, WT *PTEN*, WT *TP53*, *CDK4N* null, undetermined *MGMT*; JX6: Classical, amplified *EGFRvIII*, WT *CDK4*, WT *PTEN*, WT *TP53*, *CDK4N* null, unmethylated *MGMT*. All cells were incubated at 37 °C in a humidified 5% CO2, 95% air atmosphere. For cell viability studies and caspase 3-like enzymatic activity assays, cells were plated on 48 well-plates at a density of 25 000 cells/well- JX6 and X1016; 40 000 cells/well- U87 and U87vIII. For flow analyses and lysate collection, cells were plated on 100 mm dishes at a density of: 1.25×10^6 cells/dish- JX6 and X1016; 2×10^6 cells/dish- U87 and U87vIII. Cultures were used in experiments 24 hours postplating. Drug treatments were performed in respective media supplemented with 2% fetal bovine serum to reduce effective drug concentrations.

Cell Viability and Caspase Cleavage Assays

The calcein-AM conversion assay (Life Technologies, Carlsbad, CA C3100MP) was employed to quantify viable cell number after drug treatment. Caspase 3 cleavage was assessed using the chemical substrate DEVD-7-amino-4-methylcoumarin (AMC) (Enzo Life Sciences #ALX-260-031). Both assays were performed as previously described (30).

Calcein/Ethidium Homodimer Staining

The LIVE/DEAD Viability/Cytotoxicity Kit (Fisher Scientific, #V13241) was used to determine cell death following 24 hours of OHT treatment per the manufacturer's instructions. Samples were analyzed with a VACalibur flow cytometer (Becton Dickinson) using a 488-nm laser for calcein and a 647-nm laser for ethidium homodimer-1. Analysis was performed using CellQuest software, version 3.3.

Western Blotting

Whole cell lysates were prepared by aspirating media, washing cells with 1X PBS, removing cells with a cell lifter, and pelleting by centrifugation at 13000*g* for 10 minutes. Cell pellets were resuspended in lysis buffer containing 20 mM Tris–HCl (pH 7.4), 150 mM NaCl, 2 mM EDTA, 1% Triton X-100, 10% glycerol, and a protease/phosphatase inhibitor cocktail (Fisher Scientific #1861281). After 3 rounds of 10 minutes incubation on ice and 1 minute vortex, lysates were clarified by centrifugation at 13 000*g* for 10 minutes at 4 °C. Supernates were quantified using Pierce BCA Protein Assay Kit (Fisher Scientific #23225) and transferred to new microfuge tubes to be stored at −80 °C. Thirty-five micrograms of protein was immunoblotted per our previously described protocol (31). Primary antibodies were used at the following concentrations: LC3 (1 μg/mL), EGFR (1 μg/mL), EGFRvIII

Downloaded from http://jnen.oxfordjournals.org/ by guest on September 20, 2016

(1 μg/mL), ATG5 (0.852 μg/mL), GAPDH (0.00484 μg/mL), AKT (0.083 μg/mL), pAKT S473 (0.01 μg/mL), pAKT T308 (0.035 μg/mL), and β-tubulin (0.2 μg/mL). Secondary antibodies were HRP-conjugated goat anti-rabbit and horse anti-mouse used at 0.18 μg/mL and 0.17 μg/mL, respectively. Immunoreactive species were detected by enhanced chemiluminescence (Pierce ECL; Fisher Scientific #32106) using Classic Blue Autoradiography Film BX (MidSci #EBNU2; St. Louis, MO) and a Konica SRX-101A tabletop processor.

Immunocytochemistry

EGFR (Cell Signaling #4267) primary antibody and rabbit serum (Jackson ImmunoResearch, West Grove, PA #011-000-001) were both used at 0.00017 mg/mL. Super Picture (Invitrogen #87-9263) secondary antibody was used at 0.008 μg/mL. Immunoreactivity was detected using a tyramide signal amplification system using a Cy3 fluorophore (0.00013mg/mL) (Perkin-Elmer Life Science Products, Waltham, MA #NEL744). Hoechst (Sigma #33258, 0.02mg/mL) was used for nuclear counterstaining. Samples were examined with a Nikon A1 laser confocal microscope using a 60× plan Apo objective and a 405-nm laser for Hoechst or 561-nm laser for Cy3. Images were analyzed using NIS Elements 4.2 software.

RNA_i

ATG5 siRNA (siGENOME SMARTPool) was purchased from Thermo Scientific and reconstituted according to the manufacturer's instructions. Cells were plated in DMEM-10 and transfected 24 hours postplating using X-tremeGene siRNA transfection reagent (Roche, Indianapolis, IN #04-476-093-001) at a ratio of 5:2 (transfection reagent:siRNA). Cells were used in experiments 48 hours posttransfection. *ATG5* and nontarget (NT) siRNA sequences (used as an equimolar mixture for targeting multiple transcript sequences) are as follows: (1) 5′-GGAAUAUCCUGCAGAAGAA-3′; (2) 5′-CAUCUGAGCUACCCGGAUA-3′; (3) 5′-GACAAGAAGACAUUAGUGA-3′; and (4) 5′-CAAUUGGUUUGCUAUUUGA-3′. NT siRNA sequences: (1) 5′-UAGCGACUAAACACAUCAA-3′; (2) 5′-UAAGGCUAUGAAGAGAUAC-3′; (3) 5′-AUGUAUUGGCCCUGUAUUAG-3′; and (4) 5′-AUGAACGUGAAUUGCUACAA-3′.

Statistics

All data points represent mean ± SD. All experiments were repeated at least 3 times unless otherwise stated. Statistical significance was determined by ANOVA followed by Dunnett's post hoc test. A p value < 0.05 was considered significant.

RESULTS

OHT Mediates Caspase-Independent Cell Death in Human GBM Cells

One established human GBM cell line (U87) and 2 PDXs (JX6 and X1016) were used to assess OHT's effects on GBM cell viability. In all 3 lines tested, OHT induced a concentration-dependent decrease in viable cell number after 24 hours (Fig. 1A; Supplementary Fig. 1). To gain insight into the mechanism of OHT-induced reduction in GBM cell number, a DEVD-AMC caspase 3-like enzymatic activity assay was performed in tandem with viability studies. After 24 hours of OHT, both PDXs exhibited an induction of caspase 3-like enzymatic activity; in contrast, no increased activity was detected in U87 cells (Fig. 1B). To assess whether caspase activity was mediating the observed OHT-induced reduction in cell viability, a broad-spectrum caspase inhibitor, BAF, was used in combination with OHT and viability was assessed in JX6 cells because these exhibited the greatest caspase 3-like activity following OHT treatment. Although BAF completely suppressed OHT-induced caspase 3-like enzymatic activity (Fig. 1C), it produced only a slight but significant inhibition of OHT-induced reduction in cell viability (Fig. 1D). In keeping with the observation that OHT had no effect on caspase 3-like enzymatic activity in U87 cells, BAF had no effect on the OHT-induced loss of cell viability in U87 cells (data not shown). These data support the conclusion that caspase activity is not critical for the death promoting effects of OHT on glioma cells. To verify that the OHT-induced reduction in viable GBM cell numbers was a function of cytotoxic rather than cytostatic effects, flow cytometric analysis of calcein/ethidium homodimer double staining was performed on U87 cells after 24 hours of OHT treatment and a concentration-dependent increase in ethidium homodimer-positive (dead/dying) cells was observed (Fig. 1E). These data indicate that OHT induces a predominantly caspase-independent cell death in human GBM cells, although a statistically significant increase in caspase 3-like activity was observed.

OHT Induces Cytotoxic Autophagy in Human GBM Cells

Based on our previously published observation that OHT induces cytotoxic autophagy in MPNST cells, we hypothesized that similar effects would be observed in GBM cells. During formation of autophagic vacuoles (AV) in the early stages of autophagy, microtubule-associated protein 1 light chain 3α (LC3-I) is cleaved and lipidated to form LC3-II, a molecule requisite for AV formation (32). Accordingly, we first assessed levels of LC3-II after 24 hours OHT treatment and found a concentration-dependent increase of LC3-II in all 3 cell lines tested (Fig. 2A). It is important to note that LC3I/LC3II ratios possess significant variability between cells and tumor types. Further, our lab has previously reported considerable variability in baseline autophagy and the levels of LC3I and LC3II in human GBM PDXs (33). The antibody used to detect LC3 used in this study detects both LC3I and LC3II. Low levels of LC3I in both PDXs likely reflect a high rate of baseline autophagy and rapid conversion of LC3I to LC3II. Because elevated LC3-II levels can result from induction of AV formation as well as impairment of lysosomal AV clearance, we examined the effects of OHT on LC3-II levels in U87 cells in the presence and absence of Bafilomycin A1 (Baf A1), a vacuolar ATPase inhibitor that inhibits AV fusion with lysosomes and the subsequent degradation of AV content. When AV clearance is inhibited by Baf A1, OHT imparts an

Downloaded from http://jnen.oxfordjournals.org/ by guest on September 20, 2016

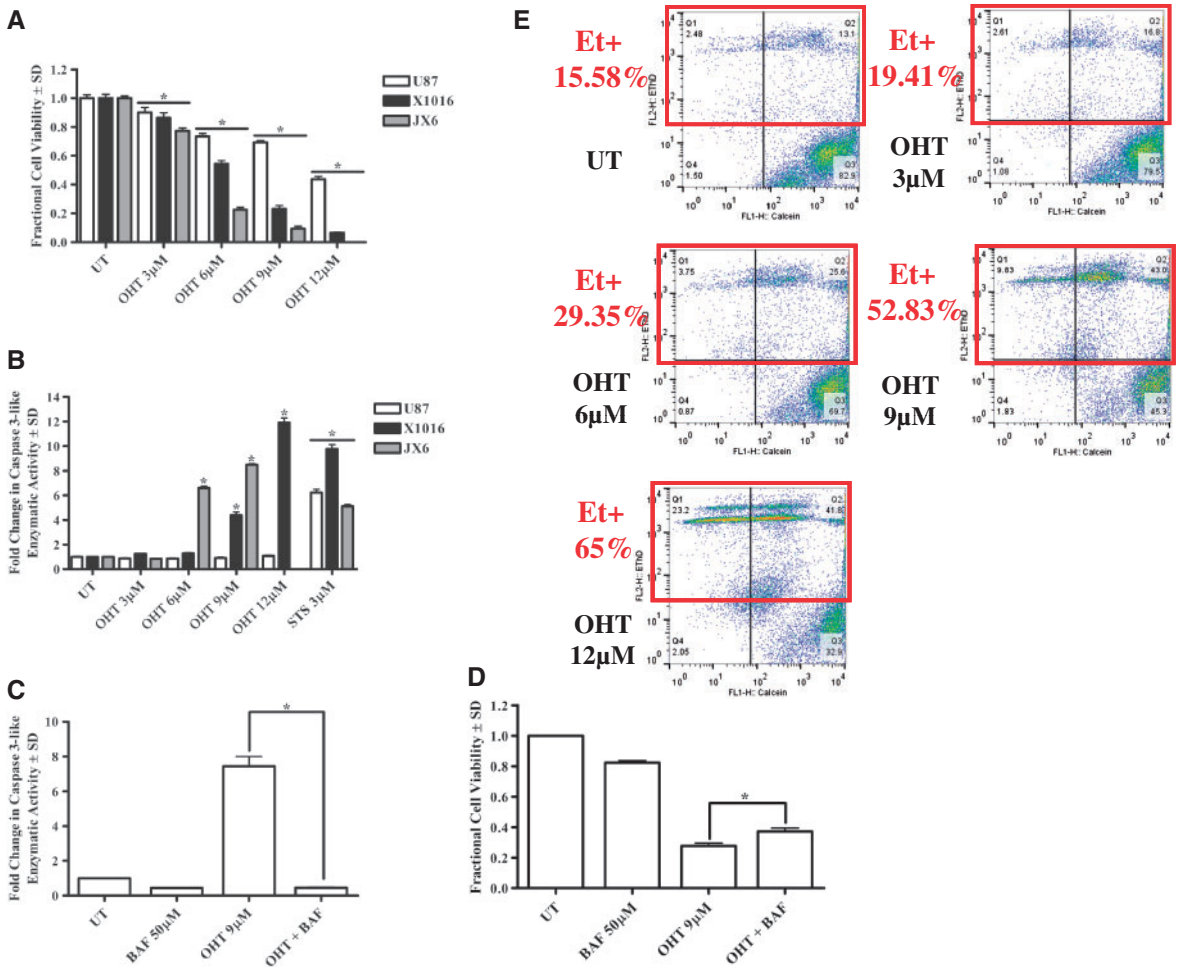


FIGURE 1. 4-Hydroxy tamoxifen (OHT) mediates caspase-independent cell death in human Glioblastoma cells. **(A)** OHT-treated cells demonstrate a concentration-dependent decrease in viable cell number after 24 hours. **(B)** Loss of cell viability is accompanied by significant caspase 3-like enzymatic activity in JX6 and X1016 cells. **(C** and **D)** Broad caspase inhibition with BOC-aspartyl (Ome)-fluoromethyl ketone modestly but significantly attenuates OHT-mediated reduction in JX6 cell viability. **(E)** OHT treatment (24 hours) produces a concentration-dependent increase in ethidium homodimer-positive (Et+) U87 cells. *$p < 0.05$. UT, untreated.

additional increase in LC3-II accumulation (Fig. 2B), indicating that OHT induces AV formation rather than simply inhibiting AV clearance. Because autophagy is typically a prosurvival cellular response and can be observed in degenerating cells without being directly involved in the cell death process per se, we evaluated the ability of OHT to kill GBM cells when AV formation was genetically inhibited. Accordingly, we performed siRNA knockdown of ATG5, a protein required for conversion of LC3-I to LC3-II (34, 35) in U87 cells. A partial knockdown of *ATG5* (46%) (Fig. 2C) resulted in a 60% reduction of OHT-induced LC3-II accumulation (Fig. 2D), verifying that a functional impairment of autophagy induction was achieved by *ATG5* knockdown. This partial inhibition of AV formation was sufficient to produce significant inhibition of OHT-induced cell death in 2 biological replicates (Fig. 2E). Taken together, these data support the conclusion that OHT mediates GBM cell death, at least in part, via induction of cytotoxic autophagy.

OHT Promotes Accelerated Degradation of EGFR

We previously showed that OHT mediates human MPNST cell death via autophagic degradation of the prosurvival protein KRAS and was additionally accompanied by a reduction in EGFR levels (16). The hypothesis that OHT induces degradation of EGFR in GBM cells is supported by both the shared lineage of MPNST and GBM cells (36, 37), and the observation that EGFR has been shown to colocalize with KRAS en route to degradation (38). Given the highly relevant contribution of EGFR to GBM growth and invasiveness (39), we evaluated the effects of OHT on this oncogenic kinase in greater detail. For these studies, we utilized the human GBM cell line U87 as well as an isogenic line stably expressing EGFRvIII (referred to hereafter as U87vIII). EGFRvIII possesses a deletion of exons 2–7, resulting in the inability to bind any currently characterized ligand due to lack of an extracellular domain (40). However, EGFRvIII confers a low level of

Downloaded from http://jnen.oxfordjournals.org/ by guest on September 20, 2016

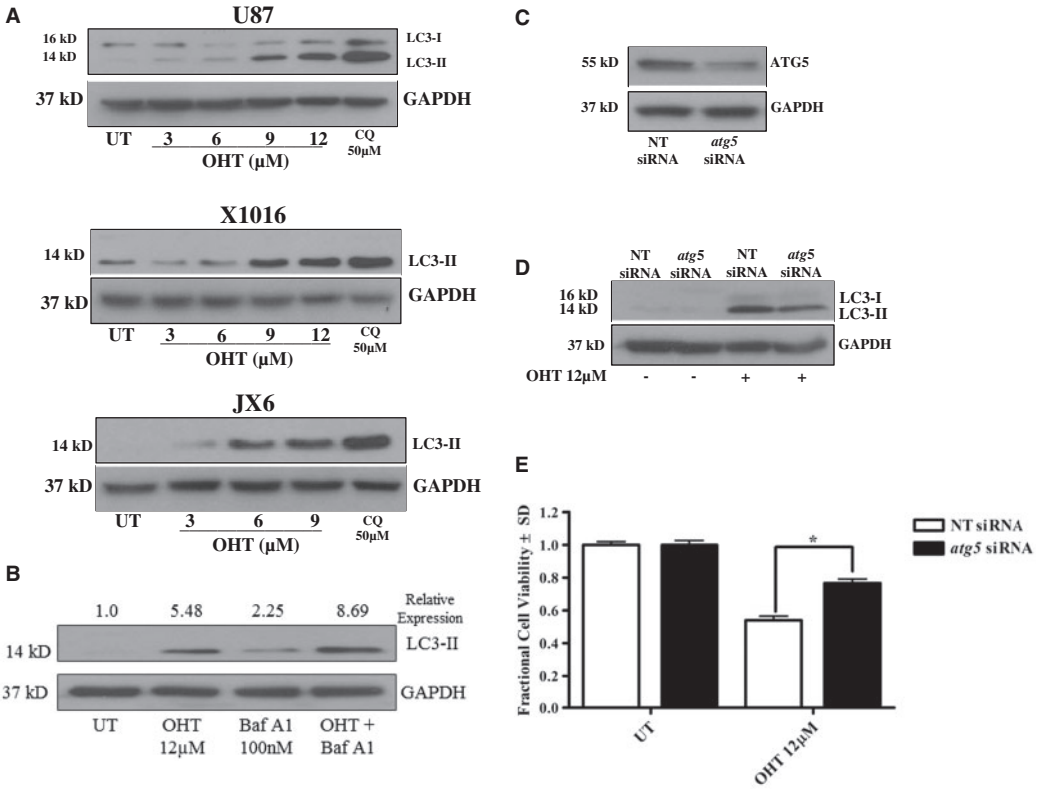


FIGURE 2. OHT-induced autophagy is cytotoxic. **(A)** Treatment with OHT (24 hours) yields a concentration-dependent increase in levels of LC3-II in U87, X1016, and JX6 cells. **(B)** OHT increases autophagic flux as indicated by increased levels of LC3-II in U87 cells treated with both OHT and Baf A1 (100 nM) relative to OHT or Baf A1 alone. **(C** and **D)** siRNA knockdown of atg5 (C) results in a 40% decrease in OHT-induced LC3-II accumulation (D), demonstrating a functional inhibition of autophagy. **(E)** atg5 knockdown results in significant protection from OHT-induced reduction in cell viability. Chloroquine (CQ) (50 μM) was used as a positive control for LC3-II accumulation. *$p < 0.05$. UT, untreated.

constitutive signaling resulting from impaired internalization and increased protein stability (41). Although multiple mutant forms of EGFR exist in GBM (42–44), EGFRvIII is the most common (44, 45). We first collected total protein from U87 and U87vIII cells after 24 hours treatment with OHT. Western blot analysis revealed a concentration-dependent decrease of EGFR in U87 but not of EGFRvIII in U87vIII cells (Fig. 3A). Although EGFR in U87 cells was evaluated 3 times, we queried EGFRvIII in U87vIII cells once. The observation that EGFRvIII levels are unaffected by OHT is possibly a result of its impaired internalization (41). Importantly, U87vIII cells are relatively refractory to OHT-induced reduction in viable cell number (Fig. 3B), suggesting that degradation of EGFR contributes to the cytotoxic effects of OHT on WT EGFR-expressing GBM cells. To determine if the observed reduction of EGFR was a function of accelerated degradation rather than suppression of protein expression, we treated U87 cells with OHT with or without 100 μM CHX, a well-established protein synthesis inhibitor. Not surprisingly given the long half-life of EGFR and the relatively short time course of the experiment (46), no decrease in EGFR was observed in the presence of CHX alone whereas CHX + OHT resulted in a significant time-dependent reduction in EGFR levels in 2 separate biological replicates (Fig. 3C). To extend these results to GBM PDXs, we examined EGFR protein levels following 24 hour OHT treatment of JX6 cells via Western blot (Fig. 3D) and by immunocytochemistry (ICC) (Fig. 3E). We observed a reduction in EGFR protein levels in 3 separate replicate experiments and EGFR-like immunoreactivity in the single experiment performed. Although Western blot data was repeated at least 3 times, ICC was performed only once. Finally, we investigated the downstream effects of OHT on EGFR signaling and observed a marked decrease in pAKT (S473) after 24 hours of OHT treatment in U87 cells (Fig. 3F). This observation was extended into GBM PDXs, as JX6 cells (Fig. 3G) also exhibited reduction in pAKT in 2 separate biological replicates. These data confirm a biological response to EGFR reduction in both established human GBM cells and PDXs. Taken together these data support the hypothesis that OHT mediates cytotoxic autophagy in human GBM cells at least in part by decreasing EGFR protein levels and signaling through AKT.

PKC Inhibition Recapitulates Effects of OHT on EGFR

Inhibition of Ca^{2+} flux through endoplasmic reticulum Ca^{2+} release channels triggers rapid autophagy (47, 48) and active PKC has been shown to inhibit autophagy (49). Because

Downloaded from http://jnen.oxfordjournals.org/ by guest on September 20, 2016

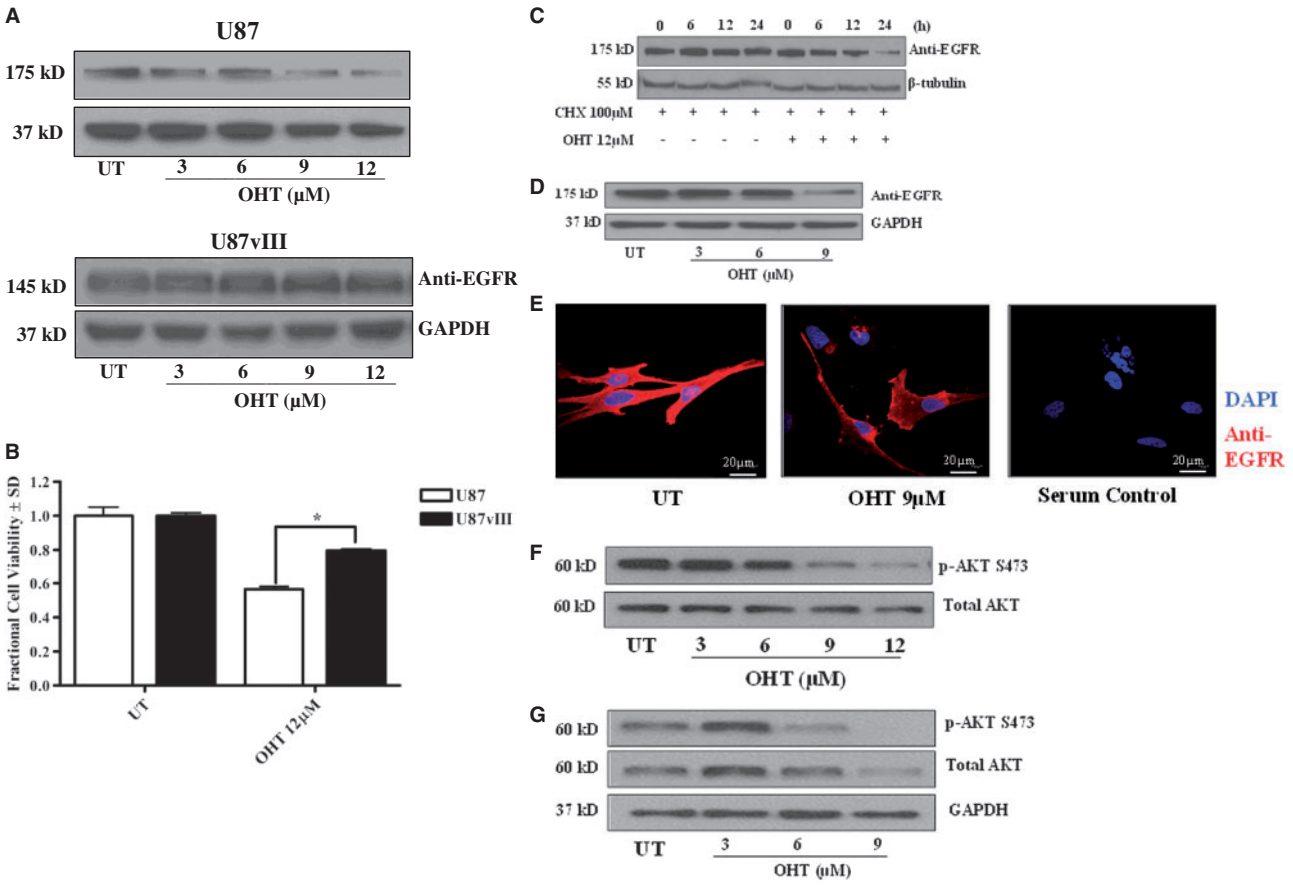


FIGURE 3. OHT accelerates degradation of epidermal growth factor receptor (EGFR). **(A)** Treatment with OHT (24 hours) results in a concentration-dependent decrease in EGFR protein levels in U87 but not U87vIII cells. **(B)** U87 cells possessing EGFRvIII (U87vIII) are significantly less sensitive to OHT's reduction in cell viability as determined by a calcein-AM conversion assay *$p < 0.001$. **(C)** Whole cell lysates from OHT-treated U87 cells demonstrate a time-dependent decrease in EGFR in the presence of the protein synthesis inhibitor cycloheximide. **(D)** EGFR protein levels are reduced in JX6 cells as determined by Western blot following OHT exposure. **(E)** Anti-EGFR immunoreactivity is reduced in JX6 cells as determined by immunocytochemistry following 24 hours of OHT exposure. **(F** and **G)** Treatment with OHT (24 hours) mediates a marked reduction in active (phosphorylated) AKT (p-AKT S473) in U87 **(F)** and JX6 **(G)** cells. UT, untreated.

OHT is known to inhibit Ca^{2+} signaling in GBM (50–52), which exerts a negative regulatory effect on autophagy (49), it is possible that Ca^{2+} signaling modulation mediates the observed effects of OHT on autophagy. Previous studies from our laboratory and others have demonstrated that inhibition of signaling through PKC can recapitulate various effects of OHT (15, 16). These investigations were based on observations made in the 1990s that TMX inhibits PKC activity (53, 54). We hypothesized that the effects of OHT on EGFR were dependent, at least in part, on Ca^{2+} signaling inhibition. To test this hypothesis, we collected total protein following treatment of U87 cells with OHT or 2 known Ca^{2+} signaling modulators that antagonize separate arms of Ca^{2+} signaling: Ro-31-8220 (Ro-31) inhibits PKC while TFP inhibits calmodulin. As expected, reduction in EGFR was observed in all drug treatments (Fig. 4A). We next queried levels of pAKT at both phosphorylation sites (S473 and T308) and observed that, as with OHT, activation of AKT was markedly inhibited by TFP while Ro-31 had no effect (Fig. 4B). These data demonstrate that Ca^{2+} modulation phenocopies the observed effects of OHT on EGFR and downstream signaling, suggesting that the effects of OHT on GBM cells are at least in part a function of Ca^{2+} signaling modulation.

DISCUSSION

GBM are the most common and deadly form of human primary malignant brain tumor (8). Patients receiving radiotherapy plus the most efficacious chemotherapeutic option, TMZ, exhibit only a slight increase in median survival from 12.2 to 14.6 months compared with radiotherapy alone (55). Compounding this dismal prognosis is the fact that roughly 50% of GBMs express the DNA repair enzyme MGMT and are consequently resistant to TMZ (10–12). Contributing significantly to GBM's resistance to other chemotherapeutic approaches is its ability to evade apoptosis. GBM cells exhibit marked overexpression of anti-apoptotic proteins such as BCL-2, BCL-X_L, and MCL-1 (5, 56), in addition to inactivation of

Downloaded from http://jnen.oxfordjournals.org/ by guest on September 20, 2016

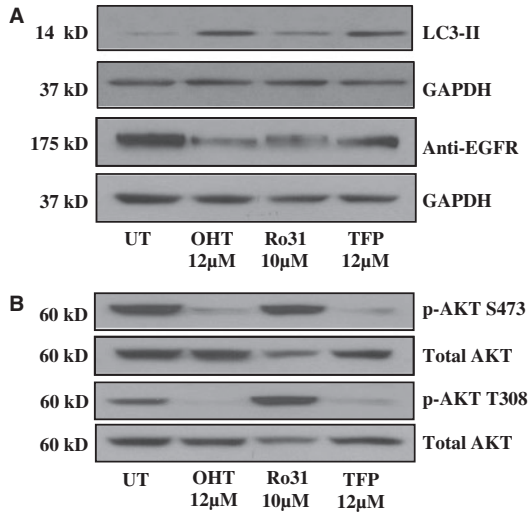


FIGURE 4. Inhibition of protein kinase C (PKC) recapitulates the effects of OHT on EGFR. **(A)** PKC inhibitors Ro31 and trifluoperazine (TFP) increase LC3-II accumulation and reduce EGFR protein levels after 24 hours as determined by Western blot. **(B)** Phosphorylation of AKT at both S473 and T308 is markedly reduced by OHT and TFP but not Ro31 in U87 cells after 24 hours of treatment.

p53, a critical proapoptotic protein (7). Considered together, additional chemotherapeutic options for GBM are desperately needed and therapies that do not rely on induction of apoptosis are a logical avenue of exploration.

The goal of this study was to explore the effects of OHT on GBM cells in vitro in an effort to provide a rationale for further investigations of OHT in GBM chemotherapy *in vivo*. In support of our hypothesis that OHT can exert cytotoxic effects on GBM cells, we demonstrate a concentration-dependent increase in GBM cell death following OHT treatment. Although OHT is typically utilized as an ER antagonist in the treatment of ER-positive breast cancer, several studies have shown that ER-negative malignancies also respond to OHT (57, 58). Further, OHT variably induces caspase 3-like activity in GBM cells and OHT-induced cell death is largely unaffected by broad-spectrum caspase inhibition, suggesting a caspase-independent cell death mechanism. Because many GBM cells are resistant to apoptotic induction (5–7), the lack of strong caspase 3-like activity after OHT exposure is not surprising. These data support the conclusion that OHT might prove useful in the treatment of patients whose tumors are refractory to apoptosis-targeting therapies.

Because OHT is known to induce autophagy in some cell types (59), we queried protein levels of LC3-II, a surrogate marker of AVs. We observed a concentration-dependent increase in LC3-II accumulation upon treatment with OHT that was further increased upon inhibition of lysosomal function with Baf A1. These data confirmed that OHT-induced autophagy in human GBM cells. Further, genetic inhibition of autophagy via partial *ATG5* knockdown in GBM cells imparted a significant protection from OHT-induced cell death. Taken together, our data support the conclusion that OHT induces human GBM cell death that at least in part results from cytotoxic autophagy.

Enhanced EGFR signaling, either through overexpression of WT EGFR or activating mutations, occurs commonly in GBM (60, 61); thus, in addition to the WT receptor, we also examined the effects of OHT on the most common EGFR mutant variant, EGFRvIII (44, 45). In contrast to the WT receptor, EGFRvIII was not only refractory to OHT-induced degradation, but it also conferred a survival advantage to U87 cells when challenged with OHT. Because EGFRvIII protein is stable in the presence of OHT and promotes a survival advantage, we speculate that accelerated degradation of WT EGFR plays a role in OHT-induced human GBM cytotoxicity. Studies from *The Cancer Genome Atlas* have defined 4 relatively distinct molecular subtypes of GBM: classical, mesenchymal, neural, and proneural (62). Given that classical GBM is characterized by aberrations in EGFR expression (63), this subtype might prove more responsive to OHT treatment than its mesenchymal, neural, or proneural counterparts. Our data provide a potential explanation for observations made in various clinical trials of TMX in GBM suggesting a 20%–40% response rate (64, 65). Considering that these trials were performed only on the basis of histologically defined GBM, patient stratification based on molecular subtype and EGFR mutation status has the potential to improve response rates.

Finally, given the literature connecting OHT and autophagy with Ca^{2+} modulation, we compared OHT with 2 specific Ca^{2+} signaling inhibitors and observed an induction of autophagy concurrent with decreased protein levels of WT EGFR and inhibition of downstream signaling (AKT) with most drugs tested. These data support previous work suggesting a role for Ca^{2+} signaling modulation in the effects of OHT on human GBM cell viability (64) and suggest a novel role for OHT and PKC inhibitors in modulation of steady state EGFR protein levels.

In summary, this study elucidated a novel mechanism of action for OHT in human GBM cells in which cytotoxicity is at least in part autophagy-dependent and occurs concurrently with accelerated degradation of EGFR. Although autophagy is typically a survival-promoting process, its cell death promoting function is recognized and characterized histologically by the large scale sequestration of portions of the cytoplasm in AVs, giving the cell a characteristic vacuolated appearance (66). We utilized established techniques to assess autophagy as well as flux through the pathway (67) and have demonstrated that partial inhibition of autophagy protects against the cytotoxic effects of OHT in human GBM cells. Additional studies are needed to determine if the effects of OHT on EGFR might prove useful in the context of other malignancies that are driven by this oncogenic kinase, such as nonsmall cell lung carcinoma (68). TMX's FDA-approved status (69) provides a basis for expeditious repurposing of this drug to non-ER driven tumor types.

ACKNOWLEDGEMENTS

The authors thank Shawn Williams of the University of Alabama at Birmingham (UAB) High Resolution Imaging Facility (supported by the Cancer Center Support Grant CA013148 and the Rheumatic Disease Core Center Grant AR048311) for his expertise and guidance with confocal imaging, Terry Lewis and Marissa Menard of the University of

Downloaded from http://jnen.oxfordjournals.org/ by guest on September 20, 2016

Alabama at Birmingham (UAB) Molecular Detection Core (supported by grant NS0474666) for assistance with immunocytochemistry, and Enid Keyser of the University of Alabama at Birmingham (UAB) Flow Cytometry Core (supported by grants AR048311 and AI027767) for support with flow cytometry analysis.

REFERENCES

1. Gallego O. Nonsurgical treatment of recurrent glioblastoma. Curr Oncol 2015;22:e273–81
2. Aldape K, Zadeh G, Mansouri S, et al. Glioblastoma: Pathology, molecular mechanisms and markers. Acta Neuropathol 2015;129:829–48
3. Friedmann-Morvinski D, Bushong EA, Ke E, et al. Dedifferentiation of neurons and astrocytes by oncogenes can induce gliomas in mice. Science 2012;338:1080–4
4. Hanahan D, Weinberg RA. The hallmarks of cancer. Cell 2000;100: 57–70
5. Tagscherer KE, Fassl A, Campos B, et al. Apoptosis-based treatment of glioblastomas with ABT-737, a novel small molecule inhibitor of Bcl-2 family proteins. Oncogene 2008;27:6646–56
6. Krakstad C, Chekenya M. Survival signaling and apoptosis resistance in glioblastomas: Opportunities for targeted therapeutics. Mol Cancer 2010; 9:135–48
7. Cancer Genome Atlas Network. Comprehensive genomic characterization defines human glioblastoma genes and core pathways. Nature 2008; 455:1061–8
8. Omuro A, DeAngelis LM. Glioblastoma and other malignant gliomas: A clinical review. JAMA 2013;310:1842–50
9. Stupp R, Mason WP, van den Bent MJ, et al. Radiotherapy plus concomitant and adjuvant temozolomide for glioblastoma. N Engl J Med 2005; 352:987–96
10. Esteller M, Garcia-Foncillas J, Andion E, et al. Inactivation of the DNA-repair gene MGMT and the clinical response of gliomas to alkylating agents. N Engl J Med 2000;343:1350–4
11. Hegi ME, Diserens AC, Godard S, et al. Clinical trial substantiates the predictive value of 0-6-methylguanine-DNA methyltransferase promoter methylation in glioblastoma patients treated with temozolomide. Clin Cancer Res 2004;10:1871–4
12. Nakamura M, Watanabe T, Yonekawa Y, et al. Promoter methylation of the DNA repair gene MGMT in astrocytomas is frequently associated with G:C → A:T mutations of the TP53 tumor suppressor gene. Carcinogenesis 2001;22:1715–9
13. Lim YC, Desta Z, Flockhart DA, et al. Endoxifen (4-hydroxy-N-desmethyl-tamoxifen) has anti-estrogenic effects in breast cancer cells with potency similar to 4-hydroxy-tamoxifen. Cancer Chemother Pharmacol 2005;55:471–8
14. Clarke R, Leonessa F, Welch JN, et al. Cellular and molecular pharmacology of antiestrogen action and resistance. Pharmacol Rev 2001;53: 25–71
15. Byer SJ, Eckert JM, Brossier NM, et al. Tamoxifen inhibits malignant peripheral nerve sheath tumor growth in an estrogen receptor-independent manner. Neuro Oncol 2011;13:28–41
16. Kohli L, Kaza N, Coric T, et al. 4-Hydroxytamoxifen induces autophagic cell death through K-Ras degradation. Cancer Res 2013;73: 4395–405
17. Eskelinen EL. New insights into the mechanisms of macroautophagy in mammalian cells. Int Rev Cell Mol Biol 2008;266:207–47
18. Kundu M, Thompson CB. Autophagy: Basic principles and relevance to disease. Annu Rev Pathol 2008;3:427–55
19. Eskelinen EL, Saftig P. Autophagy: A lysosomal degradation pathway with a central role in health and disease. Biochem Biophys Acta 2009; 1793:664–73
20. Tsujimoto Y, Shimizu S. Another way to die: Autophagic programmed cell death. Cell Death Differ 2005;12(Suppl 2):1528–34
21. Maiuri MC, Zalckvar E, Kimchi A, et al. Self-eating and self-killing: Crosstalk between autophagy and apoptosis. Nat Rev Mol Cell Biol 2007;8:741–52
22. Samara C, Syntichaki P, Tavernarakis N. Autophagy is required for necrotic cell death in *Caenorhabditis elegans*. Cell Death Differ 2008;15: 105–12
23. Berry DL, Baehrecke EH. Growth arrest and autophagy are required for salivary gland cell degradation in Drosophila. Cell 2007;131:1137–48
24. Koike M, Shibata M, Tadakoshi M, et al. Inhibition of autophagy prevents hippocampal pyramidal neuron death after hypoxic-ischemic injury. Am J Pathol 2008;172:454–69
25. Ahn SJ, Yoon MS, Hyuk S, et al.Phospholipase C-protein kinase C mediated phospholipase D activation pathway is involved in tamoxifen induced apoptosis. J Cell Biochem 2003;89:520–8
26. Baltuch GH, Couldwell WT, Villemure JG, et al. Protein kinase C inhibitors suppress cell growth in established and low-passage glioma cell lines. A comparison between staurosporine and tamoxifen. Neurosurgery 1993;33:495–501
27. Couldwell WT, Antel JP, Apuzzo ML, et al. Inhibition of growth of established human glioma cell lines by modulators of the protein kinase-C system. J Neurosurg 1990;73:594–600
28. Horgan K, Cooke E, Hallett MB, et al. Inhibition of protein kinase C mediated signal transduction by tamoxifen. Importance of antitumor activity. Biochem Pharmacol 1986;35:4463–5
29. Mishima K, Johns TG, Luwor RB, et al. Growth suppression of intracranial xenografted glioblastomas overexpressing mutant epidermal growth factor receptors by systemic administration of monoclonal antibody (mAb) 806, a novel monoclonal antibody directed to the receptor. Cancer Res 2001;61:5349–54
30. Geng Y, Kohli L, Klocke BJ, et al. Chloroquine-induced autophagic vacuole accumulation and cell death in glioma cells is p53 independent. Neuro Oncol 2010;12:473–81
31. Walls KC, Ghosh AP, Franklin AV, et al. Lysosome dysfunction triggers Atg7-dependent neural apoptosis. J Biol Chem 2010;285:10497–507
32. Tanida I, Ueno T, Kominami E. LC3 and autophagy. Methods Mol Biol 2008;445:77–88
33. Kaza N, Kohli L, Roth KA. Autophagy in brain tumors: A new target for therapeutic intervention. Brain Pathol 2012;22:89–98
34. Mizushima N, Yamamato A, Hatano M, et al. Dissection of autophagosome formation using Apg5-deficient mouse embryonic stem cells. J Cell Biol 2001;152:657–68
35. Mizushima N, Noda T, Yoshimori T, et al. A protein conjugation system essential for autophagy. Nature 1998;395:395–8
36. Woodhoo A, Sommer L. Development of the Schwann cell lineage: From the neural crest to the myelinated nerve. Glia 2008;56:1481–90
37. Jessen KR, Mirsky R. The origin and development of glial cells in peripheral nerves. Nat Rev Neurosci 2005;6:671–82
38. Lu A, Tebar F, Alvarez-Moya B, et al. A clathrin-dependent pathway leads to KRas signaling on late endosomes en route to lysosomes. J Cell Biol 2009;184:863–79
39. Tsatsanis C, Spandidos DA. The role of oncogenic kinases in human cancer. Int J Mol Med 2000;5:583–90
40. Gan HK, Cvrljevic AN, Johns TG. The epidermal growth factor receptor variant III (EGFRvIII): Where the wild things are altered. FEBS J 2013; 280:5350–70
41. Huang HS, Nagane M, Klingbeil CK, et al. The enhanced tumorigenic activity of a mutant epidermal growth factor receptor common in human cancers is mediated by threshold levels of constitutive tyrosine phosphorylation and unattenuated signaling. J Biol Chem 1997;272:2927–35
42. Libermann TA, Nusbaum HR, Razon N, et al. Amplification, enhanced expression and possible rearrangement of EGF receptor gene in primary human brain tumors of glial origin. Nature 1985;313:144–7
43. Wong AJ, Ruppert JM, Bigner SH, et al. Structural alterations of the epidermal growth factor receptor gene in human gliomas. Proc Natl Acad Sci USA 1992;89:2965–9
44. Frederick L, Wang XY, Eley G, et al. Diversity and frequency of epidermal growth factor receptor mutations in human glioblastomas. Cancer Res 2000;60:1383–7
45. Sugawa N, Ekstrand AJ, James CD, et al. Identical splicing of aberrant epidermal growth factor receptor transcripts from amplified rearranged genes in human glioblastomas. Proc Natl Acad Sci USA 1990;87:8602–6
46. Sorkin A, Duex JE. Quantitative analysis of endocytosis and turnover of epidermal growth factor (EGF) and EGF receptor. Curr Protoc Cell Biol 2010;Chapter:Unit-15.14
47. Criollo A, Maiuri MC, Tasdemir E, et al. Regulation of autophagy by the inositol triphosphate receptor. Cell Death Differ 2007;14:1029–39
48. Khan MT, Joseph SK. Role of inositol triphosphate receptors in autophagy in DT40 cells. J Biol Chem 2010;285:16912–20

Downloaded from http://jnen.oxfordjournals.org/ by guest on September 20, 2016

49. Jiang H, Cheng D, Liu W, et al. Protein kinase C inhibits autophagy and phosphorylates LC3. Biochem Biophys Res Commun 2010;395:471–6
50. O'Brian CA, Ioannides CG, Ward NE, et al. Inhibition of protein kinase C and calmodulin by the geometric isomers cis- and trans-tamoxifen. Biopolymers 1990;29:97–104
51. Gulino A, Barrera G, Vacca A, et al. Calmodulin antagonism and growth-inhibiting activity of triphenylethylene antiestrogens in MCF-7 human breast cancer cells. Cancer Res 1986;46:6274–8
52. O'Brian CA, Housey GM, Weinstein IB. Specific and direct binding of protein kinase C to an immobilized tamoxifen analogue. Cancer Res 1988;48:3626–9
53. Baltuch GH, Dooley NP, Villemure JG, et al. Protein kinase C and growth regulation of malignant gliomas. Can J Neurol Sci 1995;22:264–71
54. Gelmann EP. Tamoxifen for the treatment of malignancies other than breast and endometrial carcinoma. Sem Oncol 1997;24(1 Suppl 1):S1-65–70
55. Zhang J, Stevens MF, Bradshaw TD. Temozolomide: Mechanisms of action, repair and resistance. Curr Mol Pharmacol 2012;5:102–14
56. Krajewski S, Krajewska M, Ehrmann J, et al. Immunohistochemical analysis of Bcl-2, Bcl-X, Mcl-1 and Bax in tumors of central and peripheral nervous system origin. Am J Pathol 1997;150:805–14
57. Gelmann EP. Tamoxifen induction of apoptosis in estrogen receptor-negative cancers: New tricks for an old dog? J Natl Cancer Inst 1996;88:224–6
58. Ferlini C, Scambia G, Marone M, et al. Tamoxifen induces oxidative stress and apoptosis in oestrogen receptor-negative human cancer cell lines. Br J Cancer 1999;79:257–63
59. Cho KS, Yoon YH, Choi JA, et al. Induction of autophagy and cell death by tamoxifen in cultured retinal pigment epithelial and photoreceptor cells. Invest Ophthalmol Vis Sci 2012;53:5344–53
60. Furnari FB, Fenton T, Bachoo RM, et al. Malignant astrocytic glioma: Genetics, biology, and paths to treatment. Genes Dev 2007;21:2683–710
61. Taylor TE, Furnari FB, Cavenee WK. Targeting EGFR for treatment of glioblastoma: Molecular basis to overcome resistance. Curr Cancer Drug Targets 2012;12:197–209
62. Brennan CW, Verhaak RG, McKenna A, et al. The somatic genomic landscape of glioblastoma. Cell 2013;155:462–77
63. Verhaak RG, Hoadley KA, Purdom E, et al. Integrated genomic analysis identifies clinically relevant subtypes of glioblastoma characterized by abnormalities in PDGFRA, IDH1, EGFR, and NF1. Cancer Cell 2010;17:98–110
64. Couldwell WT, Weiss MH, DeGiorgio CM, et al. Clinical and radiographic response in a minority of patients with recurrent malignant gliomas treated with high-dose tamoxifen. Neurosurgery 1993;32:485–9
65. Vertosick FT, Jr, Selker RG, Pollack IF, et al. The treatment of intracranial malignant gliomas using orally administered tamoxifen therapy: Preliminary results in a series of "failed" experiments. Neurosurgery 1992;30:897–902
66. Kroemer G, Galluzzi L, Vandenabeele P, et al. Classification of cell death: Recommendations of the Nomenclature Committee on Cell Death 2009. Cell Death Differ 2009;16:3–11
67. Mizushima N, Yoshimori T, Levine B. Methods in mammalian autophagy research. Cell 2010;140:313–26
68. Pal SK, Figlin RA, Reckamp K. Targeted therapies for non-small cell lung cancer: An evolving landscape. Mol Cancer Ther 2010;9:1931–44
69. Brown PH, Lippman SM. Chemoprevention of breast cancer. Breast Cancer Res Treat 2000;62:1–17

Downloaded from http://jnen.oxfordjournals.org/ by guest on September 20, 2016

www.impactjournals.com/oncotarget/ Oncotarget, 2017, Vol. 8, (No. 5), pp: 8670-8678

Research Paper

BH3 mimetics suppress CXCL12 expression in human malignant peripheral nerve sheath tumor cells

Christopher D. Graham[1], Niroop Kaza[1], Hawley C. Pruitt[1], Lauren M. Gibson[1], Barbara J. Klocke[1], Lalita A. Shevde[1], Steven L. Carroll[1,2], Kevin A. Roth[1,3]

[1]Department of Pathology, University of Alabama at Birmingham, Birmingham, Alabama, United States of America

[2]Current Address: Medical University of South Carolina, Department of Pathology and Laboratory Medicine, Charleston, South Carolina, United States of America

[3]Current Address: Columbia University Medical Center, Department of Pathology and Cell Biology, New York, United States of America

Correspondence to: *Kevin A. Roth,* ***email:*** *kar2208@cumc.columbia.edu*

Keywords: *MPNST, BH3 mimetic, CXCL12, PARP1, AT101*

Received: *July 13, 2016* ***Accepted:*** *December 05, 2016* ***Published:*** *December 31, 2016*

ABSTRACT

Malignant peripheral nerve sheath tumors (MPNSTs) are aggressive, Schwann cell-derived neoplasms of the peripheral nervous system that have recently been shown to possess an autocrine CXCL12/CXCR4 signaling loop that promotes tumor cell proliferation and survival. Importantly, the CXCL12/CXCR4 signaling axis is driven by availability of the CXCL12 ligand rather than CXCR4 receptor levels alone. Therefore, pharmacological reduction of CXCL12 expression could be a potential chemotherapeutic target for patients with MPNSTs or other pathologies wherein the CXCL12/CXCR4 signaling axis is active. AT101 is a well-established BCL-2 homology domain 3 (BH3) mimetic that we recently demonstrated functions as an iron chelator and thus acts as a hypoxia mimetic. In this study, we found that AT101 significantly reduces CXCL12 mRNA and secreted protein in established human MPNST cell lines *in vitro*. This effect was recapitulated by other BH3 mimetics [ABT-737 (ABT), obatoclax (OBX) and sabutoclax (SBX)] but not by desferrioxamine (DFO), an iron chelator and known hypoxia mimetic. These data suggest that CXCL12 reduction is a function of AT101's BH3 mimetic property rather than its iron chelation ability. Additionally, this study investigates a potential mechanism of BH3 mimetic-mediated CXCL12 suppression: liberation of a negative CXCL12 transcriptional regulator, poly (ADP-Ribose) polymerase I (PARP1) from its physical interaction with BCL-2. These data suggest that clinically available BH3 mimetics might prove therapeutically useful at least in part by virtue of their ability to suppress CXCL12 expression.

INTRODUCTION

MPNSTs arise sporadically or in patients affected by neurofibromatosis type 1 (NF1) [1]. NF1 is the most commonly inherited cancer predisposition syndrome of the human nervous system, affecting 1 in 3500 newborns [2]. NF1 patients typically exhibit numerous benign neurofibromas, and 8 – 13% of patients will develop more aggressive MPNSTs [1]. Despite increased understanding of the underlying molecular mechanisms driving the development of MPNSTs, treatment advances have been limited. Surgery is the standard of care; however, complete tumor excision is often impossible as MPNSTs aggressively invade adjacent tissues and metastasize [3]. Further, radiation and chemotherapy are largely ineffective at promoting MPNST patient survival [4]. These factors result in a <50% five-year survival rate for MPNST patients [1] and MPNSTs remain the leading cause of death in patients with NF1 [5].

CXCL12 (stromal cell-derived factor-1, SDF-1) belongs to a class of small (8-12 kilodalton [kD]) cytokines, known as chemokines (chemotactic cytokines). Based on structure, CXCL12 is a member of the C-X-C sub-group of chemokines possessing a single,

non-conserved amino acid residue (X) between the first N-terminal cysteine residues. Originally described as a homeostatic chemokine with a prominent role in the trafficking of hematopoietic cells, CXCL12 is now recognized to modulate multiple physiological processes via activation of its receptor, CXCR4 [5, 6]. Such pathways include activation of phospholipase C (PLC), regulation of adenylate cyclase and stimulation of kinase cascades such as phosphoinositide 3-kinase (PI3K), mitogen-activated protein kinase (MAPK) and c-Jun N-terminal kinase (JNK) [7, 8, 9, 10]. In addition to its physiological role, CXCL12/CXCR4 signaling has been implicated in driving tumor cell proliferation, survival and migration in various solid tumors [11, 12]. The original view of stromal cell-secreted CXCL12 acting on CXCR4-expressing tumor cells in a paracrine manner has evolved in recent years. Several studies have shown that some tumor cells, in addition to expressing CXCR4, can secrete CXCL12 and so activate an autocrine loop promoting growth and metastasis [6, 13]. Parada, *et al*'s discovery of this autocrine signaling axis' involvement in NF1-derived MPNST cells provides an exciting opportunity to explore novel therapies targeting CXCL12/CXCR4 autocrine signaling to treat MPNST patients [6].

In addition to CXCR4, CXCL12 also binds a "decoy" receptor, CXCR7 [14]. While it is thought that CXCR7 does not induce the same cascade of signals mediated by CXCR4, CXCR7 has been shown to significantly increase cell proliferation and adhesion in various conditions [14, 15, 16, 17]. Speculation abounds as to the biological role(s) of CXCR7, from the idea that it sequesters CXCL12 to create a gradient leading to differential signaling through CXCR4 [18, 19], to the hypothesis that CXCR7 serves as a co-receptor for CXCR4 [20, 21]. Accordingly, inhibition of CXCR7 function may serve to increase the clinical efficacy of CXCR4 inhibitors such as AMD3100, as blockage of CXCR4 only partially inhibits tumor cell response to CXCL12 gradients in multiple animal models [22, 23, 24]. These observations strengthen the argument that inhibition of CXCL12 expression may complement or enhance the efficacy of clinically available CXCR4 antagonists such as AMD3100.

AT101 [(-)-gossypol acetic acid] is a modified enantiomer of the naturally occurring polyphenolic aldehyde gossypol, and has received significant attention as a potential chemotherapeutic agent in multiple tumor types [25]. The basis for AT101's anti-neoplastic activity has been largely attributed to its BH3 mimetic activity, which results in interaction and inhibition of anti-apoptotic B-Cell Lymphoma 2 (BCL-2) family proteins such as BCL-2, BCL-X_L and MCL-1 [25]. This BH3 mimetic property of AT101 has been shown to promote both apoptotic and non-apoptotic tumor cell death, *in vitro* and *in vivo* [26, 27]. We recently reported that AT101, independent of its BH3 mimetic property, acts as an iron chelator in established human MPNST cell lines [4].

In this report, we show that AT101 causes a significant reduction in CXCL12 mRNA and secreted protein in established human MPNST cell lines. This effect results from AT101's BH3 mimetic property rather than its iron chelation ability. Finally, we show that the BH3 mimetic ABT robustly increases PARP1 binding to the *CXCL12* promoter.

RESULTS

AT101 suppresses CXCL12 expression

Because an active CXCL12/CXCR4 signaling pathway has been shown to mediate tumor cell proliferation, survival and migration in several tumor types including MPNSTs [6, 11, 12] and BH3 mimetics have been demonstrated to modulate CXCL12 transcription [28, 33], we sought to assess CXCL12 mRNA levels in T265-2c cells treated with AT101 (5μM for 24h) by quantitative real time PCR. We found that AT101 treatment resulted in a dramatic reduction of CXCL12 mRNA expression in T265-2c cells (Figure 1A, Supplementary Figure 4). CXCL12 is a chemotactic cytokine and is rapidly secreted, making it difficult to measure levels of intracellular CXCL12 in cell extracts. Accordingly, we performed an Enzyme-Linked ImmunoSorbent Assay (ELISA) on T265-2c culture media that had been treated with or without AT101 to assess whether treatment suppressed CXCL12 protein secretion as well as mRNA expression. Our data demonstrate that AT101 treatment (5μM for 24h) significantly decreased levels of secreted CXCL12 protein compared to untreated cells (Figure 1B Supplementary Figure 5). Our findings indicate that AT101 suppresses both CXCL12 expression and secretion in T265-2c MPNST cells. ABT, OBX, SBX and DFO had varying effects on CXCL12 secretion (Supplementary Figure 10).

AT101-induced suppression of CXCL12 is a function of its BH3 mimetic property

Because AT101 has both BH3 mimetic and hypoxia mimetic effects [4], we sought to address which mechanism, if either, was responsible for the observed suppression of CXCL12 expression. We compared the effects of three BH3 mimetics (ABT, OBX, SBX) and a hypoxia mimetic (DFO) with AT101 on CXCL12 mRNA levels in T265-2c cells. BH3 mimetic drug concentrations were chosen because of the comparable reduction in viable cell number after 24h treatment. We found that all BH3 mimetics tested dramatically reduced CXCL12 mRNA levels after 24h (Figure 2, Supplementary Figure 6). DFO produced only a slight, albeit statistically significant, reduction in CXCL12 mRNA that was substantially less than that of BH3 mimetics (Figure 2, Supplementary Figure 6). These results suggest that BH3 mimetics as a class suppress CXCL12 expression and that

AT101-mediated suppression of CXCL12 is not dependent on its ability to chelate iron. Further, to determine if CXCL12 suppression was a unique effect of BH3 mimetics on T265-2c cells or represented a more general response of MPNST cells, an additional NF1-derived (90-8) and a sporadic MPNST cell line (STS26T) were treated with AT101, ABT, OBX and SBX for 24h followed by qRT-PCR analysis of CXCL12. Both the NF1-derived (Figure 3A, Supplementary Figure 7) and sporadic (Figure 3B, Supplementary Figure 8) MPNST cell lines exhibited suppression of CXCL12 similar to T265-2c cells. These results suggest that BH3 mimetics possess a conserved function of CXCL12 suppression in MPNST cells. It is important to note that the BH3 mimetics tested exhibited conserved effects in U251 established human glioblastoma cells (Supplementary Figure 9). Further, BH3 mimetics reduced cell viability in all MPNST cell lines tested (Figure 4, Supplementary Figure 1/2/3) while DFO resulted in a less robust and reproducible effect (Supplementary Figure 11/12/13) Because CXCL12 is known to stimulate autocrine cell cycle progression via induction of cyclin D1, we evaluated cyclin D1 protein levels following AT101 or ABT treatment and observed an AT101- but not ABT-dependent reduction in cyclin D1 (Supplementary Figure 14).

BH3 mimetics and PARP1

The single most defining characteristic of Type 1 diabetes (T1D) is loss of pancreatic insulin-producing beta cells [28]. Because CXCL12 has demonstrated anti-diabetogenic capability by promoting pancreatic beta cell survival [31, 32], interest in the regulatory mechanism(s) of CXCL12 transcription has increased. A recent investigation into the transcriptional regulation of CXCL12 in rat pancreatic beta cells identified PARP1 as a negative transcriptional regulator of CXCL12 [28]. Interestingly, ABT has been shown to displace PARP1 from its interaction with the BCL-2 family member BCL-2 [33]. Considered together with the observation that PARP1 is known to have a negative regulatory effect on CXCL12 transcription [28], we hypothesized that at least some BH3 mimetic-mediated suppression of CXCL12 expression may result from liberation of a negative CXCL12 transcriptional regulator (PARP1). To test this hypothesis, we developed PCR primers flanking a putative PARP1 binding site within the CXCL12 promoter (Supplementary Figure 15) and performed ChIP analysis of T265-2c cells using antibodies against PARP1 or rabbit IgG following treatment with ABT. qRT-PCR analysis of ChIP products revealed a robust increase in PARP1 interaction with the *CXCL12* promoter (Figure 5A).

DISCUSSION

The BCL-2 family of proteins mediates cellular life and death in part by regulating mitochondrial membrane integrity [34]. This regulation results from a delicate balance of interactions between BH domains of pro- and anti-apoptotic proteins within the BCL-2 family. Following various pro-death stimuli including DNA damage [35], growth factor deprivation [36] and oncogene activation [37], the balance of physical interactions between BH domains of pro- and anti-apoptotic proteins is disrupted by BH3-only proteins. This results in activation of pro-apoptotic multi-domain BCL-2 proteins (BAX/BAK) and subsequent apoptosis. It is estimated that roughly 50% of all human cancers exhibit elevated gene expression of anti-apoptotic BCL-2 family members [38], contributing to resistance to standard apoptosis-inducing therapies. Consequently, molecules possessing only the BH3 domain of BCL-2 proteins (termed BH3 mimetics), have received significant attention as potentially useful cancer therapeutic agents either alone or in combination with other drugs [34].

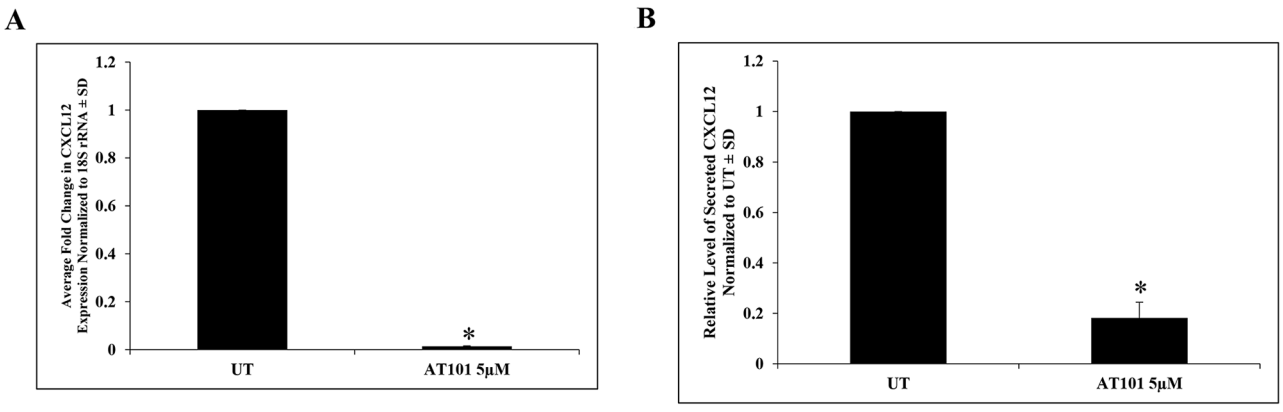


Figure 1: AT101 down-regulates CXCL12 in MPNST cells. A. qRT-PCR analysis of AT101-treated T265-2c cells (5μM, 24h). **B.** AT101 treatment (5μM, 24h) resulted in a significant reduction of secreted CXCL12 protein in T265-2c cells as demonstrated by an ELISA. **p*-value <0.05.

We have been investigating AT101, a well-known BH3 mimetic, as an alternative chemotherapeutic option for patients with MPNSTs. Previously published studies from our lab have demonstrated that AT101 can also chelate intracellular iron and induce a hypoxia-like state *in vitro*. qRT-PCR analysis demonstrated that AT101-induced suppression of CXCL12 transcription in all three MPNST cell lines tested. To gain insight into the mechanism by which AT101 exerts its suppressive effects on CXCL12, we compared AT101 with three BH3 mimetics (ABT, OBX, SBX) and a hypoxia mimetic (DFO). We found that BH3 mimetics, but not DFO, robustly suppressed CXCL12 in all three MPNST cell lines tested. These results suggest that AT101's ability to suppress CXCL12 is largely a function of its BH3 mimetic property rather than its iron chelation ability.

Understanding the mechanism behind BH3 mimetic-induced reduction of CXCL12 is critical to appropriate clinical application. To this end, we have investigated an interesting hypothesis based on the observation that ABT has been shown to displace PARP1 from BCL-2 [33] and that PARP1 exerts a strong inhibitory effect on CXCL12 transcription [28]. Our ChIP data, which demonstrates a robust BH3 mimetic-mediated increase in PARP1 binding to the *CXCL12* promoter, supports the hypothesis that disruption of the BCL-2:PARP1 interaction via BH3 mimetics results in increased negative regulation of CXCL12 transcription by PARP1. These data suggest that BH3 mimetic-mediated suppression of CXCL12 expression is, at least in part, mediated by displacement of PARP1 from its interaction with BCL-2 and subsequent binding of PARP1 to the

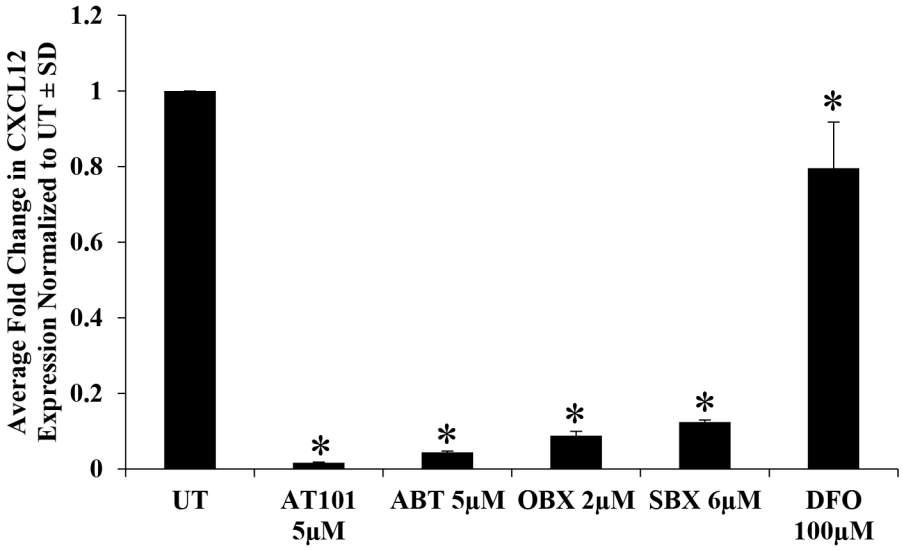


Figure 2: BH3 mimetics recapitulate the effects of AT101 on CXCL12 expression. T265-2c cells treated with AT101, ABT, OBX, SBX or DFO significantly suppress CXCL12 mRNA levels compared to no treatment as demonstrated by qRT-PCR. **p*-value <0.05. Comparison of DFO with AT101, ABT, OBX or SBX treatment resulted in a statistically significant difference in CXCL12 expression (*p*-value <0.01).

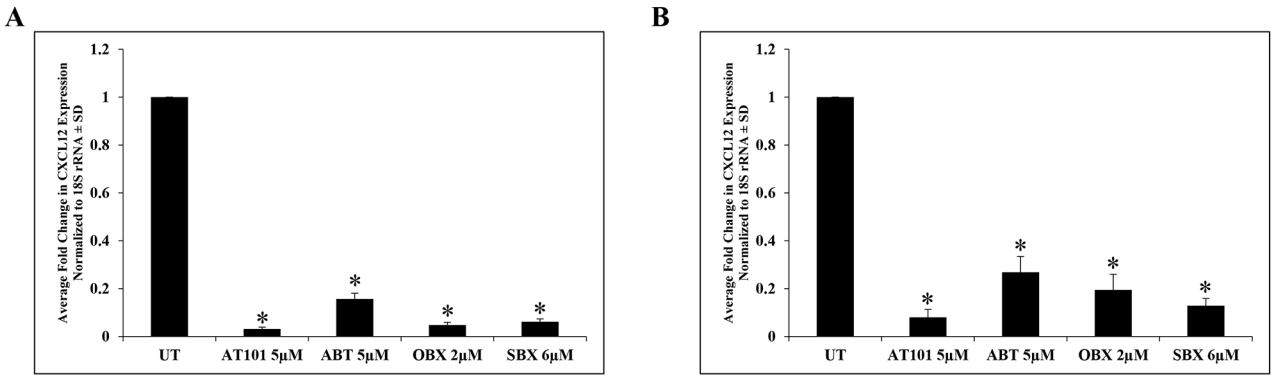


Figure 3: BH3 mimetic suppression of CXCL12 is conserved among multiple MPNST cell lines. BH3 mimetics suppress CXCL12 mRNA levels in an NF1-derived (90-8) **A.** and sporadic (STS26T) **B.** MPNST cell line as demonstrated by qRT-PCR. **p*-value <0.05.

CXCL12 promoter resulting in transcriptional down-regulation (Figure 5B, proposed model).

Targeting tumor-specific growth promoting pathways is important for successful cancer therapy, and the CXCL12/CXCR4 signaling axis is involved in tumor progression and migration in multiple tumor types [12, 39, 40]. The physiological role for chemotactic cytokines is to direct the homing of hematopoietic cells to specific sites within the body via interaction with cell-surface receptors [41–47]. This physiological role may help explain the observation that organs possessing the highest frequency of breast cancer metastasis also have the most abundant secretion of these chemotactic ligands, suggesting a significant role for these molecules in breast cancer metastasis [11]. Supporting this notion is the observation that CXCL12 expression is elevated in multiple tissues

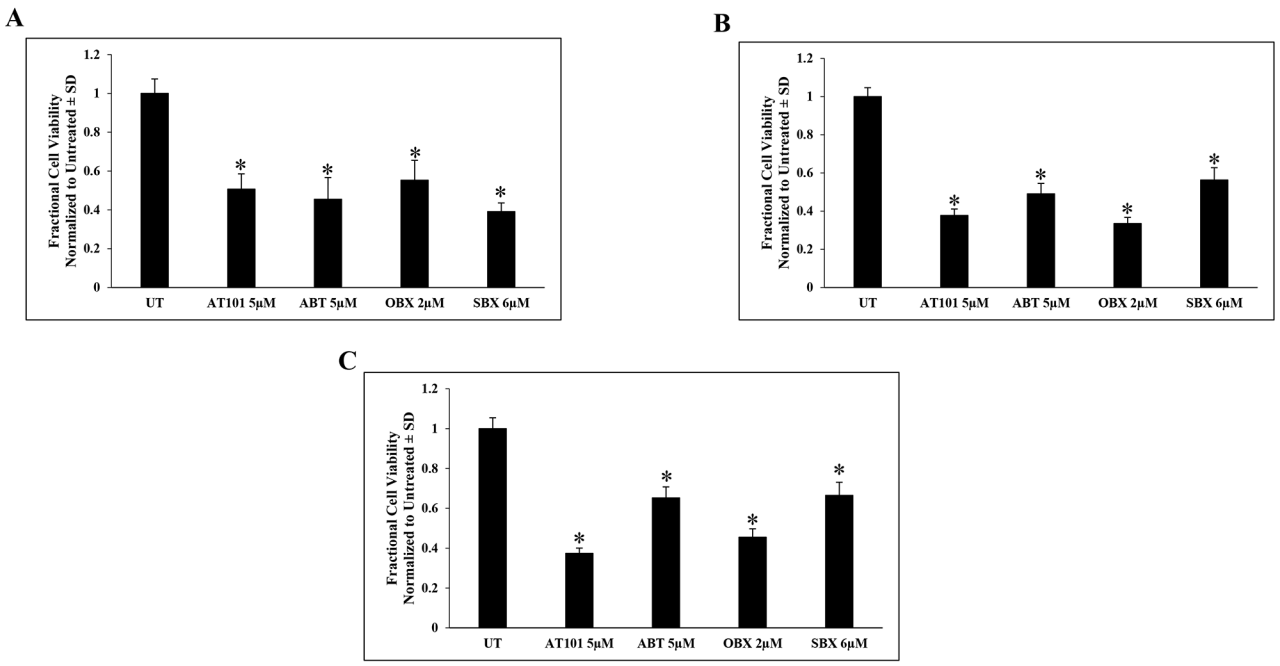


Figure 4: AT101 and BH3 mimetics mediate reduction in MPNST cell viability. AT101- or BH3 mimetic-treated T265 **A.** 90-8 **B.** and STS26 **C.** MPNST cells demonstrate a decrease in viable cell number after 24h. **p*-value <0.01.

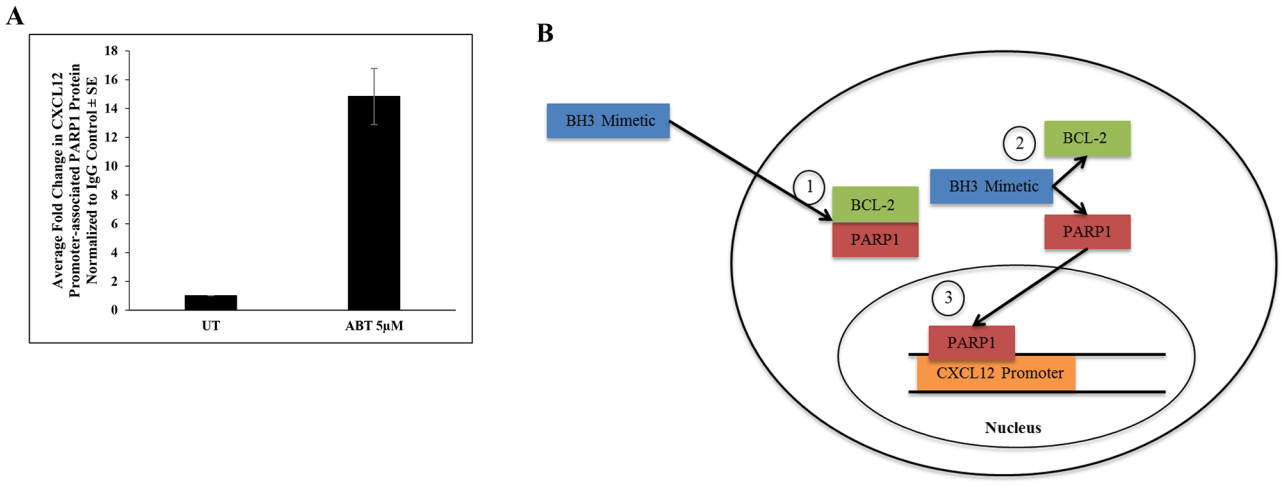


Figure 5: ABT increases PARP1 binding to the *CXCL12* promoter. A. T265-2c cells treated with ABT for 24h exhibit increased PARP1 binding to the *CXCL12* promoter as demonstrated by qRT-PCR of Chromatin Immunoprecipitation (ChIP) with PARP1 antibody or IgG control. **B.** Proposed mechanism: PARP1 dimerizes with BCL-2 under normal physiological conditions (Step 1) (ref 33, ref 55). BH3 mimetics disrupt the BCL-2:PARP1 complex via the BH3 domain (Step 2) (ref 33), freeing PARP1 to bind the CXCL12 proximal promoter and exert transcriptional repression (Step 3).

known to harbor breast cancer metastases (lymph nodes, lung, liver, bone marrow) and relatively lower in tissues not typically associated with such metastases (small intestine, kidney, skin, brain, skeletal muscle) [11]. Further, *in vivo* neutralization of the CXCL12/CXCR4 interaction in breast cancer has been shown to significantly inhibit lung and lymph node metastasis [11]. Outside the context of cancer, reduction of CXCL12 has potential significance in the field of autoimmune disorders, as neutralization of chemokines is thought to have a restraining effect on the autoimmune response [48]. Conversely, disruption of the CXCL12/CXCR4 interaction has been shown to promote hematopoietic stem cell mobilization, promoting immunologic response of patients with non-Hodgkin lymphoma and multiple myeloma [49]. Additional studies are required to determine if BH3 mimetic suppression of CXCL12 is limited to MPNST and related tumor cells or is a general phenomenon with implications for other tumor types.

Affecting the CXCL12 signaling axis has potential for significant therapeutic benefit, as CXCR4 is over-expressed in more than 20 human cancers [50]. Accordingly, CXCR4 has been targeted by numerous antagonists including AMD3100, TN14003, T22, CTCE-9908 and ALX40-4C, all of which are CXCL12 N-terminus peptide analogs [51]. The ligand-dependent nature of this signaling axis relative to other cancer-relevant pathways of which ligand-independent signal transduction occurs via means such as receptor dimerization provides additional therapeutic targeting at the ligand level. This approach has potential for therapeutic benefit alone or as a combination approach to shut down the pathway at multiple levels. Here we demonstrate that BH3 mimetics as a class have the capability to robustly suppress CXCL12 expression and secretion in MPNSTs and set a precedent for further studies into the clinical utility of targeting the CXCL12 signaling axis by ligand ablation.

MATERIALS AND METHODS

Antibodies and other reagents

PARP1 primary antibody (#sc-7150 [H-250]) and rabbit IgG (sc-2027) were obtained from Santa Cruz (Dallas, TX). Other reagents were obtained from the following sources: ABT-737 [ABT] and Obatoclax [OBX] (Selleck Chemicals, Houston, TX S1002 and S1057, respectively), desferrioxamine [DFO] (Sigma D9533), sabutoclax [SBX] (AdooQ Biosciences, Irvine, CA A12823), AT101 (Ascenta Therapeutics, Malvern, PA).

Cell culture

We have previously described the source of human NF1-derived MPNST cell lines (T265-2c, 90-8) utilized in this study [29]. STS26T sporadic MPNST cells were a gift from Dr. Steven Carroll whose source is described by Dahlberg *et al*. [30]. All cell lines were cultured in DMEM containing 1% penicillin/streptomycin (Invitrogen, Carlsbad, CA), 1% L-glutamine (Sigma), and 10% fetal bovine serum (Fisher Scientific). All cells were incubated at 37°C in a humidified 5% CO2, 95% air atmosphere. Based on cellular size and in order to achieve relative confluence, cell lines were plated at varying densities. For DNA, RNA and protein collection, cells were plated on 100mm dishes at a density of: 1×10^6/dish- 90-8, STS26T; 1.5×10^6/dish- T265-2c. Cultures were used in experiments 24 hours post-plating. Drug treatments were performed in respective media supplemented with 2% FBS.

Cell viability assay

The calcein-AM conversion assay (Life Technologies, Carlsbad, CA C3100MP) was employed to quantify viable cell number after drug treatment as previously described [54, 55].

ELISA

T265-2c cells were plated in 100mm dishes at previously described densities and were treated 24h post plating in media containing 2% FBS with or without AT101. Conditioned media was collected 24 hours after treatment and concentrated ~80-fold using Amicon Ultra-4 centrifugal filters with a molecular size exclusion of 3kD (Millipore, Billerica, MA UFC800324) and stored at -80°C. Following protein quantification, 375µg total protein was loaded per well (in duplicate) using a human CXCL12/SDF-1 ELISA kit (R&D Systems, Minneapolis, MN DSA00) per the manufacturer's instructions.

Reverse transcription and real-time quantitative PCR analysis

RNA was isolated using the RNeasy Plus mini kit (Qiagen, Germany #74134). cDNA was subsequently synthesized using the High Capacity cDNA Reverse Transcription kit (Applied Biosystems, Foster City, CA #4368814). Real-time quantitative PCR was performed using the Maxima SYBR Green/ROX qPCR master mix (Thermo Scientific, Waltham, MA #K0221) and probes were obtained from Life Technologies (Carlsbad, CA). Amplifications were run in a StepOne Plus Real-Time PCR System (Applied Biosystems). The following sense/antisense primers and probes were selected from the Harvard PrimerBank and used for detecting: human CXCL12 (5'-ATTCTCAACACTCCAAACTGTGC-3' and 5'-ACTTTAGCTTCGGGTCAATGC-3') and human 18S rRNA (5'-GTAACCCGTTGAACCCCATT-3' and 5'-CCATCCAATCGGTAGTAGCG-3'). Analysis was performed using the ΔΔCT method [52] and values were adjusted using 18S rRNA levels as reference.

Chromatin immunoprecipitation (ChIP)

T265-2c cells were plated in 100mm dishes at densities described above in the *Cell Culture* section and drug treatments were performed after 24h. To account for loss of total cell number resulting from cytotoxic effects of BH3 mimetic treatment, twice as many 100mm dishes were used for each treatment condition versus untreated and each dish of respective cells was combined after fixation. ChIP using antibodies against PARP1 (Santa Cruz H-250 [sc-7150]) (12µg/ml) or rabbit IgG (Santa Cruz sc-2027) (12µg/ml) was performed using the ChIP-IT Express Enzymatic kit from Active Motif (Carlsbad, CA #53009) per the manufacturer's instructions. DNA was amplified using primers flanking the putative PARP1 ["A/GNNA/TCAAA" [53] binding site within the *CXCL12* promoter. Negative control primers were obtained from Active Motif (#103708).

Primer sequence:
Forward: 5′-GAATCTCCCGTCCCACTCC-3′
Reverse: 5′-GCCGAGCCTCAGTTTCCT-3′

Statistics

All data points represent the mean ± standard deviation (S.D.) except for ChIP qRT-PCR data, which represents mean ± standard error (S.E.). All experiments were repeated at least 3 times (except for T265-2c ChIP and STS26T qRT-PCR) and representative data is shown; all biological replicates are included in supplementary material. Each real-time quantitative PCR was performed in triplicate and the average and S.D. (or S.E. for ChIP qRT-PCR) was used for statistical analysis. Each ELISA was performed in duplicate and averages from three biological and technical replicates were used to obtain an average and S.D. for statistical analysis. ELISA data is presented as a compilation of three replicate experiments. Statistical significance was determined by ANOVA followed by Dunnett's post-hoc test. A p-value < 0.05 was considered significant.

Abbreviations

Malignant Peripheral Nerve Sheath Tumor (MPNST); Neurofibromatosis Type 1 (NF1); ABT-737 (ABT); obatoclax (OBX); sabutoclax (SBX); desferrioxamine (DFO); B-Cell Lymphoma 2 (BCL-2); BCL-2 Homology domain 3 (BH3); Poly (ADP-Ribose) Polymerase 1 (PARP1); Phospholipase C (PLC); PhosphoInositide 3-Kinase (PI3K); Mitogen-Activated Protein Kinase (MAPK); c-Jun N-terminal Kinase (JNK).

ACKNOWLEDGEMENTS

We wish to thank the UAB Heflin Center for Genomic Studies (supported by grant CA013148) and UAB Molecular Detection Core (supported by grant NS47466) for technical assistance as well as Ascenta Therapeutics for supplying AT101. This work was supported by United States Department of Defense (DOD) grant W81XWH-14-1-0073.

CONFLICTS OF INTEREST

None.

FUNDING

This work was supported by Department of Defense grant W81XWH-14-1-0073 (K.A.R). Funding sources for this study had no involvement in study design, collection/analysis/interpretation of data, writing of the report, or decision to publish.

Author contributions

CDG, SLC, KAR conceived study; CDG, NK, HCP, LAS, SLC, KAR designed experiments; CDG, NK, HCP, LMG, BJK performed experiments; CDG, KAR, NK, HCP, LAS analyzed data; CDG, KAR wrote manuscript; CDG, NK, BJK, LMG, HCP, LAS, SLC, KAR reviewed manuscript.

REFERENCES

1. Evans DG, Baser ME, McGaughran J, Sharif S, Howard E, Moran A. Malignant peripheral nerve sheath tumours in neurofibromatosis 1. J Med Genet 2002; 39:311-314.
2. Zhu Y, Parada LF. Neurofibromin, a tumor suppressor in the nervous system. Exp Cell Res 2001; 264:19-28.
3. Ferner RE, Gutmann DH. International consensus statement on malignant peripheral nerve sheath tumors in neurofibromatosis. Cancer Res 2002; 62:1573-77.
4. Kaza N, Kohli L, Graham CD, Klocke BJ, Carroll SL, Roth KA. BNIP3 regulates AT101 [(-)-gossypol] induced death in malignant peripheral nerve sheath tumor cells. PLOS ONE 2014; 9:e96733.
5. Ma Q, Jones D, Borghesani PR, Segal RA, Nagasawa T, Kishimoto T, Bronson RT, Springer TA. Impaired B-lymphopoiesis, myelopoiesis, and derailed cerebellar neuron migration in CXCR4- and SDF-1-deficient mice. Proc Natl Acad Sci U.S.A. 1998; 95:9448-53.
6. Mo W, Chen J, Patel A, Zhang L, Chau V, Li Y, Cho W, Lim K, Xu J, Lazar AJ, Creighton CJ, Bolshakov S, McKay RM, Lev D, Le LQ, Parada LF. CXCR4/CXCL12 mediate autocrine cell-cycle progression in NF1-associated malignant peripheral nerve sheath tumors. Cell 2013; 152:1077-90.
7. Lattin J, Zidar DA, Schroder K, Kellie S, Hume DA, Sweet MJ. G-protein-coupled receptor expression, function, and signaling in macrophages. J Leukoc Biol 2007; 82:16-32.

8. Mellado M, Rodríguez-Frade JM, Mañes S, Martínez-A C. Chemokine signaling and functional responses: the role of receptor dimerization and TK pathway activation. Annu Rev Immunol 2001; 19:397-421.
9. New DC, Wong YH. Molecular mechanisms mediating the G protein-coupled receptor regulation of cell cycle progression. J Mol Signal 2007; 2:2.
10. Pierce KL, Premont RT, Lefkowitz RJ. Seven-transmembrane receptors. Nat Rev Mol Cell Biol 2002; 3:639-50.
11. Müller A, Homey B, Soto H, Ge N, Buchanan ME, McClanahan T, Murphy E, Yuan W, Wagner SN, Barrera JL, Mohar A, Verastequi E, Zlotnik A. Involvement of chemokine receptors in breast cancer metastasis. Nature 2001; 410:50-56.
12. Rempel SA, Dudas S, Ge S, Gutiérrez JA. Identification and localization of the cytokine SDF1 and its receptor, CXC chemokine receptor 4, to regions of necrosis and angiogenesis in human glioblastoma. Clin Cancer Res 2000; 6:102-111.
13. Gatti M, Pattarozzi A, Bajetto A, Würth R, Daga A, Fiaschi P, Zona G, Florio T, Barbieri F. Inhibition of CXCL12/CXCR4 autocrine/paracrine loop reduces viability of human glioblastoma stem-like cells affecting self-renewal ativity. Toxicology 2013; 314:209-20.
14. Burns JM, Summers BC, Wang Y, Melikian A, Berahovich R, Miao Z, Penfold ME, Sunshine MJ, Littman DR, Kuo CJ, Wei K, McMaster BE, Wright K, *et al*. A novel chemokine receptor for SDF-1 and I-TAC involved in cell survival, cell adhesion, and tumor development. J Exp Med 2006; 203:2201-13.
15. Raggo C, Ruhl R, McAllister S, Koon H, Dezube BJ, Früh K, Moses AV. Novel cellular genes essential for transformation of endothelial cells by Kaposi's sarcoma-associated herpesvirus. Cancer Res 2005; 65:5084-95.
16. Miao Z, Luker KE, Summers BC, Berahovich R, Bhojani MS, Rehemtulla A, Kleer CG, Essner JJ, Nasevicius A, Luker GD, Howard MC, Schall TJ. CXCR7 (RDC1) promotes breast and lung tumor growth *in vivo* and is expressed on tumor-associated vasculature. Proc Natl Acad Sci U.S.A. 2007; 104:15735-40.
17. Begley LA, MacDonald JW, Day ML, Macoska JA. CXCL12 activates a robust transcriptional response in human prostate epithelial cells. J Biol Chem 2007; 282:26767-74.
18. Boldajipour B, Mahabaleshwar H, Kardash E, Reichman-Fried M, Blaser J, Minina S, Wilson D, Xu Q, Raz E. Control of chemokine-guided cell migration by ligand sequestration. Cell 2008; 132:463-73.
19. Dambly-Chaudière C, Cubedo N, Ghysen A. Control of cell migration in the development of the posterior lateral line: antagonistic interactions between the chemokine receptors CXCR4 and CXCR7/RDC1. BMC Dev Biol 2007; 7:23.
20. Levoye A, Balabanian K, Baleux F, Bachelerie F, Lagane B. CXCR7 heterodimerizes with CXCR4 and regulates CXCL12-mediated G protein signaling. Blood 2009; 113:6085-93.
21. Sierro F, Biben C, Martínez-Muñoz L, Mellado M, Ransohoff RM, Li M, Woehl B, Leung H, Groom J, Batten M, Harvey RP, Martinez-A C, Mackay CR, *et al*. Disrupted cardiac development but normal hematopoiesis in mice deficient in the second CXCL12/SDF1 receptor, CXCR7. Proc Natl Acad Sci U.S.A. 2007; 104:14759-64.
22. Jankowski K, Kucia M, Wysoczynski M, Reca R, Zhao D, Trzyna E, Trent J, Peiper S, Zembala M, Ratajczak J, Houghton P, Janowska-Wieczorek A, Ratajczak MZ. Both hepatocyte growth factor (HGF) and stromal-derived factor-1 regulate the metastatic behavior of human rhabdomyosarcoma cells, but only HGF enhances their resistance to radiochemotherapy. Cancer Res 2003; 63:7926-35.
23. Wysoczynski M, Kucia M, Ratajczak J, Ratajczak MZ. Cleavage fragments of the third complement component (C3) enhance stromal derived factor-1 (SDF-1)-mediated platelet production during reactive postbleeding thrombocytosis. Leukemia 2007; 21:973-82.
24. Wysoczynski M, Miekus K, Jankowski K, Wanzeck J, Bertolone S, Janowska-Wieczorek A, Ratajczak J, Ratajczak MZ. Leukemia inhibitor factor: a newly identified metastatic factor in rhabdomyosarcomas. Leukemia 2007; 67:2131-40.
25. Hu W, Wang F, Tang J, Liu X, Yuan Z, Nie C, Wei Y. Proapoptotic protein Smac mediates apoptosis in cisplatin-resistant ovarian cancer cells when treated with the anti-tumor agent AT101. J Biol Chem 2012; 287:68-80.
26. Goff DJ, Court Recart A, Sadarangani A, Chun HJ, Barrett CL, Krajewska M, Leu H, Low-Marchelli J, Ma W, Shih AY, Wei J, Zhai D, Geron I, *et al*. A Pan-BCL2 inhibitor renders bone-marrow-resistant human leukemia stem cells sensitive to tyrosine kinase inhibition. Cell Stem Cell 2013; 12:316-28.
27. Voss V, Senft C, Lang V, Ronellenfitsch MW, Steinbach JP, Seifert V, Kogel D. The pan-Bcl-2 inhibitor (-)-gossypol triggers autophagic cell death in malignant glioma. Mol Cancer Res 2010; 8:1002-16.
28. Marković J, Grdović N, Dinić S, Karan-Djurašević T, Uskoković A, Arambašić J, Mihailovic M, Pavlovic S, Poznanovic G, Vidakovic M. PARP-1 and YY1 are important novel regulators of CXCL12 gene transcription in rat pancreatic beta cells. PLOS ONE 2013; 8:e59679.
29. Stonecypher MS, Byer SJ, Grizzle WE, Carroll SJ. Activation of the neuregulin-1/ErbB signaling pathway promotes the proliferation of neoplastic Schwann cells in human malignant peripheral nerve sheath tumors. Oncogene 2005 24:5589-605.
30. Dahlberg WK, Little JB, Fletcher JA, Suit HD, Okunieff P. Radiosensitivity *in vitro* of human soft tissue sarcoma cell

lines and skin fibroblasts derived from the same patients. Int J Radiat Biol 1993; 63:191-98.

31. Yu L, Cecil J, Peng SB, Schrementi J, Kovacevic S, Paul D, Su EW, Wang J. Identification and expression of novel isoforms of human stromal cell-derived factor 1. Gene 2006; 374:174-79.
32. Yano T, Liu Z, Donovan J, Thomas MK, Habener JF. Stromal cell derived factor-1 (SDF-1)/CXCL12 attenuates diabetes in mice and promotes pancreatic beta-cell survival by activation of the prosurvival kinase Akt. Diabetes 2007; 56:2946-57.
33. Dutta C, Day T, Kopp N, van Bodegom D, Davids MS, Ryan J, Bird L, Kommajosyula N, Weigert O, Yoda A, Fung H, Brown JR, Shapiro GI, *et al*. BCL2 suppresses PARP1 function and nonapoptotic cell death. Cancer Res 2012; 72:4193-203.
34. Ni Chonghaile T, Letai A. Mimicking the BH3 domain to kill cancer cells. Oncogene 2008; 27:S149-57.
35. Evan GI, Wyllie AH, Gilbert CS, Littlewood TD, Land H, Brooks M, Waters CM, Penn LZ, Hancock DC. Induction of apoptosis in fibroblasts by c-myc protein. Cell 1992; 69:119-28.
36. Oda E, Ohki R, Murasawa H, Nemoto J, Shibue T, Yamashita T, Tokino T, Taniquchi T, Tanaka N. Noxa, a BH3-only member of the Bcl-2 family and candidate mediator of p53-induced apoptosis. Science 2000; 288:1053-58.
37. Nakano K, Vousden KH. PUMA, a novel proapoptotic gene, is induced by p53. Mol Cell 2001; 7:683-94.
38. Yip KW, Reed JC. Bcl-2 family proteins and cancer. Oncogene 2008; 27:6398-406.
39. Shakir M, Tang D, Zeh HJ, Tang SW, Anderson CJ, Bahary N, Lotze MT. The chemokine receptors CXCR4/CXR7 and their primary heterodimeric ligands CXCL12 and CXCL12/high mobility group box 1 in pancreatic cancer growth and development: finding flow. Pancreas 2015; 44:528-34.
40. Yadav SS, Prasad SB, Das M, Kumari S, Pandey LK, Singh S, Pradhan S, Narayan G. Epigenetic silencing of CXCR4 promotes loss of cell adhesion in cervical cancer. Biomed Res Int 2014; 2014:581403.
41. Zlotnik A, Yoshie O. Chemokines: a new classification system and their role in immunity. Immunity 2000; 12:121-27.
42. Campbell JJ, Butcher EC. Chemokines in tissue-specific and microenvironment-specific lymphocyte homing. Curr Opin Immunol 2000; 12:336-41.
43. Butcher EC, Williams M, Youngman K, Rott L, Briskin M. Lymphocyte trafficking and regional immunity. Adv Immunol 1999; 72:209-53.
44. Morales J, Homey B, Vicari AP, Hudak S, Oldham E, Hedrick J, Orozco R, Copeland NG, Jenkins NA, McEvoy LM, Zlotnik A. CTACK, a skin-associated chemokine that preferentially attracts skin-homing memory T cells. Proc Natl Acad Sci U.S.A. 1999; 96:14470-75.
45. Homey B, Wang W, Soto H, Buchanan ME, Wiesenborn A, Catron D, Muller A, McClanahan TK, Dieu-Nosjean MC, Orozco R, Ruzicka T, Lehmann P, Oldham E, *et al*. Cutting edge: the orphan chemokine receptor G protein-coupled receptor-2 (GPR-2, CCR10) binds the skin-associated chemokine CCL27 (CTACK/ALP/ILC). J Immunol 2000; 164:3465-70.
46. Peled A, Petit I, Kollet O, Magdid M, Ponomaryov T, Byk T, Nagler A, Ben-hur H, Many A, Schultz L, Lider O, Alon R, Zipori D, *et al*. Dependence of human stem cell engraftment and population of NOD/SCID mice on CXCR4. Science 1999; 283:845-48.
47. Förster R, Schubel A, Breitfeld D, Kremmer E, Renner-Müller I, Wolf E, Lipp M. CCR7 coordinates the primary immune response by establishing function microenvironments in secondary lymphoid organs. Cell 1999; 99:23-33.
48. Karin N. The multiple faces of CXCL12 (DF-1alpha) in the regulation of immunity during health and disease. J Leukoc Biol 2010; 88:463-73.
49. Damon LE, Damon LE. Mobilization of hematopoietic stem cells into the peripheral blood. Expert Rev Hematol 2009; 2:717-33.
50. Balkwill F. Cancer and the chemokine network. Nat Rev Cancer 2004; 4:540-50.
51. Sun X, Cheng G, Hao M, Zheng J, Zhou X, Zhang J, Taichman RS, Pienta KJ, Wang J. CXCL12/CXCR4/CXCR7 chemokine axis and cancer progression. Cancer Metastasis Rev 2010; 29:709-22.
52. Livak KL, Schmittgen TD. Analysis of relative gene expression data using real-time quantitative PCR and the 2(-Delta C(T)) Method. Methods 2001; 25:402-08.
53. Ko HL, Ren EC. (2011) Novel poly (ADP-ribose) polymerase 1 binding motif in hepatitis B virus core promoter impairs DNA damage repair. Hepatology 54:1190-98 (PMID 21721027).
54. Geng Y, Kohli L, Klocke BJ, Roth KA. (2010) Chloroquine-induced autophagic vacuole accumulation and cell death in glioma cells is p53 independent. Neuro Oncol 12:473-81 (PMID 20406898).
55. Oltersdorf T, Elmore SW, Shoemaker AR, Armstrong RC, Augeri DJ, Belli BA, *et al*. (2005) An inhibitor of Bcl-2 family proteins induces regression of solid tumours. Nature 435:677-81 (PMID 15902208).

Recent Advances in the Diagnosis and Pathogenesis of Neurofibromatosis Type 1 (NF1)-associated Peripheral Nervous System Neoplasms

Jody F. Longo, PhD, Shannon M. Weber, BS,*†*
Brittany P. Turner-Ivey, PhD, and Steven L. Carroll, MD, PhD*‡*

Downloaded from https://journals.lww.com/anatomicpathology by BhDMf5ePHKav1zEoum1tQfN4a+kJLhEZgbsIHo4XMi0hCywCX1AWnYQp/IlQrHD3y/RXqG5VZA8fTmspxFW6RWqCR8mGQdtsiaCdHKPeog= on 08/15/2018

Abstract: The diagnosis of a neurofibroma or a malignant peripheral nerve sheath tumor (MPNST) often raises the question of whether the patient has the genetic disorder neurofibromatosis type 1 (NF1) as well as how this will impact the patient's outcome, what their risk is for developing additional neoplasms and whether treatment options differ for NF1-associated and sporadic peripheral nerve sheath tumors. Establishing a diagnosis of NF1 is challenging as this disorder has numerous neoplastic and non-neoplastic manifestations which are variably present in individual patients. Further, other genetic diseases affecting the Ras signaling cascade (RASopathies) mimic many of the clinical features of NF1. Here, we review the clinical manifestations of NF1 and compare and contrast them with those of the RASopathies. We also consider current approaches to genetic testing for germline *NF1* mutations. We then focus on NF1-associated neurofibromas, considering first the complicated clinical behavior and pathology of these neoplasms and then discussing our current understanding of the genomic abnormalities that drive their pathogenesis, including the mutations encountered in atypical neurofibromas. As several neurofibroma subtypes are capable of undergoing malignant transformation to become MPNSTs, we compare and contrast patient outcomes in sporadic, NF1-associated and radiation-induced MPNSTs, and review the challenging pathology of these lesions. The mutations involved in neurofibroma-MPNST progression, including the recent identification of mutations affecting epigenetic regulators, are then considered. Finally, we explore how our current understanding of neurofibroma and MPNST pathogenesis is informing the design of new therapies for these neoplasms.

Key Words: neurofibroma, malignant peripheral nerve sheath tumor, RASopathies, tumor genomics, epigenetic regulation

(*Adv Anat Pathol* 2018;25:353–368)

When diagnosing a neurofibroma or a malignant peripheral nerve sheath tumor (MPNST), pathologists often have to consider whether the patient might also have the genetic disorder neurofibromatosis type 1 (NF1). If NF1 is likely, the clinician caring for the patient may need to consider how this will impact the patient's outcome, what their risk is for developing additional neoplasms and whether treatment options differ for NF1-associated and sporadic peripheral nerve sheath tumors. These questions are reasonable but answering them can be problematic. NF1 has numerous neoplastic and non-neoplastic clinical features, which are variably present in different patients; this variable presentation can make it difficult to diagnose NF1 with confidence. To complicate matters further, several genetic diseases that dysregulate the Ras pathway (RASopathies) have clinical manifestations that overlap with those of NF1. Predicting outcomes in patients with neurofibromas and MPNSTs continues to be complicated, in part because of ongoing controversies regarding the grading of these neoplasms. Distinguishing sporadic and NF1-associated neurofibromas and MPNSTs on the basis of genomic abnormalities is also not possible because we have not yet identified abnormalities that are unique to sporadic or NF1-associated tumors. Indeed, there is a surprising degree of overlap in the driver mutations found in sporadic and NF1-associated neurofibromas and MPNSTs; there are differences, though, which suggests that there is >1 pathway to neoplasia in the peripheral nervous system (PNS). These genomic studies are also providing hope, as they are generating intriguing new ideas as to how to treat neurofibromas and MPNSTs.

In this review, we will discuss our current understanding of NF1 and the pathology of NF1-associated peripheral nerve sheath tumors. We will first consider the clinical and genetic features of NF1, comparing these features to those seen in NF1 mimics. We will then focus on NF1-associated neurofibromas and MPNSTs, considering first the complicated clinical behavior and pathology of these neoplasms and then discussing our current understanding of the genomic abnormalities that drive their pathogenesis. Finally, we will explore how recent studies have informed the design of new, potentially effective therapies for neurofibromas and MPNSTs.

PRESENTATION AND DIAGNOSIS OF NEUROFIBROMATOSIS TYPE 1

Clinical Features of NF1

NF1 (OMIM #162200) is the most common genetic disease affecting the human nervous system, occurring in every one in 2500 to 3500 newborn infants.[1–4] This condition, which is also known as peripheral neurofibromatosis or von Recklinghausen disease, is caused by the mutation of the *NF1* tumor suppressor gene located on chromosome 17 (17q11.2). In families with a history of NF1, the disease

From the *Department of Pathology and Laboratory Medicine; ‡The Center for Genomic Medicine; and †Medical Scientist Training Program, Medical University of South Carolina, Charleston, SC.

Supported by the National Institute of Neurological Diseases and Stroke (R01 NS048353), the National Cancer Institute (R01 CA122804), the Department of Defense (X81XWH-09-1-0086, W81XWH-12-1-0164, W81XWH-14-1-0073, and W81XWH-15-1-0193) and the Children's Tumor Foundation (2015-05-007 and 2016-04-001).

The authors have no conflicts of interest to disclose.

Reprints: Steven L. Carroll, MD, PhD, Department of Pathology and Laboratory Medicine, Medical University of South Carolina, 171 Ashley Avenue, MSC 908, Charleston, SC 29425-9080 (e-mail: carrolst@musc.edu).

Copyright © 2018 Wolters Kluwer Health, Inc. All rights reserved.

Copyright © 2018 Wolters Kluwer Health, Inc. All rights reserved.

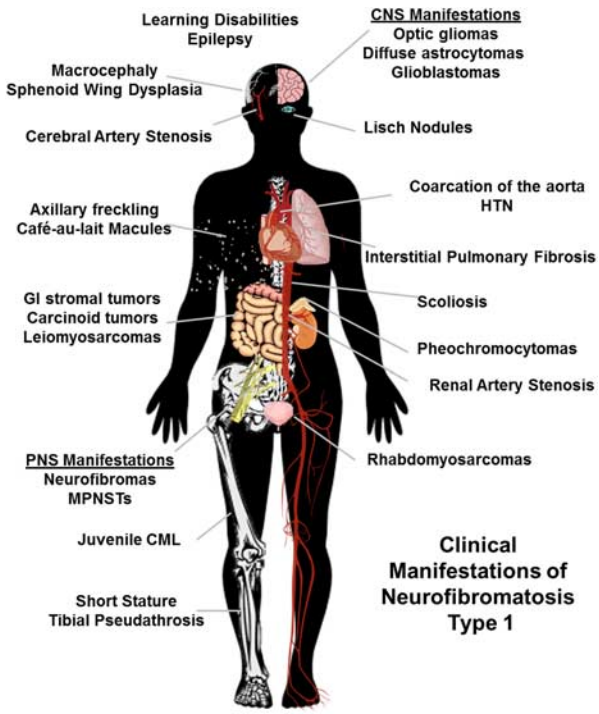


FIGURE 1. Diagram indicating the neoplastic and non-neoplastic clinical findings potentially encountered in NF1 patients. CML indicates chronic myelomonocytic leukemia; CNS, central nervous system; GI, gastrointestinal; HTN, hypertension secondary to renal artery stenosis; MPNST, malignant peripheral nerve sheath tumor; PNS, peripheral nervous system.

typically manifests as a fully penetrant autosomal dominant disorder. The absence of a family history does not eliminate NF1 as a diagnostic possibility, however, as 50% of individuals with NF1 are born into families with no previous history of the disease. This reflects the fact that the *NF1* gene has one of the highest rates of de novo mutation known for a single gene disorder. Intriguingly, these new *NF1* mutations occur in the paternally derived chromosome and so are thought to arise during spermatogenesis.[5]

The lifespan of individuals with NF1 is typically about 15 years shorter than that of the general population.[6] In large part, this shortened lifespan reflects the fact that NF1 patients are at increased risk for the development of several types of benign and malignant neoplasms (Fig. 1). Although many of these tumors arise in the central nervous system and the PNS, several types of NF1-associated neoplasms occur elsewhere including skin, the gastrointestinal tract, bone marrow, breast, and soft tissues (Fig. 1). In the central nervous system, NF1 patients develop astrocytic neoplasms, most commonly optic gliomas (pilocytic astrocytomas) that arise during childhood or adolescence. NF1-associated optic gliomas can occur anywhere along the optic nerves, the optic chiasm or the optic tracts and are found in ~15% of children with NF1.[4,7] As World Health Organization (WHO) grade I neoplasms, optic gliomas typically follow a benign clinical course. Nonetheless, they can be clinically problematic as nearly 50% of NF1 patients with optic gliomas develop moderate to severe visual impairment.[8,9] Precocious puberty also occurs in a small fraction of NF1 patients whose optic gliomas involve the optic chiasm.[10,11] Although less common than optic gliomas, NF1 patients are also at increased risk for the development of higher grade diffuse astrocytomas (WHO grade II to III) and glioblastomas (WHO grade IV), many of which occur in the brainstem.[12] Strikingly, The Cancer Genome Atlas Research Network has found that 18% of sporadic glioblastomas have homozygous deletion or mutation of the *NF1* gene,[13] underscoring the important role that *NF1* loss plays in glioblastoma pathogenesis. In the PNS, NF1 patients primarily develop neurofibromas and MPNSTs (see below for a detailed discussion of these lesions).

Although tumors of the nervous system are most commonly encountered in NF1, individuals with this disorder also develop tumors at other anatomic sites. Several series have estimated that 0.1% to 5.7% of NF1 patients will develop pheochromocytomas, typically in the fifth decade of life.[14–18] Gastric carcinoids are also associated with NF1, although this is a rare manifestation of the disorder.[19] NF1 patients are at increased risk (45-fold higher than that of the general population) for the development of gastrointestinal stromal tumors (GISTs).[20] Curiously, 60% of NF1-associated GISTs occur in the small intestine, whereas sporadic GISTs are most commonly gastric.[21] Young children with NF1 are prone to develop juvenile myelomonocytic leukemia, with boys being particularly susceptible to this malignancy.[22] Glomus tumors, which are small benign but exquisitely painful tumors that develop at the end of digits, have also been suggested to be a feature of NF1.[23] Compared with the general population, NF1 patients are also at increased risk for the development of embryonal rhabdomyosarcomas[24–26]; this is, however, one of the less common manifestations of NF1, occurring in <1% of individuals with this disorder. Likewise, leiomyosarcomas and osteosarcomas occur rarely in NF1, but still at a rate higher than that of the general population.[27] Finally, it was recently found that the lifetime risk of developing breast cancer is doubled in women with NF1 and that the survival of NF1 patients with breast cancer is poorer than that of other breast cancer patients.[28,29]

In addition to these neoplastic manifestations, there are a number of non-neoplastic findings that are commonly encountered in NF1 patients (Fig. 1). Macrocephaly is consistently present in NF1 patients; many individuals with NF1 also have a short stature, although this finding is more variable.[30–32] Melanocytic lesions of the skin (café-au-lait macules, axillary freckling) and iris (Lisch nodules) are very common findings in NF1. Skeletal abnormalities such as scoliosis, vertebral scalloping, unilateral sphenoid wing dysplasia, and tibial pseudoarthrosis are present in nearly half of NF1 patients.[33] Decreased bone mineral density is also frequent in NF1 patients. This is potentially related to the fact that serum 25-hydroxy-vitamin D concentrations are reduced in individuals with a large numbers of dermal neurofibromas[34]—in fact, 25-hydroxy-vitamin D levels are inversely proportional to the burden of these tumors. Cardiovascular abnormalities ranging from renal, coronary, and cerebral artery stenosis to pulmonary stenosis, valvular malformations, and coarctation of the abdominal aorta occur in nearly 10% of NF1 patients[6,35–38] and are another factor contributing to mortality in these patients, particularly those who die before 30 years of age.[6,39] Although their IQ scores are normal or slightly below normal, learning disabilities are reported in up to 80% of children with NF1.[40] Further, nearly 40% of these children have attention deficit/hyperactivity disorder, 30% have autism spectrum disorder,[41] and many have visual spatial deficits.[42] T2-weighted magnetic resonance imaging often

Copyright © 2018 Wolters Kluwer Health, Inc. All rights reserved.
Copyright © 2018 Wolters Kluwer Health, Inc. All rights reserved.

identifies "unidentified bright objects" (UBOs) in the basal ganglia, thalamus, brainstem, cerebellum, or subcortical white matter of these children.[43–45] These UBOs, which have variously been interpreted as hamartomas,[46] regions of abnormal myelination,[47] heterotopias[48] or vacuolated myelin,[49] are potentially related to the learning disabilities seen in children with NF1.[50] UBOs can also be confused with the radiologic abnormalities associated with a glioma.

It is thus apparent that a wide variety of clinical abnormalities can be encountered in NF1 patients. NF1 is completely penetrant and affects males and females equally. However, the constellation of findings that are present in individual patients is highly variable, even among closely related family members who have NF1. As a result of this variability, clinicians attempting to establish a diagnosis of NF1 rely on key clinical findings that are most commonly present in patients with this disorder. At least 2 of the following must be present to diagnose NF1: (1) 6 café-au-lait macules (>1.5 cm in diameter postpuberty, >0.5 cm prepuberty); (2) armpit or inguinal freckling; (3) 1 plexiform neurofibroma or ≥ 2 cutaneous neurofibromas; (4) an optic glioma; (5) ≥ 2 Lisch nodules; (6) bony dysplasia; or (7) a first-degree relative with NF1. In most instances, these criteria, which were developed by the 1988 National Institutes of Health Consensus Development Conference on Neurofibromatosis, work well. However, in patients where the diagnosis has relied primarily on pigmentary abnormalities rather than the occurrence of key neoplasms, NF1 can be confused with other NF1 mimics.

Distinguishing NF1 From NF1 Mimics Clinically

To understand why some RASopathies have clinical findings that overlap with NF1, one must first understand the signaling pathways affected by *NF1* loss. Neurofibromin, the protein encoded by the *NF1* gene, includes up to 2818 amino acids and, as the result of alternative mRNA splicing, occurs as 220 and 250 kDa protein species. Shortly after the *NF1* gene was cloned, it was noted that a domain in the neurofibromin protein was highly homologous to the yeast Ras GTPase-activating proteins (Ras GAPs) IRA1 and IRA2.[51] Functional analyses subsequently confirmed that the IRA-homologous domain of neurofibromin (amino acids 1203 to 1549 of GenBank sequence NP_000258.1), like the yeast IRA proteins, functions as a Ras GAP.[52] Ras proteins exist in 2 forms: an active GTP-bound form and an inactive GDP-bound form. The conversion of active Ras to the inactive state is dependent on a GTPase activity that is intrinsic to Ras. However, this intrinsic GTPase activity is very inefficient and Ras thus requires a "helper" protein to stimulate its own GTPase activity. The neurofibromin Ras GAP performs this function; neurofibromin interacts with Ras to stimulate its intrinsic GTPase activity, resulting in the cleavage of the terminal triphosphate of GTP, thus converting GTP (active) to GDP (inactive). In light of this neurofibromin function, it can be readily appreciated that loss-of-function mutations of the *NF1* gene and the accompanying loss of neurofibromin expression result in unopposed activation of Ras and Ras-regulated signaling pathways. The regulation of Ras signaling, however, is not the sole function of neurofibromin. Indeed, several studies have shown that neurofibromin interacts with the cytoskeleton[53] and focal adhesion kinase,[54] regulates calcium[55,56] and cAMP-modulated[57–59] signaling pathways and binds to glycerophospholipids[60–62]; all of these neurofibromin functions are independent of neurofibromin's Ras GAP domain. However, neurofibromin's ability to inhibit Ras signaling is its best understood function and it is clearly biologically relevant. Consequently, most attempts to design therapies targeting NF1-associated neoplasms have focused on Ras-associated signaling cascades (see below).

Ras proteins regulate a wide variety of cellular functions such as proliferation, survival, migration, and differentiation.[63] Given the central role of Ras signaling in the life of the cell and the need to precisely regulate this signaling, it is not surprising that a number of proteins other than neurofibromin enhance or inhibit Ras-modulated signaling pathways (Fig. 2). Mutations in several of the genes encoding these proteins also dysregulate Ras-associated signaling cascades, thereby producing the genetic syndromes that are collectively known as the RASopathies.[64,65] In addition to NF1, at least 9 RASopathies have been defined to date: Legius syndrome, Noonan syndrome, LEOPARD syndrome (also known as Noonan syndrome with multiple lentigines), Noonan-like syndrome (recently renamed CBL syndrome), Noonan-like syndrome with loose anagen hair, Costello syndrome, cardiofaciocutaneous syndrome, hereditary gingival fibromatosis, and capillary malformation-arteriovenous malformation syndrome. The clinical manifestations of many of these RASopathies overlap with one another and with NF1. Intriguingly, however, although the mutations causing these syndromes all dysregulate the Ras signaling cascade, their clinical manifestations are not identical (Table 1). Of note, the findings encountered in non-NF1 RASopathies most commonly overlap with the non-neoplastic manifestations of NF1. For example, Legius syndrome, which is also known as NF1-like syndrome, is characterized by the occurrence of multiple café-au-lait macules, skin fold freckling, macrocephaly, and learning disabilities, much as is seen in NF1. However, Legius syndrome patients, unlike NF1 patients, do not typically develop large numbers of dermal neurofibromas (we have, however, seen doubts raised by the chance co-occurrence of a sporadic neurofibroma in a Legius patient) or the spectrum of malignancies commonly encountered in NF1. Noonan syndrome patients also show a number of the non-neoplastic findings such as macrocephaly, short stature, and mild cognitive impairment often seen in NF1; individuals with Noonan syndrome are also prone to develop myeloproliferative disorders similar to juvenile myelomonocytic leukemia. However, again, classic Noonan syndrome patients do not develop numerous neurofibromas or the spectrum of other neoplasms characteristic of NF1. The clinical features of the other RASopathies indicated in Table 1 show less overlap with NF1 than either Legius or Noonan syndrome. Consequently, a careful assessment of the non-neoplastic features of these patients and an appreciation of the fact that they either do not develop malignancies or develop a spectrum of malignancies quite different from that seen in NF1 will usually keep the clinician from falling into the trap of misdiagnosing one of these RASopathies as NF1.

Although the guidelines outlined above are typically sufficient for distinguishing NF1 from other RASopathies, we would note that there are some patients where diagnosis will still be problematic. This is because a small subsets of NF1 patients exist who present with clinical features that more extensively overlap with other RASopathies. As an illustration of this, we would point to the subset of patients with the NF1 variant known as neurofibromatosis-Noonan syndrome (OMIM #601321). Individuals with neurofibromatosis-Noonan syndrome have café-au-lait macules, Lisch nodules,

Copyright © 2018 Wolters Kluwer Health, Inc. All rights reserved.

Copyright © 2018 Wolters Kluwer Health, Inc. All rights reserved.

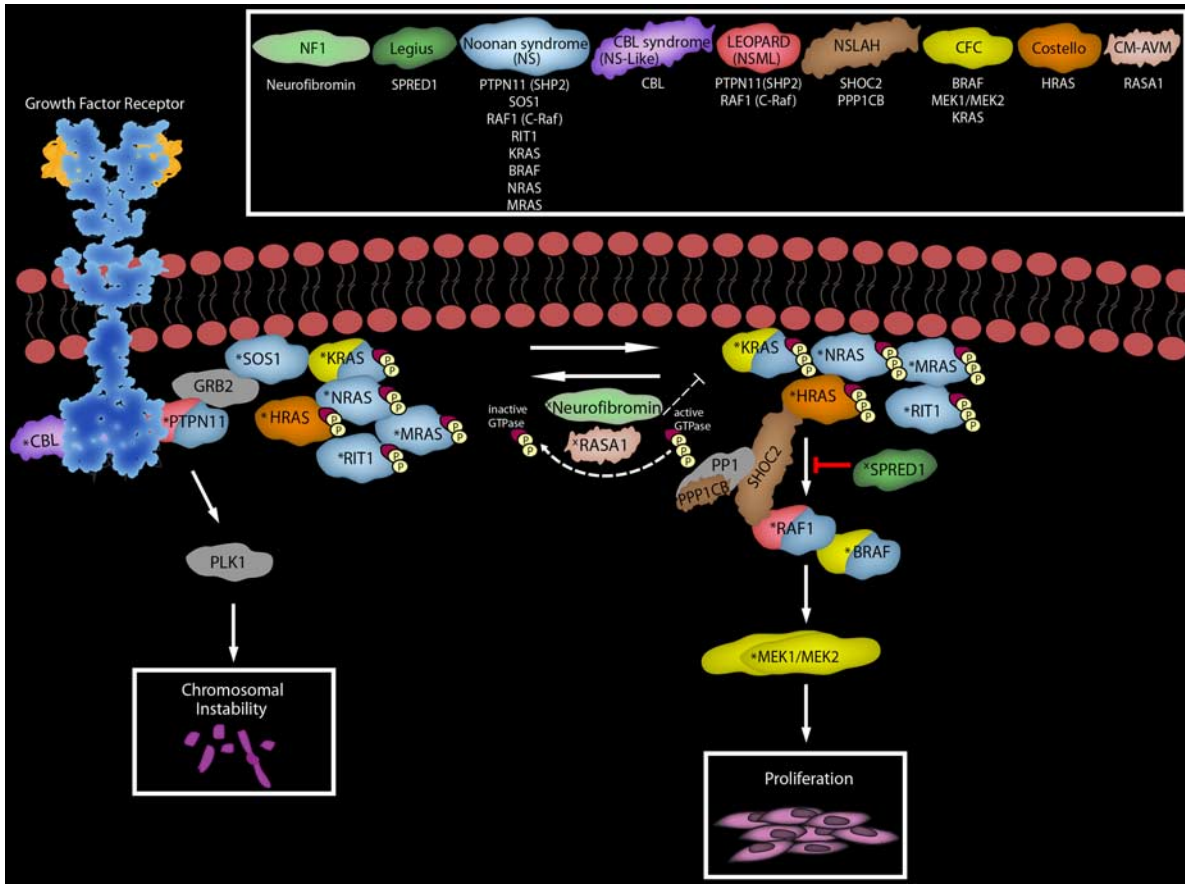


FIGURE 2. The Ras-associated signaling cascades and the inherited causative genes responsible for the clinical manifestations of RASopathies. RASopathies include NF1, Legius syndrome, NS, CBL syndrome (NS-like with or without juvenile myelomonocytic leukemia), NS with multiple lentigines (NSML or LEOPARD), NS-like disorder with loose anagen hair (NSLAH), CFC syndrome, Costello syndrome, and capillary malformation-ateriovenous malformation syndrome (CM-AVM). The most common mutated genes and the resultant proteins associated with each effected disease are color matched as indicated in the key. Note KRAS and BRAF are found mutated in both NS and CFC. Not depicted above are potential causal genes with germline mutations requiring further validation such as SOS2, A2ML1, RASA2, and LZTR1 (NS), RRAS (CBL syndrome), and BRAF (LEOPARD). RASopathy-related germline gain-of-function mutations are designated with a "*," loss-of-function mutations are designated with a "x." A2ML1 indicates alpha-2-macroglobulin like 1; BRAF, B-Raf protooncogene serine/threonine-protien kinase, CBL, the Cbl protooncogene; CFC, cardiofaciocutaneous; GRB2, growth factor receptor bound protein 2; HRAS, Harvey Ras oncogene; KRAS, Kirsten Ras oncogene; MEK1/MEK2, mitogen-activated protein kinase 1 and 2; NF1, neurofibromatosis type 1; NS, Noonan syndrome; PLK1, polo-like-kinase 1; PP1, protein phosphatase 1; PPP1CB, protein phosphatase 1 catalytic subunit beta; PTPN11, protein tyrosine phosphatase nonreceptor type 11; RAF1, Raf-1 protooncogene; RASA1, Ras p21 protein activator 1; RASA2, Ras p21 protein activator 2; RIT1, Ras-like without CAAX 1; SHOC2, SHOC2 leucine-rich repeat scaffold protein; SOS1, SOS Ras/Rac guanine nucleotide exchange factor 1; SPRED1, sprout-related EVH1 domain containing 1.

and axillary freckling in combination with features of Noonan syndrome such as hypertelorism, epicanthal folds, a webbed neck, low-set ears, and pulmonic stenosis; they do not, however, have neurofibromas.[66,67] Genomic analyses have shown that neurofibromatosis-Noonan syndrome patients carry heterozygous mutations of the *NF1* gene, with in-frame deletions affecting exons 24 and 25, which encode part of the Ras GAP sequence, being particularly common.[68] On occasion, coexisting mutations of the *PTPN11* gene, which is linked to Noonan syndrome, are present in neurofibromatosis-Noonan syndrome patients.[69] However, this seems be to the exception rather than the rule.

NF1 Mutations and Genotype-Phenotype Correlations

In families in which NF1 has not been previously encountered or properly diagnosed, genomic testing is often performed to establish the diagnosis and to facilitate genetic counseling for family members. However, this testing is complicated, both because of the large size of the *NF1* gene and because of the wide spectrum of mutations that are encountered in NF1 patients. The human *NF1* gene spans ~283,000 base pairs and contains 60 exons, some of which are alternatively spliced in the mRNAs transcribed from this locus.[70,71] In light of the high frequency of new mutations affecting the *NF1* locus, it is not surprising that the types of mutations encountered in NF1 patients are diverse. The overwhelming majority of germline *NF1* mutations are point mutations and include nonsense mutations, missense mutations, frameshift mutations, and mutations affecting mRNA splicing.[72,73] Only 5% of NF1 patients have whole gene deletion,[74] which apparently results from nonallelic homologous recombination between sequences flanking the *NF1* locus. These homologous recombination

Copyright © 2018 Wolters Kluwer Health, Inc. All rights reserved.
Copyright © 2018 Wolters Kluwer Health, Inc. All rights reserved.

TABLE 1. Clinical Features of RASopathies

Syndrome	Non-Neoplastic Features	Neoplastic Features
Legius syndrome/NF1-like syndrome	Multiple café-au-lait macules; macrocephaly; skin fold freckling; learning disability; Noonan syndrome-like facies; cardiac valvular abnormalities	Lipomas
Noonan syndrome	Macrocephaly; distinctive facies; short stature; mild cognitive impairment; webbed neck; pectus excavatum; cryptorchidism	Juvenile myelomonocytic leukemia-like myeloproliferative disorders
LEOPARD syndrome/Noonan syndrome with multiple lentigines	Multiple lentigines; electrocardiographic conduction abnormalities; ocular hypertelorism; pulmonary stenosis; abnormal genitalia; retardation of growth; sensorineural deafness	None
Noonan-like syndrome	Noonan syndrome-like facies; hyperpigmented skin lesions; microcephaly; cardiomyopathy; arrthymias; valvular abnormalities; developmental delays	None
Noonan-like syndrome with loose anagen hair	Cardiovascular abnormalities; macrocephaly; short stature; mild cognitive impairment; fine sparse and easily pluckable hair	None
Costello syndrome	Cardiovascular abnormalities; coarse facies with facial warts; short stature; failure to thrive; severe feeding difficulties; curly hair; palmar keratosis. Variant exists presenting with a congenital myopathy with excess of muscle spindles	Increased risk of malignant tumors including transitional cell carcinomas of bladder, rhabdomyosarcomas, and ganglioneuroblastomas
Cardiofaciocutaneous syndrome	Cardiovascular abnormalities; distinct facies; failure to thrive; nevi, lentigines, palmar-plantar keratosis; curly hair; seizures; severe intellectual disability	None
Hereditary gingival fibromatosis	None	Gingival fibromatosis
Capillary malformation-arteriovenous malformation syndrome	Capillary malformations; arteriovenous malformations	None

NF1 indicates neurofibromatosis type 1.

events, which are also referred to as *NF1* microdeletions, are classified as type I or type II recombination events. Type I deletions span 1.4 MB and result from recombination between the *NF1-REP A* and *NF1-REP C* clusters of paralogous loci.[75–78] Type II deletions result in the loss of 1.2 MB of sequence and arise by recombination between the *SUZ12* gene and the *SUZ12P1* pseudogene.[79,80] Interestingly, 3 genes known as *OMGP*, *EVI2B*, and *EVI2A* are encoded in an intron of the *NF1* gene (although running in the opposite direction). These genes are also deleted in type I and type II recombination events, raising the question of whether their loss might also contribute to the phenotype of patients with *NF1* microdeletions.

Germline mutations in the *NF1* gene tend to cluster in particular locations, with mutations affecting exons 10a-c and 37 being particularly common.[72] However, given the frequency with which new mutations occur in the *NF1* gene and the variety of *NF1* mutation types described above, it is not surprising that germline *NF1* mutations are also encountered at numerous other sites in this locus. To address this complexity, a comprehensive approach was developed several years ago which combined deep sequencing of all 60 *NF1* exons, copy number analyses, and screening for intronic splicing site mutations. Although complicated, this testing methodology was effective, identifying *NF1* mutations in ~95% of clinically suspicious cases[72]; the 5% of candidate cases in which an NF1 diagnosis could not be established were likely NF1 cases in which the mutation occurred in gene regions that were not examined (eg, promoter sequences of the gene), cases in which the patient was mosaic for the *NF1* mutation or an NF1 mimic such as those described above. With the advent of massively parallel sequencing methodologies, an increasing number of diagnostic laboratories have now turned to sequencing the entire sequence of the *NF1* gene to identify possible causative mutations. Curiously, however, many reference laboratories are reporting diagnostic success in only 75% to 85% of candidate cases. It is not clear whether this difference reflects a more careful selection of cases with the older diagnostic methodology or some other factor.

The question often arises as to whether the *NF1* genotype predicts the phenotype in patients. The answer is "sometimes." There is good evidence that patients with NF1 microdeletion (ie, the 5% of NF1 patients with whole gene deletion) show a strong correlation between genotype and phenotype. NF1 microdeletion syndrome patients characteristically have large numbers of dermal neurofibromas (in the thousands), dysmorphic features, and substantial cognitive impairment and are at increased risk for the development of plexiform neurofibromas and MPNSTs.[81] Another notable example is those pedigrees in which family members carry a 3 base pair in-frame deletion in exon 17 of the *NF1* gene. Although these patients do not develop

Copyright © 2018 Wolters Kluwer Health, Inc. All rights reserved.

Copyright © 2018 Wolters Kluwer Health, Inc. All rights reserved.

dermal neurofibromas, they do manifest the other features characteristic of NF1.[82]

In contrast, the manifestations of NF1 can be highly variable in patients with other mutations of the *NF1* gene. This is true even when comparing the clinical findings in family members who carry the exact same *NF1* mutation. These clinical observations have led to the suggestion that modifier genes exist that interact with the *NF1* gene and influence what manifestations of NF1 will be evident in an individual patient. As an initial assessment of this possibility, 8 traits commonly encountered in NF1 (the number of café-au-lait macules, number of dermal neurofibromas, and head circumference as well as the occurrence of plexiform neurofibromas, optic gliomas, scoliosis, epilepsy, and referral for remedial education) were examined in 48 pedigrees (a total of 175 patients) that included 6 pairs of monozygotic twins.[19] This study showed that the number of café-au-lait macules and dermal neurofibromas had the highest correlation between monozygotic twins, with a lower degree of correlation between first-degree relatives and an even lower correlation among more distant relatives. The presence or absence of plexiform neurofibromas, optic gliomas, scoliosis, epilepsy, and referral for remedial education also showed significant familial clustering, in a pattern most consistent with polygenic effects. There is also evidence that aberrant Ras activation must cross a threshold to drive tumorigenesis and that some "milder" *NF1* mutations cannot accomplish this on their own[83]; in this circumstance, other genes must interact with *NF1* mutations to drive tumorigenesis.

There is thus good evidence that modifier genes exist that interact with *NF1* to modify the phenotype of NF1 patients. However, the identity of these modifier genes has not yet been established. Thus far, the most promising approaches to identifying the relevant modifier genes have come from studies in rodent models. It is clear that the pathogenesis of MPNSTs in mice carrying cis-linked *Nf1* and *p53* null mutations (cis-NP mice) is influenced by strain background.[84] Two unlinked polymorphic loci known as nerve sheath tumor resistance 1 (*Nstr1*) and 2 (*Nstr2*) have been mapped and shown to epistatically influence MPNST pathogenesis in cis-NP mice. Genome-wide association studies in BDIV (tumor resistant) and BDIX (tumor susceptible) rats exposed to the chemical mutagen ethylnitrosourea have also identified 2 genomic regions known as *Mss1* and *Mss7* that lower the risk of developing an MPNST.[85,86] It remains to be determined whether the human counterparts of these rodent loci contribute to phenotypic variability in NF1 patients.

NEUROFIBROMAS

Pathology of Neurofibromas

It is generally accepted that multiple neurofibroma subtypes exist, that these subtypes have distinct natural histories and that they differ in their potential for undergoing malignant transformation and becoming an MPNST. However, how these neurofibroma subtypes are classified depends on the specialists' perspective—at present, pathologists, dermatologists, geneticists, and basic scientists all use different classification schemes. In an attempt to resolve this confusion, a summit that included experts from all of these specialities recently convened and devised a consensus classification scheme for neurofibromas (Ortonne et al, submitted). Hopefully, this consensus classification scheme will be widely accepted in the near future. However, at present, pathologists most commonly use the WHO criteria for defining neurofibroma subtypes. Consequently, we will use the WHO classification scheme here as a framework for discussing the biology of different neurofibroma subtypes.

The WHO classification scheme defines 5 neurofibroma subtypes (Table 2), 2 of which are found exclusively found in skin and related tissues (cutaneous or dermal neurofibromas). Localized cutaneous neurofibromas, as indicated by their designation, are well-circumscribed nonencapsulated lesions that are found in the dermis and subcutaneous tissues of the skin. Sporadic localized cutaneous neurofibromas are very commonly encountered in the general population as solitary lesions—indeed localized cutaneous neurofibromas are the most common subtype of neurofibroma encountered clinically. Only about 10% of localized cutaneous neurofibromas are NF1-associated. NF1 patients also tend to have multiple localized cutaneous neurofibromas, which are often overlain by café-au-lait macules. Curiously, localized cutaneous neurofibromas are typically not present at birth in NF1 patients. These lesions instead begin to appear when the patient enters puberty and accumulate thereafter. In addition, localized cutaneous neurofibromas increase in number and enlarge in women with NF1 who get pregnant, suggesting that these lesions are hormonally regulated. Despite their at times rapid growth, localized cutaneous neurofibromas are benign tumors that

TABLE 2. Characteristics of Neurofibroma Subtypes Defined by the World Health Organization

Subtype	Location	Relation to NF1	Malignant Potential	Comments
Localized cutaneous	Skin (dermis and subcutaneous)	10% NF1-associated, 90% sporadic	None	Most common subtype. In NF1, may be overlain by café-au-lait macules
Diffuse cutaneous	Skin (dermis and subcutaneous)	10% NF1-associated, 90% sporadic	Very low, but does occur	Uncommon lesions that present as plaque-like thickenings of skin
Localized intraneural	Cranial, spinal, or autonomic nerves	Can be either sporadic or NF1-associated	Intermediate	Second most common subtype
Plexiform	Cranial, spinal, or autonomic nerve plexuses	Exclusively NF1-associated	Highest	Key diagnostic for NF1
Massive soft tissue	Extremities, extensive soft tissue expansion with underlying large nerve	Exclusively NF1-associated	Intermediate, but low clinical impact due to rarity	Least common subtype, also known as elephantiasis neuromatosa

NF1 indicates neurofibromatosis type 1.

Copyright © 2018 Wolters Kluwer Health, Inc. All rights reserved.
Copyright © 2018 Wolters Kluwer Health, Inc. All rights reserved.

have essentially no malignant potential. The second type of skin-associated neurofibromas, which are known as diffuse cutaneous neurofibromas, are poorly defined plaque-like lesions that, like localized cutaneous neurofibromas, are localized in the dermis and subcutaneous region of skin in children and young adults. As 90% of diffuse cutaneous neurofibromas are sporadic, the presence of these uncommon lesions is not necessarily indicative of NF1. Unlike localized cutaneous neurofibromas, however, diffuse cutaneous neurofibromas do have a very low, but nonetheless real, malignant potential. Although dermal neurofibromas have long been held to originate from peripheral nerves, it typically has been difficult to find a nerve of origin in either localized or diffuse cutaneous neurofibromas; even if a small cutaneous nerve can be identified, it is difficult to rule out the possibility that the nerve was simply entrapped by the growing neurofibroma. These observations, as well as observations in genetically engineered mouse models, have led to the suggestion that dermal neurofibromas instead arise from skin-derived precursors, which are a population of neural crest-derived multipotent progenitor cells found at the base of hair follicles.[87]

The other 3 neurofibroma subtypes are more clearly associated with large nerves and are thought to originate from these structures. Localized intraneural neurofibromas, which are the second most common type of neurofibroma, occur at any point along cranial, spinal, or autonomic nerves. Localized intraneural neurofibromas may be either sporadic or NF1-associated. Grossly, localized intraneural neurofibromas are evident as a segmental fusiform enlargement of the affected nerve rather than as a diffuse enlargement of multiple nerve fascicles as is seen in a plexiform neurofibroma. Localized intraneural neurofibromas can transform into a MPNST but do so less frequently than plexiform neurofibromas. Plexiform neurofibromas occur in cranial, spinal, or autonomic nerve plexuses and are often thought to be exclusively NF1-associated. In contrast to localized intraneural neurofibromas, these produce diffuse enlargement of a nerve plexus rather than segmental enlargement of the nerve. Grossly, plexiform neurofibromas are often described as having a "bag of worms" appearance. Of the 5 neurofibroma subtypes, plexiform neurofibromas have the highest potential for undergoing transformation into a MPNST. Massive soft tissue neurofibromas are the rarest subtype of neurofibroma. These neoplasms occur in the extremities, where they trigger massive hypertrophy of soft tissue, resulting in the condition sometimes referred to as elephantiasis neurofibromatosa. An underlying plexiform neurofibroma is often found in massive soft tissue neurofibromas, which can lead to confusion as to how these neurofibromas should be subtyped. Like plexiform neurofibromas, massive soft tissue neurofibromas are solely NF1-associated neoplasms and often undergo malignant transformation. However, their clinical impact is lessened by the fact that massive soft tissue neurofibromas are by far the least common neurofibroma subtype and so are only rarely identified as the source of an MPNST.

Despite their differences in location and malignant potential, all 5 neurofibroma subtypes have an identical microscopic appearance. Examination of a hematoxylin and eosin-stained section of a neurofibroma (Fig. 3A) shows a bland, moderately cellular neoplasm composed predominantly of spindled cells set again a richly collagenous or focally mucinous background. Despite this bland appearance, however, neurofibromas are actually composed of a very complex mixture of cell types. Between 40% and 80% of the cells within a neurofibroma are Schwann cell-like elements that are immunoreactive for the calcium-binding protein S100β, the low affinity neurotrophin receptor ($p75^{LNTR}$) and the transcription factor Sox10 (Fig. 3B). Mast cells, which are recognizable by their immunoreactivity for c-Kit (CD117; Fig. 3C), are scattered throughout neurofibromas and are thought to be responsible for the pruritus that NF1 patients often experience in conjunction with their dermal neurofibromas. Neurofibromas also contain a peculiar population of CD34-immunoreactive dendritic cells (Fig. 3D). The identity of these cells remains controversial, with some investigators believing that these CD34-positive cells are a type of macrophage[88] and others suggesting that they may be another, as yet undescribed, cell type.[89] A population of cells with the ultrastructural characteristics of perineurial cells (long thin cytoplasmic processes, frequent pinocytotic vesicles, and a discontinuous basal lamina) are also present in neurofibromas; although these cells lack the epithelial membrane antigen immunoreactivity seen in normal perineurial cells, they do mark for the perineurial markers Glut1 and claudin. At least some of the CD34 immunoreactivity in neurofibromas is in small blood vessels, however, as shown by the fact that these structures also label for CD31 (Fig. 3E). Fibroblasts are also numerous in neurofibromas and can be readily identified by their immunoreactivity for the transcription factor TCF4 (Fig. 3F). In addition, it was recently pointed out that neurofibromas contain large numbers of macrophages[90] that label for the pan-macrophage marker Iba1 (Fig. 3G). These cells include both the anti-inflammatory (M2 macrophages, identifiable by CD163 staining; Fig. 3H) and proinflammatory (M1 macrophages, identifiable by immunoreactivity for CD86; Fig. 3I) subsets of macrophages.

Given the complex composition of neurofibromas, it is not surprising that for many decades pathologists argued about: (1) whether neurofibromas were hamartomas or were true neoplasms and (2) if they were neoplasms, which cell type within the neurofibroma was the neoplastic cell type. The identification of the *NF1* gene in the early 1990s provided the tools that made it possible to settle these questions. The germline of NF1 patients is heterozygous for the *NF1* mutation, carrying both a mutant allele and a wild-type allele. As clinical evidence suggested that *NF1* functions as a tumor suppressor, it was anticipated that a "second hit" deleting the remaining wild-type (functional) *NF1* gene would be required for tumorigenesis. In keeping with this, *NF1* loss of heterozygosity (LOH) was identified in cells isolated from neurofibromas. However, *NF1* LOH was evident in Schwann cells, but not fibroblasts, isolated from these tumors.[91,92] These observations both confirmed the identification of neurofibromas as true neoplasms and argued that Schwann cells were the neoplastic component within neurofibromas. The subsequent generation of genetically engineered mouse models in which the ablation of *Nf1* in Schwann cells triggered neurofibroma formation provided direct experimental proof that Schwann cells are the neoplastic element in neurofibromas.[93,94]

Although it is now clear that Schwann cells are the neoplastic component of neurofibromas, a growing body of evidence indicates that the other cell types present in these neoplasms also contribute to tumorigenesis. Loss of the remaining functional *NF1* allele in Schwann cells results in changes in the biology of Schwann cells (eg, increased proliferation) that promote tumor formation. However, *NF1*

Copyright © 2018 Wolters Kluwer Health, Inc. All rights reserved.

Copyright © 2018 Wolters Kluwer Health, Inc. All rights reserved.

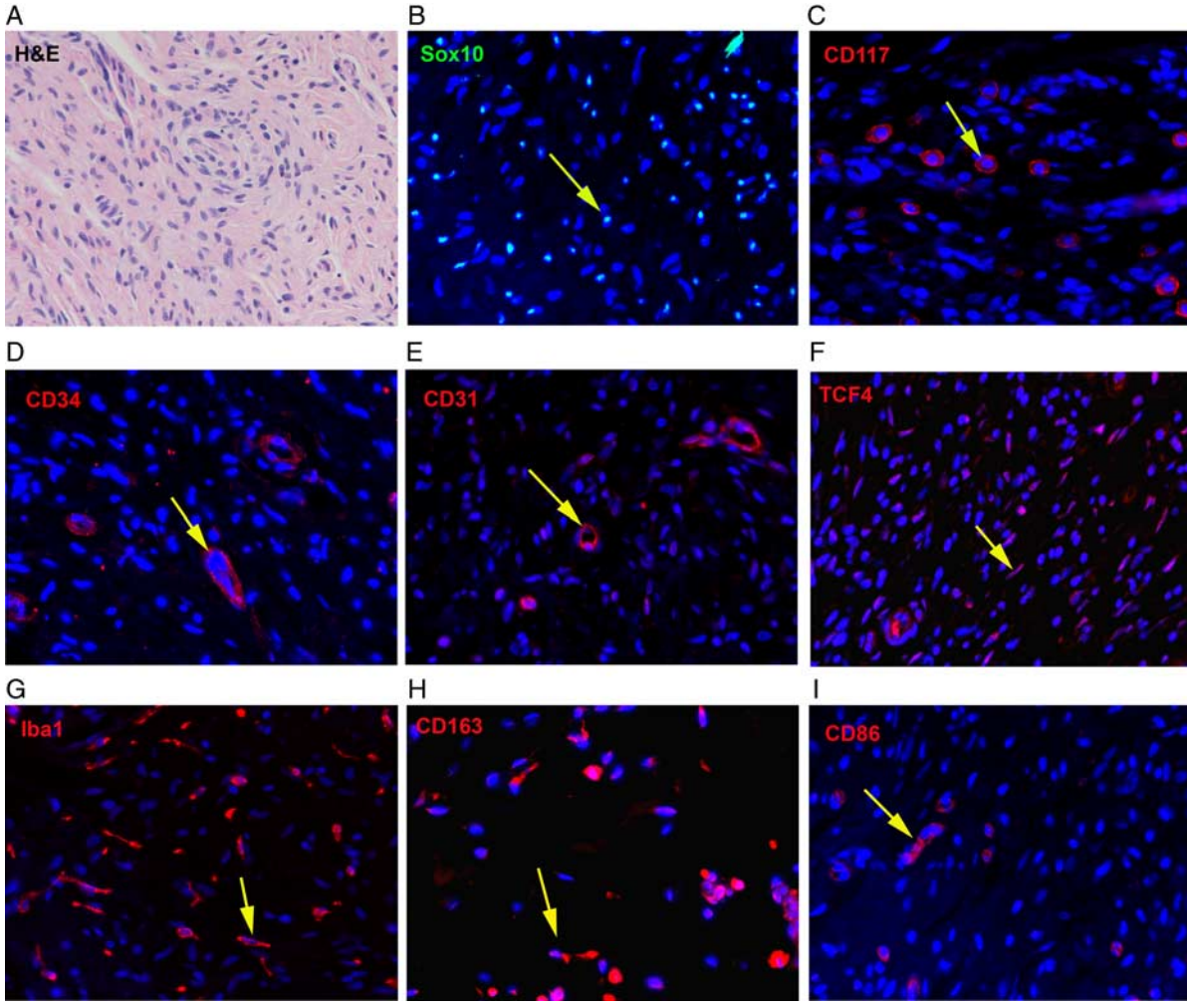


FIGURE 3. Cellular composition of neurofibromas. A, hematoxylin and eosin-stained section of a dermal neurofibroma (×40). All subsequent images are taken from this same tumor at a ×63 magnification. B, Immunoreactivity for the transcription factor Sox10 (green, representative cell indicated by an arrow) in the Schwann cell component of this dermal neurofibroma. The section has been counterstained with bisbenzamide to highlight the nuclei of all cells in the tumor. C, Immunoreactivity for the mast cell marker CD117 (also known as c-Kit; red, representative cell indicated by arrow) in the dermal neurofibroma. D, Immunoreactivity for CD34 (red) is apparent in vasculature (arrow) and in small dendritic cells in the tumor. E, Immunoreactivity (red) for CD31 in small intratumoral blood vessels (arrow). F, Immunoreactivity (red) for the fibroblast nuclear marker TCF4 (transcription factor 4; representative cell indicated by arrow) in the tumor. G, Immunoreactivity for the pan-macrophage marker Iba1 (red, representative cell indicated by arrow) in the tumor. H, Immunoreactivity for CD163 (red), a marker of the M2 (anti-inflammatory) subclass of macrophages, in the tumor (representative cell indicated by arrow). I, Immunoreactivity for CD86 (red), a marker of the M1 (proinflammatory) subclass of macrophages, in the tumor (representative cell indicated by arrow).

loss in Schwann cells also induces hyperreactive paracrine interactions that act in concert to drive neurofibroma pathogenesis. At present, the role that paracrine interactions between *NF1*$^{-/-}$ Schwann cells and *NF1*$^{+/-}$ mast cells play in neurofibroma pathogenesis is best understood. Kit ligand, which promotes the proliferation, survival, migration, and activation of mast cells is secreted by the Schwann cells within neurofibromas.[95,96] A comparison of Kit ligand secretion by Schwann cells isolated from mice with ablation of the *Nf1* gene showed that secretion of this growth factor was dependent on *Nf1* gene dosage, with *Nf1*$^{-/-}$ Schwann cells secreting 6 times more Kit ligand than either *Nf1*$^{+/-}$ or wild-type Schwann cells.[97] Intriguingly, the proliferation, survival, and migration of *Nf1*$^{+/-}$ mast cells challenged with Kit ligand is exaggerated compared with wild-type mast cells,[97–99] which facilitates the recruitment of mast cells into a developing neurofibroma. These recruited, hyperactive *Nf1*$^{+/-}$ mast cells are required for tumorigenesis, as mice with Schwann cell-specific *Nf1* ablation that are grafted with *Nf1*$^{+/-}$ bone marrow develop neurofibromas, whereas those grafted with wild-type bone marrow do not.[100]

Following Kit ligand stimulation, these recruited mast cells in turn show enhanced secretion of transforming growth factor-β,[101] which acts on fibroblasts to stimulate collagen production. As *Nf1*$^{+/-}$ fibroblasts are themselves hyperresponsive to transforming growth factor-β compared with their wild-type counterparts, this results in collagen production that is in excess of what is produced by similarly stimulated wild-type fibroblasts. The existence of a paracrine network that connects Schwann cells, mast cells, and

Copyright © 2018 Wolters Kluwer Health, Inc. All rights reserved.
Copyright © 2018 Wolters Kluwer Health, Inc. All rights reserved.

fibroblasts in neurofibroma pathogenesis suggests that other, as yet undiscovered, paracrine factors promote additional interactions between other cell types intrinsic to these neoplasms. Investigations directed toward further defining these paracrine networks and identifying key signaling molecules within them will likely be a fruitful avenue of future study that has great potential for therapeutic development.

Genomic Abnormalities in Neurofibromas

As noted above, Schwann cells derived from NF1-associated neurofibromas have both a germline *NF1* mutation and a somatic *NF1* mutation,[91,92,102] which is often evident as *NF1* LOH. The essential role of *NF1* loss in neurofibroma pathogenesis is supported by the development of neurofibromas in mice following ablation of the *Nf1* gene in Schwann cells.[93,94] Consequently, it is clear that *NF1* loss is necessary for the pathogenesis of neurofibromas in NF1 patients. However, there is also reason to think that *NF1* loss alone is not sufficient for the development of a neurofibroma and that additional genomic or other abnormalities are required for tumorigenesis. This reasoning is supported, in part, by our current understanding of the regulation of the Ras signaling pathway. Because of the central role it plays in a number of key cellular functions, surveillance mechanisms exist that reign in excessive Ras activation by triggering a process known as oncogene-induced senescence. This process is clearly relevant to the pathogenesis of NF1-associated neoplasms as experimental ablation of *NF1* expression in fibroblasts results in an initial activation of Ras and Ras-regulated signaling pathways which is then followed by inactivation of these pathways, growth arrest, and cellular senescence.[103] As senescent neurofibromin-negative Schwann cells are present in neurofibromas, oncogene-induced senescence is likely operant in *NF1*-null Schwann cells and must be overcome for tumor growth. However, the mechanism by which *NF1*-null Schwann cells overcome oncogene-induced senescence is not yet understood. In principal, this mechanism could involve the occurrence of mutations in other genes, alterations in the epigenome or biochemical alterations that oppose oncogene-induced senescence.

Several laboratories have examined the genomes of NF1-associated neurofibromas, both to search for other mutations that interact with *NF1* loss to drive tumor growth and to determine whether the multiple neurofibromas that occur in these patients arise independently or are instead clones derived from a single progenitor event. At present, there is little evidence that implicates mutations in genes other than *NF1* in neurofibroma pathogenesis. Emmerich et al[104] performed whole exome sequencing on 7 spatially distinct dermal neurofibromas and 2 reference tissues from a single NF1 patient. Although these tumors shared a common germline *NF1* mutation, the "second hit" *NF1* mutation was distinct in each tumor, indicating these neoplasms arose independently. These authors reported somatic mutations in other genes in only 2 of their 7 neoplasms, which led them to suggest that mutations in genes other than *NF1* are not necessary for the pathogenesis of NF1-associated dermal neurofibromas. In contrast, Faden and colleagues also performed whole exome sequencing on 6 dermal neurofibromas from a single individual and found 15 to 26 somatic mutations per sample.[105] Although *NF1* was the only recurrently mutated gene in their tumors, pathway analyses indicated that mutations affecting Hippo pathway components were overrepresented in their tumors. Findings similar to those of Emmerich and colleagues have been reported in plexiform neurofibromas. Whole exome sequencing, RNA-Seq, and genome-wide copy number assays performed on 23 Schwann cell cultures established from plexiform neurofibromas consistently identified *NF1* mutations in these tumors, but found no evidence of other recurrent somatic inactivating mutations or copy number changes.[106] Consequently, there little evidence at present to indicate that specific genes other than *NF1* are consistently mutated in dermal or plexiform neurofibromas. These observations suggest that it is more likely that other types of abnormalities (eg, epigenetic changes and biochemical alterations) instead interact with *NF1* loss to promote neurofibroma growth.

In contrast, there is good evidence that the accumulation of additional genomic abnormalities occurs when a benign neurofibroma transitions to become an atypical neurofibroma. In keeping with the studies cited above, array comparative genomic hybridization analyses of 16 atypical neurofibromas, 15 benign neurofibromas (11 plexiform, 4 dermal), and 34 MPNSTs [including (WHO grade II), intermediate (WHO grade III), and high-grade (WHO grade IV) lesions] showed no evidence of copy number changes in the benign neurofibromas.[107] However, 15 of the 16 atypical neurofibromas showed deletions of *CDKN2A*/*CDKN2B*, a locus encoding 2 key inhibitors of the cell cycle ($p16^{INK4A}$ and $p19^{ARF}$). This same abnormality was present in the MPNSTs, which led these investigators to suggest that *CDKN2A*/*CDKN2B* loss is an early step in neurofibroma-MPNST progression and that this loss can be used as a diagnostic marker for the premalignant state in neurofibromas.

MALIGNANT PERIPHERAL NERVE SHEATH TUMORS

Clinical Features and Diagnosis of Malignant Peripheral Nerve Sheath Tumors

MPNSTs are aggressive spindle cell neoplasms derived from the Schwann cell lineage.[2,108] As a group, MPNSTs represent ~2% to 5% of all soft tissue sarcomas.[109,110] However, MPNSTs are encountered in 3 very different clinical settings, which raises the question of whether there are distinct MPNST subtypes that arise via different pathogenic mechanisms. About 40% to 50% of MPNSTs arise in NF1 patients.[2] Indeed, MPNSTs are the most common malignancy encountered in NF1 patients—these individuals' lifetime risk of developing an MPNST has been estimated at 8% to 13%[111] and 5.9% to 10.3%.[112] Another 40% to 47% of MPNSTs are sporadic, with the remaining 10% to 13% occurring at sites of previous radiation therapy.[111,113–115] Although there is evidence that NF1-associated, sporadic, and radiation-induced MPNSTs have different prognoses, this evidence is controversial and there is an ongoing debate as to which of these groups have the worst prognosis. Some investigators have found that NF1-associated MPNSTs have a poorer outcome than sporadic or radiation-induced MPNSTs.[115–118] In contrast, other groups have reported that radiation-induced MPNSTs have the poorest outcome.[114,118] This controversy aside, there is general agreement that MPNSTs have a poor prognosis, with multiple centers reporting that the 5-year disease-free survival rates of patients with these tumors are between 34% and 60%.[113,115,117–122]

Copyright © 2018 Wolters Kluwer Health, Inc. All rights reserved.

Copyright © 2018 Wolters Kluwer Health, Inc. All rights reserved.

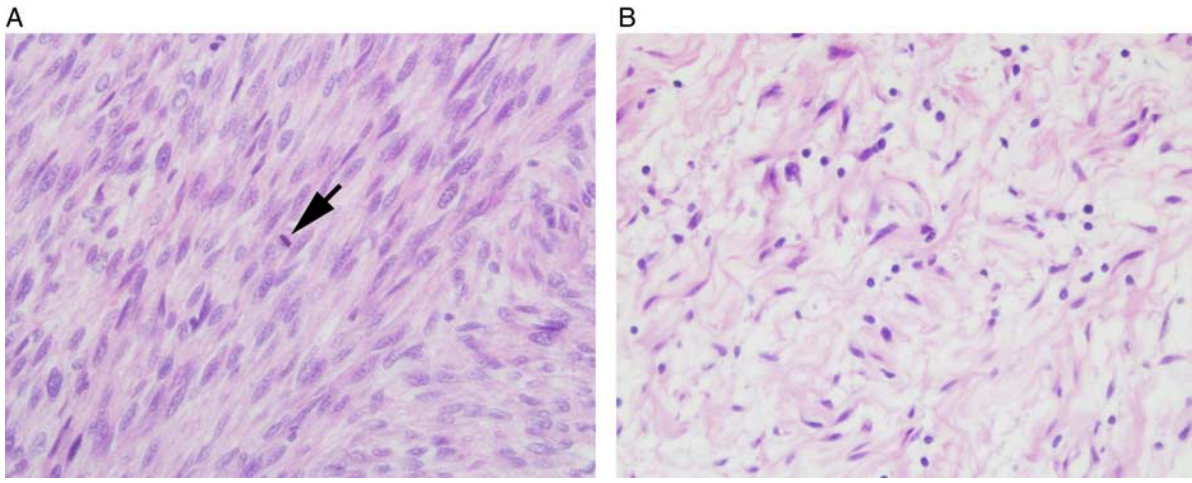


FIGURE 4. Pathology of a MPNST that arose from a plexiform neurofibroma involving the brachial plexus of a 32-year-old white man with NF1. A, Section of the MPNST, which is evident as a markedly hypercellular spindle cell neoplasm. The arrow indicates one of the numerous mitotic figures that were detected in this malignancy. B, Regions of the original plexiform neurofibroma were readily detected in this resection specimen. MPNST indicates malignant peripheral nerve sheath tumor.

Despite their different prognoses, there are no histologic features that distinguish sporadic, NF1-associated and radiation-induced MPNSTs. Irrespective of their origin, MPNSTs are poorly differentiated spindle cell neoplasms in which mitotic figures are usually readily identified (Fig. 4). Unfortunately, MPNSTs are histologically similar to several other types of spindle cell malignancies. Further, the immunohistochemical markers that are commonly used to diagnose an MPNST and eliminate other diagnostic possibilities have significant limitations. To begin with, S100β, the most widely used marker for MPNSTs, is only positive in 30% to 65% of MPNSTs. Glial fibrillary acidic protein, an intermediate filament normally expressed in nonmyelinating Schwann cells, is positive in an even smaller fraction of MPNSTs (20% to 30% of cases). Leu-7 (CD57) shows variable staining in MPNSTs, with the amount of Leu-7 immunoreactivity present being dependent on the degree of Schwannian differentiation. In our experience, basement membrane markers such as collagen type IV and laminin are patchy and tend to be more prominent only in low-grade MPNSTs. It has been reported that strong immunoreactivity for the intermediate filament nestin (despite the misconception that this is a stem cell marker, nestin is strongly expressed in non-neoplastic Schwann cells) is common in MPNSTs.[123] Again, however, other tumor types that are in the differential for MPNSTs also stain for nestin. A recent study suggested using loss of neurofibromin immunoreactivity as a means of distinguishing MPNSTs from other spindle cell neoplasms.[124] This approach likely will be useful for identifying NF1-associated MPNSTs and a subset of sporadic and radiation-induced MPNSTs, as at least some of these latter tumors also have *NF1* loss (see the Genomic abnormalities in malignant peripheral nerve sheath tumors section below). However, *NF1* is maintained in other sporadic and radiation-induced MPNSTs, so this approach likely would not distinguish all MPNSTs from their histologic mimics. Because of the often poor differentiation encountered in MPNSTS and the lack of specific ultrastructural markers, electron microscopy also has limited utility. MPNSTs typically show rudimentary to poorly formed cell junctions, long-spacing fibrous collagen (Luse bodies) and partial investment of tumor cells by basement membranes; these features may be more obvious in low-grade MPNSTs.

Grading of MPNSTs also continues to be problematic. The WHO classification scheme currently assigns 3 grades to MPNSTs (WHO grades II to IV). Per their diagnostic criteria, WHO grade II (low grade) MPNSTs are hypercellular lesions that contain cells with nuclei that are greater than 3-fold larger than typical neurofibroma nuclei and show nuclear hyperchromasia. Although the presence of mitotic figures supports the diagnosis, these features are assessed independent of mitotic activity. This is a diagnostically challenging grade, as it is quite difficult to use these findings to distinguish between an atypical neurofibroma and a low-grade MPNST. A WHO grade III (intermediate grade) MPNST is characterized by prominent hypercellularity, clear cytologic atypia and brisk mitotic activity ($\geq$4 mitoses per 10 high power fields). WHO grade IV (high grade) MPNSTs show tumor necrosis in addition to the other features present in a WHO grade III lesion. In addition to the difficulties noted for low-grade MPNSTs, this grading system has been criticized because it does not clearly predict patient outcomes. Consequently, many pathologists prefer to simply classify MPNSTs as either low-grade or high-grade tumors.

Genomic Abnormalities in Malignant Peripheral Nerve Sheath Tumors

The difficulties inherent to diagnosing and grading MPNSTs and the need for effective new therapeutic regimens has stimulated interest in understanding the genomic abnormalities in these neoplasms. In contrast to neurofibromas, the genomes of MPNSTs are highly complex. Classic karyotyping indicates that MPNSTs tend to be hypodiploid or near triploid, with multiple regions of chromosomal gain and loss, both cytogenetically and with array comparative genomic hybridization.[125–133] Initial reports were that gains are commonly seen on chromosome 7, 8p, and 19q, whereas losses are more widespread (chromosomes 1p, 9p, 11, 12p, 14q, 17q, 18, 22q, X, and Y). The genomic changes in MPNSTs are likely more complex than was indicated by these earlier studies. We recently examined

Copyright © 2018 Wolters Kluwer Health, Inc. All rights reserved.
Copyright © 2018 Wolters Kluwer Health, Inc. All rights reserved.

a series of human MPNST cell lines and surgically resected MPNSTs using high density single nucleotide polymorphism arrays capable of identifying both balanced and unbalanced regions of chromosomal gain or loss. We found a characteristic pattern in the genomes of these tumors, with unusually high levels of LOH and frequent regions of chromosomal gain. Overall, LOH occurred in up to 20 chromosomes (median, 14) with gains or high copy number gains in up to 23 chromosomes (median, 18). Analysis of the genomic segments in these tumors indicated that a massive loss of genomic material occurs early in MPNST pathogenesis that is followed by whole or partial genome reduplication. In keeping with these high density single nucleotide polymorphism array analyses, our whole exome sequencing and RNA-Seq analyses of these same specimens also shows extensive genomic rearrangement, which results in the production of multiple fusion genes.

At present, our understanding of the specific mutations that drive MPNST pathogenesis is rudimentary. Like neurofibromas, MPNSTs show biallelic inactivation of the *NF1* gene.[134] As this observation makes it clear that *NF1* loss alone is not sufficient for MPNST pathogenesis, the progression of a plexiform neurofibroma to become a MPNST must involve the mutation of additional driver genes. The first mutations other than *NF1* that were identified in MPNSTs were in genes encoding proteins in the $p19^{ARF}$-MDM2-p53 and $p16^{INK4A}$-cyclin D-Rb signaling cascades, both of which regulate the progression of the cell cycle. Mutations of *TP53* are quite common in MPNSTs, with several series reporting mutations of this tumor suppressor gene in up to 75% of MPNSTs.[135–138] Intriguingly, complete p53 loss is not required for MPNST pathogenesis as loss or mutation of only 1 copy of *TP53* is common in MPNSTs.[139] Loss of the *CDKN2A* gene, which simultaneously dysregulates the $p19^{ARF}$-Mdm2-p53 and $p16^{INK4A}$-cyclin D-Rb pathways, is evident in about half of all MPNSTs.[140,141] Further emphasizing the importance of these cell cycle regulatory pathways in MPNSTs, *RB1* loss is observed in ~25% of MPNSTs.[142,143] In addition to the mutations of genes encoding proteins in the $p19^{ARF}$-MDM2-p53 and $p16^{INK4A}$-cyclin D-Rb signaling cascades, mutations of some genes previously shown to be important in other tumor types are encountered in MPNSTs. Decreased expression of PTEN, a key inhibitor of the PI3 kinase-Akt signaling pathway, has been reported in MPNSTs[144,145]; *PTEN* deletions and epigenetic silencing of the *PTEN* locus have both been identified in MPNSTs[146,147] and likely account for this decreased expression. Amplification of the *EGFR*[148,149] gene, which encodes a key upstream activator of the Ras signaling cascade also occurs in MPNSTs. In addition to these genes, several other genes have been shown to be mutated, amplified, or deleted in MPNSTs. However, many of these mutations occur in small subsets of MPNSTs and their functional impact has not yet been thoroughly assessed.

With the advent of massively parallel sequencing methodologies, we are now getting our first comprehensive look at the genomic abnormalities present in MPNSTs. Two groups recently reported the results of using whole exome/genome sequencing, copy number analyses, and whole transcriptome sequencing on 15[150] and 4[151] MPNSTs; these tumors included NF1-associated, sporadic, and radiation-induced MPNSTs. These investigators found that *NF1* loss was uniformly present in the NF1-associated MPNSTs and in 72% of the sporadic and radiation-induced MPNSTs.[150] Both groups also found loss-of-function mutations in genes encoding proteins in polycomb repressive complex 2, an epigenetic regulator that modulates histone methylation, in up to 80% of MPNSTs. The affected genes included *SUZ12*, *EED*, *EPC1*, and *CHD4*; intriguingly, *SUZ12* is the same gene that is involved in the type II recombination events that produce *NF1* microdeletions (see the NF1 Mutations and genotype-phenotype correlations section above). *SUZ12* and *EED* mutations are associated with a loss of dimethylation and trimethylation of lysine 27 in histone H3 (H3K27me3 marks) and a transcriptome signature that is distinct from the signature of MPNSTs with intact *SUZ12* and *EED* genes. Restoring SUZ12 expression in *SUZ12*-null MPNST cells restores H3K27me3 marks and inhibits tumor growth, indicating that this gene acts as a tumor suppressor in MPNST cells. *SUZ12* and *EED* are not lost in neurofibromas, indicating that these mutations occur either during neurofibroma-MPNST progression or in MPNSTs as they progress from low grade to high grade. These observations have led to the suggestion that a loss of H3K27me3 immunoreactivity can be useful for distinguishing MPNSTs from neurofibromas and for distinguishing MPNSTs from their histologic mimics.[152–155] Undoubtedly, these findings are the first of many observations that will further clarify the role that specific genomic and epigenetic abnormalities play in MPNST pathogenesis.

NEW APPROACHES TO THE TREATMENT OF NF1-ASSOCIATED PERIPHERAL NERVE SHEATH TUMORS

The poor survival of patients with MPNSTs and the morbidity associated with neurofibromas reflects the fact that the currently used radio-therapeutic and chemotherapeutic regimens are ineffective against these tumors. This has led several laboratories to ask whether neurofibromas and MPNSTs could be treated by targeting the signaling abnormalities that result from *NF1* loss, as this mutation is present in all neurofibromas and MPNSTs arising in NF1 patients[2] as well as in the majority of sporadic and radiation-induced MPNSTs.[150] Given neurofibromin's role as a Ras GAP, most attempts to develop new therapies for neurofibromas and MPNSTs initially focused on Ras and Ras-regulated signaling cascades. In an initial clinical trial, the farnesyltransferase inhibitor tipifarnib, which prevents an essential modification of H-Ras, was used to treat children with plexiform neurofibromas. Although well tolerated in phase I trials,[156] tipifarnib ultimately proved ineffective for the treatment of these tumors. This failure likely reflects the fact that neurofibromin acts as a Ras GAP for multiple members of the classic Ras (H-Ras, K-Ras, N-Ras) and R-Ras (R-Ras, R-Ras2/TC21, and M-Ras/R-Ras3) subfamilies of small GTP-binding proteins,[52,157–159] most of which are not sensitive to tipifarnib. We have found that all 6 of these Ras proteins are expressed and activated in MPNST cells; knockdown of 1 Ras protein simply results in increased expression and activation of other Ras family members.[160] As targeting these Ras proteins by other means has proven difficult,[63] subsequent efforts instead focused on inhibiting downstream mediators of Ras signaling such as the Raf/MEK/ERK and PI3 kinase/AKT/mTOR effector pathways. Unfortunately, this approach has also had limited success. Although MEK inhibitors are effective against neurofibromas, MPNSTs are only moderately and variably responsive to these

Copyright © 2018 Wolters Kluwer Health, Inc. All rights reserved.

Copyright © 2018 Wolters Kluwer Health, Inc. All rights reserved.

agents.[161,162] The Raf inhibitor sorafenib also showed no objective responses in plexiform neurofibromas[163] or MPNSTs.[164] The mTORC1 inhibitor rapamycin showed promising effects in culture,[165] but had only transient effects on MPNST xenograft growth in vivo.[166] Although these efforts were logical and merit additional investigation, it is clear that therapeutic agents targeting key signaling pathways downstream of Ras have not yet been shown to be effective against MPNSTs.

An alternative approach to treating neurofibromas and MPNSTs would be to inhibit key molecules upstream of Ras proteins that are essential for Ras activation. As noted above, MPNST pathogenesis is driven by *NF1* mutation-induced Ras hyperactivation and other incompletely understood mutations that accumulate during neurofibroma-MPNST progression.[2] In some other sporadic cancer types that are Ras-dependent, Ras hyperactivation is promoted via multiple mechanisms that activate receptor tyrosine kinases (RTKs). This suggests that Ras-mediated increases in proliferation, invasion, and survival in MPNSTs could be inhibited by therapeutically targeting ≥ 1 RTK(s). Initiating experiments to test the effects of inhibiting the key RTK(s) in MPNSTs, however, have been confounded by varying reports in the literature. Several laboratories have presented evidence that one or another RTK drives MPNST growth. However, these reports often contradict one another and the strength of the evidence supporting each candidate RTK is variable. For instance, an amplicon involving chromosomal segment 4q12 occurs in 19% of MPNSTs; this amplicon contains genes encoding 3 RTKs (*PDGFRA*, *KIT*, and *KDR*).[167] Platelet-derived growth factor (PDGF) and its 2 receptors (PDGFRA and PDGFRB) are coexpressed in neurofibromas[168] and MPNSTs[169] and these receptors are constitutively activated in at least some MPNSTs.[170] VEGF and its KDR (VEGFR2) receptor are similarly coexpressed in MPNST cells and have been suggested to form an autocrine signaling loop.[171] Some, but not all, MPNST lines express c-Kit and the baseline proliferation of MPNST cells has reportedly been inhibited with agents targeting this RTK.[172] Coexpression of hepatocyte growth factor and its c-Met receptor have been detected in neurofibromas[173–175] and MPNSTs,[173,175] raising the possibility that these molecules also form an autocrine signaling loop in these tumors. The EGF receptor is inappropriately expressed in neurofibromas and MPNSTs[148] and the *EGFR* gene is amplified in a subset of MPNSTs.[149] Introduction of an *Egfr* hypomorphic mutation into cis-$Nf1^{+/-}$;$Trp53^{+/-}$ mice (a widely used model of NF1-associated MPNSTs) impedes tumorigenesis,[176] suggesting that EGF signaling is important for MPNST growth. Finally, we have shown that the neuregulin-1 (NRG1) receptors erbB2, erbB3, and erbB4 are present and activated in MPNSTs, where they promote proliferation[177] and migration.[178] When we overexpressed the NRG1 isoform GGFβ3 in the Schwann cells of transgenic mice, these animals developed plexiform neurofibromas that progressed to become MPNSTs at a high frequency[179]; our genetic complementation experiments indicated that GGFβ3 promotes tumorigenesis via its effects on *Nf1*-regulated signaling pathways.[180]

In light of these conflicting reports, it is clear that a comprehensive analysis needs to be performed that will look simultaneously at the role that all 58 of the RTKs encoded in the human genome play in individual MPNSTs. This is needed because at present we cannot rule out the possibility that RTKs other than those noted above also contribute to MPNST pathogenesis; indeed, the role of many of the 58 RTKs found in humans has not yet been explored in MPNSTs. On the basis of experience in other tumor types (eg, glioblastomas), we also have to consider the possibility that multiple RTKs are coactivated in MPNSTs and simultaneously contribute to tumorigenesis.[181,182] Finally, it is conceivable that there are distinct MPNST subtypes that depend on different RTKs for growth. Nonetheless, considering the large number of drugs currently available that effectively inhibit RTKs, this is a promising line of investigation that is being actively pursued by multiple laboratories. Identifying an RTK inhibitor, or more likely a combination of RTK inhibitors with or without inhibitors of key Ras-regulated pathways, would finally give us an effective means of treating MPNSTs or preventing the malignant transformation of neurofibromas.

In summary, there have been great advances in our understanding of the clinical abnormalities associated with NF1 and the features that distinguish NF1 from other RASopathies. Although distinguishing these conditions remains challenging, we now have genetic testing available that can facilitate this process. Recent advances in understanding the genomic abnormalities found in neurofibromas, atypical neurofibromas, and MPNSTs are also providing new tools that can be used better classify these lesions pathologically. As we build upon these advances in coming years, it is our hope that our growing understanding of the genomic abnormalities in NF1-associated peripheral nerve sheath tumors will allow the rational design of effective new therapies for these clinically challenging neoplasms.

REFERENCES

1. Carroll SL, Ratner N. How does the Schwann cell lineage form tumors in NF1? *Glia*. 2008;56:1590–1605.
2. Carroll SL. Molecular mechanisms promoting the pathogenesis of Schwann cell neoplasms. *Acta Neuropathol*. 2012;123:321–348.
3. Shen MH, Harper PS, Upadhyaya M. Molecular genetics of neurofibromatosis type 1 (NF1). *J Med Genet*. 1996;33:2–17.
4. Williams VC, Lucas J, Babcock MA, et al. Neurofibromatosis type 1 revisited. *Pediatrics*. 2009;123:124–133.
5. Jadayel D, Fain P, Upadhyaya M, et al. Paternal origin of new mutations in von Recklinghausen neurofibromatosis. *Nature*. 1990;343:558–559.
6. Rasmussen SA, Yang Q, Friedman JM. Mortality in neurofibromatosis 1: an analysis using US death certificates. *Am J Hum Genet*. 2001;68:1110–1118.
7. Ferner RE, Huson SM, Thomas N, et al. Guidelines for the diagnosis and management of individuals with neurofibromatosis 1. *J Med Genet*. 2007;44:81–88.
8. Balcer LJ, Liu GT, Heller G, et al. Visual loss in children with neurofibromatosis type 1 and optic pathway gliomas: relation to tumor location by magnetic resonance imaging. *Am J Ophthalmol*. 2001;131:442–445.
9. Thiagalingam S, Flaherty M, Billson F, et al. Neurofibromatosis type 1 and optic pathway gliomas: follow-up of 54 patients. *Ophthalmology*. 2004;111:568–577.
10. Listernick R, Charrow J, Greenwald M, et al. Natural history of optic pathway tumors in children with neurofibromatosis type 1: a longitudinal study. *J Pediatr*. 1994;125:63–66.
11. Listernick R, Darling C, Greenwald M, et al. Optic pathway tumors in children: the effect of neurofibromatosis type 1 on clinical manifestations and natural history. *J Pediatr*. 1995;127:718–722.
12. Rodriguez FJ, Perry A, Gutmann DH, et al. Gliomas in neurofibromatosis type 1: a clinicopathologic study of 100 patients. *J Neuropathol Exp Neurol*. 2008;67:240–249.

Copyright © 2018 Wolters Kluwer Health, Inc. All rights reserved.

Copyright © 2018 Wolters Kluwer Health, Inc. All rights reserved.

13. Cancer Genome Atlas Research Network. Comprehensive genomic characterization defines human glioblastoma genes and core pathways. *Nature*. 2008;455:1061–1068.
14. Riccardi VM. Neurofibromatosis: past, present, and future. *N Engl J Med*. 1991;324:1283–1285.
15. Walther MM, Herring J, Enquist E, et al. von Recklinghausen's disease and pheochromocytomas. *J Urol*. 1999;162:1582–1586.
16. Bausch B, Koschker AC, Fassnacht M, et al. Comprehensive mutation scanning of NF1 in apparently sporadic cases of pheochromocytoma. *J Clin Endocrinol Metab*. 2006;91:3478–3481.
17. Mannelli M, Castellano M, Schiavi F, et al. Italian Pheochromocytoma/Paraganglioma Network. Clinically guided genetic screening in a large cohort of Italian patients with pheochromocytomas and/or functional or nonfunctional paragangliomas. *J Clin Endocrinol Metab*. 2009;94:1541–1547.
18. Eisenhofer G, Lenders JW, Timmers H, et al. Measurements of plasma methoxytyramine, normetanephrine, and metanephrine as discriminators of different hereditary forms of pheochromocytoma. *Clin Chem*. 2011;57:411–420.
19. Easton DF, Ponder MA, Huson SM, et al. An analysis of variation in expression of neurofibromatosis (NF) type 1 (NF1): evidence for modifying genes. *Am J Hum Genet*. 1993;53:305–313.
20. Barahona-Garrido J, Aguirre-Gutierrez R, Gutierrez-Manjarrez JI, et al. Association of GIST and somatostatinoma in a patient with type-1 neurofibromatosis: is there a common pathway? *Am J Gastroenterol*. 2009;104:797–799.
21. Miettinen M, Fetsch JF, Sobin LH, et al. Gastrointestinal stromal tumors in patients with neurofibromatosis 1: a clinicopathologic and molecular genetic study of 45 cases. *Am J Surg Pathol*. 2006;30:90–96.
22. Stiller CA, Chessells JM, Fitchett M. Neurofibromatosis and childhood leukaemia/lymphoma: a population-based UKCCSG study. *Br J Cancer*. 1994;70:969–972.
23. Brems H, Park C, Maertens O, et al. Glomus tumors in neurofibromatosis type 1: genetic, functional, and clinical evidence of a novel association. *Cancer Res*. 2009;69:7393–7401.
24. McGaughran JM, Harris DI, Donnai D, et al. A clinical study of type 1 neurofibromatosis in north west England. *J Med Genet*. 1999;36:197–203.
25. Patil S, Chamberlain RS. Neoplasms associated with germline and somatic NF1 gene mutations. *Oncologist*. 2012;17:101–116.
26. Crucis A, Richer W, Brugieres L, et al. Rhabdomyosarcomas in children with neurofibromatosis type I: a national historical cohort. *Pediatr Blood Cancer*. 2015;62:1733–1738.
27. Afsar CU, Kara IO, Kozat BK, et al. Neurofibromatosis type 1, gastrointestinal stromal tumor, leiomyosarcoma and osteosarcoma: four cases of rare tumors and a review of the literature. *Crit Rev Oncol Hematol*. 2013;86:191–199.
28. Uusitalo E, Kallionpaa RA, Kurki S, et al. Breast cancer in neurofibromatosis type 1: overrepresentation of unfavourable prognostic factors. *Br J Cancer*. 2017;116:211–217.
29. Wang X, Teer JK, Tousignant RN, et al. Breast cancer risk and germline genomic profiling of women with neurofibromatosis type 1 who developed breast cancer. *Genes Chromosomes Cancer*. 2018;57:19–27.
30. Clementi M, Milani S, Mammi I, et al. Neurofibromatosis type 1 growth charts. *Am J Med Genet*. 1999;87:317–323.
31. Szudek J, Birch P, Friedman JM. Growth charts for young children with neurofibromatosis 1 (NF1). *Am J Med Genet*. 2000;92:224–228.
32. Szudek J, Birch P, Friedman JM. Growth in North American white children with neurofibromatosis 1 (NF1). *J Med Genet*. 2000;37:933–938.
33. Elefteriou F, Kolanczyk M, Schindeler A, et al. Skeletal abnormalities in neurofibromatosis type 1: approaches to therapeutic options. *Am J Med Genet A*. 2009;149A:2327–2338.
34. Lammert M, Friedman JM, Roth HJ, et al. Vitamin D deficiency associated with number of neurofibromas in neurofibromatosis 1. *J Med Genet*. 2006;43:810–813.
35. Lin AE, Birch PH, Korf BR, et al. Cardiovascular malformations and other cardiovascular abnormalities in neurofibromatosis 1. *Am J Med Genet*. 2000;95:108–117.
36. Oderich GS, Sullivan TM, Bower TC, et al. Vascular abnormalities in patients with neurofibromatosis syndrome type I: clinical spectrum, management, and results. *J Vasc Surg*. 2007;46:475–484.
37. Rea D, Brandsema JF, Armstrong D, et al. Cerebral arteriopathy in children with neurofibromatosis type 1. *Pediatrics*. 2009;124:e476–e483.
38. D'Arco F, D'Amico A, Caranci F, et al. Cerebrovascular stenosis in neurofibromatosis type 1 and utility of magnetic resonance angiography: our experience and literature review. *Radiol Med*. 2014;119:415–421.
39. Friedman JM, Arbiser J, Epstein JA, et al. Cardiovascular disease in neurofibromatosis 1: report of the NF1 Cardiovascular Task Force. *Genet Med*. 2002;4:105–111.
40. Schwetye KE, Gutmann DH. Cognitive and behavioral problems in children with neurofibromatosis type 1: challenges and future directions. *Expert Rev Neurother*. 2014;14:1139–1152.
41. Garg S, Green J, Leadbitter K, et al. Neurofibromatosis type 1 and autism spectrum disorder. *Pediatrics*. 2013;132:e1642–e1648.
42. Cutting LE, Levine TM. Cognitive profile of children with neurofibromatosis and reading disabilities. *Child Neuropsychol*. 2010;16:417–432.
43. Itoh T, Magnaldi S, White RM, et al. Neurofibromatosis type 1: the evolution of deep gray and white matter MR abnormalities. *AJNR Am J Neuroradiol*. 1994;15:1513–1519.
44. Van Es S, North KN, McHugh K, et al. MRI findings in children with neurofibromatosis type 1: a prospective study. *Pediatr Radiol*. 1996;26:478–487.
45. Griffiths PD, Blaser S, Mukonoweshuro W, et al. Neurofibromatosis bright objects in children with neurofibromatosis type 1: a proliferative potential? *Pediatrics*. 1999;104:e49.
46. Braffman BH, Bilaniuk LT, Zimmerman RA. The central nervous system manifestations of the phakomatoses on MR. *Radiol Clin North Am*. 1988;26:773–800.
47. Smirniotopoulos JG, Murphy FM. The phakomatoses. *AJNR Am J Neuroradiol*. 1992;13:725–746.
48. Bognanno JR, Edwards MK, Lee TA, et al. Cranial MR imaging in neurofibromatosis. *AJR Am J Roentgenol*. 1988;151:381–388.
49. DiPaolo DP, Zimmerman RA, Rorke LB, et al. Neurofibromatosis type 1: pathologic substrate of high-signal-intensity foci in the brain. *Radiology*. 1995;195:721–724.
50. Torres Nupan MM, Velez Van Meerbeke A, Lopez Cabra CA, et al. Cognitive and behavioral disorders in children with neurofibromatosis type 1. *Front Pediatr*. 2017;5:227.
51. Xu GF, O'Connell P, Viskochil D, et al. The neurofibromatosis type 1 gene encodes a protein related to GAP. *Cell*. 1990;62:599–608.
52. Xu GF, Lin B, Tanaka K, et al. The catalytic domain of the neurofibromatosis type 1 gene product stimulates Ras GTPase and complements IRA mutants of *S. cerevisiae*. *Cell*. 1990;63:835–841.
53. Bollag G, McCormick F, Clark R. Characterization of full-length neurofibromin: tubulin inhibits Ras GAP activity. *EMBO J*. 1993;12:1923–1927.
54. Kweh F, Zheng M, Kurenova E, et al. Neurofibromin physically interacts with the N-terminal domain of focal adhesion kinase. *Mol Carcinog*. 2009;48:1005–1017.
55. Korkiamaki T, Yla-Outinen H, Koivunen J, et al. Altered calcium-mediated cell signaling in keratinocytes cultured from patients with neurofibromatosis type 1. *Am J Pathol*. 2002;160:1981–1990.
56. Dang I, DeVries GH. Schwann cell lines derived from malignant peripheral nerve sheath tumors respond abnormally to platelet-derived growth factor-BB. *J Neurosci Res*. 2005;79:318–328.
57. Dasgupta B, Dugan LL, Gutmann DH. The neurofibromatosis 1 gene product neurofibromin regulates pituitary adenylate cyclase-activating polypeptide-mediated signaling in astrocytes. *J Neurosci*. 2003;23:8949–8954.
58. Dang I, De Vries GH. Aberrant cAMP metabolism in NF1 malignant peripheral nerve sheath tumor cells. *Neurochem Res*. 2011;36:1697–1705.
59. Kim HA, Ratner N, Roberts TM, et al. Schwann cell proliferative responses to cAMP and Nf1 are mediated by cyclin D1. *J Neurosci*. 2001;21:1110–1116.

Copyright © 2018 Wolters Kluwer Health, Inc. All rights reserved.

Copyright © 2018 Wolters Kluwer Health, Inc. All rights reserved.

60. D'Angelo I, Welti S, Bonneau F, et al. A novel bipartite phospholipid-binding module in the neurofibromatosis type 1 protein. *EMBO Rep*. 2006;7:174–179.
61. Welti S, Fraterman S, D'Angelo I, et al. The sec. 14 homology module of neurofibromin binds cellular glycerophospholipids: mass spectrometry and structure of a lipid complex. *J Mol Biol*. 2007;366:551–562.
62. Welti S, Kuhn S, D'Angelo I, et al. Structural and biochemical consequences of NF1 associated nontruncating mutations in the Sec. 14-PH module of neurofibromin. *Hum Mutat*. 2011;32: 191–197.
63. Cox AD, Der CJ. Ras history: the saga continues. *Small GTPases*. 2010;1:2–27.
64. Aoki Y, Niihori T, Inoue S, et al. Recent advances in RASopathies. *J Hum Genet*. 2016;61:33–39.
65. Simanshu DK, Nissley DV, McCormick F. RAS proteins and their regulators in human disease. *Cell*. 2017;170:17–33.
66. Nystrom AM, Ekvall S, Allanson J, et al. Noonan syndrome and neurofibromatosis type I in a family with a novel mutation in NF1. *Clin Genet*. 2009;76:524–534.
67. Stevenson DA, Viskochil DH, Rope AF, et al. Clinical and molecular aspects of an informative family with neurofibromatosis type 1 and Noonan phenotype. *Clin Genet*. 2006; 69:246–253.
68. De Luca A, Bottillo I, Sarkozy A, et al. NF1 gene mutations represent the major molecular event underlying neurofibromatosis-Noonan syndrome. *Am J Hum Genet*. 2005;77: 1092–1101.
69. Bertola DR, Pereira AC, Passetti F, et al. Neurofibromatosis-Noonan syndrome: molecular evidence of the concurrence of both disorders in a patient. *Am J Med Genet A*. 2005;136:242–245.
70. Viskochil D, Buchberg AM, Xu G, et al. Deletions and a translocation interrupt a cloned gene at the neurofibromatosis type 1 locus. *Cell*. 1990;62:187–192.
71. Wallace MR, Marchuk DA, Andersen LB, et al. Type 1 neurofibromatosis gene: identification of a large transcript disrupted in three NF1 patients. *Science*. 1990;249:181–186.
72. Messiaen LM, Callens T, Mortier G, et al. Exhaustive mutation analysis of the NF1 gene allows identification of 95% of mutations and reveals a high frequency of unusual splicing defects. *Hum Mutat*. 2000;15:541–555.
73. Wimmer K, Roca X, Beiglbock H, et al. Extensive in silico analysis of NF1 splicing defects uncovers determinants for splicing outcome upon 5' splice-site disruption. *Hum Mutat*. 2007;28:599–612.
74. Wimmer K, Yao S, Claes K, et al. Spectrum of single- and multiexon NF1 copy number changes in a cohort of 1,100 unselected NF1 patients. *Genes Chromosomes Cancer*. 2006;45: 265–276.
75. Dorschner MO, Sybert VP, Weaver M, et al. NF1 microdeletion breakpoints are clustered at flanking repetitive sequences. *Hum Mol Genet*. 2000;9:35–46.
76. Lopez-Correa C, Dorschner M, Brems H, et al. Recombination hotspot in NF1 microdeletion patients. *Hum Mol Genet*. 2001;10:1387–1392.
77. Jenne DE, Tinschert S, Reimann H, et al. Molecular characterization and gene content of breakpoint boundaries in patients with neurofibromatosis type 1 with 17q11.2 microdeletions. *Am J Hum Genet*. 2001;69:516–527.
78. Raedt TD, Stephens M, Heyns I, et al. Conservation of hotspots for recombination in low-copy repeats associated with the NF1 microdeletion. *Nat Genet*. 2006;38:1419–1423.
79. Kehrer-Sawatzki H, Kluwe L, Sandig C, et al. High frequency of mosaicism among patients with neurofibromatosis type 1 (NF1) with microdeletions caused by somatic recombination of the JJAZ1 gene. *Am J Hum Genet*. 2004; 75:410–423.
80. Steinmann K, Cooper DN, Kluwe L, et al. Type 2 NF1 deletions are highly unusual by virtue of the absence of nonallelic homologous recombination hotspots and an apparent preference for female mitotic recombination. *Am J Hum Genet*. 2007;81:1201–1220.
81. Pasmant E, Sabbagh A, Spurlock G, et al. NF1 microdeletions in neurofibromatosis type 1: from genotype to phenotype. *Hum Mutat*. 2010;31:E1506–E1518.
82. Upadhyaya M, Huson SM, Davies M, et al. An absence of cutaneous neurofibromas associated with a 3-bp inframe deletion in exon 17 of the NF1 gene (c.2970-2972 delAAT): evidence of a clinically significant NF1 genotype-phenotype correlation. *Am J Hum Genet*. 2007;80:140–151.
83. Brohl AS, Kahen E, Yoder SJ, et al. The genomic landscape of malignant peripheral nerve sheath tumors: diverse drivers of Ras pathway activation. *Sci Rep*. 2017;7:14992.
84. Hawes JJ, Tuskan RG, Reilly KM. Nf1 expression is dependent on strain background: implications for tumor suppressor haploinsufficiency studies. *Neurogenetics*. 2007;8:121–130.
85. Koelsch B, van den Berg L, Fischer C, et al. Chemically induced oncogenesis in the peripheral nervous system is suppressed in congenic BDIX.BDIV-Mss1 and -Mss7 rats. *G3 (Bethesda)*. 2015;6:59–65.
86. van den Berg L, Koelsch BU, Winzen-Reichert B, et al. Genetic dissection of the Mss4 locus mediating sex-biased cancer resistance in the rat peripheral nervous system. *Int J Cancer*. 2015;136:2099–2108.
87. Le LQ, Shipman T, Burns DK, et al. Cell of origin and microenvironment contribution for NF1-associated dermal neurofibromas. *Cell Stem Cell*. 2009;4:453–463.
88. Cohen PR, Rapini RP, Farhood AI. Expression of the human hematopoietic progenitor cell antigen CD34 in vascular and spindle cell tumors. *J Cutan Pathol*. 1993;20:15–20.
89. Weiss SW, Nickoloff BJ. CD-34 is expressed by a distinctive cell population in peripheral nerve, nerve sheath tumors, and related lesions. *Am J Surg Pathol*. 1993;17:1039–1045.
90. Prada CE, Jousma E, Rizvi TA, et al. Neurofibroma-associated macrophages play roles in tumor growth and response to pharmacological inhibition. *Acta Neuropathol*. 2013;125:159–168.
91. Kluwe L, Friedrich R, Mautner VF. Loss of NF1 allele in Schwann cells but not in fibroblasts derived from an NF1-associated neurofibroma. *Genes Chromosomes Cancer*. 1999;24: 283–285.
92. Rutkowski JL, Wu K, Gutmann DH, et al. Genetic and cellular defects contributing to benign tumor formation in neurofibromatosis type 1. *Hum Mol Genet*. 2000;9:1059–1066.
93. Zhu Y, Ghosh P, Charnay P, et al. Neurofibromas in NF1: Schwann cell origin and role of tumor environment. *Science*. 2002;296:920–922.
94. Wu J, Williams JP, Rizvi TA, et al. Plexiform and dermal neurofibromas and pigmentation are caused by Nf1 loss in desert hedgehog-expressing cells. *Cancer Cell*. 2008;13:105–116.
95. Hirota S, Nomura S, Asada H, et al. Possible involvement of c-kit receptor and its ligand in increase of mast cells in neurofibroma tissues. *Arch Pathol Lab Med*. 1993;117:996–999.
96. Ryan JJ, Klein KA, Neuberger TJ, et al. Role for the stem cell factor/KIT complex in Schwann cell neoplasia and mast cell proliferation associated with neurofibromatosis. *J Neurosci Res*. 1994;37:415–432.
97. Yang FC, Ingram DA, Chen S, et al. Neurofibromin-deficient Schwann cells secrete a potent migratory stimulus for Nf1+/- mast cells. *J Clin Invest*. 2003;112:1851–1861.
98. Ingram DA, Yang FC, Travers JB, et al. Genetic and biochemical evidence that haploinsufficiency of the Nf1 tumor suppressor gene modulates melanocyte and mast cell fates in vivo. *J Exp Med*. 2000;191:181–188.
99. Ingram DA, Hiatt K, King AJ, et al. Hyperactivation of p21 (ras) and the hematopoietic-specific Rho GTPase, Rac2, cooperate to alter the proliferation of neurofibromin-deficient mast cells in vivo and in vitro. *J Exp Med*. 2001;194:57–69.
100. Yang FC, Ingram DA, Chen S, et al. Nf1-dependent tumors require a microenvironment containing Nf1+/– and c-kit-dependent bone marrow. *Cell*. 2008;135:437–448.
101. Yang FC, Chen S, Clegg T, et al. Nf1+/- mast cells induce neurofibroma like phenotypes through secreted TGF-beta signaling. *Hum Mol Genet*. 2006;15:2421–2437.

Copyright © 2018 Wolters Kluwer Health, Inc. All rights reserved.

Copyright © 2018 Wolters Kluwer Health, Inc. All rights reserved.

102. Serra E, Rosenbaum T, Winner U, et al. Schwann cells harbor the somatic NF1 mutation in neurofibromas: evidence of two different Schwann cell subpopulations. *Hum Mol Genet*. 2000;9:3055–3064.
103. Courtois-Cox S, Genther Williams SM, Reczek EE, et al. A negative feedback signaling network underlies oncogene-induced senescence. *Cancer Cell*. 2006;10:459–472.
104. Emmerich D, Zemojtel T, Hecht J, et al. Somatic neurofibromatosis type 1 (NF1) inactivation events in cutaneous neurofibromas of a single NF1 patient. *Eur J Hum Genet*. 2015;23:870–873.
105. Faden DL, Asthana S, Tihan T, et al. Whole exome sequencing of growing and non-growing cutaneous neurofibromas from a single patient with neurofibromatosis type 1. *PLoS One*. 2017;12:e0170348.
106. Pemov A, Li H, Patidar R, et al. NCI DCEG Cancer Genomics Research Laboratory. The primacy of NF1 loss as the driver of tumorigenesis in neurofibromatosis type 1-associated plexiform neurofibromas. *Oncogene*. 2017;36:3168–3177.
107. Beert E, Brems H, Daniels B, et al. Atypical neurofibromas in neurofibromatosis type 1 are premalignant tumors. *Genes Chromosomes Cancer*. 2011;50:1021–1032.
108. Brossier NM, Carroll SL. Genetically engineered mouse models shed new light on the pathogenesis of neurofibromatosis type I-related neoplasms of the peripheral nervous system. *Brain Res Bull*. 2012;88:58–71.
109. Brennan MF, Antonescu CR, Moraco N, et al. Lessons learned from the study of 10,000 patients with soft tissue sarcoma. *Ann Surg*. 2014;260:416–421; discussion 21–22.
110. Ng VY, Scharschmidt TJ, Mayerson JL, et al. Incidence and survival in sarcoma in the United States: a focus on musculoskeletal lesions. *Anticancer Res*. 2013;33:2597–2604.
111. Evans DG, Baser ME, McGaughran J, et al. Malignant peripheral nerve sheath tumours in neurofibromatosis 1. *J Med Genet*. 2002;39:311–314.
112. McCaughan JA, Holloway SM, Davidson R, et al. Further evidence of the increased risk for malignant peripheral nerve sheath tumour from a Scottish cohort of patients with neurofibromatosis type 1. *J Med Genet*. 2007;44:463–466.
113. Zou C, Smith KD, Liu J, et al. Clinical, pathological, and molecular variables predictive of malignant peripheral nerve sheath tumor outcome. *Ann Surg*. 2009;249:1014–1022.
114. LaFemina J, Qin LX, Moraco NH, et al. Oncologic outcomes of sporadic, neurofibromatosis-associated, and radiation-induced malignant peripheral nerve sheath tumors. *Ann Surg Oncol*. 2013;20:66–72.
115. Stucky CC, Johnson KN, Gray RJ, et al. Malignant peripheral nerve sheath tumors (MPNST): the Mayo Clinic experience. *Ann Surg Oncol*. 2012;19:878–885.
116. Kolberg M, Holand M, Agesen TH, et al. Survival meta-analyses for 1800 malignant peripheral nerve sheath tumor patients with and without neurofibromatosis type 1. *Neuro Oncol*. 2013;15:135–147.
117. Porter DE, Prasad V, Foster L, et al. Survival in malignant peripheral nerve sheath tumours: a comparison between sporadic and neurofibromatosis type 1-associated tumours. *Sarcoma*. 2009;2009:756395.
118. Watson KL, Al Sannaa GA, Kivlin CM, et al. Patterns of recurrence and survival in sporadic, neurofibromatosis type 1-associated, and radiation-associated malignant peripheral nerve sheath tumors. *J Neurosurg*. 2017;126:319–329.
119. Ducatman BS, Scheithauer BW, Piepgras DG, et al. Malignant peripheral nerve sheath tumors. A clinicopathologic study of 120 cases. *Cancer*. 1986;57:2006–2021.
120. Anghileri M, Miceli R, Fiore M, et al. Malignant peripheral nerve sheath tumors: prognostic factors and survival in a series of patients treated at a single institution. *Cancer*. 2006;107:1065–1074.
121. Fan Q, Yang J, Wang G. Clinical and molecular prognostic predictors of malignant peripheral nerve sheath tumor. *Clin Transl Oncol*. 2014;16:191–199.
122. Valentin T, Le Cesne A, Ray-Coquard I, et al. Management and prognosis of malignant peripheral nerve sheath tumors: the experience of the French Sarcoma Group (GSF-GETO). *Eur J Cancer*. 2016;56:77–84.
123. Shimada S, Tsuzuki T, Kuroda M, et al. Nestin expression as a new marker in malignant peripheral nerve sheath tumors. *Pathol Int*. 2007;57:60–67.
124. Reuss DE, Habel A, Hagenlocher C, et al. Neurofibromin specific antibody differentiates malignant peripheral nerve sheath tumors (MPNST) from other spindle cell neoplasms. *Acta Neuropathol*. 2014;127:565–572.
125. Mertens F, Rydholm A, Bauer HF, et al. Cytogenetic findings in malignant peripheral nerve sheath tumors. *Int J Cancer*. 1995;61:793–798.
126. Plaat BE, Molenaar WM, Mastik MF, et al. Computer-assisted cytogenetic analysis of 51 malignant peripheral-nerve-sheath tumors: sporadic vs. neurofibromatosis-type-1-associated malignant schwannomas. *Int J Cancer*. 1999;83:171–178.
127. Forus A, Weghuis DO, Smeets D, et al. Comparative genomic hybridization analysis of human sarcomas: I. Occurrence of genomic imbalances and identification of a novel major amplicon at 1q21-q22 in soft tissue sarcomas. *Genes Chromosomes Cancer*. 1995;14:8–14.
128. Lothe RA, Karhu R, Mandahl N, et al. Gain of 17q24-qter detected by comparative genomic hybridization in malignant tumors from patients with von Recklinghausen's neurofibromatosis. *Cancer Res*. 1996;56:4778–4781.
129. Mechtersheimer G, Otano-Joos M, Ohl S, et al. Analysis of chromosomal imbalances in sporadic and NF1-associated peripheral nerve sheath tumors by comparative genomic hybridization. *Genes Chromosomes Cancer*. 1999;25:362–369.
130. Schmidt H, Wurl P, Taubert H, et al. Genomic imbalances of 7p and 17q in malignant peripheral nerve sheath tumors are clinically relevant. *Genes Chromosomes Cancer*. 1999;25:205–211.
131. Schmidt H, Taubert H, Wurl P, et al. Cytogenetic characterization of six malignant peripheral nerve sheath tumors: comparison of karyotyping and comparative genomic hybridization. *Cancer Genet Cytogenet*. 2001;128:14–23.
132. Schmidt H, Taubert H, Meye A, et al. Gains in chromosomes 7, 8q, 15q and 17q are characteristic changes in malignant but not in benign peripheral nerve sheath tumors from patients with Recklinghausen's disease. *Cancer Lett*. 2000;155:181–190.
133. Mertens F, Dal Cin P, De Wever I, et al. Cytogenetic characterization of peripheral nerve sheath tumours: a report of the CHAMP study group. *J Pathol*. 2000;190:31–38.
134. Legius E, Marchuk DA, Collins FS, et al. Somatic deletion of the neurofibromatosis type 1 gene in a neurofibrosarcoma supports a tumour suppressor gene hypothesis. *Nat Genet*. 1993;3:122–126.
135. Birindelli S, Perrone F, Oggionni M, et al. Rb and TP53 pathway alterations in sporadic and NF1-related malignant peripheral nerve sheath tumors. *Lab Invest*. 2001;81:833–844.
136. Holtkamp N, Atallah I, Okuducu AF, et al. MMP-13 and p53 in the progression of malignant peripheral nerve sheath tumors. *Neoplasia*. 2007;9:671–677.
137. Legius E, Dierick H, Wu R, et al. TP53 mutations are frequent in malignant NF1 tumors. *Genes Chromosomes Cancer*. 1994;10:250–255.
138. Menon AG, Anderson KM, Riccardi VM, et al. Chromosome 17p deletions and p53 gene mutations associated with the formation of malignant neurofibrosarcomas in von Recklinghausen neurofibromatosis. *Proc Natl Acad Sci U S A*. 1990;87:5435–5439.
139. Upadhyaya M, Kluwe L, Spurlock G, et al. Germline and somatic NF1 gene mutation spectrum in NF1-associated malignant peripheral nerve sheath tumors (MPNSTs). *Hum Mutat*. 2008;29:74–82.
140. Kourea HP, Orlow I, Scheithauer BW, et al. Deletions of the INK4A gene occur in malignant peripheral nerve sheath tumors but not in neurofibromas. *Am J Pathol*. 1999;155:1855–1860.
141. Nielsen GP, Stemmer-Rachamimov AO, Ino Y, et al. Malignant transformation of neurofibromas in neurofibromatosis 1 is associated with CDKN2A/p16 inactivation. *Am J Pathol*. 1999;155:1879–1884.
142. Mantripragada KK, Spurlock G, Kluwe L, et al. High-resolution DNA copy number profiling of malignant peripheral nerve sheath tumors using targeted microarray-based comparative genomic hybridization. *Clin Cancer Res*. 2008;14:1015–1024.

Copyright © 2018 Wolters Kluwer Health, Inc. All rights reserved.

Copyright © 2018 Wolters Kluwer Health, Inc. All rights reserved.

143. Mawrin C, Kirches E, Boltze C, et al. Immunohistochemical and molecular analysis of p53, RB, and PTEN in malignant peripheral nerve sheath tumors. *Virchows Arch*. 2002;440:610–615.
144. Bradtmoller M, Hartmann C, Zietsch J, et al. Impaired Pten expression in human malignant peripheral nerve sheath tumours. *PLoS One*. 2012;7:e47595.
145. Gregorian C, Nakashima J, Dry SM, et al. PTEN dosage is essential for neurofibroma development and malignant transformation. *Proc Natl Acad Sci U S A*. 2009;106:19479–19484.
146. Kawaguchi K, Oda Y, Saito T, et al. Genetic and epigenetic alterations of the PTEN gene in soft tissue sarcomas. *Hum Pathol*. 2005;36:357–363.
147. Holtkamp N, Malzer E, Zietsch J, et al. EGFR and erbB2 in malignant peripheral nerve sheath tumors and implications for targeted therapy. *Neuro Oncol*. 2008;10:946–957.
148. DeClue JE, Heffelfinger S, Benvenuto G, et al. Epidermal growth factor receptor expression in neurofibromatosis type 1-related tumors and NF1 animal models. *J Clin Invest*. 2000;105:1233–1241.
149. Perry A, Kunz SN, Fuller CE, et al. Differential NF1, p16, and EGFR patterns by interphase cytogenetics (FISH) in malignant peripheral nerve sheath tumor (MPNST) and morphologically similar spindle cell neoplasms. *J Neuropathol Exp Neurol*. 2002;61:702–709.
150. Lee W, Teckie S, Wiesner T, et al. PRC2 is recurrently inactivated through EED or SUZ12 loss in malignant peripheral nerve sheath tumors. *Nat Genet*. 2014;46:1227–1232.
151. Zhang M, Wang Y, Jones S, et al. Somatic mutations of SUZ12 in malignant peripheral nerve sheath tumors. *Nat Genet*. 2014;46:1170–1172.
152. Schaefer IM, Fletcher CD, Hornick JL. Loss of H3K27 trimethylation distinguishes malignant peripheral nerve sheath tumors from histologic mimics. *Mod Pathol*. 2016;29:4–13.
153. Cleven AH, Sannaa GA, Briaire-de Bruijn I, et al. Loss of H3K27 tri-methylation is a diagnostic marker for malignant peripheral nerve sheath tumors and an indicator for an inferior survival. *Mod Pathol*. 2016;29:582–590.
154. Asano N, Yoshida A, Ichikawa H, et al. Immunohistochemistry for trimethylated H3K27 in the diagnosis of malignant peripheral nerve sheath tumours. *Histopathology*. 2017;70:385–393.
155. Mito JK, Qian X, Doyle LA, et al. Role of histone H3K27 trimethylation loss as a marker for malignant peripheral nerve sheath tumor in fine-needle aspiration and small biopsy specimens. *Am J Clin Pathol*. 2017;148:179–189.
156. Widemann BC, Salzer WL, Arceci RJ, et al. Phase I trial and pharmacokinetic study of the farnesyltransferase inhibitor tipifarnib in children with refractory solid tumors or neurofibromatosis type I and plexiform neurofibromas. *J Clin Oncol*. 2006;24:507–516.
157. Martin GA, Viskochil D, Bollag G, et al. The GAP-related domain of the neurofibromatosis type 1 gene product interacts with ras p21. *Cell*. 1990;63:843–849.
158. Ballester R, Marchuk D, Boguski M, et al. The NF1 locus encodes a protein functionally related to mammalian GAP and yeast IRA proteins. *Cell*. 1990;63:851–859.
159. Ohba Y, Mochizuki N, Yamashita S, et al. Regulatory proteins of R-Ras, TC21/R-Ras2, and M-Ras/R-Ras3. *J Biol Chem*. 2000;275:20020–20026.
160. Brossier NM, Prechtl AM, Longo JF, et al. Classic Ras proteins promote proliferation and survival via distinct phosphoproteome alterations in neurofibromin-null malignant peripheral nerve sheath tumor cells. *J Neuropathol Exp Neurol*. 2015;74:568–586.
161. Mattingly RR, Kraniak JM, Dilworth JT, et al. The mitogen-activated protein kinase/extracellular signal-regulated kinase kinase inhibitor PD184352 (CI-1040) selectively induces apoptosis in malignant schwannoma cell lines. *J Pharmacol Exp Ther*. 2006;316:456–465.
162. Jessen WJ, Miller SJ, Jousma E, et al. MEK inhibition exhibits efficacy in human and mouse neurofibromatosis tumors. *J Clin Invest*. 2013;123:340–347.
163. Kim A, Dombi E, Tepas K, et al. Phase I trial and pharmacokinetic study of sorafenib in children with neurofibromatosis type I and plexiform neurofibromas. *Pediatr Blood Cancer*. 2013;60:396–401.
164. Maki RG, D'Adamo DR, Keohan ML, et al. Phase II study of sorafenib in patients with metastatic or recurrent sarcomas. *J Clin Oncol*. 2009;27:3133–3140.
165. Johannessen CM, Reczek EE, James MF, et al. The NF1 tumor suppressor critically regulates TSC2 and mTOR. *Proc Natl Acad Sci U S A*. 2005;102:8573–8578.
166. Johansson G, Mahller YY, Collins MH, et al. Effective in vivo targeting of the mammalian target of rapamycin pathway in malignant peripheral nerve sheath tumors. *Mol Cancer Ther*. 2008;7:1237–1245.
167. Holtkamp N, Okuducu AF, Mucha J, et al. Mutation and expression of PDGFRA and KIT in malignant peripheral nerve sheath tumors, and its implications for imatinib sensitivity. *Carcinogenesis*. 2006;27:664–671.
168. Kadono T, Soma Y, Takehara K, et al. The growth regulation of neurofibroma cells in neurofibromatosis type-1: increased responses to PDGF-BB and TGF-beta 1. *Biochem Biophys Res Commun*. 1994;198:827–834.
169. Badache A, De Vries GH. Neurofibrosarcoma-derived Schwann cells overexpress platelet-derived growth factor (PDGF) receptors and are induced to proliferate by PDGF BB. *J Cell Physiol*. 1998;177:334–342.
170. Perrone F, Da Riva L, Orsenigo M, et al. PDGFRA, PDGFRB, EGFR, and downstream signaling activation in malignant peripheral nerve sheath tumor. *Neuro Oncol*. 2009;11:725–736.
171. Zietsch J, Ziegenhagen N, Heppner FL, et al. The 4q12 amplicon in malignant peripheral nerve sheath tumors: consequences on gene expression and implications for sunitinib treatment. *PLoS One*. 2010;5:e11858.
172. Badache A, Muja N, De Vries GH. Expression of kit in neurofibromin-deficient human Schwann cells: role in Schwann cell hyperplasia associated with type 1 neurofibromatosis. *Oncogene*. 1998;17:795–800.
173. Rao UN, Sonmez-Alpan E, Michalopoulos GK. Hepatocyte growth factor and c-MET in benign and malignant peripheral nerve sheath tumors. *Hum Pathol*. 1997;28:1066–1070.
174. Fukuda T, Ichimura E, Shinozaki T, et al. Coexpression of HGF and c-Met/HGF receptor in human bone and soft tissue tumors. *Pathol Int*. 1998;48:757–762.
175. Su W, Gutmann DH, Perry A, et al. CD44-independent hepatocyte growth factor/c-Met autocrine loop promotes malignant peripheral nerve sheath tumor cell invasion in vitro. *Glia*. 2004;45:297–306.
176. Ling BC, Wu J, Miller SJ, et al. Role for the epidermal growth factor receptor in neurofibromatosis-related peripheral nerve tumorigenesis. *Cancer Cell*. 2005;7:65–75.
177. Stonecypher MS, Byer SJ, Grizzle WE, et al. Activation of the neuregulin-1/ErbB signaling pathway promotes the proliferation of neoplastic Schwann cells in human malignant peripheral nerve sheath tumors. *Oncogene*. 2005;24:5589–5605.
178. Eckert JM, Byer SJ, Clodfelder-Miller BJ, et al. Neuregulin-1 beta and neuregulin-1 alpha differentially affect the migration and invasion of malignant peripheral nerve sheath tumor cells. *Glia*. 2009;57:1501–1520.
179. Huijbregts RP, Roth KA, Schmidt RE, et al. Hypertrophic neuropathies and malignant peripheral nerve sheath tumors in transgenic mice overexpressing glial growth factor beta3 in myelinating Schwann cells. *J Neurosci*. 2003;23:7269–7280.
180. Brosius SN, Turk AN, Byer SJ, et al. Neuregulin-1 overexpression and Trp53 haploinsufficiency cooperatively promote de novo malignant peripheral nerve sheath tumor pathogenesis. *Acta Neuropathol*. 2014;127:573–591.
181. Pillay V, Allaf L, Wilding AL, et al. The plasticity of oncogene addiction: implications for targeted therapies directed to receptor tyrosine kinases. *Neoplasia*. 2009;11:448–458; 2 p following 58.
182. Stommel JM, Kimmelman AC, Ying H, et al. Coactivation of receptor tyrosine kinases affects the response of tumor cells to targeted therapies. *Science*. 2007;318:287–290.

Copyright © 2018 Wolters Kluwer Health, Inc. All rights reserved.

Copyright © 2018 Wolters Kluwer Health, Inc. All rights reserved.

ARTICLE OPEN ACCESS

Cutaneous neurofibromas

Current clinical and pathologic issues

Nicolas Ortonne, MD, PhD,* Pierre Wolkenstein, MD, PhD,* Jaishri O. Blakeley, MD, Bruce Korf, MD, PhD, Scott R. Plotkin, MD, PhD, Vincent M. Riccardi, MD, MBA, Douglas C. Miller, MD, PhD, Susan Huson, MD, Juha Peltonen, MD, PhD, Andrew Rosenberg, MD, Steven L. Carroll, MD, PhD, Sharad K. Verma, PhD, Victor Mautner, MD, Meena Upadhyaya, PhD, and Anat Stemmer-Rachamimov, MD

Correspondence
Dr. Wolkenstein
pierre.wolkenstein@aphp.fr

Neurology® 2018;91 (Suppl 1):S5-S13. doi:10.1212/WNL.0000000000005792

Abstract

Objective

To present the current terminology and natural history of neurofibromatosis 1 (NF1) cutaneous neurofibromas (cNF).

Methods

NF1 experts from various research and clinical backgrounds reviewed the terms currently in use for cNF as well as the clinical, histologic, and radiographic features of these tumors using published and unpublished data.

Results

Neurofibromas develop within nerves, soft tissue, and skin. The primary distinction between cNF and other neurofibromas is that cNF are limited to the skin whereas other neurofibromas may involve the skin, but are not limited to the skin. There are important cellular, molecular, histologic, and clinical features of cNF. Each of these factors is discussed in consideration of a clinicopathologic framework for cNF.

Conclusion

The development of effective therapies for cNF requires formulation of diagnostic criteria that encompass the clinical and histologic features of these tumors. However, there are several areas of overlap between cNF and other neurofibromas that make distinctions between cutaneous and other neurofibromas more difficult, requiring careful deliberation with input across the multiple disciplines that encounter these tumors and ultimately, prospective validation. The ultimate goal of this work is to facilitate accurate diagnosis and meaningful therapeutics for cNF.

RELATED ARTICLES

Creating a comprehensive research strategy for cutaneous neurofibromas
Page S1

The biology of cutaneous neurofibromas: Consensus recommendations for setting research priorities
Page S14

Considerations for development of therapies for cutaneous neurofibroma
Page S21

Clinical trial design for cutaneous neurofibromas
Page S31

*These authors contributed equally to this work.

From the Departments of Pathology (N.O.) and Dermatology (P.W.), French Referral Center for Neurofibromatoses, Henri-Mondor Hospital, AP-HP, University Paris Est Créteil, France; Department of Neurology (J.O.B., S.K.V.), Johns Hopkins University School of Medicine, The Neurofibromatosis Therapuetic Acceleration Program, Baltimore, MD; University of Alabama at Birmingham (B.K.); Cancer Center and Department of Neurology (S.R.P.) and Department of Pathology, Division of Neuropathology (A.S.-R.), Massachusetts General Hospital, Boston; The Neurofibromatosis Institute (V.M.R.), La Crescenta, CA; Department of Pathology & Anatomical Sciences (D.C.M.), University of Missouri School of Medicine, Columbia; Manchester Centre for Genomic Medicine (S.H.), Central Manchester University Hospitals NHS Foundation Trust, Manchester Academic Health Science Centre, UK; Institute of Biomedicine (J.P.), University of Turku, Finland; Department of Pathology and Laboratory Medicine (A.R.), Jackson Memorial Hospital/University of Miami Miller School of Medicine, FL; Department of Pathology and Laboratory Medicine (S.L.C.), Medical University of South Carolina, Charleston; Clinics and Polyclinics of Neurology (V.M.), University Hospital Hamburg-Eppendorf, Hamburg, Germany; and Division of Cancer and Genetics (M.U.), Institute of Medical Genetics, Cardiff University, UK.

Go to Neurology.org/N for full disclosures. Funding information and disclosures deemed relevant by the authors, if any, are provided at the end of the article.

The Article Processing Charge was funded by The Neurofibromatosis Therapeutic Acceleration Program at Johns Hopkins.

This is an open access article distributed under the terms of the Creative Commons Attribution License 4.0 (CC BY), which permits unrestricted use, distribution, and reproduction in any medium, provided the original work is properly cited.

Copyright © 2018 The Author(s). Published by Wolters Kluwer Health, Inc. on behalf of the American Academy of Neurology.

Glossary

cNF = cutaneous neurofibromas; **NF1** = neurofibromatosis type 1; **NOS** = not otherwise specified; **OCT** = optical coherence tomography; **pNF** = plexiform neurofibromas; **QoL** = quality of life; **US** = ultrasound.

There are many clinical features associated with the neurogenetic condition neurofibromatosis type 1 (NF1). However, the feature that affects the majority of NF1 patients is the development of cutaneous neurofibromas (cNF).[1] Neurofibromas are defined as histologically benign (WHO grade I) tumors composed of multiple cell types including Schwann cells, fibroblasts, immune cells (such as mast cells and macrophages), and other elements of nerve.[2] Regardless of their location, all neurofibromas share certain histologic and cellular characteristics.

The most common and prominent location of neurofibromas is the skin (skin is defined in this article as including epidermis and dermis). Discrete lesions are often referred to as dermal or cutaneous neurofibromas. cNF are benign and, unlike plexiform neurofibromas (pNF), are not known to have any malignant potential.[3]

Although not life-threatening, cNF have a major effect upon quality of life (QoL) for most patients with NF1 due to their prevalence and disfigurement.[4–12] Furthermore, the number of cNF increases with age after adolescence and throughout a patient's lifespan. Despite the high prevalence of cNF in people with NF1 and their documented influence on QoL, current treatment is limited to surgical removal or physical destruction.

There have been several efforts to define the various forms of neurofibromas, resulting in a number of classification systems proposed by neurologists, clinical geneticists, dermatologists, pathologists, and basic researchers (table 1).[3,13–16] Some of these schemes are incompatible with one another, which may impede, rather than enhance, the transfer of knowledge from basic and translational science to clinical care. An agreed-upon classification system would facilitate research addressing critical questions such as the comparisons between human disease and *Nf1* mouse models of cNF, whether there are specific responses to treatments based on potential subtypes of cNF, or if cNF might respond similarly or differently to therapies than other neurofibromas (potentially allowing cNF to serve as a surrogate for pNF). This article reviews the terms in current use for cNF and outlines the critical factors contributing to the definition of cNF, with the ultimate goal of creating a draft framework for a classification system to be validated in future prospective studies.

Methods

This work is the result of 2 multidisciplinary meetings, one sponsored by the Neurofibromatosis Therapeutics Acceleration Program in 2016, and another by The European Neurofibromatosis Group in 2008. Across these 2 meetings, international experts from within and outside the NF field (with expertise in dermatology, genetics, neurology, neuro-oncology, dermatopathology, neuropathology, regenerative medicine, and plastic surgery) reviewed different aspects of cNF, including clinical features, biology, effects on QoL, and existing proposed classification schemes of neurofibromas (table 1).

A literature search using the terms NF1, cNF, plexiform neurofibroma, dermal neurofibroma, classification, pain, itching, and QoL was completed. Although cNF may be sporadic in some instances, this review is focused on the cNF arising in the context of NF1. The investigators met to review these areas, including critical elements of each proposed classification system, with the intent of using this information as a framework for the longer-term goal of developing a single unified, data-driven classification system for cNF incorporating core features of cNF including pattern of growth (localized or diffuse) and anatomical location (skin, subcutaneous tissue, or deep nerve).

Results

Cutaneous neurofibromas: Clinical definitions or descriptors

This article is focused on cNF, which are benign and arise in and are limited to the skin. They are localized but not encapsulated and do not show clear association to myelinated nerves. They present clinically as a well-defined cutaneous lesion, most often as a nodule or plaque.[3] cNF is the preferred term over dermal neurofibroma, as the term cNF distinguishes between discrete neurofibromas of the skin and neurofibromas that arise in deeper tissues but invade into the dermis. The term cNF does not encompass deep, large, or diffusely infiltrating tumors that involve the dermis.[3] However, the skin may also be secondarily involved by extension of a deep or plexiform neurofibroma, either by involvement of cutaneous nerves (i.e., plexiform growth pattern) or by diffuse infiltration of the subcutaneous and cutaneous tissue (i.e., diffuse growth pattern). The importance of distinguishing true cNF from extension of deep neurofibromas into the skin is particularly important when atypical changes are present. The presence of cytologic atypia or proliferation in a cNF represents reactive or degenerative changes and is not worrisome, while similar changes in a plexiform neurofibroma that may involve the skin can be a manifestation of malignant transformation.[17]

Natural history of cNF

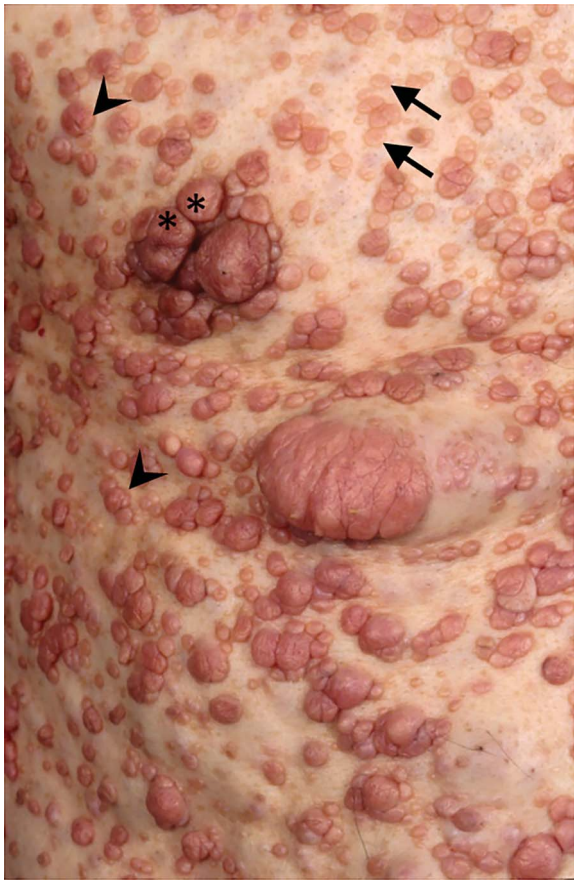
cNF most commonly become clinically apparent after puberty.[1] However, there is a wide range of clinical presentation

Table 1 Clinicopathologic classification of neurofibromas

Proposed classification	Proposed by
Cutaneous neurofibromas	Jouhilahti et al.[3]
Subcutaneous neurofibromas	
Intraneural neurofibromas	
Plexiform neurofibromas	
Localized cutaneous neurofibromas	Carroll and Ratner[13]
Diffuse cutaneous neurofibromas	
Localized intraneural neurofibromas	
Plexiform neurofibromas	
Massive soft tissue	
Localized neurofibromas	Rosenberg[14]
Plexiform neurofibromas	
Diffuse neurofibromas	
Pigmented neurofibromas	
Dermal neurofibromas	Huson[15]
Nodular neurofibromas	
Plexiform neurofibromas	
Discrete cutaneous neurofibromas of the dermis and epidermis (endoneurial neurofibroma)	Friedman and Riccardi[16]
Discrete subcutaneous neurofibromas that lie deeper in the skin (perineurial neurofibroma)	
Nodular plexiform neurofibromas (perineurial neurofibroma)	
Diffuse plexiform neurofibromas (epineurial neurofibroma)	
Cutaneous neurofibromas	Goldblum et al.[44]
Subcutaneous neurofibromas	
Diffuse neurofibromas	
Localized cutaneous neurofibromas	Stemmer-Rachamimov, Wolkenstein, and Ortonne (unpublished, 2008)
Localized subcutaneous neurofibromas	
Diffuse cutaneous and subcutaneous neurofibromas	
Localized intraneural neurofibromas	
Plexiform neurofibromas	

with select genotype–phenotype correlations. In the small subset of people with NF1 microdeletions, cNF are more likely to be apparent earlier in childhood.[18] In contrast, in people with *NF1* deletion in p.Met992del, or a missense mutation affecting p.Arg1809, there are few to no cNF throughout life.[19–22] Additional details around the biology of genotype–phenotype correlations are discussed by Brosseau et al.[23] in this series. In the majority of people with NF1, the number of cNF increases with age such that there are more tumors present in older patients.[1] There are no known predictive factors to determine the eventual number or types of cNF that will appear on an individual with NF1 (other than the small subsets with specific types of mutation listed above). Furthermore, there is dramatic variability in cNF burden between patients, and even within families harboring the same *NF1* mutation. Retrospective studies suggest that women experience an increase in the size and numbers of cNF during pregnancy.[24–26] Finally, it has been suggested that people with NF1 have low serum vitamin D concentrations, especially those with many cNF. However, it is not clear if these factors are causative or correlative.[27]

Figure 1 Polymorphism of cutaneous neurofibromas (cNF) in a single patient

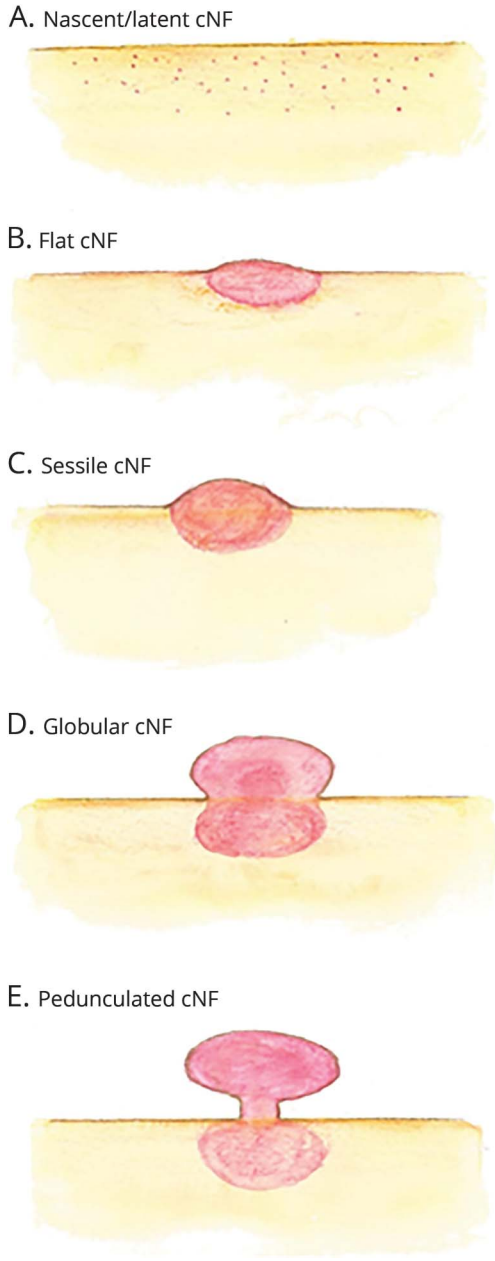


Many different aspects of cNF can be seen in this patient, including sessile cNF (arrows), globular cNF (arrowheads), and pedunculated cNF (asterisks). NF = neurofibromas.

Clinical features and effect on QoL

Patients and clinicians report multiple different appearances of cNF, ranging from barely visible flat nodules with subtle discoloration to large and pedunculated masses (figure 1). It remains unknown if this variability in appearance is an expression of the various stages of the evolution of a single tumor, or represents different subtypes of cNF. One proposed classification system assigns 1 of 5 subcategories to describe the clinical appearance of cNF[28]: nascent, flat, sessile, globular, or pedunculated (figure 2). The nascent/latent cNF (figure 2A) is not apparent by inspection or palpation of the skin, but can be appreciated by proper imaging techniques, such as high-resolution ultrasound (US) and optical coherence tomography (OCT) imaging, which are discussed by Cannon et al.[29] in this series. The flat cNF (figure 2B) is visible at the skin surface, and is distinguished primarily by its slightly raised surface. The surface may appear thinner and somewhat pale compared to adjacent uninvolved skin, or there may be some increased pigmentation and peripheral coarse hairs (bristles). Flat cNF tend to range in size from 0.5 to 12 millimeters. The sessile cNF (figure 2C) is raised compared to the adjacent skin and there is usually an apparent apex. The height of the apex may be as high as 8–10 mm. The surface and texture are essentially the same as that of the flat lesion. There may be erythema or hyperpigmentation, as well as bristle hirsutism. These lesions typically have a maximal diameter of roughly 1.0 to 10–12 mm. Imaging (US or OCT) may reveal more extensive cNF elements below the surface of the skin. The globular cNF (figure 2D) has a base at the surface of the skin that may be 20–30 mm in diameter, with a comparable height and a globular shape. Moving the raised portion of globular neurofibromas (i.e., above the surrounding uninvolved skin surface) can help a clinical examiner

Figure 2 Proposed categories of clinically observed cutaneous neurofibromas (cNF) to be considered in the prospective validation study



(A) Nascent/latent cNF. (B) Flat cNF. (C) Sessile cNF. (D) Globular cNF. (E) Pedunculated cNF.

to identify a deeper part of the lesion. The pedunculated cNF (figure 2E) has a stalk that joins the portions above and below the skin surface. The stalk is usually several millimeters long and 1–3 mm in diameter. The diameter of the superficial portion is usually between 5 and 25 millimeters.

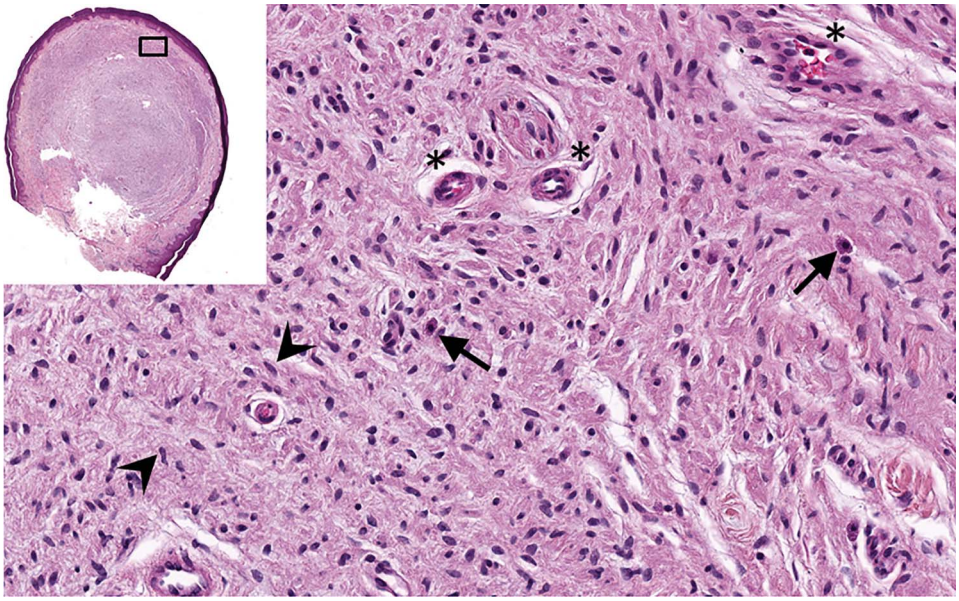
Roughly 20% of people with NF1 report pruritus.[30] Chronic pruritus can be an independent factor for altered QoL as it causes sleep disruption as well as the emotional experience of chronic pain.[30] Among those with pruritus, 52.5% complained of pruritus localized to one or more cNF. The pathophysiology of pruritus in NF1 is not well-understood. It is hypothesized that mast cells and components released from their degranulation are a major cause of pruritus, as mast cells are well-known to be present in the cNF microenvironment and may contribute to tumor initiation, progression, and angiogenesis.[31–36] However, it is also possible that pruritus is a manifestation of a neuropathy affecting the small nerve tributaries in the skin, which are integral to the development of these tumors.[30,37] Indeed, anecdotally, people with NF1 report improvement in pruritus after therapy with antineuropathic agents such as gabapentin or mast cell stabilizing agents such as ketotifen, indicating that both mechanisms may be active.

Although cNF are not life-threatening, the majority of patients report cNF-associated disfigurement as their major problem related to NF1. Combined responses from several surveys show that between 97% and 100% of adults with NF1 who participated reported skin lesions and >60% reported moderate to severe visibility of these lesions.[8,9,11,12] In all of these studies, the visibility of disease was independently associated with adverse emotional state, physical symptoms, and poor function assessed with skin-disease-specific QoL and general health measures.[11,12] The effect of disfigurement on QoL has been evaluated through the use of dermatologic scales such as Skindex.[8,9,12] Using this tool as well as measures of overall disease-associated QoL (i.e., Short Form–36), the burden of disfigurement on QoL in patients with NF1 has been highlighted across multiple studies.[5,6,8–11,38] The greatest effect on QoL from cNF is emotional: patients with more visible tumors report significantly greater overall negative effects on their skin-disease-specific QoL, and visible features of cNF are associated with severe depression. The magnitude of this effect is similar to that reported in the literature for patients with psoriasis, a skin condition traditionally regarded as causing significant disability. These results underscore the link between cNF disease visibility and psychological well-being.[11] As such, reducing deformity is a priority in adult patients with NF1.[11] For example, people with NF1 who graded themselves to be more severely affected expressed greater fear about the appearance of the lesions.[12]

Histology of cNF

Histologically, all neurofibromas are mixed tumors consisting of cells of diverse lineages. cNF are composed of neoplastic Schwann cells and non-neoplastic elements including mast cells and fibroblasts.[39] There are also often other cells including nerve sheath elements (i.e., perineurial cells) and cells from various skin adnexae (e.g., hair follicles, eccrine sweat glands, sebaceous glands).[13] On occasion, adipocytes may be sequestered in or intrinsic to the lesion.[40] Correspondingly, the use of traditional histologic stains, as well as immunohistochemistry with a variety of biomarkers and electron microscopy, has shown the involvement of S100+ Schwann cells, EMA+ perineurial cells, mast cells, lymphocytes, CD34+ fibroblasts, as well

Figure 3 Cutaneous neurofibromas (cNF), morphologic aspect

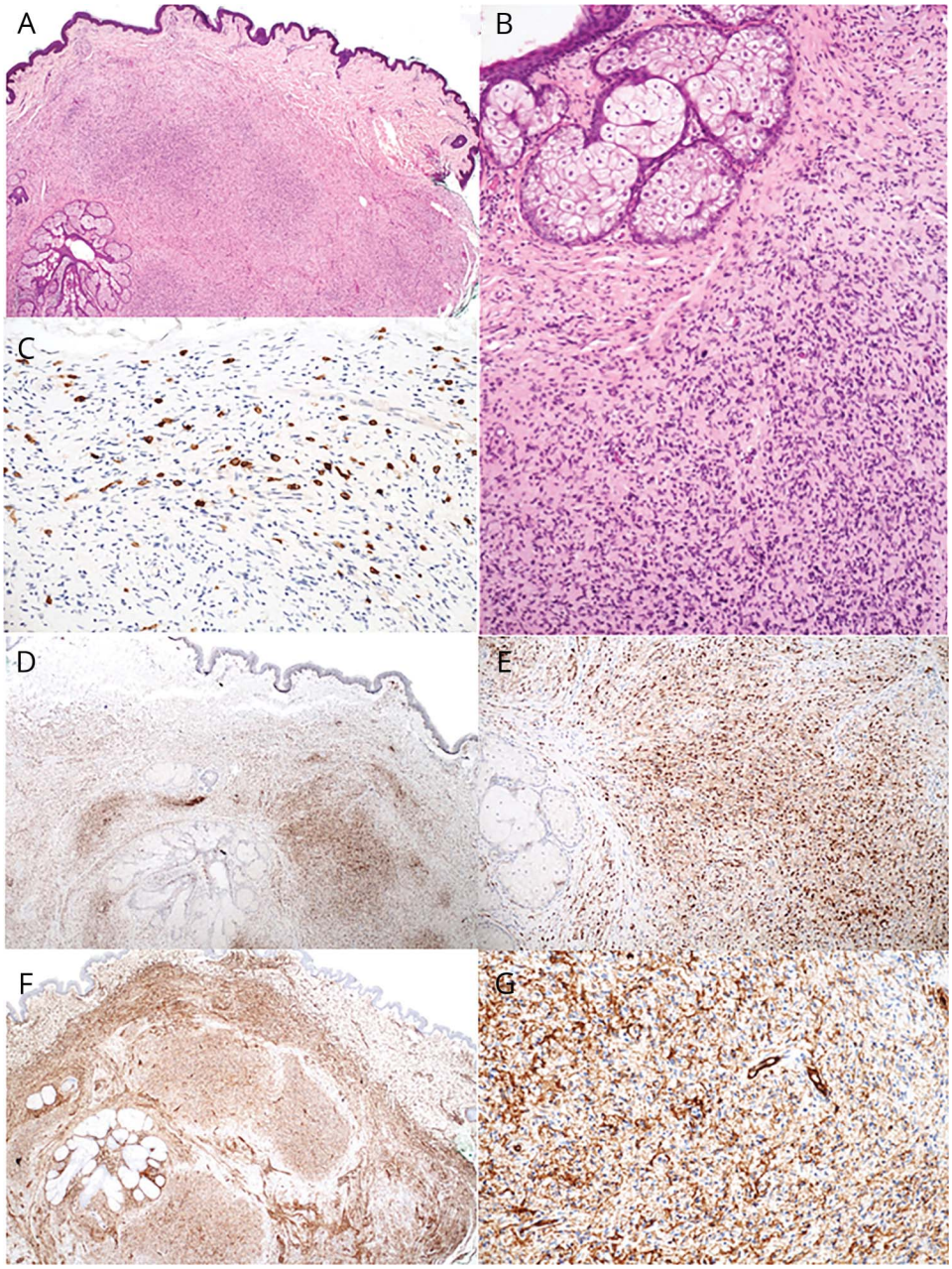


The lesion is made of scattered spindle cells (arrowheads) that correspond to Schwann cells and fibroblasts, admixed with numerous capillaries and veins (asterisks) and mast cells (arrows) (hematoxylin and eosin, ×400, and inset ×25).

as axonal elements[41,42] (figures 3 and 4). Pigmented cNF may be associated with melanocytic cells (or the neoplastic Schwann cells that may become melanotic).[43] Other notable features seen on occasion include the formation of Meissner-like corpuscles.[44] It is presumed that the Schwann cells are neoplastic ($NF1^{-/-}$) and that the other cells are either present initially or recruited into the lesion, but are not neoplastic ($NF1^{-/+}$). However, the definitive cell of origin for human cNF has yet to be defined but has been postulated to be a progenitor cell called a skin-derived precursor cell. Preclinical models suggest that these cells are distinct from the cells that give rise to pNF.[45] There are additional data indicating that multipotent neurofibroma-derived precursor cells, perhaps arising from stem cells around hair roots closely associated with cNF, are the causative cells.[3] Together, these data suggest that cNF and other forms of neurofibromas may arise from different precursor cells even though they have similar cellular compositions.

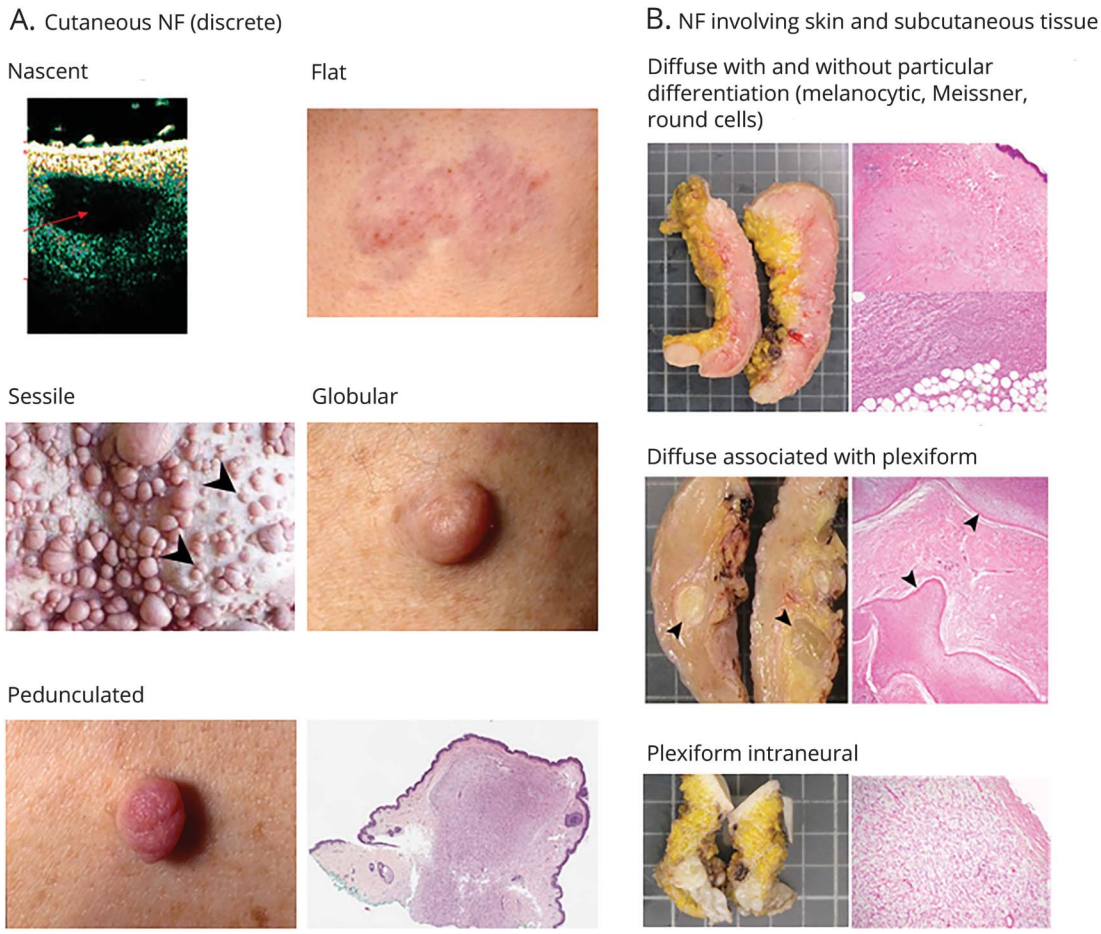
The diverse cellular components of neurofibromas are embedded in an abundant collagenous and often myxoid extracellular matrix. Histologically, cNF cannot be differentiated from neurofibromas elsewhere in the body as the features and cell composition are present in the various forms of neurofibromas. Hence, to accurately identify a lesion as cNF, the surgical specimen must include a margin of uninvolved skin.

Figure 4 Histopathologic features of cutaneous neurofibromas (cNF)



cNF in which various cell types are evidenced using immunostainings. (A, B) Hematoxylin & eosin at 25 and 200 magnification show a cNF presenting as a self-limiting tumor in the skin with no peripheral capsule and in which numerous spindle cells are seen. (C–G) Immunostainings developed with DAB with antibodies to CD117 (C, ×200), S100 protein (D ×25 and E ×100), and CD34 (F ×25 and G ×100). These stains demonstrate numerous mast cells showing strong membrane expression of CD117 (C), Schwann cells displaying heterogeneous cytoplasmic and nuclear expression of S100 protein (D, E), and CD34+ fibroblasts (F,G).

Figure 5 Unified clinicopathologic aspects of neurofibromas



(A) Clinical pictures show the various subtypes of cutaneous neurofibromas (cNF). This includes digital photographs of nascent (visible by ultrasound, but not the naked eye), flat, sessile, globular, and pedunculated cNF. The ultrasound image is courtesy of Dominique Pichard. The red arrow tip indicates the cNF involving the epidermis and dermis. (B) Gross and histologic pictures show the various NF subtypes involving skin and subcutaneous tissue (diffuse, with or without atypia). The upper panels show a cutaneous and subcutaneous NF with diffuse growth pattern replacing the dermis (upper right picture) and the subcutaneous fat tissue (hematoxylin & eosin, ×25 and ×100). The middle panels show a neurofibroma involving the dermis and subcutaneous tissue with 2 distinct growth patterns including plexiform (arrowheads) and diffuse (hematoxylin & eosin, ×25). The lower panels show a neurofibroma located entirely in the subcutaneous tissue with a plexiform neurofibroma with intraneural growth pattern (hematoxylin & eosin, ×100).

Cutaneous neurofibromas as a subset of all neurofibromas: Plan to address the challenges in creating a modern classification system

In addition to classifications already published in articles or textbooks, other unpublished classification systems have been proposed. Two unpublished systems were presented at the European NF meeting (2008) by Ortonne et al. and Stemmer-Rachamimov et al., in which a comprehensive synthesis of clinical and pathologic features was attempted (table 1 and figure 5). These 2 systems are very similar and may be the basis of a new integrated classification system, if validated prospectively. These schemes propose defining neurofibromas by their clinical appearance and histologic features: growth pattern (diffuse/infiltrating or localized), relationship to nerve (intraneural or extraneural, without any perineurial capsule), and anatomic location (cutaneous, cutaneous/subcutaneous, deep). The resulting categories proposed were cutaneous NF (discrete) and larger NF involving skin and subcutaneous tissue (diffuse, with or without atypia) (table 2). This scheme for cNF (table 2 and figure 5) aims to differentiate classic cNF from deep neurofibromas that may involve skin and subcutaneous tissues. As above, it is important to appreciate that an underlying plexiform NF extending into the skin (plexiform intraneural, diffuse associated with plexiform) has different risk profiles than cNF purely limited to the skin. This histologic distinction cannot be made if the sample provided does not reveal the underlying plexiform lesion and shows only the extraneural diffusely infiltrating portion of the tumor in skin. In such instances, histologic distinction from a true cNF is impossible and the term NF involving skin and subcutaneous tissue; diffuse, not otherwise specified (NOS) is most appropriate. Although molecular information is lacking, there is an opportunity to apply common terminology to classify neurofibromas clinically and pathologically in a systematic fashion. Based on the current state of the field, a modern classification system for cNF will be built on the defined clinical and

Table 2 Potential unified classification system for cutaneous neurofibromas

A. Cutaneous neurofibromas (discrete)
Clinical variants
• Nascent (seen on ultrasound or similar imaging only)
• Flat
• Sessile
• Globular
• Pedunculated
B. Extensive neurofibromas (with or without atypia)
Histologic variants
• Diffuse with or without particular differentiation (melanocytic, Meissner/round cells)
• Diffuse associated with plexiform (plexiform and diffuse)
• Diffuse, not otherwise specified
• Plexiform intraneural

pathologic features (table 2) with a plan to incorporate molecular and imaging data as they become available. An ongoing study is evaluating the accuracy of this system with a blinded review by dermatopathologists and neuropathologists. The long-term goal is to have an integrated molecular, clinical, and pathologic classification that best reflects the biology of cNF.

As a first step, the term cNF should be reserved for the discrete neurofibroma limited to the skin, which develop into and mainly involve the dermis, never show a plexiform architecture, and never transform into a malignant peripheral nerve sheath tumor. Further research is needed to determine if there are subtypes of cNF. The term diffuse neurofibroma is advisable for neurofibromas that involve the skin and subcutaneous tissues without clear margins. These tumors may have a diffuse, plexiform, or both patterns. Inherent in these terms is an ambiguity between neurofibromas that are clinically localized but have no perineurial capsule and so could be histologically diffuse and those that are clinically more diffuse. In the case of partial biopsies or superficial excisions, one may miss a deeper plexiform organization or the involvement of a definable nerve trunk, and so the category for diffuse, NOS was introduced. It is important to note that the approach for resection and clinical description of the lesion is particularly important for these tumors. The term plexiform is applied to intraneural neurofibromas. These initial definitions will be applied to prospective validation studies across dermatopathologists and neuropathologists to formalize the pathologic definitions of cNF.

Discussion

cNF are common and a major clinical burden for people with NF1, prominently affecting QoL and emotional well-being as well as physical comfort. Currently, the only way of treating cNF is removal by procedural methods such as electrodessication, CO_2 laser, or surgery.[46] Developing effective medical therapies for existing cNF and prevention of cNF are priorities for the majority of adults with NF1. Development of a reliable and widely accepted nosology based on clinical, genetic, and radiologic features of cNF is a crucial step in investigating these tumors to better understand their development and start to uncover opportunities for tumor-specific therapies that will allow reduction in the clinical symptoms and burdens of cNF for people with NF1. The work presented here creates a framework for prospective validation studies to more accurately define cNF. Ultimately, this will facilitate score diagnosis of these lesions and the efficient development of therapeutics.

Author contributions

N. Ortonne: drafting the manuscript, development of recommendations. P. Wolkenstein: drafting the manuscript, development of recommendations. J. Blakeley: drafting the manuscript, development of recommendations. B. Korf: review of manuscript, development of recommendations. S. Plotkin: review of manuscript, development of recommendations. V.M. Riccardi: drafting and review of manuscript, development of recommendations. D.C. Miller: review of manuscript, development of recommendations. S. Huson: review of manuscript, development of recommendations. J. Peltonen: review of manuscript, development of recommendations. A. Rosenberg: review of manuscript, development of recommendations. S. Carroll: review of manuscript, development of recommendations. S. Verma: drafting and review of manuscript, development of recommendations. V. Mautner: review of manuscript, development of recommendations. M. Upadhyaya: review of manuscript, development of recommendations. A. Stemmer-Rachamimov: drafting and review of manuscript, development of recommendations.

Study funding

This publication was supported by an agreement from The Johns Hopkins University School of Medicine and the Neurofibromatosis Therapeutic Acceleration Program (NTAP). Its contents are solely the responsibilities of the authors and do not necessarily represent the official views of The Johns Hopkins University School of Medicine.

Disclosure

N. Ortonne reports no disclosures relevant to the manuscript. P. Wolkenstein receives fees from Pierre Fabre Dermatologie. J. Blakeley reports no disclosures relevant to the manuscript. B. Korf reports consulting fees from Novartis. S. Plotkin reports ownership in NFlection and consulting fees from Novartis. V. Riccardi, D. Miller, S. Huson, J. Peltonen, A. Rosenberg, S. Carroll, S. Verma, V. Mautner, M. Upadhyaya, and A. Stemmer-Rachamimov report no disclosures relevant to the manuscript. Go to Neurology.org/N for full disclosures.

Received November 1, 2017. Accepted in final form April 16, 2018.

References

1. Duong TA, Bastuji-Garin S, Valeyrie-Allanore L, Sbidian E, Ferkal S, Wolkenstein P. Evolving pattern with age of cutaneous signs in neurofibromatosis type 1: a cross-sectional study of 728 patients. Dermatology 2011;222:269–273.
2. Jo VY, Fletcher CD. WHO classification of soft tissue tumours: an update based on the 2013 (4th) edition. Pathology 2014;46:95–104.
3. Jouhilahti EM, Peltonen S, Callens T, et al. The development of cutaneous neurofibromas. Am J Pathol 2011;178:500–505.
4. Bicudo NP, de Menezes Neto BF, da Silva de Avo LR, Germano CM, Melo DG. Quality of life in adults with neurofibromatosis 1 in Brazil. J Genet Couns 2016;25:1063–1074.
5. Ferner RE, Thomas M, Mercer G, et al. Evaluation of quality of life in adults with neurofibromatosis 1 (NF1) using the impact of NF1 on quality of life (INF1-QOL) questionnaire. Health Qual Life Outcomes 2017;15:34.
6. Graf A, Landolt MA, Mori AC, Boltshauser E. Quality of life and psychological adjustment in children and adolescents with neurofibromatosis type 1. J Pediatr 2006;149:348–353.
7. Granstrom S, Langenbruch A, Augustin M, Mautner VF. Psychological burden in adult neurofibromatosis type 1 patients: impact of disease visibility on body image. Dermatology 2012;224:160–167.
8. Kodra Y, Giustini S, Divona L, et al. Health-related quality of life in patients with neurofibromatosis type 1: a survey of 129 Italian patients. Dermatology 2009;218:215–220.
9. Page PZ, Page GP, Ecosse E, Korf BR, Leplege A, Wolkenstein P. Impact of neurofibromatosis 1 on quality of life: a cross-sectional study of 176 American cases. Am J Med Genet A 2006;140:1893–1898.
10. Vranceanu AM, Merker VL, Park E, Plotkin SR. Quality of life among adult patients with neurofibromatosis 1, neurofibromatosis 2 and schwannomatosis: a systematic review of the literature. J Neurooncol 2013;114:257–262.
11. Wolkenstein P, Zeller J, Revuz J, Ecosse E, Leplege A. Quality-of-life impairment in neurofibromatosis type 1: a cross-sectional study of 128 cases. Arch Dermatol 2001;137:1421–1425.
12. Wolkenstein P, Zeller J, Revuz J, Ecosse E, Leplege A. Visibility of neurofibromatosis 1 and psychiatric morbidity. Arch Dermatol 2003;139:103–104.
13. Carroll SL, Ratner N. How does the Schwann cell lineage form tumors in NF1? Glia 2008;56:1590–1605.
14. Rosenberg AE. WHO classification of soft tissue and bone, fourth edition: summary and commentary. Curr Opin Oncol 2013;25:571–573.
15. Huson SM. Neurofibromatosis 1: a clinical and genetic overview. In: Huson SM, Hughes RAC, editors. The Neurofibromatoses: A Pathogenic and Clinical Overview. London: Chapman & Hall Medical; 1994:167–168.
16. Friedman JM, Riccardi VM. An overview of NF-1: dysplasia and neoplasia. In: Gutmann DH, MacCollin M, Riccardi VM, editors. Neurofibromatosis: Phenotype, Natural History, and PathogenesisBaltimoreJohn Hopkins University Press; 1999.
17. Beert E, Brems H, Daniels B, et al. Atypical neurofibromas in neurofibromatosis type 1 are premalignant tumors. Genes Chromosomes Cancer 2011;50:1021–1032.
18. Leppig KA, Kaplan P, Viskochil D, Weaver M, Ortenberg J, Stephens K. Familial neurofibromatosis 1 microdeletions: cosegregation with distinct facial phenotype and early onset of cutaneous neurofibromata. Am J Med Genet 1997;73:197–204.
19. Pinna V, Lanari V, Daniele P, et al. p.Arg1809Cys substitution in neurofibromin is associated with a distinctive NF1 phenotype without neurofibromas. Eur J Hum Genet 2015;23:1068–1071.
20. Quintans B, Pardo J, Campos B, et al. Neurofibromatosis without neurofibromas: confirmation of a genotype-phenotype correlation and implications for genetic testing. Case Rep Neurol 2011;3:86–90.
21. Santoro C, Maietta A, Giugliano T, et al. Arg(1809) substitution in neurofibromin: further evidence of a genotype-phenotype correlation in neurofibromatosis type 1. Eur J Hum Genet 2015;23:1460–1461.
22. Upadhyaya M, Huson SM, Davies M, et al. An absence of cutaneous neurofibromas associated with a 3-bp inframe deletion in exon 17 of the NF1 gene (c.2970-2972 delAAT): evidence of a clinically significant NF1 genotype-phenotype correlation. Am J Hum Genet 2007;80:140–151.
23. Brosseau JP, Pichard DC, Legius EH. The biology of cutaneous neurofibromas: consensus recommendations for setting research priorities. Neurology 2018;91:S14–S20.
24. Sbidian E, Duong TA, Valeyrie-Allanore L, Wolkenstein P. Neurofibromatosis type 1: neurofibromas and sex. Br J Dermatol 2016;174:402–404.
25. Dugoff L, Sujansky E. Neurofibromatosis type 1 and pregnancy. Am J Med Genet 1996;66:7–10.
26. Roth TM, Petty EM, Barald KF. The role of steroid hormones in the NF1 phenotype: focus on pregnancy. Am J Med Genet A 2008;146A:1624–1633.
27. Lammert M, Friedman JM, Roth HJ, et al. Vitamin D deficiency associated with number of neurofibromas in neurofibromatosis 1. J Med Genet 2006;43:810–813.
28. Riccardi VM. An overview of NF-1: dysplasia and neoplasia. In: Riccardi VMNeurofibromatosis: Phenotype, Natural History, and Pathogenesis. Baltimore: The Johns Hopkins University Press; 1992:28–33.
29. Cannon A, Jarnagin K, Korf B. Clinical trial design for cutaneous neurofibromas. Neurology 2018;91:S31–S37.
30. Brenaut E, Nizery-Guermeur C, Audebert-Bellanger S, et al. Clinical characteristics of pruritus in neurofibromatosis 1. Acta Derm Venereol 2016;96:398–399.
31. Riccardi VM. Pathophysiology of neurofibromatosis: IV: dermatologic insights into heterogeneity and pathogenesis. J Am Acad Dermatol 1980;3:157–166.
32. Riccardi VM. Cutaneous manifestation of neurofibromatosis: cellular interaction, pigmentation, and mast cells. Birth Defects Orig Artic Ser 1981;17:129–145.
33. Kamide R, Nomura N, Niimura M. Characterization of mast cells residing in cutaneous neurofibromas. Dermatologica 1989;179(suppl 1):124.
34. Carr NJ, Warren AY. Mast cell numbers in melanocytic naevi and cutaneous neurofibromas. J Clin Pathol 1993;46:86–87.
35. Staser K, Yang FC, Clapp DW. Mast cells and the neurofibroma microenvironment. Blood 2010;116:157–164.
36. Korf BR, Rubenstein AE. Neurofibromatosis: a handbook for patients, families, and health care professionals. Am J Hum Genet 2005;77:681.
37. Brenaut E, Marcorelles P, Genestet S, Menard D, Misery L. Pruritus: an underrecognized symptom of small-fiber neuropathies. J Am Acad Dermatol 2015;72:328–332.
38. Krab LC, Oostenbrink R, de Goede-Bolder A, Aarsen FK, Elgersma Y, Moll HA. Health-related quality of life in children with neurofibromatosis type 1: contribution of demographic factors, disease-related factors, and behavior. J Pediatr 2009;154:420–425.e1.
39. Le LQ, Shipman T, Burns DK, Parada LF. Cell of origin and microenvironment contribution for NF1-associated dermal neurofibromas. Cell Stem Cell 2009;4:453–463.
40. Val-Bernal JF, Gonzalez-Vela MC. Cutaneous lipomatous neurofibroma: characterization and frequency. J Cutan Pathol 2005;32:274–279.
41. Brasfield RD, Das Gupta TK. Von Recklinghausen's disease: a clinicopathological study. Ann Surg 1972;175:86–104.
42. Khalifa MA, Montgomery EA, Ismiil N, Azumi N. What are the CD34+ cells in benign peripheral nerve sheath tumors? Double immunostaining study of CD34 and S-100 protein. Am J Clin Pathol 2000;114:123–126.
43. Fetsch JF, Michal M, Miettinen M. Pigmented (melanotic) neurofibroma: a clinicopathologic and immunohistochemical analysis of 19 lesions from 17 patients. Am J Surg Pathol 2000;24:331–343.
44. Goldblum JR, Folpe AL, Weiss SW, Enzinger FM, Weiss SW. Enzinger and Weiss's Soft Tissue Tumors. Philadelphia: Saunders; 2013.
45. Chen Z, Liu C, Patel AJ, Liao CP, Wang Y, Le LQ. Cells of origin in the embryonic nerve roots for NF1-associated plexiform neurofibroma. Cancer Cell 2014;26:695–706.
46. Verma S, Riccardi VM, Plotkin SR. Considerations for development of therapies for cutaneous neurofibroma. Neurology 2018;91:S21–S30.

Neurology®

Cutaneous neurofibromas: Current clinical and pathologic issues

Nicolas Ortonne, Pierre Wolkenstein, Jaishri O. Blakeley, et al.

Neurology 2018;91;S5-S13
DOI 10.1212/WNL.0000000000005792

This information is current as of July 9, 2018

Updated Information & Services	including high resolution figures, can be found at: http://n.neurology.org/content/91/2_Supplement_1/S5.full
References	This article cites 42 articles, 3 of which you can access for free at: http://n.neurology.org/content/91/2_Supplement_1/S5.full#ref-list-1
Subspecialty Collections	This article, along with others on similar topics, appears in the following collection(s): **Nerve tumor** http://n.neurology.org/cgi/collection/nerve_tumor **Neurofibromatosis** http://n.neurology.org/cgi/collection/neurofibromatosis
Permissions & Licensing	Information about reproducing this article in parts (figures,tables) or in its entirety can be found online at: http://www.neurology.org/about/about_the_journal#permissions
Reprints	Information about ordering reprints can be found online: http://n.neurology.org/subscribers/advertise

Neurology ® is the official journal of the American Academy of Neurology. Published continuously since 1951, it is now a weekly with 48 issues per year. Copyright © 2018 The Author(s). Published by Wolters Kluwer Health, Inc. on behalf of the American Academy of Neurology.. All rights reserved. Print ISSN: 0028-3878. Online ISSN: 1526-632X.

AMERICAN ACADEMY OF NEUROLOGY®

SCIENTIFIC REPORTS

OPEN

Usp9X Regulates Cell Death in Malignant Peripheral Nerve Sheath Tumors

Received: 26 March 2018
Accepted: 9 November 2018
Published online: 26 November 2018

E. Bianchetti[1], S. J. Bates[1], S. L. Carroll[2], M. D. Siegelin[1] & K. A. Roth[1]

Malignant peripheral nerve sheath tumors (MPNSTs) are the leading cause of death in neurofibromatosis type 1 (NF1) patients. Current treatment modalities have been largely unsuccessful in improving MPNST patient survival, making the identification of new therapeutic targets urgent. In this study, we found that interference with Usp9X, a deubiquitinating enzyme which is overexpressed in nervous system tumors, or Mcl-1, an anti-apoptotic member of the Bcl-2 family whose degradation is regulated by Usp9X, causes rapid death in human MPNST cell lines. Although both Usp9X and Mcl-1 knockdown elicited some features of apoptosis, broad spectrum caspase inhibition was ineffective in preventing knockdown-induced MPNST cell death suggesting that caspase-independent death pathways were also activated. Ultrastructural examination of MPNST cells following either Usp9X interference or pharmacological inhibition showed extensive cytoplasmic vacuolization and swelling of endoplasmic reticulum (ER) and mitochondria most consistent with paraptotic cell death. Finally, the Usp9X pharmacological inhibitor WP1130 significantly reduced human MPNST growth and induced tumor cell death in an *in vivo* xenograft model. In total, these findings indicate that Usp9X and Mcl-1 play significant roles in maintaining human MPNST cell viability and that pharmacological inhibition of Usp9X deubiquitinase activity could be a therapeutic target for MPNST treatment.

Neurofibromatosis type 1 (NF1) is a genetic neurocutaneous disease with an incidence of 1:3000[1,2] characterized by a predisposition to multiple peripheral nerve sheath tumors[3]. The vast majority of NF1-associated nerve sheath tumors are benign, but malignant peripheral nerve sheath tumors (MPNSTs) are the leading cause of death in NF1 patients. MPNSTs are aggressive Schwann cell-derived soft tissue sarcomas and occur in 5 to 10% of patients with NF1[4]. Approximately half of MPNSTs are associated with NF1 and often arise from benign plexiform neurofibromas[5]. Currently, standard MPNST therapy is tumor resection with wide surgical margins, but patient prognosis is poor due to variables such as tumor size, anatomic location, propensity to metastasis and limited tumor cell sensitivity to chemotherapy and radiation[1]. Therefore, identification of new therapeutic targets to treat this aggressive neoplasm is a high clinical priority.

Usp9X is a deubiquitinating enzyme which is overexpressed in various human cancers, including nervous system tumors, such as glioblastoma (GBM)[6]. Genetic and/or pharmacological inhibition of Usp9X activity has been shown to induce tumor cell death in both *in vitro* and *in vivo* models of GBM[6–8]. Previous studies have demonstrated that down-regulation of Usp9X is followed by enhanced degradation of the anti-apoptotic Bcl-2 family member, myeloid cell leukemia 1 (Mcl-1)[7,9]. Furthermore, Mcl-1 down-regulation is known to be an important determinant of apoptosis in sarcomas[10]. Our findings suggest that Usp9X and Mcl-1 are novel targets for the treatment of MPNSTs and that paraptosis, a caspase-independent type of regulated cell death, may play a role in MPNST cell death induced by Usp9X inhibition.

[1]Department of Pathology & Cell Biology, Columbia University Vagelos College of Physicians and Surgeons, New York, USA. [2]Medical University of South Carolina, Department of Pathology and Laboratory Medicine, Charleston, South Carolina, USA. Correspondence and requests for materials should be addressed to E.B. (email: eb2985@cumc.columbia.edu)

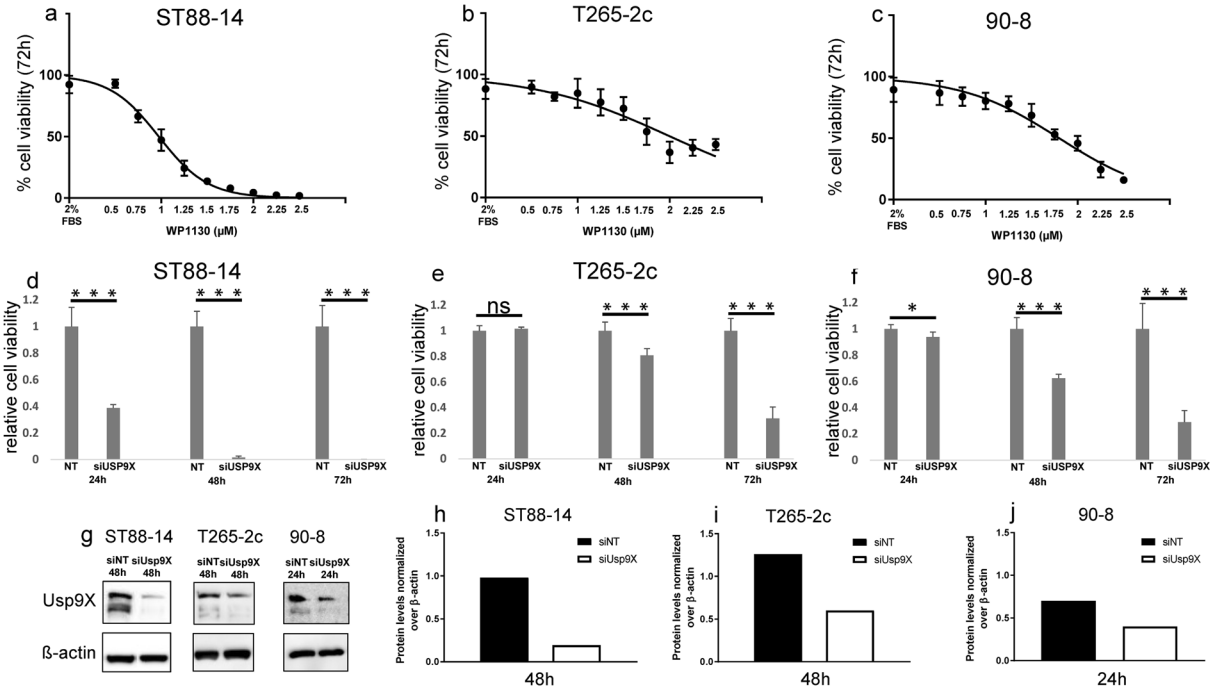


Figure 1. Usp9X inhibition causes massive reduction in cellular viability in MPNST cell lines. (**a–c**) ST88-14 (**a**), T265-2c (**b**), 90-8 cells (**c**) were treated with increasing concentrations of WP1130 for 72 h. Cellular viability was determined by CellTiter-Glo assay and the IC_{50}-values were calculated based on a non-linear regression analysis. Data are presented as mean and SD, n = 3. (**d–f**) Usp9X was silenced in ST88-14 (**d**), T265-2c (**e**), 90-8 cells (**f**) with non-targeting (NT) RNA or siUsp9X for 24, 48 and 72 h. Cellular viability was determined by CellTiter-Glo assay and relative cell viability was calculated. Data are presented as mean and SD, n = 3. * = 0.0129 *** ≤ 0.001. (**g–j**) Usp9X knock down was performed in ST88-14, T265-2c and 90-8 cells. Whole-cell extracts were examined by Western blot for Usp9X. ß-actin Western blot analysis was performed to confirm equal protein loading. Bar graphs show protein quantification analyzed through ImageJ. Data are presented as mean and SD, n = 3.

Results

Usp9x is expressed in human MPNST cell lines. Usp9X expression in MPNSTs has not previously been reported. Thus to ensure potential human clinical relevance, we first examined Usp9X expression levels in a panel of human MPNST cell lines (Suppl. Figure 1a). All MPNST cells showed Usp9X protein expression, albeit at different levels. The results confirm that the Usp9X protein is expressed in MPNST cells, reinforcing the notion that Usp9X is a viable, potential therapeutic target for MPNST.

Usp9X inhibition causes massive reduction in MPNST cell viability. To investigate the potential role of Usp9X in regulating MPNST cell survival, we first examined the effects of inhibiting Usp9X enzymatic activity with the deubiquitinase inhibitor, WP1130, a pharmacological inhibitor of Usp9X known also as Degrasyn[6], on three NF1 patient-derived MPNST cell lines (ST88-14, T265-2c and 90-8). WP1130 caused a concentration-dependent decrease in cell viability after 72 h in all three cell lines, with ST88-14 cells being particularly sensitive (Fig. 1a,b,c). In these experiments, we used a concentration range between 0.5 and 2.5 μM, established from preliminary results (Suppl. Figure 1b,c). In addition to Usp9X, WP1130 inhibits the enzymatic activity of multiple deubiquitinases; thus, to more selectively determine the effects of Usp9X inhibition on MPNST cell survival *in vitro*, we silenced Usp9X gene using siRNA. Suppression of Usp9X was confirmed by immunoblotting (Fig. 1g–j). In all three cell lines, Usp9X gene silencing resulted in a significant reduction in viable cell numbers after 72 h (Fig. 1d–f). Consistent with the results obtained with pharmacological inhibition of Usp9X activity, ST88-14 cells were most strongly affected by Usp9X silencing, with a significant reduction in cell viability observed after just 24 h treatment (Fig. 1d). These data support the conclusion that Usp9X is critical for the survival of MPNST cells.

Usp9X inhibition depletes Mcl-1. Based on our previously published observation that Usp9X induces a decline of Mcl-1 protein levels in GBM cells[9,11], we hypothesized that similar effects would be observed in MPNST cells. To test this hypothesis, ST88-14 cells were treated with WP1130 at two different concentrations (Suppl. Figure 1e) and Mcl-1 levels were assessed by Western blot after 24 and 48 h. Usp9X interference decreased endogenous Mcl-1 protein levels at both concentrations after treatment for 48 h (Suppl. Figure 1e). Consistent with these results, Usp9X knock-down in ST88-14 cells resulted in decreased Mcl-1 levels at 48 h as well (Suppl. Figure 1d).

Usp9X knock-down causes MPNST cell death with variable caspase activation and features of apoptosis. To determine if Usp9X inhibition induced apoptosis of MPNST cells, we inhibited Usp9X pharmacologically with WP1130 and silenced it by siRNA, as well, in ST88-14 and T265-2c cell lines and examined various biochemical indicators of apoptosis. Usp9X pharmacological inhibition resulted in several features of apoptosis (Fig. 2a,b), including a time-dependent decrease in mitochondrial membrane potential (Fig. 2c,d), in both cell lines. Consistent with the viability data, ST88-14 cells were more rapidly and strongly affected by Usp9X inhibition, than T265-2c cells. As with pharmacological inhibition of Usp9X activity, Usp9X knock-down produced biochemical features of apoptotic cell death including a significant loss in mitochondrial membrane potential (Fig. 2a–d). ST88-14 cells consistently showed more dramatic effects after Usp9X interference, compared to T265-2c cells (Fig. 2a–d) and caspase 3-like enzymatic activity was more pronounced after Usp9X knock-down or WP1130 treatment in ST88-14 cells compared to T265-2c cells (Fig. 2e–g).

Interference with Mcl-1 produces cell death with apoptotic features in MPNST cell lines. Usp9X regulates cell survival through both Mcl-1-dependent and –independent processes. To determine if Mcl-1 is a regulator of MPNST survival, we examined the effects of Mcl-1 knockdown on the three MPNST cell lines. As with Usp9X pharmacological inhibition or knock-down, Mcl-1 knock-down resulted in significant cell death in all cell lines tested (Fig. 3a–g), most prominently in T265-2c and 90-8 cell lines (Fig. 3d–g). All three cell lines showed time-dependent apoptotic features with enhanced DNA fragmentation, annexin V staining (Fig. 3b,f), and loss in mitochondrial membrane potential (Fig. 3c,g) with maximal response at 72 h after transfection. T265-2c cells were more sensitive to Mcl-1 depletion (Fig. 3d,e), compared to ST88-14 cells (Fig. 3a), with strong features of apoptosis (Fig. 3f,g). Suppression of Mcl-1 was confirmed by immunoblotting (Fig. 3h,i). Consistent with these results, pharmacological inhibition of Mcl-1 with A-1210477[12], caused a concentration-dependent decrease in cellular viability after 72 h in all tested cell lines (Suppl. Figure 2). These data indicate that in addition to being sensitive to Usp9X inhibition, MPNST cell lines are also susceptible to Mcl-1 loss, which appears to activate apoptosis, most prominently in the T265-2c cell line.

Caspase-inhibition provides minimal protection from cell death after Usp9X or Mcl-1 depletion. To determine if caspase-dependent apoptosis is the main cell death pathway activated by Usp9X or Mcl-1 depletion, we tested the ability of ZVAD, a broad-spectrum caspase inhibitor, to inhibit Usp9X and Mcl-1 knock-down induced MPNST cell death. Despite producing a complete inhibition of caspase 3-like enzymatic activity (Fig. 4c), ZVAD failed to significantly attenuate cell death after Usp9X or Mcl-1knock-down at 72 h in ST88-14 (Fig. 4a) or T265-2c cells (Fig. 4b), indicating that other caspase-independent death pathways are likely activated in parallel with apoptosis following Usp9X or Mcl-1 inhibition.

Usp9X inhibition causes ER stress in MPNST cell lines. Interestingly, both Usp9X pharmacological inhibition and silencing in MPNST cells elicited a significant increase in ATF3, a typical marker of ER-stress (Fig. 5a,b) and in the pro-apoptotic BH3-only protein Noxa (Fig. 5a,b). The protein expression level of a second ER stress marker, ATF4, was similarly increased in ST88-14 cells after Usp9X disruption (data not shown). Given that ATF3 and ATF4 are downstream regulators of the ER-stress response[7] and are capable of activating Noxa[7], we hypothesized that cell death induced by Usp9X inhibition may in part be mediated through an ER stress response.

Ultrastructural examination of MPNST cells following Usp9X inhibition reveals evidence of paraptosis. We used transmission electron microscopy (TEM) to determine if there was ultrastructural evidence of ER stress in MPNST cells following Usp9X inhibition. T265-2c cells were treated with vehicle or 2.5 µM WP1130 for 24 h and processed for TEM. Vehicle treated cells showed intact organelles and normal ER structure (Fig. 5c–e). In contrast, WP1130 treated T265-2c cells exhibited significant morphological changes including reduced cell size and altered cell shape (Fig. 5f). In addition, following WP1130 treatment T265-2c cells exhibited numerous small and large clear cytoplasmic vacuoles (Fig. 5f). The typical ultrastructural features of apoptosis, e.g. chromatin condensation and margination and membrane blebbing were only rarely observed in treated cells (Fig. 5f–h). Striking changes in ER and mitochondrial ultrastructure previously described in paraptotic cell death[13,14] were seen following WP1130 treatment of T265-2c cells. Compared with vehicle treated cells, WP1130 exposed cells showed significant swelling and disruption of normal ER structure with dramatic expansion of the ER lumina (Fig. 5d and g). Similarly, in contrast with normal appearing mitochondria in vehicle treated cells, numerous mitochondria in the WP1130 treated cells were markedly enlarged, edematous, disorganized and fragmented (Fig. 5e and h). Taken together, these results suggest that WP1130 induces paraptosis[13] in T265-2c cells.

WP1130 inhibits MPNST tumor growth *in vivo*. To assess the potential efficacy of Usp9X inhibition in treating MPNSTs *in vivo*, we tested WP1130 in a heterotopic xenograft MPNST model. ST88-14 cells were implanted subcutaneously and animals were divided into three groups receiving either vehicle or two different concentrations of WP1130 (12.5 and 25 mg/kg intraperitoneally) (Fig. 6 and Suppl. Figure 3). In our initial *in vivo* experiment, treatment was initiated eight days after implantation and injections were given three times/week for four weeks (Fig. 6a–f). WP1130 at 25 mg/kg per dose produced a statistically significant growth reduction with partial regression of tumors compared to vehicle treated controls (Fig. 6a). The day after the last injection, tumors were resected and the tumor volume and weight measured. WP1130 produced a significant decrease in tumor volume at both concentrations (Fig. 6b) and a statistically significant decrease in tumor weight in the 25 mg/kg dose group (Fig. 6c and d). The regression of the tumors' size suggested that this treatment not only attenuated tumor growth but induced tumor cell death. Histopathological analysis of the resected tumors in the vehicle treated control group showed densely cellular, highly pleomorphic tumors with brisk mitotic activity (Fig. 6e). In contrast, mice treated with WP1130 showed tumors with reduced cellularity and mitotic activity, multi-focal necrotic areas and the presence of scattered apoptotic nuclei throughout the tumors at both concentrations

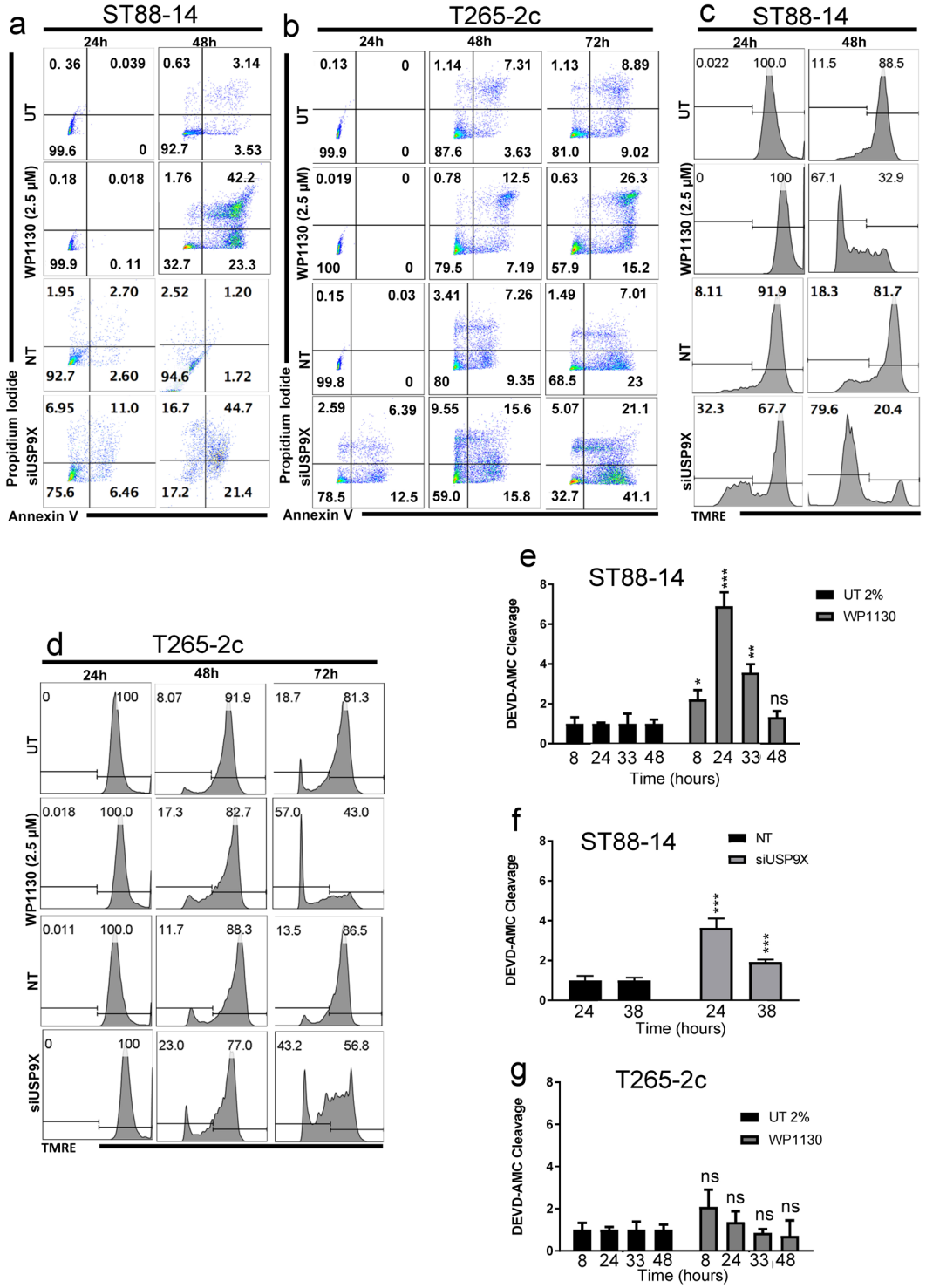


Figure 2. Usp9X inhibition induces cell death with features of apoptosis and loss of membrane potential in MPNST cell lines. (**a**–**d**) ST88-14 (**a**,**c**) and T265-2c cells (**b**,**d**) were treated with WP1130 at the concentration of 2.5 µM, or transfected either with non-targeting (NT)-siRNA or Usp9X-siRNA. (**a**,**b**) Staining for annexin V/Propidium Iodide was performed prior to flow cytometric analysis. Representative flow plots are shown. N = 3. (**c**,**d**) Cells were stained with Mitochondrial Membrane Potential Assay Kit (TMRE), then flow cytometric analysis was performed. N = 3. (**e**,**f**) ST88-14 cells were treated with WP1130 at the concentration of 2.5 µM (**e**) or transfected either with non-targeting (n.t.)-siRNA or Usp9X-siRNA (**f**), then caspase 3-like enzymatic activity was measured at different time points. Column: mean. Error bar: SD, n = 3. * = 0.0209 ** = 0.0026 *** ≤ 0.001. (**g**) T265-2c cells were treated with WP1130 at the concentration of 2.5 µM prior to caspase 3-like activity measurement at different time points.

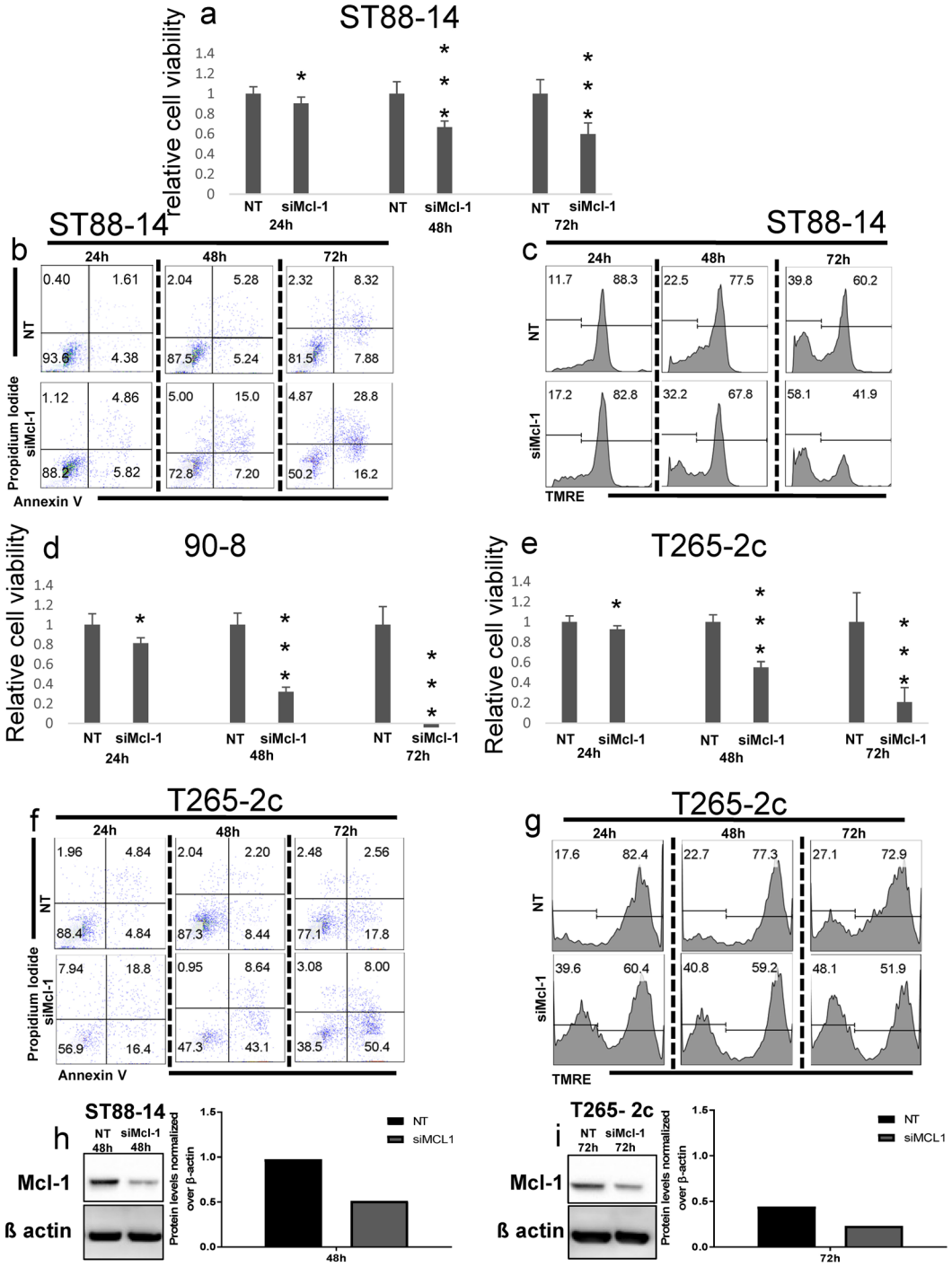


Figure 3. Mcl-1 knock-down causes massive reduction in cellular viability, cell death with features of apoptosis and loss of membrane potential in MPNST cell lines. (**a**,**d**,**e**) ST88-14 (**a**) 90-8 (d), T265-2c (**e**) cells were transfected either with non-targeting (NT)-siRNA or Mcl-1-siRNA for 24, 48 and 72 h. Cellular viability was determined by CellTiter-Glo assay and relative cell viability was calculated. Data are presented as mean and SD, n = 3. *(**a**) = 0.0161, *(**d**) = 0.0015, *(**e**) = 0.0168, *** ≤ 0.001 (**b**,**f**) Staining for annexin V/Propidium Iodide was performed prior to flow cytometric analysis. Representative flow plots are shown. N = 3. (**c**,**g**) Staining for Mitochondrial Membrane Potential Assay Kit (TMRE) was performed prior to flow cytometric analysis. Representative flow plots are shown. N = 3. (**h**,**i**) Knock down of Mcl-1 was confirmed in ST88-14 cells (**h**) and T265-2c cells (**i**) by Western blot analysis. ß-actin was used to ensure equal loading.

(Fig. 6f). WP1130 inhibition of Usp9X leads to the inhibition of Usp9X function and thus, an expected decrease in the levels of Usp9X substrates[15]. To verify the *in vivo* effectiveness of WP1130 treatment, we tested the protein levels of Mcl-1 in xenografts from vehicle and WP1130 treated mice and found a significant reduction in Mcl-1

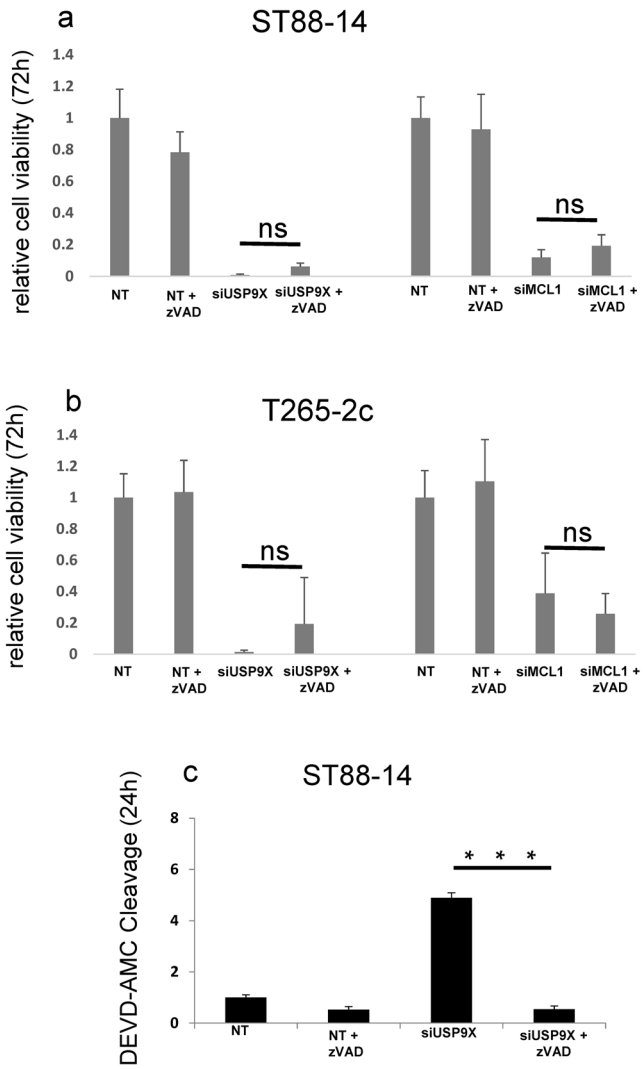


Figure 4. Caspase-dependent apoptosis is not the exclusive MPNST cell death pathway activated after Usp9X and Mcl-1 knock down *in vitro*. (**a**,**b**) ST88-14 (**a**) and T265-2c (**b**) cells were transfected with non-targeting (NT)-siRNA with or without z-VAD as controls, or Usp9X-siRNA, or Mcl-1-siRNA for 72 h. Cellular viability was determined by CellTiter-Glo assay and relative cell viability was calculated. Data are presented as mean and SD, n = 3. (**c**) Caspase-3 like activity was measured at 24 h after treatments in ST88-14 cell line. Data are presented as mean and SD, n = 3.

levels *in vivo* (Fig. 6g). To extend these findings, we performed a second *in vivo* experiment in which we allowed the tumors to grow to a significant size before initiating WP1130 therapy to better model the human situation. Therefore, we implanted ST88-14 cells and waited one month before initiating daily injections of WP1130 for five days per week for two weeks (Suppl. Figure 3). WP1130 treatment resulted in a significant attenuation in tumor growth when compared to the vehicle treated group (Suppl. Figure 3a). Histopathological analysis of the resected tumors showed features similar to those observed in the initial *in vivo* study. WP1130 reduced cellularity and induced cell death, with multiple areas of necrosis and presence of frequent apoptotic nuclei, at both concentrations (Suppl. Figure 3c), compared to the control group (Suppl. Figure 3b). WP1130 treatment also resulted in a marked increase in cleaved caspase 3 immunoreactivity and TUNEL labeling compared to tumors of the vehicle group (Suppl. Figure 4a–d). To preliminarily assess potential *in vivo* toxic effects of WP1130, we performed body weight measurements on vehicle and WP1130 treated animals throughout the experiment and found no differences between the three groups (data not shown) suggesting that WP1130 does not have obvious toxic effects. These results are consistent with several previous *in vivo* studies of WP1130[6,16,17].

Discussion

The goal of this study was to determine if Usp9X and/or Mcl-1 play(s) a role in MPNST cell survival and thus, serve as potential therapeutic targets for MPNST treatment. Usp9X is a deubiquitinating enzyme[18] that plays a role in regulating protein degradation by modulation of ubiquitin conjugation to its targets and thereby controlling their proteasomal turnover[19]. It is well established that Usp9X plays a pivotal role in various malignant

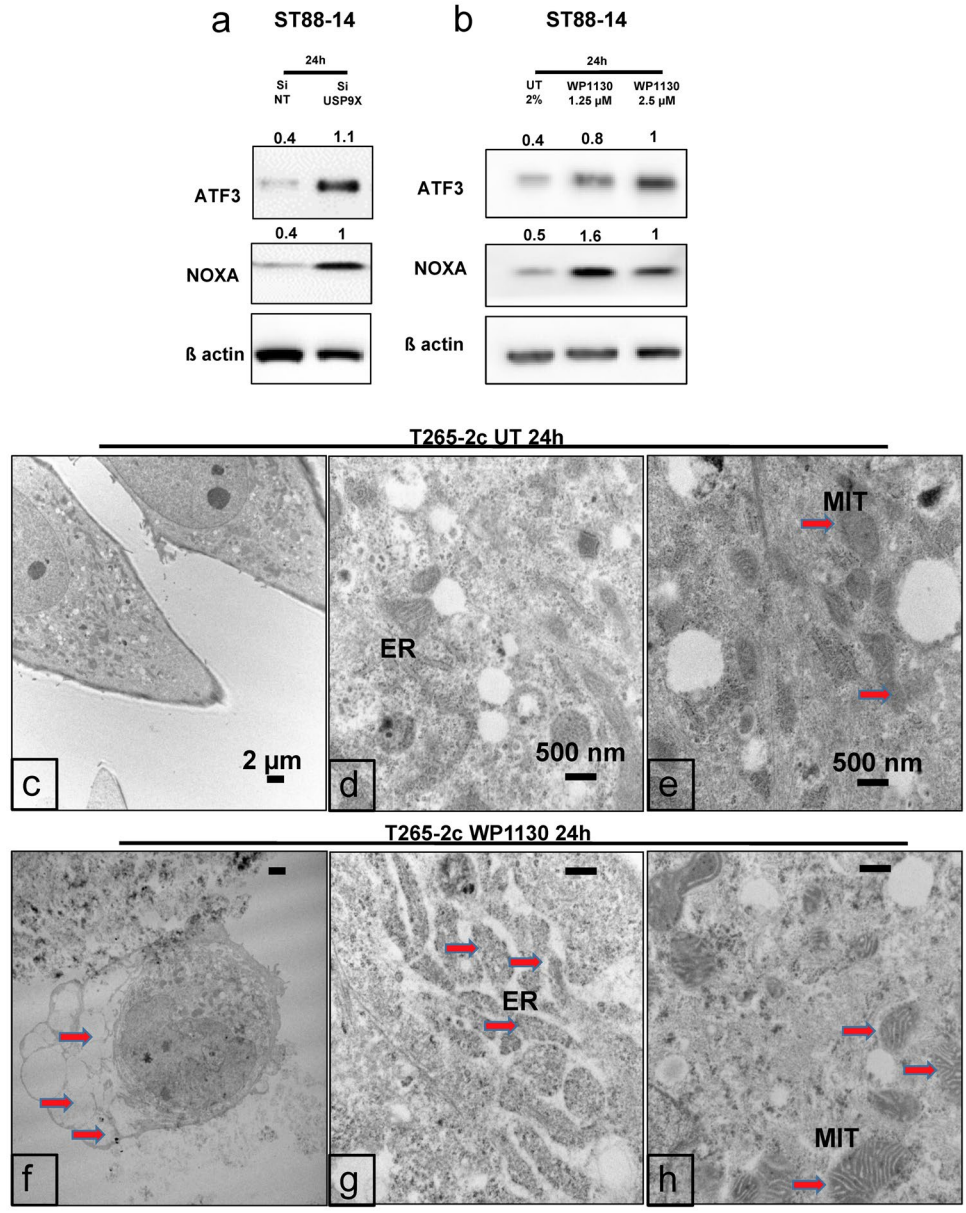


Figure 5. Usp9X inhibition causes Noxa increase and ER stress in MPNST cell lines. Ultrastructural analysis shows features of paraptosis. (**a**,**b**) ST88-14 cells were transfected for 24 h with either non-targeting (NT)-siRNA or Usp9X-siRNA (**a**) or treated with WP1130 at the concentration of 1.25 and 2.5 µM (**b**). Whole cell extracts were collected prior to Western blot analysis for ATF3, Noxa and ß-actin. Numbers shows protein quantification analyzed through ImageJ. N = 3. (**c**–**e**) Ultrastructural appearance of untreated control cells using TEM. (**f**–**h**) After treatment with WP1130 at the concentration of 2.5 µM (**f**,**g**,**h**) T265-2c cells showed extensive cytosolic vacuolization (f, red arrows) and swelling of ER (g, red arrowheads) and mitochondria (h, red arrows).

tumors affecting the nervous system, including GBM[6,11,20]. Mechanistically, Usp9X exerts its effects on cell survival at least in part by controlling the levels of anti-apoptotic Bcl-2 family members, including Mcl-1, or inhibitor of apoptosis proteins, such as XIAP[8]. Interference with Usp9X results in degradation of these survival promoting proteins[8,19]. Studies related to other malignancies, such as pancreatic cancer, demonstrated that Usp9X is necessary to drive tumor growth by inhibition of cell death[21]. However, it should be noted that the effects of Usp9X on tumors are likely to be context dependent since at least one study, involving a transgenic mouse model of pancreatic cancer, suggested that Usp9X played a tumor suppressive role[22]. Such observations do not void Usp9X as a cancer therapeutic target, but they remind us that some proteins have tumor type-specific biological roles that must be determined experimentally before advancing to human trials for any given cancer type. There might also be "context" dependent and functional differences between tumor initiation and the propagation of established malignancies. This is the first study that we are aware of examining the potential role of Usp9X in MPNST survival. Given that anti-apoptotic Bcl-2 family members are important cell death mediators in the context of

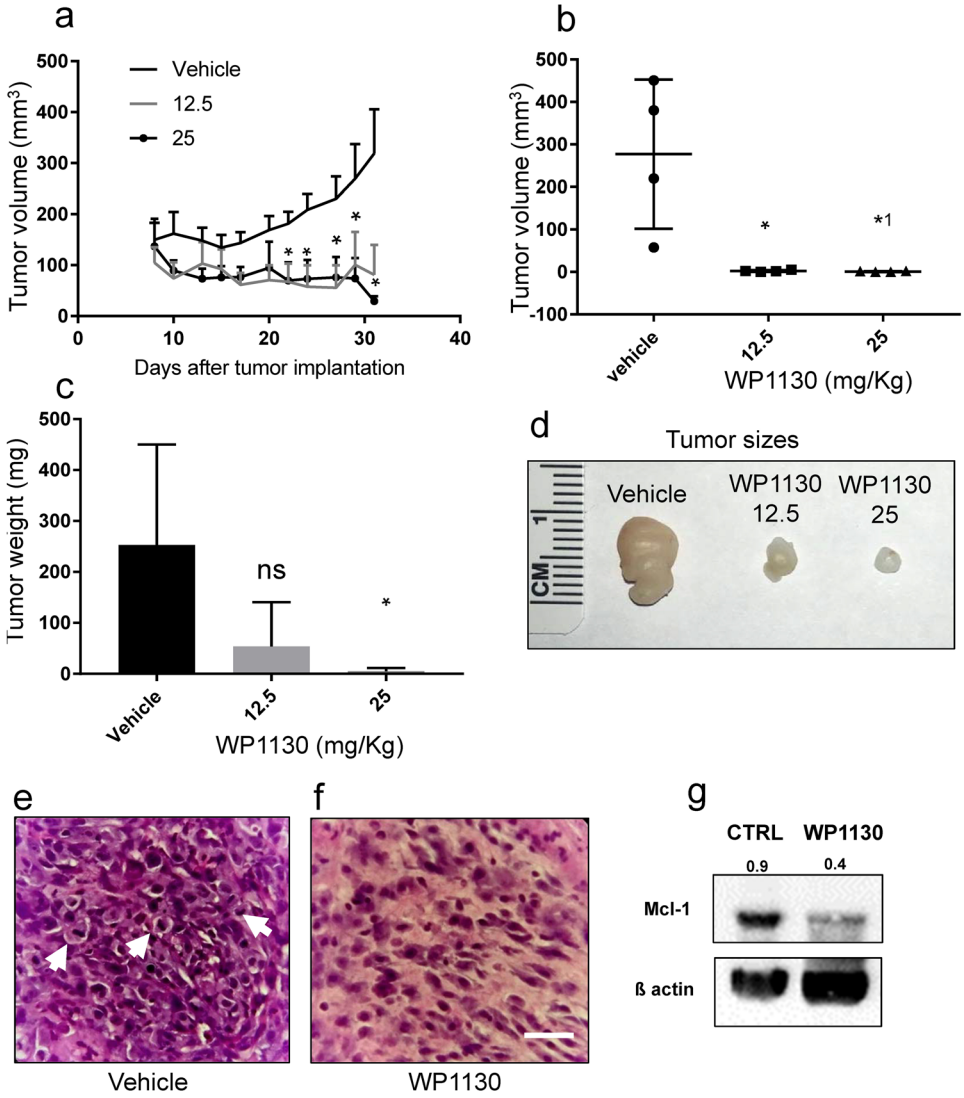


Figure 6. Treatment with WP1130 reduces tumor size in a mouse MPNST model generated by subcutaneous injection of ST88-14 cell line. (**a**) Tumor growth curves showing the increase in tumor size for each treatment group. Data are presented as mean and SEM. Asterisks shown only for 25 mg/Kg dose, compared to control group. Asterisks values, from left to right: 0.0413, 0.0321, 0.0409, 0.0479 and 0.0162. (**b**) Quantification of the tumors volume among different treatment groups 35 days after tumor implantation. * = 0.0202, *1 = 0.0198. (**c**) Quantification of the tumors weight among different treatment groups 35 days after tumor implantation. * = 0.0458. (**d**) Representative photographs of the tumors. (**e**,**f**) Representative photomicrographs showing the histological morphology (H & E staining) of tumors from mice receiving either vehicle or WP1130 at the concentration of 12.5 mg/kg. Arrows indicate mitotic figures. Scale bar, 50 µm. (**g**) Whole tissue extracts from vehicle and 25 mg/kg WP1130 treated mice were collected prior to Western blot analysis for Mcl-1 and ß-actin served as loading control. Numbers shows protein quantification analyzed through ImageJ. N = 3.

MPNST and that Mcl-1 is a central regulator of apoptosis in sarcomas[10], a pivotal role of Usp9X as a potential therapeutic target in MPNSTs appears likely.

The current study offers evidence to support the hypothesis that targeting Usp9X might significantly impact MPNST viability. In our report, by both pharmacological and genetic targeting of Usp9X *in vitro*, we detected not only inhibition of cell growth, but also massive cell death. WP1130 inhibits Usp9X deubiquitinase activity as well as that of several other deubiquitinases such as Usp5, Usp14, and UCH37[23]. First, we showed that WP1130, in a concentration- and time-dependent manner, decreases the viability of three different human NF1 patient-derived MPNST cell lines, ST88-14, T265-2c and 90-8. To determine the specific role of Usp9X in MPNST cell survival, we silenced Usp9X by siRNA. The selective knock-down of Usp9X caused a significant reduction in cell viability in all three MPNST cell lines tested. Both pharmacological inhibition and Usp9X knock down, caused time-dependent MPNST cell death with some features of apoptosis, including loss in mitochondrial membrane potential. However, the extent of caspase-3 enzymatic activity varied between cell lines being most robust in ST88-14 cells with minimal caspase activation observed in T265-2c cells. Thus, the extent of caspase-3 enzymatic

activity after WP1130 in our cell lines seems to be dependent on cell-specific factors that remain to be determined. Interestingly, treatment of MPNST cell lines with a broad caspase inhibitor failed to significantly attenuate cell death after Usp9X knock-down suggesting that caspase-independent death pathways are also activated. In all MPNST cell lines tested, but most prominently in the T265-2c cell line, Mcl-1 knock-down-induced death displayed features of apoptosis such as increased annexin V staining and decreased mitochondrial membrane potential but, as in Usp9X knock-down cells, broad caspase inhibition did not protect MPNST cells from Mcl-1 knock-down-induced death. We also tested a novel small-molecule inhibitor of Mcl-1, A1210477, since these compounds are currently in preparation for human clinical application, and our results suggest that this compound exerts anti-proliferative activity against MPNST cells. From these data, we conclude that Usp9X and Mcl-1 are central cell death regulators in MPNSTs and that although caspases may be activated following their inhibition, caspase-independent pathways contribute significantly to the MPNST cell death promoting effects of Usp9X and Mcl-1 inhibition *in vitro*.

The mechanism by which Usp9X interference induced massive reduction of viability in MPNST cell lines appears to be multiple. Biochemical analysis showed that Usp9X inhibition caused an ER stress response with an increase of ATF3 and ATF4, two markers of ER stress, followed by an increase in pro-apoptotic Noxa and a subsequent decrease in Mcl-1 protein levels. Similar to our *in vitro* observations, ST88-14 xenografts following treatment with WP1130 showed a significant reduction in Mcl-1 protein levels *in vivo*.

According to previous publications[24], upon ER stress, the ER lumen is remarkably enlarged in cells, which can be detected by electron microscopic examination. Ultrastructural examination of MPNST cells following WP1130 treatment showed features of ER stress and paraptosis, a type of caspase-independent cell death associated with ER damage. These results suggest for the first time a relation between Usp9X and ER stress in the context of MPNST. In addition, we noted an increase in pro-apoptotic Noxa, which is known to be regulated by ATF3 and ATF4[25,26] and which preceded the down-regulation of Mcl-1[7]. Although a relationship between Noxa induction and Usp9X inhibition has not been described before in MPNST cells, these results suggest that Noxa might be implicated in the death produced by Usp9X inhibition. As explained above, we found a decline in Mcl-1 levels upon Usp9X inhibition, which is in keeping with earlier findings in other model systems[7,18,27,28]. However, our study demonstrated that Noxa up-regulation precedes Mcl-1 down-regulation, suggesting that the Noxa increase is proximal of Mcl-1 with respect to cell death induction. Given that Noxa is an inhibitor of Mcl-1 and has been known to stimulate Mcl-1 mediated proteasomal degradation, Usp9X inhibition might in part lead to a reduction of Mcl-1 levels through Noxa mediated destabilization of Mcl-1. However, taking this speculation aside, at the minimum, increased Noxa levels will facilitate release of BAK and BIM from Mcl-1, thereby driving BAX/BAK mediated intrinsic apoptosis.

In seeking to identify others forms of cell death produced by Usp9X inhibition in MPNST cells, TEM analysis showed morphological features of paraptosis with extensive cytoplasmic vacuolization, swelling of ER and mitochondria and only minimal features of apoptosis[13,14]. To the best of our knowledge, presence of paraptosis has never been described before in relation to MPNSTs or in the context of Usp9X inhibition.

To determine if Usp9X inhibition has therapeutic potential *in vivo*, we tested WP1130 in a heterotopic MPNST xenograft model. WP1130 treatment resulted in a statistically significant growth reduction and partial regression of tumors. These results suggest that WP1130 might be useful for MPNST treatment. Our findings are in keeping with the results of others that have observed anti-cancer effects of WP1130 in various xenograft model systems[6,16,17]. While we found single agent efficacy with Usp9X and Mcl-1 inhibitors in MPSNT model systems, it is tempting to speculate as to whether these effects may be further enhanced by drug combination therapies. The literature suggests that in other tumor entities, including GBM, the efficacy of Mcl-1 inhibitors is dramatically increased in the presence of other drug compounds[11,29]. Similar results have been found with regards to Usp9X inhibition[15]. For instance, Bcl-2/Bcl-xL- inhibition coupled with the inhibitor WP1130 showed synergistic anti-cancer effects in several preclinical model systems[18,30]. In conclusion, our study demonstrates that MPNST cell lines are susceptible to both Usp9X and Mcl-1 loss which appears to activate both apoptotic and caspase-independent death pathways, such as paraptosis.

Materials and Methods

Ethics statement. All procedures were in accordance with Animal Welfare Regulations and approved by the Institutional Animal Care and Use Committee at the Columbia University Irving Medical Center. The study was reviewed and approved by the institutional review board at the Columbia University Irving Medical Center.

Reagents. Primary antibodies were obtained from the following sources: Usp9X (Cell Signaling, Danvers, MA #5751), Mcl-1 (Cell Signaling, Danvers, MA #5453), Noxa (Calbiochem, San Diego, CA #OP180), ATF4 (Cell Signaling, Danvers, MA #11815), ATF3 (Novus Biologicals, Littleton, CO #NBP1-85816), β-actin (Sigma, St. Louis, MO #A5316). Secondary antibodies were HRP-conjugated goat anti-rabbit (Thermo Scientific, Waltham, MA #31460) and goat anti-mouse (Thermo Scientific, Waltham, MA #31430). Degrasyn [WP1130] was obtained from Selleckchem (Houston, TX #S2243). A-1210477 was purchased from APExBIO (Houston, TX #B6011). Tunicamycin [TUN] and Staurosporine [STS] were purchased from Sigma (St. Louis, MO; TUN #T7765, STS #S5921).

Cell culture. The human NF1-associated MPNST lines used in this study are: T265-2c cells, ST88-14 cells and 90-8 cells, obtained and maintained as described[31,32]. Morphology and doubling times of cells were routinely assessed, according to the guidelines contained in the ATCC Technical Bulletin 8. The identity of cells was verified by short tandem repeat analyses. The short tandem repeat profile of each sporadic MPNST cell line was determined by examining 15 markers standardly used by the American Type Culture Collection and the amelogenin locus (included to verify the sex of the patient from which the tumor was derived) with an AmpFLSTR system

(Applied Biosystems; Foster City, CA). Cells were regularly tested for Mycoplasma infection, as well. Cells were maintained in Dulbecco's modified Eagle's medium (DMEM, Corning, Manassas, VA), containing 1% penicillin/streptomycin (Invitrogen, Carlsbad, CA), 1% L-glutamine (Sigma, St. Louis, MO), and 10% fetal bovine serum (FBS;Hyclone, Logan, UT) and incubated at 37 °C in a humidified 5% CO2, 95% air atmosphere. For cell viability studies, cells were plated on uncoated 96 well plates at a density of 4,000/well. For caspase 3-like enzymatic activity assays, on uncoated 48 well plates at a density of 20,000/well. For flow analyses and lysate collection, on uncoated 12 well plates at a density of 50,000/well, and in 100 mm dishes at a density of 10^6 cells/dish. Cultures were used in experiments 24 hours post-plating unless stated otherwise. Drug treatments were performed in media supplemented with 2% FBS.

RNAi. SignalSilence Usp9X siRNA I #6308 was purchased from Cell Signaling. Non-targeting siRNA-pool (ON-TARGETplus Non-targeting Pool, # D-001810-10-05) and Mcl-1 (SMARTpool: ON-TARGETplus Mcl-1 siRNA, L-004501-00-0005) were purchased from Thermo Fisher Scientific (Pittsburgh, PA). MPNST cell lines were transfected as previously described[33]. Cells were plated on 12 wells plates. After 24 hours, they have been incubated with the formed complexes of Lipofectamine 2000 (Invitrogen, Carlsbad, CA, USA) and the respective siRNA (12-well condition) in DMEM without FBS and antibiotics. The day after, FBS was added to a total concentration of 2%.

Cell viability and caspase cleavage assays. Cellular proliferation was measured using CellTiter-Glo assays (Promega, Madison, WI), according to the manufacturer's instructions. Briefly, cells were plated in 96-well plates. After treatments, 100 µl of CellTiter-Glo Reagent was added to each well containing 100 µl medium and cells. Cell lysis was induced by shaking for 2 min on an orbital shaker. Then cells were incubated for 10 min at RT for stabilization of the signal prior to measuring luminescence. Luminescence was measured using a plate reader (SpectraMax i3x multi-mode detection platform, Molecular Devices). Caspase activation was assessed with an *in vitro* caspase-3 like cleavage assay utilizing the chemical substrate DEVD-7-amino-4-methylcoumarin (AMC) (Enzo Life Sciences, Framingdale, NY #ALX-260-031). Assay was performed as previously described[34].

Measurement of apoptosis and mitochondrial membrane potential. For annexin V/propidium iodide (PI) staining the FITC Annexin V Apoptosis Detection Kit I (BD Pharmingen, USA) was used according to the manufacturer's instructions. TMRE staining was performed using CellSimple™ Mitochondrial Membrane Potential Assay Kit (II) (Cell Signaling #45898), in accordance with the manufacturer instructions. Fluorescence was measured using a BD FACSCalibur flow cytometer. The data were analyzed with the FlowJo software (version 8.7.1; Tree Star, Ashland, OR, USA).

Western blotting. Whole cell lysates were prepared by removing the media and lysing cells directly in Laemmli buffer, containing 5% 2-Mercaptoethanol (Bio-Rad #161-0710), 95% 2x Laemmli Sample Buffer (Bio-Rad #161-0737) and protease and phosphatase inhibitor cocktail (Thermo Scientific #1861281). Lysates were stored at −80 °C. Whole tumor lysates were prepared by lysing the tissues directly in RIPA buffer (Thermo Fisher #89900) with the addition of protease and phosphatase inhibitor cocktail (Thermo Scientific #1861281). Tumors were mechanically disaggregated followed by sonication. Insoluble material was removed by centrifugation at 12,000 r.p.m., and the supernatant was collected for protein quantification. Lysates were immediately stored at −80 °C.

Western blots were performed as described previously[35]. All primary antibodies were diluted to a final concentration of 1:500, except β-actin (1:8000). Secondary antibodies conjugated with horseradish-peroxidase were used at a dilution of 1:5000. For immunodetection, the Pierce ECL Western blotting substrate was utilized (Pierce ECL; Thermo Scientific, Waltham, MA). Membranes were developed using Azure c-300 gel doc & western blot Imaging (Azure Biosystem). Quantification of Western blot bands was performed with the open source image processing program ImageJ.

Transmission Electron Microscopy. Cells were fixed with 2.5% glutaraldehyde in 0.1 M Sorenson's buffer (PH 7.2) for at least one hour, then postfixed with 1% OsO4 also in Sorenson's buffer for one hour. After dehydration cells were embedded in a mixture of Lx-112 (Ladd Research Industries, Inc.) and Embed-812 (EMS, Fortwashington, PA). Thin sections (60 nm) were cut on the MT-Power-Trome XL ultramicrotome. Sections were stained with uranyl acetate and lead citrate and examined under a JEOL JEM-1200 EXII electron microscope. Images were taken on an ORCA-HR digital camera (Hamamatsu) and recorded with the AMT Image Capture Engine.

Subcutaneous xenograft model. 7×10^6 ST88-14 cells suspended 1:1 in Matrigel Matrix (Corning Inc., Corning, NY, USA) were implanted subcutaneously into one flank (first experiment) and into both flanks (second experiment) of 6–8 week-old SCID SHO mice as previously described[18]. 4 mice per experimental group were used. Vehicle or drug was injected intraperitoneally 3 times each week for 4 weeks during the first *in vivo* study, and for five of seven days, from Monday to Friday, for 2 weeks during the second *in vivo* experiment. For intraperitoneal application WP1130 were dissolved in a solution of 80% Cremophor EL (SIGMA, St. Louis, MO) and 20% Ethanol (Pharmco-Aaper, Brookfield, CT) (v/v), diluted 1:1 in sterile PBS.

Histological analysis. Subcutaneous tumors and samples from organs were removed from SCID SHO mice and fixed for at least 24 h in 4% PBS-buffered formalin. Then tissues were embedded in paraffin and 4 µm thick sections were cut prior to staining with hematoxylin and eosin, TUNEL (Click-iT™ TUNEL Colorimetric IHC Detection Kit, Thermo Fisher #C10625) or cleaved caspase 3 (Cell Signaling #9661). Photomicrographs were taken at X40 and X60 magnification.

Statistics. All data points represent mean ± S.D. All experiments were repeated at least 3 times unless stated otherwise. Representative data is shown. Statistical significance was determined by one-way ANOVA test for multiple comparisons and student's t-test for two groups using Graphpad Prism 6 software. A p-value ≤ 0.05 was considered significant.

Data Availability Statement

all the data are available upon request.

References

1. Kim, A. *et al*. Malignant Peripheral Nerve Sheath Tumors State of the Science: Leveraging Clinical and Biological Insights into Effective Therapies. *Sarcoma* **2017**, 7429697, https://doi.org/10.1155/2017/7429697 (2017).
2. Graham, C. D. *et al*. BH3 mimetics suppress CXCL12 expression in human malignant peripheral nerve sheath tumor cells. *Oncotarget* **8**, 8670–8678, https://doi.org/10.18632/oncotarget.14398 (2017).
3. Kiuru, M. & Busam, K. J. The NF1 gene in tumor syndromes and melanoma. *Lab Invest* **97**, 146–157, https://doi.org/10.1038/labinvest.2016.142 (2017).
4. Brooks, D. G. The neurofibromatoses: hereditary predisposition to multiple peripheral nerve tumors. *Neurosurg Clin N Am* **15**, 145–155, https://doi.org/10.1016/j.nec.2004.02.008 (2004).
5. Brossier, N. M. & Carroll, S. L. Genetically engineered mouse models shed new light on the pathogenesis of neurofibromatosis type I-related neoplasms of the peripheral nervous system. *Brain Res Bull* **88**, 58–71, https://doi.org/10.1016/j.brainresbull.2011.08.005 (2012).
6. Karpel-Massler, G. *et al*. Inhibition of deubiquitinases primes glioblastoma cells to apoptosis *in vitro* and *in vivo*. *Oncotarget* **7**, 12791–12805, https://doi.org/10.18632/oncotarget.7302 (2016).
7. Yan, J. *et al*. Usp9x- and Noxa-mediated Mcl-1 downregulation contributes to pemetrexed-induced apoptosis in human non-small-cell lung cancer cells. *Cell Death Dis* **5**, e1316, https://doi.org/10.1038/cddis.2014.281 (2014).
8. Engel, K. *et al*. USP9X stabilizes XIAP to regulate mitotic cell death and chemoresistance in aggressive B-cell lymphoma. *EMBO Mol Med* **8**, 851–862, https://doi.org/10.15252/emmm.201506047 (2016).
9. Karpel-Massler, G. *et al*. TIC10/ONC201 synergizes with Bcl-2/Bcl-xL inhibition in glioblastoma by suppression of Mcl-1 and its binding partners *in vitro* and *in vivo*. *Oncotarget* **6**, 36456–36471, https://doi.org/10.18632/oncotarget.5505 (2015).
10. Nair, J. S. & Schwartz, G. K. Inhibition of polo like kinase 1 in sarcomas induces apoptosis that is dependent on Mcl-1 suppression. *Cell Cycle* **14**, 3101–3111, https://doi.org/10.1080/15384101.2015.1078033 (2015).
11. Karpel-Massler, G. *et al*. Inhibition of Mitochondrial Matrix Chaperones and Antiapoptotic Bcl-2 Family Proteins Empower Antitumor Therapeutic Responses. *Cancer research* **77**, 3513–3526, https://doi.org/10.1158/0008-5472.CAN-16-3424 (2017).
12. Milani, M. *et al*. DRP-1 is required for BH3 mimetic-mediated mitochondrial fragmentation and apoptosis. *Cell Death Dis* **8**, e2552, https://doi.org/10.1038/cddis.2016.485 (2017).
13. Wang, W. B. *et al*. Paraptosis accompanied by autophagy and apoptosis was induced by celastrol, a natural compound with influence on proteasome, ER stress and Hsp90. *J Cell Physiol* **227**, 2196–2206, https://doi.org/10.1002/jcp.22956 (2012).
14. Zhang, J. S. *et al*. gamma-Tocotrienol induces paraptosis-like cell death in human colon carcinoma SW620 cells. *PLoS One* **8**, e57779, https://doi.org/10.1371/journal.pone.0057779 (2013).
15. Peterson, L. F. *et al*. Targeting deubiquitinase activity with a novel small-molecule inhibitor as therapy for B-cell malignancies. *Blood* **125**, 3588–3597, https://doi.org/10.1182/blood-2014-10-605584 (2015).
16. Wang, S. *et al*. Ablation of the oncogenic transcription factor ERG by deubiquitinase inhibition in prostate cancer. *Proc Natl Acad Sci USA* **111**, 4251–4256, https://doi.org/10.1073/pnas.1322198111 (2014).
17. Pham, L. V. *et al*. Degrasyn potentiates the antitumor effects of bortezomib in mantle cell lymphoma cells *in vitro* and *in vivo*: therapeutic implications. *Mol Cancer Ther* **9**, 2026–2036, https://doi.org/10.1158/1535-7163.MCT-10-0238 (2010).
18. Karpel-Massler, G. *et al*. Combined inhibition of Bcl-2/Bcl-xL and Usp9X/Bag3 overcomes apoptotic resistance in glioblastoma *in vitro* and *in vivo*. *Oncotarget* **6**, 14507–14521, https://doi.org/10.18632/oncotarget.3993 (2015).
19. Murtaza, M., Jolly, L. A., Gecz, J. & Wood, S. A. La FAM fatale: USP9X in development and disease. *Cell Mol Life Sci* **72**, 2075–2089, https://doi.org/10.1007/s00018-015-1851-0 (2015).
20. Yang, B. *et al*. Deubiquitinase USP9X deubiquitinates beta-catenin and promotes high grade glioma cell growth. *Oncotarget* **7**, 79515–79525, https://doi.org/10.18632/oncotarget.12819 (2016).
21. Cox, J. L. *et al*. Context-dependent function of the deubiquitinating enzyme USP9X in pancreatic ductal adenocarcinoma. *Cancer Biol Ther* **15**, 1042–1052, https://doi.org/10.4161/cbt.29182 (2014).
22. Perez-Mancera, P. A. *et al*. The deubiquitinase USP9X suppresses pancreatic ductal adenocarcinoma. *Nature* **486**, 266–270, https://doi.org/10.1038/nature11114 (2012).
23. Kapuria, V. *et al*. Deubiquitinase inhibition by small-molecule WP1130 triggers aggresome formation and tumor cell apoptosis. *Cancer research* **70**, 9265–9276, https://doi.org/10.1158/0008-5472.CAN-10-1530 (2010).
24. Oslowski, C. M. & Urano, F. Measuring ER stress and the unfolded protein response using mammalian tissue culture system. *Methods Enzymol* **490**, 71–92, https://doi.org/10.1016/B978-0-12-385114-7.00004-0 (2011).
25. Ishida, C. T. *et al*. BH3-mimetics and BET-inhibitors elicit enhanced lethality in malignant glioma. *Oncotarget* **8**, 29558–29573, https://doi.org/10.18632/oncotarget.16365 (2017).
26. Singleton, D. C. & Harris, A. L. Targeting the ATF4 pathway in cancer therapy. *Expert Opin Ther Targets* **16**, 1189–1202, https://doi.org/10.1517/14728222.2012.728207 (2012).
27. Schwickart, M. *et al*. Deubiquitinase USP9X stabilizes MCL1 and promotes tumour cell survival. *Nature* **463**, 103–107, https://doi.org/10.1038/nature08646 (2010).
28. Trivigno, D., Essmann, F., Huber, S. M. & Rudner, J. Deubiquitinase USP9x confers radioresistance through stabilization of Mcl-1. *Neoplasia* **14**, 893–904 (2012).
29. Leverson, J. D. *et al*. Potent and selective small-molecule MCL-1 inhibitors demonstrate on-target cancer cell killing activity as single agents and in combination with ABT-263 (navitoclax). *Cell Death Dis* **6**, e1590, https://doi.org/10.1038/cddis.2014.561 (2015).
30. Peddaboina, C. *et al*. The downregulation of Mcl-1 via USP9X inhibition sensitizes solid tumors to Bcl-xl inhibition. *BMC Cancer* **12**, 541, https://doi.org/10.1186/1471-2407-12-541 (2012).
31. Ryan, J. J. *et al*. Role for the stem cell factor/KIT complex in Schwann cell neoplasia and mast cell proliferation associated with neurofibromatosis. *J Neurosci Res* **37**, 415–432, https://doi.org/10.1002/jnr.490370314 (1994).
32. Stonecypher, M. S., Byer, S. J., Grizzle, W. E. & Carroll, S. L. Activation of the neuregulin-1/ErbB signaling pathway promotes the proliferation of neoplastic Schwann cells in human malignant peripheral nerve sheath tumors. *Oncogene* **24**, 5589–5605, https://doi.org/10.1038/sj.onc.1208730 (2005).
33. Siegelin, M. D. *et al*. Exploiting the mitochondrial unfolded protein response for cancer therapy in mice and human cells. *J Clin Invest* **121**, 1349–1360, https://doi.org/10.1172/JCI44855 (2011).

34. Geng, Y., Kohli, L., Klocke, B. J. & Roth, K. A. Chloroquine-induced autophagic vacuole accumulation and cell death in glioma cells is p53 independent. *Neuro Oncol* **12**, 473–481, https://doi.org/10.1093/neuonc/nop048 (2010).
35. Pareja, F. *et al*. PI3K and Bcl-2 inhibition primes glioblastoma cells to apoptosis through downregulation of Mcl-1 and Phospho-BAD. *Mol Cancer Res* **12**, 987–1001, https://doi.org/10.1158/1541-7786.MCR-13-0650 (2014).

Acknowledgements

This work was supported by Department of Defense grants W81XWH-14-1-0073, W81XWH-12-1-0164 and X81XWH-15-1-0193, and by National Institutes of Health grants K08 NS083732, R01 NS095848, R01 NS102366 and Louis V. Gerstner, Jr. Scholars Program (2017–2020). Research reported in this publication was supported by the National Cancer Institute Cancer Center Support Grant P30 CA013696. We thank Dr. Kristy Brown with expert technical assistance with the TEM acquisition and analysis. We thank Dr. Linda Sasset for the optimization of the protocol for protein extraction from tumors. Research reported in this publication was performed in the CCTI Flow Cytometry Core, supported in part by the Office of the Director, National Institutes of Health under award S10RR027050. The content is solely the responsibility of the authors and does not necessarily represent the official views of the National Institutes of Health.

Author Contributions

Conception and Design: E.B., K.A.R. and M.D.S. Development of methodology: E.B., M.D.S. and K.A.R. Acquisition of data: E.B., S.J.B. Analysis and interpretation of data: E.B., M.D.S. and K.A.R. Administrative, technical and material support: E.B., M.D.S., S.L.C. and K.A.R. Writing, review and revision of the manuscript: E.B., M.D.S., S.L.C. and K.A.R. Study supervision: K.A.R.

Additional Information

Supplementary information accompanies this paper at https://doi.org/10.1038/s41598-018-35806-5.

Competing Interests: The authors declare no competing interests.

Publisher's note: Springer Nature remains neutral with regard to jurisdictional claims in published maps and institutional affiliations.

Open Access This article is licensed under a Creative Commons Attribution 4.0 International License, which permits use, sharing, adaptation, distribution and reproduction in any medium or format, as long as you give appropriate credit to the original author(s) and the source, provide a link to the Creative Commons license, and indicate if changes were made. The images or other third party material in this article are included in the article's Creative Commons license, unless indicated otherwise in a credit line to the material. If material is not included in the article's Creative Commons license and your intended use is not permitted by statutory regulation or exceeds the permitted use, you will need to obtain permission directly from the copyright holder. To view a copy of this license, visit http://creativecommons.org/licenses/by/4.0/.

© The Author(s) 2018

Oridonin inhibits aberrant AKT activation in breast cancer

Bowen Sun[1,2], Geng Wang[2,3], Huidong Liu[2,3], Pian Liu[4], Waleed O. Twal[5], Hiuwing Cheung[2], Steven L. Carroll[2], Stephen P. Ethier[2], Emily E. Mevers[6], Jon Clardy[6], Thomas Roberts[6,7], Changbin Chen[8], Qian Li[8], Lanfeng Wang[8], Meixiang Yang[1], Jean J. Zhao[6,7] and Qi Wang[2]

[1]The first Affiliate Hospital, Biomedical Translational Research Institute, Guangdong Province Key Laboratory of Molecular Immunology and Antibody Engineering, Jinan University, Guangzhou 510632, China

[2]Department of Pathology and Laboratory Medicine, Medical University of South Carolina, Charleston, SC 29425, USA

[3]Department of Anatomy, Harbin Medical University, Harbin 150081, China

[4]Cancer Center, Union Hospital, Tongji Medical College, Huazhong University of Science and Technology, Wuhan 430000, China

[5]Department of Regenerative Medicine and Cell Biology, Medical University of South Carolina, Charleston, SC 29425, USA

[6]Department of Biological Chemistry and Molecular Pharmacology, Harvard Medical School, Boston, MA 02115, USA

[7]Department of Cancer Biology, Dana-Farber Cancer Institute, Boston, MA 02115, USA

[8]Institute Pasteur of Shanghai, Chinese Academy of Sciences, Shanghai 200031, China

Correspondence to: *Jean J. Zhao,* ***email:*** *jean_zhao@dfci.harvard.edu*
Qi Wang, ***email:*** *wangq@musc.edu*

Keywords: *TCM plant extracts; oridonin; PI3K/AKT signaling; mammary tumor prevention; tumorigenesis*

Received: *October 17, 2017* ***Accepted:*** *January 13, 2018* ***Published:*** *February 01, 2018*

Copyright: Sun et al. This is an open-access article distributed under the terms of the Creative Commons Attribution License 3.0 (CC BY 3.0), which permits unrestricted use, distribution, and reproduction in any medium, provided the original author and source are credited.

ABSTRACT

Aberrant activation of phosphatidylinosito-4,5-bisphosphate 3-kinase/protein kinase B (PI3K/AKT) signaling in cancer has led to pursuit of inhibitors for targeting this pathway. However, inhibitors of PI3K and AKT have failed to yield efficacious results without adverse effects. Here, we screened a library containing 441 authenticated traditional chinese medicine (TCM) plant extracts by examining their effect on cell viability of a human mammary epithelial cell line HMEC-PIK3CA^{H1047R}, which expresses mutant PIK3CA^{H1047R} and has constitutively active AKT signaling. We found that Oridonin, an extract from *Rabdosia rubescens*, reduced cell viability to the greatest extent. Oridonin binds to AKT1 and potentially functions as an ATP-competitive AKT inhibitor. Importantly, Oridonin selectively impaired tumor growth of human breast cancer cells with hyperactivation of PI3K/AKT signaling. Moreover, Oridonin prevented the initiation of mouse mammary tumors driven by PIK3CA^{H1047R}. Our results suggest that Oridonin may serve as a potent and durable therapeutic agent for the treatment of breast cancers with hyperactivation of PI3K/AKT signaling.

INTRODUCTION

The lipid phosphatidylinositol 3,4,5-trisphosphate (PIP_3) is a critical signaling molecule located at the cell membrane, the level of which is tightly regulated by the opposing activities of two enzymes: the phosphatidylinositol 3-kinase (PI3K; a lipid kinase) and phosphatase and tensin homologue (PTEN; a lipid phosphatase). Under normal physiological condition, growth factor stimulation of receptor tyrosine kinases (RTKs) activates PI3K that uses phosphatidylinositol 4,5-trisphosphate (PIP_2) as a substrate to generate PIP_3. Increased PIP_3 levels result in the activation of the serine/threonine kinase AKT and downstream effector pathways that regulate many biological processes including cell proliferation and survival. The tumor suppressor PTEN functionally antagonizes PI3K activity via its intrinsic lipid phosphatase activity by converting PIP_3 back to

PIP_2 [1, 2]. The PI3K/AKT signaling pathway is improperly activated in many types of human cancer by RTKs and somatic mutations in specific components of the signaling pathway [3]. In breast cancer, human epidermal growth factor 2 (HER2), a RTK, is constitutively activated by overexpression or gene amplification in 15–20% of breast tumors [4]. The *PIK3CA* gene, which encodes the p110α isoform of PI3K, is frequently mutated in more than 25% of breast cancer [5–8]. Loss of PTEN occurs in an additional of 25% of breast cancer [9, 10]. Genetic alterations of all three isoforms of AKT have also been observed in breast cancers [11, 12].

Many small molecule drugs targeting different isoforms or components of the PI3K/AKT signaling pathway are in clinical development. Some of these drugs inhibit all isoforms of the catalytic subunit of class IA PI3Ks (p110α, p110β, and p110δ) may cause undesired toxicity. Some inhibitors are designed to inhibit individual isoforms in cancers in which the activation of PI3K/AKT signaling relies on specific isoforms only. However, it remains unclear which type of inhibitor will be more effective clinically. Since feedback signaling has been shown to limit the efficacy of PI3K inhibitors [13], dual PI3K/mTOR inhibitors have also been developed. However, a critical issue that will influence the advantage of these inhibitors is whether complete inhibition of all isoforms of PI3K and mTORC1/2 will be tolerable in patients or whether the use of these inhibitors will necessitate sacrificing complete inhibition of one or more of the potential targets. There is still an urgent need for new inhibitors that effectively shut down PI3K/AKT signaling with minimum toxicity.

Medicinal plants, including those used in traditional chinese medicine (TCM), have historically proven their value as a source of molecules with therapeutic potential and represent an important pool for the identification of novel drugs. Here, we screened a library of authenticated TCM plants containing 441 plants extracts by the cell viability assay in a human mammary epithelial cell line HMEC-PIK3CA^{H1047R} with constitutively activated PI3K and AKT signaling. Of these, Oridonin, an extract from *Rabdosia rubescens*, reduced cell viability to the greatest extent. We demonstrated that Oridonin functioned as a potential ATP-competitive AKT inhibitor. Oridonin selectively impaired the growth of human breast cancer cells with hyperactivation of AKT signaling (p-AKT^{High}) *in vitro* and *in vivo*. Our results suggest that Oridonin may be of substantial clinical utility in breast cancers with hyperactivation of PI3K/AKT signaling.

RESULTS

Screen of compounds in TCM plant extracts that inhibit the growth of HMEC- PIK3CA^{H1047R} cells

To identify potential PI3K pathway inhibitors from TCM plant extracts we used a Celltiter-Glo cell viability assay to screen a library containing 441 partially purified plant extracts [14] in HMEC-PIK3CA^{H1047R} cells, which possess constitutively activated AKT signaling due to ectopic expression of mutant PIK3CA^{H1047R} in an immortalized human mammary epithelial cell (HMEC) line (Supplementary Figure 1). The results from the screen are represented in Figure 1 as volcano plots displaying the statistical significance against growth inhibition in the cells. We found that 54 out of 441 extracts significantly inhibited HMEC-PIK3CA^{H1047R} cell growth ($p < 0.05$) (Supplementary Table 1). Among them, 19 extracts, derived from *Rabdosia rubescens*, *Glycyrrhiza uralensis Fisch*, and *Sophora flavescens Ait*, showed more than 80% cell growth inhibition comparable to the effect of the pan PIK3 inhibitor BKM120 or the dual PI3K/mTOR inhibitor BEZ235 (Figure 1 and Supplementary Table 2). 1561-D12, an extract from *Rabdosia rubescens*, showed maximal growth inhibition (Figure 1 and Supplementary Table 2). Liquid chromatography-mass spectrometry (LC/MS) and nuclear magnetic resonance (NMR) analyses of 1561-D12 showed that the fraction contained a relatively pure major chemical entity, which was identified as Oridonin (Supplementary Table 3), a previously described compound with potential antitumor activity in a variety of cancer cells [15–19].

Oridonin preferentially suppresses AKT/mTOR signaling in human mammary epithelial cells

We then investigated whether Oridonin suppressed PI3K signaling or activated AKT itself in HMEC-PIK3CA^{H1047R} cells. We performed immunoblotting to evaluate PI3K signaling components in HMEC-PIK3CA^{H1047R} cells after treatment with increasing concentrations of Oridonin or the dual PI3K/mTOR inhibitor BEZ235. Unexpectedly, Oridonin did not significantly suppress phosphorylation of AKT as BEZ235 did, but did efficiently inhibit the phosphorylation of AKT substrates, such as AKT substrate 1 (AKTS1; also known as PRAS40) and downstream mTOR signaling proteins (Figure 2A).

To further determine whether Oridonin suppresses PI3K signaling, we treated HMEC-PIK3CA^{H1047R} cells in a time-dependent manner. Consistent with the above data, Oridonin suppressed the phosphorylation of PRAS40 and S6RP at 15 minutes post treatment but did not inhibit the phosphorylation of AKT even after 90 minutes (Figure 2B). To determine whether Oridonin inhibited PI3K signaling in other cells with activation of AKT signaling, we stably depleted PTEN via shRNA in HMEC cells. PTEN protein expression was suppressed in stable pLKO-shPTEN [20] expressing HMEC cells, and phosphorylation of AKT and its effectors increased (Figure 2C). Consistent with the effect of Oridonin in HMEC-PIK3CA^{H1047R} cells, Oridonin suppressed the phosphorylation of PRAS40 and S6RP starting from 15 minutes post treatment, but had a minimal effect on phosphorylation of AKT (Figure 2C).

To investigate the broad effect of Oridonin in AKT specifically, we evaluated the spectrum of AKT phosphorylation substrates using phospho-AKT substrate-specific antibodies that recognize the phospho-(Ser/Thr) AKT substrate motif (RXXS*/T*) in an engineered cell line HMEC-myrAKT1 that ectopically expresses myristoylated AKT1. When directed to membranes by the addition of a src *myristoylation* sequence, AKT becomes constitutively active. Oridonin gradually suppressed pan-AKT phosphorylation substrates in HMEC-myrAKT1 cells comparable to the effects of the PI3K/mTOR dual inhibitor BEZ235 (Figure 2D), pan PI3K initiator BKM120, AKT inhibitor MK2206, and mTOR inhibitor RAD001 (Supplementary Figure 2). Moreover, as expected, Oridonin suppressed the phosphorylation of PRAS40 and S6RP starting from 15 minutes post treatment, but did not inhibit phosphorylation of AKT in these cells (Figure 2E). These results indicate that Oridonin preferentially blocks AKT kinase activity by inhibiting phosphorylation of AKT substrates and subsequently suppresses downstream mTOR signaling.

To investigate whether Oridonin directly binds to AKT, we performed surface plasmon resonance (SPR) analysis to evaluate the *in vitro* binding of Oridonin with purified human recombinant AKT1. As shown in Figure 3A, Oridonin bound to AKT1 immobilized on a sensor chip. Optimal fitting of SPR data obtained by measuring the binding of Oridonin at a concentration of 2 μM to immobilized AKT1 was best achieved using a single class binding site model. As a result, an affinity constant (KD) of 2.15 nM (n = 3; χ^2 of fit < 10) was determined for Oridonin binding to AKT1. AKT protein isoforms (AKT1, 2 and 3) are structurally plastic enzymes, with large conformational differences observed between the inactive and the active kinase domain structures including order changes in the N-terminal pleckstrin homology (PH) domain, an interdomain linker, a kinase domain, and a C-terminal hydrophobic motif [21]. Using a well-documented docking software-AutoDock Vina due to its accuracy of the predictions of the experimental structure [22], we predict a docking model of Oridonin binding AKT1 (Figure 3B and 3C) based on the crystal structure of AKT1 complex with adenylyl-imidodiphosphate (AMP-PNP) [23], a non-hydrolysable analogue of ATP functions as an ATP-dependent competitive inhibitor. This model showed that Oridonin did bind AKT1 in the ATP binding

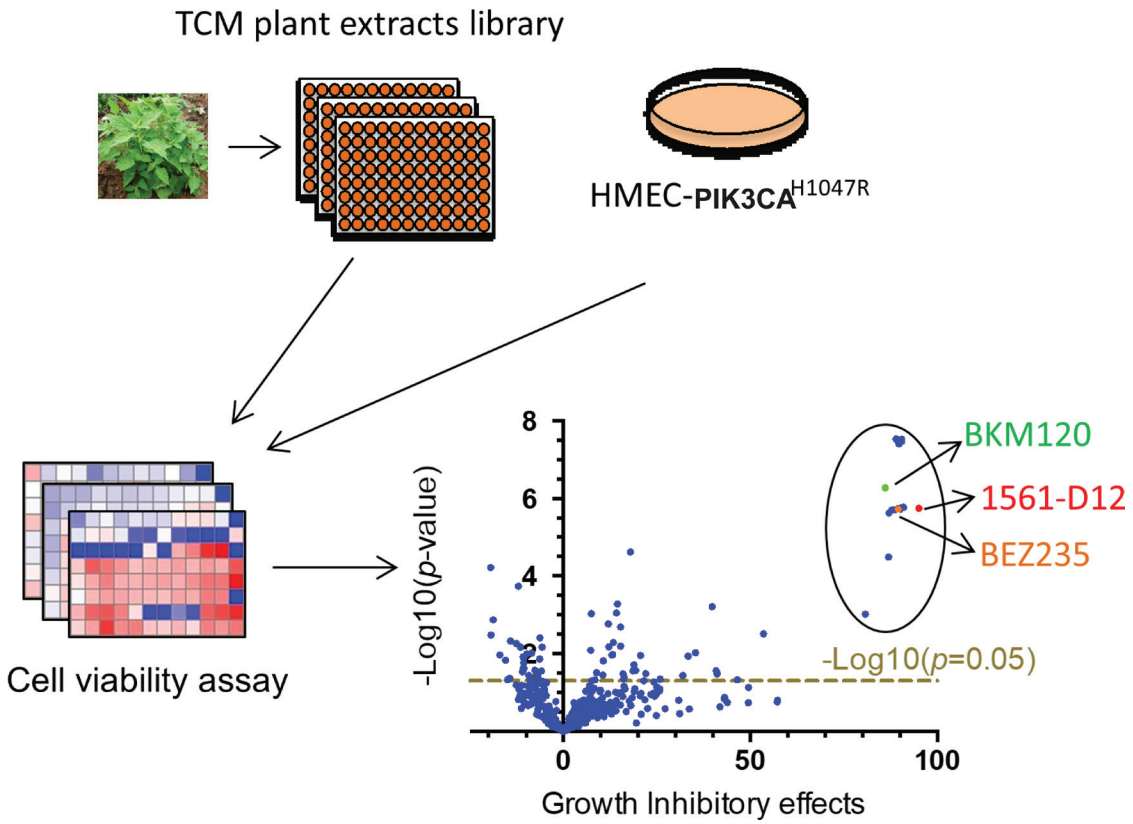


Figure 1: Schematic of the screen for TCM plant extracts. HMEC-PIK3CA^{H1047R} cells with constitutively active ATK signaling were generated by introducing oncogenic mutant PIK3CA^{H1047R} into an immortalized human mammary epithelial cell (HMEC) cell line. The cells were seeded in 96-well plates and treated in triplicate with a TCM library containing 441 extracts from plants used in traditional Chinese medicine. After 3 days of exposure to 1.5 μg/mL of extracts, cell numbers were assessed using the CellTiter-Glo luminescent cell viability assay. Volcano plots were generated by plotting the growth inhibitory effects against probability. Candidate compounds are highlighted by the circle in the upper right corner.

pocket of the kinase domains, because it has been overlaid very well with AMP-PNP (Figure 3B). Additionally, Oridonin binds the entry site of the ATP binding pocket, suggesting it might prevent ATP access to the nucleotide-binding site (Figure 3C). The active structure of AKT1 in complex with AMP-PNP was reported to limit accessibility to the phosphorylation sites [23]. Taken together, these results suggest that Oridonin may function as a potential ATP-competitive AKT inhibitor.

Oridonin selectively suppresses growth of breast cancer cells with hyperactivation of AKT signaling

To investigate whether Oridonin inhibits the cell viability of other breast cancer cells we determined dose-response curves in a panel of breast cancer cell lines with different levels of phosphorylated AKT (Figure 4A). Three breast cancer cells had high levels of AKT phosphorylation (p-AKT^{High}) due to activation by HER2 amplification (SKBR3 and HCC1569) or PTEN loss (MDAMB468), whereas MDAMB231 and the immortalized mammary epithelial cell MCF-10A expressed low levels of p-AKT. p-AKT^{High} cells were more sensitive to Oridonin treatment, with cell viability effectively suppressed by 10-to 100-fold lower concentrations of Oridonin compared with MDAMB231 and MCF-10A cells (Figure 4B and Supplementary Figure 3). To investigate whether the proliferation of these cells is inhibited by Oridonin treatment, we performed clonogenic growth assays using the above cell lines. Cells were treated with

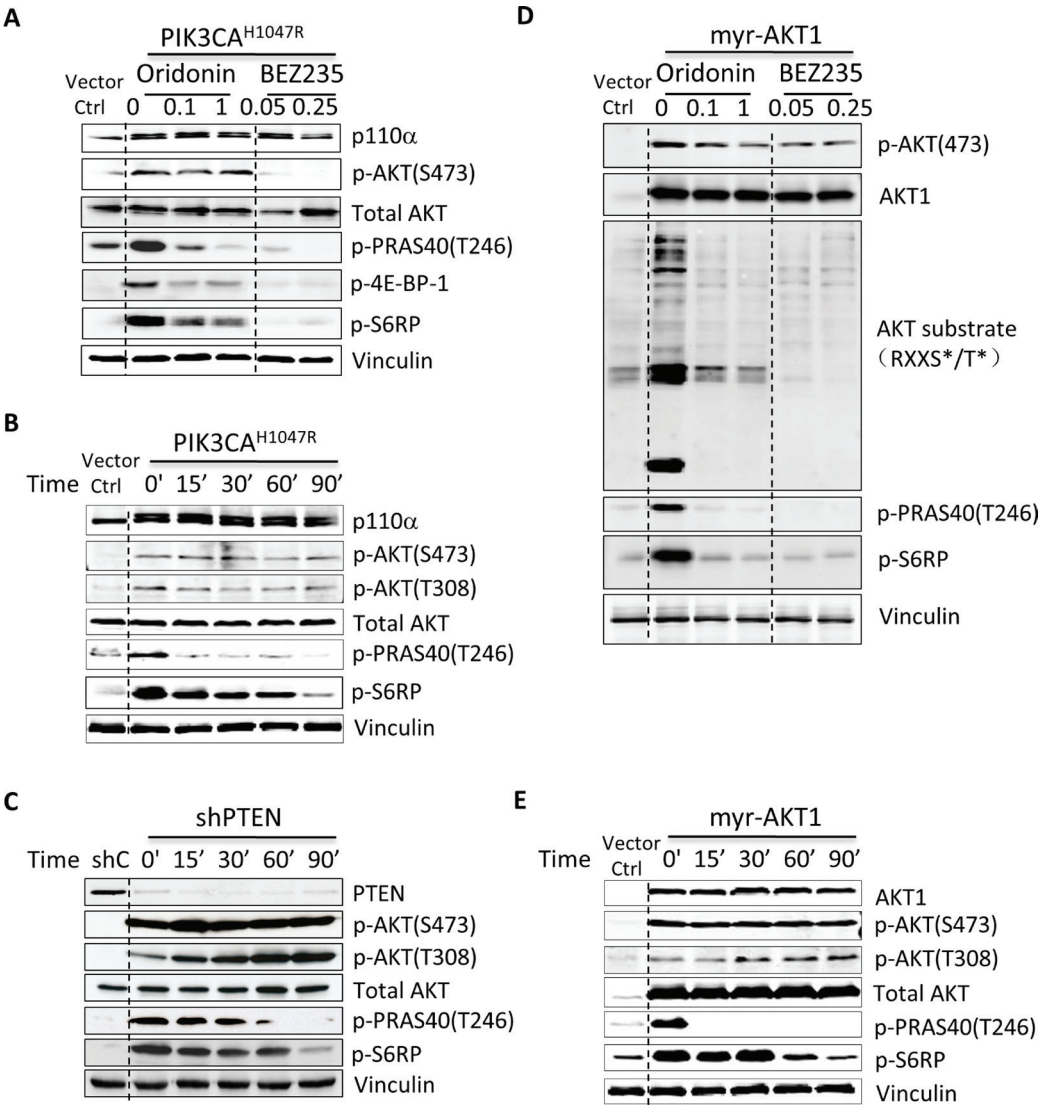


Figure 2: Oridonin preferentially suppresses AKT/mTOR signaling. HMEC-PIK3CA^{H1047R} (**A**) or HMEC-myr-AKT1 (**D**) cells were starved for 2 hrs and then treated with vehicle control (DMSO) or increasing concentrations of Oridonin (0.1 and 1 μM) or BEZ235 (50 and 250 nM) for 1 hr before preparation of lysates for immunoblotting using the indicated antibodies. HMEC-PIK3CA^{H1047R} (**B**), HMEC-shPTEN (**C**) and HMEC-Myr-AKT1 (**E**) cells were starved for 2 hrs and then treated with vehicle control (DMSO) or Oridonin (1 μM) for 0, 15, 30, 60, and 90 minutes before preparation of lysates for immunoblotting using the indicated antibodies.

1 μM Oridonin for three weeks and stained with crystal violet. Consistent with the above findings, Oridonin selectively inhibited the clonogenic growth of p-AKT^{High} cells (MDAMB468, SKBR3, and HCC1569), but did not suppress proliferation of p-AKT^{low} MDAMB231 and MCF-10A cells (Figure 4C). These findings suggest that Oridonin selectively inhibited clonogenic growth of breast cancer cells with hyperactivation of AKT.

Oridonin impairs growth of breast tumor with hyperactivation of AKT *in vivo*

To test whether Oridonin can impair the *in vivo* growth of p-AKT^{High} breast cancer cells, NCr nude mice bearing palpable MDAMB468 or HCC1569 xenografts were treated with Oridonin or vehicle control. Durable tumor regression was achieved in both

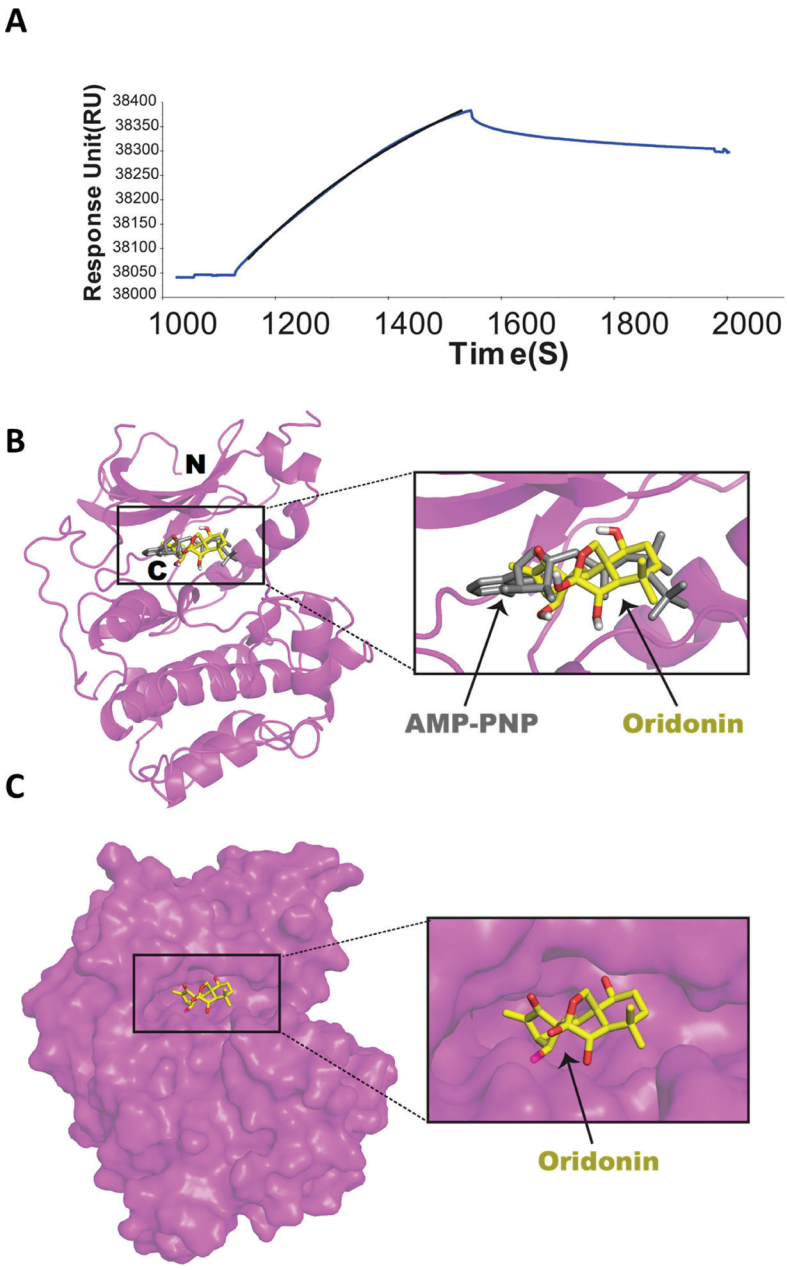


Figure 3: Surface plasmon resonance (SPR) analysis of Oridonin binding to AKT1. (**A**) SPR sensorgrams of Oridonin (2 μM) binding to purified human recombinant AKT1 on a sensor chip CM5 are shown. Data depicted were normalized to 100 response units (RU) and are representative of three independent experiments. To obtain affinity constants (KD), SPR profiles in a given series were simultaneously fit to a 1:1 binding site model using BIAevaluation Version 3.1 software. Original sensogram is shown in blue and best fit association line from BIA evaluation software is in black. (**B**) Docking model of Oridonin binding AKT1. Ribbon representation of overlaid Oridonin docking model with the complex structure of AKT1 with AMP-PNP (PDB ID: 4EKK; magenta, protein; gray, ligand). (**C**) Surface representation of Oridonin binding in the nucleotide-binding pocket. For oridonin, $C_{20}H_{28}O_6$ (C, yellow; O, red) and hydrogens were hidden to simplify the 3D structure.

MDAMB468 and HCC1569 xenograft tumor models following Oridonin treatment (Figure 5A and 5D). To evaluate signaling and pharmacodynamic responses of MDAMB468 and HCC1569 xenografts during Oridonin treatment, tumors were isolated 72 hrs after drug administration and molecular markers were analyzed by immunohistochemical staining. Oridonin decreased phosphorylation of the AKT substrate PRAS40 and AKT downstream mTOR target (S6), blocked proliferation (as assessed by Ki67 index), and induced apoptosis (as assessed by cleaved caspase 3) (Figure 5B, 5C, 5E, and 5F). These results indicate that Oridonin effectively impairs tumor growth in p-AKT^{High} breast cancers by inhibiting proliferation and inducing apoptosis via suppressing AKT-mTOR signaling pathway.

Oridonin prevents the initiation of mammary tumors carrying PIK3CA^{H1047R} by blocking AKT-mTOR signaling

We previously reported that expression of PIK3CA^{H1047R} could initiate transformation of mammary epithelium in inducible MMTV-rtTA-tetO-PIK3CA^{H1047R} (iPIK3CA^{H1047R}) female mice [24]. To examine whether Oridonin can prevent PIK3CA^{H1047R}-induced mammary epithelial cell transformation, we transplanted PIK3CA^{H1047R} mammary tissue fragments into cleared fat pads of 3-week-old NCr nude female mice. PIK3CA^{H1047R} expression in iPIK3CA^{H1047R} mammary epithelial cells is coupled to a luciferase reporter, allowing transgene expression to be followed *in vivo* [24]. Expression of

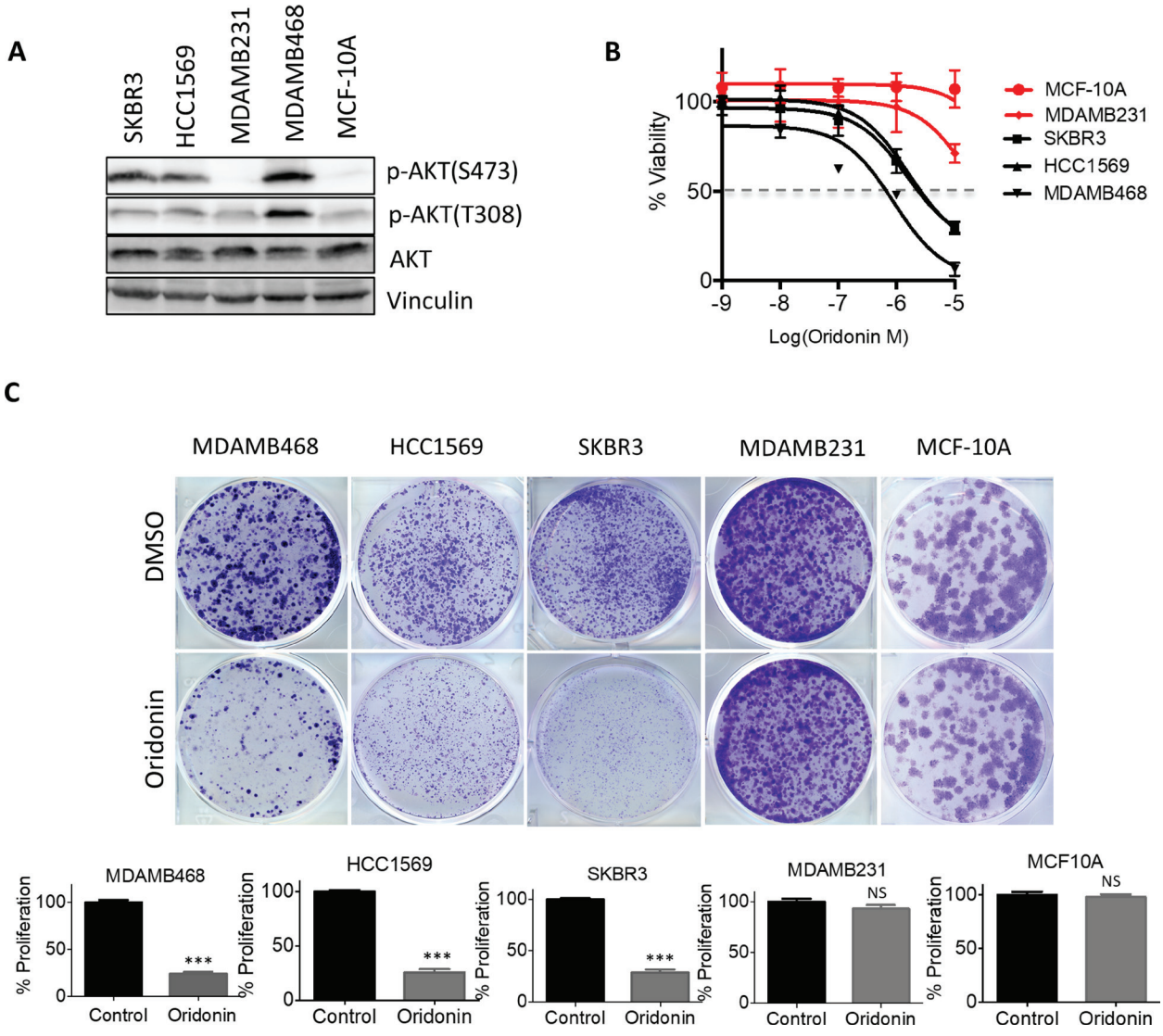


Figure 4: Oridonin selectively impairs cell growth and tumorigenesis in breast cancer with hyperactivation of AKT signaling. (**A**) Immunoblot analysis of AKT phosphorylation levels in breast cancer cell lines. (**B**) Dose-response curve of breast cancer cells after treatment with increasing concentrations of Oridonin for 72 hrs. Percent viability relative to that of DMSO-treated cells is shown. Data represent mean ± SD of three replicates. (**C**) Crystal violet staining of cells and quantification of cell growth. Data are presented as mean ± SD of three replicates, $^{*}p < 0.01$, $^{***}p < 0.001$ (Student's *t* test).

PIK3CA^{H1047R} in transplanted mammary epithelial cells was induced by treating the mice with doxycycline at 8 weeks post transplantation. Mice were concurrently treated with Oridonin, BEZ235 or vehicle control. The increased luciferase reporter activity in transplanted iPIK3CA^{H1047R} epithelium induced by doxycycline treatment was blocked by treatment with Oridonin and BEZ235 (Figure 6A). Histological examination showed increased mammary ductal side-branching and enlarged focal nodular structures filled with hyperproliferative cells characteristic of early neoplastic lesions in the vehicle control group whereas normal mammary epithelium structures were observed in mice treated with Oridonin or BEZ235 (Figure 6B). Immunohistochemical analyses showed that Oridonin significantly eliminated AKT effector phosphorylation and blocked cell proliferation in the iPIK3CA^{H1047R} mammary outgrowths (Figure 6C–6E). These results establish that Oridonin prevents cell transformation by blocking AKT and downstream mTOR signaling in response to the induction of PIK3CA^{H1047R}.

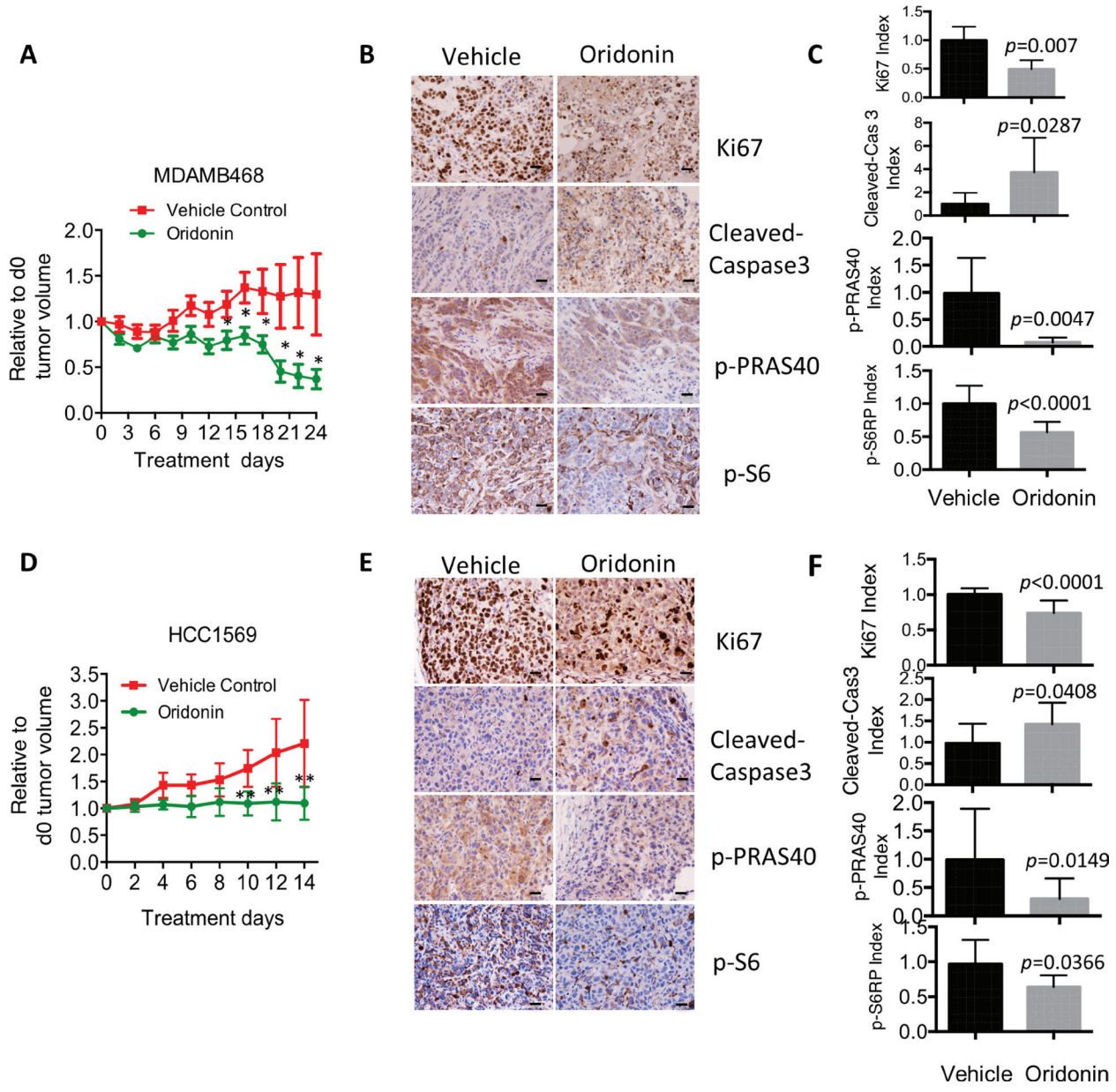


Figure 5: Oridonin impairs *in vivo* cell growth in breast cancer with hyperactivation of AKT signaling. (**A**) Growth of triple negative breast cancer cells (MDAMB468) in nude mice treated with vehicle (Tn = 7) or Oridonin (Tn = 8, 15 mg/kg) by intraperitoneal injection. Mean ± SD values are presented. $^{*}p < 0.05$ (Student's *t* test). (**B**) Growth of HER2-positive breast cancer cells (HCC1569) in nude mice treated with vehicle (Tn = 6) or Oridonin (Tn = 10, 15 mg/kg) by intraperitoneal injection. Mean ± SD values are presented. $^{**}p < 0.01$ (Student's *t* test). (**C**, **D**) Immunohistochemical (IHC) analysis of AKT pathway, proliferation (Ki67), and apoptosis (cleaved caspase 3) in tumors harvested from animals treated with vehicle or Oridonin for 3 days. Scale bar represents 20 um. (**E**, **F**) Quantitative analyses of 6 IHC images randomly obtained from three mice. *p* values were assessed by Student's *t* test.

DISCUSSION

In this study, we screened a library of 441 TCM plant extracts by examining their effect on cell viability in a HMEC-PIK3CA^{H1047R} cell model with constitutively active AKT signaling. Nineteen of the extracts impaired cell growth as efficiently as the pan PI3K inhibitor BKM120 or dual PI3K/mTOR inhibitor BEZ235. We showed that Oridonin, an extract from *Rabdosia rubescens*, reduced cell viability most efficiently. Rather than inhibit PI3K activity directly, Oridonin bound to AKT1 and may function as a potential ATP-competitive AKT inhibitor. Oridonin selectively impaired the cell growth of p-AKT^{High} human breast cancers *in vitro* and *in vivo* by preferentially blocking AKT-mTOR signaling. Oridonin also efficiently prevented the initiation of mouse mammary tumors driven by PIK3CA^{H1047R} *in vivo*. Our results suggest that Oridonin may serve as a potent and selective therapeutic agent in patients bearing breast cancers with hyperactivation of AKT signaling.

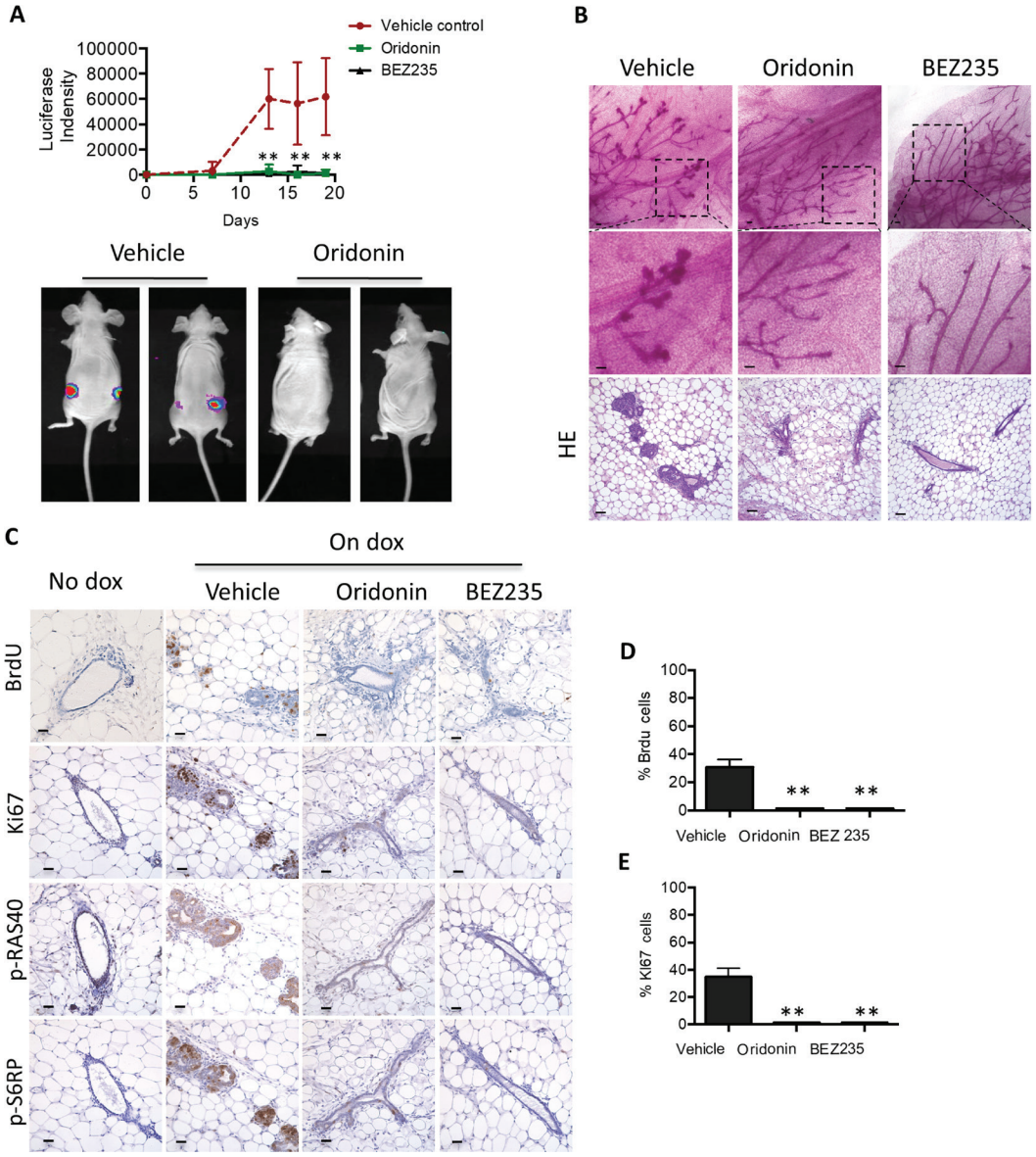


Figure 6: Oridonin prevents initiation of mouse mammary tumors carrying PIK3CA$_{H1047R}$. (**A**) Mammary glands from bitransgenic mice MMTV-rtTA-tetO-PIK3CA$_{H1047R}$ were transplanted into NCr nude mice. Doxycycline was introduced into the diet 8 weeks after transplantation. Intensities of luciferase were analyzed in mice bearing doxycycline-inducible PIK3CA$_{H1047R}$ mammary glands after treatment with vehicle ($n = 9$), Oridonin ($n = 9$) or BEZ235 ($n = 4$) (top panel). $^{*}p < 0.01$, $^{**}p < 0.001$ (Student's t test). Representative images at the time of the last treatment are shown (bottom panel). (**B**) Mammary gland whole mounts prepared from mice at the end of treatment with vehicle, Oridonin, or BEZ325, Scale bars represent 20 um. **(C–E)** Immunohistochemical analysis of proliferation, assessed by Brdu and Ki67 staining, and AKT signaling in tumors harvested from animals treated with vehicle, Oridonin, or BEZ325 at 18 days. Scale bars represent 20 um. Quantitative analyses of 6 images randomly obtained from three mice. $^{*}p < 0.01$, $^{**}p < 0.001$ (Student's t test).

Although the popularity of herbal therapies has increased globally in recent years, their efficacy, safety, mechanisms of action, and potential as novel therapeutic agents remain poorly defined. *Rabdosia rubescens* and its extracts were shown to suppress disease progression, reduce tumor burden, and prolong survival in patients with esophageal cancer, gastric carcinoma, or liver cancer [15–18]. The antitumor activity of Oridonin, a bitter tetracycline diterpenoid compound isolated from *Rabdosia rubescens*, was demonstrated in many types of cancers including prostate, breast, non-small cell lung cancers, acute leukemia, glioblastoma, and human melanoma [15–19]. However, the mechanisms underlying the antitumor activity of Oridonin remain largely unknown. Here, we showed for the first time that Oridonin directly bound to AKT1 and may function as a potential ATP-competitive AKT inhibitor. Oridonin impaired cell proliferation and induced apoptosis in a p-AKT dependent manner. Oridonin effectively inhibited the phosphorylation of pan-AKT substrates and subsequently blocked downstream effector mTOR signaling in breast tumor cells with HER2 amplification/overexpression (SKBR3 and HCC1569), PTEN loss (MDAMB468, HMEC-shPTEN), mutant PI3K (HMEC-PIK3CA^{H1047R}, mouse mammary epithelium with PIK3CA^{H1047R}), and AKT1 overexpression (HMEC-myr-ATK1) (Figures 2 and 4), suggesting broad therapeutic benefits of Oridonin in breast cancer cells with hyperactivation of AKT signaling. Importantly, breast cancer cells without AKT activation (MDAMB231) were less sensitive to Oridonin, with IC50 values 10 times higher than those in cells with AKT activation. The non-transformed cell line MCF10A was far less sensitive to Oridonin, with IC50 value 100 times higher than that in breast cancer cells with AKT activation (Supplementary Figure 3), leading to potent and selective cytotoxicity while sparing normal cells. The selective cytotoxicity of Oridonin in p-AKT^{High} breast cancer cells provides a therapeutic advantage that cannot be achieved by the pan PI3K inhibitor BKM120, dual PI3K/mTOR inhibitor BEZ235, AKT inhibitor MK2206 (Supplementary Figure 4). In view of potential AKT-independent signaling, which exhibits only minimal AKT activation, downstream of oncogenic PI3KCA mutation in human cancers [25], the phosphorylation level of AKT should be considered as a therapeutic marker of Oridonin treatment. Notably, Oridonin efficiently prevented the initiation of mouse mammary tumors with PI3KCA mutant cells (Figure 6) suggesting the potential application and advantages of *Rabdosia rubescens* or its extracts for carriers of breast cancer susceptibility genes who are at high risk of developing breast cancer; for example, carriers of germline PTEN mutation or BRAC1 mutation show increased AKT signaling [26–28]. In addition to Oridonin, another 18 extracts from *Glycyrrhiza uralensis Fisch* or *Sophora flavescens Ait* inhibited the growth of HMEC-PIK3CA^{H1047R} cells by more than 80% compared to cells treated with DMSO (Supplementary Table 1), suggesting the potential role of other TCM plant extracts in inhibition of PI3K signaling and cancer therapy.

Our results provide concrete evidence that *Rabdosia rubescens* extract Oridonin decreases AKT signaling and selectively inhibits tumor growth in p-AKT^{High} breast tumors cells. Of note, to date pan-or isoform-selective inhibitor of PI3K inhibitors, AKT inhibitors, mTOR inhibitors, and dual PI3K/mTOR inhibitors have not yielded durable or efficacious clinical results, Oridonin offers promise of both increased efficacy and reduced toxicity compared with single PI3K, AKT, or even dual PI3K/mTOR inhibitors. Together, our data suggest that in the context of p-AKT^{High} breast cancers, Oridonin may serve as a potent and durable therapeutic agent and should be considered for clinical application.

MATERIALS AND METHODS

TCM plant extract library

The production of the plant extract library was obtained by the ICCB-Longwood Screening Facility at Harvard Medical School (https://iccb.med.harvard.edu). The library contains 441 extracts from plants used in traditional Chinese medicine. Crude extracts from the plants were obtained and further fractionated to eliminate nuisance compounds, especially those of high molecular weight or high polarity [14].

LC/MS and NMR techniques for compound characterization

HPLC purifications were carried out using an Agilent 1200 series HPLC system equipped with a photo-diode array detector and a Phenomenex 4 µm Hydro semi-preparative column. Compounds eluted at minute 25 when run using the following gradient: holding 20% ACN + 0.1% formic acid (FA)/H_2O + 0.1% FA for 5 min, followed by a shallow gradient to 40% ACN + 0.1% FA/H_2O + 0.1% FA over 30 min and then fast gradient to 100% ACN + 0.1% FA over 5 min. LR-LCMS data was obtained using an Agilent 1200 series HPLC system equipped with a photo-diode array detector and a 6130 quadrupole mass spectrometer. NMR spectra were recorded with pyridine as an internal standard (δ_H 8.71, 7.58, and 7.22; δ_C 150.4, 135.9, and 123.9) on a Varian Oxford 600 MHz spectrometer equipped with a 5 mm AutoX HCN triple res inverse probe. Compounds were identified either using authentic samples or comparing their chemical shifts with those reported in the literature [14].

Cell culture

MDAMB468 and MDAMB231 cells were cultured in 10% fetal bovine serum (FBS) DMEM with penicillin/

streptomycin. SKBR3 and HCC1569 cells were cultured in 10% FBS RPMI1640 with penicillin/streptomycin. HMEC-PIK3CA^{H1047R}, HMEC-shPTEN, and HMEC-myr-AKT1 cells were cultured in 2.5% FBS DMEM/F12 supplemented with insulin, epidermal growth factor, and hydrocortisone, as described previously [29].

Cell viability assay

Cell viability was assessed using a CellTiter-Glo luminescent cell viability assay (Promega). Equal numbers of cells were plated in 96-well plates and treated with serial dilutions of inhibitors for 72 hrs. Two independent experiments were performed per cell line, each with triplicate measurements.

Western blotting

Cells were lysed in 1% NP-40 buffer supplemented with protease and phosphatase inhibitors (Roche). Equal amounts of proteins were resolved by SDS-PAGE and transferred to nitrocellulose membranes for western blotting. The primary antibodies used were specific for the following proteins: p-PRAS40-T246 (Invitrogen), p-AKT S473, p-AKT T308, p-S6 S240/244, p-4EBP1, p110a, PTEN, AKT1, p-AKT substrate (RXXS*/T*), and AKT (all from Cell Signaling Technology). Secondary anti-mouse and anti-rabbit IgG fluorophore conjugated antibodies were used to visualize the indicated proteins on an Odyssey scanner (Li-Cor).

Kinetic analysis of oridonin-AKT1 binding

Surface plasmon resonance (SPR) measurements of the interaction of Oridonin with purified human recombinant AKT1 protein (Abcam) were performed on a BIAcore 3000 instrument. AKT1 was immobilized on BIAcore sensor chips (type CM5, GE Healthcare Life Sciences) at 14450 RU using an amine coupling kit. Oridonin was dissolved in 1% Pluronic F68 (Sigma) detergent by sonication at 1 mg/mL. Running buffer used in the experiment was HEPES/NaCl buffer containing 1% Pluronic F68 detergent at a flow of 20 µl/minute Oridonin (diluted to 2 µM) was injected for 7 minutes over the chip surface in a Biacore 3000 machine and then allowed to dissociate for a further 7 minutes. The binding analysis was performed using BIA evaluation software.

Histology and immunohistochemistry (IHC)

Formalin-fixed paraffin-embedded tissue sections were prepared by the Biorepository & Tissue Analysis Shared Resource, Hollings Cancer Center. BrdU labeling and staining were done according to the manufacturer's instructions (BD Biosciences). IHC was performed with antibodies against Ki67 (Vector labs), p-PRAS40-T246 (Invitrogen), p-S6 (Cell Signaling Technology), and cleaved-caspase 3 (Cell Signaling Technology). For quantification of IHC, 6 images were taken per tumor section and analyzed using the Visiopharm Integrator System (Visiopharm).

Xenograft studies

All animal experiments were conducted in accordance with animal use guidelines of the National Institutes of Health using protocols approved by the Medical University of South Carolina and the Dana-Farber Cancer Institute Animal Care and Use Committee. Breast cancer cells were harvested and resuspended in 40% Matrigel-Basement Membrane Matrix, LDEV-free (BD Biosciences), and then injected (100 µl per site) into the fourth pair of mammary fat pads of nude mice (CrTac: NCr-Foxn1nu). Tumors were measured in two dimensions using manual calipers. Tumor volume was calculated using the formula: Volume = 0.5 × length × width × width. Tumor volume was measured every 2–3 days. Upon harvesting, tumors were fixed in formalin overnight and then in 70% ethanol for histopathology analysis.

Inhibitor administration

Animals were treated with Oridonin (15 mg/kg; Chengdu Purification Technology Development Co., Ltd, Chuengdu, China) in 1% Pluronic F68 (Sigma) or vehicle (1% Pluronic 68) daily by intraperitoneal (IP) injection as described previously [19]. BEZ235 (Haoyuan Chemo express Co. Ltd, Shanghai, China) was reconstituted 1:9 in 1-methyl-2 pyrolidone (NMP; Sigma) and polyethylene glycol 300 (PEG300; Fluka Analytical). Mice were treated with this compound formulation at 45 mg/kg daily (QD) by oral gavage.

Mammary fragment transplantation

Mammary glands were isolated from 8-week-old female MMTV-rtTA-tetO-PIK3CA^{H1047R} mice [24]. Mammary gland fragments were transplanted into cleared fat pads of 3-week-old NCr nude female mice as described previously [30]. Doxycycline induction was performed 8 weeks post-transplantation by introduction of a 2500 ppm doxycycline containing diet [31].

Bioluminescence imaging

Mice were anesthetized with ketamine and xylazine and administered D-luciferin (Promega) IP to monitor luciferase gene expression *in vivo*. Images were analyzed using KODAK Molecular Imaging Software (version 4.5.0b6 SE).

Mammary gland whole mounts

Transplanted mammary glands were harvested and mounted on glass slides. Slides were fixed in an

ethanol-glacial acid mixture and stained with carmine red, followed by dehydration and a final clearing in toluene as described previously [30].

Statistical analyses

Statistical analysis was performed as described for each experiment. All data are presented as mean ± s.d. Student's *t*-test (two-tailed) was used to compare two groups ($p < 0.05$ was considered significant) for independent samples.

ACKNOWLEDGMENTS AND FUNDING

We thank C. Shamu for providing TCM library. This work was supported by the Institutional Research Grant of Hollings Cancer Center and the Medical University of South Carolina (IRG-97-219-14)(QW); NIH grants R35 CA210057 CA187918 (TMR and JJZ), 1P50CA168504 (TMR and JJZ); the Breast Cancer Research Foundation (JJZ); Rosanna's Rush for Research (JJZ); The Starr Foundation; and the Marcus Foundation to the Osher Institute of Medicine at Harvard Medical School. The BIAcore facility at the Department of Regenerative Medicine and Cell Biology was supported by the South Carolina Center of Biomedical Research Excellence (SC COBRE) for Developmentally Based Cardiovascular Diseases grant from The National Institute of General Medical Sciences (NIGMS) of the National Institutes of Health (NIH) (Award Number P30GM103342 to R.R. Markwald).

CONFLICTS OF INTEREST

The authors declare no conflicts of interest.

REFERENCES

1. Cully M, You H, Levine AJ, Mak TW. Beyond PTEN mutations: the PI3K pathway as an integrator of multiple inputs during tumorigenesis. Nature Reviews Cancer. 2006; 6:184–192.
2. Parsons R. Human cancer, PTEN and the PI-3 kinase pathway. Seminars In Cell & Developmental Biology. 2004; 15:171–176.
3. Engelman JA. Targeting PI3K signalling in cancer: opportunities, challenges and limitations. Nature Reviews Cancer. 2009; 9:550–562.
4. Hynes NE, Lane HA. ERBB receptors and cancer: the complexity of targeted inhibitors. Nature Reviews Cancer. 2005; 5:341–354.
5. Bachman KE, Argani P, Samuels Y, Silliman N, Ptak J, Szabo S, Konishi H, Karakas B, Blair BG, Lin C, Peters BA, Velculescu VE, Park BH. The PIK3CA gene is mutated with high frequency in human breast cancers. Cancer Biol Ther. 2004; 3:772–775.
6. Buttitta F, Felicioni L, Barassi F, Martella C, Paolizzi D, Fresu G, Salvatore S, Cuccurullo F, Mezzetti A, Campani D, Marchetti A. PIK3CA mutation and histological type in breast carcinoma: high frequency of mutations in lobular carcinoma. J Pathol. 2006; 208:350–355.
7. Lee JW, Soung YH, Kim SY, Lee HW, Park WS, Nam SW, Kim SH, Lee JY, Yoo NJ, Lee SH. PIK3CA gene is frequently mutated in breast carcinomas and hepatocellular carcinomas. Oncogene. 2005; 24:1477–1480.
8. Levine DA, Bogomolniy F, Yee CJ, Lash A, Barakat RR, Borgen PI, Boyd J. Frequent mutation of the PIK3CA gene in ovarian and breast cancers. Clinical Cancer Research. 2005; 11:2875–2878.
9. Stemke-Hale K, Gonzalez-Angulo AM, Lluch A, Neve RM, Kuo WL, Davies M, Carey M, Hu Z, Guan Y, Sahin A, Symmans WF, Pusztai L, Nolden LK, et al. An integrative genomic and proteomic analysis of PIK3CA, PTEN, and AKT mutations in breast cancer. Cancer Research. 2008; 68:6084–6091.
10. Yuan TL, Cantley LC. PI3K pathway alterations in cancer: variations on a theme. Oncogene. 2008; 27:5497–5510.
11. Carpten JD, Faber AL, Horn C, Donoho GP, Briggs SL, Robbins CM, Hostetter G, Boguslawski S, Moses TY, Savage S, Uhlik M, Lin A, Du J, et al. A transforming mutation in the pleckstrin homology domain of AKT1 in cancer. Nature. 2007; 448:439–444.
12. Clark AR, Toker A. Signalling specificity in the Akt pathway in breast cancer. Biochemical Society Transactions. 2014; 42:1349–1355.
13. Fruman DA, Rommel C. PI3K and cancer: lessons, challenges and opportunities. Nature Reviews Drug Discovery. 2014; 13:140–156.
14. Eisenberg DM, Harris ES, Littlefield BA, Cao S, Craycroft JA, Scholten R, Bayliss P, Fu Y, Wang W, Qiao Y, Zhao Z, Chen H, Liu Y, et al. Developing a library of authenticated Traditional Chinese Medicinal (TCM) plants for systematic biological evaluation—rationale, methods and preliminary results from a Sino-American collaboration. Fitoterapia. 2011; 82:17–33.
15. Chen S, Gao J, Halicka HD, Huang X, Traganos F, Darzynkiewicz Z. The cytostatic and cytotoxic effects of oridonin (Rubescenin), a diterpenoid from Rabdosia rubescens, on tumor cells of different lineage. International Journal Of Oncology. 2005; 26:579–588.
16. Fujita T, Takeda Y, Sun HD, Minami Y, Marunaka T, Takeda S, Yamada Y, Togo T. Cytotoxic and antitumor activities of Rabdosia diterpenoids. Planta Medica. 1988; 54:414–417.
17. Ikezoe T, Chen SS, Tong XJ, Heber D, Taguchi H, Koeffler HP. Oridonin induces growth inhibition and apoptosis of a variety of human cancer cells. International Journal Of Oncology. 2003; 23:1187–1193.

18. Li XT, Lin C, Li PY, Zhang TM. [Comparative study on the sensitivities of seven human cancer cell lines to rubescensine A]. Acta Pharmaceutica Sinica. 1985; 20:243–246.

19. Zhou GB, Kang H, Wang L, Gao L, Liu P, Xie J, Zhang FX, Weng XQ, Shen ZX, Chen J, Gu LJ, Yan M, Zhang DE, et al. Oridonin, a diterpenoid extracted from medicinal herbs, targets AML1-ETO fusion protein and shows potent antitumor activity with low adverse effects on t(8;21) leukemia *in vitro* and *in vivo*. Blood. 2007; 109:3441–3450.

20. Filbin MG, Dabral SK, Pazyra-Murphy MF, Ramkissoon S, Kung AL, Pak E, Chung J, Theisen MA, Sun Y, Franchetti Y, Sun Y, Shulman DS, Redjal N, et al. Coordinate activation of Shh and PI3K signaling in PTEN-deficient glioblastoma: new therapeutic opportunities. Nature Medicine. 2013; 19:1518–1523.

21. Yang J, Cron P, Good VM, Thompson V, Hemmings BA, Barford D. Crystal structure of an activated Akt/protein kinase B ternary complex with GSK3-peptide and AMP-PNP. Nature Structural Biology. 2002; 9:940–944.

22. Trott O, Olson AJ. AutoDock Vina: improving the speed and accuracy of docking with a new scoring function, efficient optimization, and multithreading. Journal Of Computational Chemistry. 2010; 31:455–461.

23. Lin K, Lin J, Wu WI, Ballard J, Lee BB, Gloor SL, Vigers GP, Morales TH, Friedman LS, Skelton N, Brandhuber BJ. An ATP-site on-off switch that restricts phosphatase accessibility of Akt. Science Signaling. 2012; 5:ra37.

24. Liu P, Cheng H, Santiago S, Raeder M, Zhang F, Isabella A, Yang J, Semaan DJ, Chen C, Fox EA, Gray NS, Monahan J, Schlegel R, et al. Oncogenic PIK3CA-driven mammary tumors frequently recur via PI3K pathway-dependent and PI3K pathway-independent mechanisms. Nature Medicine. 2011; 17:1116–1120.

25. Vasudevan KM, Barbie DA, Davies MA, Rabinovsky R, McNear CJ, Kim JJ, Hennessy BT, Tseng H, Pochanard P, Kim SY, Dunn IF, Schinzel AC, Sandy P, et al. AKT-independent signaling downstream of oncogenic PIK3CA mutations in human cancer. Cancer Cell. 2009; 16:21–32.

26. Juvekar A, Burga LN, Hu H, Lunsford EP, Ibrahim YH, Balmana J, Rajendran A, Papa A, Spencer K, Lyssiotis CA, Nardella C, Pandolfi PP, Baselga J, et al. Combining a PI3K inhibitor with a PARP inhibitor provides an effective therapy for BRCA1-related breast cancer. Cancer Discovery. 2012; 2:1048–1063.

27. Wang Q, Von T, Bronson R, Ruan M, Mu W, Huang A, Maira SM, Zhao JJ. Spatially distinct roles of class Ia PI3K isoforms in the development and maintenance of PTEN hamartoma tumor syndrome. Genes Dev. 2013; 27:1568–1580.

28. Wang Q, Weisberg E, Zhao JJ. The gene dosage of class Ia PI3K dictates the development of PTEN hamartoma tumor syndrome. Cell Cycle (Georgetown, Tex). 2013; 12:3589–3593.

29. Zhao JJ, Gjoerup OV, Subramanian RR, Cheng Y, Chen W, Roberts TM, Hahn WC. Human mammary epithelial cell transformation through the activation of phosphatidylinositol 3-kinase. Cancer Cell. 2003; 3:483–495.

30. Utermark T, Rao T, Cheng H, Wang Q, Lee SH, Wang ZC, Iglehart JD, Roberts TM, Muller WJ, Zhao JJ. The p110alpha and p110beta isoforms of PI3K play divergent roles in mammary gland development and tumorigenesis. Genes Dev. 2012; 26:1573–1586.

31. Goel S, Wang Q, Watt AC, Tolaney SM, Dillon DA, Li W, Ramm S, Palmer AC, Yuzugullu H, Varadan V, Tuck D, Harris LN, Wong KK, et al. Overcoming Therapeutic Resistance in HER2-Positive Breast Cancers with CDK4/6 Inhibitors. Cancer Cell. 2016; 29:255–269.

Manuscript Details

Manuscript number	AJPA_2019_139
Title	The Family Misfit: Mechanisms of ErbB3 Action in Human Neoplasia
Short title	Role of erbB3 in Human Cancers
Article type	Review Article

Abstract

It is well established that the epidermal growth factor receptor (EGFR), erbB2/HER2 and, to a lesser extent, erbB4/HER4 promote the pathogenesis of many types of human cancer. In contrast, the role that erbB3/HER3, the fourth member of the erbB family of receptor tyrosine kinases, plays in these diseases is poorly understood and, until recently, underappreciated. In large part, this was because early structural and functional studies suggested that erbB3 had little, if any, intrinsic tyrosine kinase activity and thus was unlikely to be an important therapeutic target. Since that time, however, numerous publications have demonstrated an important role for erbB3 in carcinogenesis, metastasis and acquired drug resistance. Further, somatic ERBB3 mutations are frequently encountered in many types of human cancers. Dyregulation of erbB3 trafficking as well as cooperation with other receptor tyrosine kinases further enhances erbB3's role in tumorigenesis and drug resistance. As a result of these advances in our understanding of the structure and biochemistry of erbB3, and a growing focus on the development of precision and combinatorial therapeutic regimens, erbB3 is increasingly considered to be an important therapeutic target in human cancers. In this review, we discuss the unique structural and functional features of erbB3 and how this information is being used to develop effective new therapeutic agents that target erbB3 in human cancers.

Keywords	Cancer genomics; receptor tyrosine kinases; oncogenes; cytoplasmic signaling cascades; cancer therapeutics
Taxonomy	Cell Signaling, Receptor Tyrosine Kinase, Antibody Therapy of Cancer

Corresponding Author	Steven Carroll
Order of Authors	Laurel Black, Jody Longo, Steven Carroll

Submission Files Included in this PDF

File Name [File Type]

ErbB3 Submission Letter 5 March 2019.pdf [Cover Letter]

erbB3 Review Submitted Version.docx [Manuscript File]

Figure 1.tif [Figure]

Figure 2.tif [Figure]

Figure 3.tif [Figure]

ErbB3 Review Table 1.docx [Table]

To view all the submission files, including those not included in the PDF, click on the manuscript title on your EVISE Homepage, then click 'Download zip file'.

MUSC Health
Medical University of South Carolina

Steven L. Carroll, MD, PhD, FASCP, FCAP
Professor and Chair
Gordon R. Hennigar, Jr., MD, Endowed Chair in Pathology
Chief, Pathology and Lab Medicine ICCE
Director, Carroll A. Campbell, Jr. Brain Bank
Director, HCC Biorepository & Tissue Analysis Shared Resource

Pathology & Laboratory Medicine
171 Ashley Avenue, MSC 908
Charleston, SC 29425-9080
Tel 843 792 3121
Fax 843 792 0555

musc.edu/pathology
muschealth.org

March 5, 2019

Martha Furie, Ph.D.
Editor-in-Chief, *The American Journal of Pathology*

Dear Dr. Furie,

In response to your request that Associate Editors consider submitting a review article to the American Journal of Pathology, enclosed please find our Invited Review article entitled "The Family Misfit: Mechanisms of ErbB3 Action in Human Neoplasia". The role of the epidermal growth factor receptor (EGFR/HER1), erbB2 (HER2) and, to a lesser extent, erbB4 (HER4) in the pathogenesis of human cancers is well established. In contrast, the contributions that erbB3 (HER3) make to these disease processes have historically been less well understood, in part because investigations into erbB3 action were hampered by the widely held perception that this receptor is "kinase-dead". This is beginning to change, however, as new studies are increasingly acknowledging the role that erbB3 plays in the pathogenesis of human cancers. Further, we have a growing appreciation of the fact that the dimerization of erbB3 with other erbB receptors results in the formation of signaling complexes with distinct characteristics, in large part due to the unique interactions that erbB3 fosters with other cytoplasmic signaling molecules. In addition, the identification of numerous point mutations in the *ERBB3* gene in human cancers has allowed us to identify key amino acid residues and associated cytoplasmic signaling molecule docking sites that are involved in mediating erbB3 actions. These and other advances have now stimulated the development of promising new therapeutic agents designed to specifically target erbB3. We discuss all of these topics in detail in our review.

Best regards,

Steven L. Carroll, MD, PhD, FASCP, FCAP

REVIEW ARTICLE

The Family Misfit: Mechanisms of ErbB3 Action in Human Neoplasia

LAUREL BLACK, JODY FROMM LONGO AND STEVEN L. CARROLL

Department of Pathology and Laboratory Medicine, Medical University of South Carolina, Charleston, SC 29425-9080

Running head: Role of erbB3 in Human Cancers

Words in Abstract: 216

Words in Text: 5,998

Number of References: 91

Number of Figures: Three

Number of Tables: One

Key Words: Cancer genomics; receptor tyrosine kinases; oncogenes; cytoplasmic signaling cascades; cancer therapeutics.

Supported by: The National Institute of Neurological Diseases and Stroke (R01 NS048353), the National Cancer Institute (R01 CA122804), the Department of Defense (X81XWH-09-1-0086, W81XWH-11-1-0498, W81XWH-12-1-0164, W81XWH-14-1-0073 and W81XWH-15-1-0193) and The Children's Tumor Foundation (2014-04-001 and 2015-05-007).

Address correspondence to:
Steven L. Carroll, MD, PhD
Professor and Chair
Department of Pathology and Laboratory Medicine
171 Ashley Avenue, MSC 908
Medical University of South Carolina
Charleston, SC 29425-9080
Phone: (843) 792-3121
Fax: (843) 792-0555
E-mail: carrolst@musc.edu

Abstract

It is well established that the epidermal growth factor receptor (EGFR), erbB2/HER2 and, to a lesser extent, erbB4/HER4 promote the pathogenesis of many types of human cancer. In contrast, the role that erbB3/HER3, the fourth member of the erbB family of receptor tyrosine kinases, plays in these diseases is poorly understood and, until recently, underappreciated. In large part, this was because early structural and functional studies suggested that erbB3 had little, if any, intrinsic tyrosine kinase activity and thus was unlikely to be an important therapeutic target. Since that time, however, numerous publications have demonstrated an important role for erbB3 in carcinogenesis, metastasis and acquired drug resistance. Further, somatic *ERBB3* mutations are frequently encountered in many types of human cancers. Dyregulation of erbB3 trafficking as well as cooperation with other receptor tyrosine kinases further enhances erbB3's role in tumorigenesis and drug resistance. As a result of these advances in our understanding of the structure and biochemistry of erbB3, and a growing focus on the development of precision and combinatorial therapeutic regimens, erbB3 is increasingly considered to be an important therapeutic target in human cancers. In this review, we discuss the unique structural and functional features of erbB3 and how this information is being used to develop effective new therapeutic agents that target erbB3 in human cancers.

Nearly four decades ago, a 170 kDa cell surface glycoprotein was identified as the elusive receptor for epidermal growth factor (EGF)[1]. Shortly thereafter, it was recognized that the EGF receptor (EGFR) was encoded by the c-*erbB1* proto-oncogene[2, 3] and that it was closely related to three other cell surface glycoproteins known as erbB2 [also known as c-Neu or HER2 (human EGF receptor 2)][4], erbB3 (HER3)[5, 6] and erbB4 (HER4)[7]. Today, we know these four glycoproteins as the erbB family of receptor tyrosine kinases (RTKs). This family of growth factor receptors transmits signals from the extracellular milieu into the cellular interior, resulting in the activation of multiple cytoplasmic and nuclear signaling cascades that regulate myriad cellular functions. ErbB receptors are widely expressed in a variety of neuronal, epithelial and mesenchymal cell types[8, 9]. In keeping with their wide expression, careful analyses of the phenotypes of knockout mouse models and results obtained in other experimental systems have demonstrated that erbB receptors play key roles in the development of essential cell types within the cardiovascular, nervous, musculoskeletal and other organ systems. It is also becoming increasingly apparent that erbB receptors are essential for the pathogenesis of a wide variety of human cancer types[10]. This has motivated the development of numerous therapeutic agents that target erbB receptors such as the monoclonal anti-erbB2 antibody trastuzumab and gefitinib, a small molecular inhibitor of EGFR. To date, the majority of studies examining the role that erbB receptors play in cancer pathogenesis have focused on EGFR or erbB2. Pharmaceutical development has paralleled this focus, emphasizing the development of agents that target EGFR or erbB2.

In comparison to EGFR and erbB2, the functions of erbB3 and erbB4 and their role in human disease have been less well studied. In the case of erbB3, this reflects, in part, the widely held perception that erbB3 is completely “kinase-dead”. However, recent findings have begun to

challenge this widely-held perception. Furthermore, there is a growing body of evidence indicating that erbB3 is essential for the pathogenesis of many human cancers. It is also becoming apparent that the physical interaction of erbB3 with other erbB receptors results in the formation of potently pro-tumorigenic signaling complexes[11], in large part due to the unique ability of erbB3 to activate key cytoplasmic signaling pathways. These studies, together with the identification of numerous somatic and germline mutations in the *ERBB3* gene in human cancers, are now fueling the functional characterization of key amino acid residues in this RTK. In light of these and other advances, it is quite understandable that several laboratories have begun to pursue the development of new therapeutic agents that specifically target and inhibit erbB3.

In this review, we will consider new findings about the unique functional characteristics of erbB3 and its role in human carcinogenesis. To explain what makes erbB3 special and how it differs from other erbB family members, we will first discuss our current understanding of the erbB family of RTKs, including their structure, their distinct activating ligands, the structural changes induced by ligand binding and how this leads to the formation of signaling complexes with distinct functional characteristics. We will turn to the unique functional characteristics of erbB3, including the disparate opinions regarding its tyrosine kinase activity, how its structural features modify its function during the formation of active signaling complexes and the mechanisms by which erbB3 activity is modulated. We will discuss how erbB3 signaling regulates cellular function, contrasting erbB3 function in normal development with its function in cancer. We will then conclude by discussing how this new understanding of erbB3 action is guiding the development of promising new therapeutic agents.

The ErbB Subfamily of RTKs: Their Structure, Their Upstream Activators and the Downstream Consequences Triggered by Receptor Activation

The four members of the erbB family of receptor tyrosine kinases (sometimes referred to as the epidermal growth factor receptor family) share a common structure that includes an N-terminal extracellular ligand binding domain (the ectodomain), a single transmembrane domain, an intracellular juxtamembrane domain, a tyrosine kinase domain and a C-terminal autophosphorylation domain; the latter three domains are collectively referred to as the endodomain. This shared structure reflects the fact that all four erbB receptors function similarly—after binding a ligand, they share the common property of interacting with one another, thereby activating their intrinsic tyrosine kinase activity which in turn results in the phosphorylation of each receptor's endodomain and the recruitment of cytoplasmic signaling proteins that dock to these phosphorylated residues. Despite their similarities in structure and function, though, numerous studies have shown that the EGFR, erbB2, erbB3 and erbB4 also have unique functional characteristics. In keeping with this, although the erbB domains noted above do show partial sequence homology, the precise amino acid sequence of each of these domains differs between erbB family members. The degree of sequence divergence is variable from domain to domain—the domains with the highest degree of sequence homology are those that mediate overlapping functions shared by different erbB receptors, while the least conserved domains are typically those that mediate distinct functions performed by individual erbB family members. In addition, the size of these domains and the amino acid positions where they are located varies slightly between different erbB receptors. Overall, the juxtamembrane and tyrosine kinase domains have the greatest degree of sequence homology (59-81% sequence identity) amongst the erbB family members[12]. The high degree of sequence conservation in the

erbB tyrosine kinase domains undoubtedly reflects the constraints imposed by the enzymatic activity of this domain. Given this high degree of sequence homology, it is also not surprising that many small molecular erbB inhibitors, which bind to the ATP-binding pocket in the tyrosine kinase domain, "cross-hit" multiple erbB receptors. In contrast, the ectodomain and the autophosphorylation domain (12-30% sequence identity) are the two most structurally divergent domains[12]. The limited conservation of the ectodomain reflects, in part, the fact that each erbB receptor binds a different cocktail of ligands. The autophosphorylation domain contains binding sites for specific docking proteins that orchestrate the activation or repression of downstream signal transduction pathways. The low sequence homology within the erbB autophosphorylation domains is thus consistent with the observation that many of the intracellular signaling cascades regulated by specific erbB receptors are unique to that receptor.

In addition to the variations in the domains shared by all erbB receptors, some erbB genes can generate structural variants in which alternative mRNA splicing introduces additional functional domains. Perhaps the best known of these are the erbB4 structural variants seen in tissues that express this RTK. In addition to the regions noted above, erbB4 can contain either of two domains in the "stalk" region N-terminal to the transmembrane domain that are known as juxtamembrane-A (JM-A) and juxtamembrane-B (JM-B). Unlike JM-B, JM-A contains a site which can be targeted for proteolytic cleavage. Proteolytic cleavage of JM-A by tumor necrosis factor-α converting enzyme (TACE)/ADAM17[13, 14] followed by intramembranous cleavage by the γ-secretase complex[15, 16] releases the 80 kDa erbB4 intracellular domain into the cellular interior where it can interact with mitochondria to promote apoptosis[17, 18]. The erbB4 intracellular domain can also enter the nucleus, where it interacts with TAB2 and N-CoR to form a transcriptional regulatory complex[19]. In addition, erbB4 variants exist that differ in the

presence or absence of an alternatively spliced intracellular 16 amino acid Cyt1 domain[20, 21], which contains a docking site for the p85 regulatory subunit of phosphatidylinositol 3-kinase (PI3K). Although we (Brosius et al., submitted) and others[22] have demonstrated that these erbB4 variants do indeed modulate PI3K signaling, the physiologic impact of this mode of erbB4 signaling at an organismal level remains incompletely understood, a knowledge gap that hopefully will be filled by the analysis of *Erbb4*-Cyt1$^{flox/flox}$ mice that we have recently developed in collaboration with Dr. Andres Buonanno. As is discussed below, splice variants that modify the structure of erbB3 (e.g., nuclear 50 and 80 kDa variants) also exist. Consequently, although the masses usually cited for the different erbB receptors (170 kDa for EGFR; 180 kDa for erbB2; 185 kDa for erbB3 and erbB4) in most publications are certainly accurate, investigators can and do encounter erbB proteins that differ significantly from these norms.

With the exception of erbB2, multiple EGF family ligands can bind to the ectodomain of each of the erbB receptors, resulting in their activation. Based on their relative affinity for individual erbB receptors, EGF family ligands can be divided into three groups. The first group of ligands, which share the common property of binding only to EGFR, includes EGF, amphiregulin, transforming growth factor α (TFGα), and epigen (Figure 1A). The second group of ligands, which can activate both EGFR and erbB4, is represented by epiregulin, betacellulin and heparin-binding EGF. The third group of EGF family ligands encompasses multiple splice variants of neuregulin-1 (NRG1), NRG2, NRG3 and NRG4; this growth factor subfamily binds to both erbB3 and erbB4 (NRG1, NRG2) or to erbB4 only (NRG3, NRG4)[23]. None of the EGF family ligands noted above bind directly to and activate erbB2. However, mucin-4 (Muc4), a

transmembrane protein that contains two EGF-like domains, is capable of activating erbB2 via direct interaction. For this to occur, erbB2 and Muc4 must be coexpressed in the same cell[24].

Unlike many other RTK ligands, EGF family ligands bind to the ectodomains of erbB receptors as monomers rather than as dimers. Ligand binding occurs at specific sites in the erbB receptor ectodomain. Structural analyses have shown that the erbB receptor ectodomain can be further divided into four functionally distinct subdomains (I-IV; Figure 1A) whose conformation is shaped by disulfide bonds[25]. Subdomains I and III (also known as L1 and L2, respectively) are leucine-rich regions that mediate receptor binding of activating growth factors[26, 27]; subdomains I and III have an amino acid sequence identity of only approximately 37% between the different erbB receptors, consistent with the fact that each erbB receptor binds different growth factors. Ligand binding to subdomains I and III of an erbB receptor triggers extracellular and intracellular conformational changes that ultimately result in the formation of an asymmetric dimer[28] in which one partner contains bound ligand and the other partner does not (this is not to imply that the ligand does not ultimately come into contact with the second receptor subunit; some models indicate that the ligand does in fact form contacts with the second erbB receptor recruited to the signaling complex).

ErbB receptor dimerization following ligand activation is mediated, in part, by subdomains II (CR1) and IV (CR2) of the ectodomain, the cysteine-rich regions that separate and follow subdomains I and III, respectively[27]. Prior to ligand binding, inactive erbB receptors exist in a tethered state confirmation, in which the dimerization arm loop of subdomain II binds to the subdomain IV tethering arm (Figure 1A), thereby preventing aberrant activation[27]. The conformational changes induced by the binding of an EGF family ligand to subdomains I and III of an erbB receptor include disruption of this tethered state conformation and the extension of

subdomains II and IV. As a result of this extension, subdomains II and IV are now available to participate in homo- or heterodimerization with subdomains II and IV of another erbB receptor. This nascent dimerization event is further stabilized by interactions between the transmembrane domains of the now partnered erbB receptors; GXXXG consensus sequences, which occur in pairs in all of the erbB receptors except erbB3, appear to play a particularly important role in mediating interactions between erbB receptor transmembrane domains[29]. In this newly formed asymmetric dimer, the receptor with bound ligand is referred to as the "activator" receptor; an "activator" receptor uses its poised tyrosine kinase domain to allosterically activate the tyrosine kinase domain of its partner "receiver" receptor.

The erbB tyrosine kinase domain contains four functional subdomains known as the N-lobe, helix αC, the activation loop and the C-lobe. All of these tyrosine kinase subdomains play distinct roles in receptor activation. The active site of the tyrosine kinase domain is located between the N-and C-lobes (Figure 1A). In the inactive state, the N- and C-lobes are more open; during activation, the lobes will assume a closed conformation that properly positions ATP and the receptor's substrate within the binding pocket[30]. This conformational shift is triggered in the kinase domain when the C-lobe of the "activator" kinase physically interacts with the N-lobe of the "receiver" kinase and stabilizes it[31]; this stabilization event occurs when the hydrophobic bottom region of the C-lobe of the "activator" receptor interacts with the hydrophobic top region of the N-lobe of the "receiver" receptor[32]. This interaction forces the helix αC region of the "activator" to swing inward on the "receiver" kinase, further stabilizing the interaction and allowing the extension of the activation loop[33]. The end result of these conformational changes is activation of the tyrosine kinase domain of the "receiver" receptor, which is then poised to perform *trans* or *cis* (auto) phosphorylation of tyrosine residues in the C-terminal tails of each

receptor[34]. By this process, the ligand-bound receptor (the "activator") activates the tyrosine kinase of the receptor lacking bound ligand (the "receiver"). The preference of the "receiver" receptor to perform *trans* or *cis* phosphorylation is thought to depend upon which growth factor binds to the activator receptor and the identity of its heterodimeric partner.

The specific tyrosine residues that become phosphorylated within the intracellular domains of the dimerized erbB receptors are dictated by several factors including the sequence of each receptor protein, which homo- or heterodimeric pair formed, the activating ligand, receptor stoichiometry and receptor expression levels at the plasma membrane as well as the presence of other extracellular matrix components. The specific tyrosine residues that are phosphorylated determines the specific cytoplasmic signaling molecules recruited to the signaling complex. The downstream signaling pathways known to be regulated by erbB kinases in this manner include the phosphatidylinositol 3-kinase (PI3K)/Akt [protein kinase B (PKB)] pathway, the Ras/Raf/MEK/ERK1/2 pathway, JAK/STAT pathways and the phospholipase C (PLCγ)/protein kinase C (PKC) pathway[35]. As these downstream signaling pathways orchestrate many cellular processes that are essential for normal pre- and postnatal development[36], it is not surprising that aberrant activity of erbB receptors triggered by overexpression or mutation disrupts cellular homeostasis and triggers the development of multiple types of cancer.

As indicated above, which tyrosine residues are phosphorylated following ligand binding and receptor dimerization is determined, in part, by which erbB receptors dimerize with one another. Preferred erbB dimerization partners exist amongst the family members, with erbB2 being the preferred dimerization partner for the other erbB family members in most cellular contexts. This appears to reflect a conformational difference between non-activated erbB2 and other non-activated erbB receptors. In contrast to the EGFR, erbB3 and erbB4, which adopt a

"tethered" intramolecular conformation in the absence of bound ligand, erbB2 assumes a constantly active conformation in which subdomains II and IV are extended and continually available for interaction with other erbB receptors even in the absence of ligand stimulation[37]. It is also likely that differences in the sequences of subdomains II and IV in other erbB receptors play a role in determining which erbB receptors are more likely to dimerize with each other. Subdomains II and IV are among the most divergent regions in the erbB receptors, with an average amino acid sequence identity of only 17%. Although the structural consequences of this extreme sequence variability remain incompletely understood, it is highly likely that this divergence translates into different preferences for receptor dimerization.

A hierarchy also exists regarding which erbB receptors are most likely to function as "receiver" kinases. Among the erbB receptors, EGFR is the strongest "receiver" kinase followed by erbB2 and then erbB4. In fact, erbB4 only functions only as a "receiver" when it homodimerizes with another erbB4 receiver or when it heterodimerizes with erbB3. This hierarchical process, which determines which erbB kinase is activated and which erbB kinase is subsequently phosphorylated within an erbB homo- or heterodimer, adds to the complexity and cellular control of the cytoplasmic signaling cascades regulated by erbB receptors[38].

Distinct Features of ErbB3, the Functional Peculiarities That Result from its Structural Differences and its Key Regulatory Partners

Studies of mice with targeted null mutations of the *Erbb3* gene (*Erbb3* "knockout" mice) provided some of the earliest evidence indicating that erbB3 was functionally distinct from other erbB family members (Figure 1B). Most *Erbb3*$^{-/-}$ mice die *in utero* at embryonic day 13.5 (E13.5)[39, 40]. Death in these embryos results from the presence of endocardial cushion defects

that lead to blood reflux through defective valves[40] as well as a loss of Schwann cell precursors[39]. Multiple other abnormalities of the central and peripheral nervous system are also evident in *Erbb3*$^{-/-}$ embryos including a loss of dorsal root ganglia sensory neurons[39] and spinal cord motor neurons[39] as well as hypoplasia of the primary sympathetic ganglion chain[41] and malformation of the midbrain and hindbrain with poor differentiation of the cerebellar plate[40]. In contrast, *Nrg1*$^{-/-}$, *Erbb2*$^{-/-}$ and *Erbb4*$^{-/-}$ mice die *in utero* at E10.5 due to a failure of cardiac ventricular myocyte differentiation and show defects in their nervous systems that differ from those seen in *Erbb3*$^{-/-}$ mice[40, 42, 43]. Certainly at least some of these differences can be explained by differences in the cell types expressing each erbB receptor and the ligands activating these receptors. However, when we carefully mapped the expression of each erbB receptor in the central nervous system via immunohistochemistry and *in situ* hybridization, we found that many cell types in the areas impacted by erbB receptor knockout co-expressed multiple erbB receptors, indicating that they were not functionally redundant[9]. Conditional *Erbb3* knockout mice have implicated erbB3 in additional functions such as maintaining luminal-basal homeostasis in breast epithelium[44]; erbB3 is also essential for the survival and proper formation of extravillous trophoblasts during placental development[45]. Observations such as these have motivated several labs to take a closer look at the structural and functional characteristics of erbB3.

ErbB3 contains 1,342 amino acids and has a predicted molecular weight of 145 kDa. However, its observed mass is typically 185 kDa. This difference occurs because erbB3 is heavily post-translationally glycosylated at ten potential N-linked glycosylation sites (Figure 2). In this regard, it is similar to other erbB receptors; approximately 30% of the mature molecular weight of EGFR (11 glycosylation sites), erbB2 (7 glycosylation sites) and erbB4 (9 glycosylation sites) is due to N-glycosylation. A growing body of evidence indicates that this

glycosylation is important for ligand-dependent and -independent functions of mature erbB receptors, as well as, protein stability and activation of downstream signaling events[46, 47]. However, it is also becoming apparent that site-specific glycosylation has distinct effects on the function of each receptor. As an example, glycosylation of Asn-418 in erbB3 prevents tumor progression by blocking aberrant uncontrolled dimerization of erbB3 with erbB2[48].

In mature 185 kDa erbB3 [the form after removal of the signal peptide (amino acids 1-19) and post-translational modification], the extracellular domain spans amino acids 20-630, with the transmembrane domain encoded by residues 642-666, the juxtamembrane domain by amino acids 667-709, the tyrosine kinase domain by residues 709-965 (with the activation loop spanning amino acids 830-890) and the C-terminal tail being located at amino acids 990-1342[49]. Several different isoforms of erbB3 have been documented that vary from this structure. In prostate cancer, a truncated and secreted 45kDa erbB3 isoform (p45-sErbB3; also known as MDA-BF-1) was discovered in bone metastases[50]. ErbB3 expression in prostate cancer is both cytoplasmic and nuclear, with much higher nuclear staining evident in malignant tissue relative to non-transformed prostate tissue[51]; these observations are consistent with the presence of a nuclear localization signaling near the erbB3 C-terminus. The expression pattern of erbB3 in Schwann cells also demonstrates cytoplasmic and nuclear localization. In Schwann cells, however, an alternative transcription initiation site leads to the production of a 50 kDa truncated form of erbB3. This truncated erbB3 protein, which is referred to as the nuclear variant of erbB3 (nuc-erbB3) contains the C-terminal nuclear localization site and thus localizes to Schwann cell nuclei[52]. Chromatin immunoprecipitation (ChIP)-chip experiments have shown that nuc-erbB3 associates with the promoters of several genes involved in myelination; inhibition of nuc-erbB3 inhibits myelination and alters the distribution of ezrin within nodes of Ranvier. Although a

similarly produced 80 kDa erbB3 variant was also, the functional characteristics of this variant in Schwann cells was unclear. However, in prostate[53] and lung carcinoma[54] cells, this 80 kDa erbB3 variant similarly enters the nucleus and acts as a transcriptional regulator.

There are two key features of the 185 kDa form of erbB3 that impact its ability to dimerize with other erbB receptors and form an active signaling complex. First, erbB3 possesses only one GXXXG consensus sequence in its transmembrane domain; as other erbB receptors have two GXXXG consensus sequences that mediate interactions between erbB receptor transmembrane domains during dimerization, this potentially weakens erbB3's ability to homodimerize[29]. Second, the tyrosine kinase activity of erbB3 is widely thought to be impaired compared to other erbB family members. Although the ATP-binding site (GlyXGlyXXGly, aa 716-721) of erbB3 is conserved, a key amino acid residue in the catalytic domain is altered in erbB3[55]; as a result of this Asp to Asn815 alteration, the kinase activity of erbB3 is two orders of magnitude lower than that of the EGFR[56]. Based on these observations, it has been suggested that erbB3 is a "pseudokinase" that instead functions either as a scaffold protein that mediates the assembly of signaling complexes or as an allosteric regulator of other proteins[57, 58]. The combination of a single GXXXG consensus sequence and impaired tyrosine kinase activity potentially explains why erbB3 homodimers are rarely, if ever, encountered as an active signaling complex (erbB3 can, however, form oligomers when inactive; see below).

The impaired tyrosine kinase activity of erbB3 also has important implications for its ability to function as an "activator" or "receiver" in a signaling complex (Figure 2A). As described above, the activation of the kinase domains in asymmetric erbB dimers occurs when the C-lobe of the "activator" receptor physically interacts with the N-lobe of the "receiver" receptor and activates the tyrosine kinase domain of the "receiver" receptor[31]. Given this sequence of events,

it is easy to understand why the kinase-impaired erbB3 receptor would be expected to function primarily as an "activator" partner[59]; with its impaired tyrosine kinase activity, erbB3 would be ineffective as a "receiver" receptor. This supposition is based on the prevalent view that active erbB3 signaling complexes are represented by erbB heterodimers. We would be remiss, however, if we did not note that some investigators have suggested that active signaling complexes that include erbB3 may take other forms. For instance, evidence has been presented arguing that erbB2 and erbB3 instead form tetrameric structures following ligand binding[58].

It should also be noted that there is not uniform agreement that erbB3 is kinase-dead. Shi and colleagues have presented evidence that erbB3 does bind ATP and has weak tyrosine kinase activity despite the alterations in the sequence of its tyrosine kinase domain[60]. X-ray crystallography indicates that the activation loop of ATP-bound erbB3 has a structure similar to that of inactive EGFR and erbB4. It has been suggested that this unique conformation allows erbB3 to activate its dimerization partner via an associative mechanism, rather than the more efficient dissociative mechanism; since activation via an associative mechanism is not as robust, this may explain the difficulty that erbB3 has phosphorylating exogenous substrates[60]. In keeping with this suggestion, a quantum mechanics/molecular mechanics (QM/MM) simulation study similarly argued that erbB3 catalyzes phosphorylation via a mechanism distinct from that used by other erbB family members. This study indicated that the hydrophobic interface that erbB3 forms with partner receptors facilitates the allosteric trans-activation of its dimerization partner, thereby eliminating the requirement for strong intrinsic HER3 kinase activity[61]. At present, we cannot rule out the possibility that this model represents an alternative and distinct mode of erbB3 signaling.

That is not to say that erbB3 is ineffective in signaling—indeed, erbB2-erbB3 heterodimers are the most prominent and potent transforming erbB signaling complex encountered in a plethora of cancers[62]. The intracellular domain of erbB3 contains nine tyrosines with known functional impact when phosphorylated (Y1054, Y1197, Y1199, Y1222, Y1260, Y1262, Y1276, Y1289, and Y1328; Figure 2B, yellow circles) and an additional five sites that can be phosphorylated but whose function is unknown (Y680, Y868, Y1132, Y1159 and Y1307; Figure 2B, blue circles). Any combination of these tyrosines can be phosphorylated to drive downstream signal transduction pathways. Six of these tyrosines (Y1054, Y1197, Y1222, Y1260, Y1276 and Y1289), when phosphorylated, serve as docking sites for the p85 regulatory subunit of PI3 kinase[63]. As a consequence, erbB3 is a highly potent activator of the PI3 kinase pathway which potently drives the pathogenesis of multiple cancer types. However, erbB3 also activates other signaling pathways by providing docking sites for Src family members, Shc (Y1328) and Grb2 (Y1199, Y1262), an adapter protein that binds Son of Sevenless (SOS), a guanine nucleotide exchange factor that activates Ras proteins. In addition, erbB3 contains multiple serine and threonine residues that can be phosphorylated. The proteins mediating phosphorylation of these serine and threonine residues and the consequences of these phosphorylation events remain incompletely understood.

The half-life of erbB3, which impacts the period and amplitude of signal transduction following activation, is heavily dependent upon receptor recycling, N-linked glycosylation and/or degradation; this occurs in both in a ligand-dependent and -independent manner[64]. In its inactive state, erbB3 appears to exist in oligomerized pools; this oligomerization of self-associated erbB3 receptors occurs via a ligand-independent mechanism when erbB3 is located at the plasma membrane. However, when NRG1β binds erbB3, these oligomers are destabilized,

freeing erbB3 to heterodimerize with a partner (typically erbB2)[65]. Ligand binding also affects the stability of erbB3. In the absence of ligand, erbB3 has a half-life of approximately 2.5-3.5 hours at the plasma membrane[64]. Following NRG1β stimulation, though, the half-life of erbB3 is reduced to approximately 0.5 hours[66]. In addition, the half-life of erbB3 can be modified by other cellular proteins. For instance, the RING finger E3 ubiquitin ligase, Nrdp1, acts in a ligand-independent manner to reduce levels of both mature erbB3 and nascent erbB3 emerging from the endoplasmic reticulum; loss of Nrdp1 results in increased erbB3 expression in many breast cancers[67]. With the exception of erbB4, which undergoes ligand-induced endocytosis, all of the erbB receptors undergo constitutive endocytosis at a relatively slow rate (~1-2%/minute)[68]. ErbB3 is endocytosed by both clathrin-mediated (CME) and clathrin-independent endocytosis (CIE). Interestingly, cytoplasmic trafficking favors the fast clathrin-dependent endocytosis pathway while nuclear translocation of erbB3 relies heavily upon the high capacity clathrin-independent pathway[69]. This provides yet another mechanism by which erbB3 levels in the cytoplasm and nucleus can be independently adjusted, thereby allowing erbB3 regulation of cytoplasmic signaling to be modified independent of nuclear signaling.

ErbB3 in Human Cancer

Over the last two decades, it has become increasingly evident that erbB3 plays a key role in cancer biology. This appreciation was initially driven by findings such as the observation that erbB3 has an important role in erbB2-driven breast cancer (even though the mechanism by which this occurred was, at the time, unknown)[70]. Signaling by erbB2-erbB3 heterodimers was subsequently shown to regulate a number of key functions in human cancers such as proliferation, migration and tumor cell survival[71]. However, other erbB3-containing dimers have

been shown to be key drivers of neoplasia in other settings. For example, erbB3 serves as a powerful mediator of EGFR-dependent cellular proliferation in pancreatic cancer[72], in large part because this allows the activation of EGFRs to promote PI3 kinase signaling via dimerization with erbB3. An association study that examined the expression of all four erbB receptors and their interacting partners in 159 samples from 79 tissues found that erbB3 is usually co-expressed with erbB2 and EGFR or erbB2 and erbB4 receptors[73]. As erbB3 is similarly co-expressed with other erbB family members in human cancers[10], it clearly has the opportunity to form multiple heterodimers in these neoplasms.

Among the erbB receptors, cancer-associated mutations have been most often found in EGFR and erbB2, followed by erbB3 and then erbB4[74]. Our review of the COSMIC database indicates that erbB3 is mutated and/or overexpressed in a wide variety of cancers including several types of adenocarcinomas (breast, urinary tract, stomach, large intestine, biliary tract, bladder, endometrium, ovarian, uterine cervical, prostate, lung), melanomas and gliomas; overexpression is often associated with copy number gains that encompass the *ERBB3* gene. In contrast, COSMIC did not report any tumor types with *ERBB3* copy number loss and only a very small fraction of cancers had lowered erbB3 expression (liver, endometrium, breast, and prostate). Although mutations occur at multiple sites, the vast majority of cancer-associated *ERBB3* mutations are missense mutations that occur in subdomains II (~169-332 residues) and IV (~353-475 residues) of the extracellular domain (stars in Figure 3A indicate hot spots for *ERBB3* mutation). In contrast, fewer mutations have been found in the *ERBB3* tyrosine kinase domain. Experimental validation of the functional significance of *ERBB3* mutations has been limited. However, V104M, A232V, P262H/S, G284R, T389K, Q809R, S846I and E928G were shown to promote anchorage-independent growth compared to wild type controls in the presence

of erbB2; the T355I mutation has similar effects in the absence of erbB2[74, 75]. Approximately half of all *ERBB3* point mutations are G to A or A to G transitions; the other half are a G to T transversions or C to T transitions.

ErbB3 signaling in cancer is additionally diversified by "cross-talking" with other RTKs and by the variety of ligands that can activate it. ErbB3 has been demonstrated to form complexes with IGF1R, FGFR2, and HGFR (c-MET) in both ligand-dependent and -independent manners[76]. The erbB3 ligands NRG1 and NRG2 drive erbB3 signaling in a variety of cancers including breast, ovarian, colorectal, non-small cell lung carcinoma, prostate, and head and neck squamous cell carcinoma via overexpression and act in an autocrine, juxtacrine and paracrine fashion[77]. Of note, the NRG1 and NRG2 genes give rise, via alternative splicing and the use of multiple promoters, to numerous isoforms. Although incompletely studied, there is evidence indicating that these different NRG isoforms exert different biological effects when they activate erbB3 signaling.

It is likely that we currently underestimate how widely erbB3 is expressed in human cancers. In part, this reflects the fact that detecting erbB3 protein expression can be challenging because of its very short half-life following activation. However, some provocative recent studies suggest that the widespread use of two-dimensional (2D) cell culture models to study erbB3 expression, function and drug responsiveness may also be a factor. In comparison to 2D monolayer cultures, erbB3 protein expression has been found to be much higher in multicellular aggregate (MCA) 3D cultures of head and neck squamous carcinomas; furthermore, erbB3 signaling pathways operate continuously in these MCA cultures despite low levels of erbB2 and EGFR expression[78]. In addition, responses to drugs targeting erbB receptors differ between 2D monolayer and MCA cultures[79]. Although relatively few such comparisons have been performed to date, it will be

important to bear in mind the impact of culture methodologies as we continue to dissect the role that erbB3 plays in human cancer and assess new therapeutic agents targeting this receptor tyrosine kinase.

Approaches Used to Develop New Therapeutic Agents Targeting erbB3

Our growing understanding of the structure and function of erbB3 has paved the way for the development of several therapeutic strategies targeting erbB3 in human cancers (Figure 3B). These strategies include: 1) creating soluble receptors (ligand traps) that bind erbB3 ligands (e.g., RB200[80]), thereby making them unavailable for binding to erbB3 receptors expressed by tumor cells; 2) designing bivalent ligands (e.g., bivalent NRG1) that promote erbB3 homodimerization at the expense of heterodimerization with other erbB receptors; 3) blocking the ligand binding sites of erbB3; 4) promoting erbB3 destruction by internalization or other means; 5) locking erbB3 in a tethered conformation; or 6) using immunotherapy designed to target erbB3-expressing tumor cells[81]. Broadly speaking, the agents employed to promote blockade of ligand binding sites, erbB3 destruction or locking erbB3 in a tethered conformation are most often monoclonal antibodies; for an excellent review of specific monoclonal antibodies used for each of these strategies, we refer the reader to Mishra et al[81]. The promise of these agents is demonstrated by the fact that a wide variety of them are currently in clinical trials for multiple cancer types (Table 1). However, these are not the only type of agents that effectively target erbB3. Antisense oligonucleotides such as EZN-3920 have been shown to reduce erbB3 expression, the activation of erbB3-dependent signaling pathways and *in vivo* tumor growth[82], particularly when used in combination with small molecular erbB inhibitors such as lapatinib (targets EGFR and erbB2) or gefitinib (targets EGFR). Small molecular inhibitors that bind to

the ATP-binding pocket of erbB3 (TX1-85-1, TX-121-1) have also proven effective at promoting erbB3 degradation, interfering with erbB3 heterodimerization and inhibiting erbB3-dependent pathways[83]. Anti-erbB3 antibodies conjugated to cytotoxic drugs such as saponin[84] and monomethyl auristatin F[85] have shown promise against melanomas in mouse models and human melanoma cell lines, respectively. Finally, vaccines utilizing peptides derived from erbB3 exert anti-tumor effects against breast and pancreatic cancers[86].

The observation that erbB3 can physically interact with other receptor tyrosine kinases has led several laboratories to develop agents that simultaneously target erbB3 and these other receptors. In some cases, these studies have been motivated by a growing awareness that interactions between erbB kinases and other RTKs contributes to resistance to erbB-targeted therapeutics. For instance, Martins et al have presented evidence that in non-HER2 amplified breast cancers, the formation of erbB3/IGFR1 heterodimers is driven by HSP90 inhibitor treatment; these tumors are sensitive to combinatorial therapy targeting erbB3 and IGF1R[87]. In other settings, drug resistance can arise when erbB3 stabilizes the activation of the PI3K and MAPK pathways that was previously driven by MET amplification, HER2 amplification (which drives ligand independent activation of erbB3) or NRG1-fusion gene mediated activation of erbB3[76]. Similarly, gefitinib-sensitive lung cancer can develop therapeutic resistance via focal amplification of *MET* which in turn drives erbB3-dependent activation of the PI3K pathway. In response to observations such as these, monoclonal antibodies such as MM-141 have been developed that simultaneously target erbB3 and another receptor tyrosine kinase (IGF1 receptor in this case; Figure 3B, Table 1). It is also clear that interactions with other erbB receptors can contribute to resistance to agents targeting an individual erbB receptor. For instance, shortly after it was established that erbB3 facilitated therapeutic resistance in erbB2-driven breast cancers, a

similar role was elucidated for erbB3 in EGFR-driven lung cancers[88]. These observations have driven the development of monoclonal antibodies that simultaneously target the EGFR and erbB3 [duligotuzumab (MEHD7945A)] or erbB2 and erbB3 (MM-111, MCLA-128; Table 1).

Despite these advances, several important questions essential for the future design of erbB3-directed therapeutic agents remain unanswered. For example, although there is evidence that patients with specific mutations in the tyrosine kinase domain of erbB3 mutations respond better to erbB inhibitors[89], the effect that mutations at other sites have on responsiveness to these agents is unknown. In addition, it is unclear whether common somatic mutations of erbB3 have structural consequences that affect endodomain phosphorylation and drug responsiveness. We also do not wish to leave the reader with the impression that therapeutic resistance in erbB-expressing tumors uniformly occurs via mechanisms such as outlined above. A growing body of evidence indicates that resistance to tyrosine kinase inhibitors is instead often triggered when erbB3 protein expression is upregulated. This upregulation can occur via multiple mechanisms. The small molecular inhibitors lapatinib and erlotinib induce erbB3 expression by promoting FOXO mediated transcription[90]. Rapamycin enhances erbB3 expression by repressing the expression of miRNAs that stabilize erbB3 mRNA levels or by promoting PI3K-mTOR-4EBP1 mediated upregulation of 5'cap binding translation[91], while inhibitors of mTOR kinases such as PP242 and BE235 enhance erbB3 phosphorylation by decreasing phosphatase activity[91]. In light of the intricate regulation of erbB3 action that we have described here, it is not surprising that we continue to encounter unexpected mechanisms by which erbB3 promotes tumorigenesis or therapeutic resistance. In light of the explosion of evidence implicating erbB3 in the pathogenesis of human cancer, though, this is likely to be an important field of investigation for many years to come.

FIGURE LEGENDS

Figure 1. The erbB family of RTKs orchestrate biological processes via distinct ligands in normal cells. **A:** Each erbB family member has distinct ligand binding specificity. EGFR (orange) is shown in the tethered (inactive) conformation with its potential ligands: amphiregulin (AREG), epiregulin (EREG), epigen (EPGN), epidermal growth factor (EGF), heparin binding-epidermal growth factor (HB-EGF), betacellulin (BTC) and transforming growth factor alpha (TGFα). ErbB2 (blue) is shown in its constitutive open conformation. ErbB3 (green) is shown in the tethered conformation with its potential ligands: neuregulin-1 and neuregulin-2 (NRG1 and NRG2). ErbB4 (red) is shown in the tethered conformation with its associated ligands: EREG, HB-EGF, NRG1, NRG2, NRG3 and NRG4. N and C in the intracellular domain indicates the N-lobe and C-lobe, respectively, of the tyrosine kinase domain, which flank the tyrosine kinase active site (red). **B:** Full-length erbB3 as well as a 50 kDa nuclear variant of erbB3 (not shown) regulates multiple critical biological functions in normal cells (indicated in each box). The oval in the center highlights erbB3-regulated signaling pathways that have been implicated in the regulation of some of these biological functions.

Figure 2 Ligand binding creates an untethered erbB3 structure primed for heterodimerization. A) ErbB3 in its tethered (inactive) conformation, is structurally poised to bind ligand (NRG1/NRG2) within domain I of the ectodomain. Ligand binding induces a conformational change bringing together domains I/III allowing for heterodimerization with other erbB receptors to occur. In this schematic, erbB3 is the activator receptor and erbB2 serves as the receiver receptor. Asymmetric dimer formation involves interaction between the bottom of the C-lobe on the activator receptor with the top of the N-lobe of the receiver receptor, allowing for activation

loop extension followed by phosphorylation of each receptor's autophosphorylation domain. The phosphorylated receptors provides docking sites within their autophosphorylation domains for kinase mediated signal transduction; signaling pathways activated as a result of these interactions are indicated in gray. B) Schematic of key erbB3 post-translational modifications. Red circles in the ectodomain represent the ten N-glycosylation sites in erbB3. Yellow circles in the endodomain represent the nine functionally validated phosphorylation sites. The blue circles represent five additional tyrosines that could potentially be phosphorylated but have not yet been shown to undergo this modification.

Figure 3 ErbB3 somatic mutation "hotspots" and current therapeutics targeting erbB3. A) The erbB3 receptor is shown with stars indicating nine somatic mutations that were found to be recurrent in multiple human tumor types. Seven of these mutations are within the extracellular domain of the receptor and two of the mutations are within the kinase domain. These mutations possibly have roles in altering the functions of ligand binding, heterodimerization with other RTKs and signaling mechanism due to their locations within the specific domains of the receptor. B) MM-141 is a bivalent antibody that binds both the erbB3 receptor and IGF1R. Next is shown a bivalent neuregulin (NRG) trap which promotes the homotypic association of erbB3 receptors, "trapping" them so that they are unable to bind other partners. A bivalent ligand trap, RB200, has also been created to sequester ligands that activate the erbB3 and EGF receptors. RB200 consists of Fc domains of IgG1 fused to full-length erbB3 and EGFR extracellular domain dimers. Two other bivalent antibodies are MCLA-128 and MM-111 which target erbB2 and erbB3. Monoclonal antibodies that have been created to target erbB3 are as follows: U3-1287, MM-121, KTN3379, AV-203 & REGN1400 of which the domain targeted is

unknown and RG7116, LJM716 and GSK2849330 which target within domain I, between domains II-IV and domain III, respectively, in the ECD.

References

[1] Carlin CR, Knowles BB: Identity of human epidermal growth factor (EGF) receptor with glycoprotein SA-7: evidence for differential phosphorylation of the two components of the EGF receptor from A431 cells. Proc Natl Acad Sci U S A 1982, 79:5026-30.

[2] Downward J, Yarden Y, Mayes E, Scrace G, Totty N, Stockwell P, Ullrich A, Schlessinger J, Waterfield MD: Close similarity of epidermal growth factor receptor and v-erb-B oncogene protein sequences. Nature 1984, 307:521-7.

[3] Ullrich A, Coussens L, Hayflick JS, Dull TJ, Gray A, Tam AW, Lee J, Yarden Y, Libermann TA, Schlessinger J, et al.: Human epidermal growth factor receptor cDNA sequence and aberrant expression of the amplified gene in A431 epidermoid carcinoma cells. Nature 1984, 309:418-25.

[4] Coussens L, Yang-Feng TL, Liao YC, Chen E, Gray A, McGrath J, Seeburg PH, Libermann TA, Schlessinger J, Francke U, et al.: Tyrosine kinase receptor with extensive homology to EGF receptor shares chromosomal location with neu oncogene. Science 1985, 230:1132-9.

[5] Kraus MH, Issing W, Miki T, Popescu NC, Aaronson SA: Isolation and characterization of ERBB3, a third member of the ERBB/epidermal growth factor receptor family: evidence for overexpression in a subset of human mammary tumors. Proc Natl Acad Sci U S A 1989, 86:9193-7.

[6] Plowman GD, Whitney GS, Neubauer MG, Green JM, McDonald VL, Todaro GJ, Shoyab M: Molecular cloning and expression of an additional epidermal growth factor receptor-related gene. Proc Natl Acad Sci U S A 1990, 87:4905-9.

[7] Plowman GD, Culouscou JM, Whitney GS, Green JM, Carlton GW, Foy L, Neubauer MG, Shoyab M: Ligand-specific activation of HER4/p180erbB4, a fourth member of the epidermal growth factor receptor family. Proc Natl Acad Sci U S A 1993, 90:1746-50.

[8] Olayioye MA, Neve RM, Lane HA, Hynes NE: The ErbB signaling network: receptor heterodimerization in development and cancer. EMBO J 2000, 19:3159-67.

[9] Gerecke KM, Wyss JM, Karavanova I, Buonanno A, Carroll SL: ErbB transmembrane tyrosine kinase receptors are differentially expressed throughout the adult rat central nervous system. J Comp Neurol 2001, 433:86-100.

[10] Hynes NE, MacDonald G: ErbB receptors and signaling pathways in cancer. Curr Opin Cell Biol 2009, 21:177-84.

[11] Kaushansky A, Gordus A, Budnik BA, Lane WS, Rush J, MacBeath G: System-wide investigation of ErbB4 reveals 19 sites of Tyr phosphorylation that are unusually selective in their recruitment properties. Chem Biol 2008, 15:808-17.

[12] Jorissen RN, Walker F, Pouliot N, Garrett TP, Ward CW, Burgess AW: Epidermal growth factor receptor: mechanisms of activation and signalling. Exp Cell Res 2003, 284:31-53.

[13] Vecchi M, Carpenter G: Constitutive proteolysis of the ErbB-4 receptor tyrosine kinase by a unique, sequential mechanism. J Cell Biol 1997, 139:995-1003.

[14] Rio C, Buxbaum JD, Peschon JJ, Corfas G: Tumor necrosis factor-alpha-converting enzyme is required for cleavage of erbB4/HER4. J Biol Chem 2000, 275:10379-87.

[15] Ni CY, Murphy MP, Golde TE, Carpenter G: gamma -Secretase cleavage and nuclear localization of ErbB-4 receptor tyrosine kinase. Science 2001, 294:2179-81.

[16] Lee HJ, Jung KM, Huang YZ, Bennett LB, Lee JS, Mei L, Kim TW: Presenilin-dependent gamma-secretase-like intramembrane cleavage of ErbB4. J Biol Chem 2002, 277:6318-23.

[17] Naresh A, Long W, Vidal GA, Wimley WC, Marrero L, Sartor CI, Tovey S, Cooke TG, Bartlett JM, Jones FE: The ERBB4/HER4 intracellular domain 4ICD is a BH3-only protein promoting apoptosis of breast cancer cells. Cancer Res 2006, 66:6412-20.

[18] Naresh A, Thor AD, Edgerton SM, Torkko KC, Kumar R, Jones FE: The HER4/4ICD estrogen receptor coactivator and BH3-only protein is an effector of tamoxifen-induced apoptosis. Cancer Res 2008, 68:6387-95.

[19] Sardi SP, Murtie J, Koirala S, Patten BA, Corfas G: Presenilin-dependent ErbB4 nuclear signaling regulates the timing of astrogenesis in the developing brain. Cell 2006, 127:185-97.

[20] Sawyer C, Hiles I, Page M, Crompton M, Dean C: Two erbB-4 transcripts are expressed in normal breast and in most breast cancers. Oncogene 1998, 17:919-24.

[21] Elenius K, Choi CJ, Paul S, Santiestevan E, Nishi E, Klagsbrun M: Characterization of a naturally occurring ErbB4 isoform that does not bind or activate phosphatidyl inositol 3-kinase. Oncogene 1999, 18:2607-15.

[22] Nielsen TO, Sorensen S, Dagnaes-Hansen F, Kjems J, Sorensen BS: Directing HER4 mRNA expression towards the CYT2 isoform by antisense oligonucleotide decreases growth of breast cancer cells in vitro and in vivo. Br J Cancer 2013, 108:2291-8.

[23] Stein RA, Staros JV: Insights into the evolution of the ErbB receptor family and their ligands from sequence analysis. BMC Evol Biol 2006, 6:79.

[24] Carraway KL, Theodoropoulos G, Kozloski GA, Carothers Carraway CA: Muc4/MUC4 functions and regulation in cancer. Future Oncol 2009, 5:1631-40.

[25] Lemmon MA: Ligand-induced ErbB receptor dimerization. Exp Cell Res 2009, 315:638-48.

[26] Ward CW, Garrett TP: The relationship between the L1 and L2 domains of the insulin and epidermal growth factor receptors and leucine-rich repeat modules. BMC Bioinformatics 2001, 2:4.

[27] Ferguson KM, Berger MB, Mendrola JM, Cho HS, Leahy DJ, Lemmon MA: EGF activates its receptor by removing interactions that autoinhibit ectodomain dimerization. Mol Cell 2003, 11:507-17.

[28] Zhang X, Gureasko J, Shen K, Cole PA, Kuriyan J: An allosteric mechanism for activation of the kinase domain of epidermal growth factor receptor. Cell 2006, 125:1137-49.

[29] Escher C, Cymer F, Schneider D: Two GxxxG-like motifs facilitate promiscuous interactions of the human ErbB transmembrane domains. J Mol Biol 2009, 389:10-6.

[30] Jura N, Zhang X, Endres NF, Seeliger MA, Schindler T, Kuriyan J: Catalytic control in the EGF receptor and its connection to general kinase regulatory mechanisms. Mol Cell 2011, 42:9-22.

[31] Macdonald-Obermann JL, Piwnica-Worms D, Pike LJ: Mechanics of EGF receptor/ErbB2 kinase activation revealed by luciferase fragment complementation imaging. Proc Natl Acad Sci U S A 2012, 109:137-42.

[32] Kovacs E, Zorn JA, Huang Y, Barros T, Kuriyan J: A structural perspective on the regulation of the epidermal growth factor receptor. Annu Rev Biochem 2015, 84:739-64.

[33] Qiu C, Tarrant MK, Choi SH, Sathyamurthy A, Bose R, Banjade S, Pal A, Bornmann WG, Lemmon MA, Cole PA, Leahy DJ: Mechanism of activation and inhibition of the HER4/ErbB4 kinase. Structure 2008, 16:460-7.

[34] Linggi B, Carpenter G: ErbB receptors: new insights on mechanisms and biology. Trends Cell Biol 2006, 16:649-56.

[35] Brossier NM, Byer SJ, Peavler LT, Carroll SL: ErbB Membrane Tyrosine Kinase Receptors: Analyzing Migration in a Highly Complex Signaling System. Protein Kinase Technologies, 2012. pp. 105-31.

[36] Yarden Y, Pines G: The ERBB network: at last, cancer therapy meets systems biology. Nat Rev Cancer 2012, 12:553-63.

[37] Hu S, Sun Y, Meng Y, Wang X, Yang W, Fu W, Guo H, Qian W, Hou S, Li B, Rao Z, Lou Z, Guo Y: Molecular architecture of the ErbB2 extracellular domain homodimer. Oncotarget 2015, 6:1695-706.

[38] Ward MD, Leahy DJ: Kinase activator-receiver preference in ErbB heterodimers is determined by intracellular regions and is not coupled to extracellular asymmetry. J Biol Chem 2015, 290:1570-9.

[39] Riethmacher D, Sonnenberg-Riethmacher E, Brinkmann V, Yamaai T, Lewin GR, Birchmeier C: Severe neuropathies in mice with targeted mutations in the ErbB3 receptor. Nature 1997, 389:725-30.

[40] Erickson SL, O'Shea KS, Ghaboosi N, Loverro L, Frantz G, Bauer M, Lu LH, Moore MW: ErbB3 is required for normal cerebellar and cardiac development: a comparison with ErbB2-and heregulin-deficient mice. Development 1997, 124:4999-5011.

[41] Britsch S, Li L, Kirchhoff S, Theuring F, Brinkmann V, Birchmeier C, Riethmacher D: The ErbB2 and ErbB3 receptors and their ligand, neuregulin-1, are essential for development of the sympathetic nervous system. Genes Dev 1998, 12:1825-36.

[42] Gassmann M, Casagranda F, Orioli D, Simon H, Lai C, Klein R, Lemke G: Aberrant neural and cardiac development in mice lacking the ErbB4 neuregulin receptor. Nature 1995, 378:390-4.

[43] Meyer D, Birchmeier C: Multiple essential functions of neuregulin in development. Nature 1995, 378:386-90.

[44] Balko JM, Miller TW, Morrison MM, Hutchinson K, Young C, Rinehart C, Sanchez V, Jee D, Polyak K, Prat A, Perou CM, Arteaga CL, Cook RS: The receptor tyrosine kinase ErbB3 maintains the balance between luminal and basal breast epithelium. Proc Natl Acad Sci U S A 2012, 109:221-6.

[45] Fock V, Plessl K, Draxler P, Otti GR, Fiala C, Knofler M, Pollheimer J: Neuregulin-1-mediated ErbB2-ErbB3 signalling protects human trophoblasts against apoptosis to preserve differentiation. J Cell Sci 2015, 128:4306-16.

[46] Takahashi M, Hasegawa Y, Ikeda Y, Wada Y, Tajiri M, Ariki S, Takamiya R, Nishitani C, Araki M, Yamaguchi Y, Taniguchi N, Kuroki Y: Suppression of heregulin beta signaling by the single N-glycan deletion mutant of soluble ErbB3 protein. J Biol Chem 2013, 288:32910-21.

[47] Lee HS, Qi Y, Im W: Effects of N-glycosylation on protein conformation and dynamics: Protein Data Bank analysis and molecular dynamics simulation study. Sci Rep 2015, 5:8926.

[48] Yokoe S, Takahashi M, Asahi M, Lee SH, Li W, Osumi D, Miyoshi E, Taniguchi N: The Asn418-linked N-glycan of ErbB3 plays a crucial role in preventing spontaneous heterodimerization and tumor promotion. Cancer Res 2007, 67:1935-42.

[49] Wieduwilt MJ, Moasser MM: The epidermal growth factor receptor family: biology driving targeted therapeutics. Cell Mol Life Sci 2008, 65:1566-84.

[50] Vakar-Lopez F, Cheng CJ, Kim J, Shi GG, Troncoso P, Tu SM, Yu-Lee LY, Lin SH: Up-regulation of MDA-BF-1, a secreted isoform of ErbB3, in metastatic prostate cancer cells and activated osteoblasts in bone marrow. J Pathol 2004, 203:688-95.

[51] Koumakpayi IH, Diallo JS, Le Page C, Lessard L, Gleave M, Begin LR, Mes-Masson AM, Saad F: Expression and nuclear localization of ErbB3 in prostate cancer. Clin Cancer Res 2006, 12:2730-7.

[52] Adilakshmi T, Ness-Myers J, Madrid-Aliste C, Fiser A, Tapinos N: A nuclear variant of ErbB3 receptor tyrosine kinase regulates ezrin distribution and Schwann cell myelination. J Neurosci 2011, 31:5106-19.

[53] El Maassarani M, Barbarin A, Fromont G, Kaissi O, Lebbe M, Vannier B, Moussa A, Seite P: Integrated and Functional Genomics Analysis Validates the Relevance of the Nuclear Variant ErbB380kDa in Prostate Cancer Progression. PLoS One 2016, 11:e0155950.

[54] Andrique L, Fauvin D, El Maassarani M, Colasson H, Vannier B, Seite P: ErbB3(80 kDa), a nuclear variant of the ErbB3 receptor, binds to the Cyclin D1 promoter to activate cell proliferation but is negatively controlled by p14ARF. Cell Signal 2012, 24:1074-85.

[55] Sithanandam G, Anderson LM: The ERBB3 receptor in cancer and cancer gene therapy. Cancer Gene Ther 2008, 15:413-48.

[56] Guy PM, Platko JV, Cantley LC, Cerione RA, Carraway KL, 3rd: Insect cell-expressed p180erbB3 possesses an impaired tyrosine kinase activity. Proc Natl Acad Sci U S A 1994, 91:8132-6.

[57] Scheeff ED, Eswaran J, Bunkoczi G, Knapp S, Manning G: Structure of the pseudokinase VRK3 reveals a degraded catalytic site, a highly conserved kinase fold, and a putative regulatory binding site. Structure 2009, 17:128-38.

[58] Zhang Q, Park E, Kani K, Landgraf R: Functional isolation of activated and unilaterally phosphorylated heterodimers of ERBB2 and ERBB3 as scaffolds in ligand-dependent signaling. Proc Natl Acad Sci U S A 2012, 109:13237-42.

[59] Littlefield P, Liu L, Mysore V, Shan Y, Shaw DE, Jura N: Structural analysis of the EGFR/HER3 heterodimer reveals the molecular basis for activating HER3 mutations. Sci Signal 2014, 7:ra114.

[60] Shi F, Telesco SE, Liu Y, Radhakrishnan R, Lemmon MA: ErbB3/HER3 intracellular domain is competent to bind ATP and catalyze autophosphorylation. Proc Natl Acad Sci U S A 2010, 107:7692-7.

[61] Telesco SE, Shih A, Liu Y, Radhakrishnan R: Investigating Molecular Mechanisms of Activation and Mutation of the HER2 Receptor Tyrosine Kinase through Computational Modeling and Simulation. Cancer Res J 2011, 4:1-35.

[62] Stortelers C, van der Woning SP, Jacobs-Oomen S, Wingens M, van Zoelen EJ: Selective formation of ErbB-2/ErbB-3 heterodimers depends on the ErbB-3 affinity of epidermal growth factor-like ligands. J Biol Chem 2003, 278:12055-63.

[63] Roskoski R, Jr.: The ErbB/HER family of protein-tyrosine kinases and cancer. Pharmacol Res 2014, 79:34-74.

[64] Sak MM, Breen K, Ronning SB, Pedersen NM, Bertelsen V, Stang E, Madshus IH: The oncoprotein ErbB3 is endocytosed in the absence of added ligand in a clathrin-dependent manner. Carcinogenesis 2012, 33:1031-9.

[65] Landgraf R, Eisenberg D: Heregulin reverses the oligomerization of HER3. Biochemistry 2000, 39:8503-11.

[66] Cao Z, Wu X, Yen L, Sweeney C, Carraway KL, 3rd: Neuregulin-induced ErbB3 downregulation is mediated by a protein stability cascade involving the E3 ubiquitin ligase Nrdp1. Mol Cell Biol 2007, 27:2180-8.

[67] Fry WH, Simion C, Sweeney C, Carraway KL, 3rd: Quantity control of the ErbB3 receptor tyrosine kinase at the endoplasmic reticulum. Mol Cell Biol 2011, 31:3009-18.

[68] Baulida J, Carpenter G: Heregulin degradation in the absence of rapid receptor-mediated internalization. Exp Cell Res 1997, 232:167-72.

[69] Reif R, Adawy A, Vartak N, Schroder J, Gunther G, Ghallab A, Schmidt M, Schormann W, Hengstler JG: Activated ErbB3 Translocates to the Nucleus via Clathrin-independent Endocytosis, Which Is Associated with Proliferating Cells. J Biol Chem 2016, 291:3837-47.

[70] Holbro T, Beerli RR, Maurer F, Koziczak M, Barbas CF, 3rd, Hynes NE: The ErbB2/ErbB3 heterodimer functions as an oncogenic unit: ErbB2 requires ErbB3 to drive breast tumor cell proliferation. Proc Natl Acad Sci U S A 2003, 100:8933-8.

[71] Citri A, Skaria KB, Yarden Y: The deaf and the dumb: the biology of ErbB-2 and ErbB-3. Exp Cell Res 2003, 284:54-65.

[72] Liles JS, Arnoletti JP, Tzeng CW, Howard JH, Kossenkov AV, Kulesza P, Heslin MJ, Frolov A: ErbB3 expression promotes tumorigenesis in pancreatic adenocarcinoma. Cancer Biol Ther 2010, 10:555-63.

[73] Schulze WX, Deng L, Mann M: Phosphotyrosine interactome of the ErbB-receptor kinase family. Mol Syst Biol 2005, 1:2005 0008.

[74] Mishra R, Hanker AB, Garrett JT: Genomic alterations of ERBB receptors in cancer: clinical implications. Oncotarget 2017, 8:114371-92.

[75] Jaiswal BS, Kljavin NM, Stawiski EW, Chan E, Parikh C, Durinck S, Chaudhuri S, Pujara K, Guillory J, Edgar KA, Janakiraman V, Scholz RP, Bowman KK, Lorenzo M, Li H, Wu J, Yuan W, Peters BA, Kan Z, Stinson J, Mak M, Modrusan Z, Eigenbrot C, Firestein R, Stern HM, Rajalingam K, Schaefer G, Merchant MA, Sliwkowski MX, de Sauvage FJ, Seshagiri S: Oncogenic ERBB3 mutations in human cancers. Cancer Cell 2013, 23:603-17.

[76] Karachaliou N, Lazzari C, Verlicchi A, Sosa AE, Rosell R: HER3 as a Therapeutic Target in Cancer. BioDrugs 2017, 31:63-73.

[77] Mota JM, Collier KA, Barros Costa RL, Taxter T, Kalyan A, Leite CA, Chae YK, Giles FJ, Carneiro BA: A comprehensive review of heregulins, HER3, and HER4 as potential therapeutic targets in cancer. Oncotarget 2017, 8:89284-306.

[78] Humtsoe JO, Pham E, Louie RJ, Chan DA, Kramer RH: ErbB3 upregulation by the HNSCC 3D microenvironment modulates cell survival and growth. Oncogene 2016, 35:1554-64.

[79] Jacobi N, Seeboeck R, Hofmann E, Schweiger H, Smolinska V, Mohr T, Boyer A, Sommergruber W, Lechner P, Pichler-Huebschmann C, Onder K, Hundsberger H, Wiesner C, Eger A: Organotypic three-dimensional cancer cell cultures mirror drug responses in vivo: lessons learned from the inhibition of EGFR signaling. Oncotarget 2017, 8:107423-40.

[80] Sarup J, Jin P, Turin L, Bai X, Beryt M, Brdlik C, Higaki JN, Jorgensen B, Lau FW, Lindley P, Liu J, Ni I, Rozzelle J, Kumari R, Watson SA, Zhang J, Shepard HM: Human epidermal growth factor receptor (HER-1:HER-3) Fc-mediated heterodimer has broad antiproliferative activity in vitro and in human tumor xenografts. Mol Cancer Ther 2008, 7:3223-36.

[81] Mishra R, Patel H, Alanazi S, Yuan L, Garrett JT: HER3 signaling and targeted therapy in cancer. Oncol Rev 2018, 12:355.

[82] Wu Y, Zhang Y, Wang M, Li Q, Qu Z, Shi V, Kraft P, Kim S, Gao Y, Pak J, Youngster S, Horak ID, Greenberger LM: Downregulation of HER3 by a novel antisense oligonucleotide, EZN-3920, improves the antitumor activity of EGFR and HER2 tyrosine kinase inhibitors in animal models. Mol Cancer Ther 2013, 12:427-37.

[83] Xie T, Lim SM, Westover KD, Dodge ME, Ercan D, Ficarro SB, Udayakumar D, Gurbani D, Tae HS, Riddle SM, Sim T, Marto JA, Janne PA, Crews CM, Gray NS: Pharmacological targeting of the pseudokinase Her3. Nat Chem Biol 2014, 10:1006-12.

[84] Capone E, Giansanti F, Ponziani S, Lamolinara A, Iezzi M, Cimini A, Angelucci F, Sorda R, Laurenzi V, Natali PG, Ippoliti R, Iacobelli S, Sala G: EV20-Sap, a novel anti-HER-3 antibody-drug conjugate, displays promising antitumor activity in melanoma. Oncotarget 2017, 8:95412-24.

[85] Capone E, Lamolinara A, D'Agostino D, Rossi C, De Laurenzi V, Iezzi M, Iacobelli S, Sala G: EV20-mediated delivery of cytotoxic auristatin MMAF exhibits potent therapeutic efficacy in cutaneous melanoma. J Control Release 2018, 277:48-56.

[86] Miller MJ, Foy KC, Overholser JP, Nahta R, Kaumaya PT: HER-3 peptide vaccines/mimics: Combined therapy with IGF-1R, HER-2, and HER-1 peptides induces synergistic antitumor effects against breast and pancreatic cancer cells. Oncoimmunology 2014, 3:e956012.

[87] Martins CD, Da Pieve C, Burley TA, Smith R, Ciobota DM, Allott L, Harrington KJ, Oyen WJG, Smith G, Kramer-Marek G: HER3-Mediated Resistance to Hsp90 Inhibition Detected in Breast Cancer Xenografts by Affibody-Based PET Imaging. Clin Cancer Res 2018, 24:1853-65.

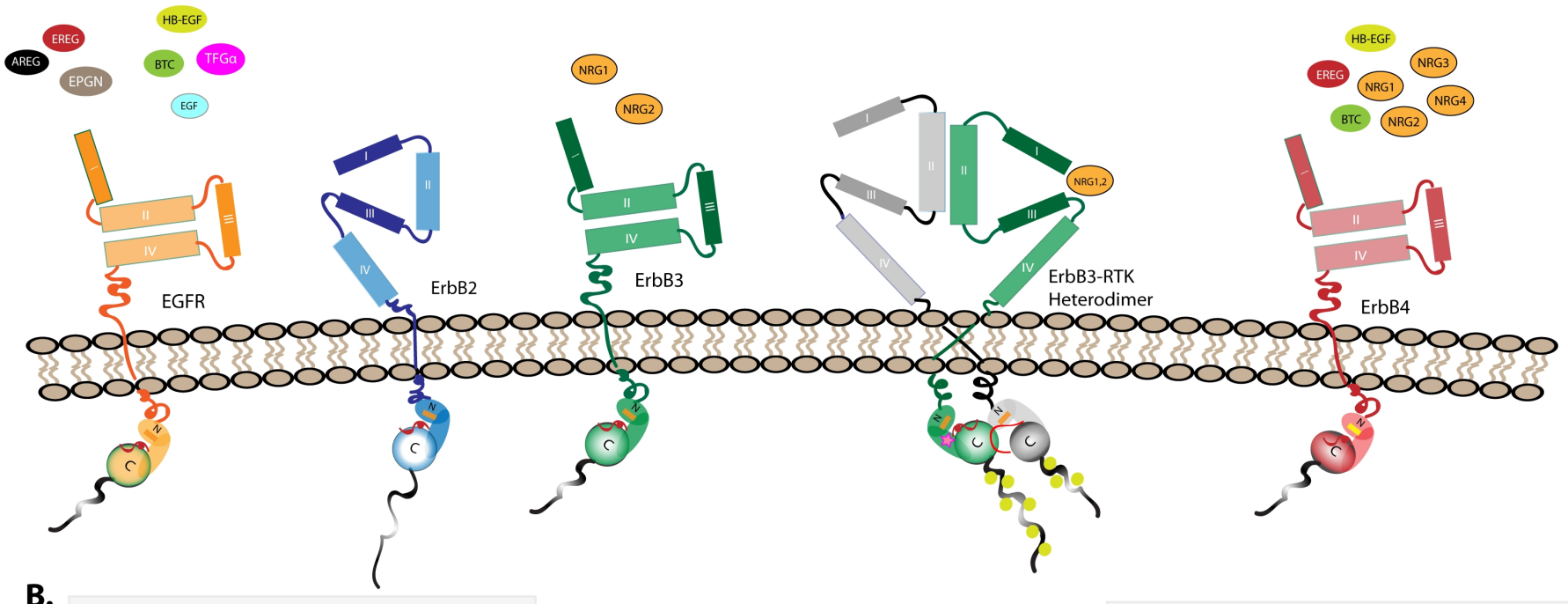
[88] Hamburger AW: The role of ErbB3 and its binding partners in breast cancer progression and resistance to hormone and tyrosine kinase directed therapies. J Mammary Gland Biol Neoplasia 2008, 13:225-33.

[89] Verlingue L, Hollebecque A, Lacroix L, Postel-Vinay S, Varga A, El Dakdouki Y, Baldini C, Balheda R, Gazzah A, Michot JM, Marabelle A, Mir O, Arnedos M, Rouleau E, Solary E, De Baere T, Angevin E, Armand JP, Michiels S, Andre F, Deutsch E, Scoazec JY, Soria JC, Massard C: Human epidermal receptor family inhibitors in patients with ERBB3 mutated cancers: Entering the back door. Eur J Cancer 2018, 92:1-10.

[90] Amin DN, Sergina N, Lim L, Goga A, Moasser MM: HER3 signalling is regulated through a multitude of redundant mechanisms in HER2-driven tumour cells. Biochem J 2012, 447:417-25.

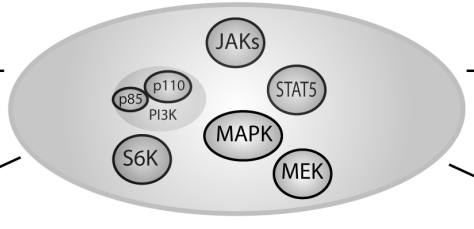
[91] Lyu H, Huang J, Edgerton SM, Thor AD, He Z, Liu B: Increased erbB3 promotes erbB2/neu-driven mammary tumor proliferation and co-targeting of erbB2/erbB3 receptors exhibits potent inhibitory effects on breast cancer cells. Int J Clin Exp Pathol 2015, 8:6143-56.

A.



B.

A nuclear variant form (nuc-erbB3) functions as a transcriptional regulator in human Schwann cells and is required for proper myelination

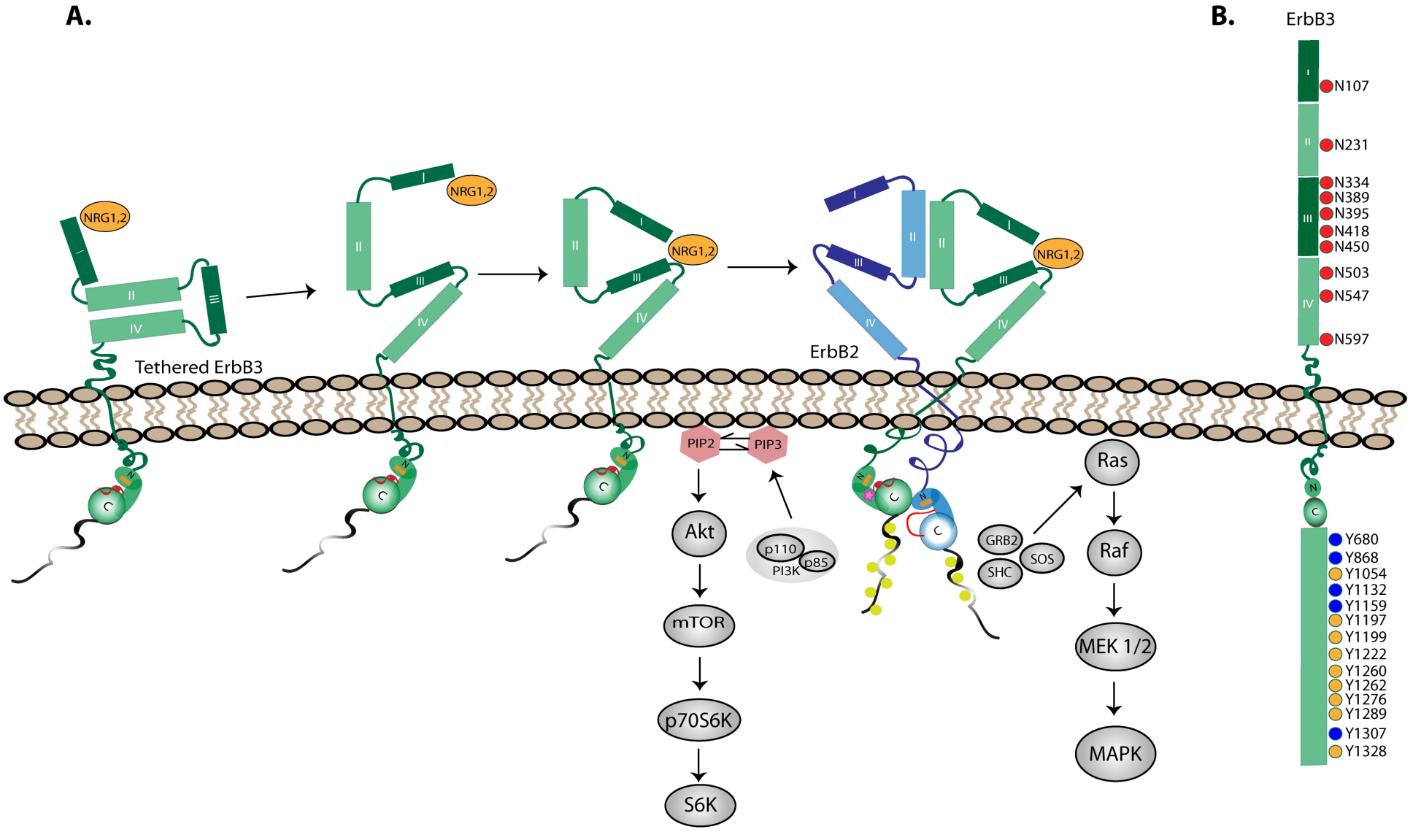


ErbB3 is important for cell differentiation and the luminal-epithelium homeostasis in breast tissue

ErbB3 is required for proper endocardial mesenchyme cushion development

ErbB2-ErbB3 is required for survival and proper formation of extravillous trophoblasts (EVTs) during placental development

ErbB3 is required for normal midbrain/hindbrain and cerebellar development



ErbB Regulation of Cellular Survival and Growth Pathways

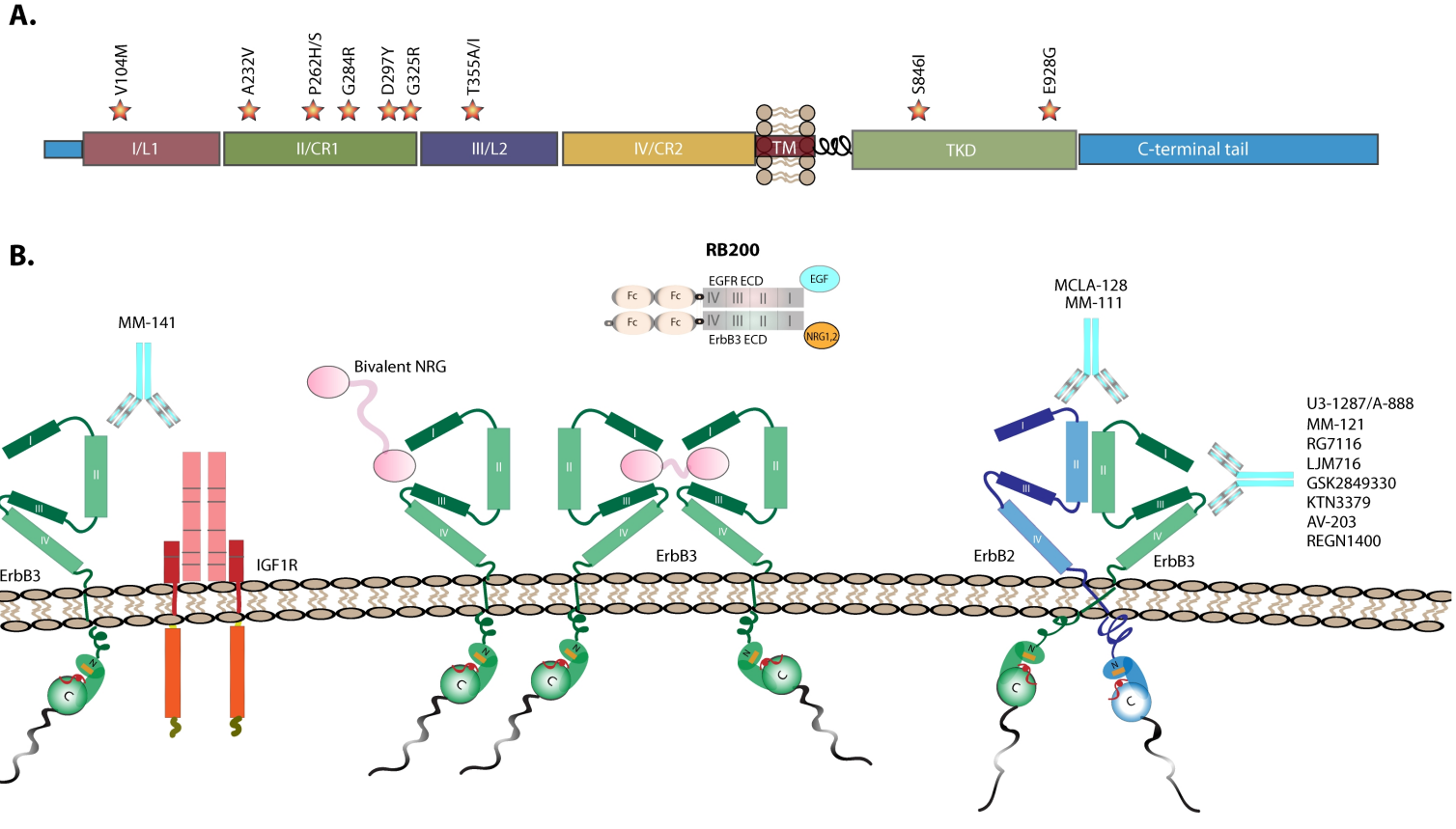

A.
V104M
A232V
P262H/S
G284R
D297Y
G325R
T355A/I
S846I
E928G
I/L1
II/CR1
III/L2
IV/CR2
TM
TKD
C-terminal tail
B.
RB200
EGFR ECD
EGF
Fc
IV III II I
ErbB3 ECD
NRG1,2
MM-141
Bivalent NRG
MCLA-128
MM-111
U3-1287/A-888
MM-121
RG7116
LJM716
GSK2849330
KTN3379
AV-203
REGN1400
ErbB3
IGF1R
ErbB3
ErbB2
ErbB3

Table 1. Anti-ErbB3 Monoclonal and Bi-specific Antibodies Currently in Clinical Trials

Anti-ErbB3 Monoclonal Antibodies	ClincalTrials.gov Identifier	Status	Indication	Combinatory?	Manufacturer	Begin Date/Date of Last Update
Patritumab – U3-1402	NCT03260491	Recruiting Phase I	Metastatic or Unresectable NSCLC	No	Daiichi Sankyo, Inc.	August 24, 2017/July 12, 2018
Patritumab – U3-1402	NCT02980341	Phase II/III	HER3+ Metastatic Breast Cancer	No	Daiichi Sankyo, Inc.	December 2, 2016/January 28, 2019
Patritumab - U3-1287 (AMG888)	NCT01042379	Phase II	Breast Cancer/I-SPY2	Trastuzumab	Daiichi Sankyo, Inc.	January 5, 2010/October 31, 2018
Patritumab - U3-1287 (AMG888)	NCT01957280	Completed Phase I	Solid Tumors (Assess Pharmacokinetics, Immunogenicity and Safety/ Tolerability)	No	Daiichi Sankyo, Inc.	October 8, 2013/May 14, 2014
Patritumab - U3-1287 (AMG888)	NCT01211483	Completed Phase Ib	NSCLC	+/- Erlotinib	Daiichi Sankyo, Inc.	September 29, 2010/November 20, 2017
Patritumab - U3-1287 (AMG888)	NCT02350712	Completed Phase I	Head and Neck Cancer	Cetuximab and a Platinum Containing Therapy	Daiichi Sankyo, Inc.	January 30, 2015/September 11, 2018
Patritumab - U3-1287 (AMG888)	NCT00730470	Completed Phase I	Advanced Solid Tumors	No	Daiichi Sankyo, Inc.	August 8, 2008/July 29, 2010
Seribantumab – MM-121	NCT02387216	Recruiting Phase II	HRG+ NSCLC	+/- Chemotherapy	Merrimack Pharmaceuticals	March 12, 2015/May 1, 2018
Seribantumab – MM-121	NCT03241810	Recruiting Phase II	Metastatic Breast Cancer	Fulvestrant	Merrimack Pharmaceuticals	August 8, 2017/September 18, 2018
Seribantumab – MM-121	NCT01451632	Completed Phase I	Colorectal Cancer, Squamous Cell Head and Neck Cancer, NSCLC, Triple Negative Breast Cancer, Other tumors with EGFR Dependence	Cetuximab, Irinotecan	Merrimack Pharmaceuticals	October 13, 2011/September 8, 2016
Seribantumab – MM-121	NCT01209195	Completed Phase I	Locally Advanced/Metastatic or Recurrent Ovarian Cancer, Fallopian Tube Cancer, Primary Peritoneal Cancer or Endometrial	Paclitaxel	Merrimack Pharmaceuticals	September 27, 2010/September 8, 2016
Seribantumab – MM-121	NCT01421472	Completed Phase II	ER+, HER2- Breast Cancer Patients, Triple Negative Breast Cancer Patients	Paclitaxel	Merrimack Pharmaceuticals	August 22, 2011/May 3, 2016
Seribantumab – MM-121	NCT01447706	Completed Phase II	Epithelial Ovarian Cancer (Platinum resistant),	Paclitaxel	Merrimack Pharmaceuticals	October 6, 2011/May 12, 2016

			Fallopian Tube Cancer, Peritoneal Cancer			
Seribantumab – MM-121	NCT00994123	Completed Phase I	Advanced Carcinoma, Non-Small-Cell Lung	Erlotinib	Merrimack Pharmaceuticals	October 14, 2009/August 22, 2016
Seribantumab – MM-121	NCT01151046	Completed Phase II	Her2 Negative Breast Cancer Patients	+/- Exemestane	Merrimack Pharmaceuticals	June 25, 2010/May 12, 2016
Seribantumab – MM-121	NCT01447225	Completed Phase I	Advanced Solid Tumors	+/- Carboplatin, Pemetrexed, Cabazitaxel orGemcitabine	Merrimack Pharmaceuticals	October 6, 2011/September 14, 2016
Seribantumab – MM-121	NCT01436565	Completed Phase I	Solid Tumors	SAR245408	Merrimack Pharmaceuticals	September 19, 2011/June 13, 2014
LJM716	NCT02167854	Active, not recruiting Phase I	Metastatic HER2+ Breast Cancer	BYL719 and Trastuzumab	Novartis	June 19, 2014/October 22, 2018
LJM716	NCT01602406	Completed Phase I	Advanced HER2-positive Breast Cancer or Gastric Cancer	Trastuzumab	Novartis	May 21, 2012/July 26, 2018
LJM716	NCT01822613	Completed Phase I	Esophageal Squamous Cell Carcinoma	BYL719	Novartis	April 2, 2013/June 1, 2017
LJM716	NCT01598077	Completed Phase I	Squamous Cell Carcinoma of Head and Neck, or HER2+ Breast Cancer or Gastric Cancer		Novartis	May 15, 2012/April 23, 2014
AV-203	NCT01603979	Completed Phase I	Advanced Solid Tumors		AVEO	May 23, 2012/April 8, 2015
REGN1400	NCT01727869	Completed Phase I	Unresectable or Metastatic Cancer	+/- Erlotinib, Cetuximab	Regeneron	Nov 16, 2012/April 6, 2015
GSK2849330	NCT01966445	Completed Phase I	Advanced Her3-Positive Solid Tumors		GlaxoSmithKline	October 21, 2013/July 19, 2018
GSK2849330	NCT02345174	Completed Phase I	Immuno Positron Emission Tomography Study of HER3+ Tumors		GlaxoSmithKline	January 26, 2015/September 13, 2018
Lumretuzumab/RG 7116/RO5479599	NCT01918254	Completed Phase I	HER2+,HER3+ Metastatic Breast Cancers	Paclitaxel, Pertuzumab	Hoffmann-La	August 7, 2013/September 12, 2017
Lumretuzumab/RG 7116/RO5479599	NCT01482377	Completed Phase I	HER3+ Solid Tumors of Epithelial Cell Origin	+/- Cetuximab, Erlotinib	Hoffmann-La	November 30, 2011/January 27, 2017
KTN3379	NCT02456701	Completed Phase I	BRAF Mutant Thyroid Cancers	Vemurafenib	Celldex Therapeutics	May 28, 2015/September 5, 2017
KTN3379	NCT02014909	Completed Phase I	Advanced Tumors		Celldex Therapeutics	December 18, 2013/July 24, 2017
KTN3379	NCT02473731	Completed Phase I	Squamous Cell Carcinoma of the Head and Neck		Celldex Therapeutics	June 17, 2015/May 12, 2017
Bispecific Antibodies	**ClincalTrials.gov Identifier**	**Status**	**Indication**	**Combinatory**	**Manufacturer**	**Begin Date/Date of Last Update**

Duligotuzumab (MEHD7945A) EGFR & erbB3 Targeted	NCT01986166	Completed Phase I	Locally Advanced or Metastatic Cancers With Mutant KRAS	Cobimetinib	Genentech, Inc.	November 18, 2013/July 18, 2016
	NCT01207323	Completed Phase I	Locally Advanced or Metastatic Epithelial Tumors		Genentech, Inc.	September 22, 2010/May 1, 2018
	NCT01911598	Completed Phase I	Recurrent/ Metastatic Squamous Cell Carcinoma of the Head and Neck	Cisplatin and 5-Fluorouracil (5-FU) OR Paclitaxel and Carboplatin	Genentech, Inc.	July 30, 2013/July 6, 2017
	NCT01652482	Completed Phase II	KRAS Wild-Type Metastatic Colorectal Cancer	5-fluorouracil	Genentech, Inc.	July 30, 2012/November 2, 2016
	NCT01577173	Completed Phase II	Recurrent/ Metastatic Squamous Cell Carcinoma of The Head And Neck		Genentech, Inc.	April 13, 2012/November 2, 2016
MM-111 erbB2 & erbB3 Targeted	NCT01097460	Completed Phase I	Advanced Her2 Amplified, Heregulin Positive Breast Cancer	Herceptin	Merrimack	April 1, 2010/January 7, 2015
	NCT00911898	Completed Phase I	Advanced, Refractory Her2 Amplified, Heregulin Positive Cancers		Merrimack	June 3, 2009/January 13, 2015
	NCT01304784	Completed Phase I	HER2 Positive Cancer	Cisplatin, Capecitabine, Trastuzumab ; Lapatinib +/- Trastuzumab; Paclitaxel, Trastuzumab; Lapatinib, trastuzumab, paclitaxel; Docetaxel, trastuzumab	Merrimack	February 25, 2011/December 16, 2015
MM-141 IGF1R & erbB3 Targeted	NCT01733004	Completed Phase I	Hepatocellular Carcinoma		Merrimack	November 26, 2012/August 4, 2016
	NCT02399137	Completed Phase II	Pancreatic Cancer	Nab-Paclitaxel, Gemcitabine	Merrimack	March 26, 2015/September 18, 2018
MCLA-128 erbB2 & erbB3 Targeted	NCT02912949	Recruiting Phase I and II	Malignant Solid Tumor, Breast Cancer, Gastric Cancer, Ovarian Cancer, Endometrial Cancer, NSCLC		Merus N.V.	September 23, 2016/March 28, 2017
	NCT03321981	Recruiting Phase II	Breast Cancer Metastatic	Trastuzumab, Vinorelbine, Endocrine therapy	Merus N.V.	October 26, 2017/August 13, 2018

Cell Communication and Signaling

ErbB4 Promotes Malignant Peripheral Nerve Sheath Tumor Pathogenesis via Ras-Independent Mechanisms

--Manuscript Draft--

Manuscript Number:	CCAS-D-19-00153
Full Title:	ErbB4 Promotes Malignant Peripheral Nerve Sheath Tumor Pathogenesis via Ras-Independent Mechanisms
Article Type:	Research

Funding Information:		
	National Institute of Neurological Disorders and Stroke (R01NS048353)	Dr. Steven Carroll
	National Institute of Neurological Disorders and Stroke (F31NS081824)	Dr STEPHANIE N. BROSIUS
	National Cancer Institute (R01CA122804)	Dr. Steven Carroll
	National Cancer Institute (R01CA134773)	Dr KEVIN A. ROTH
	Congressionally Directed Medical Research Programs (X81XWH-09-1-0086)	Dr. Steven Carroll
	Congressionally Directed Medical Research Programs (W81XWH-12-1-0164)	Dr. Steven Carroll
	Congressionally Directed Medical Research Programs (W81XWH-15-1-0193)	Dr. Steven Carroll
	Congressionally Directed Medical Research Programs (W81XWH-14-1-0073)	Dr KEVIN A. ROTH
	Children's Tumor Foundation (2014-04-001)	Dr. Steven Carroll
	Children's Tumor Foundation (2015-05-007)	Dr. Steven Carroll

Abstract:

Background

We have found that erbB receptor tyrosine kinases drive Ras hyperactivation and growth in NF1-null malignant peripheral nerve sheath tumors (MPNSTs). However, MPNSTs variably express multiple erbB receptors with distinct functional characteristics and it is not clear which of these receptors drive MPNST pathogenesis. Here, we test the hypothesis that altered erbB4 expression promotes MPNST pathogenesis by uniquely activating key cytoplasmic signaling cascades.

Methods

ErbB4 expression was assessed using immunohistochemistry, immunoblotting and real-time PCR. To define erbB4 functions, we generated mice that develop MPNSTs with floxed Erbb4 alleles (P0-GGFβ3;Trp53+/-;Erbb4flox/flox mice) and ablated Erbb4 in these tumors. MPNST cell proliferation and survival was assessed using 3H-thymidine incorporation, MTT assays and Real-Time Glo assays. Control and Erbb4-null MPNST cells were orthotopically xenografted in immunodeficient mice and the growth, proliferation (Ki67 labeling), apoptosis (TUNEL labeling) and angiogenesis of these grafts compared. Antibody arrays querying cytoplasmic kinases were used to identify erbB4-responsive kinases. Pharmacologic or genetic inhibition was used to identify erbB4-responsive kinases that drive proliferation.

Results

Aberrant erbB4 expression was evident in 25/30 surgically resected human MPNSTs and in MPNSTs from genetically engineered mouse models (P0-GGFβ3 and P0-

Powered by Editorial Manager® and ProduXion Manager® from Aries Systems Corporation

	GGFβ3;Trp53+/- mice); multiple erbB4 splice variants that differ in their ability to activate PI3 kinase and nuclear signaling were present in MPNST-derived cell lines. Erbb4-null MPNST cells demonstrated decreased proliferation and survival and altered morphology relative to non-ablated controls. Orthotopic allografts of Erbb4-null cells were significantly smaller than controls, with reduced proliferation, survival and vascularization. ERBB4 knockdown in human MPNST cells similarly inhibited DNA synthesis and viability. Although we have previously shown that broad-spectrum erbB inhibitors inhibit Ras activation, Erbb4 ablation did not affect Ras activation, suggesting that erbB4 drives neoplasia via non-Ras dependent pathways. An analysis of 43 candidate kinases identified multiple NRG1β-responsive and erbB4-dependent signaling cascades including the PI3K, WNK1, STAT3, STAT5 and phospholipase-Cγ pathways. Although WNK1 inhibition did not alter proliferation, inhibition of STAT3, STAT5 and phospholipase-Cγ markedly reduced proliferation. Conclusions ErbB4 promotes MPNST growth by activating key non-Ras dependent signaling cascades including the STAT3, STAT5 and phospholipase-Cγ pathways. ErbB4 and its effector pathways are thus potentially useful therapeutic targets in MPNSTs.
Corresponding Author:	Steven Carroll, MD, PhD Medical University of South Carolina - College of Medicine Charleston, SC UNITED STATES
Corresponding Author Secondary Information:	
Corresponding Author's Institution:	Medical University of South Carolina - College of Medicine
Corresponding Author's Secondary Institution:	
First Author:	STEPHANIE N. BROSIUS
First Author Secondary Information:	
Order of Authors:	STEPHANIE N. BROSIUS
	JODY FROMM LONGO
	LAUREL BLACK
	STUART J. WORLEY
	KEVIN A. ROTH
	Steven Carroll, MD, PhD
Order of Authors Secondary Information:	
Opposed Reviewers:	Nancy Ratner
	Thomas de Raedt
Additional Information:	
Question	**Response**
Is this study a clinical trial?<hr>A clinical trial is defined by the Word Health Organisation as 'any research study that prospectively assigns human participants or groups of humans to one or more health-related interventions to evaluate the effects on health outcomes'.	No

Manuscript
Click here to access/download;Manuscript;MPNST erbB4 Manuscript Submitted Version.docx
Click here to view linked References

RESEARCH ARTICLE

ErbB4 Promotes Malignant Peripheral Nerve Sheath Tumor Pathogenesis via Ras-Independent Mechanisms

STEPHANIE N. BROSIUS*, JODY FROMM LONGO*, LAUREL BLACK, STUART J. WORLEY, KEVIN A. ROTH and STEVEN L. CARROLL

Department of Pathology (SNB, KAR) and the Medical Scientist Training Program (SNB), University of Alabama at Birmingham, Birmingham, AL 35294-0017
Department of Pathology and Laboratory Medicine (JFL, LB, SJW, SLC), Medical University of South Carolina, Charleston, SC 29425-9080

Author E-mail Addresses: Stephanie N. Brosius, stephanie.brosius@gmail.com; Jody Fromm Longo, longoj@musc.edu; Laurel Black, blackl@musc.edu; Stuart J. Worley, worleystuart@gmail.com; Kevin A. Roth, kar2208@cumc.columbia.edu; Steven L. Carroll, carrolst@musc.edu

Running head: ErbB4 function in MPNST pathogenesis

Abstract Word Count: 350

Number of Figures: Seven

Additional Files: One

Address correspondence to:
Steven L. Carroll, MD, PhD
Professor and Chair, Dept. of Pathology and Laboratory Medicine
171 Ashley Avenue, MSC 908
Medical University of South Carolina
Charleston, SC 29425-9080
Phone: (843) 792-3121; Fax: (843) 792-0555
E-mail: carrolst@musc.edu

Footnote: *These authors contributed equally to the manuscript. SNB is currently in the Department of Pediatrics at The Children's Hospital of Philadelphia. KAR is currently affiliated with the Department of Pathology and Cell Biology, Vagelos College of Physicians and Surgeons, Columbia University.

Abstract

Background: We have found that erbB receptor tyrosine kinases drive Ras hyperactivation and growth in *NF1*-null malignant peripheral nerve sheath tumors (MPNSTs). However, MPNSTs variably express multiple erbB receptors with distinct functional characteristics and it is not clear which of these receptors drive MPNST pathogenesis. Here, we test the hypothesis that altered erbB4 expression promotes MPNST pathogenesis by uniquely activating key cytoplasmic signaling cascades.

Methods: ErbB4 expression was assessed using immunohistochemistry, immunoblotting and real-time PCR. To define erbB4 functions, we generated mice that develop MPNSTs with floxed *Erbb4* alleles (P_0-GGFβ3;*Trp53*$^{+/-}$;*Erbb4*$^{flox/flox}$ mice) and ablated *Erbb4* in these tumors. MPNST cell proliferation and survival was assessed using ^{3}H-thymidine incorporation, MTT assays and Real-Time Glo assays. Control and *Erbb4*-null MPNST cells were orthotopically xenografted in immunodeficient mice and the growth, proliferation (Ki67 labeling), apoptosis (TUNEL labeling) and angiogenesis of these grafts compared. Antibody arrays querying cytoplasmic kinases were used to identify erbB4-responsive kinases. Pharmacologic or genetic inhibition was used to identify erbB4-responsive kinases that drive proliferation.

Results: Aberrant erbB4 expression was evident in 25/30 surgically resected human MPNSTs and in MPNSTs from genetically engineered mouse models (P_0-GGFβ3 and P_0-GGFβ3;*Trp53*$^{+/-}$ mice); multiple erbB4 splice variants that differ in their ability to activate PI3 kinase and nuclear signaling were present in MPNST-derived cell lines. *Erbb4*-null MPNST cells demonstrated decreased proliferation and survival and altered morphology relative to non-ablated controls. Orthotopic allografts of *Erbb4*-null cells were significantly smaller than controls, with reduced proliferation, survival and vascularization. *ERBB4* knockdown in human MPNST cells similarly inhibited DNA synthesis and viability. Although we have previously shown that broad-spectrum erbB inhibitors inhibit Ras activation, *Erbb4* ablation did not affect Ras activation, suggesting that erbB4 drives neoplasia via non-Ras dependent pathways. An analysis of 43 candidate

kinases identified multiple NRG1β-responsive and erbB4-dependent signaling cascades including the PI3K, WNK1, STAT3, STAT5 and phospholipase-Cγ pathways. Although WNK1 inhibition did not alter proliferation, inhibition of STAT3, STAT5 and phospholipase-Cγ markedly reduced proliferation.

Conclusions: ErbB4 promotes MPNST growth by activating key non-Ras dependent signaling cascades including the STAT3, STAT5 and phospholipase-Cγ pathways. ErbB4 and its effector pathways are thus potentially useful therapeutic targets in MPNSTs.

Key words: Neurofibromatosis type 1; Schwann cell; erbB kinases; cytoplasmic signaling pathways.

Background

Malignant peripheral nerve sheath tumors (MPNSTs) are highly aggressive spindle cell neoplasms derived from the Schwann cell lineage [1]. These neoplasms are the most common malignancy occurring in patients with neurofibromatosis type 1 (NF1) [2]; they also occur sporadically in the general population and at sites of previous radiation therapy. There is an ongoing controversy as to whether NF1-associated, sporadic or radiation-induced MPNSTs have a worse prognosis [3-7]. However, it is generally agreed that in all of these clinical settings, MPNSTs have a poor prognosis, with several academic centers reporting 5-year disease-free survival rates of 34-60% [4, 6-12]. In large part, these poor outcomes reflect the fact that surgical resection is currently the only effective means of treating MPNSTs and achieving a complete surgical resection is often impossible. Developing effective new chemotherapeutic regimens is thus essential if we are to improve the survival of patients with these aggressive neoplasms.

Loss-of-function mutations of the *NF1* tumor suppressor gene, which encodes the Ras inhibitor neurofibromin, are present in all NF1-associated MPNSTs and a major subset of

sporadic and radiation-induced MPNSTs [13, 14]. In the absence of neurofibromin, Ras activation is unopposed, resulting in Ras hyperactivation. Given this, it was reasonable to expect that agents targeting Ras or Ras-regulated cytoplasmic signaling cascades would be effective against MPNSTs. However, attempts to treat MPNSTs in this manner have thus far been unsuccessful. This reflects the fact that multiple Ras proteins are hyperactivated in MPNSTs [15] and that the key Ras-regulated signaling pathways in these tumors are poorly understood. This led us to hypothesize that an alternative approach, namely targeting the upstream proteins that drive Ras hyperactivation in *NF1*-null MPNSTs would be effective against MPNSTs. Prior to testing this hypothesis, though, we must identify the key Ras activating proteins in MPNSTs. Several lines of evidence suggest that one or more members of the erbB family of receptor tyrosine kinases (RTKs) fulfill this role in MPNSTs. We and others have shown that MPNSTs variably express erbB1 (the EGF receptor), erbB2, erbB3 and erbB4 [16]. These erbB kinases are constitutively activated in MPNST cells [16] and promote their proliferation [16] and migration [17]. Further, when we overexpressed an erbB3/erbB4-specific ligand [the neuregulin-1 (NRG1) isoform glial growth factor-β3 (GGFβ3)] in the Schwann cells of transgenic mice (P_0-GGFβ3 mice), these animals developed neurofibromas [18] that transformed into MPNSTs *in vivo* [18, 19] with genomic abnormalities analogous to those seen in human MPNSTs [18]. Our subsequent genetic complementation experiments showed that NRG1 promotes MPNST pathogenesis by activating erbB3 and erbB4-mediated signaling cascades that are dysregulated by neurofibromin loss [20].

These observations present a conundrum, though—NRG1 activates both erbB3 and erbB4 and these receptors are often coexpressed in MPNSTs. Consequently, it is not clear which of them drives MPNST pathogenesis. This distinction has important mechanistic and therapeutic implications. NRG1 binds to erbB4 with an affinity an order of magnitude greater than that of erbB3 and, when activated, erbB4 has greater tyrosine kinase activity [21]. ErbB4 also responds to several ligands (NRG3, NRG4, betacellulin, epiregulin, heparin-binding EGF) that do not

activate erbB3. As their intracellular domains contain distinct docking sites for cytoplasmic signaling molecules, the downstream signaling pathways activated by erbB4 differ from those regulated by erbB3 [21, 22]. Further, erbB4, unlike other erbB kinases, can be proteolytically cleaved post-activation [23, 24], releasing a cytoplasmic fragment that functions as a transcriptional regulator [25]. It is thus likely that if erbB4 promotes MPNST pathogenesis, it does so via mechanisms different from erbB3. If erbB4 promotes MPNST pathogenesis, it would also represent a potential target for new therapeutic agents such as the monoclonal anti-erbB4 antibodies that are currently in development. Consequently, here we test the hypothesis that erbB4 promotes MPNST pathogenesis and that it does so by activating cytoplasmic signaling cascades distinct from those regulated by erbB3.

Methods

Reagents and antibodies

A mouse anti-GAPDH monoclonal antibody (clone 6C5) was purchased from Fitzgerald Antibodies and Antigens (Concord, MA). Rabbit anti-erbB4 antibodies were from Santa Cruz (sc-284) and Abcam (ab35374; Cambridge, MA). Rabbit anti-actinin (# 6487) and anti-S100β antibodies were purchased from Cell Signaling and Dako (Carpinteria, CA), respectively. Nestin (clone rat-401), pan-Ras (clone Ras-10), and erbB4 (HFR1; #05-1133) mouse monoclonal antibodies were from Millipore (Billerica, MA). Anti-Ki67 and anti-CD31 antibodies were obtained from Abcam (ab15580 and ab23364). Actin Green, Alexa Fluor 568 were purchased from Invitrogen,;Cy3-, fluorescein isothiocyanate (FITC)- and horseradish peroxidase-conjugated secondary antibodies were from Jackson Immunoresearch (West Grove, PA). IRDye 680RD and IRDye800CW secondary antibodies were from LI-COR (Lincoln, NE). Cy3 Tyramide Signal Amplification kits were from Perkin Elmer (Waltham, MA), while Immpress Polymer Detection Reagents were purchased from Vector Laboratories (Burlingame, CA). The PLCγ inhibitor

U73122 (#112648-68-7) was from Selleckchem. Stat5 (CAS 285986-31-4; #573108) and Stat3 (5, 15-DPP; #D4071) inhibitors were from Sigma.

Human MPNST specimens and lines

Paraffin blocks of surgically resected human MPNSTs were from the files of the UAB Department of Pathology. We have previously described the sources of our human MPNST cell lines [16, 17, 26, 27]. MPNST cells were maintained in Dulbecco's modification of Eagle's medium (DMEM) supplemented with 10% fetal calf serum, 10 µg/mL streptomycin and 10 IU/mL penicillin (DMEM10). Cell line identities were validated by short tandem repeat analyses as recommended by ATCC Technical Bulletin 8. The morphology and doubling times of these cultures were monitored and cells were tested at regular intervals by PCR for *Mycoplasma*.

Immunoblotting and immunohistochemistry

Cells were lysed and immunoblotted using our previously described methodology [20]. Immunoreactive species were identified using enhanced chemiluminescence (Pierce) or Licor IRDye secondaries. We have found that detection of erbB4 is highly dependent on lysis conditions; for details and a comparison of erbB4 detection under different lysis conditions, see Figure S1. Activated Ras was pulled down using the Raf1-Ras binding domain (ThermoFisher; Waltham, MA) and detected with a pan-Ras antibody as previously described [20]. Nestin, S100β, and Ki67 immunohistochemistry, TUNEL labeling and determination of Ki67 and TUNEL labeling indices was performed per our previously described methodologies [20]. To quantify vascular densities, 3-4 independent images of CD31-immunostained sections from each graft (Cre-ablated and control) of UBI-1 and UBI-2 cells were analyzed with ImageJ using the "automated counting of single-color image" function.

RNA interference

A pool of four siRNAs targeting erbB4 (L-003128-00-005) and a non-targeting control pool (D-001810-10-05) were purchased from Thermo Scientific (Waltham, MA), while WNK1 (Sigma TRCN0000000919, TRCN0000219718) and erbB4 shRNAs (TRCN00000001410, TRCN00000001411) were obtained from the Hollings Cancer Center shRNA Shared Resource. Cells plated in DMEM-10 (200,000 cells/well in 6 well plates) were transfected with siRNAs using X-TREME Gene siRNA transfection reagent (Roche, Indianapolis, IN; 5:2 transfection reagent:siRNA). Cells were transduced with shRNAs using our previously described methodology [15].

Quantitative PCR (QPCR)

1000 ng of total RNA isolated using Trizol (Life Technologies) was converted to cDNA using a SuperScript Vilo RT Kit (Invitrogen). 5-20 ng of cDNA was used for QPCR with TaqMan primer sets following the manufacturers' protocol. The TaqMan primer sets used were: pan-erbB4: Hs00171783_m1 (spans exons 12-13, detects all isoforms), Hs00955522_m1 (spans exons 26-27; CYT1 specific), Hs00955509_m1 (spans exons 14-15; JMb specific), Hs00955511_m1 (spans exons 16-17; JMa specific), a custom set for CYT2 (spans exons 25-27; 5' primer: 5′-CAACATCCCACCTCCCATCTATAC-3′, 3' primer: 5′ACACTCCTTGTTCAGCAGCAAA-3′, probe a: 5′AATTGACTCGAATAGGAACCAGTTTGTATACCGAGAT-3′) and GAPDH (Hs99999905_m1, Mm99999915_g1).

***In vitro* proliferation and survival assays**

Tritiated thymidine incorporation assays were performed as previously described [26] with cells plated at a density of 20,000 cells per well in 48 well plates. For Real-Time Glo and MTT assays, 4,000 or 20,000 log phase cells per well were plated in 96 or 48 well plates, respectively, and assays performed following the manufacturers' instructions.

Genetically engineered mouse models

Mice were maintained according to the *NIH Guide for the Care and Use of Laboratory Animals* (Eighth Edition). Standard cages were used to house mice, with food and water available *ad libitum.*

We have previously described the generation and characterization of P_0-GGFβ3;*Trp53*$^{+/-}$ mice [20]. *Erbb4*$^{-/-}$; α-MHC-*Erbb4* mice [28] were provided by Dr. Andres Buonanno. Mice with exon 2 of the *Erbb4* gene flanked by loxP sites (*Erbb4*$^{flox/flox}$ mice) were obtained from Dr. Kent Lloyd [29]. P_0-GGFβ3;*Trp53*$^{+/-}$ mice were mated to *Erbb4*$^{flox/flox}$ mice and the resulting progeny then mated to each other to generate P_0-GGFβ3;*Trp53*$^{+/-}$;*Erbb4*$^{flox/flox}$ mice. Offspring were screened via PCR using previously described primers for the P_0-GGFβ3 transgene, *Trp53* null alleles [19, 20], *Erbb4*^{flox} and *Erbb4* wild-type alleles [30].

Diagnosis of mouse tumors

Mice were examined daily for our previously described indicators of tumor development [20]; complete necropsies were performed on mice with suspected tumors and early passage cultures prepared from tumors per our previously established methods [18, 20]. Tumor diagnoses were performed following World Health Organization (WHO) diagnostic criteria as we previously described [20].

***Erbb4* ablation with adenoviral vectors**

Mouse MPNST cells were plated (100,000 cells/mL) in DMEM10. The next morning, cultures were rinsed with PBS and infected with Ad5CMVCre-eGFP or Ad5-eGFP (Gene Transfer Vector Core, University of Iowa; Iowa City, IA) in 10mL DMEM (MOI 100) for 8 hours; 10mL DMEM10 was then added. 24-48 hours post-transfection, GFP-positive cells were sorted on a BD Biosciences FACS Aria machine using FACS Diva software (Franklin Lakes, NH). *Erbb4*

deletion was assessed using previously described primers [31] which generate a 250 base pair band from recombined *ErbB4*^{flox} alleles and a 350 base pair band from non-recombined alleles.

Orthotopic allografts

48 hours after transduction with Ad5CMVCre-eGFP or Ad5-eGFP and FACS sorting, 50,000 GFP-positive MPNST cells were orthotopically allografted into the sciatic nerves of Hsd: Athymic Nude-Foxn1^{nu} mice (Harlan Laboratories; Indianapolis, IN) per our previously published protocol [32].

Antibody arrays

The phosphorylation of 43 kinases and two related proteins was assessed using Proteome Profiler Phospho-Kinase Arrays (#ARY003B; R&D Systems, Minneapolis, MN). MPNST cells were serum starved overnight and then stimulated with 10nM NRG1β for 5 minutes. Cells were lysed and arrays processed and developed per the manufacturer's recommendations. Signals were quantified using the Protein Array Analyzer Plug In for FIJI.

Results

Aberrant expression of erbB4 is evident in MPNSTs

Our previous analyses of two MPNST cell lines and six tumor samples indicated that erbB4 was variably expressed in these neoplasms [16]. To determine how commonly erbB4 is expressed in MPNSTs *in vivo* and examine its distribution in these tumors, we immunostained thirty surgically resected human MPNSTs (see Table S1 for the demographics and NF1 status of these patients). Twenty-five tumors (83%) were positive for erbB4 and demonstrated prominent membranous (Fig. 1A, erbB4 stain; 1B, control non-immune IgG stain) and/or nuclear (Fig. 1C) immunoreactivity. The membranous staining was often punctate, consistent with our previous observations in MPNST cells [17]. Intratumoral variability was evident, with both erbB4-positive

and –negative tumor cells present in the same neoplasm. Upon scoring the number of erbB4 positive tumor cells in each MPNST, we found that in most (16/25) tumors, the majority [>75% (4+; Fig. 1D) or 50-75% (3+; Fig. 1E)] of the tumor cells were erbB4 immunoreactive. In another seven tumors, erbB4 staining was less widely distributed, with 25-50% of the tumor cells being erbB4 positive (2+; Fig. 1F). The remaining two erbB4-positive MPNSTs contained <10-25% erbB4-immunoreactive cells (data not shown).

To compare erbB4 expression in MPNST cells to that in non-neoplastic human Schwann cells, we performed real time PCR quantification of *ERBB4* mRNA levels in 16 MPNST cell lines (Fig. 1G), with MCF7 cells serving as a positive high expressing control. Eleven lines had *ERBB4* expression greater than that in Schwann cells, with the highest levels observed in MPNST642, NMS2, NMS2-PC and T265-2c cells, and intermediate expression levels in 2XSB, sNF02.2, S462, 90-8TL, MPNST2, sNF96.2, and sNF94.3 cells. Four lines (ST88-14, STS-26T, HS-PSS, Hs-Sch2) had *ERBB4* expression that was slightly lower than Schwann cells. A comparison of erbB4 protein and mRNA expression in a selected subset of MPNST lines showed that all of the lines that expressed *ERBB4* mRNA also had detectable erbB4 protein (Fig. 1H). However, *ERBB4* mRNA levels were not necessarily predictive of erbB4 protein levels, suggesting that post-translational factors regulate erbB4 protein levels in MPNST cells.

Alternative splicing of *ERBB4* mRNAs results in the production of functionally distinct protein variants that contain different juxtamembrane domains (JMa, JMb variants) and either include or lack a sequence in the autophosphorylation domain of the receptor (CYT1 and CYT2 variants, respectively). JMa variants, unlike JMb isoforms, can undergo proteolytic cleavage to release a 120kDa fragment that acts as a transcriptional regulator. The CYT1 sequence contains a p85 docking site that allows erbB4-mediated activation of the PI3 kinase/Akt signaling cascade. To determine which *ERBB4* splice variants are predominantly expressed in MPNST cells, we performed real-time PCR with isoform specific primer/probe sets (Figure S2A). We found that most MPNST cell lines had higher expression of JMa than JMb variants while

CYT1 and CYT2 variant expression was comparable across our panel of cell lines (Figure S2B and C).

ErbB4 promotes proliferation, survival and angiogenesis in MPNSTs

To determine whether erbB4 promotes the proliferation and survival of human MPNST cells, we targeted *ERBB4* expression using siRNAs in cell lines (S462 and T265-2c) with increased erbB4 mRNA and protein expression compared to Schwann cells (Fig. 2A). MTT and ^{3}H-thymidine incorporation assays showed that cultures with transient *ERBB4* knockdown contained smaller numbers of viable cells relative to cultures receiving nonsense control siRNAs (Fig. 2B), a change due, at least in part, to decreased proliferation (Fig. 2C). Stable knockdown of *ERBB4* in MPNST642 cells, tumor cells with a very high level of *ERBB4* mRNA expression and protein expression (Figure S1B), similarly showed reductions in erbB4 protein levels (Fig. 2D) and the number of viable cells (Fig. 2E).

Our previously described P_0-GGFβ3;*Trp53*$^{+/-}$ genetically engineered mouse (GEM) model develops MPNSTs *de novo* with complete penetrance [20]; like human MPNSTs, these GEM tumors and early passage cultures derived from them express erbB4 (Fig. 2F; Fig. S2D). We therefore decided to use this model to further dissect erbB4's role in MPNST pathogenesis *in vivo*. Unfortunately, however, we could not generate P_0-GGFβ3;*Trp53*$^{+/-}$ mice with germline *Erbb4* deletion as germline *Erbb4* loss produces cardiac defects that result in embryonic lethality [33]. The approach of introducing floxed *Erbb4* alleles into MPNSTs and deleting them with CreER^{T2} was also problematic as our initial experiments indicated that mosaicism would complicate the interpretation of these experiments. We therefore tried crossing P_0-GGFβ3;*Trp53*$^{+/-}$ mice to mice in which *Erbb4*$^{-/-}$ lethality is rescued by re-expressing erbB4 in the heart (*Erbb4*$^{-/-}$;α-MHC-*Erbb4* mice). However, out of 65 pups expected to have the desired P_0-GGFβ3;*Trp53*$^{+/-}$;*Erbb4*$^{-/-}$;α-MHC-*Erbb4* genotype, we obtained only one pup with this genotype and it did not produce any progeny.

We thus took the alternative approach of producing P_0-GGFβ3;*Trp53*$^{+/-}$;*Erbb4*$^{flox/flox}$ mice, with the goal of deleting *Erbb4 ex vivo*, grafting the cells back into mice and then assessing the effects of *Erbb4* ablation on tumor growth. The survival of P_0-GGFβ3;*Trp53*$^{+/-}$;*Erbb4*$^{flox/flox}$ mice (average survival, 210 days; Fig. 2G) was indistinguishable from that of P_0-GGFβ3;*Trp53*$^{+/-}$ mice [20]. Peripheral nervous system tumors were present in nearly 100% of the P_0-GGFβ3;*Trp53*$^{+/-}$;*Erbb4*$^{flox/flox}$ mice; these tumors were most commonly associated with trigeminal nerves, with some evident in sciatic nerve or dorsal root ganglia (Table S2). The tumors in P_0-GGFβ3;*Trp53*$^{+/-}$;*Erbb4*$^{flox/flox}$ mice were markedly hypercellular MPNSTs with brisk mitotic activity (Fig. 2H) and immunoreactivity for S100β and nestin (Fig. 2 I-K). As tumor penetrance and lifespan in P_0-GGFβ3;*Trp53*$^{+/-}$;*Erbb4*$^{flox/flox}$ mice and P_0-GGFβ3; *Trp53*$^{+/-}$; mice was similar, we concluded that the floxed *Erbb4* alleles did not impede tumorigenesis or worsen the survival of these mice.

To determine what effects erbB4 loss had in these tumors, we established early passage P_0-GGFβ3;*Trp53*$^{+/-}$;*Erbb4*$^{flox/flox}$ MPNST cultures, transduced them with adenovirus expressing eGFP or eGFP-Cre recombinase. eGFP-positive cells were isolated via FACS from each treatment group. PCR analyses verified the presence of recombined *Erbb4* alleles and *Erbb4* mRNA reductions (Figure S3A and B) in the presence of Cre recombinase, but not in controls. *Erbb4* ablation did not reduce the expression of *Egfr*, *Erbb2* or *Erbb3* mRNAs (Fig. S3C) indicating that the changes described below are unlikely to reflect indirect effects on the expression of other erbB family members. The purified tumor cells were viable but demonstrated morphologic changes. In contrast to the spindled morphology of cells with intact *Erbb4* alleles (Fig. 2L), the *Erbb4* knockout cells were ameboid with shorter, thicker processes and often showed nuclear blebbing (Fig. 2M-N). To determine whether *Erbb4* ablation in P_0-GGFβ3;*Trp53*$^{+/-}$;*Erbb4*$^{flox/flox}$ MPNSTs inhibited viability, we performed MTT assays on transduced cultures of three independently arising MPNSTs. We found that cultures transduced with Cre-expressing adenovirus showed decreased numbers of viable cells compared to cells

infected with the control vector (Fig. 2O). As in human MPNST cells, ^{3}H-thymidine incorporation assays demonstrated that this decrease in cell numbers was due, in part, to reduced proliferation (Fig. 2P).

To examine the effects of *Erbb4* ablation *in vivo*, the three distinct P_0-GGFβ3;*Trp53*$^{+/-}$;*Erbb4*$^{flox/flox}$ early passage MPNST cultures previously assessed by MTT and ^{3}H-thymidine incorporation assays (Fig. 2O-P) were transduced with eGFP- or eGFP-Cre expressing adenovirus, FACs sorted and then orthotopically allografted in the sciatic nerves of nude mice. The grafts were excised 35 days post-grafting, and their masses and volumes determined. Grafts of *Erbb4*-ablated tumor cells showed up to an 80% reduction in volume and mass relative to grafts of cells transduced with eGFP-expressing adenovirus (Fig. 3A, B). The cellularity of the *Erbb4*-null tumors was lower than that of the eGFP controls (Fig. 3C, D) and the *Erbb4* knockout cells had more prominently vacuolated cytoplasm. To determine whether this decrease in graft mass and volume reflected decreased tumor cell proliferation or survival, we quantified the Ki67 and TUNEL labeling indices in five *Erbb4*-ablated and five control grafts established from each of the three early-passage cultures. In all instances, there were statistically significant decreases in Ki67 labeling in the *Erbb4*-null grafts relative to eGFP controls (Fig. 3E). In addition, the *Erbb4*-ablated allografts demonstrated a 3-4-fold increase in the percentage of TUNEL positive cells relative to the control grafts (Fig. 3F). *Erbb4* loss thus results in both decreased proliferation and increased apoptosis in these grafts.

During our gross examination of the grafts, we noted that the *Erbb4* ablated grafts were paler than the controls, raising the question of whether vascular density was decreased in the grafts lacking *Erbb4*. Upon immunostaining our grafts for the vascular marker CD31, we found that the vascular density in the *Erbb4* ablated grafts (Fig. 3K-M) did indeed appear to be lower than that in the control allografts (Fig. 3G-J). Quantification of the vascular densities in these grafts showed that the vascular density in the *Erbb4* ablated grafts was approximately half that of the control grafts (Fig. 3N). As *Erbb4* is intact in the vasculature within these grafts, this

suggests that the decreases in vascular density observed in *Erbb4* ablated grafts are an indirect effect of *Erbb4* loss in MPNST cells via mechanisms such as erbB4-mediated enhancement of the production and/or secretion of angiogenic factors by MPNST cells.

ErbB4 mediates basal and NRG1-stimulated phosphorylation of multiple cytoplasmic kinases, but is not essential for Ras hyperactivation

Although MPNSTs co-express erbB3 and erbB4, our demonstration that *Erbb4* ablation decreased proliferation, survival and angiogenesis in MPNSTs indicates that these receptors are not functionally redundant and suggest that erbB4 activates distinct signaling cascades essential for MPNST tumorigenesis. As many growth factors, including NRG1 [34], activate Ras, we first asked whether *Erbb4* ablation diminished the erbB-dependent Ras hyperactivation we have previously observed in P_0-GGFβ3;*Trp53*$^{+/-}$ MPNSTs [20]. To answer this question, we generated lysates from early passage P_0-GGFβ3;*Trp53*$^{+/-}$;*Erbb4*$^{flox/flox}$ MPNST cells transduced with eGFP or eGFP-Cre expressing adenovirus, pulled down the activated Ras proteins with Raf-1 and then probed the captured Ras proteins using a pan-Ras antibody (Fig. 4A). Surprisingly, we found that Ras activation was not reduced by *Erbb4* ablation, indicating that *Erbb4* loss impairs MPNST proliferation and survival via effects on Ras-independent pathways.

To identify the erbB4-regulated signaling cascades potentially driving proliferation, survival and angiogenesis in MPNSTs, we stimulated *Erbb4* intact and *Erbb4*-null GGFβ3;*Trp53*$^{+/-}$;*Erbb4*$^{flox/flox}$ MPNST cells with 10nM NRG1β for 5 minutes, a time that our preliminary analyses indicated was sufficient to maximally activate NRG1β-responsive signaling pathways. Lysates from these cells were used to probe arrays containing phosphorylation site-specific antibodies that query 43 different cytoplasmic kinases and other key proteins (Figure S4). We then asked which of these proteins showed altered phosphorylation following NRG1β stimulation and *Erbb4* ablation.

We first identified the NRG1β responsive proteins and kinases in *Erbb4* intact GGFβ3;*Trp53*$^{+/-}$;*Erbb4*$^{flox/flox}$ MPNST cells; as NRG1β activates both erbB3 and erbB4, alterations in the phosphorylation of the proteins queried by our arrays in these cells could reflect the action of either erbB3 or erbB4. Kinases whose phosphorylation levels were changed by at least 1.5-fold compared to unstimulated cells were considered NRG1β responsive. Using this criterion, we identified 16 NRG1β responsive sites with increased phosphorylation and 2 NRG1β responsive events in which the phosphorylation of the targeted protein was decreased (Fig. 4B). The proteins in which NRG1β increased phosphorylation included Akt (T308), RSK, PRAS40 [also known as AKT1S1 (Akt1 substrate 1)], Src, Hck, Fyn, STAT3 (S727 and Y705), PYK2, PLCγ1, p53 (S46) and Chk-2; of particular note, given that we have previously shown that Ras is activated in P_0-GGFβ3;*Trp53*$^{+/-}$ MPNSTs by NRG1 [20], we found that the phosphorylation of ERK was also increased by NRG1β stimulation in these experiments. In contrast, the phosphorylation of S473 in pAKT (unlike T308, another activation site in Akt, where phosphorylation was increased by NRG1β; see above), JNK, STAT5a/b (Y694/Y699) and β-catenin was decreased following NRG1β stimulation. However, since decreased phosphorylation of β-catenin results in increased transcriptional activity, this latter change reflects increased activation of the β-catenin pathway downstream of NRG1β.

To determine which phosphorylation events noted above required NRG1β-mediated activation of erbB4, we compared the stimulated the phosphorylation profile of *Erbb4* intact cells to that of *Erbb4* ablated cells (Fig. 4C). We found that two of the 18 NRG1β-responsive phosphorylation events were partially dependent on the presence of *Erbb4* (PRAS40, Akt-T308) suggesting that erbB3 and erbB4 redundantly regulate these PI3K pathway proteins downstream of NRG1β through distinct heterodimers. The phosphorylation of six kinases (Src, Hck, Chk-2, p53-S46, STAT5a and b) was completely dependent on NRG1β and intact *Erbb4*, indicating that NRG1β-driven phosphorylation of these targets is mediated, directly or indirectly,

by erbB4. Interestingly, several of the changes we observed suggested that erbB3 and erbB4 play opposing roles in activating some signaling pathways in MPNSTs. For instance, the phosphorylation of STAT5a/b at Y694/699, two sites that are required for activation, was weakly (0.66 fold down) decreased by NRG1β in the presence of *Erbb4*. However, in the absence of *Erbb4*, NRG1β stimulation resulted in an almost complete loss of STAT5a/b activation, suggesting that erbB4 opposes erbB3-mediated inhibition of STAT5a/b. The reduction in pAkt-S473 phosphorylation observed in response to NRG1β stimulation (Fig. 2B) was also rescued by *Erbb4* ablation, with pAkt-S437 returning to baseline levels in the presence of NRG1β. In contrast, the reduction in β-catenin phosphorylation levels observed in response to NRG1β stimulation was further exaggerated when *Erbb4* was ablated, suggesting both erbB3 and erbB4 activate this signaling cascade. The remaining six NRG1β -responsive proteins (RSK, Fyn, STAT3-Y705/S727, PLCγ-1, PYK2) had phosphorylation that was enhanced by erbB4, both in the presence and absence of exogenous NRG1β (Fig. 4C). This latter observation may reflect erbB4 activation mediated by endogenous NRG1β expressed by the tumor cells themselves or, alternatively, the action of other erbB4 ligands expressed by the MPNST cells that similarly activate downstream signaling cascades.

We next asked whether there were additional proteins whose phosphorylation was dependent upon *Erbb4* but unaffected by NRG1β stimulation. We identified 15 proteins whose phosphorylation was not altered when challenged with exogenous NRG1β but that were sensitive to *ErbB4* ablation. *Erbb4* ablation decreased the phosphorylation of five of these proteins [WNK1, p53 (S15), p70S6K, eNOS, and HSP60; Fig. 4D), suggesting that *Erbb4* is a key upstream activator of these kinases. *Erbb4* loss increased the phosphorylation of the other ten proteins in a NRG1β independent manner suggesting that erbB4 negatively regulates the activation of these proteins. This latter group of proteins included two RTKs, EGFR and PDGFRβ, as well as HSP27, five Src-related kinases (Lck, Lyn, FAK, Fgr, Yes), mTOR and

MSK1/2 kinases (Fig. 4E). The majority of these proteins are associated with the plasma membrane and their activation in the absence of erbB4 may be a direct result of altered receptor heterodimerization and cellular architecture at the plasma membrane.

Gene ontology analyses of both the NRG1β-dependent and –independent targets of erbB4 indicated that the biological pathways regulated by erbB4 promote migration and survival (Fig. 5). Specifically, these analyses indicated that the erbB4/NRG1β-dependent kinases drive proliferation and cell communication, response to stress, migration, survival and response to nitrogen compounds, whereas the NRG1β-independent actions of erbB4 include migration, survival and blood vessel cell migration. Importantly, the results of these gene ontology analyses are consistent with our experimental findings demonstrating that erbB4 promotes survival, proliferation and angiogenesis in MPNST cells.

MPNSTs are sensitive to inhibitors targeting erbB4 activated signaling pathways

To directly assess whether the proteins whose phosphorylation is altered by *Erbb4* loss include molecules that promote MPNST proliferation and/or survival, we inhibited the actions of four of these proteins (WNK1, PLCγ, STAT3 and STAT5a). Although our shRNAs effectively knocked down WNK1 expression in T265-2c and S462 cells, MTT assays did not show a reproducible decrease in the number of viable cells following knockdown (Fig. 6A). In contrast, the PLCγ inhibitor U73122 inhibited the viability of T265-2c, S462 and MPNST462 cells in a concentration-dependent manner (Fig. 6B). Likewise, the STAT3 inhibitor Cas285986-31-4 also inhibited the viability of three MPNST cell lines in a concentration-dependent manner (Fig. 6C). The STAT5 inhibitor 5,15-DPP also decreased the number of viable cells in cultures of these lines in a concentration-dependent manner, although its effects were not as pronounced as those of the STAT3 inhibitor (Fig. 6D). We conclude that PLCγ, STAT3 and STAT5 are among the erbB4 targets that mediate the proliferation and/or survival of MPNST cells (Fig. 7).

Discussion

The erbB4 receptor tyrosine kinase has been implicated in the pathogenesis of several human cancers including glioblastomas [35], melanomas [36, 37], medulloblastomas [38], pulmonary adenocarcinomas [39], ovarian carcinomas [40] and esophageal carcinomas [41]. Many of these cancer types also express erbB3, a second NRG1 receptor that is functionally distinct from erbB4. Surprisingly, it has not been clearly established whether the co-expression of two NRG1 receptors in these neoplasms promotes tumorigenesis and, if they do, whether they do so by increasing receptor numbers (thereby rendering tumor cells more responsive to NRG1 or other erbB ligands) or whether these two receptors instead make distinct, critically important contributions to tumor initiation and progression. The evidence we have obtained using MPNSTs as a model system argues that, at least in this setting, erbB3 and erbB4 promote tumorigenesis by regulating different essential signaling cascades. However, our findings also raise intriguing new questions regarding the mechanisms by which erbB4 drives tumor pathogenesis.

Several lines of evidence reported in this manuscript support the hypothesis that erbB4 promotes MPNST pathogenesis. Our immunohistochemical, real time PCR and immunoblotting results demonstrate that multiple erbB4 splice variants, including variants capable of activating PI3K signaling and mediating transcription, are expressed in the overwhelming majority of human and mouse MPNSTs. Ablation of *Erbb4* in P_0-GGFβ3;*Trp53*$^{+/-}$;*ErbB4*$^{flox/flox}$ MPNST cells results in altered cellular morphology, increased cell death and reduced proliferation. Further, when allografted in nude mice, *Erbb4*-null P_0-GGFβ3;*Trp53*$^{+/-}$;*Erbb4*$^{flox/flox}$ MPNST allografts produce tumors up to 80% smaller than controls with evidence of decreased mitogenesis, increased cell death and decreased vascular density. Finally, knocking down *ERBB4* expression in human MPNST cells has effects on proliferation and survival analogous to those seen in *Erbb4*-null mouse MPNSTs. We found that loss of erbB4 expression did not reduce the expression of erbB3, the other NRG1 receptor, in these MPNST cells. Further, the *Erbb4*-null

tumor cells are still NRG1-responsive, as demonstrated by our phosphorylation-specific antibody array experiments. It is thus apparent that the erbB3 receptors expressed in MPNST cells cannot completely compensate for the loss of erbB4 expression.

Our findings also indicate that erbB3 and erbB4 mediate distinct effects in MPNST cells. The erbB3 receptors expressed in MPNST cells are clearly functional as the phosphorylation of the Ras downstream effectors Erk-1/2 and JNK-1/2/3 were similarly increased in NRG1-stimulated *Erbb4*-null cells and unmodified controls. Consequently, the effects we observed following *Erbb4* ablation are not due to a loss of NRG1 responsiveness. These changes are also not the result of decreased Ras activation as Ras activation was unaffected by *Erbb4* loss. As both erbB3 and erbB4 can activate Ras, this suggests that erbB3 and/or other erbB receptors compensate for erbB4 loss in MPNST cells to maintain Ras activation. Our demonstration that erbB4 loss results in decreased proliferation and survival thus indicates that erbB4 must promote the proliferation and survival of MPNST cells by regulating other non-Ras dependent signaling cascades.

By comparing kinase phosphorylation in NRG-1β stimulated and unstimulated *Erbb4*-null and control cells, we identified several candidate kinases that potentially represent the downstream effectors of erbB4-mediated proliferation, survival, angiogenesis and, potentially, other effects in MPNSTs. In keeping with our demonstration that MPNST cells express erbB4 splice variants containing the Cyt1 domain, *Erbb4*-null MPNST cells demonstrated altered phosphorylation of Akt and key Akt targets such as, eNOS, ribosomal p70S6 kinase (S6K) and ribosomal p90S6 kinase (RSK1/2/3); the phosphorylation of these molecules was decreased in Cre-treated *Erbb4* ablated tumor cells, indicating that erbB4 positively regulates the PI3K/Akt/mTOR signaling cascades in MPNST cells. However, erbB-mediated regulation of Akt action in MPNST cells is likely complex. We have found that NRG1β, acting through erbB4, reduced the phosphorylation of Akt residue S473 yet we observed an increase in T308 phosphorylation that was at least partially dependent on erbB4. A similar inverse response on

Akt has been previously reported in response to ER-stress and is a context dependent mechanism that diversifies Akt signaling [42]. Although the phosphorylation of both of these sites activates Akt, the phosphorylation of these two amino acids is orchestrated by different kinases; S473, which resides in the regulatory domain of Akt, is phosphorylated by mTORC2 and DNA-PK, while T308 which is located in the Akt kinase domain, is a direct target of PDK1. The fact that both S473 and T308 were found to be increased by NRG1 stimulation in the absence of erbB4 suggest that this increase is mediated partially by erbB3. The fact that we see positive regulation of eNOS, a major regulator of angiogenesis, apoptosis, invasion and metastasis, strongly suggests that PDK1-Akt (T308) promotes MPNST growth downstream of erbB4 and thus may be a useful therapeutic target. However, regulation of the PI3K pathway is often further complicated by the expression of multiple PDK1 isoforms that have opposing effects on mTORC1 activity. We would also point out that erbB3, which is also activated by NRG1, contains multiple docking sites for the regulatory p85 subunit of PI3 kinase and thus also likely plays an important role in the regulation of the PI3K/Akt signaling cascade in MPNST cells. It will be of great interest to determine how erbB3 and erbB4 inputs into the PI3K/Akt signaling pathway interact in MPNST cells.

We have also found that erbB4 promotes the phosphorylation of PLC-γ, a protein that promotes the pathogenesis of many tumor types. Inhibition of PLC-γ action in MPNST cells reduced the number of viable cells, indicating that PLC-γ has a similar role in MPNSTs. In addition, we discovered that erbB4 regulates the phosphorylation of two molecules—with-no-lysine kinase 1 (WNK1), a kinase that is phosphorylated at Thr60 by Akt [43], and heat shock protein 60 (HSP60)—that promote tumorigenesis in other cancer types. In glioma cells, WNK1 associates with multiple ion transporters and contributes to migration by modulating volumetric changes [44]. This action is consistent with our observation that *Erbb4* ablation alters the morphology of MPNST cells. However, in HeLa cells, WNK1 associates with mitotic spindles and promotes mitosis and abscission; loss of this kinase results in aberrant mitotic spindle

formation, defective cell division and cell death [45]. In contrast to the findings in HeLa cells, we found that WNK1 knockdown did not impair the proliferation and survival of MPNST cells. Further, we commonly observed multinucleated cells in control tumors but not *ErbB4*-null tumors; this is the opposite of what we would expect based on the earlier findings in HeLa cells. These findings thus suggest that WNK1 functions in MPNST cells differ from those observed in other tumor types. Heat shock proteins are upregulated in response to cellular stress and chaperone protein folding. However, heat shock protein expression in tumors is not strictly linked to stress [46]; these proteins also facilitate evasion of apoptosis [47] and help tumor cells escape or inhibit immune system surveillance. These latter HSP60 actions raise the question of whether erbB4 promotes MPNST pathogenesis via analogous mechanisms.

In MPNSTs, we found that erbB4 promotes nuclear signaling by phosphorylating STAT3 and STAT5, two downstream targets of the mTOR and Jak/Stat signaling pathways. Our demonstration that pharmacologic inhibition of STAT3 and STAT5 action decreases the number of viable cells *in vitro* indicates that phosphorylation of STAT3 and STAT5 is essential for MPNST proliferation and/or survival. This suggestion is consistent with previous observations indicating that elevated expression of both of these STAT proteins is seen in numerous cancers, where their phosphorylation results in enhanced expression of cell cycle progression (e.g., cyclin D1 [48, 49]) and survival (e.g., Bcl-xL and Bcl-2 [50-52]) genes. The absence of STAT5 activation that we observed in *Erbb4*-null cells is consistent with earlier reports that erbB4 activates STAT5, leading to its transport to the nucleus. However, the changes in STAT3 activity were unexpected, as STAT3 is activated by erbB2 or EGFR in other cell types, not erbB4. It is unlikely that erbB2 drives STAT3 phosphorylation in these tumors as *ErbB4*-null MPNST cells remain NRG-1-responsive and express erbB3, a receptor that dimerizes with erbB2 to form an active NRG1 signaling complex. These observations thus raise the interesting possibility that erbB4 regulates STAT3 phosphorylation in MPNST cells via a previously unknown mechanism.

Interestingly, although some signaling cascades were activated in MPNST cells by NRG1β stimulation, others such as p70S6 kinase, STAT3, WNK1 and HSP60 displayed equivalent levels of phosphorylation in the presence and absence of exogenous NRG1β. Nonetheless, *Erbb4* ablation reduced the phosphorylation of these proteins, indicating that erbB4 regulated their phosphorylation. One potential explanation for this conundrum is that the basal level of stimulation provided by tumor cell-derived NRG1 [16] is sufficient to maximally drive the phosphorylation of these proteins. An alternative explanation, however, reflects the fact that erbB4 is not just a NRG1 receptor; it also responds to NRG2, NRG3, NRG4, heparin-binding EGF, betacellulin and epiregulin. We have previously shown that heparin-binding EGF, betacellulin and epiregulin expression is much lower in human MPNST cells than non-neoplastic Schwann cells [27], making it unlikely that these factors play major roles in promoting erbB4 activation. To the best of our knowledge, however, NRG2, NRG3 and NRG4 action has not been carefully examined in MPNSTs. Consequently, we cannot rule out the possibility that one or more of these growth factors contributes to the baseline activation of erbB4 in MPNST cells and drives the phosphorylation of some erbB4 target molecules.

Conclusions

In summary, multiple erbB4 splice variants are commonly expressed in MPNSTs. Acting in a cell-autonomous manner, these erbB4 variants promote the proliferation and survival of tumor cells. ErbB4 receptors expressed by MPNST cells also indirectly promote angiogenesis in MPNSTs. Despite our anticipation that erbB4 would drive Ras activation, we found that erbB4 instead promotes MPNST pathogenesis via Ras-independent effects; these signaling events include alterations in the PI3K/Akt/mTOR and PLC-γ signaling cascades, activation of transcription via STAT proteins, and the phosphorylation of other molecules with oncogenic potential, such as HSP60. Our findings thus identify erbB4 and key erbB4-dependent signaling pathways as potentially important chemotherapeutic targets in MPNSTs. Future studies will be

needed to further investigate the role of the other erbB4 targets that we have identified in MPNST pathogenesis. It will also be of great interest to establish the relative contributions that canonical membrane-based erbB4 signaling and transcriptional signaling by the erbB4 intracellular domain make to the development of these aggressive spindle cell neoplasms.

Abbreviations

MPNST: malignant peripheral nerve sheath tumor; NF1: neurofibromatosis type 1; NRG: neuregulin; PI3K: phosphatidylinositol-3 kinase; PLCγ: phospholipase C γ; RTK: receptor tyrosine kinase; WNK1: with no lysines 1

DECLARATIONS

Ethics approval and consent to participate

The human studies presented in this manuscript were reviewed and approved by the University of Alabama at Birmingham and the Medical University of South Carolina Institutional Review Boards for Human Use and were performed in accordance with the ethical standards of the 1964 Helsinki Declaration and its later amendments. The University of Alabama at Birmingham and the Medical University of South Carolina Institutional Animal Care and Use Committees approved all animal experiments.

Consent for Publication

Not applicable.

Availability of data and materials

All data generated or analyzed during this study are included in this published article and supplementary information files.

Competing Interests

The authors declare that they have no competing interests.

Funding

This work was supported by grants from the National Institute of Neurological Diseases and Stroke (R01 NS048353 to SLC, F31 NS081824 to SNB), the National Cancer Institute (R01 CA122804 to SLC and R01 CA134773 to KAR), the Department of Defense (X81XWH-09-1-0086, W81XWH-12-1-0164 and W81XWH-15-1-0193 to SLC and W81XWH-14-1-0073 to KAR) and The Children's Tumor Foundation (2014-04-001 and 2015-05-007 to SLC).

Authors' Contributions

KAR and SLC conceived and designed the experiments and provided oversight of the research project and grant funding. SNB, JFL, LB and SJW performed the experiments. SNB, JFL, KAR and SLC prepared the manuscript. All authors have read and approved the final manuscript.

Acknowledgements

We thank the Medical University of South Carolina Hollings Cancer Center Biorepository & Tissue Analysis Shared Resource (P30 CA138313) and the Genomics/shRNA Shared Resource for providing crucial specimens and reagents.

References

1. Carroll SL: **Molecular mechanisms promoting the pathogenesis of Schwann cell neoplasms.** *Acta Neuropathol* 2012, **123:**321-348.
2. Rasmussen SA, Yang Q, Friedman JM: **Mortality in neurofibromatosis 1: an analysis using U.S. death certificates.** *Am J Hum Genet* 2001, **68:**1110-1118.

3. LaFemina J, Qin LX, Moraco NH, Antonescu CR, Fields RC, Crago AM, Brennan MF, Singer S: **Oncologic outcomes of sporadic, neurofibromatosis-associated, and radiation-induced malignant peripheral nerve sheath tumors.** *Ann Surg Oncol* 2013, **20:**66-72.

4. Stucky CC, Johnson KN, Gray RJ, Pockaj BA, Ocal IT, Rose PS, Wasif N: **Malignant peripheral nerve sheath tumors (MPNST): the Mayo Clinic experience.** *Ann Surg Oncol* 2012, **19:**878-885.

5. Kolberg M, Holand M, Agesen TH, Brekke HR, Liestol K, Hall KS, Mertens F, Picci P, Smeland S, Lothe RA: **Survival meta-analyses for >1800 malignant peripheral nerve sheath tumor patients with and without neurofibromatosis type 1.** *Neuro Oncol* 2013, **15:**135-147.

6. Porter DE, Prasad V, Foster L, Dall GF, Birch R, Grimer RJ: **Survival in Malignant Peripheral Nerve Sheath Tumours: A Comparison between Sporadic and Neurofibromatosis Type 1-Associated Tumours.** *Sarcoma* 2009, **2009:**756395.

7. Watson KL, Al Sannaa GA, Kivlin CM, Ingram DR, Landers SM, Roland CL, Cormier JN, Hunt KK, Feig BW, Ashleigh Guadagnolo B, et al: **Patterns of recurrence and survival in sporadic, neurofibromatosis Type 1-associated, and radiation-associated malignant peripheral nerve sheath tumors.** *J Neurosurg* 2017, **126:**319-329.

8. Zou C, Smith KD, Liu J, Lahat G, Myers S, Wang WL, Zhang W, McCutcheon IE, Slopis JM, Lazar AJ, et al: **Clinical, pathological, and molecular variables predictive of malignant peripheral nerve sheath tumor outcome.** *Ann Surg* 2009, **249:**1014-1022.

9. Ducatman BS, Scheithauer BW, Piepgras DG, Reiman HM, Ilstrup DM: **Malignant peripheral nerve sheath tumors. A clinicopathologic study of 120 cases.** *Cancer* 1986, **57:**2006-2021.

10. Anghileri M, Miceli R, Fiore M, Mariani L, Ferrari A, Mussi C, Lozza L, Collini P, Olmi P, Casali PG, et al: **Malignant peripheral nerve sheath tumors: prognostic factors and**

survival in a series of patients treated at a single institution. *Cancer* 2006, **107:**1065-1074.

11. Fan Q, Yang J, Wang G: **Clinical and molecular prognostic predictors of malignant peripheral nerve sheath tumor.** *Clin Transl Oncol* 2014, **16:**191-199.

12. Valentin T, Le Cesne A, Ray-Coquard I, Italiano A, Decanter G, Bompas E, Isambert N, Thariat J, Linassier C, Bertucci F, et al: **Management and prognosis of malignant peripheral nerve sheath tumors: The experience of the French Sarcoma Group (GSF-GETO).** *Eur J Cancer* 2016, **56:**77-84.

13. Lee W, Teckie S, Wiesner T, Ran L, Prieto Granada CN, Lin M, Zhu S, Cao Z, Liang Y, Sboner A, et al: **PRC2 is recurrently inactivated through EED or SUZ12 loss in malignant peripheral nerve sheath tumors.** *Nat Genet* 2014, **46:**1227-1232.

14. Zhang M, Wang Y, Jones S, Sausen M, McMahon K, Sharma R, Wang Q, Belzberg AJ, Chaichana K, Gallia GL, et al: **Somatic mutations of SUZ12 in malignant peripheral nerve sheath tumors.** *Nat Genet* 2014, **46:**1170-1172.

15. Brossier NM, Prechtl AM, Longo JF, Barnes S, Wilson LS, Byer SJ, Brosius SN, Carroll SL: **Classic Ras Proteins Promote Proliferation and Survival via Distinct Phosphoproteome Alterations in Neurofibromin-Null Malignant Peripheral Nerve Sheath Tumor Cells.** *J Neuropathol Exp Neurol* 2015, **74:**568-586.

16. Stonecypher MS, Byer SJ, Grizzle WE, Carroll SL: **Activation of the neuregulin-1/ErbB signaling pathway promotes the proliferation of neoplastic Schwann cells in human malignant peripheral nerve sheath tumors.** *Oncogene* 2005, **24:**5589-5605.

17. Eckert JM, Byer SJ, Clodfelder-Miller BJ, Carroll SL: **Neuregulin-1 beta and neuregulin-1 alpha differentially affect the migration and invasion of malignant peripheral nerve sheath tumor cells.** *Glia* 2009, **57:**1501-1520.

18. Kazmi SJ, Byer SJ, Eckert JM, Turk AN, Huijbregts RP, Brossier NM, Grizzle WE, Mikhail FM, Roth KA, Carroll SL: **Transgenic mice overexpressing neuregulin-1 model neurofibroma-malignant peripheral nerve sheath tumor progression and implicate specific chromosomal copy number variations in tumorigenesis.** *Am J Pathol* 2013, **182:**646-667.

19. Huijbregts RP, Roth KA, Schmidt RE, Carroll SL: **Hypertrophic neuropathies and malignant peripheral nerve sheath tumors in transgenic mice overexpressing glial growth factor beta3 in myelinating Schwann cells.** *J Neurosci* 2003, **23:**7269-7280.

20. Brosius SN, Turk AN, Byer SJ, Brossier NM, Kohli L, Whitmire A, Mikhail FM, Roth KA, Carroll SL: **Neuregulin-1 overexpression and Trp53 haploinsufficiency cooperatively promote de novo malignant peripheral nerve sheath tumor pathogenesis.** *Acta Neuropathol* 2014, **127:**573-591.

21. Carraway KL, 3rd, Cantley LC: **A neu acquaintance for erbB3 and erbB4: a role for receptor heterodimerization in growth signaling.** *Cell* 1994, **78:**5-8.

22. Sawyer C, Hiles I, Page M, Crompton M, Dean C: **Two erbB-4 transcripts are expressed in normal breast and in most breast cancers.** *Oncogene* 1998, **17:**919-924.

23. Vecchi M, Carpenter G: **Constitutive proteolysis of the ErbB-4 receptor tyrosine kinase by a unique, sequential mechanism.** *J Cell Biol* 1997, **139:**995-1003.

24. Zhou W, Carpenter G: **Heregulin-dependent trafficking and cleavage of ErbB-4.** *J Biol Chem* 2000, **275:**34737-34743.

25. Sardi SP, Murtie J, Koirala S, Patten BA, Corfas G: **Presenilin-dependent ErbB4 nuclear signaling regulates the timing of astrogenesis in the developing brain.** *Cell* 2006, **127:**185-197.

26. Byer SJ, Eckert JM, Brossier NM, Clodfelder-Miller BJ, Turk AN, Carroll AJ, Kappes JC, Zinn KR, Prasain JK, Carroll SL: **Tamoxifen inhibits malignant peripheral nerve**

sheath tumor growth in an estrogen receptor-independent manner. *Neuro Oncol* 2011, **13:**28-41.

27. Byer SJ, Brossier NM, Peavler LT, Eckert JM, Watkins S, Roth KA, Carroll SL: **Malignant peripheral nerve sheath tumor invasion requires aberrantly expressed EGF receptors and is variably enhanced by multiple EGF family ligands.** *J Neuropathol Exp Neurol* 2013, **72:**219-233.

28. Tidcombe H, Jackson-Fisher A, Mathers K, Stern DF, Gassmann M, Golding JP: **Neural and mammary gland defects in ErbB4 knockout mice genetically rescued from embryonic lethality.** *Proc Natl Acad Sci U S A* 2003, **100:**8281-8286.

29. Long W, Wagner KU, Lloyd KC, Binart N, Shillingford JM, Hennighausen L, Jones FE: **Impaired differentiation and lactational failure of Erbb4-deficient mammary glands identify ERBB4 as an obligate mediator of STAT5.** *Development* 2003, **130:**5257-5268.

30. Golub MS, Germann SL, Lloyd KC: **Behavioral characteristics of a nervous system-specific erbB4 knock-out mouse.** *Behav Brain Res* 2004, **153:**159-170.

31. Jackson-Fisher AJ, Bellinger G, Shum E, Duong JK, Perkins AS, Gassmann M, Muller W, Kent Lloyd KC, Stern DF: **Formation of Neu/ErbB2-induced mammary tumors is unaffected by loss of ErbB4.** *Oncogene* 2006, **25:**5664-5672.

32. Turk AN, Byer SJ, Zinn KR, Carroll SL: **Orthotopic xenografting of human luciferase-tagged malignant peripheral nerve sheath tumor cells for in vivo testing of candidate therapeutic agents.** *J Vis Exp* 2011.

33. Gassmann M, Casagranda F, Orioli D, Simon H, Lai C, Klein R, Lemke G: **Aberrant neural and cardiac development in mice lacking the ErbB4 neuregulin receptor.** *Nature* 1995, **378:**390-394.

34. Tansey MG, Chu GC, Merlie JP: **ARIA/HRG regulates AChR epsilon subunit gene expression at the neuromuscular synapse via activation of phosphatidylinositol 3-kinase and Ras/MAPK pathway.** *J Cell Biol* 1996, **134:**465-476.

35. Carrasco-Garcia E, Saceda M, Grasso S, Rocamora-Reverte L, Conde M, Gomez-Martinez A, Garcia-Morales P, Ferragut JA, Martinez-Lacaci I: **Small tyrosine kinase inhibitors interrupt EGFR signaling by interacting with erbB3 and erbB4 in glioblastoma cell lines.** *Exp Cell Res* 2011, **317:**1476-1489.

36. Easty DJ, Gray SG, O'Byrne KJ, O'Donnell D, Bennett DC: **Receptor tyrosine kinases and their activation in melanoma.** *Pigment Cell Melanoma Res* 2011, **24:**446-461.

37. Xia J, Jia P, Hutchinson KE, Dahlman KB, Johnson D, Sosman J, Pao W, Zhao Z: **A meta-analysis of somatic mutations from next generation sequencing of 241 melanomas: a road map for the study of genes with potential clinical relevance.** *Mol Cancer Ther* 2014, **13:**1918-1928.

38. Gilbertson R, Hernan R, Pietsch T, Pinto L, Scotting P, Allibone R, Ellison D, Perry R, Pearson A, Lunec J: **Novel ERBB4 juxtamembrane splice variants are frequently expressed in childhood medulloblastoma.** *Genes Chromosomes Cancer* 2001, **31:**288-294.

39. Nakaoku T, Tsuta K, Ichikawa H, Shiraishi K, Sakamoto H, Enari M, Furuta K, Shimada Y, Ogiwara H, Watanabe S, et al: **Druggable oncogene fusions in invasive mucinous lung adenocarcinoma.** *Clin Cancer Res* 2014, **20:**3087-3093.

40. Paatero I, Lassus H, Junttila TT, Kaskinen M, Butzow R, Elenius K: **CYT-1 isoform of ErbB4 is an independent prognostic factor in serous ovarian cancer and selectively promotes ovarian cancer cell growth in vitro.** *Gynecol Oncol* 2013, **129:**179-187.

41. Silva SD, Alaoui-Jamali MA, Hier M, Soares FA, Graner E, Kowalski LP: **Cooverexpression of ERBB1 and ERBB4 receptors predicts poor clinical outcome**

in pN+ oral squamous cell carcinoma with extranodal spread. *Clin Exp Metastasis* 2014, **31:**307-316.

42. Szymonowicz K, Oeck S, Malewicz NM, Jendrossek V: **New Insights into Protein Kinase B/Akt Signaling: Role of Localized Akt Activation and Compartment-Specific Target Proteins for the Cellular Radiation Response.** *Cancers (Basel)* 2018, **10**.

43. Vitari AC, Deak M, Collins BJ, Morrice N, Prescott AR, Phelan A, Humphreys S, Alessi DR: **WNK1, the kinase mutated in an inherited high-blood-pressure syndrome, is a novel PKB (protein kinase B)/Akt substrate.** *Biochem J* 2004, **378:**257-268.

44. Zhu W, Begum G, Pointer K, Clark PA, Yang SS, Lin SH, Kahle KT, Kuo JS, Sun D: **WNK1-OSR1 kinase-mediated phospho-activation of Na+-K+-2Cl- cotransporter facilitates glioma migration.** *Mol Cancer* 2014, **13:**31.

45. Tu SW, Bugde A, Luby-Phelps K, Cobb MH: **WNK1 is required for mitosis and abscission.** *Proc Natl Acad Sci U S A* 2011, **108:**1385-1390.

46. Rappa F, Unti E, Baiamonte P, Cappello F, Scibetta N: **Different immunohistochemical levels of Hsp60 and Hsp70 in a subset of brain tumors and putative role of Hsp60 in neuroepithelial tumorigenesis.** *Eur J Histochem* 2013, **57:**e20.

47. Campanella C, Bucchieri F, Ardizzone NM, Marino Gammazza A, Montalbano A, Ribbene A, Di Felice V, Bellafiore M, David S, Rappa F, et al: **Upon oxidative stress, the antiapoptotic Hsp60/procaspase-3 complex persists in mucoepidermoid carcinoma cells.** *Eur J Histochem* 2008, **52:**221-228.

48. Leslie K, Lang C, Devgan G, Azare J, Berishaj M, Gerald W, Kim YB, Paz K, Darnell JE, Albanese C, et al: **Cyclin D1 is transcriptionally regulated by and required for transformation by activated signal transducer and activator of transcription 3.** *Cancer Res* 2006, **66:**2544-2552.

49. Kong J, Kong F, Gao J, Zhang Q, Dong S, Gu F, Ke S, Pan B, Shen Q, Sun H, et al: **YC-1 enhances the anti-tumor activity of sorafenib through inhibition of signal transducer and activator of transcription 3 (STAT3) in hepatocellular carcinoma.** *Mol Cancer* 2014, **13:**7.

50. Gu L, Vogiatzi P, Puhr M, Dagvadorj A, Lutz J, Ryder A, Addya S, Fortina P, Cooper C, Leiby B, et al: **Stat5 promotes metastatic behavior of human prostate cancer cells in vitro and in vivo.** *Endocr Relat Cancer* 2010, **17:**481-493.

51. Gu L, Dagvadorj A, Lutz J, Leiby B, Bonuccelli G, Lisanti MP, Addya S, Fortina P, Dasgupta A, Hyslop T, et al: **Transcription factor Stat3 stimulates metastatic behavior of human prostate cancer cells in vivo, whereas Stat5b has a preferential role in the promotion of prostate cancer cell viability and tumor growth.** *Am J Pathol* 2010, **176:**1959-1972.

52. Sanchez-Ceja SG, Reyes-Maldonado E, Vazquez-Manriquez ME, Lopez-Luna JJ, Belmont A, Gutierrez-Castellanos S: **Differential expression of STAT5 and Bcl-xL, and high expression of Neu and STAT3 in non-small-cell lung carcinoma.** *Lung Cancer* 2006, **54:**163-168.

FIGURE LEGENDS

Fig. 1. ErbB4 is commonly expressed in human MPNSTs and MPNST-derived cell lines. A-F) Representative images of erbB4 immunostaining of FFPE sections of human MPNSTs demonstrates different grades of erbB4 staining compared to isotype matched negative control (B). A subset of erbB4 positive tumor samples displayed prominent nuclear staining (C, F) and others displayed exclusive non-nuclear membranous staining (A). Red channel (Alexa 565, erbB4). Blue channel (Hoechst, nuclei). G) Real time PCR analysis showing relative mRNA expression of erbB4 mRNA using non-isoform discriminatory PCR primers; mRNA levels are

shown relative to human Schwann cells. GAPDH mRNA was used as the loading control for normalization. H) ErbB4 protein expression of by immunoblot analysis of whole cell lysates derived from human MPNST derived cell lines. GAPDH was used as a loading control.

Fig. 2. Loss of ErbB4 in human and mouse MPNST cells inhibits proliferation and survival. A) Immunoblots demonstrating reduced erbB4 expression in T265-2c and S462 cells transfected with erbB4 siRNA relative to cells transfected with non-targeting controls. B, C) Compared to non-targeting controls, erbB4 knockdown cells had decreased numbers of viable tumor cells (B) and decrease cellular proliferation (C). D) Immunoblot of MPNST642, a high erbB4 expressing cell line, demonstrating shRNA targeting of erbB4 expression. E) Compared to non-targeting shRNA controls, erbB4 shRNA knockdown cells had decreased numbers of viable tumor cells **, *p*-value≤0.01; ***, *p*-value≤0.001; ****, *p*-value≤0.0001. F) Representative erbB4 immunostaining of P_0-GGFβ3;*Trp53*$^{+/-}$;*Erbb4*$^{flox/flox}$ GEM mouse tumors showing erbB4 positivity compared to isotype matched negative controls (K). These representative erbB4 immunostains also show punctate membranous staining, with immunoreactivity present in almost all tumor cells (4+ staining). G) Kaplan-Meier survival curve of $^{/flox}$ mice shows that these animals survive an average of 210 days, similar to the parent line P_0-GGFβ3;*Trp53*$^{+/-}$ mice. H) Like their parent line, P_0-GGFβ3;*Trp53*$^{+/-}$;*Erbb4*$^{flox/flox}$ mice develop hypercellular neoplasms comprised of atypical spindled cells with numerous mitotic figures. As in human MPNSTs, these tumors are also immunoreactive for both S100β (I) and nestin (J). K) Isotype-matched negative control for erbB4 staining of mouse tumors. L) MPNST cells with intact *Erbb4* alleles (non-recombined) have a spindled morphology similar to that of wild-type Schwann cells, whereas knockout cells (M) are more ameboid. N) Nuclear blebbing was evident in a subset of *Erbb4*-ablated tumor cells. O, P) Decreased cellular viability (O) and proliferation (P) was observed in the *Erbb4* knockout cells (Cre) compared to the control cells from three independent tumor cultures. *, *p*-

value≤0.05; ****p-value≤0.0001 for comparisons of recombined (*Erbb4 -)* with non-recombined (*Erbb4+)* alleles. Red channel (Alexa 565, erbB4). Blue channel (Hoechst, nuclei).

Fig. 3. *Erbb4* ablation inhibits allograft growth and alters tumor histopathology in Nude mice. A, B) *Erbb4*-null cells from three separate tumor lines show reduced graft volume and mass compared to erbB4 expressing controls. *, p-value≤0.05. C-D) Representative histologic images of a UBI GFP control tumor (C) and a UBI Cre tumor (D). Arrows in C indicate the multinucleated cells that are commonly seen in these tumors-Check figure arrow. Note that these multinucleated cells are virtually absent in the *Erbb4*-null grafts. E) Quantification of Ki67 labeling indices in three allografted tumor lines. F) Quantification of TUNEL labeling indices in the same tumor lines. ****, p-value≤0.0001 for comparisons of recombined *Erbb4* allele (erbB4 -) grafts to grafts with non-recombined *Erbb4* alleles (erbB4+). G-M) Representative CD31 staining of control erbB4 positive tumors (G, J) and erbB4 negative tumors (H, L) with Hoechst counterstain (J,N) for cell nuclei detection. A non-immune isotype matched primary was used as a negative control (J). P) Quantification of representative immunofluorescent images using FIJI. . *, p-value≤0.05; ****p-value≤0.0001 for comparisons of recombined (*Erbb4 -)* with non-recombined (*Erbb4+)* alleles.

Fig. 4. *Erbb4* is not essential for Ras hyperactivation, but does increase the phosphorylation of a number of other cytoplasmic kinases. A) A comparison of Ras activation in *Erbb4*-null (Cre) and *Erbb4*-expressing control (Ctl) UBI MPNST cells shows that *Erbb4* loss does not affect Ras activation. B) Graphical representation of quantified kinase arrays comparing the levels of baseline phosphorylation to NRG1 stimulated phosphorylation in *Erbb4*-expressing UBI MPNST cells. The graph includes the subset of kinases whose phosphorylation was altered following NRG1β stimulation. C) Graphical representation of quantified kinase arrays comparing the levels of baseline phosphorylation of control *Erbb4*- intact cells to NRG1 stimulated *ErbB4*-intact

and *Erbb4-null* UBI MPNST cells to determine NRG1 dependent and *ErbB4* dependent kinases. D) Quantification of a subset of the non-responsive kinases *ErbB4*-intact compared to *ErbB4*-ablated to identify targets positively regulated by *ErbB4* independent of stimulation. E) Quantification of a subset of the non-responsive kinases *ErbB4*-intact compared to *ErbB4*-ablated to identify compensatory targets resulting from *ErbB4*-ablation independent of stimulation. Quantification of the kinases differentially phosphorylated was quantified per the manufacturer's protocol using ImageJ.

Fig. 5. Venn diagrams of the NRG1β- and erbB4-dependent signaling molecules identified in MPNST cells by analysis of phosphorylation events (A) and the functions that these signaling molecules mediate as identified by Ingenuity Pathway Analyses.

Fig. 6. MPNSTs are sensitive to inhibition of specific erbB4 activated signaling pathways. A) Downregulation of WNK1 expression did not affect cell viability. Cell viability was assessed six days after shRNA selection. Values represent cell viability after 72 hours normalized to 0 hr. After normalization, cell viability for each WNK1 knockdown was compared to non-targeting control. B-D) Cell viability was assessed in three log phase MPNST cell lines in the presence of designated inhibitor. Values represent cell viability after 72 hours of drug treatment normalized to 0 hr. After normalization, cell viability for each drug dose was compared to vehicle control. PLC-γ inhibition effects cell viability in a dose dependent manner (B). STAT3 inhibition significantly affects cell viability (C). STAT5 inhibition modestly affects cell viability (D).

Fig. 7. Schematic highlighting the signaling cascades that are dependent on erbB4 in MPNSTs. The STAT3/5 and PI3K pathway is positively regulated by erbB4 in a NRG1β-dependent manner.

Additional File

Additional file 1: **Fig. S1**. ErbB4 lysates are sensitive to denaturing detergents. **Table S1.** Patient demographics for immunostained MPNSTs. **Fig. S2**. Real-time PCR analyses of erbB4 splice variants and mouse MPNST erbB4 expression. **Table S2.** MPNST locations in P_0-GGFβ3;*Trp53*$^{+/-}$;*Erbb4*$^{flox/flox}$ mice. **Fig. S3**. Validation of *Erbb4* ablation and effects on expression of other erbB receptors. **Fig S4**. Kinase array blots for NRG1β and unstimulated control and *Erbb4*-null MPNST cells.

Legends for Additional File 1 Components

Fig. S1. **ErbB4 lysates are sensitive to denaturing detergents.** We observed that some cell lines showed low and/or inconsistent erbB4 protein isolation detection. Our investigations revealed that erbB4 containing lysates were very sensitive to lysis buffer composition in some lines. **A)** Immunoblot analysis of whole cell lysates isolated from MPNST cell liens using RIPA (ionic and non-ionic detergents) and MPER (non-ionic detergent). The use of lysis buffers devoid of ionic detergents such as mPER, an NP-40 (non-ionic) based detergent, improved recovery of erbB4 protein in these lines compared to other lysis buffers. RIPA lysis buffer (ionic and non-ionic containing detergents) consistently generated insoluble erbB4 in many of the cell lines (B). **B)** ErbB4 immunoblot analysis of RIPA lysates showing insolubility of erbB4 in the majority of cell lines. **C)** ErbB4 immunoblot analysis of HES (detergent free) lysates from a panel of normal human Schwann cells (HSC) and MPNST cell lines. When a detergent free, hypotonic lysis buffer was used we were able to detect multiple post-translational modifications of erbB4. MCF7 and T24 served as a positive and negative control, respectively. **D)** A subset of lysates from (C) (HSC, NMS2, MPNST642, T265-2c) were re-run on a lower percentage PAGE to highlight multiple post-translational modifications of erbB4 observed in HES lysates.

Table S1. Patient demographics for immunostained MPNSTs.

Fig. S2. Real-time PCR analyses of erbB4 splice variants and mouse MPNST erbB4 expression. **A)** Schematic of ERBB4 gene and QPCR primer location. **B-C)** Real time PCR analysis showing relative mRNA expression of *ERBB4* mRNA using isoform discriminatory PCR primers for JMa, JMb, CYT1, CYT2. Human Schwann cell (H.Sch) expression levels were set to one and all other lines were compared to that control line. *GAPDH* mRNA levels were used for normalization. D) Immunoblots of early passage mouse cultures from P0-GGFβ3 and P0-GGFβ3;Trp53+/- MPNST showing that mouse tumor derived cells from both GEM colonies retain erbB4 expression in culture.

Table S2. MPNST locations in P_0-GGFβ3;*Trp53*$^{+/-}$;*Erbb4*$^{flox/flox}$ mice.

Fig. S3. Validation of *Erbb4* ablation and effects on expression of other erbB receptors. **A)** PCR validation of *ErbB4* gene recombination (knockout) post-infection with adeno-Cre (knockout, recombined) or adeno-GFP (control, non-recombined) of three separate early-passage mouse cultures; the 250 bp band is derived from the adeno-Cre mediated recombined allele (*ErbB4* -), while the 350 bp band is the adeno-control virus mediated non-recombined allele (*ErbB4* +). **B-C)** Real-time PCR showing the normalized levels of *ErbB4* (B) or *ErbB* 1-3 (C) mRNA in Cre (*ErbB4* -, recombined) cells relative to control (*ErbB4* +, non-recombined) cells. *Gapdh* mRNA was used as the loading control normalization. Taqman probes were used for all genes.

Fig S4. Kinase array blots for NRG1β and unstimulated control and *Erbb4*-null MPNST cells. **A)** Kinase array blots for the both NRG1β stimulated (5 min) and unstimulated UB1 control (Ctl) and *ERBB4*-null (Cre) cells. Lysates were blotted onto the kinase array and signals were detected via chemiluminescence.

Figure 1

Click here to access/download;Figure;Fig 1.tif

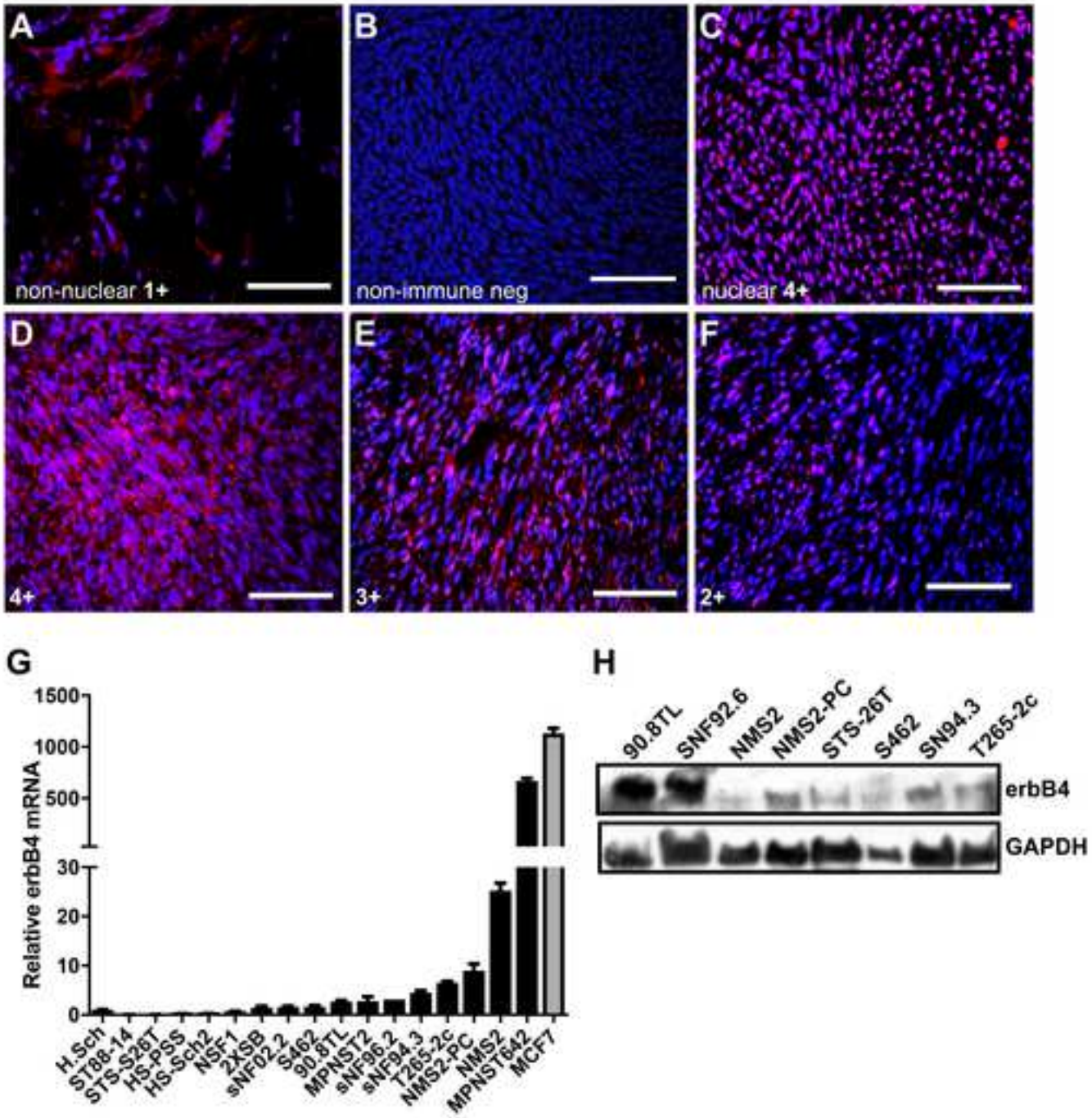


Figure 2

Click here to access/download;Figure;Fig 2.tif

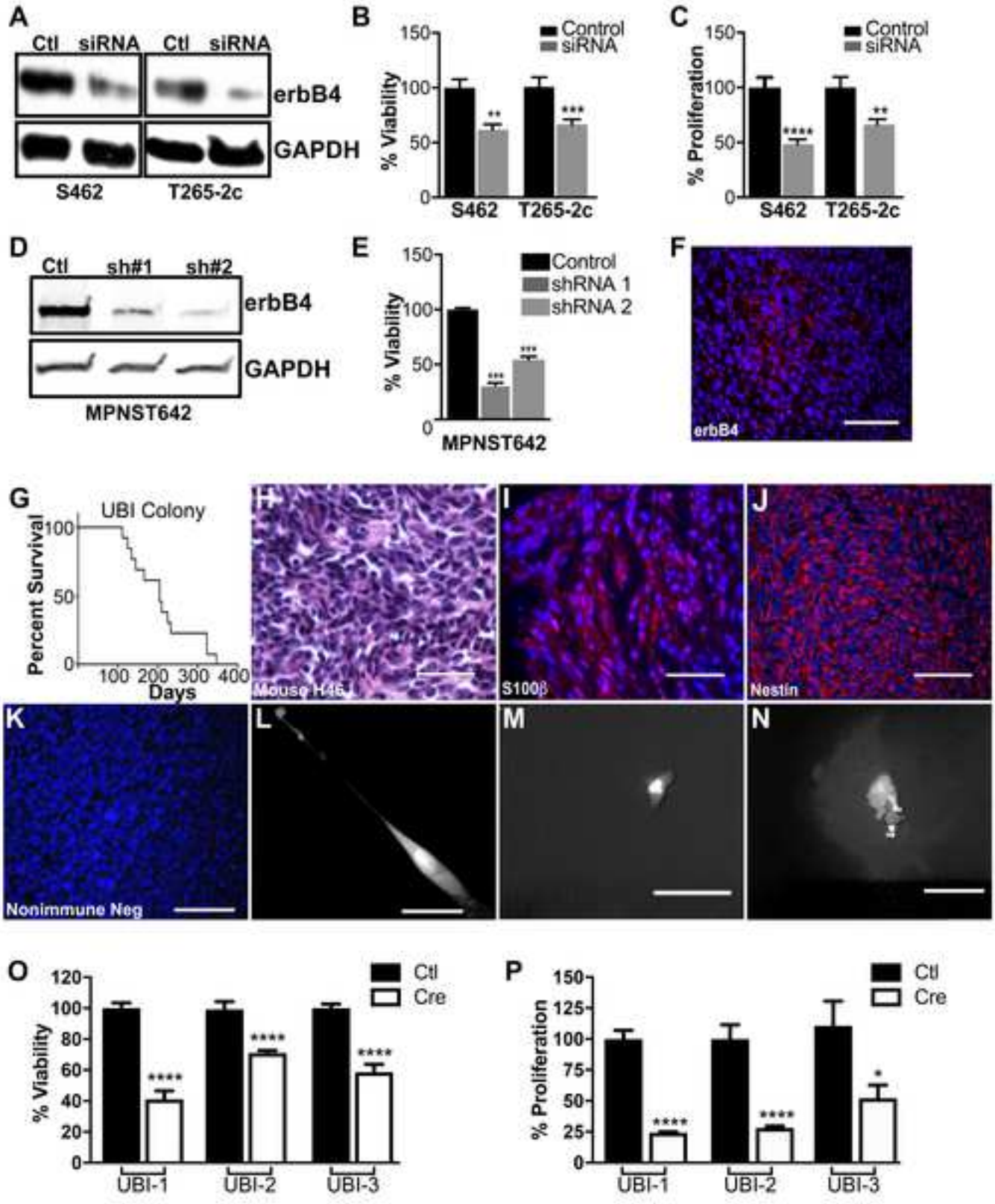


Figure 3

Click here to access/download;Figure;Fig 3.tif

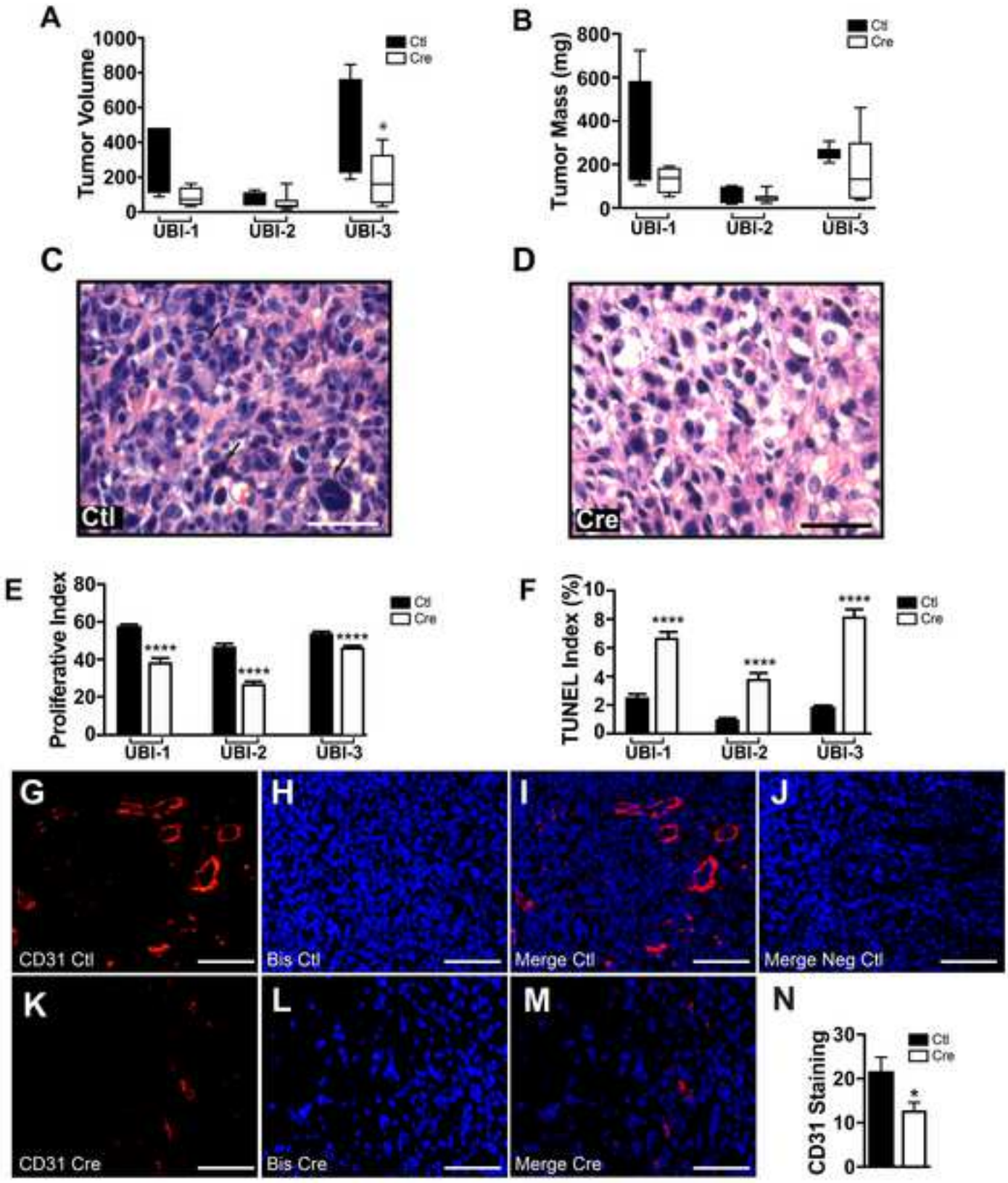


Figure 4

Click here to access/download;Figure;Fig 4.tif

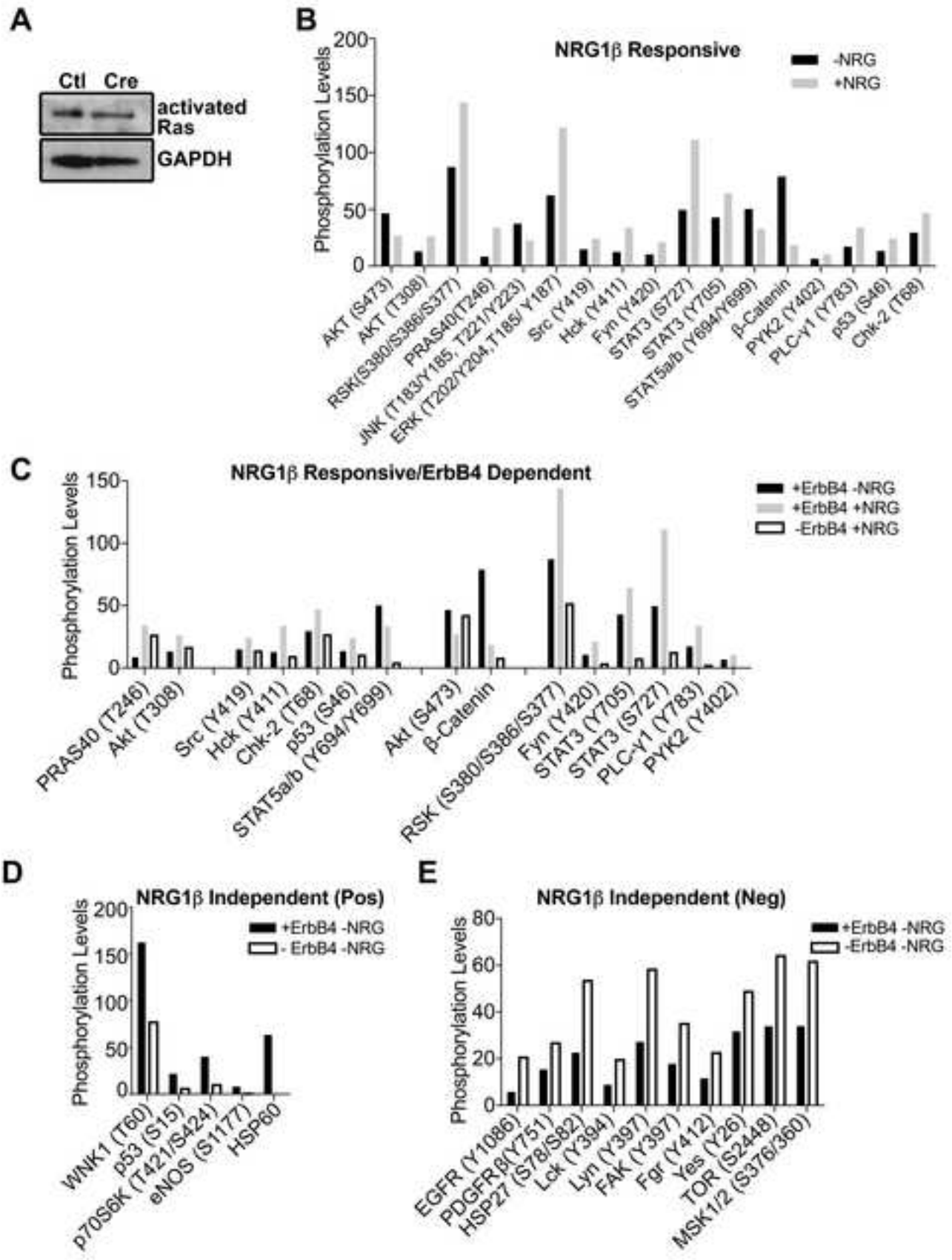
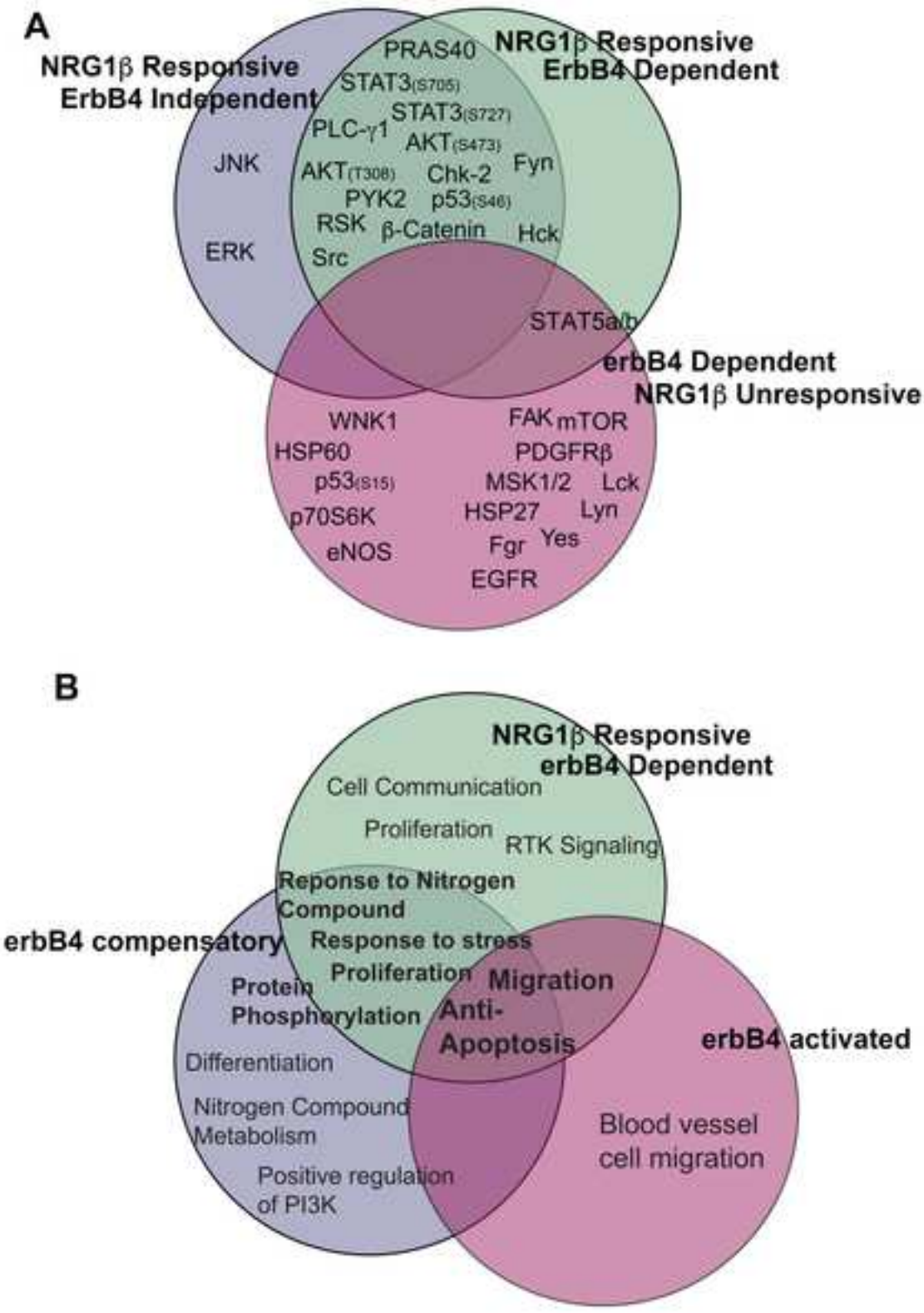


Figure 5

Click here to access/download;Figure;Fig 5.tif



Click here to access/download;Figure;CellSigComm_Fig 6.tif

Fig 6

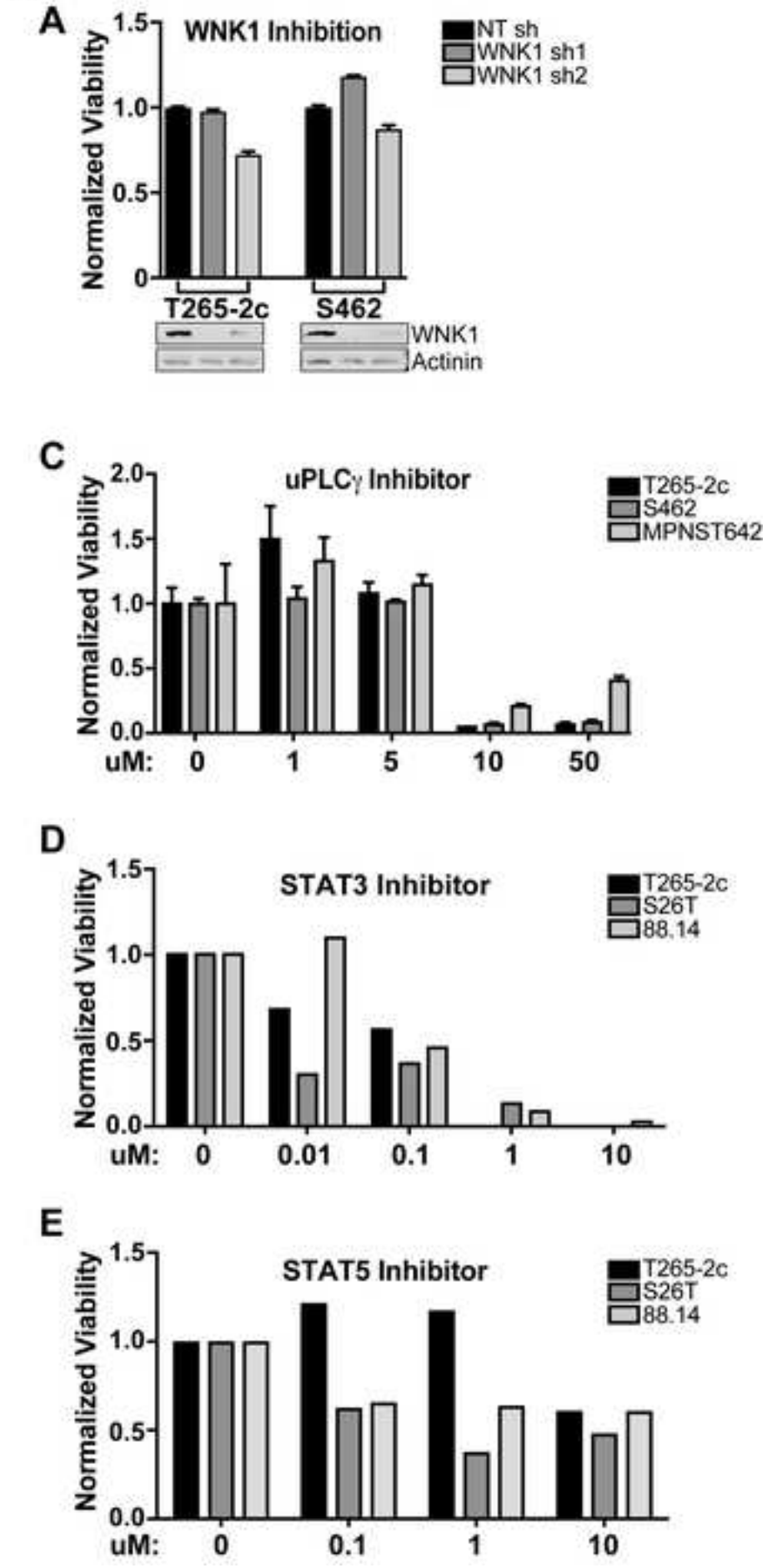


Figure 7

Click here to access/download;Figure;CellSigComm_Fig 7.tif

